A FINITE ELEMENT AND EXPERIMENTAL STUDY OF

REINFORCED CONCRETE IN TORSION

By

Mudathir Sulieman Mohamed, B.Sc., M.Sc.

A thesis submitted for the degree of

Doctor of Philosophy

Department of Civil Engineering

Glasgow University

September, 1986

بِسْمِ اللهِ الرَّحْمٰنِ الرَّحِيمِ

IN THE NAME OF ALLAH, THE MOST MERCIFUL,

THE MOST GRACIOUS

To my parents

and

my family

ACKNOWLEDGEMENTS

The work described in this thesis was carried out in the Department of Civil Engineering at the University of Glasgow under the general guidance of Professor A. Coull. The author would like to express his appreciation to Professor Coull, and to Professor H. B. Sutherland for the facilities of the department.

The author is indebted to Dr. D. V. Phillips for his valuable supervision, encouragement and advice throughout the course of this study.

Many thanks are due to:

The staff members of Glasgow University Computing Service in particular Mr. D. Fildes for their help in various matters related to programming.

The computer staff of the Civil Engineering Department, in particular Mrs. Carol John and Mr. G. Irving for their help with the computer.

Mr. W. Thomson for his patience and valuable effort in the construction of the experimental test-rig and his help during the course of the experimental programme.

Mr. J. Thomson, Mr. T. Montgomery, and Mr. J. Coleman for assissting in the experimental work and for all the tedious work involved in the preparation of the specimens.

The late Mr. J. Love and Mr. A. Burnet for their help in various matters during the experimental work.

Mr. I. Todd and Mr. A. Yuill for their help with the electrical connections and the operation of the data logger.

The staff of the University Library for all the trouble

SUMMARY

This thesis describes a study into the torsional behaviour of reinforced concrete members, in particular solid L-sections under pure torsion. It consists of three distinct but linked phases: (1) development, assessment and application of a three dimensional nonlinear finite element model for short-term behaviour of reinforced concrete, (2) an experimental programme and (3) a numerical parametric study. Nonlinear behaviour takes into account concrete cracking, nonlinear triaxial stress-strain relations of concrete, concrete crushing and yielding of steel reinforcement.

Cracking behaviour is modelled by a fixed orthotropic smeared crack approach, allowing up to three cracks to occur at any sampling point. Modelling of post-cracking behaviour allows for shear transfer and tension stiffening effects. Concrete behaviour under all multiaxial stress states is governed by a short-term constitutive law and a peak stress failure criterion. A bilinear uniaxial stress-strain law allowing for isotropic strain hardening is used for steel reinforcement.

20-noded isoparametric brick element is used to represent concrete, with single bars embedded within the concrete elements to simulate reinforcement. A modified Newton-Raphson approach was used for solving the nonlinear problem, based on the evaluation of a secantial elasticity matrix.

The program was assessed by studying the behaviour of deep beams, shallow beams simulating beam-column behaviour, rectangular beams subject to pure and combined torsion and

L-sections under pure torsion. Through systematic study, the influence of some of the major nonlinear material and solution parameters was established for these applications and limits on their values were set.

The experimental programme involved testing a series of solid reinforced concrete models of L-shaped cross sections under pure torsion in a specially designed and built test-rig. The tests were devised to: (1) assess the current British Code design procedure for torsion of solid L-sections, (2) obtain an insight into the torsional behaviour of these types of sections and (3) provide detailed results to assess the reliability of the finite element model in the analysis of torsion of fully reinforced flanged sections.

A dual approach of complementing the experimental results with a numerical parametric study, using the developed finite element model, is adopted where more variables not included in the experimental programme were investigated.

The current British Code design procedure for torsion was found to be too conservative for solid flanged sections, and it is concluded that the code's rules can be less stringent. Some recommendations that might help bring the code's torsion design procedure in line with other major codes of practice are given.

CONTENTS

NOTATION

Major symbols used in the text are listed below, others are defined as they first appear. Some symbols have different meanings in different contexts; these are clearly defined.

General symbols

[   ]   Square brackets denote rectangular matrices, T over the bracket denotes the transpose and -1 over the square matrices denotes the inverse. The symbols is also used for column vectors.

Scalars:

A_s	Cross sectional area of steel
b	total width of flange for L-section
b_w	width of web for L-section
dA	Elementary area
dv	Elementary volume
E_c	Modulus of elasticity for concrete
E_s	Modulus of elasticity for steel
E_w	Strain hardening modulus for steel
f'_c	Uniaxial compressive strength of concrete
f_{cu}	Cube strength of concrete
f_r	Modulus of rupture of concrete
f_s	Stress in steel
f_{sp}	Cylinder splitting strength of concrete
f'_t	Tensile strength of concrete
f_y	Yield stress of steel
f_{yl}	Yield stress of longitudinal reinforcement
f_{yv}	Yield stress of transverse reinforcement
G, G'	Shear modulus
h	total height of web for L-section

h_f	Height of flange for L-section
I_1, I_2, I_3	First, second and third invariants of the symbol that follows in parenthesis
J_2	Second invariant of the deviator of the symbol that follows in parenthesis
P_e	Strain energy of an element e
P_i, $P_i(\xi,\eta,\zeta)$	Shape functions
R_i	Norm of the total applied load
T_u	Ultimate (failure) torque of a reinfoced concrete section
u_i, v_i, w_i	Component of displacement at node i
u,v,w	Component of displacement in x, y, z
x,y,z	Global three dimentional cartesian coordinate
x^*,y^*,z^*	Principal axes
α_p	Torsion plastic coefficient
β	Shear retention factor
α	Tension stiffening parameter
$\xi \eta \zeta$	Normalized local curvilinear coordinates
ϵ	Strain
ϵ_c	Concrete strain
ϵ'_t	Uniaxial cracking strain of concrete
ϵ_{cu}	Uniaxial crushing strain of concrete
σ_s	Steel strain
σ_1, σ_2, σ_3	Principal stresses
ϵ_1, ϵ_2, ϵ_3	Principal strains
ν_c	Poisson's ratio for concrete
$[\sigma]$	Stress vector
σ_c	Cylinder strength of concrete
σ_y	Yield stress of steel

Vectors and Matrices:

[B]	Strain matrix
[D], [D_c]	Elasticity matrix
[F]$_e$	Nodal forces at nodes of an element e
[F]$_e$	Nodal forces vector due to initial strains
[F]$_p$	Nodal forces vector due to distributed load per unit volume
[F]$_g$	Nodal forces vector due to boundary pressure
[F]	Nodal forces vector due to external load
[F_u]	Unbalanced nodal forces vector
[J]	Jacobian matrix
[K], [K_o], [$\bar{K}$]	Overall stiffness matrix
[K]$_e$	Element stiffness matrix
[P]$_i$	Vector of total applied load
[P]	Vector of distributed load per unit Volume
[R]	Rotation matrix
[δ]	Overall displacement vector
[B], [δ]$_i$, [δ]$_u$	Nodal displacements
[δ]$_e$	Nodal displacements associated with element e
[Ψ]$_i$	Vector of residual nodal forces
[σ], [σ]$_n$	Total stress vector
[$σ_o$]	Initial stress vector
[ε], [ε]$_n$	Total strain vector
[$ε_o$]	Initial strain vector

Tensors:

δ_{ij}	Kronecker delta
ε_{ij}, ε_k	Strain tensor
ε_{kk}	Volumetric strain tensor
σ_{ij}	Stress tensor
ε_{ij}	Deviatoric strain tensor

Finite Element Analysis

Incr.	Increment number
Nalgo	Solution algorithm to indicate when the full stiffness matrix is to be reformulated
Toler.	Convergence tolerance
TS	Tension stiffening used
NTS	No tension stiffening used
$0.5 < \beta < 0.1$	Limits of the shear retention factor

N.B. 1   All dimensions in the figures are in mm units unless otherwise stated.

N.B. 2 $\varepsilon_{cu} = 0.0035$ for all analyses unless otherwise stated.

CHAPTER ONE

INTRODUCTION

1.1 General Background

This work is primarily concerned with torsional behaviour of reinforced concrete, where three approaches were followed to study its various aspects. A three dimensional nonlinear finite element model for the analysis of short-term behaviour of reinforced concrete, with particular reference to pure and combined torsion, was developed and tested. An experimental investigation on the pure torsional behaviour of reinforced concrete solid L-sections, designed to assess some aspects of torsion design procedure of current British Codes, was undertaken. A dual approach, in which a numerical parametric study complements experimental results, was adopted as more variables were investigated on concrete L-sections subject to torsion, prior to offering additional conclusions and some design recommendations. Applications of the developed finite element model include a variety of reinforced concrete structures in addition to the torsional specimens tested in this study.

In the past 30 years structural analysis has changed dramatically with the advent, and then the enormous expansion, of the power of digital computers in terms of both speed and storage capacity. This has also been accompanied by continuously decreasing unit cost of computing. Modern technology of computer hardware ensures that this trend is set to continue.

On the software front, the development of programs for specific applications led to the development of large

packages. Whereas these large packages do undoubtedly have their place, in general the majority of industrial users require smaller and more efficient packages, and often individual programs. The main advantage of an individual program is that it can be easily understood and developed by a single programmer. Furthermore, the finer aspects of behaviour to be modelled can be better catered for in an individual program and the parameters affecting it can be easily investigated. Various methods of analysis can be conveniently programmed for the study of different behaviours in various fields.

The finite element method is now recognised as a very powerful method of analysis in the field of structural and solid mechanics. Its basic concepts and methodology are well established and have been published widely. New applications are being developed continuously particularly in nonlinear analysis. It has proved a remarkably adaptable method, capable of including various levels of complex behaviour.

In structural engineering the behaviour of reinforced concrete members and structural systems has been the subject of intensive investigation since the beginning of the present century. Current design methods continue in many respects to be based on the empirical approach, using the results of large amounts of experimental data. This is mainly because of the complexities associated with the development of rational analytical procedures. However, the finite element method lends itself to serve in these circumstances.

For example in the analysis of reinforced concrete, cracking

of concrete, tension-stiffening, nonlinear multiaxial material properties, complex steel-concrete interface behaviour, and other effects previously ignored or treated in a very approximate manner can be modelled rationally. Through such studies, in which the important parameters may be varied conveniently and systematically, new insights are gained that may provide a finer basis for codes and specifications on which ordinary design is based.

The reliability of the finite element models to be used in these studies must be carefully examined beforehand so that the effects of the important material and numerical parameters involved are known. This is necessary to provide an acceptable level of quality assurance.

The need for experimental research continues, both to provide a firm basis for empirical equations still likely to be used for many aspects of ordinary design, and to provide information for finite element analysis. It is necessary to obtain experimental information on material properties and interface behaviour, both of which are fundamental input for finite element analysis. Experimental results are required against which the finite element analysis must be compared. However, tests can be fewer in number and more fundamental and the need for testing of members over the full range of variables is greatly reduced. Instead systematic parametric studies can be performed by finite element models. This will be both cheaper and quicker and will cover a larger range of important variables than laboratory or full-scale experiment alone.

A look into the literature on reinforced concrete reveals that torsion is the most neglected stress resultant; flexure, shear and axial forces are all better studied and consequently more codified. It was usual to ignore torsional moments and assume instead that they could be taken care of by the large safety factors used in flexure and shear design. Nowadays, design techniques are more refined and structures are being designed which frequently carry large torsional moments. So explicit torsional design is often necessary.

Torsional distress has in fact been observed in many real life situations. Figure (1.1) shows torsional cracks caused by the San Fernando earthquake of 1971, on the outer columns of a building (ref. 1). Major torsional cracks in a spandrel beam of a parking garage were also observed in South Florida (ref. 8), in 1964 (Figure 1.2). A complete collapse of a six storey building, in the United States, occured due to the shear and torsion failure of the ribbed reinforced concrete raft foundation as recently as 1979 (Figure 1.3), as one corner of the building settled about 3.5 meters (ref. 8).

Examples of structural members that carry significant torsional moments are many. In modern monolithic reinforced concrete structures, the spandrel beams generally carry substantial torsional moments. Edge beams of shells and some girder systems also receive some torsion that must be accounted for in design. In highway engineering, curved beams have been in extensive use in recent years. These beams are usually supported on minimum number of piers for elevated roadways. As a result, significant torsional

moments are created.

A more complex situation arises in non-rectangular three dimensional structures. Staircases without intermediate supports and spiral stairs are notable examples which can give rise to high twisting moments. In many of the above examples the large torsional stresses are created because of structural and/or architectural reasons. Indeed, many new structural forms that introduce out-of-plane loadings have been developed and are in growing use. As a result, many structures are required to function as three dimensional frames. This often results in members that are subjected to torsional moments too large to be ignored.

Two well known examples of major edge beams, from British practice, where torsional moments exercised a controlling influence over the design are the Waterloo Bridge (Figure 1.4) and the balcony of the Royal Festival Hall (Figure 1.5), both in London (refs. 4, 5). The transfer girders of the American Hospital Association Buildings in Chicago, Figure (1.6), were the first to be designed using the ACI design criterion (refs. 8, 11). These examples illustrate the need for investigations into the torsional behaviour of reinforced concrete to help add sufficient code provisions to match those for shear and flexure.

Although torsional moments rarely act in isolation, many studies have been made to understand basic behaviour under this condition. Studies have also been made of the interaction between torsion, shear and flexure (ref. 2 for example). As a result design recommendations have been included in various national codes of practice. Enhancements

to these provisions are continuously made as new evidence becomes available.

Codification of torsion provisions for reinforced concrete began in earnest in the 1950s (ref. 8). It generally started with partial provisions and some full specifications. For partial provisions only the permissible torsional stresses for concrete were given whereas for full specifications these were accompanied by the formulae for the design of torsional reinforcement. The specifications were generally based on Rausch's space truss analogy or Cowan's theory (both discussed in more detail in Chapter Two). However, the validity of these theories had not then been substantiated by systematic testing. Furthermore, the majority of experimental studies carried out since then to verify these equations have been done on rectangular sections (refs. 2, 8).

In 1958, ACI Committee 438 - Torsion, was created to study the torsion problem and to recommend suitable provisions for the 1963 ACI Building Code. However, owing to the lack of knowledge on the torsional behaviour of reinforced concrete members, the committee decided that it could not recommend any detailed provisions for the 1963 code. So only one clause was included stating: "In edge or spandrel beams the stirrups provided shall be closed and at least one longitudinal bar shall be placed in each corner of the beam section, the bar to be at least the diameter of the stirrups or 1/2 in., whichever is greater".

It was in 1969 when the ACI torsion criteria were first

formulated, based on extensive experimental research during the 1960s promoted by ACI Committee 438. The criteria were incorporated into the ACI Building Code (ref. 9), and further enhancements have been made in the later versions of the document.

The British Code incorporated torsion provisions for the first time in 1972 (ref. 3). The provisions were immediately criticized as being too conservative (ref. 10). The same provisions are used in the new version of the code (ref. 3) with only minor changes regarding the maximum permissible torsional stresses in concrete. These are increased by about 6% which would not make any appreciable difference for most practical cross sections. The code recommendations are also noted for their limited nature, as compared to other major codes of practice, for example the Russian, American and CEB-FIP Model Code. An example of this is the limit on the effective overhanging flange width in torsion. Both the ACI and the CEB-FIP codes specify the limit as 3 whereas no such provision is given in BS:8110 - 1985. Another example is the torsion provisions for box sections, which are very limited in the British code compared to the ACI specifications.

Torsional behaviour becomes inextricably three dimensional once cracking of concrete occurs and St. Venant's theory is no longer applicable. Previous studies have established that the reinforcement has no significant contribution to torsional stiffness prior to cracking of concrete and that the behaviour is essentially linear up to the cracking stage. Great reduction of stiffness occurs after cracking and the reinforcement only then assumes its major share of

responsibility in resisting the applied torque. The main feature of torsional cracking is its 45° helical nature, as distinct from flexural and shear types of cracks. All reinforcement carries tensile stresses and the concrete between the cracks carry the compressive forces.

Torsion differs from transverse shear in one important respect: diagonal tensile stresses exist on all four faces of a rectangular section subject to torsion, whereas they extend over the two vertical faces in a section subject to transverse shear. Consequently U-stirrups and bent-up bars are unsuitable for torsional shear reinforcement, and closed hoops, properly anchored at the end must be used. Inclined hoops, running to resist the diagonal tension on one face, would run in the wrong direction on the opposite face: hoops must therefore be normal to the longitudinal axis of the member. Similarly, the longitudinal reinforcement must be suitably distributed over all the faces of the section. The above illustrates the three dimensional nature, and hence the complexity, of the treatment of torsional analysis of reinforced concrete.

Most concrete elements subject to torsion are flanged sections, more commonly L-beams comprising the external wall beams of structural floor. The general procedure of designing such elements for torsion is to divide them into their component rectangles and design each rectangle separately ensuring proper interaction between the reinforcements of all components. Extensive studies have been conducted on torsion of reinforced concrete rectangular sections and to a much lesser extent on flanged sections

(refs. 2 and 6 for example). This activity will be reviewed in Chapter Two in more detail.

The majority of previous studies on torsion of reinforced concrete flanged sections were conducted on members with either unreinforced flanges or flanges having only one layer of reinforcement. The category of fully reinforced solid flanged sections, i.e. with closed stirrups in all component rectangles as recommended by the codes of practice, still lacks proper investigation in contrast to rectangular sections. Studies on such members will provide the opportunity of directly assessing the current codes provisions for torsion design as well as giving more insight into the behaviour.

Torsion theories, mainly lower bound space truss analogies and upper bound skew-bending theories, have increased basic understanding. Indeed the truss analogy, first proposed by Rausch in 1929 (ref. 6), gives a very clear idea of the main function of reinforcement and concrete in resisting torsion. The skew-bending theory, originally proposed by Lessig (ref. 7) and later undergone many developments, is based on the plane deformation approach of plane sections subjected to bending and torsion.

The space truss analogy is an extension of the model used in the design of the shear-resisting stirrups, in which the diagonal tension cracks, once they start to develop, are resisted by the stirrups. Because of the nonplanar shape of the cross sections due to the twisting moments, a space truss composed of the stirrups is used as the diagonal tension members, and the idealized concrete strips at 45°

between the cracks are used as the compression members. It is assumed that the concrete member behaves in torsion similar to a thin-walled box with a constant shear flow in the wall cross section, producing a constant torsional moment.

The skew-bending theory considers in detail the internal deformational behaviour of the series of transverse warped surfaces along the member. The basic characteristic of this theory is the assumption of a skew failure surface. This surface is initiated by a helical crack on three faces of a rectangular beam, while the ends of this helical crack are connected by a compression zone near the fourth face. The failure surface intersects both the longitudinal reinforcement and the closed stirrups. The forces in this reinforcement provides the internal forces and moments to resist the external forces and moments. At failure of a beam, the two parts of the beam separated by the failure surface rotate against each other about a neutral axis on the inside edge of the compression zone. More details on the truss analogy and the skew-bending theory will be given in Chapter Two.

In finite element terms certain special structures, such as thin walled sections, could be analysed by using membrane or plate finite elements, but in general, and in particular for solid sections, full three dimensional analysis must be used. With decreasing computing cost, three dimensional nonlinear finite element analysis is becomming a more feasible proposition. Yet it is still inherently the most expensive idealisation and care must always be taken when

setting up a model.

1.2 Objectives and Scope

The objectives of this study were:

(1) To develop a three dimensional nonlinear finite element program for the analysis of the short-term behaviour of reinforced concrete. The model was to incorporate the basic causes of the nonlinear behaviour which include concrete cracking, post-cracking effects, multiaxial stress-strain behaviour, concrete crushing and steel yielding. Proper simulation of steel reinforcement was considered important in the analysis of the torsional behaviour of reinforced concrete sections which normally include discrete longitudinal bars and stirrups. The program was written so that it could be used for other reinforced concrete applications. Therefore a critical assessment of its performance in a variety of structural applications was undertaken in order to establish a clear picture of the effects of the main nonlinear solution and material parameters in each particular situation.

(2) To conduct a series of experiments to study the behaviour of reinforced concrete specimens of L-shaped cross sections under pure torsion designed and detailed according to the British Code (BS:8110 - 1985, formerly CP110 - 1972) specifications. The aim of this part was three fold: (a) to assess the code requirements for torsion design, with particular reference to solid L-sections as a special case of solid flanged section, (b) to obtain an insight into the torsional behaviour of fully reinforced L-sections and (c) to provide detailed experimental results to assess the

capability of the developed finite element model in the analysis of these types of cross sections.

(3) To use the finite element model, having set up limits and guidelines on the important material parameters, to perform a parametric study on torsional behaviour of solid reinforced concrete L-sections to complement the experimental data. This was to provide more information on the effects of major parameters not included in the experimental programme.

(4) To combine the results of both the experimental investigation and the parametric study to offer some design recommendations that might help bring the British Code design procedure for torsion in line with other major codes of practice.

1.3 Layout of Thesis

Chapter Two reviews the torsion problem of reinforced concrete. The historical background to the current knowledge regarding the problem is summarised. The current two major methods of torsion analysis, namely the truss analogies and the skew-bending theories, are reviewed together with some of the relevant recent work reported in literature. Torsion design procedures in some of the major codes of practice are summarised and compared. The difficulties regarding the torsion analysis of reinforced concrete are also highlighted.

Chapter Three is concerned mainly with the finite element method. As the method is now firmly established, it is only briefly reviewed. The main contribution in this area is the

incorporation of embedded bars for the simulation of steel reinforcement. This allows accurate representation of stirrups and longitudinal bars within the 20-noded isoparametric element chosen to simulate concrete. Full derivation of the matrices for their implementation is given and the advantages of using these types of embedded bars are discussed. The chapter also reviews nonlinear methods of solution and describes the methods used in this work.

The mathematical material models describing the behaviour of concrete and steel are presented in Chapter Four. These include cracking, three dimensional stress-strain laws and crushing of concrete and steel stress-strain behaviour. The post-cracking behaviour of concrete is also described which includes tension stiffening and shear retention effects.

Assessment of the capability of the developed finite element model in different reinforced concrete applications is reported in Chapter Five. These include the following cases: (1) deep beams, (2) shallow beams simulating beam-column behaviour, (3) rectangular beams under pure torsion and (4) rectangular beams subjected to combined bending and torsion. Some basic aspects of modelling were carefully studied because they proved crucial for better simulation of behaviour, such as the boundary conditions for the torsional application. The effects of some important nonlinear solution and material parameters were studied and are reported. Major conclusions and general guidelines regarding the suitability of the model for these different applications are given.

Chapter Six describes in detail the test-rig which was designed and built in order to carry out the torsion tests that form the experimental portion of this study. The instrumentation employed for measurement of the various quantities is shown. The test programme and the test specimens are fully described and the concrete and steel characteristics given.

In Chapter Seven the experimental results are presented. Specimen behaviour is described and the results are thoroughly discussed. The British code design procedure is critically assessed in the light of the test results and also from reported work in literature. The conservative nature of the current code recommendations is demonstrated and the main reasons considered to be causing it are discussed.

Chapter Eight presents analysis of the test specimens using the finite element model developed and described earlier. Experimental and theoretical results are compared. The applicability of the model in the torsion analysis of solid reinforced concrete L-sections is assessed.

A numerical parametric study, devised to complement the experimental work, is presented in Chapter Nine. The purpose of the study and the parameters chosen are given and the results are presented and analysed. The outcome of the parametric study is combined with that of the experimental portion in an attempt to suggest improvements to the current British Code torsion design procedure.

The main conclusions drawn from the various aspects of this

study are compiled in Chapter Ten. General comments are given and suggestions for further work are made.

Figure (1.1) Torsional cracks caused by the San Fernando Earthquake (ref. 1)
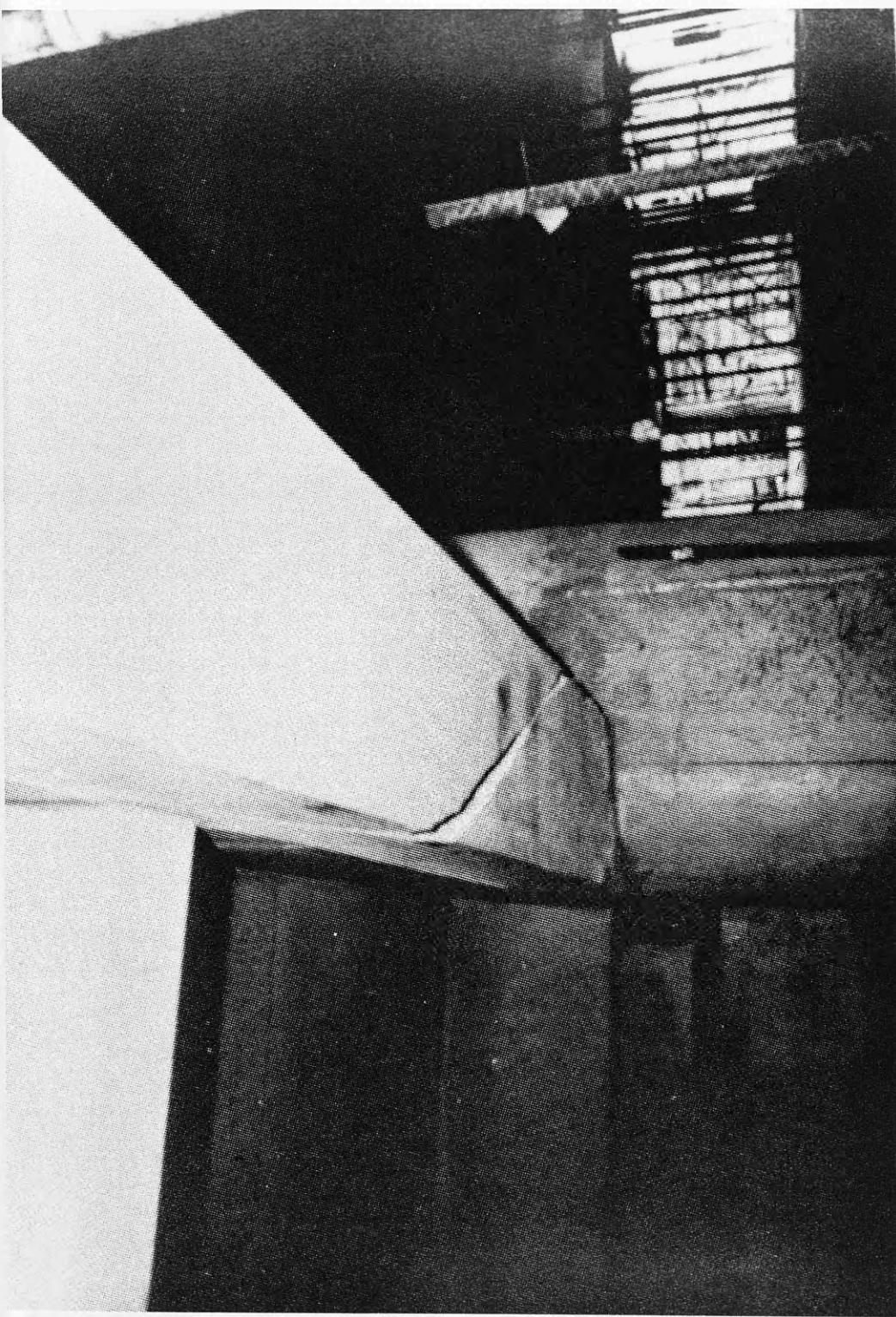
Figure (1.2) A large torsional crack near the support of a spandrel beam in a reinforced concrete parking garage in South Florida, USA, 1964 (ref. 8)
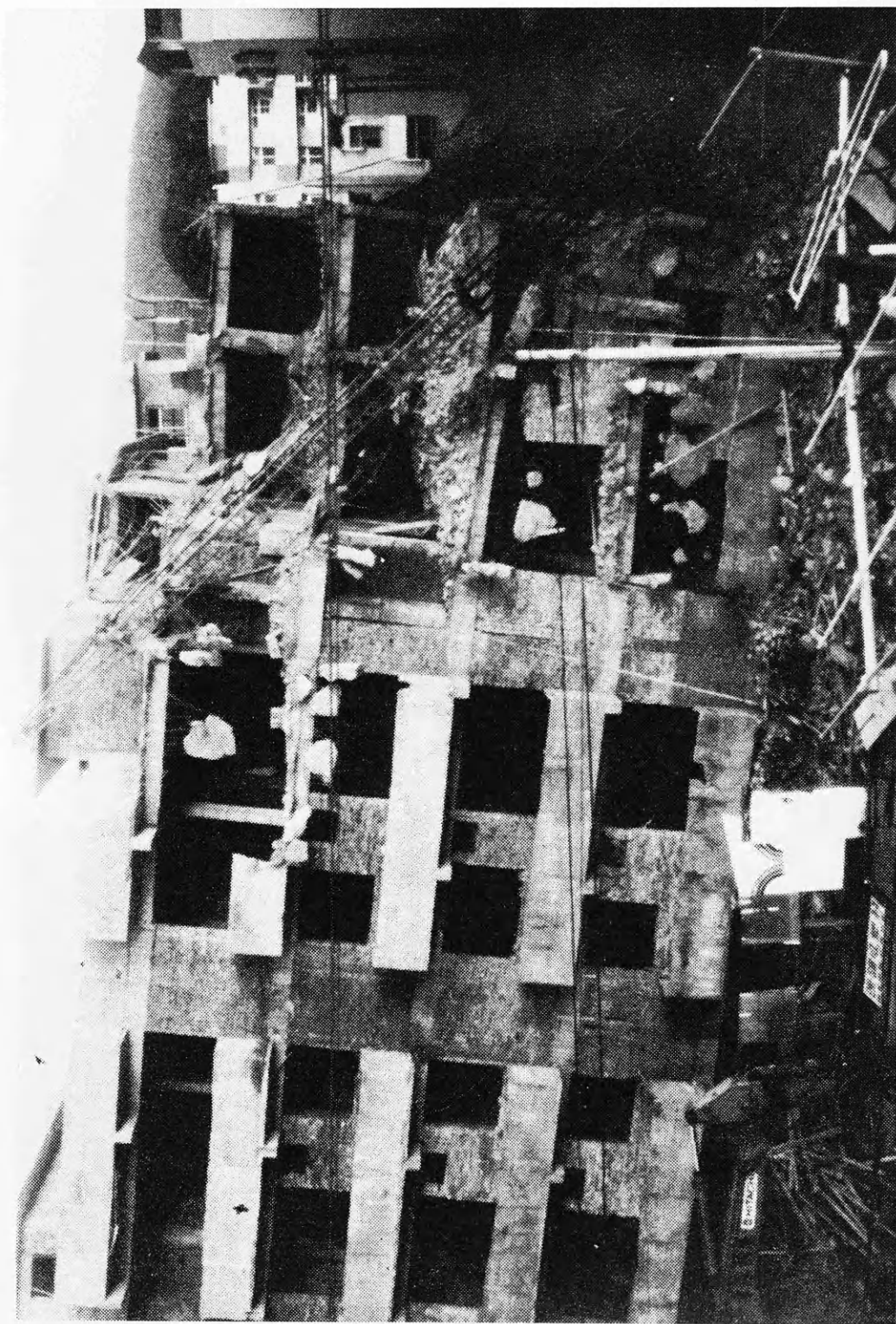
Figure (1.3) Collapse of a six storey building due to shear and torsion failure of the reinforced concrete ribbed raft foundation, 1979. One corner of the building has sunk 3.5 m. (ref. 8)
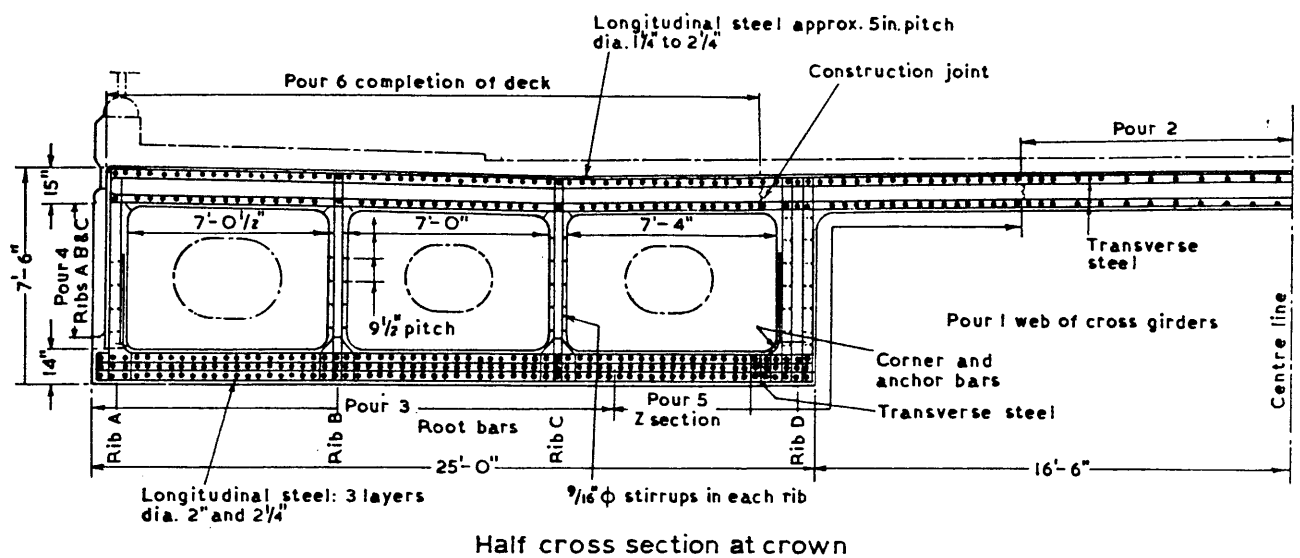
Figure (1.4) Half section through the crown of the Waterloo
Bridge, London, showing the triple box girders
(ref. 4)
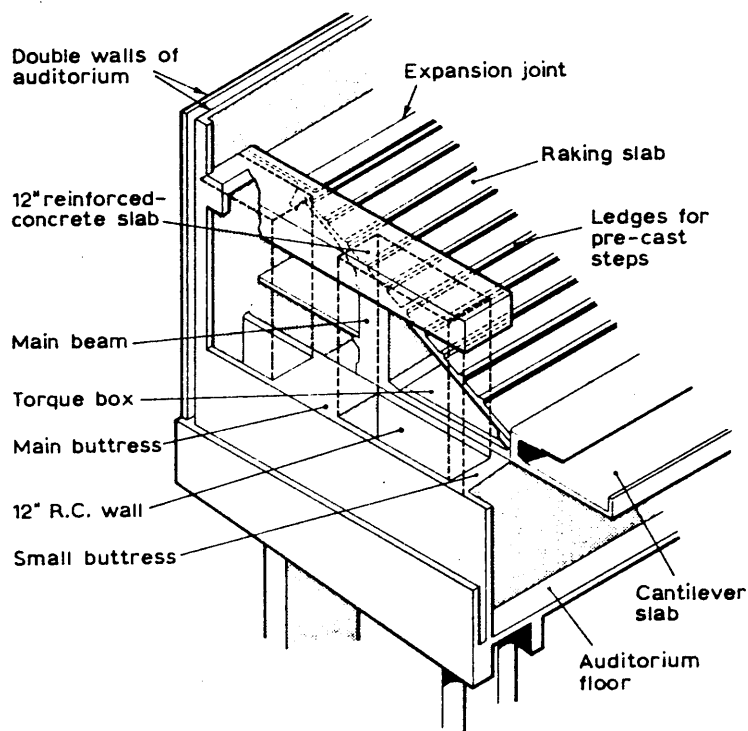
Figure (1.5) Axonometric view of the main balcony beam of the
Royal Festival Hall, London, showing the triangular
box girder which resists the twisting moments (ref. 5)
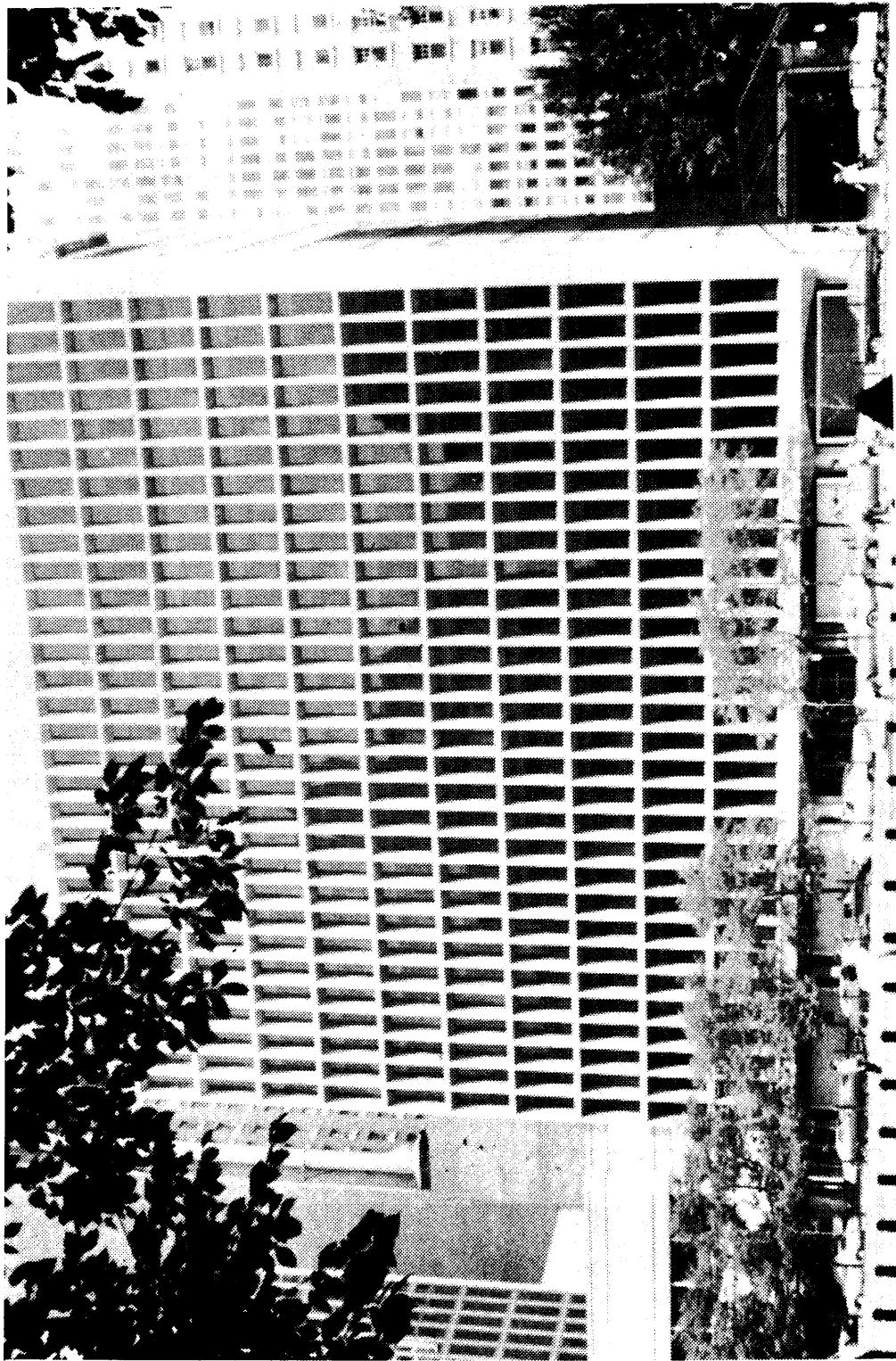
Figure (1.6) American Hospital Association Buildings, Chicago. The continuous transfer girder with 5 ft by 9 ft cross section floor level was the first to be designed by the ACI torsion criterion (refs. 8, 11)

References

(1) White, R.N., Gergely, P. and Sexsmith, R.G., "Structural Engineering", Vol. 3, Behaviour of Members and Systems, Wiley, 1972.

(2) ACI Special Publication,"Torsion of Reinforced Concrete", SP18, 1968.

(3) (a) British Standard Institution, CP110 - 1972, "The Structural Use of Concrete", Part 1, "Design, Material and Workmanship", London, 1972.

(3) (b) British Standard Institution, BS:8110 - 1985, "British Standard Structural Use of Concrete", Part 2, "Code of Practice for Special Circumstances", London, 1985.

(4) Buckton,E.J. and Cuerel, "The New Waterloo Bridge", Jour. ICE, Vol. 20, 1943, pp. 145-203.

(5) Measor,E.O. and New,D.H., "The Design and Construction of the Royal Festival Hall", Jour. ICE, Vol. 36, 1951, pp. 241-318.

(6) Rausch,E., "Design of Reinforced Concrete in Torsion" (Berechnug des Eisenbetons gegen Verderhung), Technische Hochschule, Berlin, 1929, 53 pp. (in German). A second edition was published in 1938. The third edition was titled "Drillung (Torsion), Schub and Scheren in Stahlbetonbau", Deutcher Ingenieur-Verlag GmbH, Dusseldorf, 1953, 168 pp.

(7) Lessig,N. N., "Determination of Load Carrying Capacity of Rectangular Reinforced Concrete Elements Subjected to Flexure and Torsion", Trudy No. 5, Institut Betona i Zhelezobetona (Concrete and Reinforced Concrete Institute),

Moscow, 1959, PP. 5-28 (in Russian). Translated by Portland Cement Association, Foreign Literature Study No. 371.

(8) Hsu, T.T.C., "Torsion of Reinforced Concrete", Wiley, 1984.

(9) (a) ACI Standard 318-71, "Building Code Requirements for Reinforced Concrete ACI 318-71", American Concrete Institute, Detroit, 1971.

(9) (b) ACI Standard 318-77, "Building Code Requirements for Reinforced Concrete ACI 318-77", American Concrete Institute, Detroit, 1977.

(9) (c) ACI Standard 318-83, "Buiding Code Requirements for Reinforced Concrete ACI 318-83", American Concrete Institute, Detroit, 1983.

(10) Marshall, W.T., "Torsion in Concrete and CP110 1972", The Structural Engineer, Vol. 52, No. 3, March, 1974, pp. 83-88.

(11) ACI Committee 438, "Tentative Recommendations for the Design of Reinforced Concrete Members to Resist Torsion", Jour. Amer. Conc. Instit., Proc., Vol. 66, No. 1, Jan., 1969, pp. 1-8.

CHAPTER TWO

TORSION OF REINFORCED CONCRETE

2.1 Introduction

Although torsion rarely acts in isolation, a thorough understanding of this phenomenon is essential in structural engineering and several useful studies of behaviour under this condition have been made. These studies ranged from the purely theoretical to the purely experimental. Some of these studies considered the case of pure torsion although the majority dealt with combined bending, shear and torsion. As a result of this work design recommendations were incorporated in various national codes of practice. Hsu (ref. 10) has thoroughly reviewed this activity. In the following sections the background material relevant to this work is reviewed.

The basic aspects of the torsional behaviour of reinforced concrete are the pre-cracking stiffness, the cracking torque, the post-cracking stiffness and the failure (or ultimate) torque.

2.2 Torsion of Plain and Reinforced Concrete
2.2.1 Early History

The torsion problem of a homogeneous circular member was thought about as early as 1784 by Coulomb (ref. 1), when he first found that the torque, T, is proportional to the angle of twist, θ .

The clear understanding of equilibrium, compatibility and stress-strain equations, enabled Navier (ref. 2), about 40 years later, to derive theoretical equations for torsion of an elastic circular shaft and rectangular sections. However,

the equations for rectangular sections were not supported by experiments on iron square members conducted by Duleau in 1820 (ref. 3).

In 1855, and after development of the necessary mathematical tools which included the Fourier series and the theory of elasticity, St. Venant (ref. 4) solved the puzzle regarding the torsion problem of homogeneous elastic rectangular members. The concept of warping and the so-called St. Venant constant , C, were introduced. Consequently, theoretical equations relating the applied torque to the angle of twist, and the resulting shear stresses to the applied torque were derived.

Approximate torsion equations for thin-walled flanged sections were suggested by Bach in 1911 (ref 5). Although these equations were originally intended for structural steel sections, where the thicknesses of the rectangular components are smaller than the overall dimensions by an order of magnitude, they were later found to be useful for concrete flanged sections with rather bulky sections.

Simple equations were derived by Bredt (ref. 6), in 1896, for prismatic thin tubes by assuming the cross section remained unchanged after twisting, and taking the warping effect to be uniform through the length. These equations were also found to be useful for torsion of reinforced concrete members.

The membrane analogy, which uses the similarity between the stress function in torsion problem and the deflection of a membrane under uniform loading, was discovered by Prandtl in

1903 (ref. 7). The analogy provided a convenient tool for visulization of magnitudes and directions of the elastic torsional shear stresses. This concept was later extended to the case of a plastic material by Nadai in 1923 (ref. 8) who proposed the sand heap analogy.

The attempts highlighted above greatly advanced basic understanding of the torsion problem of homogeneous members. They invariably, however, used crude assumptions. It can be said that St. Venant's theory can reasonably describe the torsion behaviour of plain concrete members at low torques. At high torques, there is a noticeable gradual deviation from the theory. This may be attributed to the presence of microcracking at this level of loading. This necessitated the search for development of new theories or use of previous ones with some modifications for torsion of plain and reinforced concrete.

2.2.2 Plain Concrete Members

Three theories have been developed to predict the torsional strength of plain concrete members: elastic theory, plastic theory, and skew-bending theory.

The elastic theory is based on St. Venant method. In applying this theory it is assumed that the torsional failure of a plain concrete member occurs when the maximum principal tensile stress, σ_{max}, equals the tensile strength of concrete, f'_t. Since $\sigma_{max} = \tau_{max}$ in pure shear, the elastic failure torque, T_e, is given by:

$$T_e = \alpha x^2 y f'_t \qquad (2.1)$$

where α is termed St. Venant's coefficient, and is a function of the ratio y/x (see for example ref. 10). The shear stress distribution for a rectangular section is shown in Figure (2.1), with the maximum values occuring at the middle of the longer side. The elastic theory was found to considerably underestimate the failure strength of plain concrete beams by up to 50% in some cases (ref. 11).

Attributing the extra strength to the plastic property of concrete, Nylander (ref.9) proposed a plastic coefficient, α_p, to replace St.Venant's elastic coefficient. Hence the torsional strength of a rectangular plain concrete beam becomes:

$$T_p = \alpha_p x^2 y f'_t \qquad\qquad (2.2)$$

where α_p = (1/2 - x/6y). Although the plastic coefficient is about 50% greater than the elastic coefficient, whic can roughly account for the observed extra strength, the plastic theory suffers from the following two weaknesses: (1) it is theoretically unsound as the principal tension is the prime cause of torsional beam failure, but no significant plastic behaviour has been observed in tension of concrete. The torsional failure of plain concrete members is quite brittle; there is no sign of plastic rotation, and (2) the theory can not account for a size effect; tests indicated that for small torsional specimens the calculated plastic torques are usually smaller than the test values, whereas the opposite is true for large specimens (ref. 10).

In view of the difficulties in using the classical elastic and plastic theories, Hsu (ref. 11) re-examined the

torsional failure process of rectangular plain concrete beams with the aid of a high speed movie camera. He indicated that, for such members under pure torsion, failure is caused by bending about an axis parallel to the wider face and inclined at an angle of $45°$ to the longitudinal axis of the beam. These characteristics were earlier suggested by Marshal and Tempe (ref. 12) for pure torsion, and by Lessig (ref. 13) for combined torsion. These are the characteristics of the so-called skew-bending failure mechanism. Hsu also suggested the following equation, based on the bending mechanism of torsional failure, for the torsional strength of plain concrete rectangular members:

$$T_{np} = \frac{x^2 y}{3} (0.85 f_r) \qquad\qquad (2.3)$$

where f_r is the modulus of rupture of concrete, and 0.85 is a reduction factor accounting for the effect of the perpendicular compressive stress on the tensile strength of concrete. This is because on a typical element on the surface of a rectangular beam, loaded in torsion, the shear stresses produce two principal stresses, one tensile and one compressive, perpendicular to each other.

Comparison of the elastic theory (Equation 2.1), plastic theory (Equation 2.2) and the skew-bending theory (Equation 2.3) reveals the following points: (1) they all have the same geometric parameter, $x^2 y$, (2) the only differences are the nondimensional coefficient and the material constant. In both the elastic and plastic theories, the material constant is the direct tensile strength of concrete, f'_t. In the skew-bending theory, it is the reduced modulus of rupture, 0.85 f_r. A comparison of the coefficients is shown in Figure

(2.2); the skew-bending coefficient (a constant = 1/3) always lies between the elastic and plastic coefficients, the latter two being functions of the ratio y/x.

For flanged sections (I, T or L), an approximation of the rectangular section equations is often adopted. This is done by assuming that the torsional strength of a flanged section is the sum of the torsional strength of its component rectangles.

2.2.3 Reinforced Concrete Members

Reinforced concrete members subjected to torsional moments can be divided into two groups: (1) members with longitudinal steel only, and (2) members with longitudinal steel and stirrups. The first group, in fact, does not have significant practical importance. Moreover, longitudinal steel alone was found ineffective in resisting torsional moments; the ultimate strength may exceed the cracking torque, but seldom exceeds it by more than 15% (ref. 10)

For concrete members reinforced with longitudinal steel and stirrups, commonly used in practice, the torsional strengths and the post-cracking torsional stiffnesses (slopes of the torque-twist curves) are strong functions of the steel percentage (see ref. 14 for example). Torque-twist curves for rectangular concrete members having the same cross section with different reinforcement ratios, taken from reference 14,are shown in Figure (2.3). Each curve can be divided into two distinct regions - before and after cracking. Before cracking the percentage of steel has negligible effect on the torsional stiffness, i.e all

members behave as plain concrete members. Therefore, St. Venant's torsional stiffness is applicable to members with longitudinal steel and stirrups before cracking.

After cracking, Figure (2.3) shows that the behaviour can no longer be predicted by St. Venant's theory. The main reason is that cracking terminates the basic assumption of the theory of elasticity that the material must be continuous. Hence a new equilibrium condition is established after cracking, in which the steel picks up the tensile stresses and the concrete carries the compression.

An interesting phenomenon was also observed (ref. 14) after cracking; the length of the beam increases with increasing torque. The unit lengthening of the beam resembles the average longitudinal steel strain (Figure 2.4), indicating that the lengthening of the beam is due to the stretching of the longitudinal bars. The effect of this lengthening may have a favourable effect in a building's torsional beam, which is normally longitudinally restrained by either columns or walls. A self-generated compression will be induced in the beam acting like a concentric prestress which will increase the torsional strength of the beam. This may be a contributing factor in explaining that complete torsional collapse is seldom observed in the interior spans of continuous beams.

The lessons learned from the accumulated theoretical and experimental studies on torsion of reinforced concrete are many, and are no doubt very useful in any further investigation. Concrete in torsion fails with a 45° helical fracture, at right angles to the direction of the diagonal

tensile stress. Consequently, 45° spiral reinforcement normal to the crack is the most effective. This is probably due to the better anchorage of the continuous spirals, as compared with individual hoops, particularly when there is no definite flexural compression zone. In specimens of circular cross section spirals are easily made, even at 45° to the axis. In rectangular specimens, however, the manufacturing as well as placing difficulties are many. Furthermore,there may be a possibility of a reversal of the sign of the torsional moment; this requires two systems of spirals to be installed, creating additional manufacturing difficulties and cost. A further objection to the use of spirals is that spiral reinforcement is not the most suitable for resisting bending shear, which normally combines with torsion shear in practical situations.

Since practical reinforced concrete sections are not normally circular, or even square, and torsion is seldom the only important criterion, spiral reinforcement is mainly of academic interest as the ideal torsion reinforcement. Nevertheless, and because of simplicity of mathematical derivations, it may be noticed that many of the torsion theories generally start by assuming spiral reinforcement, later taking closed stirrups as a special case (refs. 16, 17 for example).

The existing theories for calculating the torsional strength of members with longitudinal steel and stirrups can be roughly divided into two prominent categories: (1) the truss analogy type, and (2) the skew-bending type. Although they have later undergone many improvements, as will be seen in

the following sections of this chapter, the original
theories served to greatly improve basic understanding of
the torsional phenomenon.

2.2.3.1 Space Truss Analogy

The first theory for reinforced concrete subjected to
torsion was proposed by Rausch (ref. 17) in 1929. A concrete
member, with an arbitrary cross section, reinforced with
longitudinal and hoop steel is assumed to act like a hollow
section, so that the applied torsional moment is resisted by
the circulatory shear flow in the wall of the section.

After cracking, the concrete is separated by $45°$ cracks into
a series of helical members. These helical concrete members
are assumed to interact with the longitudinal and hoop steel
bars to form a space truss. Each of the helical members is
idealized into a series of $45°$ short straight struts
connected at the joints. The compression force in the
concrete struts will produce an outward radial force (i.e
perpendicular to both the longitudinal and lateral
directions) at each joint, that will be resisted by the
lateral hoop reinforcement. These lateral hoop bars are also
idealized as chains of short straight bars connected to the
concrete struts at the joints. The chains of diagonal
concrete struts and the chains of hoop bars thus form a
mechanism that will lengthen under an infinitismal external
torque. This tendency to lengthen is resisted by the
longitudinal reinforcement. Each longitudinal bar is assumed
to be a chain of short bars connected at the joints to the
diagonal struts and the hoop bars. In this way a space
truss, (Figure 2.5), that consists of $45°$ concrete struts in

compression and longitudinal and hoop bars in tension, is formed. Thus the space truss formed will resist a large external torque.

Through equilibrium of external and internal forces and compatibility of deformations, Rausch derived the following equation for the torsional strength of a reinforced concrete section:

$$T_n = \frac{2A_1 A_t f_s}{s} = \frac{2A_1 \hat{A}_l f_l}{u} \qquad (2.4\ a)$$

where T_n = nominal torsional resistance of the member

A_1 = area bounded by the centre line of a transverse

hoop bar = $x_1 y_1$ for a rectangular section with

closed stirrups

A_t = cross sectional area of a transverse hoop bar

f_s = steel strength of hoop bars

s = spacing of transverse hoop bars

$\hat{A}_l$ = total area of the longitudinal bars

f_l = steel strength of longitudinal bars

u = perimeter of the area bounded by the centre line

of a complete hoop bar

Equation (2.4 a), based on the working stress design method, was adopted by several codes of practice in the 1950s. Using current ultimate strength concept, the nominal torsional strength, T , can be expressed as:

$$T_n = \frac{2A_1 A_t f_{sy}}{s} = \frac{2A_1 \hat{A}_l f_{yl}}{u} \qquad (2.4\ b)$$

where f_{sy} = yield strength of transverse hoop bars

f_{yl} = yield strength of longitudinal bars

It follows from Equations (2.4 a) and (2.4 b) that the total area of the longitudinal steel is related to that of the hoop bars through the equation:

$$\frac{A_l f_y}{u} = \frac{A_t f_{sy}}{s}$$ (2.4 c)

On the assumption that both longitudinal and hoop steel has the same yield strength Equation (2.4 c) becomes:

$$\hat{A}_l s = A_t u$$ (2.4 d)

which states that the volume of all longitudinal steel within the spacing s should be equal to the volume of one complete hoop bar. This is the so-called equal volume principle employed by many codes of practice for the calculation of the longitudinal torsional reinforcement.

For a reinforced rectangular section, for example, the ultimate torsional strength is given by:

$$T_n = \frac{2x_1 y_1 A_t f_{sy}}{s}$$ (2.5)

where x_1 and y_1 are the smaller and larger dimensions of the closed stirrups, A_t is the area of one leg of stirrup, f_{ty} is the stirrup yield strength, and s is the stirrup spacing.

In the space truss formed, however, many assumptions were used. These are summarised and criticized in the following:

(1) The space truss is made up of $45°$ diagonal concrete struts; longitudinal bars, and hoop bars connected at the joints by hinges. This may be a fair assumption to make easy mathematical derivations.

(2) A diagonal concrete member carries only axial compression; i.e., shear resistance is neglected. Torsion is

primarily a shear problem. After cracking, which is normally very extensive, shear transfer becomes a major contribution in resisting the applied torque. Hence it should be, in some way, accounted for in the derivation of the ·torsional equations.

(3) Longitudinal and lateral bars carry only axial tension; i.e., dowel action is neglected. The dowel effect, near ultimate strength, has been widely observed in torsion (ref. 14 for example). As it is a result of shear deformations, its effects must be accounted for.

(4) For a solid section, the concrete core does not contribute to the ultimate torsional resistance. Although this has been shown to be reasonably applicable for rectangular sections (ref. 14), its validity for bulky flanged sections has not been reported. Furthermore, even for solid rectangular sections, the determination of the equivalent wall thickness is quite a problem. An empirical approach has been suggested by Hsu (ref. 27), using his own results on rectangular beams, to evaluate this quantity. This will be described in section (2.2.3.5).

(5) Uniform stress distribution is assumed along all the reinforcement. This contradicts St. Venant's stress distribution of torsional shear stress for all cross-sections except circular. For a rectangular section, for example, the maximum shear stress occurs at the middle of the longer side and decreases to zero at the corner. However, even St. Venant's distribution is questionable after cracking and the situation is indeed complicated.

(6) The theory has another weakness: it does not address the question of post-cracking torsional stiffness, as only the ultimate torque is determined. Hsu (ref. 27) later combined the space truss analogy and the thin tube theory to derive an equation for the post-cracking torsional stiffness. This will be discussed later in section (2.2.3.5).

Despite these comments Rausch's space truss analogy has given a very clear idea of the main functions of concrete and reinforcement in resisting torsion. The equation so derived is very simple and straightforward. For these reasons the space truss analogy has provided very useful service right up to the present time. Nevertheless, tests have shown that the theory over-estimates the torsional strength of reinforced concrete members (ref. 10). This has led to subsequent efforts to modify the original equation.

Pointing out that the non-uniform distribution of stress would result in a less effective contribution by the reinforcement, Andersen (ref. 18) suggested an efficiency coefficient, λ , less than unity, for the reinforcement. Furthermore, and analogous to the design of web reinforcement of beams to resist flexure and shear (common American practice), he suggested that concrete contribution to the ultimate strength, i.e. a separate term in the equation, must be taken into account. Accordingly Rausch's equation (Equation 2.4 b) becomes:

$$T_n = T_e + \lambda \frac{2A_1 A_t f_{ty}}{s} \qquad (2.6)$$

where T_e = St. Venant's elastic torque for plain concrete

$\qquad$ (= $\alpha x^2 y f'_t$ for a rectangular section)

λ = efficiency coefficient for reinforcement, which varies from 2/3 to 1.0, depending on the shape of the cross section and the number of bars

However, Andersen's coefficient is tedious to calculate and lacks rigour in derivation (ref. 10) and so has not been widely accepted. Using a strain energy method, Cowan (ref. 16) was able to overcome Andersen's difficulty in obtaining a logical and simple efficiency coefficient. Based strictly on St. Venant's stress and strain distribution, he derived the following equation for the torsional strength:

$$T_n = T_e + 1.6 \frac{A_1 A_t f_{ty}}{s} \qquad (2.7)$$

In the above equation the factor 1.6 implies that Cowan's efficiency coefficient, λ, is taken as 0.8 for all cases (in fact it varies between 0.798 and 0.844 for y_1/x_1 less than 3). Because Cowan's efficiency coefficient is based on St. Venant's stress and strain distribution, its validity after cracking is questionable. Nevertheless, the concept of using an efficiency coefficient to improve Rausch's torsional resistance has been widely accepted (for example the ACI Code uses it, as will be shown later).

A second approach was suggested by Lampert and Thurliman (ref. 19) for members subjected to torsion or combined torsion and bending. In trying to reduce the area A_1, in order to bring down the sum of the two terms of Equation (2.7), an arbitrary definition for the centre line of the shear flow was adopted; it was assumed that the centre line of the shear flow coincides with the lines connecting the centres of the corner bars. Furthermore, the angle of the

concrete struts was taken as variable, , instead of 45 originally used by Rausch. Also, a value for the concrete contribution different from T_e was used. Hence the torsional strength of a reinforced concrete member becomes: ·

$$T_n = T_c + 2 \frac{A_2 A_t f_{ty}}{s} \cot \alpha \qquad (2.8)$$

where A_2 = area bounded by the lines connecting the centres of the corner bars

α = angle of inclination of the concrete struts

T_c = concrete contribution =

2.5 $\tau_r t_d (2A_2)$ when $T_n < 3T_c$; T_c = 0 when $T_n > 3T_c$

$\tau_r = f'_t / 4$ where f'_t is taken as $0.214(f'_c)^{2/3}$; f'_t and f'_c in N/mm^2

t_d = effective wall thickness, taken as one-sixth of the diameter of the largest circle which can be contained within the area A_2.

For all practical purposes Equation (2.8) will be less than Equation (2.4 b) even with the incorporation of T_c and $\cot \alpha$ In the CEB-FIP Model Code (which adopts this approach and will be discussed later), the concrete struts are assumed to be inclined at a variable angle not necessarily $45°$.

More recently, Collins and Mitchell (ref. 20) adopted a third approach to modify Rausch's equation. The approach also tries to reduce the area A_1 by making an arbitrary assumption. They suggested:

$$T_n = 2 \frac{A_o A_t f_{ty}}{s} \cot \alpha \qquad (2.9 \text{ a})$$

where A_o is defined as the area bounded by the centre line of the shear flow, which is assumed to coincide with the

centroidal line of the equivalent compression stress block in the concrete struts. The concrete cover, outside the centre line of a hoop bar, is assumed to be ineffective for the determination of the equivalent stress block. So the value of A_o is approximated by:

$$A_o = A_1 - \frac{a_o}{2} P_1 \qquad (2.9\ b)$$

where a_o = depth of the equivalent rectangular compression stress block

P_1 = perimeter of the centre line of a hoop bar

In Equation (2.9 b) the depth a_o is found from equilibrium and compatibility as:

$$a_o = \frac{A_1}{P_1} \left[1 - \sqrt{1 - \frac{T_n P_1}{0.85 f_c' A_1^2} \left(\tan\alpha + \frac{1}{\tan\alpha}\right)} \right] \qquad (2.9\ c)$$

It is to be pointed out that Collins and Mitchell's approach, yet again, involved crude assumptions (for example neglecting the concrete cover) to bring the theory closer to experiments. Furthermore, a difficulty stems from the fact that the depth a_o, as calculated from Equation (2.9 c), is too small, because the standard cylinder strength of concrete has been used for the concrete struts (ref. 21). In fact, the strength of concrete is greatly reduced by the presence of diagonal cracking.

Hsu and Mo (refs. 21, 22) termed the reduction of strength in the struts due to diagonal cracking "softening of concrete". They pointed out that this softening effect can explain why Rausch's equation overestimates the torsional strength of reinforced concrete members. Using a softened

concrete compressive stress-strain curve, they derived a set of 8 equations, based on the truss model, for the prediction of the torsional strength as well as the angle of twist and steel and concrete strains at any loading stage. The equations were applied to 108 beams available in the literature and were considered satisfactory. However, the proposed equations failed in four cases due to the following reasons (ref. 22):

(1) Insufficient reinforcement; the member fails in a brittle manner upon cracking.

(2) Overreinforcement; crushing of concrete precedes yielding of longitudinal steel and stirrups, resulting in a brittle failure.

(3) Excessive stirrup spacing; the theoretical derivations assumed the struts to be continuously smeared along the length of the member.

(4) Excessive or insufficient cover; if the cover is excessive it may spall before the maximum torque is reached, or if it is too small the actual torsional strength may exceed the predicted value to an undesirable degree.

The set of equations offered by Hsu and Mo, however, need to be solved by trial and error. This is certainly a serious disadvantage as far as design is concerned.Because of this the same authors (ref. 23) made simplifications to arrive at a set of design recommendations. The recommendations included limitations on overreinforcement, insufficient reinforcement and concrete cover.

2.2.3.2 Skew-Bending Strength Theory

The other prominent category of theories for reinforced concrete members subjected to torsion is the skew-bending type. The basic characteristic of skew-bending theories is the assumption of a skew failure surface. This failure surface is initiated by a helical crack on three faces of a rectangular beam, while the ends of this helical crack are connected by a compression zone near the fourth face as shown in Figure (2.6). The failure surface intersects both the longitudinal reinforcement bars and the closed stirrups. The forces in this reinforcement provide the internal forces and moments to resist the external applied loads. At the failure of a beam, the two parts of the beam separated by the failure surface rotate against each other about a neutral axis on the inside edge of the compression zone. It is often assumed that both the longitudinal steel and stirrups will yield at the collapse of the beam.

The first skew-bending theory was proposed by Lessig (ref. 13) for combined loading in conjunction with two modes of failure; mode (1) where the compression zone is near the top face of the beam, and mode (2) where the compression zone is along a side face (see Figure 2.6). By taking two equilibrium conditions and a minimization of the strength of the section, she was able to offer a set of three basic equations which could be solved by a trial and error procedure. The theory was further simplified and incorporated in the Russian Code of 1962 (ref. 32) with empirical limits to prevent crushing of concrete before the yielding of steel and also to avoid partially overreinforced beams. However, the procedure was quite tedious and lengthy.

Moreover, it was found to overestimate the torsional strength in the case of pure torsion (ref. 14).

An overreinforced beam is reinforced with an unbalanced amount of longitudinal bars and stirrups. Therefore only the longitudinal bars or only the stirrups yield before crushing of concrete. This failure could be ductile, but not as ductile as underreinforced beams where a moderate amount of steel is provided resulting in a ductile failure (much desired in practice) caused by tensile yielding of both types of reinforcement. A third group can be defined, namely completely overreinforced beams, where an excessive amount of steel has been provided. Brittle failure caused by the crushing of concrete, before yielding of either the longitudinal bars or stirrups, is expected in this case.

Re-examining the failure process and mechanism, Hsu (refs. 14, 15) conducted experimental studies on a series of solid and hollow rectangular sections under pure torsion. Confirming the skew-bending nature of the torsion failure and suggesting that the source of the first term of the torsional strength equations, (Equation 2.8 for example), is the shear resistance of the concrete struts which was neglected in Rausch's theory, he suggested the following equation for the torsional strength of an underreinforced rectangular beam:

$$T_n = \frac{x^2 y}{3}(2.4\sqrt{f_c'}) + \underbrace{(0.66m\,\frac{f_{ly}}{f_{ty}} + 0.33\,\frac{y_1}{x_1})}_{\alpha_t}\frac{x_1 y_1 A_t f_{ty}}{s}$$

(2.10)

where x,y = smaller and larger overall section dimensions

x_1, y_1 = smaller and larger dimensions of c/c dimensions of the closed stirrups

f'_c = cylinder crushing strength of concrete

m = ratio of volume of longitudinal steel to volume

of stirrups = $\hat{A}_1 s / [A_t 2(x_1 + y_1)]$; $\hat{A}_1 = nA_1 =$

total area of longitudinal bars

(n = total number of bars and A_1 = area of one

bar)

f_{ly}, f_{ty} = yield strength of longitudinal bars and stirrups

respectively

A_t = area of one leg of stirrup

s = stirrup spacing

It can be seen that the proposed equation, 2.10, (adopted by the ACI Code), takes the same form as Equations (2.6 - 2.8) offered by the truss analogies. However, after some more test results became known, Hsu (ref. 24) updated Equation (2.10) to:

$$T_n = \frac{x^2 y}{3} \left(2.4\sqrt{f'_c}\right) + \underbrace{\sqrt{m} \frac{f_{ly}}{f_{ty}} \left(1 + 0.2 \frac{y_1}{x_1}\right)}_{\alpha_t} \frac{x_1 y_1 A_t f_{ty}}{s} \qquad (2.11)$$

It is clear, however, that the only difference between Equations (2.10) and (2.11) is the coefficient α_t, which still remains a function of m, f_{ly}/f_{ty} and y_1/x_1.

In view of the differences between various codes of practice as to the effect of the aspect ratio y/x of rectangular sections (particularly in the range 1.0 - 2.0), McMullen and Rangan (ref. 25) conducted an experimental study on 10 rectangular reinforced concrete beams. They correlated their results and others from literature using the ACI design criterion ,(Equation 2.10), to offer the following modified

equation:

$$T_u = 2.4\sqrt{f_c'}\, kx^2y + 1.4\sqrt{m}\; A_t \frac{x_1 y_1 f_{ty}}{s} \qquad (2.12)$$

where $k = 0.5/(1+x/y) < 0.33$

The equation is an improvement of Equation (2.10), a little simpler and appeared to have predicted well the ultimate torque of the beams tested. However, it is restricted to square or rectangular underreinforced beams with stirrup spacing less than $(x_1+y_1)/4$.

2.2.3.3 Classification

In structural analysis, plasticity theory provides the following two general approaches:

(1) The static approach, which searches for a stress distribution that is everywhere in equilibrium internally and balances the external loads without violating the yield criterion. As a result, it produces a lower-bound solution.

(2) The kinematic approach, which searches for a deformation mechanism that satisfies the geometric boundary conditions and for which the internal dissipation of energy equals the expenditure of energy due to external loads. This approach produces an upper-bound solution.

In general, all the skew-bending theories, that assume the yield of both longitudinal reinforcement and stirrups, belong to the kinematic approach, and hence should give upper-bound solutions. In contrast, the truss model theories belong to the static approach and theoretically should give lower-bound solutions.

2.2.3.4 Pre-cracking Stiffness

St. Venant's theory has widely been regarded as suitable for the description of torsional behaviour of reinforced concrete members before cracking (refs. 10, 14, 15). This is because reinforced concrete members before cracking behave like plain concrete members and the steel has negligible effect.

For rectangular sections, the relationship between the applied torque, T, and the resulting angle of twist, θ, is given by:

$$T = G\beta x^3 y\, \theta \qquad\qquad (2.13)$$

where G = shear modulus = $0.5E_C/(1+\nu)$

$\quad E_C$ = Young's modulus of concrete

$\quad \nu$ = Poisson's ratio

$\quad \beta$ = St. Venant's coefficient depending on the aspect ratio y/x approximated by Hsu (ref. 14) for rectangular sections as 0.155 y/x < 0.29

$\quad$ x,y = smaller and larger dimensions of the cross section

For flanged sections, however, Weinberger's approximation (ref. 26) is used. This states that the overall stiffness of a flanged section can be taken as the sum of the stiffnesses of its rectangular components. Thus Equation (2.13) becomes:

$$T = (G\sum \beta x^3 y)\,\theta \qquad\qquad (2.14)$$

where x,y = smaller and larger dimensions of each component rectangle.

Equations (2.13) and (2.14) give linear relationship between the applied torque and the resulting angle of twist.

However, they are only applicable before cracking starts. Once cracking is initiated, the basic assumptions of St. Venant's theory are broken and the relationship is no more linear. Substantial loss of stiffness has been reported (refs. 15, 48) as a new equilibrium condition is reached where the steel begins to contribute to the stiffness and carry significant stresses.

2.2.3.5 Post-cracking Stiffness

As discussed in the previous sections, all the equations are for the ultimate strength predictions. Few attempts, however, have been made to evaluate the torsional stiffness after cracking. Hsu (ref. 27) derived an equation for the post-cracking torsional stiffness of reinforced concrete sections, using Rausch's space truss idealization and the thin tube theory. Figure (2.7) shows a typical torque-twist curve for a reinforced concrete member. The first part of the curve is a straight line, the stiffness of which can be obtained by St.Venant's theory (Equations 2.13 or 2.14). After cracking, the stiffness is only a fraction of that before cracking. The curve starts out as a straight line and then gradually curves towards the horizontal when the maximum torque is approached. The slope of the initial straight portion is taken as the post-cracking torsional stiffness, the equation of which is given by (assuming a tube of thickness h):

$$G_{cr}C_{cr} = \frac{4E_s A_1^2 A_c}{u^2 \dfrac{4 m^* A_c}{uh} + \dfrac{1}{\rho_\ell} + \dfrac{1}{\rho_h}} \qquad (2.15)$$

where $G_{cr}C_{cr}$ = post-cracking torsional stiffness

E_s = Young's modulus of elasticity of steel

A_1 = area bounded by the centre line of the hoop reinforcement

A_c = solid cross sectional area within the outer perimeter of concrete

u = perimeter of the area bounded by the centre line of a complete hoop bar

m^* = ratio of steel Young's modulus to the concrete Young's modulus = E_s/E_c

h = wall thickness of the tube

ρ_ℓ = ratio of longitudinal steel area to the area of the cross section = nA_ℓ/A_cs

ρ_h = reinforcement ratio of the hoop steel

$\quad = A_h u/(A_c s)$

A_ℓ = area of one longitudinal bar

n = number of longitudinal bars

A_h = area of a hoop bar (area of one leg of stirrup)

s = stirrup spacing

For a rectangular section Equation (2.15) becomes:

$$G_{cr}C_{cr} = \frac{E_s x_1^2 y_1^2 xy}{(x_1+y_1)^2 \frac{2m^* xy}{(x_1+y_1)h} + \frac{1}{\rho_\ell} + \frac{1}{\rho_h}} \qquad (2.16)$$

where x,y = shorter and longer dimensions of the cross section

x_1, y_1 = shorter and longer dimensions of a rectangular closed stirrup

Equation (2.15) has been further simplified by Hsu (ref. 10) by neglecting the contribution of the concrete struts, and assuming that the vertical intercept of the post-cracking portion of the curve passes through the origin. This is because of the observation that the pre-cracking rotations are very small compared to those after cracking, hence can be ignored. The simplified equation becomes:

$$G_{cr}C_{cr} = \frac{4E_s A_1^2}{u(\frac{u}{nA_\ell} + \frac{s}{A_h})} \tag{2.17}$$

It can be noticed that in Equations (2.15) and (2.16) an arbitrary thickness is assumed for the wall of the thin tube representing the solid section. There is an obvious, though serious, question here; what is the effective wall thickness for solid sections or thick hollow sections ? Using his own experimental results, Hsu (ref. 15) suggested the following empirical equation:

$$h_e = 1.4(\rho_1 + \rho_h)x \tag{2.18}$$

Equation (2.17) has been used by Hsu et. al. (ref. 28) for post-cracking analysis of horizontally curved beams, an important example in highway engineering of members that carry significant torsional moments.

It has to be pointed out that the post-cracking portion of the torque-twist curve is not a straight line. So Equations (2.15) - (2.17) are an over-simplification. Equation (2.18), on the other hand, has been described by Hsu himself (ref. 10) as "an empirical quantity that fitted test results and should not be construed as the actual required wall

thickness at ultimate strength". Furthermore, the simplified equation, (2.17), has been checked on rectangular sections (refs. 15,28) only. Its validity for bulky flanged sections remains to be investigated.

Using an energy method, Sandegren and Yu (ref. 29) derived an expression for the torsional stiffness of reinforced concrete rectangular members at the end of the state of transition that follows first cracking. Approximating the solid rectangular section by an equivalent box section (Figure 2.8) and assuming plastic shear stress distribution on the wall thickness, the following expression was put forward:

$$K_t = \frac{4(b_o h_o)^2/u}{\dfrac{s}{A_{sw}E_{sw}} + \dfrac{u}{A_{slt}E_{sl}} + \dfrac{4}{tE_c}} \qquad (2.19)$$

where b_o = distance between the centres of reinforcement

h_o = vertical distance between two longitudinal bars

u = $2(b_o x h_o)$

s = spacing of stirrups

A_{sw} = area of cross section of one leg of a stirrup

E_{sw} = Young's modulus of web reinforcement

A_{slt} = total area of longitudinal steel

E_{sl} = Young's modulus of longitudinal steel

t = equivalent box wall thickness, taken as

   $b/6$ or $b_o/5$ whichever is less

b = overall breadth of section

E_c = Young's modulus of concrete

Equation (2.19) was applied on the rectangular sections of a reinforced concrete frame (ref. 29) and was found

reasonable. Its validity for other types of cross sections was not, however, substantiated. Furthermore, and as mentioned before, the post-cracking portion of the torque-twist curve is in no part of it a straight line. This is because of the continuous process of crack propagation before steel yielding and/or concrete crushing.

2.3 Torsion of Flanged Sections

The majority of torsion tests of reinforced concrete have been centerd on rectangular sections. The theoretical outcome of the investigations, however, is considered to be applicable to flanged sections by summing up the behaviour of their rectangular components. This procedure is adopted by many current codes of practice, for example the ACI and the British codes, as will be discussed later.

The majority of studies made on flanged sections concentrated on the combined behaviour and interaction of bending, shear and torsion (refs. 39, 40 for example).

The prediction of the pure torsional strength of a concrete section and its general behaviour are needed mainly as a basis for its strength and behaviour under combined loading. For L-sections, as a special case of flanged sections, some useful studies have been made to understand the basic behaviour under both pure and combined torsion. Although they undoubtedly enhanced basic understanding, they did not represent all cases of L-sections commonly used in practice.

Erosy and Ferguson (ref. 41) reported tests on small semicontinuous reinforced concrete L-beams , loaded and supported by diaphrgam-type cross members to prevent section

warping so as to simulate an edge beam, under combined torsion, shear and flexure. Their test program was designed to study the effect of the percentage of longitudinal steel, flange width and eccentricity of loading. No transverse reinforcement was used and welded wire fabrics were placed at the centre of the flanges to provide for the slab reinforcement. This was made to account for slab shrinkage and temperature changes. Placement of the slab reinforcement is unrealistic, however, as the normal case is that either top or bottom steel is used. Furthermore, the longitudinal steel alone would not add significant strength to the section (ref. 14, 15).

Osburn et. al. (ref. 42) tested L-beams, designed according to an earlier proposal (ref. 43), under combined torsion, shear and bending. They concluded that the ACI procedure, based generally on Hsu's approach (ref. 14, 15), and the procedure presented in reference (37) are both reasonably conservative. They also suggested that the slab flexural reinforcement in the flange of an L-beam does not act to increase the torsional strength of the beam. However, this last point needs further investigation because it was based on L-beams in which the flange reinforcement was provided at the top only and it did not form a closed stirrup with that of the web.

Results on L-beams subjected to pure and combined torsion were reported by Liao and Ferguson (ref. 37).The influence of stirrups was studied, and their marked influence on the behaviour and the ultimate load was reported. The stirrups, however, were provided in the web only. The flanges were

reinforced with mesh cages placed at the centre. Yet again, this may result in a case that does not represent the normal practice of L-beam reinforcement. They indicated an important point, in the author's view, which is that the torsional design procedures for beams with stirrups may eventually be less restrictive.

Behara and Ferguson (ref. 44) examined L-beams under combined bending, shear and torsion. The amounts of longitudinal steel and stirrups were varied. However, and similar to the previous studies, the flanges were reinforced at the top only. They indicated the insignificant influence of the steel amount on the pre-cracking torsional behaviour. They clearly indicated the complexity of Lessig's approach (ref. 13), which resulted in the skew-bending failure mechanism, if applied to a flanged beam. Indicating also that no theoretical solution was available, they proposed an empirical three dimensional interaction surface for the prediction of ultimate strength of a beam under combined bending, shear and torsion.

In an attempt to study the effect of the flange width on the torsional capacity of reinforced concrete flanged beams, Victor (ref. 45) tested T- and L-beams under different combinations of torque and moment. The primary variables were flange width and torque/moment ratio. He indicated that, although the design recommendations treat T- and L-beams alike, the performance of T-beams is superior. A strong conclusion of his study is that the ACI recommendation (ref. 31) to restrict the flange overhang to three times the flange thickness for both T- and L-beams

appears to be too conservative. A similar point is also concluded in a more recent study by Zararis and Penelis (ref. 52), who reported results of an experimental investigation aimed at studying the contribution of properly reinforced flanges (i.e. having closed stirrups) to the torsional capacity of reinforced concrete T-beams. They found that the effect of properly reinforced flanges is much more than that considered by the existing codes, and proposed an effective flange width of six times the flange thickness.

An experimental programme on T-beams subjected to combined bending and torsion was undertaken by Kirk and Lash (ref. 36). Based on the skew-bending failure mechanism, methods for the prediction of ultimate strength of T-beams subjected to combined bending and torsion were proposed. However, the suggested equations were limited to the case of T-beams containing the same longitudinal steel in the bottom as in the top. This may not always be the case in practical situations. The proposed equations require the steel to be proportioned so that failure would be characterised by yielding of the steel rather than crushing of the concrete, which makes sense as ductile failure is desired.

L-beams were tested by Rajagopalan et al. in pure torsion (ref. 46). Ratios of longitudinal to stirrup reinforcement above the boundaries set up by previous investigators (refs. 13, 14) were studied, and an empirical method for the prediction of the ultimate torsional strength of such "partially overreinforced beams" was proposed. The reinforcement of the tested beams was provided only in the

web. This might have resulted in the flange not sufficiently contributing towards the overall stiffness of the section.

Syamal et al. (ref. 47) presented results on L-beams subjected to combined flexure, shear and torsion. The skew-bending mechanism of failure was observed, and simplified interaction surfaces were constructed. They pointed out that a transition from a torsional failure mode to a flexural shear failure mode may occur in combined loading, depending on loading combination, beam cross section and longitudinal and transverse reinforcement. No measurements on steel were made, however, to indicate the cause of failure.

To check Behara and Ferguson's interaction surfaces (ref. 44), Rajagopalan tested L-beams with web height-to-breadth ratio > 3.0 under combined torsion, bending and shear (ref. 48). However, the flange was unreinforced as steel was provided in the web only. A substantial reduction of the torsional stiffness after diagonal cracking was observed, associated with excessive tension in the longitudinal reinforcement.

To obtain information on torsional behaviour of thin-walled reinforced concrete structures, Krpan and Collins (ref. 49) recently reported a test on a large reinforced concrete thin-walled channel section. The experiment was conducted to compare the results with the predictions of an analytical procedure suggested by the same author's (ref. 50). It was found necessary, for good strain predictions in the two legs of the transverse steel, to take into account the interaction of both circulatory and warping torsions. Although a reasonable prediction of longitudinal steel

strain was possible, that across the wall thickness was more difficult.

2.4 Code Formulations

2.4.1 Introduction

Compared to flexure and shear, torsion was the late in being codified. In a literature survey by Fisher and Zia (ref. 30) it was revealed that by 1960 there were only eight countries in the world that had "full" specifications and five countries that had "partial" specifications (see Table 2.1). "Full" specifications imply that the provisions give both the permissible torsional stresses for concrete and the formulae for the design of torsional reinforcement. "Partial" specifications give the former. The specifications were generally based on either Rausch's theory (Equation 2.6) or Cowan's theory (Equation 2.7), both of which were not then systematically tested.

Based on experimental tests carried out during the 1960s, the first detailed ACI torsion design criteria were formulated in 1969. These criteria were first embodied in the "Tentative Recommendations for the Design of Reinforced Concrete Members to Resist Torsion" (ref. 31). With minor modifications these recommendations were incorporated into the 1971 ACI Building Code (ref. 33). They were also continued, though in a slightly different format, in the 1977 and 1983 codes, with the addition of a new torsional limit design for spandrel beams.

The British Code, on the other hand, incorporated some clauses dealing with torsion for the first time in 1972

(ref. 34). These recommendations, however, were soon critisized as being conservative (ref. 35). This aspect will be discussed in detail in Chapter Seven. The same recommendations were continued with a minor change (an increase of about 6% on the maximum permissible shear stress of concrete) in the updated version of the code (ref. 34). The CEB-FIP Model Code (ref. 53) also contains some advanced provisions for torsion.

In the next sections a description of these recommendations is given.

2.4.2 ACI Procedure

The ACI design criterion for torsion follows very closely the design philosophy for flexural shear in that the reinforcement is assumed to carry the torsional stresses in excess of the concrete capacity.

Equation (2.10), based on the skew-bending theory, is simplified for practical design by assuming m = 1, $f_{ly} = f_{ty} = f_y$. The value m = 1 implies balanced ratio according to Rausch's space truss analogy (equal volume principle). For rectangular sections the torsional strength is given by:

$$T_n = \underbrace{\frac{x^2 y}{3} \left(2.4 \sqrt{f_c'}\right)}_{T_c} + \underbrace{\alpha_t \frac{x_1 y_1 A_t f_y}{s}}_{T_s} \qquad (2.20)$$

where $\alpha_t = 0.66 + 0.33 \, y_1/x_1 < 1.5$

T_n = nominal torsional moment strength of the section

T_c = nominal torsional moment strength provided by concrete

T_s = nominal torsional moment strength provided by torsion reinforcement

For practical design, the applied factored torque, T_u, should satisfy the condition $T_u = \Phi T_n = \Phi(T_c + T_s)$, where Φ is the strength reduction factor depending on the type of loading (equals 0.85 in this case). The second term of the equation is used for the calculation of stirrup reinforcement. The principle of equal volume is utilized for the calculation of the longitudinal steel, as m is assumed to be unity in Equation (2.10). Hence the total area of longitudinal steel, A_l, is given by:

$$A_l = A_t \frac{2(x_1 y_1)}{s} \qquad (2.21)$$

The following limitations are stated:

(1) A minimum torsional reinforcement is specified to ensure ductility of the beam when it cracks; this is based on theoretical considerations and is given by:

$$A_{t,min} = \frac{100xs}{f_y} \qquad (2.22)$$

(2) Torsional moment strength due to reinforcement, T_s, is specified as:

$$T_s < 4T_c \qquad (2.23)$$

This is based on test results on pure torsion (refs. 54, 55) and aims at avoiding overreinforced sections, as underreinforced beams are desirable in practice.

(3) To avoid a drastic drop of shear or torsional strength when stirrup spacing is too large, and to control crack widths, based on theoretical considerations later supported by test results (ref. 10), the maximum stirrup spacing is limited to:

$$s_{max} < \frac{x_1 y_1}{4} \qquad \text{or 12 in.} \qquad (2.24)$$

For an arbitrary bulky section without re-entrant corners, a more general equation for the maximum stirrup spacing is given as:

$$s_{max} = \frac{u}{8} \quad \text{or 12 in.} \quad (2.25)$$

where u is the periphery of the stirrup. Equation (2.25) reduces to (2.24) in the special case of a rectangular section. The maximum limit of 12 in. for the stirrup spacing was introduced to control crack width in large size girders (ref. 10).

(4) It is required that the yield strength of the torsional reinforcement shall not exceed 60,000 psi (about 415 N/mm^2). This is to ensure yielding of steel before failure, since all torsional design provisions are based on this criterion.

(5) The torsional reinforcement is to be provided at least a distance (d+b) beyond the point theoretically required. This requirement is more stringent than the corresponding one for flexure (ref. 10), but important to account for the helical nature of torsional cracks.

(6) Spacing of longitudinal bars, distributed around the perimeter of the closed stirrups, shall not exceed 12 in.

(7) Torsion can be neglected if the factored torsional moment, T_u, is less than $1.5(\sqrt{f'_c} \, x^2 y)$, or, in terms of stresses, if the torsional stress τ_u is less than $1.5 x \sqrt{f'_c}$.

For flanged sections, the assumption that the torsional strength of the section is the sum of the strengths of its

rectangular components is adopted. Hence Equation (2.20) becomes:

$$T_n = \Sigma\left[\frac{x^2y}{3}(2.4\sqrt{f'_c}) + \alpha_t\frac{x_1y_1A_tf_y}{s}\right] = \Sigma\frac{x^2y}{3}(2.4\sqrt{f'_c}) + \Sigma\alpha_t\frac{x_1y_1A_tf_y}{s}$$

(2.26)

As the quantity x^2y influences the arrangement of the component rectangles, the ACI code specifies the maximization of this quantity when dividing the flanged section to its component rectangles. To design the reinforcement for each individual rectangles, the total stirrup strength, T_s, is distributed among the rectangles in proportion to the parameter x^2y; i.e. for a typical component rectangle the allocated torsional strength will be:

$$T_{s\ell} = T_s\frac{x^2y}{\Sigma x^2y}$$

(2.27)

Thereafter, the design continues in the same way as for rectangular sections, ensuring proper detailing to tie the various reinfocements together. An effective flange width equals three times its thickness is specified. However, a recent study (ref. 52) revealed that this limit is too conservative for properly reinforced T-beams and a value of 6 is suggested. The procedure of adding up the reinforcements of the individual rectangles, on the other hand, was also found conservative (refs. 36, 37).

For box sections, if the wall thickness h is at least equal to x/4, the torsional strength is taken as equal to that of a solid section. If h < x/4, however, the first term of Equation (2.20) is modified by a reduction factor of 4h/x,

based on theoretical considerations using the thin-tube theory (ref. 10 for example). Therefore the equation becomes:

$$T_n = \left(\frac{4h}{x}\right) \frac{x^2 y}{3} \left(2.4\sqrt{f_c'}\,\right) + \alpha_t \frac{x_1 y_1 A_t f_y}{s} \qquad (2.28)$$

Equation (2.28) was checked directly by torsion tests on box sections with longitudinal steel and stirrups (refs. 56, 57) and was found reasonably valid for h down to 0.15x. However, in view of the lack of enough test results and the possibility of local wall failure when h < 0.1x, the ACI code limits the applicability of the equation to h > x/10.

The ACI code distinguishes between two cases of design for torsion, namely:

(a) Equilibrium torsion, where the torsional moment is required for the structure to be in equilibrium; a typical example is a cantilever canopy supported on a portal frame (Figure 2.9 a). In this case the design torque may not be reduced, because moment redistribution is not possible, and the restrict design procedure discussed above must be followed.

(b) Compatibility torsion, where the torsional moment can be reduced by redistribution of internal forces after cracking; a typical example is that of an edge beam into which floor beams or a slab are framed from one side only (Figure 2.9 b). In this case torsion arises from the beam twisting in order to maintain compatibility of deformations, and the design torque may be reduced. If moment is transfered to such a torsional member from a uniformly distributed loaded slab or closely spaced beams, the torsional moment will be

zero at midspan. Therefore, the torsion reinforcement may be reduced toward the midspan according to a straight line distribution of torsional moment, but not less than the minimum reinforcement specified (ref. 54).

The code apparently accepts that large percentage of torsional stiffness is lost after cracking, up to 80% to 90% in some cases (ref. 54), and allows for reasonable assumptions to be made for analysis purposes.

2.4.3 BS:8110 - 1985 (previously CP110 - 1972) Procedure

The British code, CP110 - 1972, has now become BS:8110 - 1985. The same torsion design procedure has been continued in the new code apart from a slight increase (about 6%) in the maximum permissible torsional shear stress, v_{tu},. The code considers torsion, like shear and bond, in terms of the limit state of collapse. The torsional rigidity, GC, may be calculated taking G as $0.42E_C$, where E_C is the Young's modulus of uncracked concrete, implying a Poisson's ratio of about 0.2 in the elasticity equation G = E/2(1+ν). The torsion constant, C, is taken as half the St. Venant's value calculated for plain concrete section, to allow for the likely cracking of concrete.

The sand-heap analogy which assumes plastic distribution of the torsional shear stress (refs. 8, 38) is utilized. Accordingly, for a rectangular section, the torsion shear stress, v_t, is calculated as:

$$v_t = \frac{2T}{x^2(y - \frac{x}{3})} \qquad (2.29)$$

where T = torsional moment due to ultimate loads

   x,y = minimum and maximum dimensions of the cross
       section

If v_t exceeds the ultimate torsional shear stress, v_{tmin}, specified by the code for the concrete grade used, then torsional reinforcement must be provided. If it exceeds the maximum permissible value, v_{tu}, then the section has to be redesigned. Unlike the ACI Code, and in accordance with current European thinking (refs. 57,58), BS:8110 considers the total torque, T, for the design, implying the neglect of concrete contribution. The space truss analogy is adopted and the stirrups area is calculated from:

$$\frac{A_{sv}}{s} = \frac{T}{0.8x_1y_1(0.87f_{yv})} \qquad (2.30)$$

where A_{sv} = area of the legs of closed stirrups at the
                section

     s = stirrup spacing

x_1,y_1 = smaller and larger dimensions of the stirrup

   f_{yv} = characteristic strength of the stirrups

The area of longitudinal reinforcement , A_{sl}, is given by the volume of steel which equals that of the links (principle of equal volume) suitably adjusted for any differences in the yield strength; hence:

$$A_{sl} = \frac{A_{sv}}{s} \ \frac{f_{yv}}{f_{yl}} \ (x_1+y_1) \qquad (2.31)$$

The following limitations are stated:

(1) The sum of the shear stresses resulting from shear and torsion, $v+v_t$, should in no case exceed the limiting value, v_{tu} , specified for each concrete grade.

(2) In case of small sections, when yl<550, the value of vt should not exceed $v_{tu}yl/550$, apparently to allow for the size effect.

(3) The stirrup spacing should not exceed the lesser of x_1, $y_1/2$ or 200 mm, to control crack spacing and to resist the tendency for the corners to spall (ref. 57, 59).

(4) neither f_{yv} nor f_{yl} should exceed 425 N/mm^2, to avoid premature failures caused by concrete crushing.

(5) The longitudinal steel should be distributed evenly inside the perimeter of the links. The clear distnace between these bars should not exceed 300 mm and at least four bars, one at each corner of the links, should be provided.

(6) The torsion reinforcement must extend a distance at least equal to the largest dimension of the section beyond where it ceases to be required.

Flanged sections are treated in a similar fashion as for the ACI procedure, i.e. as composed of their component rectangles. But the total torsional strength, T, is proportioned according to the ratio $x^3y/\Sigma x^3y$ instead of $x^2y/\Sigma x^2y$ as in the ACI's case. This is basically because the BS:8110 considers the component rectangles for an elastic stress distribution instead of plastic.

Box sections are treated as solid sections if the wall thickness exceeds one quarter of the width. However, unlike the ACI procedure, the code does not suggest any treatment for box sections when this condition is not fulfilled.

2.4.4 CEB-FIP Model Code Procedure

The 1978 CEB-FIP Model Code (ref. 53) separates torsion to equilibrium torsion and compatibility torsion, using the same definitions as the ACI code. For equilibrium torsion it is required that the full torsional moment should be used for the design. Compatibility torsion, on the other hand, can be ignored. The code's procedure is based on the variable-truss model (Equation 2.8).

The terms "circulatory torsion" and "warping torsion" appear in the code to distinguish between two types of torsional resistance. In circulatory torsion (known also as St. Venant's torsion) the torsional resistance is generated by the shear stresses flowing in a circulatory manner on the cross section of a member. In contrast, warping torsion furnishes the torsional resistance from the differential in-plane bending and shear in the component walls of a member.

Generally, both circulatory and warping torsional resistances occur side by side in any member subjected to torsion; circulatory torsion predominates in members with solid or hollow bulky sections, while warping torsion predominates in thin-walled sections. Unlike the previous two codes, which ignore warping torsion, the CEB-FIP code provides brief instructions for the design of open sections having three walls in separate planes, i.e. subject to warping torsion.

Simplifications were made in defining the centre line of the shear flow and the effective wall thickness in a solid or

hollow section. The centre line of the shear flow is assumed to coincide with the perimeter connecting the centroids of the corner longitudinal bars as shown by the dotted polygon in Figure (2.10) for an arbitrary section. From this dotted polygon the area, A_{ef}, and the perimeter, u_{ef}, are determined.

The effective wall thickness is defined in the following manner. Draw the largest circle that can be contained within the effective perimeter, u_{ef}, and denote the diameter of this circle, d_{ef}. Then the effective wall thickness, h_{ef}, will be given by $h_{ef} = d_{ef}/6$.

The design of web reinforcement is governed by the equation:

$$T_n = \frac{A_t f_{ty}}{s} \, 2A_{ef} \cot \alpha \qquad\qquad (2.32)$$

where T_n = nominal torsional strength (the same ACI definition is used for comparison)

A_t = area of the link

f_{ty} = yield strength of the links

A_{ef} = area of the polygon constructed by joining the centres of all longitudinal bars

s = spacing of links

α = assumed inclination of the concrete struts to the longitudinal axis of the member ($3/5 < \cot \alpha < 5/3$).

The limits of $\cot \alpha$ are prudently chosen to allow for reasonable control of concrete cracking in the service conditions (ref. 53)

This equation is applicable to the case of high torsion when $T_u > 3 \, \Phi \, T_c$. The quantity ϕ is the material reduction

factor, taken as 1/1.5 in the code, and T_c is an empirical torsional resistance given by:

$$T_c = 2.5 \, \tau_R \, h_{ef} \, 2A_{ef} \qquad (2.33)$$

where $\tau_R = f'_t/4$, the tensile strength of concrete, f'_t, is taken as $0.214(f'_c)^{2/3}$, where f'_t and f'_c are in N/mm^2. The values are also tabulated in the code.

h_{ef} = effective thickness of the wall = $d_{ef}/6$ (defined above - see also Figure 2.10)

For the case of low torsion, i.e. $T_u < 3 \, \Phi T_c$, Equation (2.32) is modified by adding an empirical torsional resistance, T_{cv}, so that:

$$T_n = T_{cv} + \frac{A_t f_{ty}}{s} \, 2A_{ef} \, \cot\alpha \qquad (2.34)$$

The term T_{cv} is known as the concrete resistance, which actually includes all the effects that are neglected in the truss model, such as shear resistance of concrete, dowel action of reinforcement, aggregate interlock, etc. (ref. 10). In the above equation:

$$
\begin{aligned}
T_{cv} &= T_c & \text{for} \quad T_u < T_c \\
T_{cv} &= 0 & \text{for} \quad T_u > 3 \, T_c
\end{aligned}
\qquad (2.35)
$$

Intermediate values can be determined by interpolation.

Equations (2.32) and (2.34) are used for the calculation of the web reinforcement (i.e. the closed stirrups). For the design of the longitudinal reinforcement the following equation is used:

$$T_n = \frac{A_l f_{ly}}{u_{ef}} \, 2A_{ef} \, \tan\alpha \qquad (2.36)$$

where A_l = total area of longitudinal reinforcement

f_{ly} = yield value of longitudinal reinforcement

u_{ef} = perimeter of the area A_{ef}

The code specifies an upper limit of resistant torque, based on crushing of concrete struts. This is obtained by considering the effective strength of concrete at failure as $0.5f'c$ (ref. 10), and is given by:

$$T_{n,max} = 0.5 \, f'_c \, A_{ef} h_{ef} \, \sin 2\alpha \qquad (2.37)$$

This equation was derived originally from large size box sections used in bridges and was calibrated for such structures (ref. 10). It was found, however, unreasonably conservative for smaller size solid sections used normally in buildings. The source of difficulty is thought to be the definitions of the area, A_{ef}, and the effective wall thickness, h_{ef}.

For large box sections, where the concrete cover and the size of the steel bars are small in comparison to the overall dimensions, the dotted polygon represents the centre of the shear flow with reasonable accuracy. However, for small solid sections the concrete cover and the steel bars are quite significant with respect to the section dimensions; hence the area within the polygon becomes considerably smaller than the area within the outer concrete perimeter, and the polygon (representing the centre line of the shear flow) may lie completely outside the effective wall thickness. Moreover, the maximum torque obtained by Equation (2.37) may become smaller than the cracking torque, resulting in an awkward situation.

To overcome this situation, Hsu (ref. 10) proposed a modification for Equation (2.37). The modified equation, checked on the PCA test results (ref. 14), and claimed to be applicable to both large box sections used in bridges and small solid sections used in buildings, is given by:

$$T_{n,max} = 0.5 \, f'_c A_c t_c \sin 2\alpha \qquad (2.38 \ a)$$

where
$$t_c = \frac{0.45 \, A_c}{P_c} \qquad (2.38 \ b)$$

In these two equations:

A_c = cross sectional area within the outer perimeter of concrete

p_c = outer perimeter of concrete

t_c = wall thickness given by Equation (2.38 b)

The following points are provided in the code dealing with various aspects:

(1) The code does not specify a minimum web reinforcement, but presumably the shear provisions are also applicable to torsion.

(2) The maximum spacing for the stirrups is limited to $u_{ef}/8$. However, there is no such specific limit for the longitudinal steel.

(3) An interesting provision is embodied in the code dealing with torsion combined with a large bending moment. Such a combination may cause critical principal compressive stresses in the compression zone, particularly in box sections, because of the small wall thickness as compared to solid sections. The principal compressive stress can be calculated from the mean longitudinal compression due to

flexure and from the tangential stress due to torsion, taken as $T_u/(A_{ef}h_{ef})$. The combined stress so obtained must not exceed $0.85f'_c$.

(4) For open sections having three walls in separate planes, the following procedure is given:

The tangent stress components due to shear and torsion in each of the three walls should be determined from static equilibrium calculations. These components and the axial components due to the bending moments and axial forces determine the local effects in each wall. The ultimate limit state of the whole section is governed by the ultimate state of one wall and can arise by:

(1) bending (longitudinal reinforcement or compression zone), or

(2) shear (reinforcement or compression struts).

Each wall can be treated as an independent beam; the calculations for which should be based on the ultimate limit state rules (sections 10 and 11 of the code, ref. 53).

(5) In the absence of any accurate methods, the code provides the following equations for calculating the torsional stiffness:

$$K_1 = 0.30 \ E_c C/(1+1.0\alpha)$$

$$K_{m2} = 0.10 \ E_c C/(1+0.3\alpha) \tag{2.39}$$

$$K_{m3} = 0.05 \ E_c C/(1+0.3\alpha)$$

where K_1 = stiffness in state 1, uncracked

K_{m2} = stiffness in state 2, bending cracks

K_{m3} = stiffness in state 2, torsional and shear cracks

C = torsional moment of inertia in the uncracked state

α = creep coefficient to be used for long term loading (tabulated in the code)

E_c = Elastic modulus of uncracked concrete

In Equation (2.39), the stiffness is given as the rotation per unit length ($d\theta/dx = T/K$). The coefficient 0.3 in the first equation takes account of the nonlinear behaviour of concrete before cracking. In the second and third equations, the influence of steel is neglected for simplicity. However, the full expression which takes account of steel contribution is also given as:

$$K_2 = \frac{E_s A_{ef}^2}{\frac{u_{ef} s}{2A_t} + 1.5 \frac{E_s}{E_c} \frac{u_{ef}}{h_{ef}} (1 + \alpha)} \qquad (2.40)$$

where A_{ef}, u_{ef} and h_{ef} are previously defined, A_t denotes the area of a stirrup or a fraction of that area which balances the torsional moment (in the case of combined loading), s is the stirrup spacing and E_s is the steel elastic modulus.

(6) The code gives a brief guide for checking torsional deformations. In the usual type of buildings checking of torsional deformations is not necessary if the torsional resistance is not needed for equilibrium. However, if the equilibrium of the structure depends on the torsional stiffness, checking of the rotations is necessary if the principal tensile stress is such that:

$$\sigma_1 > 0.7 \, f_{ctk0.05} \qquad\qquad (2.41)$$

where $f_{ctk0.05}$ = a value less than the tensile strength of concrete tabulated in the code.

Equations (2.39) can be used for the calculation of the rotations. The code, however, does not set limits on the maximum rotations.

2.4.5 General Comparisons and Criticisms

On the whole the three documents, among other national codes, contain useful provisions for torsion design. However, there are several differences among these provisons, mainly because of the different criteria employed in each case. As can be seen from the above descriptions, the ACI code appears to contain more advanced provisions than the British code, although it has been criticized as being conservative in many situations (refs. 44, 45, 52 for example). The CEB-FIP Model Code, on the other hand, defines clearly the various types of torsion for the design, namely equilibrium, compatibility, circulatory and warping torsions and goes further than the other two codes in giving some provisions for open sections having three walls in different planes. However, it permits the designer to neglect the compatibility torsion, and this has been criticized as dangerous (ref. 10).

The ACI code has seen continuous enhancements since its torsion provisions first appeared. In contrast, the British code provisions continued in the new version of the code (ref. 34) without any significant change despite the earlier criticizms (ref. 35) of being too conservative. This aspect

will be elaborated later in Chapter Seven when the experimental results are discussed. The code still lacks proper treatment of box sections. Both BS:8110 and the ACI code adopt the principle of equal volumes in determining the amount of longitudinal steel to try and ensure that both stirrups and longitudinal bars yield simultaneously. Hsu (refs. 10, 14) have shown that this ratio can vary between 0.7 and 1.5. Other criticizms have already been mentioned in the previous sections with the description of each code provisions.

2.5 Summary of Previous Work

The theories presented in the previous sections invariably involved mathematical difficulties. There were also several assumptions introduced to make derivation of the respective mathematical formulae possible. This resulted in the discrepancies often reported between experimental and predicted ultimate torques and justifies the enhancing of existing theories or introducing new methods of analysis/design.

As most of these theories attempt to predict ultimate torsional moments, they omit the prediction of some basic behavioural characteristics such as the pre- and post-cracking stiffnesses, reinforcement response and unit lengthening of members at every stage of loading. These are often important to assess the performance of the structure at important stages, for example the serviceability and ultimate conditions. Moreover, the torsion problem is mainly a cracking problem. Hence a reliable theory must essentially provide for good treatment of shear transfer across cracks, involving both aggregate interlocking and dowel action.

All previous work on torsion of reinforced concrete has undoubtedly resulted in better understanding of the basic problem. Some of this work helped directly in codification; the PCA - Portland Cement Association studies (ref. 14, 15) for example, when combined with other test results available at the time, led to the ACI torsion design criteria. However, in general, and as always expected with limited number of variables in each individual study, the results are often insufficient for major changes in the codes of practice despite the various criticisms raised. Hence the need for further studies on this particular topic.

In general, the majority of tests on solid flanged sections were carried out on models either reinforced in the web only or else having one layer of reinforcement in the flange. The codes of practice, however, recommend the use of "full" reinforcement; i.e. closed stirrups in all rectangular components of a flanged section, properly tied together to ensure that the section will act as one unit and to avoid premature or brittle failures. This category of section received little attention so far (ref. 52).

For solid rectangular and bulky flanged sections, the torsion problem becomes essentially three dimensional, particularly after cracking of concrete. This further complicates the situation for any nonlinear analytical treatment and require careful attention.

Applications of the finite element method of reinforced concrete nonlinear behaviour, however, were mainly on flexure and shear. This is because most of the finite element models developed were two dimensional. Very limited

work has been reported on torsion, reference (51) being the only one known to the author. In that particular reference no detailed results were presented.

Because of these reasons, this thesis offers on one hand a nonlinear three dimensional finite element method for short-term loading of reinforced concrete. The method is applied to a range of reinforced concrete beams under various load types including pure and combined torsion. On the other hand an experimental part was undertaken in which a series of reinforced concrete models of L-shaped cross section , designed to directly assess the British Code (BS:8110) design procedure for torsion, were tested to destruction under pure torsion in a special test-rig designed and built especially for this purpose.

To complement the experimental data, a numerical parametric study was also performed on L-sections, using the developed finite element model, to investigate more parameters not included in the experimental programme. This dual approach is highly attractive and effective, once limits on the effects of the important numerical and material parameters on the finite element model's performance, were established. Valuable time and effort is thus saved at a reasonable cost and certainly a lot more variables can be investigated than at all possible within an experimental programme alone. Indeed this approach can provide, much quicker, results that can be useful for the purpose of drawing code specifications in a time when the new nonlinear methods of analysis are becomming increasingly acceptable by the codes of practice.

The new British Code, BS:8|10 - 1985 (ref. 34), states in

clause 2.3.3 that nonlinear analysis can be used to confirm the suitability of the design. This is a very encouraging sign for such dual approach. No specific methods are suggested apart from mentioning that the method must suit the structure under consideration. The nonlinear analysis of reinforced concrete is nowadays, however, carried out by the finite element method where various sources of nonlinearity can be rationally modelled. Moreover, modern technology ensures that high speed digital computers with very large storage capacities are increasingly available to perform these tasks. Three dimensional nonlinear finite element analysis of reinforced concrete, largely avoided in the past only because of the prohibitively unjusifiable high cost, is gaining grounds and becomming viable nowadays.
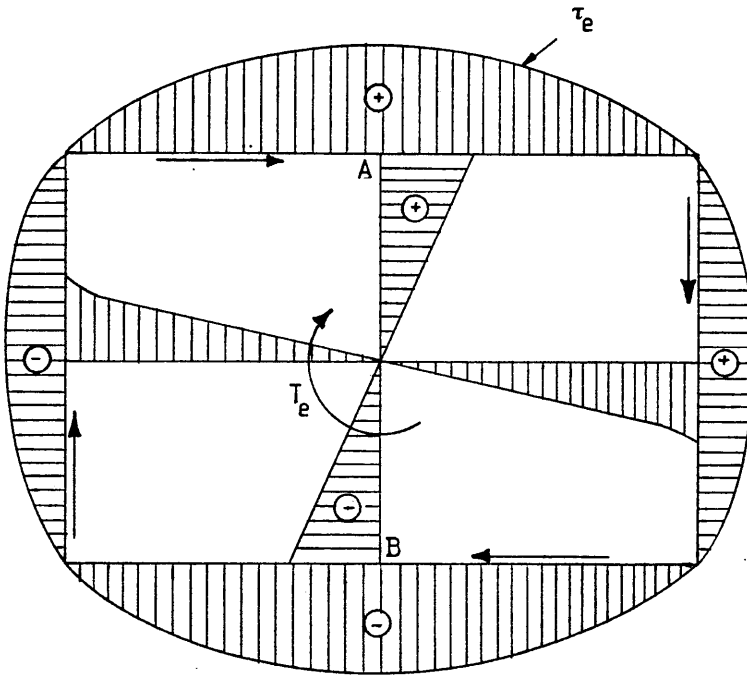
Figure (2.1) Shear stress distribution in a rectangular plain
concrete section according to St. Venant's
method (ref. 4)
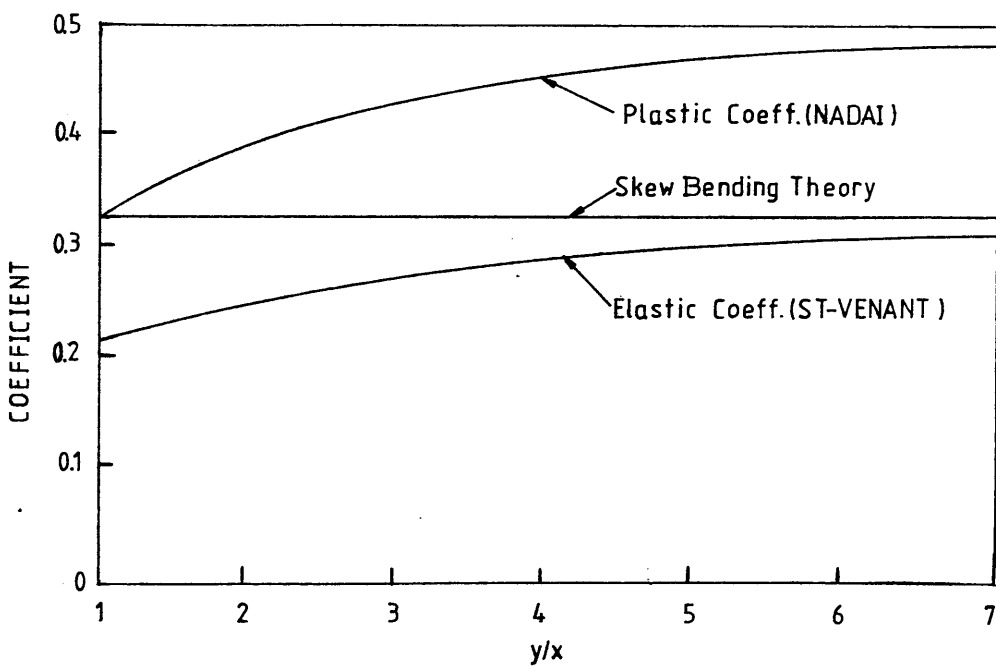
Figure (2.2) Comparison of elastic, plastic and skew-bending
coefficients (ref. 11)
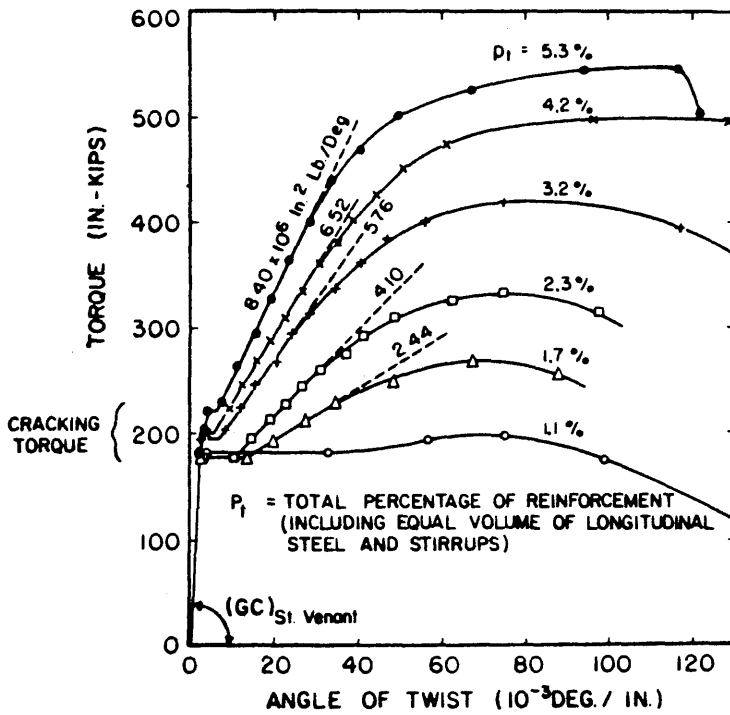
Figure (2.3) Torque-twist curves for series B of Hsu's rectangular beams (ref. 14)
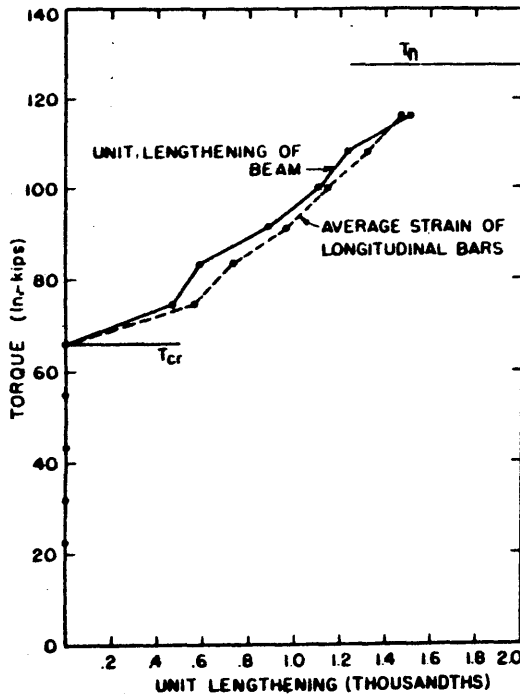
Figure (2.4) Beam unit lengthening and average longitudinal steel strain for Hsu's beam N2 (ref. 14)
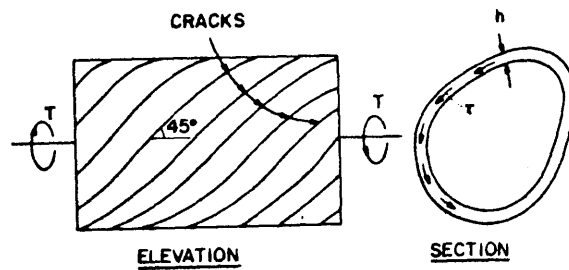
(a) DIAGONAL CRACKING IN A REINFORCED
CONCRETE MEMBER
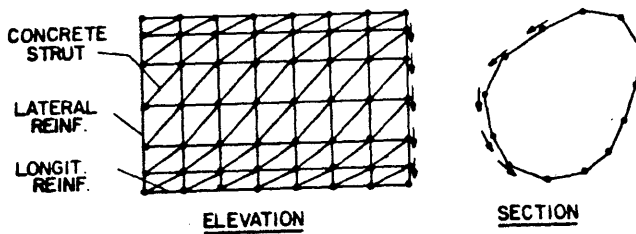
(b) SPACE TRUSS IDEALIZATION
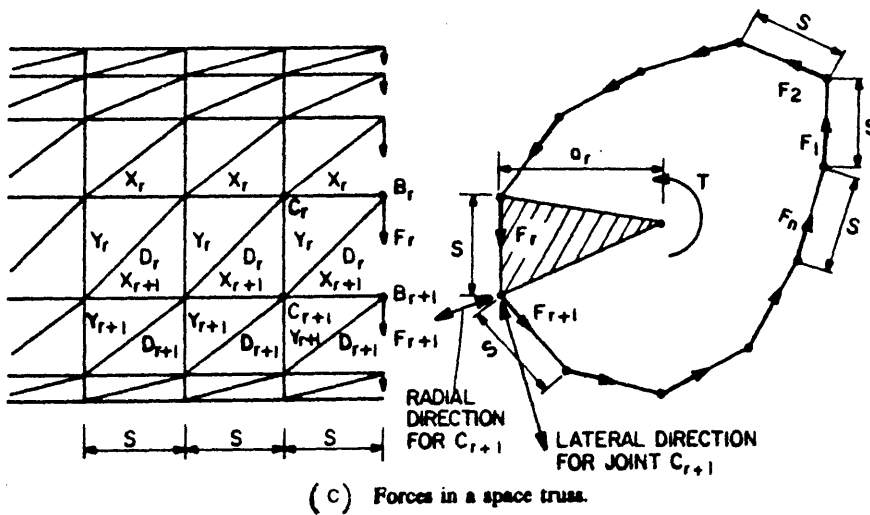
(c)   Forces in a space truss.

Figure (2.5) Space truss idealization (refs. 10, 17)

(a) Proposed failure surface.

(b) The composition of force P.
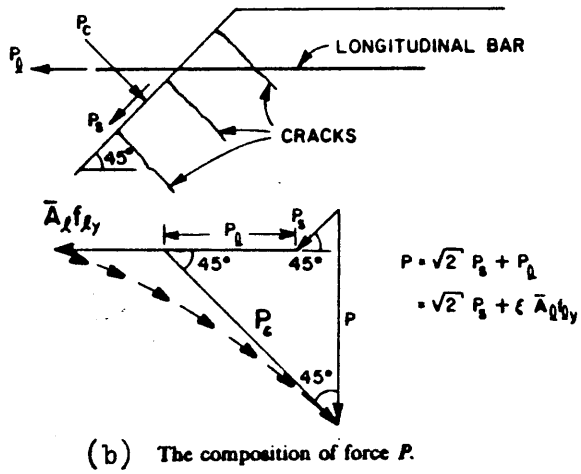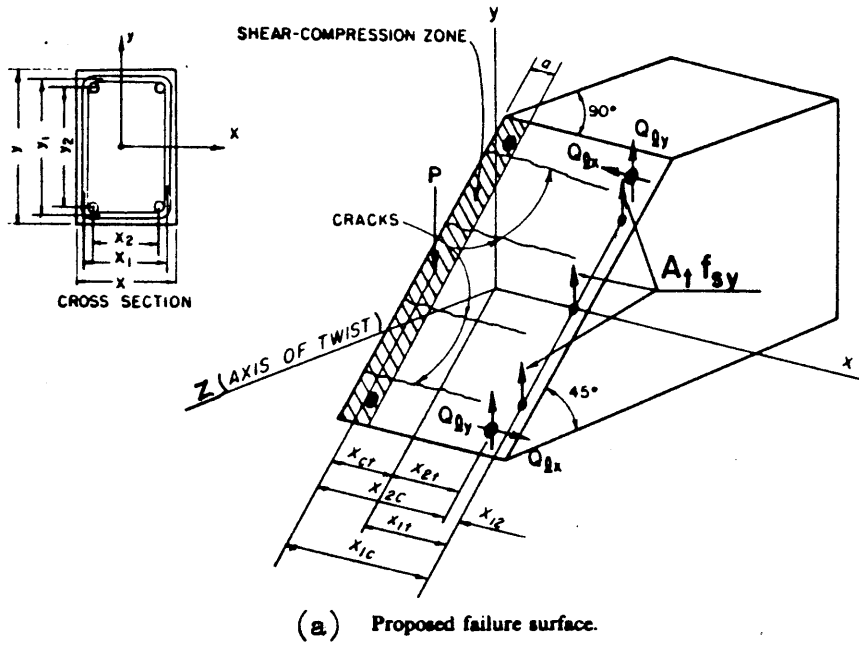
Figure (2.6) Skew-bending idealization (ref. 10, 13)
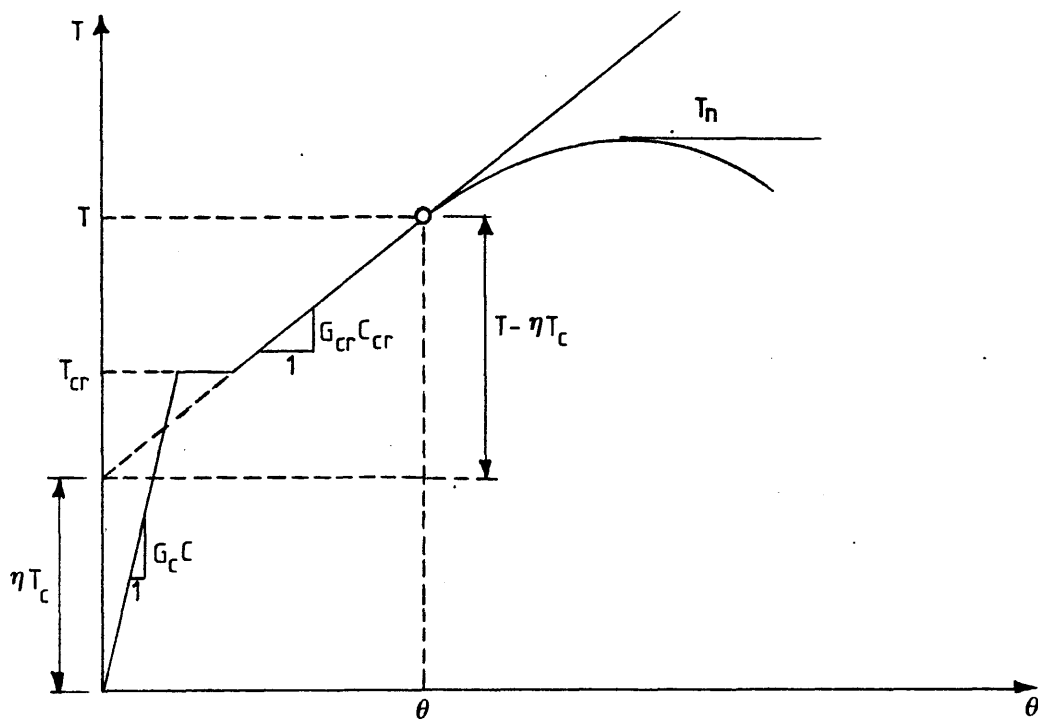
Figure (2.7) Typical torque-twist curve for reinforced concrete
beams (ref. 27)
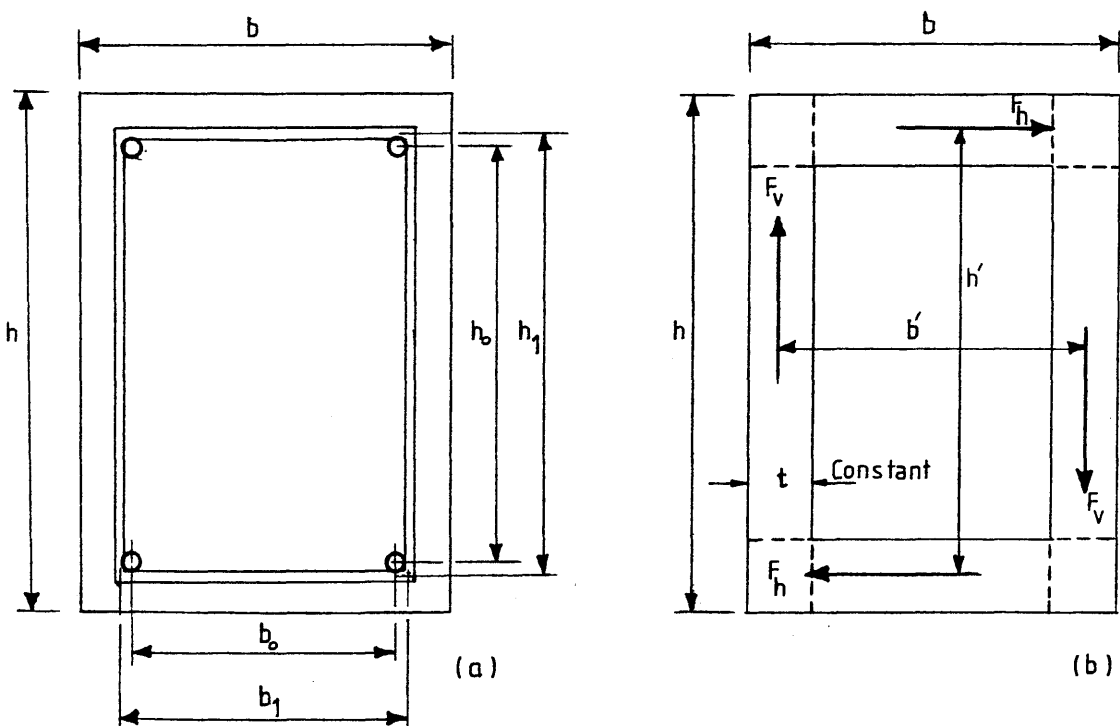
Figure (2.8) Box section model for evaluation of torsional
stiffness of rectangular sections (ref. 29)

Design torque may <u>not</u> be reduced, because moment redistribution is <u>not</u> possible.
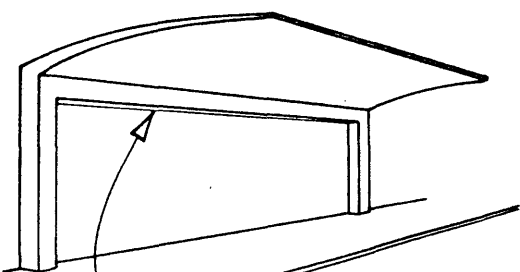
Design torque for this spandrel beam may be reduced because moment redistribution is possible.

(a) No redistribution torsion (equilibrium torsion)

(b) Torsion redistribution (compatibility torsion), isometric view of one end panel

Figure (2.9) Equilibrium and compatibility torsion (ref. 33)

A_{ef}

u_{ef}

Mean perimeter

d_{ef}

$h_{ef} = d_{ef}/6$

Longitudinal reinforcement
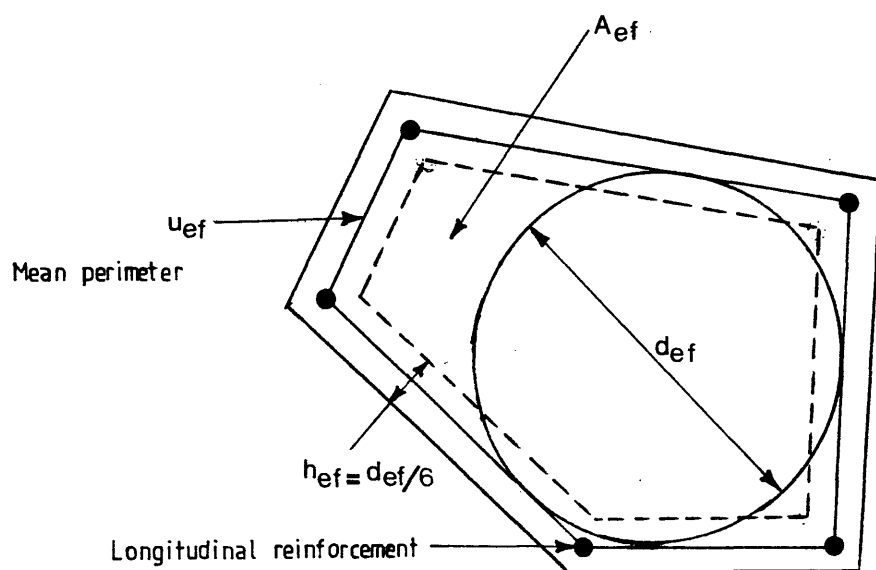
Figure (2.10) CEB-FIP Model Code definitions for an arbitrary hollow section (ref. 53)

Table (2.1) Survey of torsion design specifications during the
1960s (ref. 30)

(1) "Full specifications"	(2) Permissible stress only	(3) No mention
France,1960	Netherlands,1962	ACI 318-63, 1963
Egypt,1960 (provisional)	Norway,1962	Canada NBCC,1960
Germany,1959	Brazil,1960	Canada CSA,1959
Australia,1958	Austria,1957	Japan,1958
GSA (USA),1956	Switzerland,1956	India,1957
Poland,1956	Greece,1950	Great Britain,1957
Russia,1955	Sweden,1949	Denmark,1949
Hungary,1953		

References

(1) Coulomb, C.A., "Recherches theoriques et experimentales sur la force de torsion et sur l'elasticite des fils de metal", Histoire de l'Academie Royale des Sciences, Paris, 1784; L'Imprimerie Royale, Paris, 1787, pp. 229-269.

(2) Navier, C.L., Resume des lecons donnees a l'eocle des ponts et chaussees sur l'applicaion de la meacanique a l'establissement des constructions et des machines. Premiere practice, "continant les lecons sur la resistance des materiaux et sur l'establissement des constructions en terre, en maconnerie et en charpente", Firmin Didet, Paris, 1826. (Article V, "de la resistance d'un corps prismatique a la torsion", pp. 71-76. Article VI, "de la resistance d'un corps prismatique a la rupture causee par la torsion", pp. 76-80.)

(3) Duleau, A., "Essai theorique et experimental sur la resistance du fer forge", Paris, 1820.

(4) Saint-Venant, B.de., Memoire sur la torsion des prisms (lu a l'Academie le 13 juin 1853). Memoires des savants etrangers, Memoires presentes par divers savants a l'Academie des Sciences, de l'Institut Imperial de France et imprime par son ordre, V. 14, Imprimerie imperiale, Paris, 1856, pp. 233-560.

(5) Bach, B., "Elasticitat und Festigkeit", 6th ed., 1911.

(6) Bredt, R., "Kritische Bemerkungen zur Drehungselastizitat", Zeitschrift des Vereines Deutscher Ingenieure, Band 40, No. 28, July 11, 1896, pp. 785-790; No. 29, July 18, 1896, pp. 813-817.

(7) Prandtl, L., "Zur Torsion von prismatischen Staben", Physik Zeitschrift 4, 1903, p. 758.

(8) Nadai, A., "Theory of Flow and Fracture of Solids", Vol. 1, McGraw-Hill Book Co., New York, 1950, Chapter 35.

(9) Nylander, H., "Vridning och Vridningsinspanning vid Betong Konstruktiener (Torsion and Torsional Restraint by Concrete Structures), Statens Kommittee for Byggnadsfor-skning, Stockholm, Bulletin No. 3, 1945.

(10) Hsu, T.T.C., "Torsion of Reinforced Concrete", Van Nostrand, 1984.

(11) Hsu, T.T.C., "Torsion of Reinforced Concrete - Plain Concrete Rectangular Sections", ACI Special Publication, Torsion of Reinforced Concrete, SP18, 1968, pp. 203-238.

(12) Marshal, W.T and Tempe, N.R., "Experiments on Plain and Reinforced Concrete in Torsion", Structural Engineer, London, Vol. 19, No. 11, Nov., 1941, pp. 177-191.

(13) Lessig, N.N., "Determination of Load-Carrying Capacity of Rectangular Concrete Elements Subjected to Flexure and Torsion", Trudy No. 5, Institut Betona i Zhelezobetona (Concrete and Reinforced Concrete Institute), Moscow, 1959, pp. 5-28 (in Russian, Translated by Portland Cement Association, Foreign Literature Study No. 371.

(14) Hsu, T.T.C., "Torsion of Structural Concrete - Behaviour of Reinforced Concrete Rectangular Members", ACI Special Publication, Torsion of Structural Concrete, SP18, 1968, pp. 261-306.

(15) Hsu, T.T.C., "Ultimate Torque of Reinforced Rectangular Beams", Jour. Struct. Div., ASCE, Vol. 94, ST2, Feb., 1968, pp. 485-510.

(16) Cowan, H.J., "An Elastic Theory for the Torsional Strength of Rectangular Reinforced Concrete Beams", Mag. Conc. Res., Vol. 2, No. 4, July, 1950, pp. 3-8.

(17) Rausch, E., "Design of Reinforced Concrete in Torsion" (Berechnung des Eisenbetons geng Verdrehung), Ph.D. thesis, Technische Hochschule, Berlin, 1929, 53 pp. (in German). A second edition was published in 1938 and a third in 1952. The third edition was a technical book entitled "Drillung (Torsion), Schub and Stahlbetonban", Deutcher Ingenieur - Verlag GmbH, Dusseldorf, 168 pp.

(18) Andersen, P., "Experiments with Concrete in Torsion", Transactions, ASCE, Vol. 100, 1935, pp. 949-983. Also, Proceedings, ASCE, Vol. 60, May, 1934, pp. 641-652.

(19) Lampert, P. and Thurliman, B., "Torsionsversuche an Stahlbetonbalken" (Torsion Tests of Reinforced Concrete Beams), Bericht Nr. 6506-2, June, 1968; "Torsion-Biege-Versuche an Stahlbetonbalken" (Torsion-Bending Tests on Reinforced Concrete Beams), Bericht Nr. 6506-3, Jan., 1969, Institut fur Baustatik, ETH, Zurich, (in German).

(20) Collins, M.P. and Mitchell, "Shear and Torsion Design of Prestressed and Non-Prestressed Concrete Beams", Jour. Pres. Conc. Inst., Vol. 25, No. 5, Sep.-Oct., 1980, pp. 32-100.

(21) Hsu, T.T.C. and Mo, Y.L., "Softening of Concrete in Torsional Members", Research Report No. ST-TH-001-83, Dept. of Civil Eng., University of Houston, Houston, Texas, March, 1983.

(22) Hsu, T.T.C. and Mo, Y.L., "Softening of Concrete in Torsional Memebers - Theory and Tests", Jour. Amer. Conc. Inst., Proceedings, Vol. 82, No. 3, May-June, 1985, pp. 290-303.

(23) Hsu, T.T.C. and Mo, Y.L., "Softening of Concrete in Torsional Members - Design Recommendations", Jour. Amer. Conc. Inst., Proceedings, Vol. 82, No. 4, July-August, 1985, pp. 443-452.

(24) Hsu, T.T.C., Disscussion of "Pure Torsion in Recangular Sections - A Re-examination" ,(ref. 25), Jour. Amer. Conc. Inst., Proceedings, Vol. 76, No. 6, June, 1979, pp. 741-746.

(25) McMullen, A.E. and Rangan, B.V., "Pure Torsion in Rectagular Sections - A Re-Examination", Jour. Amer. Conc. Inst., Proceedings, Vol. 76, No. 5, Oct., 1978, pp. 511-519.

(26) Weinberger, H.F., "Upper and Lower Bounds for Torsional Rigidity", Jour. of Math. Phys., Vol. 32, 1953, pp. 54-61.

(27) Hsu, T.T.C., "Post-Cracking Torsional Rigidity of Reinforced Concrete Sections", Jour. Amer. Conc. Inst., Proceedings, Vol. 70, No. 5, May, 1973, pp. 352-360.

(28) Hsu, T.T.C., Inan, M. and Fonticiella, L., "Behaviour of Reinforced Concrete Horizontally Curved Beams", Jour. Amer. Conc. Inst., Proceedings, Vol. 75, No. 4, April, 1978,

pp. 112-123.

(29) Sandegren, D.S. and Yu, C.W., "Torsional Stiffness of Reinforced Concrete Rectangular Members", Mag. Conc. Res., Vol. 31, No. 109, Dec., 1979, pp. 193-201.

(30) Fisher, G.P. and Zia, P., "Review of Code Requirements for Torsion Design", Jour. Amer. Conc. Inst., Proceedings, Vol. 61, No. 1, Jan., 1964, pp. 1-44.

(31) ACI Committee 438, "Tentative Recommendations for the Design of Reinforced Concrete Members to Resist Torsion", Jour. Amer. Conc. Inst., Proceedings, Vol. 66, No. 1, Jan., 1969, pp. 1-8.

(32) State Committee on Construction of the USSR Council of Ministers, "Structural Standards and Regulations", SNiP II-B, 1-62, State Publishing Offices for Literature on Structural Engineering, Architecture and Structural Materials, Moscow, 1962 (in Russian).

(33) a. ACI Standard 318-71, "Building Code Requirements for Reinforced Concrete ACI 318-71", Amer. Conc. Inst., Detroit, 1971.

   b. ACI Standard 318-77, "Building Code Requirements for Reinforced Concrete ACI 318-77", Amer. Conc. Inst., Detroit, 1971.

   c. ACI Standard 318-83, "Building Code Requirements for Reinforced Concrete ACI 318-83", Amer. Conc. Inst., Detroit, 1971.

(34) a. CP110-1972, "Code of Practice for the Structural Use of Concrete", Part 1, Design, Material and Workmanship,

Brit. Stand. Inst., London, 1972.

b. BS8110-1985, "British Standard Structural Use of Concrete", Part 2, Code of Practice for Special Circumstances, Brit. Stand. Inst., London, 1985.

(35) Marshall, W.T, "Torsion in Concrete and CP110 1972", The Structural Engineer, Vol. 52, No. 3, March, 1974, pp. 83-88.

(36) Kirk, D. W. and Lash, S.D., "T-Beams Subjected to Combined Bending and Torsion", Jour. Amer. Conc. Inst., Proceedings, Vol. 68, No. 2, Feb., 1971, pp. 150-159.

(37) Liao, H.M. and Ferguson, F.M, "Combined Torsion in Reinforced Concrete L-Beams with Stirrups", Jour. Amer. Conc. Inst., Proceedings, Vol. 66, No. 17, Dec., 1969, pp. 986-993.

(38) Hughes, B.P., "Limit State Theory for Reinforced Concrete Design", Pitman, 2nd ed., 1976.

(39) Victor, D.J. and Ferguson, F.M., "Beams Under Distributed Load Creating Moment, Shear and Torsion", Jour. Amer. Conc. Inst., Vol. 65, No. 4, April, 1968, pp. 295-308.

(40) Erosy, U. and Ferguson, P.M., "Concrete Beams Subjected to Cobmined Torsion and Shear - Experimental Trends", ACI Special Publication, Torsion of Structural Concrete, SP18, 1968, pp. 441-460.

(41) Erosy, U. and Ferguson, P.M., "Behaviour of Concrete L-Beams Under Combined Torsion and Shear", Jour. Amer. Conc. Inst., Proceedings, Vol. 64, No. 12, Dec., 1967, pp. 793-

801.

(42) Osburn, D.L., Mayoglou, B. and Mattock, A.H., "Strength of Reinforced Concrete Beams with Web Reinforcement in Combined Torsion, Shear and Bending", Jour. Amer. Inst., Proceedings, Vol. 66, No. 1, Jan., 1969, pp. 31-41.

(43) Mattock, A.H., "How to Design for Torsion", ACI Special Publication, Torsion of Structural Concrete, SP18, 1968, pp. 469-498.

(44) Behara, U. and Ferguson, P.M., "Torsion, Shear and Bending on Stirruped L-Beams", Jour. Struct. Div., ASCE, Vol. 69, No. ST7, July, 1970, pp. 1271-1286.

(45) Victor, D.J., "Effective Flange Width in Torsion", Jour. Amer. Conc. Inst., Proceedings, Vol. 68, No. 1, Jan., 1971, pp. 42-46.

(46) Rajagopalan, K.S., Behara, U. and Ferguson, P.M., "Partially Over-Reinforced Concrete Beams Under Pure Torsion", Jour. Amer. Conc. Inst., Proceedings, Vol. 68, No. 10, Oct., 1971, pp. 740-747.

(47) Syamal, P.K., Mirza, M.S., and Pay, D.P., "Plain and reinforced Concrete L-Beams Under Combined Flexure, Shear and torsion", Jour. Amer. Conc. Inst., Proceedings, Vol. 68, No. 11, Nov., 1971, pp. 848-860.

(48) Rajagopalan, K.S., "Combined Torsion, Bending and Shear on L-Beams", Jour. Struct. Div., ASCE, Vol. 106, No. ST12, Dec., 1980, pp. 2475-2492.

(49) Krpan, P. and Collins, M.P., "Testing Thin-Walled Open

RC Structures in Torsion", Jour. Struct. Div., ASCE, Vol. 107, No. ST6, June, 1981, pp. 1129-1140.

(50) Krpan, P. and Collins, M.P., "Predicting the Torsional Response of Thin-Walled Open RC Members", Jour. Struct. Div., ASCE, Vol. 107, No. ST6, June, 1981, pp. 1107-1127.

(51) Melhorn, G. and Schmidt-Gonner, G., "A Calculation for Reinforced Concrete Beams Under Bending and torsion Using Three Dimensional Finite Elements", IABSE, Collequium on Advanced Mehanics of reinforecd Concrete, Delft, 1981, pp. 591-601.

(52) Zararis, P.D. and Penelis, G. Gr., "Reinforced Concrete T-Beams in Torsion and Bending", ACI Jour., Vol. 83, Jan.-Feb., 1986, pp. 145-155.

(53) CEB-FIP, "Model Code for Concrete Structures", CEB-FIP International Recommendations, third edition, Comite-International du Beton (CEB), 1978.

(54) ACI 318-83, "Commentary on Building Code Requirements fro Reinforecd Concrete", Amer. Conc. Inst., Detroit, 1983.

(55) Leonhardt, F., Walther, R. and Schelling, A., "Torsion Tests on Reinforced Concrete Beams", Proceedings, International Conference on Shear, Torsion and Bond in Reinforced and Prestressed Concrete, Coimbatore, India, Jan., 1969.

(56) Leonhardt, F. and Schelling, A., "Torsionsversuche an Stahlbetonbalken", Heft 239, Deutscher Ausschuss Fur Stahlbeton, Berlin, 1974, pp. 122.

(57) Handbook on the Unified Code for Structural Concrete (CP110 1972), Cement and Concrete Association, 1972.

(58) COMITE EUROPEEN DU BETON - FEDERATION INTERNATIONAL DE LA PRECONTRAINTE. International Recommendations for the Design and Construction of Concrete Structures. English edition, London, Cement and Concrete Association, 1970. Principles and recommendations, pp. 80, Appendixes pp. 47.

(59) Swann, R.A., "The Effect of Size on the Torsional strength of Rectangular Reinforced Concrete Beams", Cement and Concrete Association, Publication 42.453, London, March, 1971, pp. 8.

(60) Timoshenko, S.P. and Goodier, J.N., "Theory of Elasticity", McGraw Hill, 3rd ed., 1982.

CHAPTER THREE

DEVELOPMENT OF THE FINITE ELEMENT METHOD

3.1 Introduction

In recent years, the finite element method has emerged as the most powerful general method for structural analysis and has provided engineers with a tool of very wide applicability. For reinforced concrete, in particular, cracking, tension stiffening, nonlinear multiaxial material properties, complex interface behaviour, creep, shrinkage and other effects previously ignored or treated in a very approximate manner can now be considered rationally. The finite element approach can provide not only new insights into behaviour and design of ordinary reinforced concrete structures such as beams, columns, frames, slabs, and shear walls and panels but is an essential tool to be used directly for the analysis and design of complex structures such as offshore oil platforms, hyperbolic cooling towers, and nuclear containment structures.

The application of the finite element method to nonlinear problems is associated with an increasing numerical operations as compared with linear problems. However, development in the last two decades have ensured that high speed digital computers which meet this need are now available.

A nonlinear structural problem must obey the fundamental conditions of continuum mechanics, namely equilibrium, compatibility and the constitutive relations of the material. As the finite element method automatically satisfies the compatibility requirements at any stage, the

solution process must satisfy the given nonlinear relationships whilst maintaining equilibrium . During each stage, "out-of-balance" residual forces will generally exist due to departure from linear behaviour, resulting in a lack of equilibrium. The removal of these residuals by successive linear solutions is the basic step in the methods used.

In this and the next chapter, a three dimensional nonlinear finite element technique for reinforced concrete is presented, based on the displacement approach. Only material nonlinearity is considered. Because the developed computer program is intended to be used for different types of reinforced concrete structures, an appraisal of its application on a range of reinforced concrete structures reported in literature was undertaken. This will be presented in Chapter Five. A study of the different material and solution parameters affecting the different types of analyses is also reported in the same chapter. The primary objectives of the study were to check the reliability of the developed model as well as to identify limits on those parameters. Thereafter the model is used to analyse reinforced concrete L-beams subjected to pure torsion. Theoretical results and their comparisons with the experimental results are reported in Chapter Eight.

As the main procedure of the finite element method is now well documented (refs. 1, 2) no attempt will be made to describe it in detail. But in order to define terms for the sake of completeness a brief review of the method will be presented instead. Embedded bars to simulate steel reinforcement in three dimensions were developed. Their

features and theoretical derivations will be presented in this chapter.

The successful application of a nonlinear finite element model to the analysis of reinforced concrete structures depends much upon proper modelling of the complex behaviour of concrete under multiaxial stress states, initiation and propagation of cracks, shear transfer across the cracked concrete, tension stiffening effects, bond-slip, yielding of reinforcement and time-dependent effects (if long-term behaviour is considered).

3.2 The Finite Element Discretisation Technique

The finite element method started as an extension of the stiffness method and was applied to two- and three-dimensional problems in structural mechanics. However, unlike skeletal structures, there are no well-defined joints where equilibrium of forces can be established and, therefore, the continuum must be discretised into a number of elements of arbitrary shapes and also artificial joints or nodes must be created.

For structural applications, one convenient method of obtaining the governing equilibrium equations is by minimizing the total potential energy of the system. The total potential energy, π , can be expressed as:

$$\pi = \frac{1}{2} \int_V [\sigma]^T [\epsilon] dV - \int_V [\delta]^T [p] \, dV - \int_S [\delta]^T [q] \, dS \qquad (3.1)$$

where $[\sigma]$ and $[\epsilon]$ are the stress and strain vectors respectively , $[\delta]$ the displacement at any point, $[p]$ the body force per unit volume, and $[q]$ the applied surface tractions. Integrations are taken over the volume "V" of

the structure and loaded surface "S".

The first term on the right hand side of Equation (3.1) represents the internal strain energy; and the second and third terms are respectively the work contributions of the body forces and the distributed surface loads.

In the finite element displacement approach, which is used execlusively in this work, the displacement is assumed to have unknown values only at the nodal points so that the variation within any element is described in terms of the nodal values by means of interpolation functions. Thus:

$$[\delta] = [N] [\delta^e]$$ (3.2)

where [N] is the set of interpolation functions termed as the shape functions, and [δ] is the vector of nodal displacements.

The strains within the elements can be expressed in terms of the element nodal displacements as:

$$[\varepsilon] = [B] [\delta^e]$$ (3.3)

where [B] is the strain matrix generally composed of derivatives of shape functions.

Finally the stresses may be related to the strains by use of an elasticity matrix [D] as follows:

$$[\sigma] = [D][\varepsilon]$$ (3.4)

Provided that no singularities exist in the integrals of the functional, the total potential energy of the continuum will be the sum of the energy contribution of the individual

elements. Thus:

$$\pi = \sum_e \pi_e \qquad (3.5)$$

where π_e represents the total potential energy of element e which, using Equation (3.1), can be written as:

$$\pi_e = \frac{1}{2} \int_{V_e} [\delta^e]^T [B]^T [D][B][\delta^e]dV -$$
$$\int_{V_e} [\delta^e]^T [N]^T [p]\, dV - \int_{S_e} [\delta^e]^T [N]^T [q]dS \qquad (3.6)$$

where V_e is the element volume and S_e the loaded element surface area. Performance of minimisation for element e with respect to the nodal displacement δ^e for the element results in:

$$\frac{\partial \pi_e}{\partial \delta^e} = \int_{V_e} ([B]^T[D][B])[\delta^e]dV - \int_{V_e} [N]^T[p]dV - \int_{S_e} [N]^T[q]dS$$
$$= [K^e][\delta^e] - [F^e] \qquad (3.7)$$

where:

$$[F^e] = \int_{V_e} [N]^T[p]dV + \int_{S_e} [N]^T [q]dS \qquad (3.8)$$

are the equivalent nodal forces for the element, and

$$[K^e] = \int_{V_e} [B]^T[D][B]dV \qquad (3.9)$$

is termed the element stiffness matrix. The summation of the terms in Equation (3.7) over all the elements, when equated to zero, results in a system of equilibrium equations for the complete continuum. These equations are then solved by any standard technique to yield the nodal displacements. The strains and thereafter the stresses within each element can be calculated from the displacements using Equations

(3.3) and (3.4).

3.3 The 20-Noded Isoparametric Brick Element

3.3.1 Introduction

The selection of the element type is always related to the type of problem to be solved. As three dimensional nonlinear analysis is the prime concern of the analytical portion of this study, the 20-noded isoparametric brick element (ref. 1), illustrated in Figure (3.1), is used throughout this work to represent concrete. Reinforcing steel is simulated by bars embedded inside the concrete element at their actual locations in the structure without imposing any restrictions on the mesh choice. The mathematical derivations of these bars will be shown later.

The element is chosen to consider the effect of the six stress components σ_x σ_y σ_z τ_{xy} τ_{yz} τ_{zx} as shown in Figure (3.2). Each nodal point has three degrees of freedom, namely:

translation in x-direction = u,

translation in y-direction = v, and

translation in z-direction = w.

Each element has its own local coordinate system, $\xi \eta \zeta$, shown in Figure (3.1), with the origin at the centre of the element such that each local coordinate ranges from -1 to +1 only.

3.3.2 Shape Functions

Shape functions are interpolation functions that define the variation of the field variable, and its derivatives, through an element in terms of its values at the nodes.

Therefore, the shape functions are closely related to to the number of nodes and hence type of elements. Therefore, in the displacement finite element approach

$$[\delta] = \sum_{i=1}^{n} [N_i][\delta_i] \qquad\qquad (3.10)$$

where N_i is the shape function at the ith node at which the nodal displacement is δ.

The efficiency of any particular element type will depend on how well the shape functions are capable of representing the true displacement field.   The isoparametric family are a group of elements in which the shape functions are used to define the geometry as well as the displacement field.   This leads to reduced computing effort and efficiency.   The isoparametric elements are better known for their accuracy and versatility over simpler type of elements. Moreover a considerable saving of computer effort is obtained, even though a complex element requires more time to formulate. This is because it requires fewer elements compared with more simple elements.

For three dimensional applications, the displacement field at a particular local coordinate (ξ,η,ζ) are $u(\xi,\eta,\zeta)$, $v(\xi,\eta,\zeta)$, $w(\xi,\eta,\zeta)$ and are defined using three displacement degrees of freedom u_i , v_i , w_i , at each of the twenty nodes and a quadratic interpolation scheme.

The coordinate values $x(\xi,\eta,\zeta)$, $y(\xi,\eta,\zeta)$ and $z(\xi,\eta,\zeta)$ at any point (ξ,η,ζ) within the element may be defined by the expressions:

$$x(\xi,\eta,\zeta) = \sum_{i=1}^{20} N_i(\xi,\eta,\zeta) \cdot x_i$$

$$y(\xi,\eta,\zeta) = \sum_{i=1}^{20} N_i(\xi,\eta,\zeta) \cdot y_i \qquad (3.11)$$

$$z(\xi,\eta,\zeta) = \sum_{i=1}^{20} N_i(\xi,\eta,\zeta) \cdot z_i$$

where (x_i, y_i, z_i,) are the coordinates of node i and $N_i(\xi, \eta,\zeta)$ are three dimensional quadratic shape functions. In this work the shape functions for the 20-noded isoparametric brick element used are given by :

For corner nodes $\xi_i = \pm 1$ $\eta_i = \pm 1$ $\zeta_i = \pm 1$

$$(3.12)$$

$$N_i(\xi,\eta,\zeta) = \frac{1}{8}(1+\xi\xi_i)(1+\eta\eta_i)(1+\zeta\zeta_i)(\xi\xi_i + \eta\eta_i + \zeta\zeta_i - 2)$$

For mid-side node $\xi_i = 0$ $\eta_i = \pm 1$ $\zeta_i = \pm 1$

$$(3.13)$$

$$N_i(\xi,\eta,\zeta) = \frac{1}{4}(1-\xi^2)(1 + \eta\eta_i)(1 + \zeta\zeta_i)$$

For mid-side node $\xi_i = \pm 1$ $\eta_i = 0$ $\zeta_i = \pm 1$

$$(3.14)$$

$$N_i(\xi,\eta,\zeta) = \frac{1}{4}(1 + \xi\xi_i)(1-\eta^2)(1 + \zeta\zeta_i)$$

For mid-side node $\xi_i = \pm 1$ $\eta_i = \pm 1$ $\zeta_i = 0$

$$(3.15)$$

$$N_i(\xi,\eta,\zeta) = \frac{1}{4}(1+\xi\xi_i)(1 + \eta\eta_i)(1-\zeta^2)$$

Each of the twenty shape functions has a value of unity at the node to which it is related. They also have the property that their sum at any point within an element is also equal to unity, since it is required that a rigid body displacement of the element results in no element straining.

To calculate the displacements $u(\xi,\eta,\zeta)$, $v(\xi,\eta,\zeta)$ and $w(\xi,\eta,\zeta)$ at any point within the element, use is made of the expressions:

$$u(\xi,\eta,\zeta) = \sum_{i=1}^{20} N_i(\xi,\eta,\zeta) \cdot u_i$$

$$v(\xi,\eta,\zeta) = \sum_{i=1}^{20} N_i(\xi,\eta,\zeta) \cdot v_i \qquad (3.16)$$

$$w(\xi,\eta,\zeta) = \sum_{i=1}^{20} N_i(\xi,\eta,\zeta) \cdot w_i$$

3.3.3 Strain Matrix

From theory of elasticity, and for the three-dimensional case, the strain-displacement relationships may be written as:

$$\varepsilon_x = \partial u/\partial x$$

$$\varepsilon_y = \partial v/\partial y$$

$$\varepsilon_z = \partial w/\partial z$$

$$\gamma_{xy} = \partial u/\partial y + \partial v/\partial x \qquad (3.17)$$

$$\gamma_{yz} = \partial v/\partial z + \partial w/\partial y$$

$$\gamma_{zx} = \partial w/\partial x + \partial u/\partial z$$

in which ε_x, ε_y, ε_z are the normal strain components and γ_{xy} γ_{yz} and γ_{zx} are the shear strain components. Equations (3.17) may be written in matrix form as follows:

$$[\varepsilon] = \begin{bmatrix} \varepsilon_x \\ \varepsilon_y \\ \varepsilon_z \\ \gamma_{xy} \\ \gamma_{yz} \\ \gamma_{zx} \end{bmatrix} \begin{bmatrix} \partial/\partial x & 0 & 0 \\ 0 & \partial/\partial y & 0 \\ 0 & 0 & \partial/\partial z \\ \partial/\partial y & \partial/\partial x & 0 \\ 0 & \partial/\partial z & \partial/\partial y \\ \partial/\partial z & 0 & \partial/\partial x \end{bmatrix} \begin{bmatrix} U \\ V \\ W \end{bmatrix} \qquad (3.18)$$

using the finite element idealisation we can write:

$$[\epsilon] = \sum_{i=1}^{20} \begin{bmatrix} \partial N_i/\partial x & 0 & 0 \\ 0 & \partial N_i/\partial y & 0 \\ 0 & 0 & \partial N_i/\partial z \\ \partial N_i/\partial y & \partial N_i/\partial x & 0 \\ 0 & \partial N_i/\partial z & \partial N_i/\partial y \\ \partial N_i/\partial z & 0 & \partial N_i/\partial x \end{bmatrix} \begin{bmatrix} U_i \\ V_i \\ W_i \end{bmatrix} \qquad (3.19)$$

or simply:

$$[\epsilon] = \sum_{i=1}^{20} [B_i][\delta_i] \qquad (3.20)$$

where $[B_i]$ is the 6x3 strain matrix in Equation (3.19), which contains the cartesian derivatives of the shape functions.

Since the shape functions N_i are defined in terms of the local coordinates of the element ξ, ζ, η, a transformation from local to global coordinates is required to obtain the B matrix in Equation (3.19). This is done through the well known Jacobian matrix which is written as:

$$[J] = \begin{bmatrix} \partial x/\partial\xi & \partial y/\partial\xi & \partial z/\partial\xi \\ \partial x/\partial\eta & \partial y/\partial\eta & \partial z/\partial\eta \\ \partial x/\partial\zeta & \partial y/\partial\zeta & \partial z\,\partial\zeta \end{bmatrix} \qquad (3.21)$$

thus:

$$[J] = \sum_{i=1}^{20} \begin{bmatrix} \dfrac{\partial N_i}{\partial\xi}\cdot x_i & \dfrac{\partial N_i}{\partial\xi}\cdot y_i & \dfrac{\partial N_i}{\partial\xi}\cdot z_i \\[2mm] \dfrac{\partial N_i}{\partial\eta}\cdot x_i & \dfrac{\partial N_i}{\partial\eta}\cdot y_i & \dfrac{\partial N_i}{\partial\eta}\cdot z_i \\[2mm] \dfrac{\partial N_i}{\partial\zeta}\cdot x_i & \dfrac{\partial N_i}{\partial\zeta}\cdot y_i & \dfrac{\partial N_i}{\partial\zeta}\cdot z_i \end{bmatrix} \qquad (3.22)$$

the inverse of which is:

$$[J]^{-1} = \begin{bmatrix} \dfrac{\partial\xi}{\partial x} & \dfrac{\partial\eta}{\partial x} & \dfrac{\partial\zeta}{\partial x} \\[2ex] \dfrac{\partial\xi}{\partial y} & \dfrac{\partial\eta}{\partial y} & \dfrac{\partial\zeta}{\partial y} \\[2ex] \dfrac{\partial\xi}{\partial z} & \dfrac{\partial\eta}{\partial z} & \dfrac{\partial\zeta}{\partial z} \end{bmatrix} \tag{3.23}$$

Therefore the cartesian derivatives will be given by:

$$\begin{bmatrix} \partial N_i/\partial x \\[1ex] \partial N_i/\partial y \\[1ex] \partial N_i/\partial z \end{bmatrix} = [J]^{-1} \begin{bmatrix} \partial N_i/\partial \xi \\[1ex] \partial N_i/\partial \eta \\[1ex] \partial N_i/\partial \zeta \end{bmatrix} \tag{2.24}$$

3.3.4 Three Dimensional Stress-Strain Relations

From theory of elasticity, for isotropic material ,and in the absence of initial stresses and strains, the stress-strain relationship may be written in the form:

$$[\sigma] = [D] \, [\epsilon] \tag{3.25}$$

where [D] is the elasticity matrix which takes the form:

$$[D] = \frac{E(1-\nu)}{(1+\nu)(1-2\nu)} \begin{bmatrix} 1 & \nu/(1-\nu) & \nu/(1-\nu) & 0 & 0 & 0 \\ & 1 & \nu/(1-\nu) & 0 & 0 & 0 \\ & & 1 & 0 & 0 & 0 \\ & & & \dfrac{(1-2\nu)}{2(1-\nu)} & 0 & 0 \\ \text{symmetric} & & & & \dfrac{(1-2\nu)}{2(1-\nu)} & 0 \\ & & & & & \dfrac{(1-2\nu)}{2(1-\nu)} \end{bmatrix} \tag{3.26}$$

where E is the Young's modulus of elasticity, and ν is the Poissons' ratio. As the concrete nonlinearity considered in

this work is only the material nonlinearity all changes in material properties enter through the material property matrix [D]. This will be fully discussed in Chapter Four.

3.3.5 Element Stiffness Matrix

So far all the information needed to evaluate the stiffness matrix $[K^e]$ have been explained. Hence from Equation (3.9):

$$[K^e] = \iiint [B]^T [D][B] \, dv \tag{3.27}$$

where $\quad dv = dxdydz \tag{3.28}$

Again transformation from global to local coordinate system results in:

$$dv = \det[J]d\xi \, d\eta \, d\zeta \tag{3.29}$$

where the limits of integration become -1 to 1 in each one of the three directions.

3.3.6 Numerical Integration

Analytical integration of Equation (3.27) is impossible. Therefore some form of numerical integration must be resorted to. In this study Gauss-Legendre quadrature rules have been used execlusively because of their higher efficiency over other forms of quadrature. They can integrate exactly a polynomial $f(\xi)$ of degree (2n-1), where n is the number of sampling points. Also they are suitable for isoparametric elements because the range of these integration rules are ±1 which coincides with the local coordinate system limits of ±1 on element boundaries. A 3x3x3 Gauss rule has always been used for monitoring nonlinear behaviour especially cracking, as shown in Figure (3.3), although 2x2x2 and 4x4x4 are also available.

3.3.7 Evaluation of the Principal Stresses and Their Directions

The evaluation of the principal stresses and their respective directions in the global cartesian system of axes is important for the determination of the occurance and orientation of cracking in concrete. The solution of the resulting set of linear equations yields the nodal displacements and hence the strains. The strains are used to obtain the stresses at each sampling point in the structure. From Equation (3.25) there are six cartesian stress components at each Gauss point that can be evaluated, namely:

$$[\sigma] = [\sigma_x \quad \sigma_y \quad \sigma_z \quad \tau_{xy} \quad \tau_{yz} \quad \tau_{zx}]^T \qquad (3.30)$$

The values of the principal stresses, σ_i, can be obtained by solving the following cubic equation:

$$\sigma_i^3 - I_1 \sigma_i^2 + I_2 \sigma_i - I_3 = 0 \qquad (3.31)$$

where I_1, I_2, and I_3 are the stress invariants (ref. 3), which can be expressed as follows:

$$I_1 = \sigma_x + \sigma_y + \sigma_z \qquad (3.32)$$

$$I_2 = \sigma_x \sigma_y + \sigma_y \sigma_z + \sigma_z \sigma_x - \tau_{xy}^2 - \tau_{yz}^2 - \tau_{zx}^2 \qquad (3.33)$$

I = determinant of the stress tensor:

$$\begin{vmatrix} \sigma_x & \tau_{xy} & \tau_{xz} \\ \tau_{yx} & \sigma_y & \tau_{yz} \\ \tau_{zx} & \tau_{zy} & \sigma_z \end{vmatrix} \qquad (3.34)$$

Therefore the cubic equation (3.31), upon substitution, becomes:

$$\sigma_i^3 - (\sigma_x + \sigma_y + \sigma_z)\sigma_i^2$$
$$+(\sigma_x\sigma_y + \sigma_y\sigma_z + \sigma_z\sigma_x - \tau_{xy}^2 - \tau_{yz}^2 - \tau_{zx}^2)\sigma_i \qquad (3.35)$$
$$-(\sigma_x\sigma_y\sigma_z - \sigma_x\tau_{zx}^2 - \sigma_z\tau_{xy}^2 + 2\tau_{xy}\tau_{yz}\tau_{zx}) = 0$$

The principal directions which determine the principal planes can be expressed through the direction cosines such that:

$$l_i = \cos\theta_{xi}; \quad m_i = \cos\theta_{yi}; \quad n_i = \cos\theta_{zi}$$

Therefor the direction cosines of σ_1 are l_1, m_1, n_1, those for σ_2 are l_2, m_2, n_2, and those for σ_3 are l_3, n_3, n_3.

The detailed method for the evaluation of these direction cosines is fully described elsewhere (ref. 3), but will be briefly illustrated here.

The three direction cosines for σ_1 can be determined by solving Equation (3.35) in its determinant form:

$$\begin{vmatrix} \sigma_x - \sigma_1 & \tau_{yx} & \tau_{zx} \\ \tau_{xy} & \sigma_y - \sigma_1 & \tau_{zy} \\ \tau_{xz} & \tau_{yz} & \sigma_z - \sigma_1 \end{vmatrix} = 0 \qquad (3.36)$$

calling

$$A = \begin{vmatrix} \sigma_y - \sigma_i & \tau_{zy} \\ \tau_{yz} & \sigma_z - \sigma_i \end{vmatrix}, \quad B = -\begin{vmatrix} \tau_{xy} & \tau_{zy} \\ \tau_{xz} & \sigma_z - \sigma_i \end{vmatrix}, \quad C = \begin{vmatrix} \tau_{xy} & \sigma_y - \sigma_i \\ \tau_{xz} & \tau_{yz} \end{vmatrix}$$

$$(3.37)$$

it can be shown that the three direction cosines can be
expressed as:

$$\frac{\ell_i}{A} = \frac{m_i}{B} = \frac{n_i}{C} = K \qquad (3.38)$$

where K is a non-zero constant to be determined. The
subsidiary trigonometric condition:

$$\ell_i^2 + m_i^2 + n_i^2 = 0 \qquad (3.39)$$

determines K, upon substitution from Equation (3.38), as:

$$K = \frac{1}{\sqrt{A^2 + B^2 + C^2}} \qquad (3.40)$$

therefore

$$\ell_i = A.K \quad , \quad m_i = B.K \quad , \quad n_i = C.K \qquad (3.41)$$

3.4 Simulation of Steel Reinforcement

3.4.1 General

In modelling reinforced concrete by finite element methods
at least the following three alternative representations of
the reinforcement have been used:

(a) distributed

(b) discrete

(c) embedded

For a distributed representation (Figure 3.4), the steel is
assumed to be distributed over the concrete element, with a
particular orientation angle θ. A composite concrete-
reinforcement constitutive relation need to be used in this
case. To derive such a relation, perfect bond must be
assumed between the concrete and steel (refs. 4, 5). This

type of representation, though easy to implement, is very unrealistic in the sense that the reinforcing bars are no longer uniaxial members embedded inside the concrete and bonded to it.

A discrete representation of the reinforcement, using one-dimensional elements (Figure 3.5), has been widely used (ref. 5). Axial force members may be used and assumed to be pin connected with two degrees of freedom at the nodal points (ref. 6 for example). Alternatively, beam elements assumed to be capable of resisting axial force, shear, and bending can be used; in this case three degrees of freedom are assigned at each end. In either case, the one-dimensional reinforcement element is superimposed on a two-dimensional finite element mesh representing concrete. The approach is simple and it is possible to account for possible displacement of the reinforcement with respect to the surrounding concrete. A serious disadvantage, however, is that the location of steel often dictates the concrete mesh. This may result in slender elements, where the reinforcing bars are too close together, violating the concept of aspect ratios being close to unity as possible. This is specially unadvantageous with the powerful higher order isoparametric elements often used to represent concrete.

An embedded representation (Figure 3.6) may be used in connection with higher order isoparametric concrete elements. The reinforcing bar is considered to be an axial member built into the isoparametric element such that its displacements are consistent with those of the element.

Perfect bond was used in the original derivations of such bars (refs. 7, 8).

3.4.2 Embedded Bars for Three Dimensional Analyses

The concept of embedding isoparametric elements with reinforcing bars was first suggested for plane stress, plane strain, and axisymmetric analysis (refs. 7, 8). It allows an isoparametric element to cover a large volume whilst including the finer detail of reinforcement. Indeed the reinforcing steel can be placed in its exact position without imposing any restrictions on mesh choice.

In this study, reinforcing bars are embedded in the 20-noded isoparametric brick element used for concrete. The basic two-dimensional theoretical formulation (refs. 7, 8) is extended here to the three-dimensional case. The derivation requires that bars are restricted to lie along the local coordinate lines ξ, η, and ζ of the basic element as shown in Figure (3.7).

3.4.3 Theoretical Derivations

Consider a bar lying along a direction parallel to the local coordinate axis ξ as shown in Figure (3.7), i.e. lying along the line of constant $\eta = \eta_c$ and $\zeta = \zeta_c$. Bars lying along directions parallel to η and ζ axes will obviously follow a similar derivation. It is further assumed that bars are capable of transmitting axial forces only. The line of the bar is defined by using the same shape functions as the main element. Thus the cartesian co-ordinates of any point P are given by:

$$x = \sum_{i=1}^{20} N_i(\xi) x_i \qquad (3.42)$$

Full compatibility between the bar and the basic element is assumed, therefore the displacements of the bar are obtainable from the displacement field of the basic element, i.e:

$$[\delta] = \begin{bmatrix} u \\ v \\ w \end{bmatrix} = [N(\xi)][\delta]^e \qquad (3.43)$$

For bars, only one component of strain contributes to the strain energy and is defined locally by:

$$\varepsilon_p' = \partial u'/\partial x' \qquad (3.44)$$

where x, y, z are a local coordinate system at point P with y and z being normal to the line of the bar, and u, v, w are the corresponding displacements.

Now at any point it is possible to define a distortion matrix [j] as:

$$j] = \begin{bmatrix} \dfrac{\partial u}{\partial x} & \dfrac{\partial v}{\partial x} & \dfrac{\partial w}{\partial x} \\[2mm] \dfrac{\partial u}{\partial y} & \dfrac{\partial v}{\partial y} & \dfrac{\partial w}{\partial y} \\[2mm] \dfrac{\partial u}{\partial z} & \dfrac{\partial v}{\partial z} & \dfrac{\partial w}{\partial z} \end{bmatrix} = \begin{bmatrix} \dfrac{\partial N_i}{\partial x}, & \dfrac{\partial N_j}{\partial x}, & \dfrac{\partial N_m}{\partial x} \cdots \\[2mm] \dfrac{\partial N_i}{\partial y}, & \dfrac{\partial N_j}{\partial y}, & \dfrac{\partial N_m}{\partial y} \cdots \\[2mm] \dfrac{\partial N_i}{\partial z}, & \dfrac{\partial N_j}{\partial z}, & \dfrac{\partial N_m}{\partial z} \cdots \end{bmatrix} \begin{bmatrix} u_i & v_i & w_i \\[2mm] u_j & v_j & w_j \\[2mm] u_m & v_m & w_m \\ \vdots & \vdots & \vdots \end{bmatrix} \qquad (3.45)$$

and, as mentioned earlier, a Jacobian matrix given by:

$$] = \begin{bmatrix} \dfrac{\partial x}{\partial \xi} & \dfrac{\partial y}{\partial \xi} & \dfrac{\partial z}{\partial \xi} \\[2mm] \dfrac{\partial x}{\partial \eta} & \dfrac{\partial y}{\partial \eta} & \dfrac{\partial z}{\partial \eta} \\[2mm] \dfrac{\partial x}{\partial \zeta} & \dfrac{\partial y}{\partial \zeta} & \dfrac{\partial z}{\partial \zeta} \end{bmatrix} \begin{bmatrix} \dfrac{\partial N_i}{\partial \xi} ; & \dfrac{\partial N_j}{\partial \xi}, & \dfrac{\partial N_m}{\partial \xi} \cdots \\[2mm] \dfrac{\partial N_i}{\partial \eta}, & \dfrac{\partial N_j}{\partial \eta}, & \dfrac{\partial N_m}{\partial \eta} \cdots \\[2mm] \dfrac{\partial N_i}{\partial \zeta}, & \dfrac{\partial N_j}{\partial \zeta}, & \dfrac{\partial N_m}{\partial \zeta} \cdots \end{bmatrix} \begin{bmatrix} x_i & y_i & z_i \\[2mm] x_j & y_j & z_j \\[2mm] x_m & y_m & z_m \\ \vdots & \vdots & \vdots \end{bmatrix} \qquad (3.46)$$

Therefore from the relation:

$$
\begin{bmatrix}
\dfrac{\partial N_i}{\partial \xi}, & \dfrac{\partial N_j}{\partial \xi}, & \dfrac{\partial N_m}{\partial \xi} \cdots \\[2ex]
\dfrac{\partial N_i}{\partial \eta}, & \dfrac{\partial N_j}{\partial \eta}, & \dfrac{\partial N_m}{\partial \eta} \cdots \\[2ex]
\dfrac{\partial N_i}{\partial \zeta}, & \dfrac{\partial N_j}{\partial \zeta}, & \dfrac{\partial N_m}{\partial \zeta} \cdots
\end{bmatrix}
= [J]
\begin{bmatrix}
\dfrac{\partial N_i}{\partial x}, & \dfrac{\partial N_j}{\partial x}, & \dfrac{\partial N_m}{\partial x} \cdots \\[2ex]
\dfrac{\partial N_i}{\partial y}, & \dfrac{\partial N_j}{\partial y}, & \dfrac{\partial N_m}{\partial y} \cdots \\[2ex]
\dfrac{\partial N_i}{\partial z}, & \dfrac{\partial N_j}{\partial z}, & \dfrac{\partial N_m}{\partial z} \cdots
\end{bmatrix}
\tag{3.47}
$$

it follows that:

$$
[j] = [J]^{-1}
\begin{bmatrix}
\dfrac{\partial N_i}{\partial \xi}, & \dfrac{\partial N_j}{\partial \xi}, & \dfrac{\partial N_m}{\partial \xi} \cdots \\[2ex]
\dfrac{\partial N_i}{\partial \eta}, & \dfrac{\partial N_j}{\partial \eta}, & \dfrac{\partial N_m}{\partial \eta} \cdots \\[2ex]
\dfrac{\partial N_i}{\partial \zeta}, & \dfrac{\partial N_j}{\partial \zeta}, & \dfrac{\partial N_m}{\partial \zeta} \cdots
\end{bmatrix}
\begin{bmatrix}
u_i & v_i & w_i \\[1.5ex]
u_j & v_j & w_j \\[1.5ex]
u_m & v_m & w_m \\
\vdots & \vdots & \vdots
\end{bmatrix}
\tag{3.48}
$$

As [j] is a second order tensor, it transforms on coordinate rotation from x, y, z to x′, y′, z′ according to:

$$
[j'] =
\begin{bmatrix}
\dfrac{\partial u'}{\partial x'} & \dfrac{\partial v'}{\partial x'} & \dfrac{\partial w'}{\partial x'} \\[2ex]
\dfrac{\partial u'}{\partial y'} & \dfrac{\partial v'}{\partial y'} & \dfrac{\partial w'}{\partial y'} \\[2ex]
\dfrac{\partial u'}{\partial z'} & \dfrac{\partial v'}{\partial z'} & \dfrac{\partial w'}{\partial z'}
\end{bmatrix}
= [R][j][R]^T
\tag{3.49}
$$

where [R] is the rotation matrix of direction cosines at point P, given by:

$$[\, R \,] = \begin{bmatrix} \dfrac{\partial x}{\partial x'} & \dfrac{\partial y}{\partial x'} & \dfrac{\partial z}{\partial x'} \\[2mm] \dfrac{\partial x}{\partial y'} & \dfrac{\partial y}{\partial y'} & \dfrac{\partial z}{\partial y'} \\[2mm] \dfrac{\partial x}{\partial z'} & \dfrac{\partial y}{\partial z'} & \dfrac{\partial z}{\partial z'} \end{bmatrix} \tag{3.50}$$

and, by noting that x and ξ coincide and differ only in magnitude, can be shown to be:

$$[\, R \,] = \frac{1}{\sqrt{\left(\dfrac{\partial x}{\partial \xi}\right)^2 + \left(\dfrac{\partial y}{\partial \xi}\right)^2 + \left(\dfrac{\partial z}{\partial \xi}\right)^2}} \begin{bmatrix} \dfrac{\partial x}{\partial \xi} & \dfrac{\partial y}{\partial \xi} & \dfrac{\partial z}{\partial \xi} \\[2mm] \dfrac{\partial y}{\partial \xi} & \dfrac{\partial x}{\partial \xi} & \dfrac{\partial y}{\partial \xi} \\[2mm] \dfrac{\partial z}{\partial \xi} & \dfrac{\partial z}{\partial \xi} & \dfrac{\partial x}{\partial \xi} \end{bmatrix} \tag{3.51}$$

Finally from Equations (3.44), (3.49) and (3.51) it follows that:

$$\epsilon'_p = \frac{1}{h^2}\left[\left\{ c_1 \frac{\partial N_i}{\partial x} + c_2 \frac{\partial N_i}{\partial y} + c_3 \frac{\partial N_i}{\partial z} \right\}, \left\{ c_2 \frac{\partial N_i}{\partial x} + c_4 \frac{\partial N_i}{\partial y} + c_5 \frac{\partial N_i}{\partial z} \right\} \right.$$
$$\left. \left\{ c_3 \frac{\partial N_i}{\partial x} + c_5 \frac{\partial N_i}{\partial y} + c_6 \frac{\partial N_i}{\partial z} \right\}, \right] \times \begin{bmatrix} u_i \\ v_i \\ w_i \\ \cdot \\ \cdot \\ \cdot \end{bmatrix} \tag{3.52}$$

where:

$$h = \sqrt{\left(\frac{\partial x}{\partial \xi}\right)^2 + \left(\frac{\partial y}{\partial \xi}\right)^2 + \left(\frac{\partial z}{\partial \xi}\right)^2} \tag{3.53}$$

and:

$$c_1 = \left(\frac{\partial x}{\partial \xi}\right)^2$$

$$c_2 = \frac{\partial x}{\partial \xi} \cdot \frac{\partial y}{\partial \xi}$$

$$c_3 = \frac{\partial x}{\partial \xi} \cdot \frac{\partial z}{\partial \xi}$$

$$c_4 = \left(\frac{\partial y}{\partial \xi}\right)^2 \qquad\qquad (3.54)$$

$$c_5 = \frac{\partial y}{\partial \xi} \cdot \frac{\partial z}{\partial \xi}$$

$$c_6 = \left(\frac{\partial z}{\partial \xi}\right)^2$$

For bars lying along a direction parallel to the local co-ordinate axis η, the following formulae can be derived in a similar fashion:

$$[R] = \frac{1}{h}\begin{bmatrix} \dfrac{\partial y}{\partial \eta} & \dfrac{\partial x}{\partial \eta} & \dfrac{\partial x}{\partial \eta} \\[2mm] \dfrac{\partial x}{\partial \eta} & \dfrac{\partial y}{\partial \eta} & \dfrac{\partial z}{\partial \eta} \\[2mm] \dfrac{\partial y}{\partial \eta} & \dfrac{\partial z}{\partial \eta} & \dfrac{\partial y}{\partial \eta} \end{bmatrix} \qquad (3.55)$$

where h will be:

$$h = \sqrt{\left(\frac{\partial x}{\partial \eta}\right)^2 + \left(\frac{\partial y}{\partial \eta}\right)^2 + \left(\frac{\partial z}{\partial \eta}\right)^2} \qquad (3.56)$$

and for bars lying along a direction parallel to ζ,

$$[R] = \frac{1}{h}\begin{bmatrix} \dfrac{\partial z}{\partial \zeta} & \dfrac{\partial x}{\partial \zeta} & \dfrac{\partial x}{\partial \zeta} \\[2mm] \dfrac{\partial y}{\partial \zeta} & \dfrac{\partial z}{\partial \zeta} & \dfrac{\partial y}{\partial \zeta} \\[2mm] \dfrac{\partial x}{\partial \zeta} & \dfrac{\partial y}{\partial \zeta} & \dfrac{\partial z}{\partial \zeta} \end{bmatrix} \qquad (3.57)$$

and h will be:

$$h = \sqrt{(\frac{\partial x}{\partial \zeta})^2 + (\frac{\partial y}{\partial \zeta})^2 + (\frac{\partial z}{\partial \zeta})^2} \qquad (3.58)$$

For all the three cases of bar directions, Equations (3.54) hold.

The stiffness matrix $[k']^e$ of the bar is evaluated from:

$$[\acute{K}]^e = \int_V [B']^T [D'] [B'] \, d(vol) \qquad (3.59)$$

where $[B]$ = strain matrix obtained from Equation (3.52)

and $[D'] = E_S$ $\qquad (3.60)$

where E_S is the modulus of elasticity of steel.

The elemental volume $d(vol)$ is given by:

$d(vol) = A_S \, dx' = A_S \, h \, d\xi \qquad$ for bars parallel to ξ $\quad (3.61)$

$d(vol) = A_S \, dy' = A_S \, h \, d\eta \qquad$ for bars parallel to η $\quad (3.62)$

$d(vol) = A_S \, dz' = A_S \, h \, d\zeta \qquad$ for bars parallel to ζ $\quad (3.63)$

where A_S = bar cross-sectional area, and h is taken from Equations (3.53) or (3.56) or (3.51) depending on the bar direction. Clearly numerical integration must be used again, but now applied in one direction only.

The value of stress which will be induced in the steel bar will be:

$$\sigma'_p = \epsilon'_p \cdot E_s \qquad (3.64)$$

The equivalent nodal loads contributed by the steel bar will be:

$$[P_i]_{steel} = \int_V [B']^T [\sigma_i]_{steel} \, d(vol) \qquad (3.65)$$

where $[\sigma_i]_{steel}$ are the bar stresses.

It is a major content of this study to incorporate these embedded bars in three-dimensional isoparametric elements.

3.5 Nonlinear Method of Solution

3.5.1 Introduction

A nonlinear structural problem must obey the basic laws of continuum mechanics, i.e. equilibrium, compatibility, and the constitutive relations of the material. Displacement compatibility is automatically satisfied in the displacement finite element technique. Common nodes between elements ensure continuity and compatibility of displacements along internal element boundaries, and polynomial shape functions ensure continuity and single valued displacements internally. Therefore it becomes only necessary to enforce that the nonlinear constitutive relations are correctly satisfied whilst at the same time preserving the equilibrium of the structure.

There can be several causes of nonlinear behaviour in a structure, which can be divided into three categories (ref. 9):

     1 - Material nonlinearity

     2 - Geometric nonlinearity

     3 - Mixed material and geometric nonlinearity

Stress-strain relations are a major source of nonlinearity. These can vary from short-term nonlinear relationships between stress and strain such as plasticity, cracking, nonlinear elasticity, etc. , to time-dependent effects such as creep and shrinkage.

Only nonlinearity caused by short-term nonlinear behaviour of concrete and steel is considered in this study. These include the tensile cracking of concrete, the nonlinear stress-strain relations of concrete, and the yielding and work-hardening of steel. Details of the laws representing these behaviours will be discussed later in Chapter Four.

A nonlinear solution is obtained by solving a series of linear problems such that the appropriate nonlinear conditions are satisfied at any stage to a specified degree of accuracy. This technique is required because contrary to linear equations there is no general method which uniquely solves nonlinear equations. In fact it is usually impossible to obtain the explicit form of these equations in the first place. One way of achieving this goal is to ensure that at any loading stage the solution results in stresses consistent with the displacement field and satisfying the given constitutive equations. These stresses will be statically equivalent to a set of internal nodal forces which should be in equilibrium with the externally applied loads. In general these equivalent nodal forces are not equal and the differences between the external and internal forces are termed "residual forces". These residuals must be removed by repeatedly applying them on the structure until an acceptable tolerance is achieved (refs. 1, 10).

3.5.2 Numerical Techniques for Nonlinear Analysis

The solutions of nonlinear problems by the finite element method are usually attempted by one of the following three basic techniques :

(a) Incremental (step-wise procedure)

(b) Iterative (Newton methods)

(c) Incremental-Iterative (mixed procedure)

where the nonlinearity occurs in the stiffness matrix [K] which, in the case of short-term behaviour of reinforced concrete, is a function of nonlinear material properties.

The general basis of each method is similar. For problems where only the material behaviour is nonlinear, as in our case, the relationship between stress and strain is assumed to be of the form:

$$f (\sigma , \varepsilon) = 0 \qquad (3.66)$$

The element stiffness matrix is a function of the material properties and can be written as:

$$[K] = k (\sigma , \varepsilon) \qquad (3.67)$$

The external nodal forces [R] are related to the nodal displacements through the element stiffness and can be expressed by:

$$[R] = [K] [\delta] \qquad (3.68)$$

which on inversion becomes:

$$[\delta]^{-1} = [K]^{-1} [R] \qquad (3.69)$$

or
$$[\delta] = [k(\sigma , \varepsilon)]^{-1} [R] \qquad (3.70)$$

This derivation illustrates the basic nonlinear relationship between [δ] and [R], due to the influence of the material laws on [K].

Equation (3.70) is solved by a succession of linear

approximations. The three methods mentioned above are now briefly discussed. Further details can be obtained from references (1, 6, 9, 10).

3.5.2.1   Incremental Method

The basis of the incremental method is the subdivision of the total applied load vector into smaller increments, which do not necessarily need to be equal. During each load increment Equation (3.68) is assumed to be linear, i.e. a fixed value of [K] is assumed using material data existing at the end of the previous increment. Nodal displacements can be obtained for each increment and these are added to the previously accumulated displacements. The process is repeated until the total load is reached. No account is taken of the force redistribution during the application of the incremental load (i.e. no iteration process exists to restore equilibrium).

The accuracy of the incremental method can be improved by using small increments size, but this results in a more computational effort. The mid-point Runge-Kutta scheme (ref. 9) is a modification of the incremental method which utilizes the additional computational effort, where two cycles of analysis are performed for each load increment. The first step is to apply half the load increment and to calculate new stiffnesses corresponding to the total stresses at this value. These stiffnesses are then utilized to compute an approximation for the full load increment.

3.5.2.2 Iterative Method

In this method, the full load is applied in one increment.

Stresses are evaluated at that load according to the material law. Then the equivalent nodal forces are computed using these stresses. These may not be in equilibrium with the externally applied loads. The unbalanced nodal forces $[F_u]$, i.e. the difference between the external and internal forces, is calculated. These unbalanced forces are then used to compute an additional increment of displacement, and hence new stresses, which give a new set of equivalent nodal forces. This process is repeated until equilibrium is approximated to some acceptable degree. When this stage is reached the total displacement is taken as the sum of the accumulated displacements from each iteration.

3.5.2.2.1 Computation of the Unbalanced Nodal Forces

In general, the linear constitutive law can be written in the form :

$$[\sigma] = [D]([\varepsilon]-[\varepsilon_o]) + [\sigma_o] \qquad (3.71)$$

where $[D]$ is the rigidity matrix, $[\sigma_o]$ and $[\varepsilon_c]$ are the initial stress and strain vectors. Equation (3.71) is in essence the linear approximation of the nonlinear relation between stress and strain :

$$f(\sigma ,\varepsilon) = 0 \qquad (3.72)$$

Adjustments to any of the quantities $[D]$, $[\sigma_o]$, or $[\varepsilon_o]$ in Equation (3.71) can be made so that Equation (3.72) can be approximated. If $[\varepsilon_o]$ is adjusted the process is called the "initial strain" method (ref. 1) and is used when strains are expressed in terms of stresses. If $[\sigma_o]$ is adjusted the process becomes the "initial stress method (ref. 1) and is used when stresses can be given in terms of strains.

In the present work the initial stress method was used and therefore will be discussed. Equation (3.71) can be simplified to:

$$[\sigma] = [D] [\varepsilon] + [\sigma_0] \tag{3.73}$$

Assuming $[\sigma_0] = 0$ initially, Equation (3.73) is solved with an appropriate [D] matrix and $[\varepsilon_A]$ to obtain a certain level of stress $[\sigma_{A1}]$ where:

$$[\sigma_{A1}] = [D] [\varepsilon_A] \tag{3.74}$$

The stress which should have occurred is:

$$[\sigma_{A2}] = [D] [\varepsilon] \tag{3.75}$$

The difference between the stresses:

$$[\sigma_0] = [\sigma_{A2}] - [\sigma_{A1}] \tag{3.76}$$

is used as an initial stress in Equation (3.73) and the equivalent unbalanced nodal forces $[F_u]$ are calculated from:

$$[F_u] = -\int_V [B]^T [\sigma_0] \, dv \tag{3.77}$$

These forces are removed by applying them to the structure to obtain a correction to $[\delta]$. This process is repeated until $[\sigma_0]$ or $[F_u]$ become negligible.

3.5.2.2.2 Methods of Computing Stiffnesses (ref. 2, 7, 9)
Generally the stiffness can either be constant or variable throughout a solution. In the constant stiffness method (Figure 3.8) the initial linear stiffness $[K] = k(\sigma, \varepsilon)$ is used at every stage in the analysis. The unbalanced nodal forces are calculated using either the initial stress or strain method.

Because calculating the stiffness and fully solving the resulting set of equations is an expensive operation, this method has economical advantages as the stiffness is calculated only once. Its main disadvantage, however, is that usually a large number of iterations is required to obtain equilibrium, particularly when nonlinearity caused by concrete cracking and steel yielding occurs. Attempts to use accelerators to overcome this disadvantage have been tried (refs. 10, 11), although they have not always met with success especially when cracking is involved.

In the variable stiffness method (Figure 3.8), a linear solution is performed but the material property matrix [D] is adjusted during the iteration process. The adjustment can be done by using either a tangential or secantial modulus approach. Yet again the unbalanced nodal forces are calculated using either the initial stress or strain method. In this work the concrete material law presented in Chapter Four requires the use of the secantial modulus.

If the stiffnesses are updated during all iterations, then the method is a form of the well known "Newton-Raphson" method. Compared to the constant stiffness method, the variable stiffness method requires considerably less number of iterations, but the full solution is more expensive than a resolution with a constant stiffness.

A cheaper variation of the variable stiffness approach can be obtained by using a modified "Newton-Raphson" technique, where the stiffnesses are only updated occasionally during certain iterations. Hence retaining the advantages of quicker convergence with a lesser number of full solutions.

3.5.2.3 Mixed Method (Incremental-Iterative)

The step-iteration or mixed method utilizes a combination of the incremental and iterative schemes. In this case the load is applied in increments, but after each increment successive iterations are performed until equilibrium is achieved to the acceptable level of accuracy. Because the mixed method combines the advantages of both the incremental and iterative procedures and tends to minimize the disadvantages of each (ref. 9), the method is widely used. The additional computational effort is justified by the fact that the iterative part of the procedure permits one to assess the quality of the approximate equilibrium at each stage. Further discussions on the merits and demerits of each technique can be found in references (1, 2, 9). Figure (3.9) illustrates schematically the various techniques.

3.5.2.4 Methods Used in This work

A modified version of the mixed procedure is used in the present work. The modified "Newton-Raphson" approach is used to evaluate the stiffnesses. The stiffnesses are evaluated using a secant material property matrix; and different optional algorithms are programmed to be chosen at will, these are :

(1) Initial Stiffness method: The element stiffnesses are computed at the beginning of the analysis and remain unchanged thereafter.

(2) Variable stiffness method: The element stiffnesses are recomputed during each iteration of each load increment.

(3) Combined algorithm: The element stiffnesses are recopmuted for the first iteration of each load increment only.

(4) Combined algorithm: The element stiffnesses are recomputed for the second iteration of each load increment (of course for the first load increment the element stiffnesses must be calculated for the first iterartion also).

(5) Combined algorithm: The element stiffnesses are recomputed for the first and eighth iteration of each load increment.

(6) Combined algorithm: The element stiffnesses are recomputed for the first, sixth, eleventh and fifteenth iteration of each load increment. A maximum number of iterations of 15 was used in this work if convergence has not been achieved by then. More about the results obtained using different algorithms will be presented in Chapter Five.

For the calculation of the unbalanced nodal forces, a modification of the initial stress method is used, termed the method of "Residual Forces" (refs. 6, 10, 12). The basic technique is that, at any stage a load system equivalent to the total stress level is evaluated and checked against the applied loading system. The difference between the two will result in a set of residuals that are a measure of lack of equilibrium. These residuals are then applied to the structure to restore equilibrium. The process is then repeatedly continued to dissipate the out-of-balance forces (or the residuals) to a sufficiently small value. Thus for equilibrium it is required that:

$$[F_u] = \int_V [B]^T [\sigma] \, dv - [R] = 0 \qquad (3.78)$$

where $[\sigma]$ are the actual stresses depending on the constitutive law being used, $[R]$ lists all forces due to the external loads, initial stresses, etc., and $[F_u]$ the residual forces.

3.6 Convergence Criteria

3.6.1 General

Since the main purpose of the iteration process is the redistribution of the out-of-balance residual forces, a reliable convergence criterion must be used to monitor this gradual elimination and terminate the iterative process when the desired accuracy has been achieved. The accuracy is specified by the user through what is called "convergence tolerances" (refs. 1, 6, 10, 12). These convergence tolerances are quantitative values that determine the accuracy of equilibrium acceptable to the user. The convergence tolerances must be realistic; if generally they are too loose, inaccuracy may result, if they are too tight, much expensive effort is spent to obtain needless accuracy.

One possible method of checking convergence is to compare each individual nodal value (displacement) with the corresponding value obtained on the previous iteration (ref. 12). Then, provided that this change is negligibly small for all nodal points, convergence can be deemed to have occured. This local process is difficult and expensive, therefore a global check based on some norm is preferable. The convergence criteria can be based on various quantities; either directly on the unbalanced forces, indirectly on displacements, on energy changes or on changes in stress values.

Three types of convergence criteria have been in common use for structural analysis, namely:

(1) Force convergence criteria

(2) Displacement convergence criteria

(3) Energy convergence criteria

Each of the three alternatives has its merits, and the selection of a suitable one depends on many factors. In the displacement criteria inconsistencies in units (e.g. displacements and rotations) may occur and must be avoided. The same holds true for force criteria (i.e. inconsistencies of force and moment units). Although the use of a combination of displacement and force criteria may seem ideal and has been recommended by some investigators (refs. 13, 14), the equilibrium of forces is sometimes difficult to achieve even when iterative displacements are converging within tight tolerances. This is particularly true for rein-forced concrete structures when cracking of concrete usually makes it very difficult to achieve equilibrium because large residual forces are released.

This observation is supplemented by the findings of Cope and Rao (ref. 15), in their study on the monitoring indices for nonlinear analysis of reinforced concrete. However, the rate of convergence depends on the method used in the solution (e.g. constant or variable stiffness). It is also required to specify a maximum number of iterations, irrespective of the state of convergence. The maximum number of iterations may influence the predicted shape of the load-deflection curve, but it is an important safeguard against unlimitted and often unneeded cycles of resolutions

or full solutions.

An energy convergence criterion has been used by Cope and Rao (ref. 15), where they found that a convergence tolerance of 1-2.5% was appropriate to yield acceptable results in an analysis of reinforced concrete skew slabs. However, whatever criterion is chosen, care must be taken to avoid spending much effort trying to obtain unattainable and perhaps needless accuracy. Special attention must be given to the cracking stage when tensile forces are suddenly released onto the system. The author's experience with such situation together with some numerical studies in this phenomenon will be compiled in Chapter Five.

3.6.2 Convergence Criterion Used in This Work

In this study the convergence process is based on a force convergence criterion because it is a direct measure of equilibrium between the internal and external forces. A global approach is adopted, where convergence is monitored using norms as follows:

$$\frac{\sqrt{\sum_{i=1}^{N} (F_{ui}^{r})^2}}{\sqrt{\sum_{i=1}^{N} (R_i)^2}} \times 100 \leqslant \text{Toler} \qquad (3.79)$$

where N is the total number of nodal points in the system, r denotes the iteration number, F_u is the the residual force at node i and R is the total external applied load at node i.

This criterion states that the convergence occurs if the norm of the residual forces becomes less than a specified tolerance times the norm of the total applied forces.

3.7 Analysis Termination Criterion

The analysis program must be provided with some means of detecting the collapse of the analysed structure. The failure of the structure takes place when no further loading can be sustained. This is indicated in the nonlinear solution by successively iterative displacements. The growth of iterative displacements results in a lack of convergence of the nonlinear solution. It also results in the growth of the work done by the out of balance forces on these displacements.

A maximum deflection can be used as a criterion to stop the analysis at failure (ref. 22). An emperical expression can be used to detect maximum deflection, but obviously this needs great care and no one expression can fit all situations.

The maximum number of iterations can also be used. When a specified number of iterations has been performed without achieving convergence, the structure is deemed to have failed and the failure load can then be estimated. It must be mentioned here that this criterion is not always sufficient to indicate the failure of the structure, since it could be satisfied while the solution is slowly converging when severe discontinuity occurs due to extensive cracking or in the event of large displacements. It may also occur when large load increments are used or very tight convergence tolerances are specified. However, if realistic maximum number of iterations (which may be expensive) is used and the solution continued not to converge, for a number of load increments, then this can be a realistic

indication of failure.

A scalar quantity, termed the current stiffness parameter S_p, has also been suggested by Bergan et. al. (ref. 23) to serve as a way of characterizing the overall structural stiffness during load application. The norm of the incremental load and the corresponding norm of the incremental displacements are used to obtain this scalar quantity. The stiffer the structure, the greater S_p will be and vice versa.

In this study, however, the maximum number of iterations is used to detect failure. This is coupled with a search through the diagonal terms of the stiffness matrix to detect zero or negative values, in which case the analysis is terminated. It was found, as will be shown in Chapter Five, that negative or zero pivots were always associated with very large displacements at or immediately beyond the failure loads and always occured after 2-3 unconverged (sometimes diverged) increments. This was also associated with severe cracking, yielding and eventually crushing situations.

3.8 The Frontal Solution Technique

Workers in the finite element field are now more interested in using elements with high number of degrees of freedom. This inevitably results in a large set of simultaneous equations to be solved, thus creating greater demand for computer core storage. This is primarily true in the case of this study, where the 20-noded isoparametric brick element has been used.

In engineering practice, costs for productive computer runs are usually small compared with the cost of man-hours required for input preparation and output interpretation, unless solutions of very large equation systems with several thousand degrees of freedom are involved. This point may not always be true in work of academic nature. However, it is always good engineering practice to use the best technology available. In a state-of-the-art report Meyer (ref.16) summarized the most common solution techniques for equation systems used in engineering problems.

The three main solution strategies for large equation systems are bandsolvers, partitioning methods, and frontal solutions (ref. 17). The definition of those systems of equations as large is in itself computer-dependent, and with good reason, because a set of equations that can be solved in the core of a large machine may require elaborate peripheral processing if solved on a small computer. Further discussion on various techniques can be found in references (16, 17).

In this work a version of the frontal solution, originally introduced by Irons (ref. 18), and later modified by Hinton and Owen (ref. 12), is used. The main feature of the frontal solution technique is that it assembles the equations and eliminates the variables at the same time. This means that the total stiffness matrix of the structure is never formed as such, since after elimination the reduced equations corresponding to the eliminated variables are stored in core in a temporary array called a buffer area (ref. 12). As soon as this array is full, the information

is then transfered to disc. This process results in a considerable efficiency in the way core storage is handled. Thus much valuable computer time is saved through proper housekeeping. The saving due to use of buffer area may amount to about 50% compared with the use of ordinary backing disc store (ref. 6). Another important feature of the frontal technique is that, in contrast to a banded solver, node numbering is irrelevant and it is the element numbering that matters (refs. 19, 20). This is so because in a banded solver the storage allocation is determined by the order in which the nodes are presented for assembly, while in the front solver the storage is determined by the order in which the elements are presented. Further details about the frontal method can be found in references (6, 12, 16, 17, 19, 20).

A broad idea about the distribution of computing effort for a typical application has been given by Brockman (ref. 21), as shown in Table (3.1). The proportions of total computing effort associated with various operations in a three dimensional nonlinear solution are summarized in the table. The percentages quoted are based upon a number of complete analyses of moderate size ($\sim$ 1000 DOF), all using three dimensional high-order elements and Newton-Raphson iteration. It is evident, from the table, that the computations performed at the element level (stiffness, strains, stresses, internal forces,....etc) often represent the bulk of the computing effort in three dimensional applications. Equation-solving effort, which is typically the most expensive operation in a linear or a two-dimensional nonlinear analysis, assumes a secondary

importance in the context of a nonlinear three dimensional solution.

3.9 Computations Procedure

Consider the analysis at a particular iteration within a load increment

(1) For every Gauss point, evaluate the incremental values of strains $[\Delta\varepsilon_i]$ and stresses $[\Delta\sigma_i]$ using the appropriate material property matrix $[D]$.

(2) Check whether the Gauss point under consideration has previously suffered crushing, if so execute step (8).

(3) Check whether this point has previously suffered from tensile cracking, if so execute step (8).

(4) Using the stress-strain relationships described in the concrete material law, evaluate the total stresses in concrete $[\sigma_i]$ which correspond to the linearly calculated total strains. $\varepsilon_i = \varepsilon_{i-1} + \Delta\varepsilon_i$

(5) Check for crushing of concrete using the chosen crushing criterion for the new total stress $[\sigma_i]$, if crushing occurs then set all components of stress to zero at this Gauss point and set an indicator to ensure they remain zero for all subsequent load cycles; i.e. $[\sigma_i] = 0.0$. Also the material property matrix will be set to zero; i.e. $[D]_{x,y,z} = 0.0$

(6) Check for cracking of concrete using the cracking criterion previously discussed. If a crack occurs then the offending principal stress is indicated and set to zero while its direction is fixed in the cartesian x y z space. A

new material property matrix $[D_C]_{x,y,z}$ will be formulated depending on the number and directions of cracks.

(7) If the Gauss point is previously cracked in one direction, it is required to check for further cracking as follows :

(a) For the previous load cycle, the principal stresses σ_1, σ_2, σ_3 had the direction cosines l_1 ,m_1 ,n_1 ;l_2 ,m_2 ,n_2 ;l_3 ,m_3 ,n_3. These direction cosines are used for the stiffness calculation in the present load cycle to obtain the new stress vector $[\sigma_i]$, with regard to the appropriate material property matrix $[D_C]$.

(b) Now for principal stress calculation in cracked material, the new stress vector $[\sigma_i]$ will be transformed form x, y, z space to the principal stress space using the appropriate transformation matrix previously mentioned. This yields σ'_1, σ'_2, σ'_3.

(c) Because l_1 , m_1 , n_1 , correspond to σ_1 (which caused the crack) which are known and already fixed, Equations (4.25) must be simultaneously solved to obtain the remaining six direction cosines corresponding to σ'_2 and σ'_3.

(d) σ'_2 and σ'_3 are then used to check for further cracking by direct comparison with the allowable tensile strength of concrete. If further cracking occurs, the corresponding offending stress is indicated, its direction fixed and the appropriately modified material property matrix must be used.

(8) Evaluate the equivalent nodal forces contributed by the concrete element as:

$$[P_i]_{conc} = \int_V [B]^T [\sigma_i] \, dv$$

(9) Add the equivalent nodal forces by concrete elements to those contributed by steel reinforcement to obtain the total equivalent nodal forces:

$$[P_i] = [P_i]_{conc} + [P_i]_{steel}$$

(10) Check for convergence.

(a) Local coordinates   (b) Cartesian coordinates
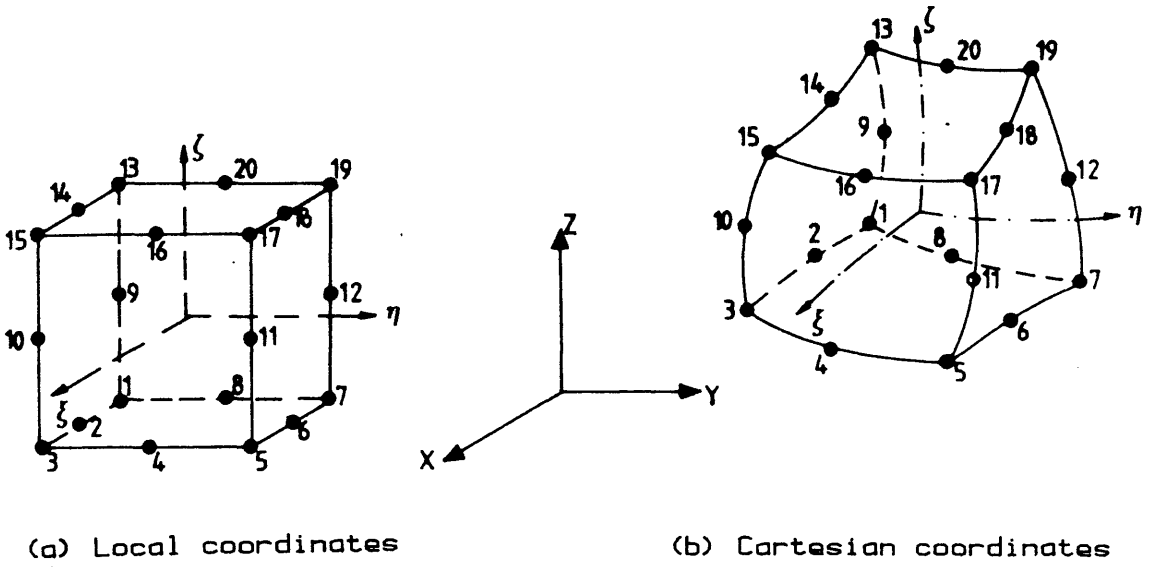
Figure (3.1) 20-Noded isoparametric brick element
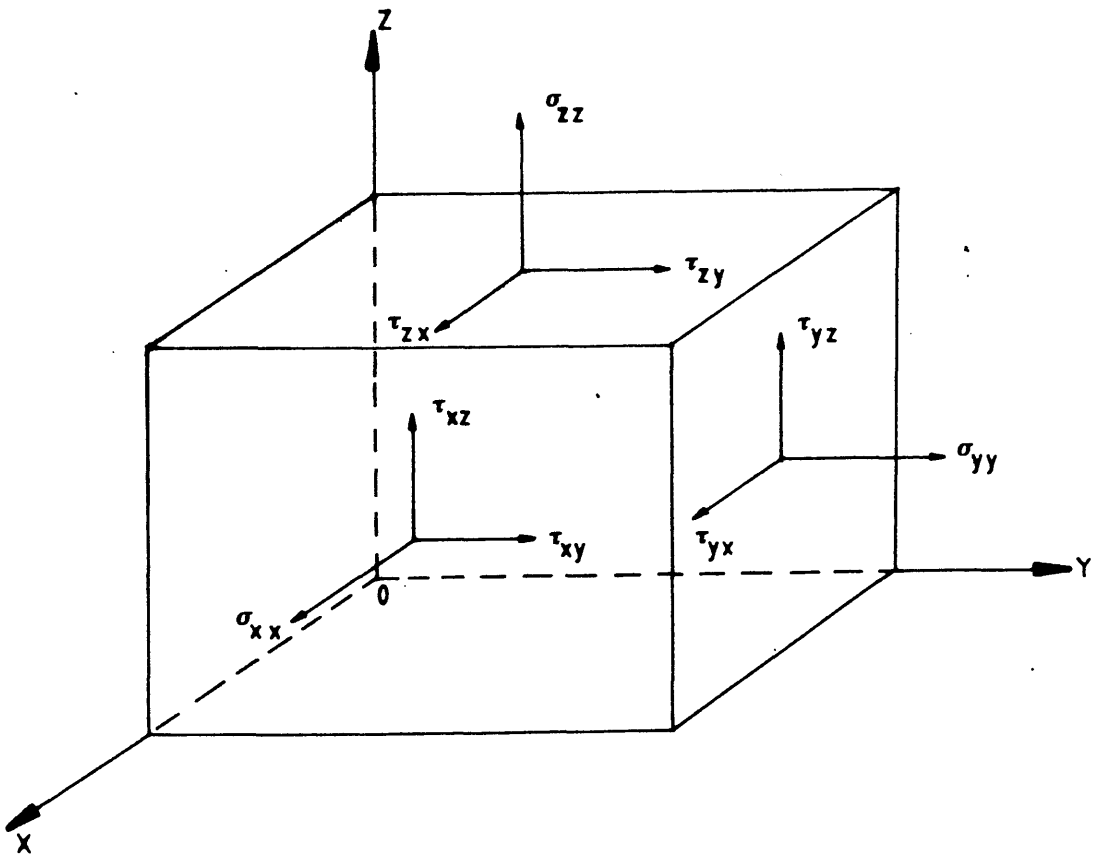
Figure (3.2) Cartesian stress components
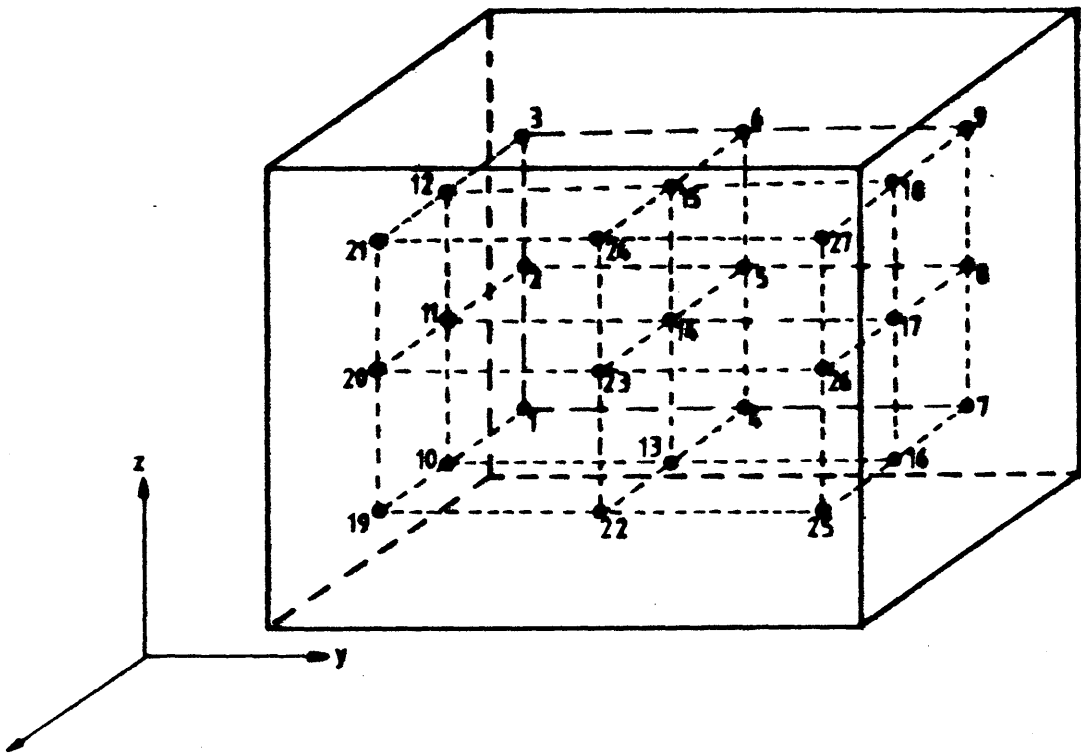
Figure (3.3) Location of Gauss points for the 3x3x3
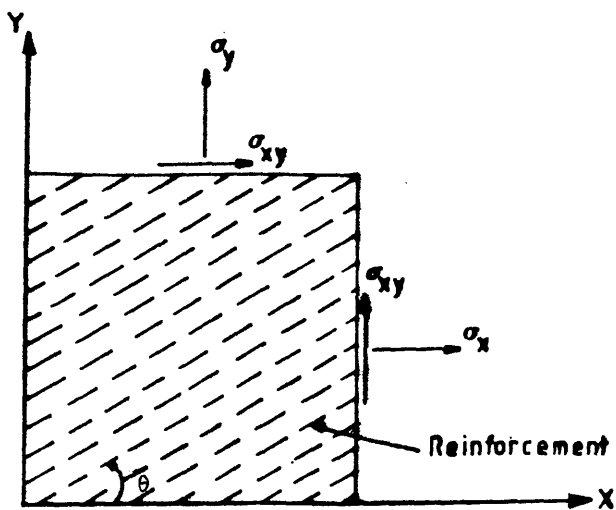integration rule; those for the 2x2x2 and
4x4x4 rules follow the same order

Figure (3.4) Distributed representation of steel
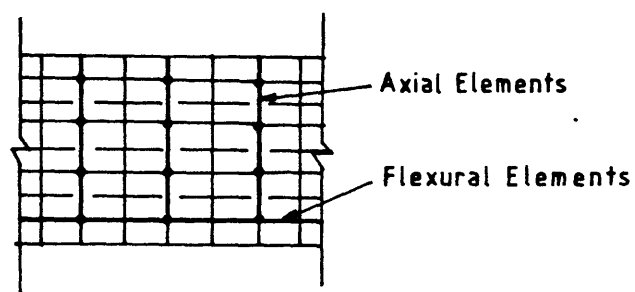
Figure (3.5) Discrete representation of steel
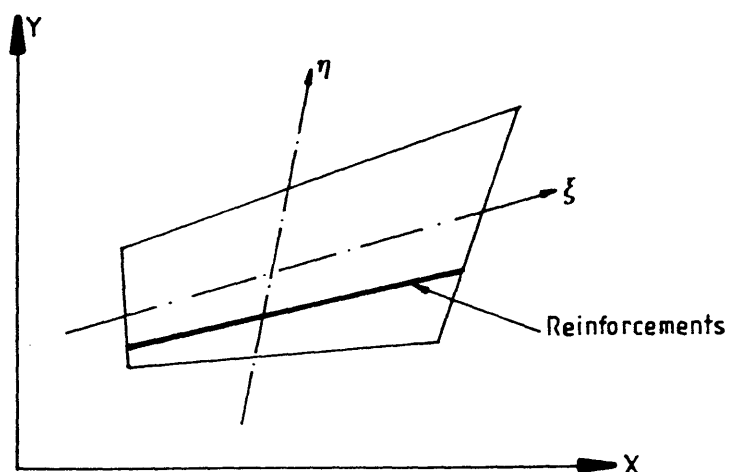
Figure (3.6) Embedded representation of steel
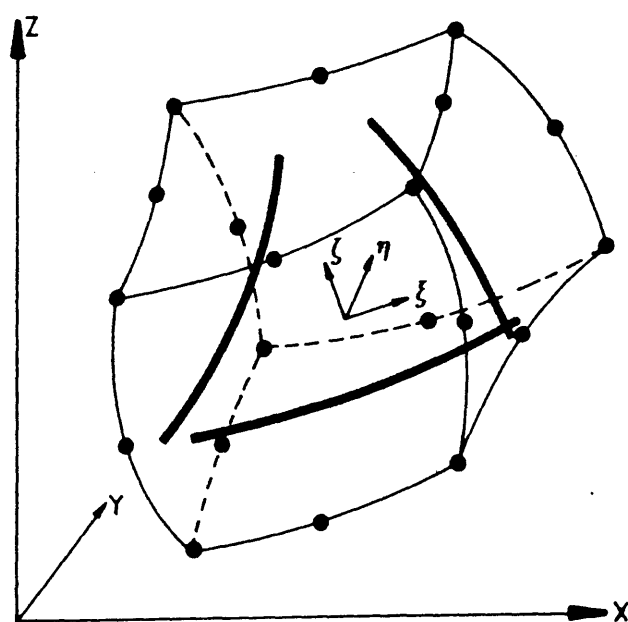
Figure (3.7) Embedded bars within the 20-noded
isoparametric brick element

Constant stiffness
procedure

Variable stiffness
procedure
Secant Modulus
Approach

Variable stiffness
procedure
Tangent Modulus
Approach

(a) Iteration process

Constant stiffness
procedure

Variable stiffness
procedure
Secant Modulus
Approach

Variable stiffness
procedure
Tangent Modulus
Approach
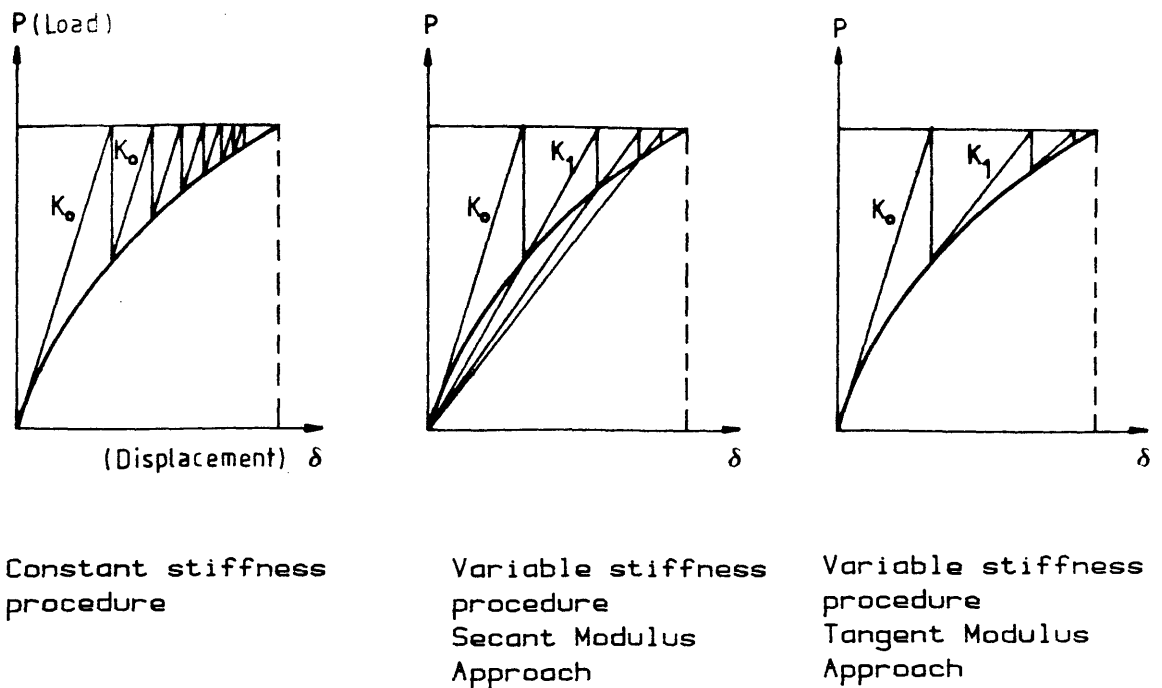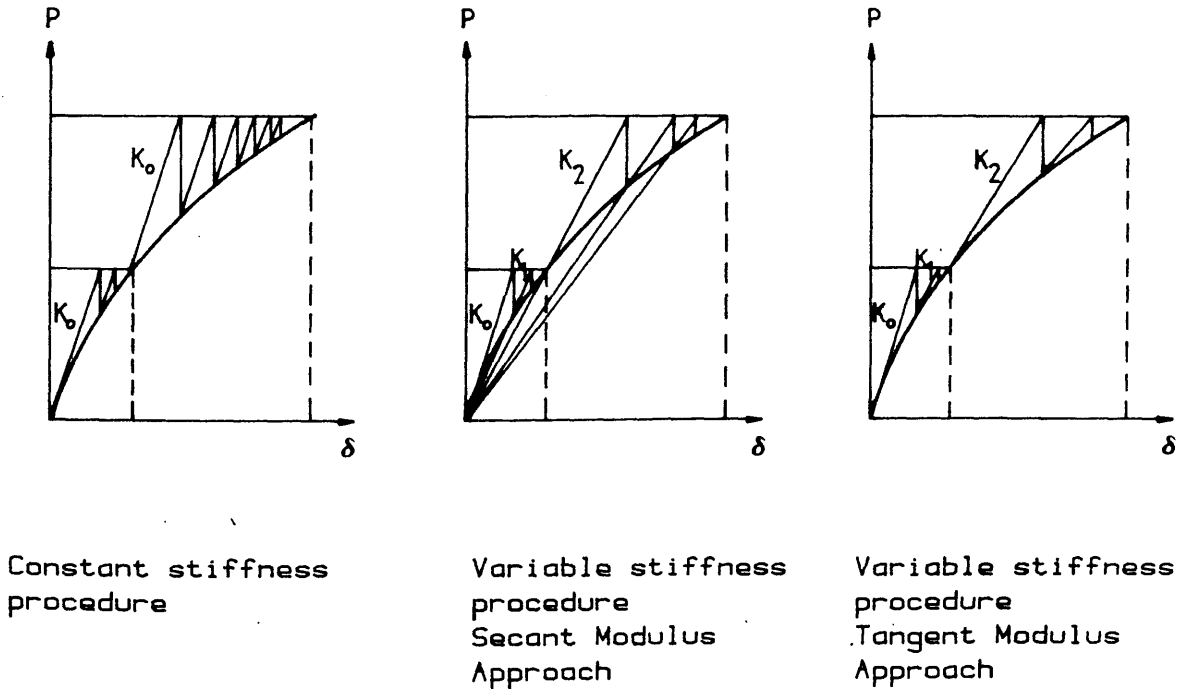
(b) Mixed procedure

Figure (3.8) Basic procedure for nonlinear solution

ble (3.1) Distribution of computing times in three

dimensional nonlinear analysis (ref. 21)

Function	% of CPU time
Input and setup	1-2
Element Calculations	45-75
Equation Solutions	25-50
Loads Calculations	2-10
Checkpoints/Restarts	0-5

Refrences

(1) Zienkiewicz, O.C., "The Finite Element Method", McGraw Hill, 3rd. Ed., 1977.

(2) Cook, R.D., "Concepts and Applications of Finite Element Analysis", Wiley, 1981.

(3) Durelli, A.J., Phillips, E.A., and Tsao, C.H., "Introduction to the Theoretical and Experimental Analysis of Stress and Strain", McGraw-Hill, 1958.

(4) Suidan, M., and Shnobrich, W.C., "Finite Element Analysis of Reinforced Concrete", Journal of the Structural Division, ASCE, Vol. 99, No. ST10, October, 1973, pp. 2109-2122.

(5) "Finite Element Analysis of Reinforced Concrete ", State of the Art Report, ASCE, 1982.

(6) Al-Manaseer, A.A., "A Nonlinear Finite Element Study of Reinforced Concrete Beams", Ph.D. Thesis, University of Glasgow, 1983.

(7) Zienkiewicz, O.C., Owen, D.R.J., Phillips; D.V., and Nayak, G.C., "Finite Element Methods in the Analysis of Reactor Vessels", Nuclear Engineering and Design, Vol. 20, No. 2, 1972, pp. 507-541.

(8) Phillips, D.V., and Zienkiewicz, O.C., "Finite Element Nonlinear Analysis of Concrete Structures", Proceedings Institution of Civil Engineers, Vol. 61, Part 2, 1976, pp. 59-88.

(9) Desai, C.S., and Abel, J.F.,"Indroduction to the Finite

Element Method - A Numerical Method for Engineering Analysis", Van-Nostrand, 1972.

(10) Phillips, D.V., "Nonlinear Analysis of Structural Concrete by Finite Element Methods", Ph.D. Thesis, University of Wales, Swansea, 1972.

(11) Duncan W. and Johnarry, T., "Further Studies on the Constant Stiffness Method of Nonlinear Analysis of Concrete Structres", Proceedings Instit. Civil Engineers, Part 2, Vol. 67, 1879, pp. 951-969.

(12) Owen, D.R.J., and Hinton, E., "Finite elements in plasticity - Theory and Practice", Pineridge Press, Swansea, 1980.

(13) Bathe, K.J. and Cimento, A.P., "Some Practical Procedures for the Solution of Nonlinear Finite Element Equations", Computer Methods in Applied Mechanics and Engineering, Vol. 22, pp. 59-85, 1980.

(14) Crisfield, M.A., "A Faster Modified Newton Raphson Iteration", computer Methods in Applied Mechanics and Engineering, Vol. 20, pp. 267-278, 1979.

(15) Cope, R.J. and Rao, P.V., "Nonlinear Finite Element Strategies for Bridge Slabs" , in : "Advanced Mechanics of Reinforced Concrete Structures", working paper, IABSE., Delft, pp. 275-290, 1981.

(16) Meyer, C., "Solution of Linear Equations State-of-the Art", Journal of the Structural Division, ASCE, Vol. 99, No. 77, Proc., paper 9861, July, 1973, pp. 1507-1526.

(17) Meyer, C., "Special Problems Related to Linear Equation Solvers", Journal of the Structural Division, ASCE, Vol. 101, NO. ST4, April, 1975, pp. 869-890.

(18) Irons, B.M., "A Frontal Solution Program for Finite Element Analysis", International Journal for Numerical Methods in Engineering,Vol. 2, 1970, pp. 5-32.

(19) Hinton, E. and Owen, D.R.J., "Finite Element Programming", Academic, 1977.

(20) Cheung, Y.K. and Yeo, M.F., "A Practical Introduction to Finite Element Analysis, Pitman, 1979.

(21) Brockman, R.A., "Economical Stiffness Formulations For Nonlinear Finite Elements", Computers and Structures, Vol. 18, No. 1, 1984, pp. 15-22.

(22) Johnary,T., "Elastic-Plastic Analysis of Concrete Structures Using Finite Elements", Ph.D. Thesis, University of Strathclyde, 1979.

(23) Bergan, P.G., Holland, I. and Soreide, T.H., "Use of the Current Stiffness Parameter in Solution of Nonlinear Problems", in:"Energy Methods in Finite Element Analysis",J. Wiley & Sons, 1979, pp. 265-282.

CHAPTER FOUR

MATHEMATICAL MODELLING OF THE MATERIAL BEHAVIOUR OF
REINFORCED CONCRETE

4.1 Introduction

A reliable prediction of the behaviour of reinforced
concrete requires a knowledge of the behaviour of concrete
in its elastic, inelastic, and nonlinear ranges, coupled
with a knowledge of the reinforcing steel behaviour.
Although the steel behaviour is better defined and generally
agreed upon, concrete behaviour shows considerable
statistical scatter. Furthermore, the bond between concrete
and the reinforcing steel is also not well defined.

Nowadays more and more experimental knowledge is becomming
available regarding the deformational behaviour and strength
properties of concrete under various loading systems (refs.
1, 2, 3). The accuracy of these data, however, is often in
question because of the uncertainties regarding the
efficiency of the various testing systems. The differences
among test methods are predominantly a function of the
specimen boundary conditions as determined by the different
loading systems. So, basically the scatter of results can
be attributed to two principal factors: variation of the
materials tested, and the variation in the test methods. A
comparative study (refs. 2, 3) has recently been undertaken
by several research laboratories which had been active in
multiaxial concrete testing for the purpose of isolating
these two variables. This effort has, at least, indicated
the possibility of conducting more systematic testing of
concrete, particularly in the multiaxial stress states.

Having obtained such experimental data, it must be transformed into sets of mathematical formulae, adequately describing the basic characteristics, to be of real use to reinforced concrete analysts. This process might also be reversed. These mathematical formulae are normally called "constitutive equations" or, sometimes, "constitutive models" for concrete. In recent years a lot of work have been carried out on this front, resulting in different models being offered (refs. 4, 5, 6, 7, 8 for example) for the description of the behaviour of concrete under different stress states. These can be broadly grouped as : (1) uniaxial and equivalent uniaxial models; (2) linear elastic-fracture models; (3) nonlinear elastic and variable models; (4) elastic-perfectly plastic-fracture models; (5) elastic-strain hardening plastic and fracture models and (6) endochronic theory of plasticity for behaviour of concrete. An attempt at critically evaluating these models, within the context of their use in the numerical analysis of concrete structures, is given by Chen and Ting (ref. 9). A good summary is also given by Chen (refs. 10, 11).

The power of modern computers have ensured that more sophisticated and complex, but reasonably "accurate", constitutive laws can be incorporated into theoretical models without much difficulty. One such set of laws, used in this work to model concrete compressive triaxial behaviour, is due to Ottosen (refs. 12, 13). The features of the model and its attractiveness will be discussed later.

As cracking of concrete is probably the major cause of nonlinearity in most reinforced concrete structures, a

separate three dimensional cracking model is developed and incorporated in the finite element program. This will be dealt with in section (4.3). Particular attention is paid to proper modelling of shear transfer across a cracked concrete surface, tension-stiffening phenomenon of the sound concrete between cracks, and dowel action of the reinforcing steel crossing these cracks.

A biaxial stress-strain law is used for reinforcing steel accounting for strain hardening effects. Full bond is assumed between concrete and steel as demanded by the theoretical derivations of the embedded bars presented in Chapter Three. These aspects will be presented in detail later on.

4.2 Ottosen Constitutive Laws for Concrete

4.2.1 General

The structural behaviour of concrete is complex because both its strength and stiffness are strongly dependent on all stress components. In the ideal case, a constitutive model for concrete should reflect the strain hardening before failure, the failure itself and the strain softening in the post-failure region. The post-failure behaviour is of particular importance. An ideal plasticity formulation with indefinite ductility, for example, might result in an improper redistribution of stresses. It is desirable if the model is easy to incorporate in a computer program. Moreover, it should be applicable to all stress states and should also be easy to calibrate for a particular type of concrete. It would be an important advantage if a model would be calibrated, for example, by means of uniaxial test

data, as these are readily obtainable for concrete. The term "failure" is used to indicate the peak of the stress-strain curve in this discussion.

A constitutive model, for short-time loading, that embodies all the above features, proposed by Ottosen (ref. 12), is chosen to simulate concrete compressive behaviour. The model is based on nonlinear elasticity, where the secant values of Young's modulus and Poisson's ratio are changed appropriately. The model is able, in a simple fashion, to represent most of the concrete behavioural characteristics. The main features of the model can be stated as: (1) the inclusion of all three stress invariants; (2) consideration of dilation of concrete; (3) stress-strain curves are completely smooth; (4) prediction of realistic failure stresses; (5) simulation of different post-failure behaviours and (6) applicability to all stress states including those where tensile stresses occur. The most attractive features of the model, in addition to the above, are that it is simple to incorporate in a computer program and its calibration requires concrete data obtained from standard uniaxial tests.

The implementation of the model in the computer program can be achieved through the following basic four steps: (1) failure and cracking criterion; (2) nonlinearity index; (3) change of secant value of Young's modulus and (4) change of secant value of Poisson's ratio. It must be mentioned here that the model can be used in conjunction with any failure criterion. In this work two failure criteria have been incorporated so that any one can then be chosen at will.

These are: (1) the more recent and sophisticated Ottosen failure criterion (ref. 14) and the comparatively old, well known, but simple modified Coulumb criterion. These are presented in sections (4.2.4) and (4.2.5).

A description of the model is given in the following sections. Referenecs (11, 12, 13) give fuller description with verification of the model against experimental results.

4.2.2. Nonlinearity Index

For the construction of the constitutive equations for concrete a measure of the actual loading, termed the nonlinearity index, β, is introduced by Ottosen. For an arbitrary choice of failure criterion, the nonlinearity index is defined as:

$$\beta = \frac{\sigma_3}{\sigma_{3f}} \qquad (4.1)$$

where σ_3 = the actual largest compressive principal stress; and σ_{3f} is the corresponding failure value, provided that other principal stresses, σ_2 and σ_3, are unchanged ($\sigma_1 > \sigma_2 > \sigma_3$). It is thus noted that the nonlinearity index, β, depends on all three stress invariants, if the failure criterion does so. Moreover, the values of $\beta < 1$, $\beta = 1$, and $\beta > 1$ correspond to stress states located inside, on, and outside the failure surface respectively.

When tensile stresses occur, a modification of the nonlinearity index is required; as concrete behaviour becomes more linear with the presence of tensile stresses. In this case, i.e. when at least σ_1 is tensile, a hydrostatic pressure $-\sigma_1$ is to be superposed on the stress state (σ_1, σ_2, σ_3). This results in a new stress state

$(\sigma_1', \sigma_2', \sigma_3') = (0, \sigma_2-\sigma_1, \sigma_3-\sigma_1)$; i.e, a biaxial compressive stress state. The nonlinearity index, β, is then defined as:

$$\beta = \frac{\sigma_3'}{\sigma_{3f}'} \qquad (4.2)$$

where σ_{3f}' is the failure value of σ_{3f} provided that σ_1' and σ_2' are unchanged. This procedure has the required effect of reducing the value appropriately when tensile stresses occur and $\beta < 1$ will always apply. Contour surfaces of β values are smooth, except for points where tensile stresses have just become involved.

4.2.3 Stress-Strain Relations

Full derivations of the stress-strain relations are given in references (12, 13). In this section, however, they will be presented in order to define terms and discuss their merits. For triaxial compressive loading the secant modulus of concrete, E_s, is given by

$$E_s = \tfrac{1}{2}E_i - \beta(\tfrac{1}{2}E_i - E_f) \pm \sqrt{\tfrac{1}{2}E_i - \beta(\tfrac{1}{2}E_i - E_f)\,^2 + E_f\beta\,D(1-\beta) - 1} \qquad (4.3)$$

in which the positive and negative signs correspond to the ascending and descending parts of the curve, respectively. In Equation (4.3) the parameter value, E_f, denotes the secant value of Young's modulus at general triaxial compression failure, replacing E_c which is the secant value at uniaxial compression failure (see Figure 4.1). D (0.0 < D < 1.0) is a parameter affecting mainly the descending part of the curve in the post-failure region, without a significant effect on the ascending part as shown in Figure (4.1). E_i is the initial uniaxial Young's modulus and the

nonlinearity index. The figure shows a uniaxial stress-strain curve demonstrating Equation (4.3). The basic features of the curve are: (1) A correct initial slope; (2) a zero slope at failure; (3) the correct failure stresses when the failure strains are given; (4) a realistic post-failure behaviour. The value of E_f remains to be determined before the application of Equation (4.3) is possible. In general, the value of E_f is a function of the type of loading, the type of concrete, etc. A sufficiently accurate expression, in general compressive loading, is

$$E_f = \frac{E_c}{1+4(A-1)x} \tag{4.4}$$

in which x represents the dependence on the actual loading and is given by:

$$x = \left(\frac{\sqrt{J_2}}{\sigma_c}\right)_f - \frac{1}{\sqrt{3}} \tag{4.5}$$

where the term $\left(\frac{\sqrt{J_2}}{\sigma_2}\right)_f$ denotes the failure value of the invariant $\frac{\sqrt{J_2}}{\sigma_c}$, and A a parameter given by:

$$A = \frac{E_i}{E_c} \tag{4.6}$$

where Ec is the secant uniaxial modulus at failure. Equation (4.4) applies for compressive stress states, where the nonlinearity index is determined by Equation (4.1) and E_f value is given by Equation (4.4). A realistic value for the parameter A normally lies between 2.0 and 2.5. When tensile stresses occur, however, the behaviour becomes more linear and it is assumed that $E_f = E_c$ holds in this case, while the nonlinearity index is given by Equation (4.2).

The model must be augmented by a cracking model. If cracking occurs, the situation will be dealt with in the manner

described in section (4.3). However, a situation in the post-failure region might occur in which there are small tensile stresses present but there is neither cracking nor crushing of concrete. Such a situation has apparently not been determined experimentally, but the following hybrid procedure was suggested by Ottosen (ref. 12) for the determination of the secant value of the Young's modulus. A failure value of the nonlinearity index β , less than unity, is determined by Equation (4.2). Then, as in Figure (4.2), the post-failure curve AB is assumed to be obtained by a translation of the part MN of the original descending branch of the curve parallel to the horizontal axis. The secant value, Es, corresponding to some actual β value can be determined by:

$$E_s = \frac{\beta E_{MN} E_A E_M}{\beta E_A E_M + \beta_f E_{MN} (E_M - E_A)} \qquad (4.7)$$

in which E_{MN} , depending on β , is the secant value along the original post-failure curve MN obtained by means of equation (4) using the negative sign. Likewise, the constants E_A and E_M are secant values at failure also obtained by equation (4) using the positive and negative signs, respectively, and the nonlinearity index value at failure, i.e. $\beta = \beta_f$. Equation (4.7) implies a gradual change of the post-failure behaviour, both when the stress state is changed towards purely compressive, or towards stress states where cracking occurs.

The variation of the secant value of the Poisson's ratio, on the other hand, is determined by the equation:

$$\nu_s = \nu_i \quad \text{when } \beta < \beta_a$$

$$\nu_s = \nu_s - (\nu_f - \nu_i) \sqrt{1 - \frac{(\beta - \beta_a)^2}{1 - \beta_a}} \quad \text{when } \beta > \beta_a \qquad (4.8)$$

in which ν_i is the initial Poisson's ratio; and ν_f is the secant value of Poisson's ratio at failure. Equation (4.8) is shown in Figure (4.3). The second of these equations, which represents one-quarter of an ellipse, is valid only until failure. Very little is known of the increase of ν_s in the post-failure region, but it is an experimental fact that dilation of concrete continues in this region. In this work, and according to Ottosen's suggestions, the values of β_a and ν_i are taken as 0.8 and 0.36 respectively. ν_i for concrete, however, is normally taken between 0.15 and 0.2. As before, the β value to be applied in Equation (4.8) is determined by Equation (4.1) when only compressive principal stresses occur and by Equation (4.2) when at least one principal stress is tensile.

Experimental verification of Ottosen's model can be found in references (12, 13) for uniaxial, biaxial and triaxial loading. In summary it is concluded that the model provides realistic predictions over a wide range of stress states also including tensile stresses; that it is calibrated by parameters obtainable from simple uniaxial test data; that it reflects the dilation which occurs when concrete is loaded in compression; that it considers all three stress invariants; and that it is suitable for use in computer codes. Application of the model have also been reported in references (15, 16, 17, 18) where reasonable predictions have been obtained.

These laws, however, have been modified in this study to cut off post-peak stress behaviour by a triaxial von Mises failure surface in strain space to simulate crushing of

concrete because it was noticed that some overestimation of ultimate loads occur without such treatment. This modification will be discussed in detail in section (4.6).

For realistic predictions of failure loads of reinforced concrete structure an accurate failure criterion is important. At present there are several proposed failure criteria and reference (11) contains a review of the most important ones.

It was stated earlier that Ottosen's model can be used in conjunction with any concrete failure criterion. In the computer program developed in this study two concrete failure criteria have been incorporated, namely: (1) Ottosen four-parameter failure criterion and (2) the modified Coulumb criterion, which will now be discussed.

4.2.4 Ottosen's Four-Parameter Failure Criterion (ref. 14)

The criterion involves the three stress invariants I_1, J_2 and $\cos 3\theta$, where:

$$I_1 = \sigma_1 + \sigma_2 + \sigma_3 = \sigma_{ii}$$

$$J_2 = \tfrac{1}{2}(s_1^2 + s_2^2 + s_3^2) = \tfrac{1}{2}s_{ij}s_{ij} \qquad (4.9)$$

$$J = \frac{3\sqrt{3}}{2}\ \frac{J_3}{J_2^{3/2}} = \cos 3\theta$$

where $\sigma_1, \sigma_2, \sigma_3$ are the three principal stresses (tensile stresses are considered positive) and J_3 is defined as:

$$J_3 = (\tfrac{1}{3})(s_1^3 + s_2^3 + s_3^3) = \tfrac{1}{3}s_{ij}s_{jk}s_{ki} \qquad (4.10)$$

where s_{ij} is the stress deviator tensor, i.e. $s_{ij} = \sigma_{ij} - (\tfrac{1}{3})\delta_{ij}\sigma_{kk}$ and s_1, s_2, s_3 = the principal stress deviators.

The octahedral normal stress, σ_o, and the shear stress, τ_o, are related to the preceding invariants by $\sigma_o = I_1/3$ and $\tau_o^2 = \frac{2 J_2}{3}$. Figure (4.4) shows the Haigh-Westergaard Coordinate System and the deviatoric plane where the various invariant relations are illustrated.

The failure surface is given by the following equation:

$$f(I_1, J_2, \cos 3\theta) = a \frac{J_2}{\sigma_c^2} + \lambda \frac{\sqrt{J_2}}{\sigma_c} + b \frac{I_1}{\sigma_c} - 1 = 0 \qquad (4.11)$$

where $\lambda = f(\cos 3\theta) > 0$, a and b are constants. The value of $f(I_1, J_2, \cos 3\theta) < 0$ corresponds to stress states inside the failure surface. σ_c is the uniaxial compressive cylinder strength. The function $\lambda = f(\cos 3\theta)$ is given by:

$$\lambda = k_1 \cos\left[\tfrac{1}{3}\text{arc cos}(k_2 \cos 3\theta)\right] \text{ for } \cos 3\theta \geqslant 0$$

$$\lambda = k_1 \cos\left[\tfrac{\pi}{3} - \tfrac{1}{3}\text{arccos}(-k_2 \cos 3\theta)\right] \text{ for } \cos 3\theta \leqslant 0 \qquad (4.12)$$

in which k_1 and k_2 are parameters (k_1 is a size factor, while k_2 is a shape factor, with $0 < k_2 < 1$). The parameter λ and the constants a, b are functions of the uniaxial tensile to compressive ratio, k, of the concrete in question. Tables (4.1) and (4.2) show their values for k values of 0.08, 0.1 and 0.12.

The characteristics of the failure surface, given by Equations (4.11) and (4.12) are : (1) only four parameters a, b, k_1 and k_2 are used which are functions of uniaxial properties of concrete; (2) use of invariants makes determination of the principal stresses unnecessary; (3) the surface is smooth and convex with the exception of the vertix; (4) the meridians are parabolic and do not intersect

the negative hydrostatic axis; (5) the trace in the deviatoric plane changes from nearly triangular to circular shape with increasing hydrostatic pressure; (6) it contains several earlier proposed criteria as special case, in particular, the criterion of Drucker-Prager (ref. 19) for a=0, λ =constant and the well known von Mises criterion for a=b=0 and λ = constant. Figure (4.5) illustrates the above properties.

Verification of Ottosen's failure criterion against experimental test data for various loadings is shown in Figure (4.6). Further details of that can also be found elsewhere (refs.11, 12, 13, 14). The agreement between the experimental and predicted values is considered satisfactory and therefore the ability of the criterion to represent realistic experimental values is good.

The mathematical form of the criterion, on the other hand, is feasible for computer applications. The sophisticated formulation, however, requires internal iteration in its implementation (see Apendix C). This results in additional computer effort when compared with other simpler, but less accurate, failure criteria. However, it is incorporated in this work because a better simulation of concrete behaviour in the multiaxial stress states is sought.

4.2.5 Modified Coulomb Criterion

The other optional failure criterion, incorporated in the developed computer program, is the more simpler classical modified Coulomb criterion which reads:

$$m\sigma_1 - \sigma_3 = \sigma_c \qquad (4.13)$$

$$\sigma_1 = \sigma_t$$

where $\sigma_1 > \sigma_2 > \sigma_3$ are the principal stresses (tension positive). The criterion contains three parameters and does not consider the intermediate principal stress. It also includes a cracking criterion given by the second of the above two equations.

The coefficient m is related to the friction angle , ϕ , by the relation:

$$m = \frac{(1 + \sin\phi)}{(1 - \sin\phi)} \qquad (4.14)$$

Different m values have been suggested for concrete, but a value of about 4.0 is adopted corresponding to a friction angle of $37°$ proposed by Cowan (ref. 20) and Johansen (ref. 21).

As can be seen from Figure (4.7) the modified Coulomb criterion correspond to an irregular hexagonal pyramid with straight meridians and with tension cut-offs. The trace in the deviatoric plane is shown in Figure (4.8) together with the Ottosen criterion. It appears from the figure that, for most stress states of practical interest, the modified Coulomb criterion underestimates the failure stresses. This is quite obvious when considering, for instance, the case of plane stress (Figure 4.6). However, it is important to note that the modified Coulomb criterion provides a fair approximation that is comparable in accuracy to many recently proposed failure criteria with a unique simplicity. It is also important to mention that its calibration

requires only the readily available uniaxial tensile and compressive strengths of the concrete in question. Figure (4.9) shows further verification of both criteria against experimental results.

In conclusion, each of the two failure criteria incorporated in the computer program provides realistic failure predictions for general stress states. While Ottosen criterion is superior when considering accuracy and sophistication the modified Coulomb criterion possesses an attractive simplicity.

The cracking model developed in this work to accompany Ottosen's constitutive equations will now be discussed in detail.

4.3 Modelling of Concrete Cracking in Three Dimensions
4.3.1 Introduction
The tensile weakness of concrete results in cracking which is regarded as a major factor contributing to the nonlinear behaviour of reinforced concrete structures. Early studies on modelling reinforced concrete nonlinear behaviour resulted in two methods of representing the cracking of concrete. The first approach, termed discrete crack representation (ref. 22), uses a predefined discrete crack system. The major drawbacks of this procedure, however, are that the topology of the structure has to be continuously altered as cracking progresses and that a previous knowledge of the crack pattern might be necessary. There is also a lack of generality in the possible crack directions as these are dictated by element boundaries rather than the resulting principal stresses or strains.

The second approach, known as the smeared crack model (refs. 23, 24, 25), assumes the cracked concrete remains a continuum. This implies that an infinite number of parallel cracks occur at a specific point if a certain cracking criterion is satisfied. By using the smeared cracking approach the problem of changing the topology of the structure with crack propagation is overcome. Moreover, the initiation, orientation and propagation of cracks at the sampling points are automatically generated resulting in complete generality. Figure (4.10) illustrates both cracking models as applied in two dimensional analysis.

The selection of which cracking model to use depends largely upon the purpose of the finite element study undertaken and the nature of the output desired (ref. 26). Generally, if overall load-displacement behaviour, without regard to local stresses and completely realistic crack patterns, is desired the smeared crack representation is probably the best choice. If, on the other hand, detailed local behaviour is of prime importance adaptations of the discrete cracking model are useful. The element type, size and grid pattern have significant effects on both models. The smeared crack approach is the most commonly used because it is easy to implement. Further details on this aspect can be found elsewhere (refs. 11, 26).

In this study the overall structural behaviour is of particular importance. Furthermore, the efficient 20-noded isoparametric brick element is used to represent concrete with embedded bars developed to adequately simulate the reinforcing steel at its exact locations in the structure.

Therefore, the smeared crack simulation is adopted.

4.3.2 Three Dimensional Smeared Cracking Model

In three dimensional stress space ; σ_1, σ_2 σ_3; cracks might occur normal to any of the principal stresses as shown in Figure (4.11). It is also quite possible for any point to be cracked in more than one direction. Up to three cracks are allowed at a point in this study, provided that they are orthogonal as shown in Figure (4.12). Once a crack occurs, its direction in the cartesian xyz space is fixed and retained as such in all subsequent loading.

A crack is said to have occured at a Gauss point if either : (1) the failure criterion described in sections (4.2.4) is violated or (2) the maximum principal stress, σ_1, exceeded the tensile strength of concrete. In the first case (i.e. violation of the failure criterion) the first crack is assigned perpendicular to σ_1. All subsequent cracks at the same point are checked by the second criterion using the other two "principal" stresses σ_2 and σ_3.

4.3.2. Material Property Matrix for Cracked Concrete

It was shown in chapter Three that the material property matrix for three dimensional isotropic uncracked concrete is given by:

$$[D] = \frac{E(1-\nu)}{(1+\nu)(1-2\nu)} \begin{bmatrix} 1 & \nu/1-\nu & \nu/1-\nu & 0 & 0 & 0 \\ & 1 & \nu/1-\nu & 0 & 0 & 0 \\ & & 1 & 0 & 0 & 0 \\ & & & \frac{1-2\nu}{2(1-\nu)} & 0 & 0 \\ & \text{symmetric} & & & \frac{1-2\nu}{2(1-\nu)} & 0 \\ & & & & & \frac{1-2\nu}{2(1-\nu)} \end{bmatrix}$$

(4.15)

Now, in the principal stress space and depending on the adopted cracking criterion, if the Gauss point in concrete is cracked in direction 1 (Figure 4.11 a), then the material property matrix becomes:

$$[D_c]_1 = \begin{bmatrix} D_{11}^* & 0 & 0 & 0 & 0 & 0 \\ & D_{22} & D_{23} & 0 & 0 & 0 \\ & & D_{33} & 0 & 0 & 0 \\ & \text{symmetric} & & \beta G & 0 & 0 \\ & & & & D_{55} & 0 \\ & & & & & \beta G \end{bmatrix} \quad (4.16)$$

where D_{ij} are the corresponding values in the [D] matrix as obtained from the constitutive equations and β is the shear retention factor which will be dealt with in section (4.4.2). G is the shear modulus for uncracked concrete.

If the point is cracked in direction 2 (Figure 4.11 b), then the material property matrix becomes:

$$[D_c]_2 = \begin{bmatrix} D_{11} & 0 & D_{13} & 0 & 0 & 0 \\ & D_{22}^* & 0 & 0 & 0 & 0 \\ & & D_{33} & 0 & 0 & 0 \\ & & & \beta G & 0 & 0 \\ & \text{symmetric} & & & \beta G & 0 \\ & & & & & D_{66} \end{bmatrix} \quad (4.17)$$

and if it is cracked in direction 3 (Figure 4.11 c), then the material property matrix will be:

$$[\,D_c\,]_3 = \begin{bmatrix} D_{11} & D_{12} & 0 & 0 & 0 & 0 \\ & D_{22} & 0 & 0 & 0 & 0 \\ & & D_{33}^* & 0 & 0 & 0 \\ & & & D_{44} & 0 & 0 \\ & \text{symmetric} & & & \beta G & 0 \\ & & & & & \beta G \end{bmatrix} \quad (4.18)$$

Multi-directional cracks may be achieved by combinations of the material property matrices $[\,D_c\,]_1$, $[\,D_c\,]_2$ and $[\,D_c\,]_3$ as follows :

if cracked in directions 1 and 2, then:

$$[\,D_c\,]_{1,2} = \begin{bmatrix} D_{11}^* & 0 & 0 & 0 & 0 & 0 \\ & D_{22}^* & 0 & 0 & 0 & 0 \\ & & D_{33} & 0 & 0 & 0 \\ & & & \beta G & 0 & 0 \\ & \text{symmetric} & & & \beta G & 0 \\ & & & & & \beta G \end{bmatrix} \quad (4.19)$$

if cracked in directions 2 and 3, then:

$$[\,D_c\,]_{2,3} = \begin{bmatrix} D_{11} & 0 & 0 & 0 & 0 & 0 \\ & D_{22}^* & 0 & 0 & 0 & 0 \\ & & D_{33}^* & 0 & 0 & 0 \\ & \text{symmetric} & & \beta G & 0 & 0 \\ & & & & \beta G & 0 \\ & & & & & \beta G \end{bmatrix} \quad (4.20)$$

if cracked in directions 3 and 1, then:

$$[\ D_c\ ]_{3,1} = \begin{bmatrix} D_{11}^* & 0 & 0 & 0 & 0 & 0 \\ & D_{22} & 0 & 0 & 0 & 0 \\ & & D_{33}^* & 0 & 0 & 0 \\ & \text{symmetric} & & \beta G & 0 & 0 \\ & & & & \beta G & 0 \\ & & & & & \beta G \end{bmatrix} \qquad (4.21)$$

and finally if the point is cracked in all three principal directions, then:

$$[D_c]_{1,2,3} = \begin{bmatrix} D_{11}^* & 0 & 0 & 0 & 0 & 0 \\ 0 & D_{22}^* & 0 & 0 & 0 & 0 \\ & & D_{33}^* & 0 & 0 & 0 \\ & & & \beta G & 0 & 0 \\ & \text{symmetric} & & & \beta G & 0 \\ & & & & & \beta G \end{bmatrix} \qquad (4.22)$$

In Equations (4.16) through (4.22) the terms D_{jj}^* are given very small value if no tension stiffening is used, allowing the stiffness normal to the cracked plane to vanish immediately upon cracking and remains zero thereafter. Their values will be determined from the descending branch of the uniaxial stress-strain curve if tension-stiffening is used. Tension stiffening will be dealt with is section (4.5).

Depending on the number of cracks occuring at any load level the appropriate material property matrix will be evaluated at every stress sampling point (Gauss point), and for simplicity of discussion the material property matrix will be termed $[D_c]$ from now on.

The matrix $[D_c]$ is for an orthotropic material and can be directly used in stiffness calculations only in the directions of the cracks at the Gauss point under consideration. To be used in the global xyz space a transformation process must be performed. This is a standard procedure and is given by the equation (ref. 27):

$$[D_c]_{x,y,z} = [T_\epsilon]^T [D_c] [T_\epsilon] \qquad (4.23)$$

where $[T_\epsilon]$ is the strain transformation matrix which takes the form :

$$[T_\epsilon] = \begin{bmatrix} \ell_1^2 & m_1^2 & n_1^2 & \ell_1 m_1 & m_1 n_1 & n_1 \ell_1 \\ \ell_2^2 & m_2^2 & n_2^2 & \ell_2 m_2 & m_2 n_2 & n_2 \ell_2 \\ \ell_3^2 & m_3^2 & n_3^2 & \ell_3 m_3 & m_3 n_3 & n_3 \ell_3 \\ 2\ell_1 \ell_2 & 2m_1 m_2 & 2n_1 n_2 & (\ell_1 m_2 + \ell_2 m_1) & (m_1 n_2 + m_2 n_1) & (n_1 \ell_2 + n_2 \ell_1) \\ 2\ell_2 \ell_3 & 2m_2 m_3 & 2n_2 n_3 & (\ell_2 m_3 + \ell_3 m_2) & (m_2 n_3 + m_3 n_2) & (n_2 \ell_3 + n_3 \ell_2) \\ 2\ell_3 \ell_1 & 2m_3 m_1 & 2n_3 n_1 & (\ell_3 m_1 + \ell_1 m_3) & (m_3 n_1 + m_1 n_3) & (n_3 \ell_1 + n_1 \ell_3) \end{bmatrix}$$

$$(4.24)$$

where l_1, m_1, n_1 are the direction cosines of the first principal stress; l_2, m_2, n_2 are those for the second prinicpal stress ; and l_3, m_3, n_3 are for the third principal stress.

The three principal planes are and must always be orthogonal to each other. This is checked by satisfying the following set of equations (ref. 28):

$$
\begin{aligned}
\ell_1^2 + m_1^2 + n_1^2 &= 1 \\
\ell_2^2 + m_2^2 + n_2^2 &= 1 \\
\ell_3^2 + m_3^2 + n_3^2 &= 1 \\
\ell_1\ell_2 + m_1 m_2 + n_1 n_2 &= 0 \\
\ell_2\ell_3 + m_2 m_3 + n_2 n_3 &= 0 \\
\ell_3\ell_1 + m_3 m_1 + n_3 n_1 &= 0
\end{aligned} \qquad (4.25)
$$

The three principal directions at any point can vary during loading before cracking is initiated, but they are fixed if at least two cracks exist at that point. One crack fixes only one principal direction but constraints the other two cracks, when they occur, to be perpendicular to it.

The process described earlier in section (3.3.7) for the evaluation of the principal stresses and their directions in three dimensional stress analysis applies to concrete before cracking when none of the principal stress directions is fixed. Once a crack occurs due to any principal stress, say σ_1, this stress will be rendered zero (or obtained from the tension stiffening law) and the crack plane must be perpendicular to the direction of this principal stress. In

subsequent loading the crack direction will be fixed and a procedure of transforming the normal and shear stresses is followed, as   explained in section (3.9), to obtain the other two principal stresses for checking new crack formation. In actual fact these will not be "true" principal stresses as some shear stresses will result, following the transformation process, on the crack planes.

Another fact in this particular situation is that the principal strain directions may not coincide with those of the principal stresses after cracking. The principal strains evaluation is required for the tension stiffening, shear retention and the crushing models as will be shown later. In this study, and because of the difficulty of evaluating their values for a cracked point, the principal strains (can be termed ficticious principal strains) are obtained by transforming the normal and shear strains into the principal stress space using the relationship:

$$[\epsilon_p] = [T_\sigma] [\epsilon] \qquad\qquad (4.26)$$

where $[\epsilon_p]$ is the "ficticious" principal strain vector which contains six components (due to the transformation process). The first three of them are the principal strains ϵ_1, ϵ_2, ϵ_3, while the remaining three are some shear strains which inevitably result. These shear strains vanish in the ideal case of the "true" principal strains being obtained. In Equation (4.26), $[\epsilon]$ is the normal and shear strains vector and $[T_\sigma]$ is the stress transformation matrix given by (ref. 29) as:

$$[T_\sigma] = \begin{bmatrix}
\ell_1^2 & m_1^2 & n_1^2 & 2\ell_1 m_1 & 2m_1 n_1 & 2n_1 \ell_1 \\
\ell_2^2 & m_2^2 & n_2^2 & 2\ell_2 m_2 & 2m_2 n_2 & 2n_2 \ell_2 \\
\ell_3^2 & m_3^2 & n_3^2 & 2\ell_3 m_3 & 2m_3 n_3 & 2n_3 \ell_3 \\
\ell_1 \ell_2 & m_1 m_2 & n_1 n_2 & (\ell_1 m_2 + \ell_2 m_1) & (m_1 n_2 + m_2 n_1) & (n_1 \ell_2 + n_2 \ell_1) \\
\ell_2 \ell_3 & m_2 m_3 & n_2 n_3 & (\ell_2 m_3 + \ell_3 m_2) & (m_2 n_3 + m_3 n_2) & (n_2 \ell_3 + n_3 \ell_2) \\
\ell_3 \ell_1 & m_3 m_1 & n_3 n_1 & (\ell_3 m_1 + \ell_1 m_3) & (m_3 n_1 + m_1 n_3) & (n_3 \ell_1 + n_1 \ell_3)
\end{bmatrix}$$

$$(4.27)$$

If the material cracks in two directions, say σ_1 and σ_2, all principal directions will be fixed and the values of these two principal stresses will be set to zero.

4.4 Modelling of Shear Transfer Across Cracks

4.4.1 General

After cracking of concrete two main mechanisms develop through which shear is transferred from the weak cracked section to the surrounding sound concrete; namely (1) aggregate interlocking on the two adjacent surfaces and (2) dowel action of any reinforcing bars crossing these cracks. The two mechanisms are interrelated and several factors govern their relative contribution towards the total shear transfered. The main known factors are: (1) crack spacing, (2) presence or otherwise of reinforcement crossing the cracks, (3) bar size, (4) total number of bars crossing, (5) bar orientation relative to the crack direction, (6) aggregate size and roughness, (7) concrete strength, (8) crack width and (9) mode of failure. Other factors, not yet fully defined, may probably also have some influence.

The mechanisms of shear transfer have been investigated experimentally and consequently several analytical expressions have been suggested. In the finite element modelling, however, these expressions can not be directly used. In the smeared cracking approach the shear transfer is modelled through the so-called "shear retention factor", β , which varies between 0 and 1, and is defined as:

$$\beta = G'/G \qquad\qquad (4.28)$$

where G' is the reduced shear modulus for cracked concrete and G is the shear modulus for the uncracked concrete. Many investigators have used a constant value for β (refs. 25, 30, 31, 32), the value of which was normally determined by trying several reduction factors and finally choosing the value that gave predictions closest to the experimental results of the problem in question. Others used a gradually decreasing value for β (refs. 33, 34), following either linear or nonlinear curves. In both cases it seems that the shear retention factor has been used more as a numerical device to obtain good results to match experimental data than a real physical phenomenon. This seems inevitable because of the following reasons: (1) the actual contribution of the shear transfer mechanisms, i.e. aggregate interlocking and dowel action is not precisely known yet, (2) more experimental data and also a unification of existing data is needed, (3) even if all that is done, the treatment of shear transfer with all its components is still uncertain to produce a single finite elements model to suit all stress states at one stroke because of the

variation of the reinforced concrete behaviour under different loading conditions, (4) the shear transfer is interrelated with the other aspects of nonlinear behaviour of reinforced concrete such as tension stiffeneing and bond-slip behaviour and (5) in nonlinear finite element analysis numerical factors, e.g. convergence tolerance, maximum number of iterations, increment size etc., also affect results obtained using whatever shear retention model is used (ref. 32). More discussion on these points will be presented when applying the developed finite element model in Chapters Five and Eight.

4.4.2 Shear Retention Factor Used in This Work

To achieve an aim of incorporating a realistic shear retention factor to model shear transfer across cracked concrete a quadratic function is used, based on of the "ficticious" direct strain ϵ normal to the crack as shown in Figure (4.13). This is given by:

for $\epsilon/\epsilon_t' \leqslant 1$, $\beta = 1.0$;   uncracked concrete

for $1 < \epsilon/\epsilon_t' \leqslant \beta_3$,

$$\beta = \beta_1 - \beta_4 \left[(1-2\beta_3) + 2\beta_3 (\epsilon/\epsilon_t') - (\epsilon/\epsilon_t')^2 \right] \qquad (4.29)$$

where $\beta_4 = (\beta_1 - \beta_2)/(1-\beta_3)^2$ and $d\beta/d\epsilon = 0$ at $\epsilon/\epsilon_t' = \beta_3$;

for $\epsilon/\epsilon_t' > \beta_3$, $\beta = \beta_2$.

In Equation (4.29) ϵ' is the uniaxial cracking strain of concrete, given by $\epsilon_t' = f_t'/E_c$, where f_t' is the uniaxial tensile strength of concrete and Ec is the concrete Young's modulus. β_1, β_2 and β_3 are shear retention parameters

defining the shape of the curve. β_1 represent the sudden loss of stiffness at crack formation; β_2 represents the residual shear stiffness due to dowel action of any steel once a crack has opened sufficiently for aggregate interlocking to cease; and β_3 represents the rate of decay of stiffness as the crack widens and the crack surface deteriorates.

The exact values of β_1, β_2 and β_3 are difficult to obtain experimentally. Nevertheless, the fact that the retention factor is based on the strain normal to the crack can be justified on the basis that this can be taken as a measure of the crack width. The use of a quadratic function can also be substantiated by the crack width measurements made in this study as reported in Chapter Seven. Nonlinear variation of crcak width with applied load was observed.

Studies have shown that β can markedly influence a solution, especially if shear behaviour dominates (ref. 25, 32, 33, 34, 35, 36). Therefore a study of β was made for each application of the finite element model as will be presented in Chapter Five.

Another useful numerical role for the shear retention factor, β, is to suppress the singularity that might result when all the elements surrounding a particular node have cracked in the same direction. Such a node would then be free to move normal to the crack direction because the resulting extensional and shear deformations do not give any restraint without such a shear retention factor (ref. 26).

4.5 <u>Tension Stiffening Phenomenon and its Modelling</u>

4.5.1 <u>Introduction</u>

The physical situation in the vicinity of a crack in reinforced concrete is illustrated in Figure (4.14). As the concrete reaches its tensile strength primary cracks form. The number and extent of these cracks is mainly controlled by the size, position and orientation of any reinforcing bars crossing the crack. At the position of the primary crack the stress in concrete drops to zero and the steel carries the full load. The concrete between the cracks, however, can still carry some tensile stress. This tensile stress drops as the load increases and this drop is associated primarily with bond deterioration between steel and concrete. This phenomenon is termed tension stiffening and has seen limited experimental studies (ref. 37 for example) to verify its importance and effects, although it is being normally included in finite element models.

In modelling tension stiffening effect two procedures have normally been used. In the first procedure the tensile portion of the concrete stress-strain curve is given a descending tail (ref. 32, 36, 38, 39, 40). The second procedure treats tension stiffening by increasing the steel stiffness (ref. 41. 42). The additional stress in the reinforcement represents the total tensile force carried by both the steel and the sound concrete between the cracks.

4.5.2 <u>Tension Stiffening Model Used in This Work</u>

Tension Stiffening is modelled by a gradual release of stress normal to the crack plane and by a gradual decrease in stiffness. This is specified by a linear descending

stress-strain curve beyond the uniaxial cracking strain ϵ_t', shown in Figure (4.15) and given by:

for $\epsilon/\epsilon_t' \leqslant 1$, linear-elastic conditions exist;

for $1 < \epsilon/\epsilon_t' \leqslant \alpha_2$

$$\sigma = \frac{\alpha_1 f_t'}{(\alpha_2 - 1)} (\alpha_2 - \epsilon/\epsilon_t') \qquad (4.30)$$

and $E_T = \sigma/\epsilon$, the secant modulus at strain ϵ;

for $\epsilon/\epsilon_t' > \alpha_2$, $\qquad \sigma = 0.0$ and $E_T = 0.0$

where α_1 and α_2 are the tension stiffening parameters which define the shape of the curve. α_1 represents the sudden loss of stiffness at crack formation; α_2 represents the rate of decay of stiffness as a crack spreads and widens, and as bond and concrete deteriorate in the vicinity of the crack. The value of E_T is evaluated from Equation (4.29) at any iteration during the loading process and is used in the material property matrix $[D_c]$ depending on whether the crack is caused by σ_1, σ_2 or σ_3.

There are no generally accepted values for α_1 and α_2. Studies have shown that they can have a strong influence on the behaviour especially when flexure dominates (ref. 32, 35, 36, 38, 39, 40). This greatly depends on the type of structure and loading conditions and can be imperically derived. Cope (ref. 40) used a value of $\alpha_2 = 15$ for concrete slabs. He argued that accuracy in predictions of behaviour may be an illusory goal and suggested the use of simple models for such phenomenon. Al-Manaseer (ref. 32) reviewed various tension stiffening models. He argued that tension stiffening can produce satisfactory results to match

experimental curves, but is very much interrelated to the convergence tolerance and other factors.

There has been some strong discussions as to whether the retention of the shear modulus meets the same numerical goals as the addition of tension stiffening even though they represent different phenomenon (ref. 26). Furthermore, a recent numerical approximation has also been put forward by Phillips and Al-Manaseer (ref. 38) suggesting the use of coarse residual force convergence tolerances and ignoring the effect of tension stiffening altogether. However, there is no unified reported evidence of adequate depth to support either of the two arguments to finally settle the discussion. In Chapter Five a study of the above two aspects is reported for different applications in an attempt to contribute to the above discussions and also identify limits on those parameters for the finite element model developed in this study.

4.6 Crushing Model

Crushing indicates the complete rupture and disintegration of the material under compressive stress states. In physical terms, the material after crushing can no longer sustain any stresses and the current stresses drop abruptly to zero. Concrete is assumed to lose its resistance to further deformations. In finite element modelling this is accomplished by releasing all current stresses at the Gauss (sampling) point, once crushing is detected, and setting the whole of the [D] matrix to almost zero in all subsequent loading.

In order to cut-off the post-peak compressive stress behaviour, modelled by Ottosen's constitutive laws as previously described, the following two crushing criteria were used:

(1) The First Crushing Model

In this model a uniaxial criterion is used. A Gauss point is considered crushed if the minimum principal compressive strain exceeds (in absolute value) the uniaxial crushing strain of concrete, ϵ_{cu}, regardless of whether the Gauss point is already cracked or not.

(2) The Second Crushing Model

In this model a combination of two criteria is used depending on the state of cracking at the Gauss point in consideration. It states:

(a) If the point is cracked in at least one direction then the first crushing criterion is used.

(b) If the point is uncracked then the von Mises triaxial failure surface in strain space is used to check for crushing. This is given by the following equation:

$$f(\epsilon) = \sqrt{(\epsilon_1 - \epsilon_2)^2 + (\epsilon_2 - \epsilon_3)^2 + (\epsilon_3 - \epsilon_1)^2} - \sqrt{2}\ \epsilon_{cu} \qquad (4.31)$$

where ϵ_1, ϵ_2, ϵ_3 are the three principal strains and ϵ_{cu} is the uniaxial crushing strain of concrete, the value of which is often taken as 0.0035 but actually depends on concrete strength.

4.7 Bond Anchorage

It is well recognized that the carrying capacity of reinforced concrete structures depends on the bond behaviour between concrete and the reinforcing steel. Several studies

have been made to determine the mechanisms of bond, bond-slip and bond-splitting of deformed reinforcing bars (refs. 44-49). Bond between smooth bars and concrete depends on chemical adhesion and friction. On the other hand, the bond behaviour of deformed bars, which are in extensive use nowadays, is fundamentally different and depends primarily on the bearing of the steel ribs against the intervening concrete keys. Bond conditions at a rib on a deformed bar differ significantly from those at locations between the ribs, therefore it is impossible to obtain a bond stress distribution which is applicable to all points (ref. 26).

Pull-out tests are generally used for the development of bond force-displacement relations base on either the anchorage approach or the transfer approach. In the former the load is applied at one side of a steel bar embedded in a concrete cylinder, while in the latter the force is applied on both sides of the bar (Figure 4.16). To be useful in finite element modelling, however, the constitutive relations between bond stress and bond-slip must necessarily be expressed on a local basis, i.e. at representative locations along the steel/concrete interface because stresses and strains are calculated at sampling points along the reinforcing bars.

A comparison of the bond stress-slip by a number of workers, shown in Figure (4.17), reveals the staggering variation of results obtained by different tests. This seems to strongly indicate the need for further research in this area in order to get more insight into this important property.

So-called linkage elements were introduced by Ngo and

Scordelis (ref. 22) to model bond-slip behaviour in a two-dimensional nonlinear finite element model. The linkage element, shown in Figure (4.18), consists of two orthogonal springs which connect and transmit shear and normal forces between two adjacent nodes. The stiffness matrix of the linkage element is calculated in the local coordinates, transformed to the global system of coordinates and then added to the overall stiffness matrix of the structure. The linkage element, therefore, lumps all the interface behaviour at a nodal point in a discrete manner in contrast to the actual distributed behaviour. This was soon realised as a serious drawback and was later improved by the so-called "bond-interface elements" (refs. 50, 51), being arranged along the steel/concrete interface (Figure 4.19).

However, due to the lack of enough evidence to aid modelling the bond-slip behaviour, and as dictated by the embedded bar's formulations, presented in Chapter Three, full bond is assumed between concrete and steel. Also its overall effects are taken into account in the tension stiffening model.

4.8 Steel Constitutive Laws

In contrast to concrete behaviour, reinforcing steel is a comparatively well behaved material. Its properties can be determined within close tolerances and there does not seem to be much problem in modelling its behaviour in finite element codes. Its presence in reinforced concrete structures is normally in the form of slender bars and thus the behaviour is essentially uniaxial.

Typical steel stress-strain curves in tension are shown in Figure (4.20). The steel behaviour is generally assumed to

be identical in tension and compression. Figure (4.21) shows four different finite element idealizations in common use for reinforcing steel behaviour. For each case it is necessary to determine, experimentally, the value of the stresses and strains at the onset of yield, strain hardening modulus after yield and at the ultimate tensile strength as well as the elastic modulus.

In conjunction with reinforcing steel simulation presented in Chapter Three, the first two idealizations of Figure (4.21) were incorporated in the finite element program. The idealization of steel behaviour as an elastic-perfectly-plastic is quite acceptable particularly for mild steel. For high yield steel, however, a strain-hardening effect may be important. Elastic unloading is not included.
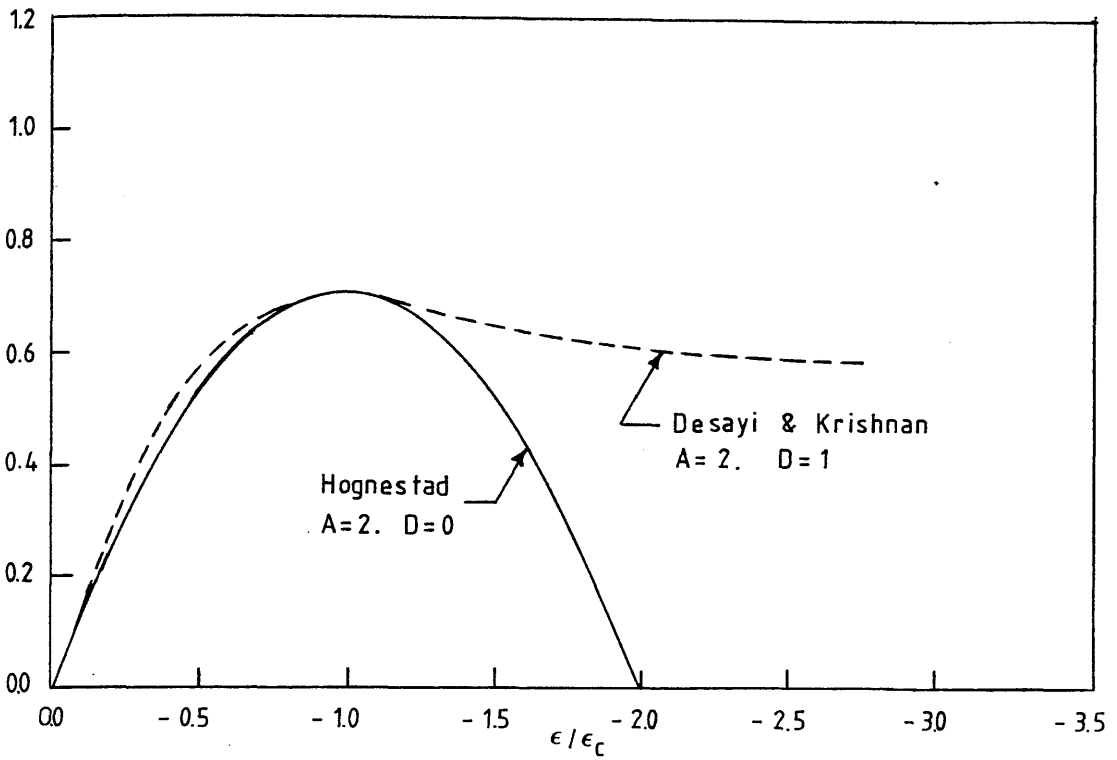
Figure (4.1) Uniaxial stress-strain curve illustrating
Ottosen's parameters A and D, and in particular
the effect of the parameter D on the post-failure
behaviour
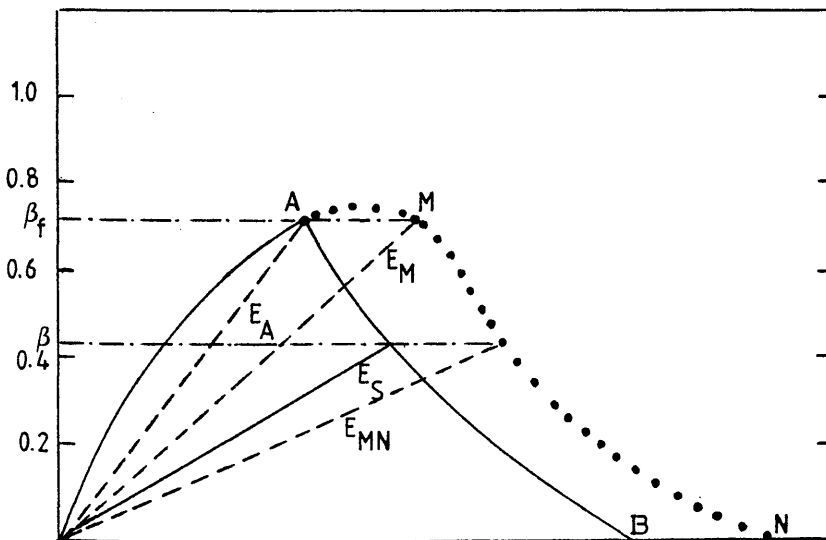
Figure (4.2) Post-failure behaviour for intermediate stress
states that do not result in cracking or
compressive crushing of concrete
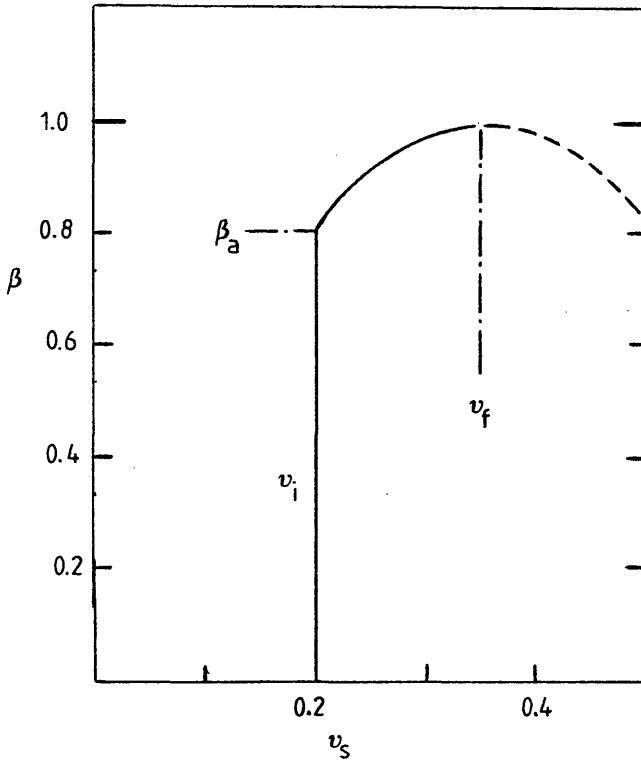
Figure (4.3) Variation of secant value of Poisson's ratio
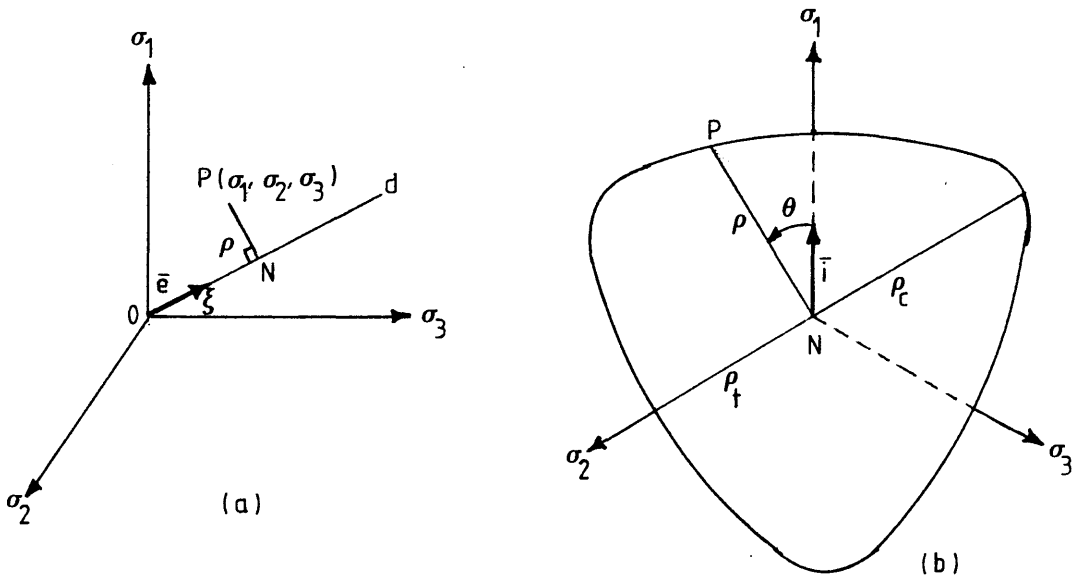
Figure (4.4) Haigh-Westergaard coordinate system

Table (4.1) Parameter values and their dependence on the σ_t/σ_c ratio for Ottosen's concrete constitutive laws (ref. 12)

σ_t/σ_c	A	B	K_1	K_2
0.08	1.8076	4.0962	14.4863	0.9914
0.10	1.2759	3.1962	11.7365	0.9801
0.12	0.9218	2.5969	9.9110	0.9647

Table (4.2) λ-values and their dependence on the σ_t/σ_c ratio for Ottosen's failure criterion (ref. 14)

σ_t/σ_c	λ_t	λ_c	λ_c/λ_t
0.08	14.4725	7.7834	0.5378
0.10	11.7109	6.5315	0.5577
0.12	9.8720	5.6979	0.5772
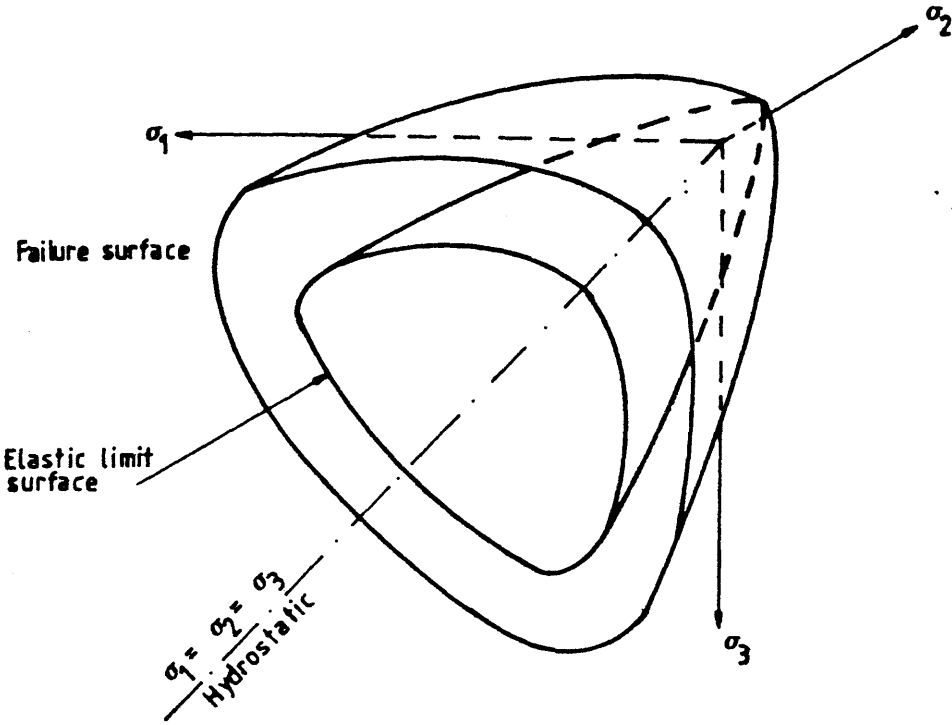
Figure (4.5) Schematic failure surface of concrete in
three dimensional stress space
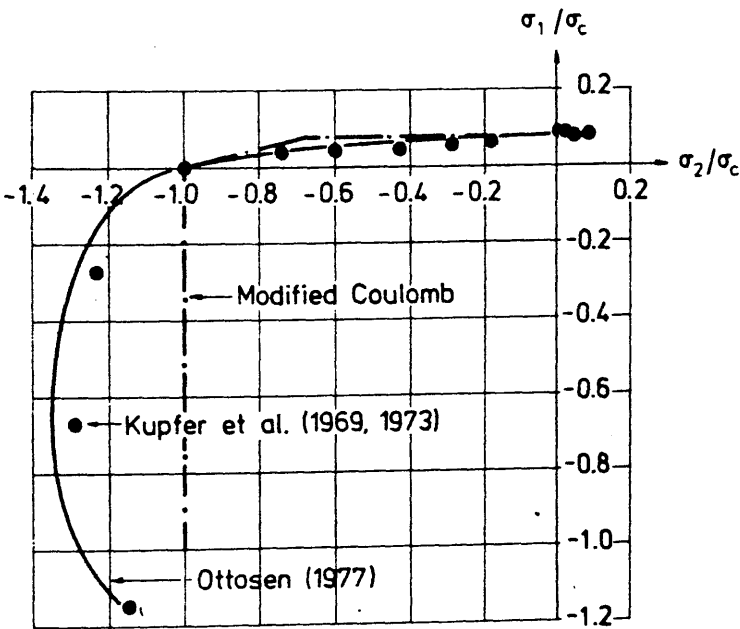
Figure (4.6) Verification of Ottosen's failure criterion
against biaxial test results (ref. 13)
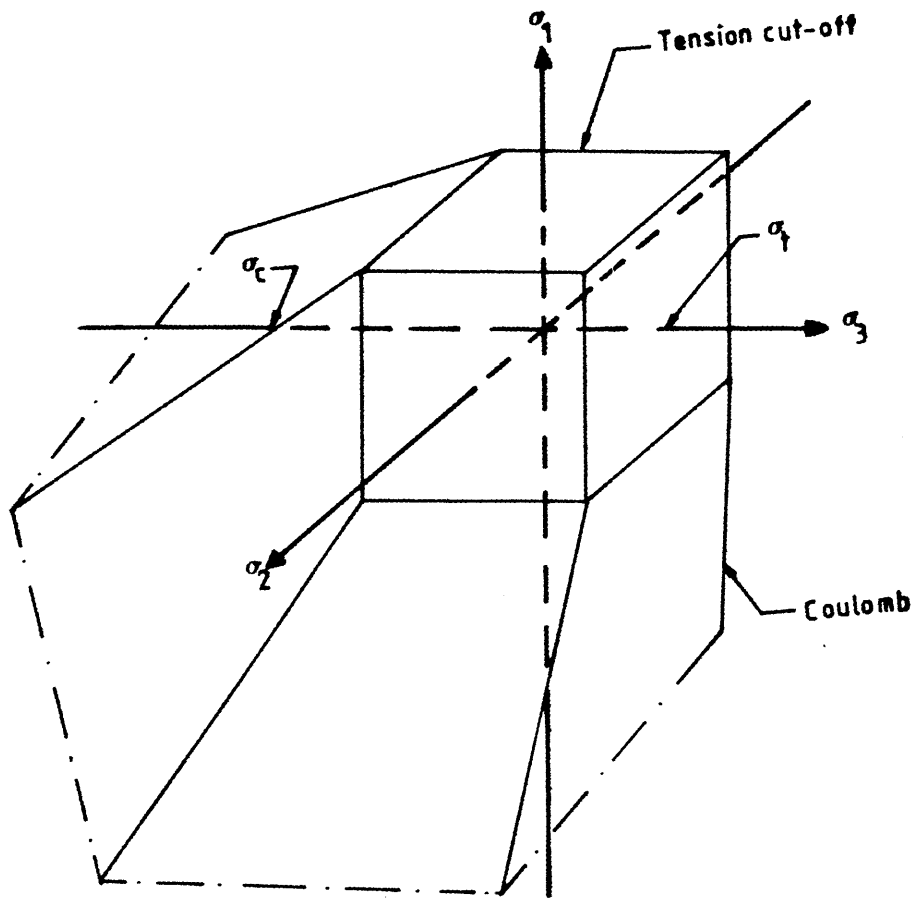
Figure (4.7) Appearance of the modified Coulomb criterion
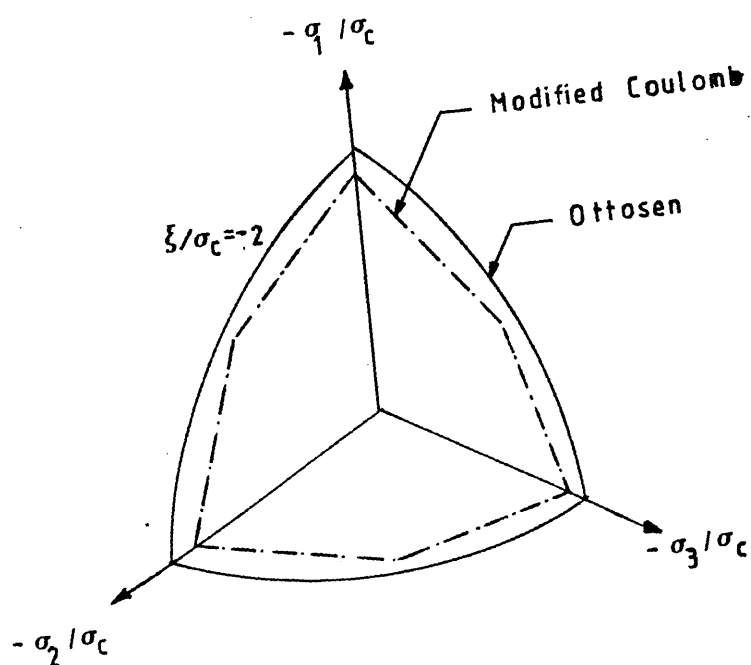
Figure (4.8) Trace of Ottosen's and the modified Coulomb criteria on the deviatoric plane
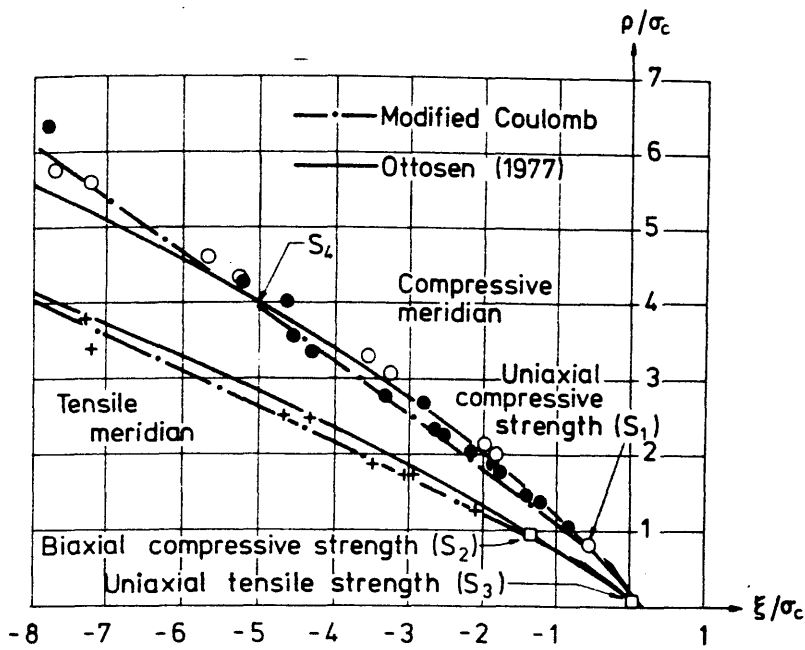
Figure (4.9) More verification of Ottosen's and the modified
              Coulomb criteria against test results (ref. 13)
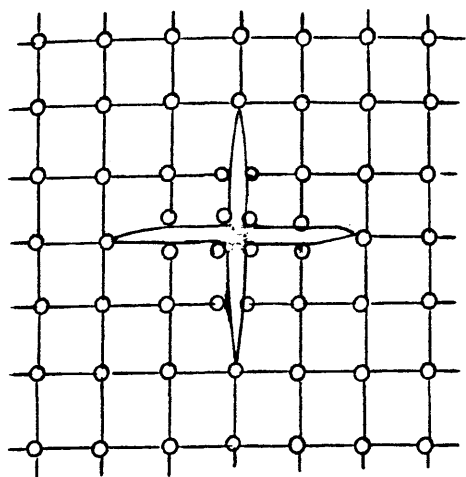
(a)   Two-directional cracking   (b) One-directional cracking
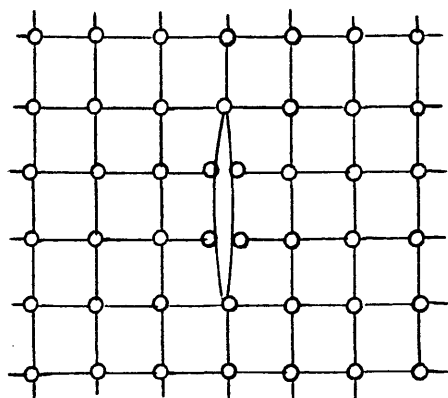
(i) Discrete cracking model
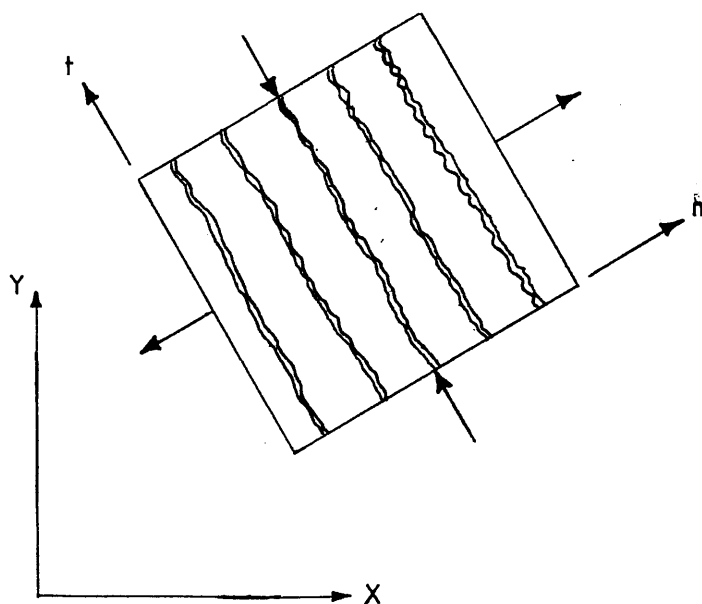
(ii) Smeared cracking model

Figure (4.10) Discrete and smeared cracking models
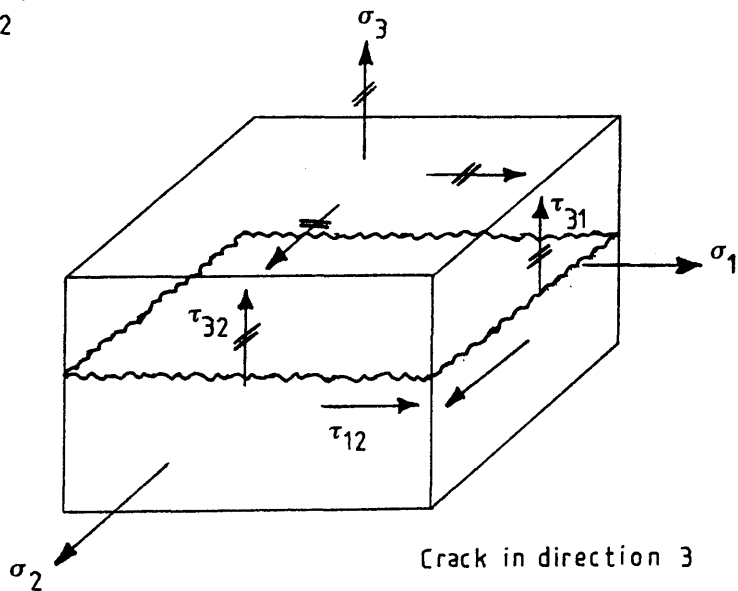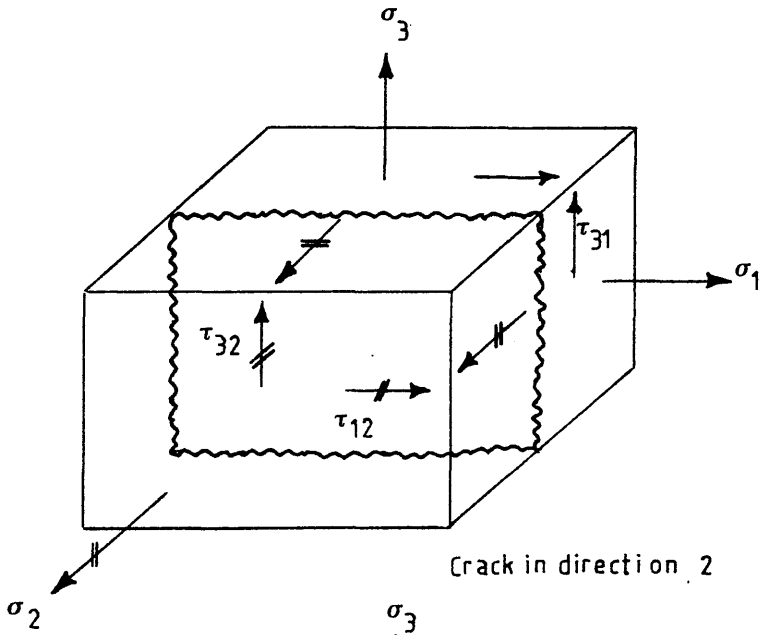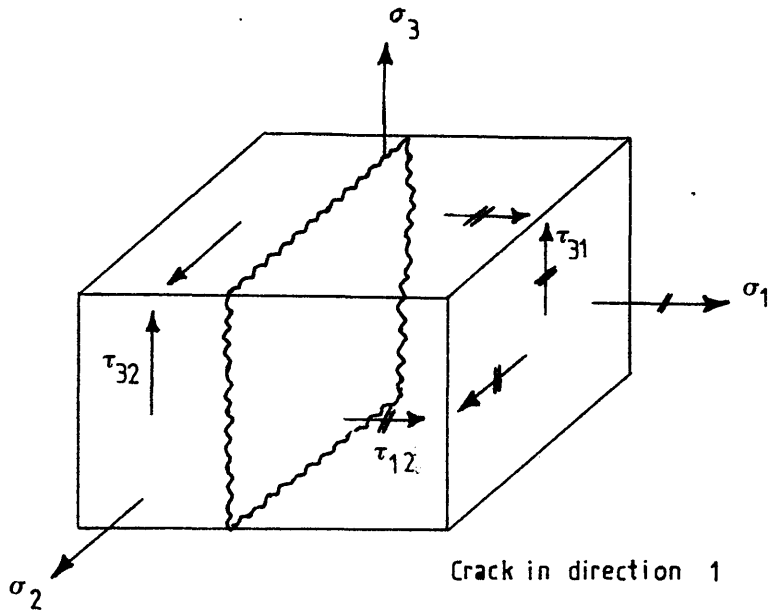
Figure (4.11) Three dimensional fixed orthogonal smeared
crack model
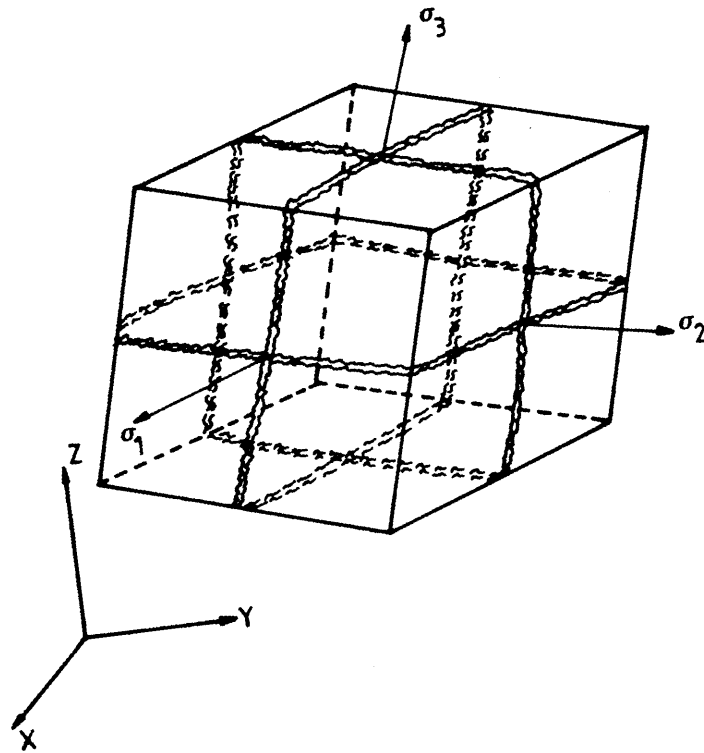
Figure (4.12) Three orthogonal cracks at a Gauss point
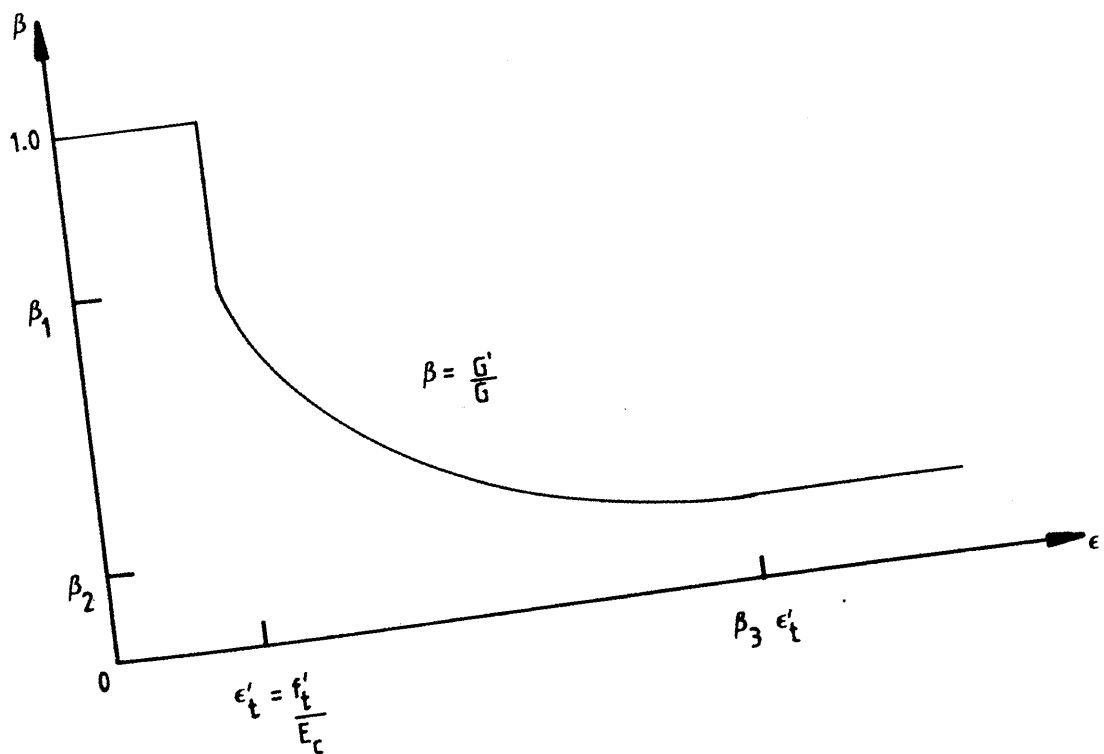
Figure (4.13) Variable shear retention factor
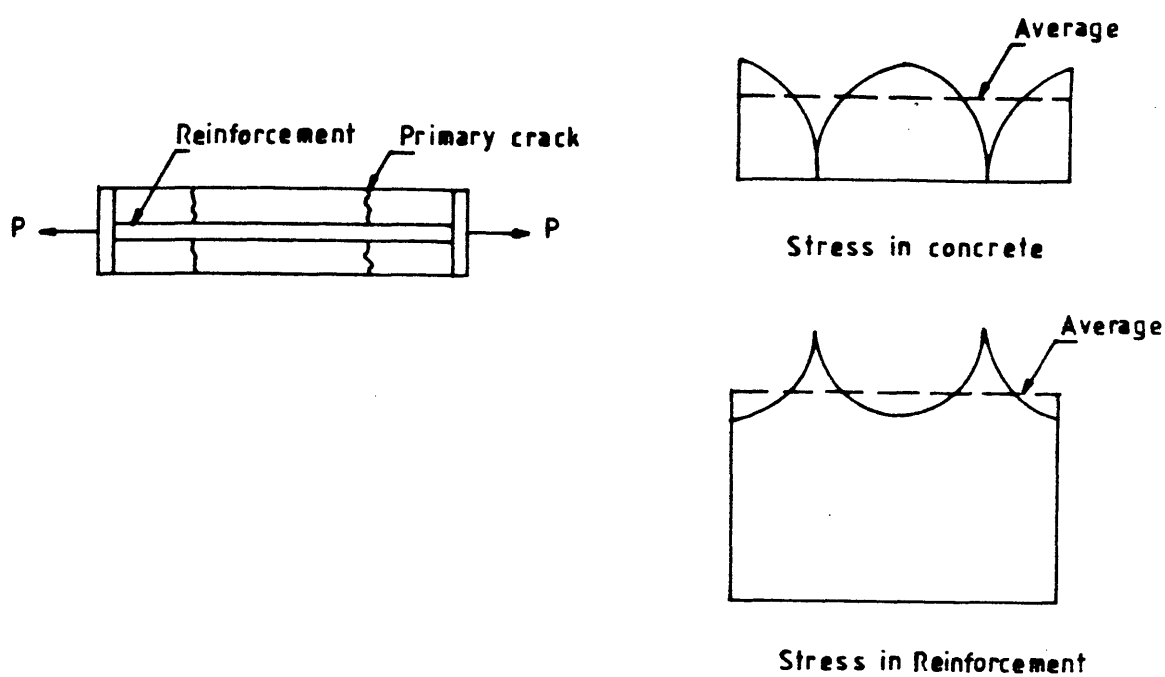
Figure (4.14) Physical situation in the vicinity of a crack in reinforced concrete (ref. 26)
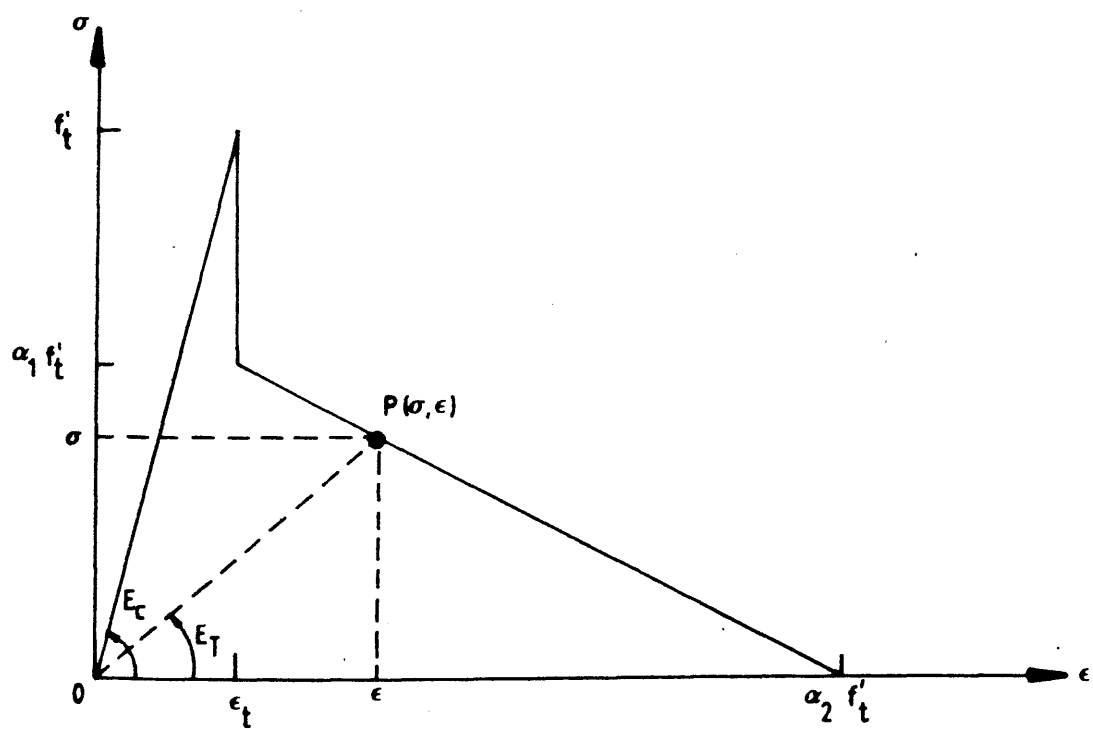
Figure (4.15) Tension stiffening model
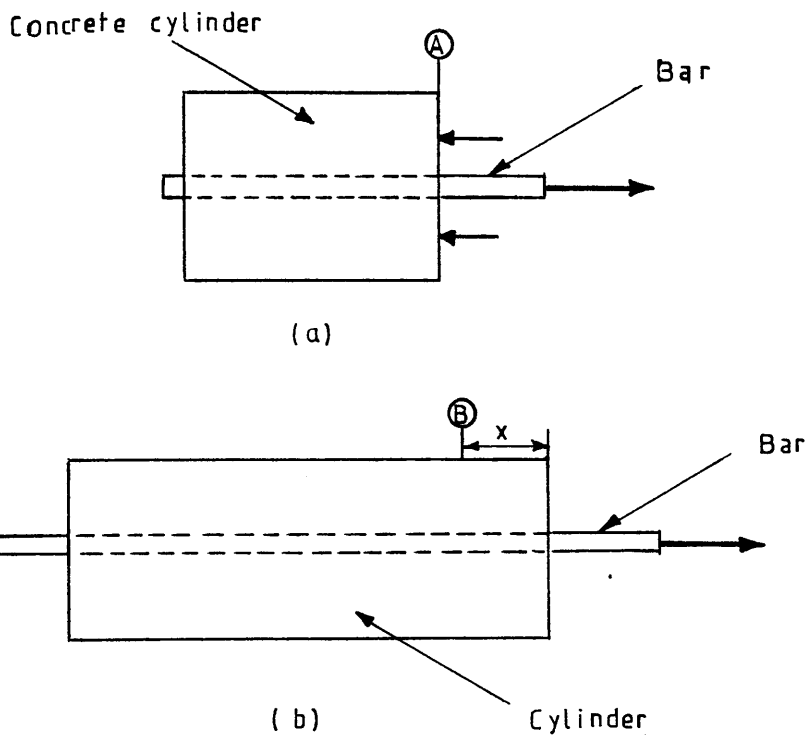
Figure (4.16) Types of pull-out tests used for bond studies
             (ref. 26)
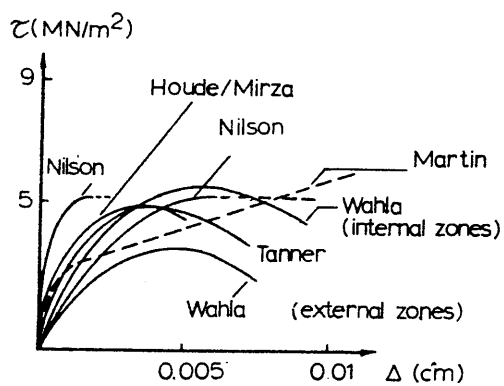
Figure (4.17) Comparison of bond slip relations (ref. 26)
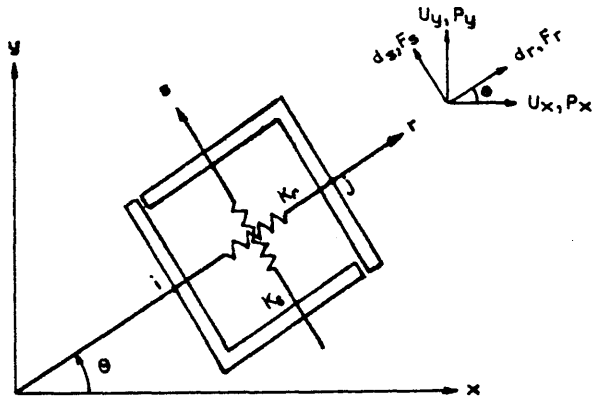
Figure (4.18) Linkage element for modelling of bond behaviour
of reinforced concrete (ref. 22)
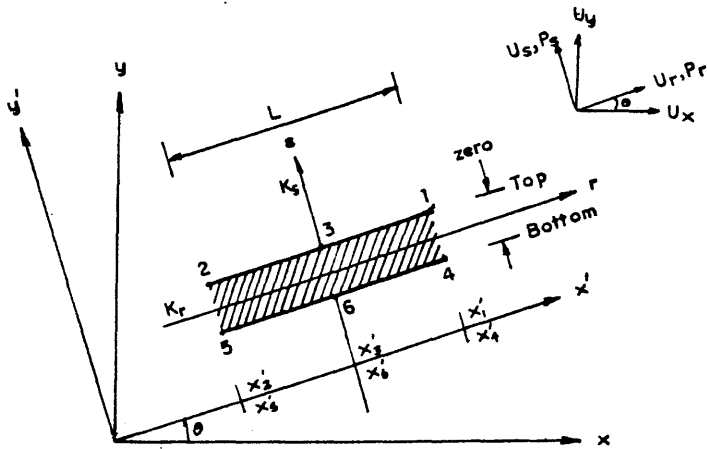
Figure (4.19) Bond interface elements (ref. 51)
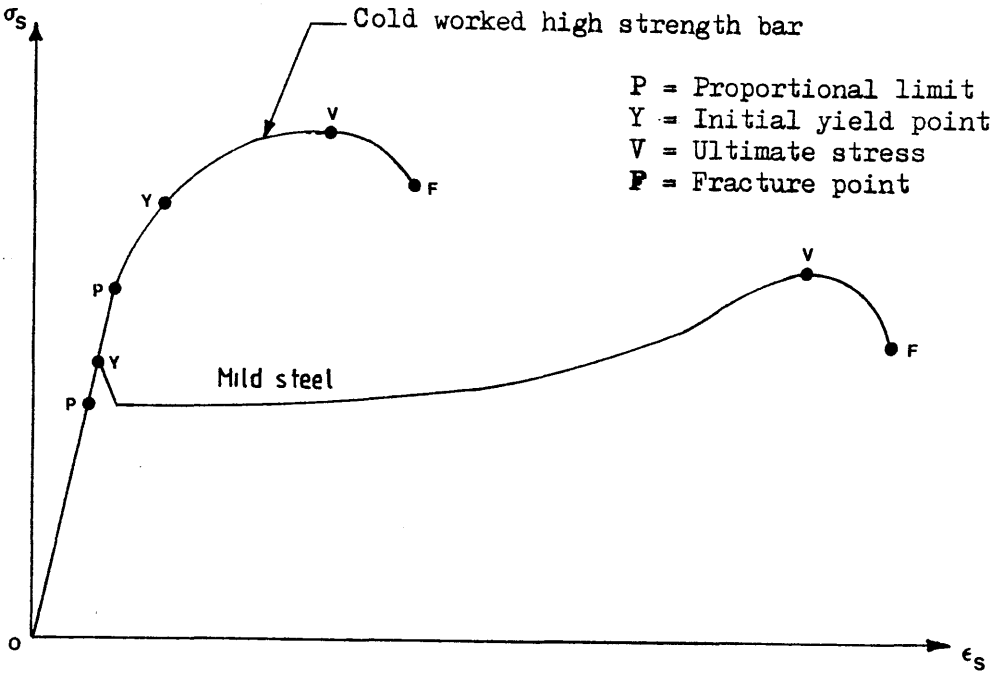
Figure (4.20) Typical steel stress-strain curves (ref. 11)
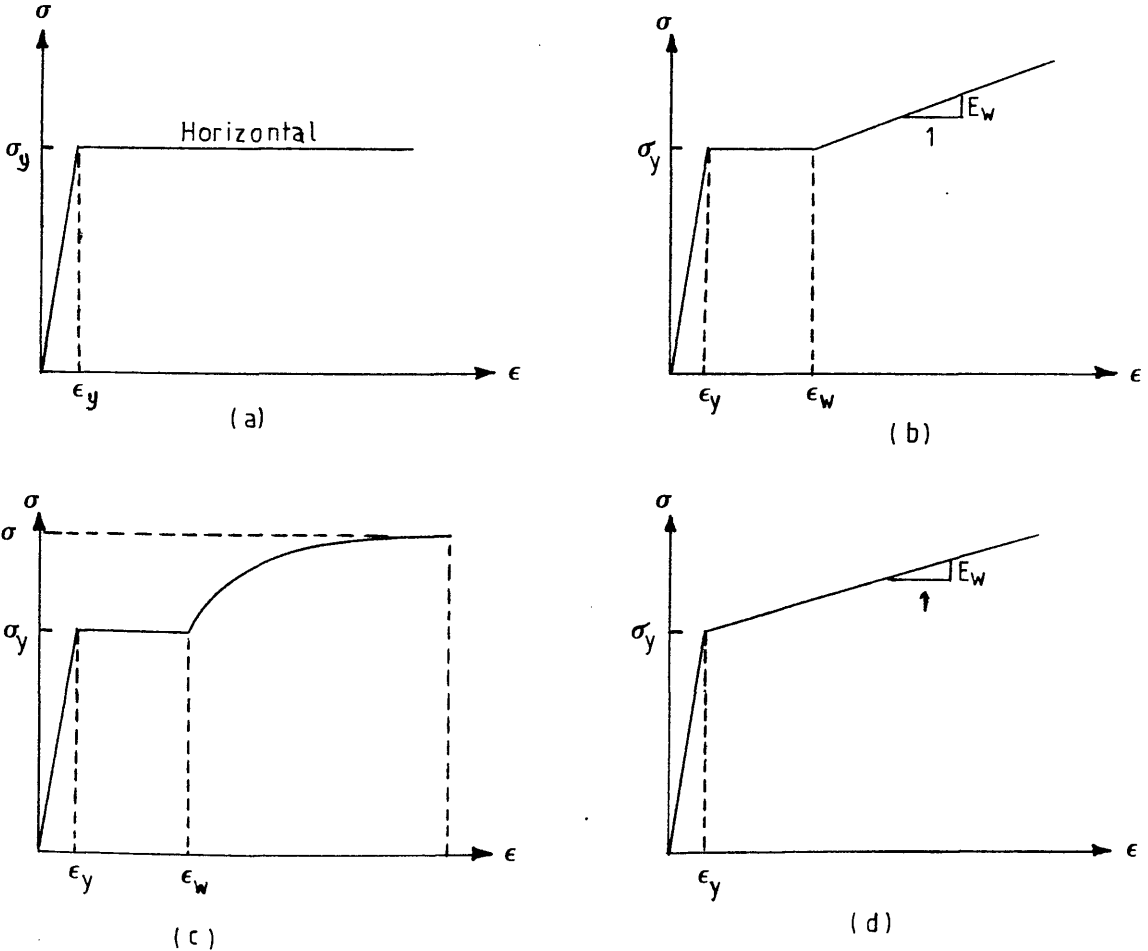
Figure (4.21) Different idealizations for the stress-strain curve
of steel in tension or compression:
(a) elastic perfectly plastic, (b) trilinear
approximation, (c) complete curve, (d) bilinear
approximation

References

(1) Kupfer, H.B. and Gerstle, K. H., "Behaviour of Concrete Under Biaxial Stresses" , Jour. Engng. Mech. Div., ASCE, Vol. 99, No. EM4, August, 1973, pp. 853-866.

(2) Gerstle, K. H., Linse, D.L., Bertacchi, P., Kotosovos, M.D., Ko, H.Y., Newman, J.B., Rossi, P., Schickert, Taylor, M.A., Traina, L.A., Zimmerman, R.M., and Bellotti R., "Strength of Concrete Under Multiaxial stress States", Proceedings, McHenry international Symposium on Concrete and Concrete Structures, Mexico City, Mexico, 1976, American Concrete Institute, pp. 103-131.

(3) Gerstle, K.H., Aschl, H., Bellotti, R., Bertacchi, p., Kotsovos, M.D., Ko, H.Y., Linse, D., Newman, J.B., Rossi, P., Schickert, G., Taylor, M.A., Traina, L.A., Winkler, H., Zimmerman, R.M., "Behaviour of Concrete Under Multiaxial Stress States", Jour. Engng. Mech. Division, ASCE, Vol. 106, No. EM6, December, 1980, pp. 1383-1403.

(4) Palaniswamy, R. and Shah, S.P.,"Fracture and Stress-Strain Relation of Concrete Under Triaxial Compression", Jour. Struc. Div., ASCE, Vol. 100, No. ST5, May, 1974, pp. 901-916.

(5) Cedolin, L., Crutzen, Y.R.J. and Poli, S.D.,"Triaxial Stress-Strain Relationship for Concrete", Jour. Engng. Mech. Div., ASCE, Vol. 103, No. EM3, June, 1977, pp. 423-439.

(6) Kotsovos, M.D.and Newman J.B., "Generalized Stress-Strain Relationsfor Concrete", Jour. Engng. Mech. Div., ASCE, Vol. 104, NO. EM4,August, 1978, pp. 845-855.

(7) Kotsovos, M.D. and Newman, J.B.,"A Mathematical Description of the Deformational behaviour of Concrete Under Complex Loading", Magazine of Concrete Research, Vol. 31, NO. 107, June, 1979, pp. 77-90.

(8) Ahmed, S.H. and Shah, S.P., "Complete Triaxial Stress-Strain Curves for Concrete", Jour. Struc. Div., ASCE, Vol. 108, No. ST4, April, 1982, pp. 728-742.

(9) Chen, W.F. and Ting, E.C., "Constitutive Models for Concrete structures", Jour. Engng. Mech. Div., ASCE, Vol. 106, No. EM1, February, 1980, pp. 1-19.

(10) Chen, W.F., "Constitutive Equations for Concrete", IABSE Colloquiuum, Vol. 28, "Plasticity in Reinforced Concrete", Copenhagen, 1979, pp. 11-34.

(11) Chen, W.F., "Plasticity in Reinforced Concrete", McGraw Hill, 1982.

(12) Ottosen, N.S., "Constitutive Model for Short-Time Loading of Concrete", Jour. Eng. Mech. Div., ASCE, Vol. 105, No. EM1, Feb. 1979, pp. 127-141.

(13) Ottosen, N.S., "Nonlinear Finite Element Analysis of Concrete Structures", Report Risφ-R-411, Risφ National Laboratory, Denmark, 1980.

(14) Ottosen, N.S., "A Failure Criterion for Concrete", Jour. Engng. Mech. Div. ,ASCE, Vol. 103, No. EM4, August 1977, pp. 527-535.

(15) Ottosen, N.S. and Andersen, S.I., "Structural Failure of Thick-Walled Concrete Structures", Paper H4/3,

Transactions, 4th Inter. Confer. on Structural Mechanics in Reactor Technology, San Fransisco, Aug., 1977.

(16) Ottosen, N.S., "2-D Finite Element Analysis of Massive RC Structures", Jour. Struct. Div., ASCE, Vol. 108, NO. ST8, Aug., 1982, pp. 1874-1893.

(17) Ottosen, N.S., " Nonlinear Finite Element Analysis of Pull-Out Test", Jour. Struc. Div., Vol. 107, No.ST4, Apr., 1981, pp. 591-603.

(18) Ottosen, N.S., "Evaluation of Concrete Cylinder Tests Using Finite Elements", Jour. Engng. Mech., Vol. 110, No. 3, March, 1984, pp. 465-481.

(19) Drucker, D.C. and Prager, W., "Soil Mechanics and Plasticity Analysis of Limit Design", Quarterly of Applied Mathematics, Vol. 10, No.2, 1952, pp. 157-165.

(20) Cowan, H.J., "The Strength of plain, Reinforced and Prestressed Concrete Under Action of Combined Stresses, with Particular Reference to the Combined Bending and torsion of Rectangular Sections", Mag. Conc. Res., Vol. 5, 1953, pp. 75-86.

(21) Johansen, J.W., "Discussion of: Strength of Concrete Under Combined Stresses", Proceedings of the Amer. Conc. Instit., Vol.56, Feb., 1959, pp. 1043-1045.

(22) Ngo, D. and Scordelis, A.C., "Finite Element Analysis of Reinforced Concrete Beams", Jour. Amer. Conc. Instit., Vol. 64, No.3, March, 1967, pp. 152-163.

(23) Rashid, Y.R., "Analysis of Prestressed Concrete

Pressure Vessels", Nuclear Engineering and Design, Vol. 7, No. 4, April, 1968, pp. 334-344.

(24) Phillips, D.V., "Nonlinear Anaysis of Structural Concrete by Finite Element Methods", Ph.D. Thesis, University of Wales, Swansea, 1972.

(25) Suidan, M. and Schnobrick, W.C., "Finite Element Analysis of Reinforced Concrete", Jour. Struct. Div., ASCE, Vol. 99, No. ST10, October, 1973, pp. 2109-2122.

(26) ASCE, "Finite Element Analysis of reinforced Concrete", State-of-the-Art Report, 1982.

(27) Cook, R.D., "Concepts and Applications of Finite Element Analysis", Second Edition, wiley, 1981.

(28) Durelli, A.J., Phillips, E.A.and Tsao, C.H., "Introduction to the Theoretical and Experimental Analysis of Stress and Strain", McGraw Hill, 1958.

(29) Brebbia, C.A. and Connor, J.J., "Fundamentals of Finite Elements Techniques", Butterworths, 1973.

(30) Phillips, D.V. and Zienkiewitcz, O.C., "Finite Element Nonlinear Analysis of Concrete Structures", Proc. Instit. Civil Engrs., Vol. 61, Part 2, 1976, pp. 59-88.

(31) Hand, F.R., Pecknold, D.A. and Schnobrich, W.C., "Nonlinear Layered Analysis of R.C. Plates and Shells", Jour. Struc. Div., ASCE, Vol.99, No. S77, July, 1973, pp. 1491-1505.

(32) Al-Manaseer, A.A., "a Nonlinear Finite Element Study of reinforced Concrete Beams", Ph.D. Thesis, Glasgow

University, 1983.

(33) Al-Mahaidi, R.S.H., "Nonlinear Finite Element Analysis of Reinforced Concrete Deep Members", Report No. 79-1, Dept. of Structural Engineering, School of Civil and Enviromental Engineering, Cornell University, January, 1979.

(34) Cedolin, L. and Dei Poli, S., "Finite Element Studies of Shear Critical Reinforced Concrete Beams", Jour. Engng. Mechanics Div., ASCE, Vol. 103, No. EM3, June, 1977, pp. 395-410.

(35) Damjanic, F. and Owen, D.R.J., "Practical Considerations for Modelling of Post-Cracking Concrete Behaviour for Finite Element Analysis of Reinforce Concrete Structures", Proc. Int. Conf. Computer Aided Analysis and Design of Concrete Structures, Split, Yugoslavia, 1984, pp. 693-706.

(36) Al-Manaseer, A.A. and Phillips, D.V., "Numerical Study of Parameters Affecting Nonlinear Solutions in Reinforced Concrete Beams", Proc. Annual Conf. Canadian Soc. Civ. Engng., Saskatoon, Canada, May, 1985, pp. 163-183.

(37) Clarck, L.A. and Speirs, D.M., "Tension Stiffening in Reinforced Concrete Beams and Slabs Under Short-Term Load", Technical Report 42.521, Cement and Concrete Association, July, 1978.

(38) Phillips,D.V. and AL-Manaseer, A.A., "Simple Nonlinear Analysis of T-Beams Using Plane Stress Elements", Proc. Int. Conf. Computer Aided Analysis and Design of Concrete Structures, Split, Yuogoslavia, 1984, pp. 677-691.

(39) Lin, C.S. and Scordelis, A., "Nonlinear Analysis of RC shells of General Form', Jour. Struc. Div., ASCE, No. ST3, Vol. 101, March, 1975, pp. 523-538.

(40) Cope, R.J., "Material Modelling of Real Reinforced Concrete Slabs", Proc. Int. Conf. Computer Aided Analysis and Design of Concrete Structures", Split, Yugoslavia, 1984, pp. 85-117.

(41) Gilbert, R.I. and Warner, R.F., "Nonlinear Analysis of Reinforced Concrete Slabs with Tension Stiffening", UNICIV Report No. R-167, University of New South Wales, Kensington, N.S.W., Australia, January, 1977.

(42) Van Greunen, J., "Nonlinear Geometric, Material and Time Dependent Analysis of Reinforced and Prestressed Concrete Slabs and Panels", UC-SESM Report No. 79-3, University of California at Berkeley, October, 1979.

(43) Scanlon, A. and Murray, A., "Time Dependent Reinforced Concrete Slab Deflections", Jour. Struc. Div., ASCE, Vol. 100, No. ST9, 1979, pp. 1911-1924.

(44) Lutz, L.A. and Gergely, P.,"Mechanics of Bond and Slip of Deformed Bars in Concrete", ACI Journal, Proc., Vol. 64, No. 11, November, 1967, pp. 711-721.

(45) Ingraffa, A.R., Gerstle, W.H., Gregley, P. and Saouma,V., "Fracture Mechanics of Bond in Reinforced Concrete", Jour. Struc. Engng., ASCE, Vol. 110, No. 4, April, 1984, pp. 871-890.

(46) Giuriani,E., "Experimental Investigation on the Bond-

Slip Law of Deformed Bars in Concrete", IABSEColloquiuum, "Advanced Mechanics of Reinforced Concrete", Delft, 1981, pp. 135-168.

(47) Jiang, D.H., Shah, S.P. and Andonian, A.T., "Study of the Transfer of Tensile Forces by Bond", ACI Journal, Vol. 81, May-June, 1984, pp. 251-259.

(48) Yankelevsky, D.Z., "Bond Action Between Concrete and Deformed Bar - A New Model", ACI Journal, Vol. 82, March-April, 1985, pp. 154-161.

(49) Copley, J.D. and Burdett, E.G., "Behaviour of Steel-to-Concrete Anchorage in High Moment Regions", ACI Journal, Vol. 82, March-April, 1985, pp. 180-187.

(50) Ngo, D., "A Network-Topological Approach to the Finite Element Analysis of Progressive Crack Growth in Concrete Members", Ph.D. Thesis, University of California, Berkeley, California, 1975.

(51) Saouma, V.E., "Interactive Finite Element Analysis of Reinforced Concrete: A Fracture Mechanics Approach", Ph.D. Thesis, Cornell University, N.Y., January, 1981.

CHAPTER FIVE

APPRAISAL OF THE DEVELOPED NONLINEAR FINITE ELEMENT PROGRAM

5.1 Introduction

The three dimensional nonlinear finite element program developed as part of this study is applicable to many types of reinforced concrete structures. The full nonlinear torsional behaviour of solid rectangular or flanged sections is only one application. Therefore the object of this chapter is to present an examination of the reliability of the developed method on a variety of reinforced concrete structures under different loading types. This is done prior to applying the model for the analysis of L-sections subjected to pure torsion which will be presented later. One objective of this appraisal, in addition to testing the model reliability, is to identify the important material and solution parameters which affect the types of applications considered. Experimental results reported elsewhere are used to carry out this appraisal. Use was also made of literature to provide previous finite element models for comparisons (for example refs. 1, 2, 3, 4 ,5).

Numerical parameters can be classified into three groups: solution parameters, quasi-material parameters, and actual material parameters. The quasi-material parameters are factors which are treated as if they were material parameters but in fact are really numerical devices used to produce a required effect (ref. 5). The most important of these parameters are:

(1) Solution parameters

    (a) Convergence tolerances

(b) Number of iterations

(c) Method of updating the stiffness

(d) Mesh size

(2) Quasi-material parameters

(a) Shear retention parameters

(b) Tension stiffening parameters

(3) Actual material parameters

(a) Crushing criterion for concrete

(b) Tensile strength of concrete

(c) Young's modulus

Some of these parameters are investigated in the present work and will be reported in this chapter for the following applications:

(1) Deep beams

(2) Shallow beams simulating beam-column connection

(3) Rectangular beams subjected to pure torsion

(4) Rectangular beams subjected to combined bending and torsion

5.2 Application to Deep Beams

5.2.1 Introduction

When the span/depth ratio of simply supported beams is less than 2, or less than 2.5 for any span of a continuous beam, it is customary to define these beams as deep (ref. 6). Most commonly, these structures are encountered in foundation walls supported by strip footings or raft slabs,

in parapet walls, in shear wall structures that resist
lateral force in buildings and in tall buildings.

The traditional principles of stress analysis are neither
suitable nor adequate to determine the strength of
reinforced concrete deep beams. Plane sections in these
beams do not remain essentially plane under loading; but
this is also true at the end of every simple span beam (ref.
7). The dimensions of deep beams promote shear deformations
to become more important in comparison to pure flexure.
Furthermore, deep beams are rather sensitive with respect to
the loading at the boundaries. The length of the bearings at
the beam supports or load application would affect the
principal stresses, which can be very critical in the
immediate vicinity of these bearings.

There is no intention to review deep beams behaviour in the
following sections. The main aim is to assess the
reliability of the developed three dimensional nonlinear
finite element model when applied to this category of
structures. In recent years a good deal of analytical and
experimental work has been undertaken in attempts to study
reinforced concrete deep beams behaviour (refs. 8, 9, 10,
11, 12, 13, 14). The complexity of their behaviour was
highlighted as were the limitations of the various proposed
methods of treatment.

5.2.2 Beam Chosen for the Study

The beam chosen for this analysis, denoted beam 101, was
experimentally investigated by Lin (ref. 13) as part of a

series of tests on eleven simply supported normal weight concrete deep beams. The beams were loaded by a central concentrated load and were divided into two main groups. One group with a span/depth ratio of 1.8 and one group with 0.9. The main objective of the test was to examine the effect of concrete strength and orientation of reinforcement directions. Concrete strength was found to be very important in these beams as an increase of its value produced an increase of the ultimate strength. An increase in the amount of reinforcement was found not to have an important influence on the load at which diagonal cracks appear, but has the advantage of restricting the crack width and thus increasing the ultimate load.

5.2.3 Beam Description and Outline of the Numerical Study

The beam's dimensions and reinforcement details are shown in Figure (5.1). The beam was simply supported on an effective span of 900.0 mm and was loaded at the centre. Bearing plates were provided at the two supports and the load point. Local reinforcement cages were provided to increase the bearing capacity at the supports and the load point. details of concrete and steel properties are given in Tables (5.1) and (5.2). While all reported material properties were used in the analysis, some additional ones had to be assumed, when demanded by the material laws incorporated in the model.

Because of symmetry only half of the beam was considered in the analysis. Two finite element meshes were used as shown in Figures (5.2) and (5.3). The first mesh consisted of 9

elements and the other of 12 elements. All reinforcing bars were placed at their exact locations in the actual structure without imposing any restrictions on mesh choice.

It can be seen that in the 9-element mesh only the effective span (i.e. from the beam centre line to the middle of the supports) was considered and the loading was applied as a concentrated point load. On the other hand, the 12-element mesh was constructed to account for both bearing plates at the support and at the load point. This was a more realistic modelling as these plates have a significant effect in deep beam behaviour as already mentioned. In this particular beam their dimensions are quite considerable in comparison with the beam span. Because of this a study on the effects of boundary conditions and load application was undertaken using elastic analysis.

Figure (5.4) and Table (5.3) summarise the results of this study. The results show clearly the great difference that can be produced by using different boundary conditions and/or different load application which, on the face of it, might seem to be applicable for the same problem. Case 4 of Figure (5.4) was finally chosen for the full nonlinear analysis using the 12-element mesh because it gave the closest elastic deflection when compared to the experimental value. This choice is also justified by the fact that the applied load was actually distributed over the area under the loading plate in the experiment. Although a similar argument may apply to the reactions, the difference between the two is that the plates at the supports can allow some

rotation of the beam ends.

Further study on numerical parameters effecting the behaviour of this deep beam included the following:

(1) The effect of shear retention parameters

(2) The effect of tension stiffening parameters

(3) The effect of the convergence tolerance associated with both the above parameters

The following assumptions/parameters were used in the analysis:

(1) A 3x3x3 Gauss rule was used throughout

(2) The load was applied in small equal increments of 40.32 KN until failure.

(3) The stiffness is recomputed at the beginning of each load increment

The comparison of the theoretical and experimental results are based on the load-deflection curves, steel response and crack patterns as will be discussed in the following sections.

5.2.4 Effect of Shear Retention Parameters

Because shear stresses are dominant in deep beams it was considered important to first investigate the effect of the shear retention parameters on the behaviour of this particular beam. The 12-element mesh was employed (case 4 of Figure 5.4). Different values of shear retention parameters were examined, coupled with two values for the convergence tolerance, namely 10% and 1%. In order to isolate other

effects, the tension stiffening model was set inactive and equal increments of load were applied in all cases. For discussion of results, the shear retention parameters (β_1, β_2 and β_3) together with the tension stiffening parameters(α_1 and α_2), discussed in Chapter Four, are recalled here.

Figure (5.5) shows the results of this study. The experimental and predicted pre-cracking parts of the load-deflection curves are almost identical, confirming the adequacy of the boundary conditions, load application and the various assumed material properties necessary for concrete stress-strain laws. After cracking and up to a load of about 330.0 KN (57.4% of the experimental ultimate load) all theoretical curves are very close to each other, probably because the spread of cracking was not enough to produce significant differences due to the shear components in the stiffness matrix. All curves up to this stage are predicting the post-cracking stiffness reasonably well, despite all giving slightly higher displacement than the experimental curve (about 12% on average) for the same applied load.

The effect of the limits on the shear retention parameters and the value of the convergence tolerance are more profound beyond this load level. Higher limits on β_1 and β_2 resulted in higher ultimate load, higher stiffness and also closer curve to the experimental. The values β_1 = 1.0, β_2 = 0.5 and Toler = 10% gave the best ultimate load prediction (98.17% of the experimental) but it is not clear whether these limits are reasonable, particularly β_2 = 0.5 because this

implies that 50% of the shear stiffness is assumed to have been retained by the dowel action beyond a normal tensile strain across the cracks of 4000 microstarin.

However, the lower values of $\beta_1 = 0.5$ and $\beta_2 = 0.1$, used with a convergence tolerance of 10%, produced an ultimate load of 91.16% of the experimental, judged as fairly acceptable given the complexity of deep beam behaviour and the too many solution and material parameters involved with not enough experimental evidence to support or suggest any particular combination. The curve for $\beta_1 = 1.0$, $\beta_2 = 0.1$ and a convergence tolerance of 10% produced only little effect, with the curve only slightly stiffer than the previous one, indicating probably the small effect of the upper limit on the shear retention factor, β . Similar reduction of β_1 from 1.0 to 0.75 for the same values of β_2 (=0.1) and Toler (=1%) produced only a mild effect apparentley near ultimate conditions. An ultimate load of 84.15% of the experimental was predicted in this case. This may confirm the previous observation regarding the upper limit on the shear retention factor.

The strong influence of the convergence tolerance, for the same combination of shear retention parameters, is clearly evident from the first two theoretical curves in Figure (5.5), with $\beta_1 = 1.0$ and $\beta_2 = 0.1$ where two values of convergence tolerance were used, namely 10% and 1%. Noticeably higher displacement was obtained at the same applied load for Toler = 1%. Furthermore, after the load of 330 KN the curve for 1% Tolerance deviates considerably

giving even much higher displacement for the same applied load than the curve for 10%. More importantly, the ultimate load predictions were considerably different, being 98.17% and 84.15% of the experimental respectively.

The above observations demonstrate clearly the difficulties associated with nonlinear finite element analysis as the same results could be obtained using different combinations of parameters and also illustrate the care that should be exercised when dealing with any particular application especially if the behaviour itself is complicated.

It is reported that the beam failed experimentally in a diagonal compression failure. The experimental load-deflection curve seem to suggest that crushing occured at a load of about 500.0 KN as can be seen in the sudden sharp decrease in stiffness beyond this load. The slope of almost all theoretical curves beyond a load of about 400.0 - 450.0 KN is practically the same as the slope of the experimental curve after the sharp reduction of stiffness, indicating that even at this critical stage the failure mechanism was apparently predicted well. This is coupled with the reasonable prediction of the crack propagation and final pattern which will be presented later.

Horizontal stress and strain distributions at a section near the midspan are shown in Figure (5.6) at four different load levels. It can be seen that at elastic load level there was minor nonlinearity in the stresses at the top of the beam. However, as cracks started to appear the stresses dropped to

zero in the cracked region as the compressive stresses increased in the top of the beam.

A more interesting behaviour is seen from the strain distribution. Again, before cracking and similar to the stresses minor nonlinearity is present at the top the beam. The neutral axis is located practically at the mid-depth of the cross section. On further loading, both tensile strains (below N.A.) and compressive strains (above N.A.) increases as expected, resulting in a continuous shift of the neutral axis upwards. This observation, coupled with the previous one regarding stress distribution, gives a certain degree of satisfaction on the performance of the finite element model as cracking spreads upwards, indicating that the tensile stresses are well redistributed onto the structure and that the neutral axis moves upwards as expected with increasing load. At a load of 403.2 KN (70.1% of the experimental failure load) the tensile strain at the bottom fibre is about 3600 microstrain, the compressive strain at the top fibre is about -2000 microstrain and the neutral axis depth is about 100 mm (20% of the total depth of the section approximately).

5.2.5 Effect of Tension Stiffening Parameters

The 12-element mesh was used in this study. All reported concrete and steel properties were used. Al-Manaseer (ref. 15), using a two-dimensional plane stress model, used a constant shear retention factor of 0.5 for this beam. This value was chosen for β_1 in this study to simulate the sudden drop of the shear stiffness immediately upon

cracking. The value $\beta_2 = 0.1$ was chosen to simulate the effect of dowel action after the cracks open widely enough for aggregate interlocking to cease. $\beta_3 \varepsilon_t' = 0.004$ determined the rate of decay of shear stiffness and also the normal strain at which aggregate interlocking was assumed to cease (i.e. at 4000 microstrain).

There was not enough experimental evidence to give precise choice of β_1, β_2 and $\beta_3 \varepsilon_t'$. However, experimental results (ref. 26) indicated significant loss of shear strength of beams in hogging regions of up to about 40% depending on various parameters such as the position of the top and bottom reinforcement and whether or not the main bars are curtailed or lapped. It must be pointed out that such results are not immediately ready for use in finite element models, but they can serve at least to indicate the directions to follow when setting up models for different aspects of behaviour. Hence the choices of the three shear retention parameters at $\beta_1 = 0.5$, $\beta_2 = 0.1$ and $\beta_3 \varepsilon_t' = 0.004$. The value of 4000 microstrain amounts roughly to twice the yield strain (or the proof strain) of most types of steel which seem to be high enough to allow the cracks to open sufficiently wide for dowel action to assume the main share of shear stiffness of the cracked section.

Having thus fixed the values of the shear retention parameters, the tension stiffening parameters (α_1 and α_2) and the convergence tolerance (Toler) were systematically varied. The results are shown in Figure (5.7) where the load deflection curves are compared. It is clear from the figure

that the use of tension stiffening has a significant effect in the early nonlinear part of the load-deflection curve. However, the ultimate load predictions did not suffer an appreciable increase when tension stiffening was used. This can be attributed to the fact that the ultimate failure is normally brought about by the effects of yielding of reinforcement, shear and diagonal cracking, and concrete crushing all of which have a stronger effect than tension stiffening at higher load levels.

It is interesting to note that the tension- and no-tension stiffening curves in Figure (5.7) formed two distinct groups with the experimental curve in between for the early nonlinear part of the curve. This tend to suggest that some element of tension stiffening takes place in this type of structure at early loading. However, it may be extremely difficult to quantify. From the figure the values of $\alpha_1 = 0.5$ and $\alpha_2 = 5.0$ with Toler = 1% gave the best fit to the experimental curve. The predicted ultimate load was 91.16% of the experimental.

Figure (5.8) shows the effect of tension stiffening on the steel strains. It seems from the curves that the no-tension stiffening results are in better comparison with the experiment unlike the load-deflection curves. The effect of tension stiffening in underestimating the steel strains is clearly seen here. This seems to suggest that although tension stiffening can be used to enhance comparison of load-deflection curves it may produce undesired effects on the steel response. It follows that low values of tension

stiffening parameters are recommended when using this model for deep beams, $\alpha_1 < 0.5$ and $\alpha_2 < 5.0$ for example. It would be extremely difficult, in the author's view, either to set exact values for such parameters or to generalize such conclusions once particular values are offered.

The policy adopted here, from the different cases studied and presented in this chapter, is to derive conclusions regarding numerical parameters for each category of problems individually. This is because of the differences in stress distributions resulting from different loading types on different types of structures. Therefore conclusions regarding effects of certain parameters on one category of problems may not necessarily suit the others.

Because of the reason that analyses are always carried out for reinforced concrete structures in order to provide the deformations and forces in concrete and steel at various loading stages, conclusions in this study will always be drawn from results that show good comparisons for overall behaviour (load-deflection curves, torque-rotation curves etc.) as long as the basic behavioural characteristics, such as steel response, crack propagation and patterns and failure loads are predicted within reasonable accuracy. The fact that reinforced concrete is a complex material is always in mind.

It can also be seen from Figure (5.8) that after yielding of steel the theoretical curves show a more flexible response than experiment. Very high steel strains were obtained. This

could be attributed to the fact that in the experiment a great deal of bond was lost at this stage while in the analysis full bond was assumed up to failure. Deterioration of bond between concrete and steel results in slip and hence relaxation of steel strains.

Theoretical crack patterns are shown in Figure (5.9) together with the final experimental crack pattern. It can be observed that vertical cracks appeared near the midspan at low load levels. On further loading these cracks spread first off-centre towards the supports and later upward. The cracks within the midspan were vertical, those off-centre were continually inclined towards the centre line of the beam forming struts between the supports and the load point. Yielding of steel occured upon further loading near midspan followed by crushing of concrete, which first occured along the diagonal struts closer to the support points before causing the final collapse of the beam. The final theoretical crack pattern agrees reasonably well with that from the experimental results.

The effect of tension stiffening can also be illustrated by studying the rate of decay of the residual forces during the iteration process. Figure (5.10) shows such a study where it is clear that tension stiffening reduces the amount of residual forces. This is because the tensile stresses in concrete are not completely released onto the structure unless the limiting strain, after which the tension stiffening ceases, is exceeded. The gradual release of concrete tensile stresses is responsible of the stiffer

load-deflection curves when using tension stiffening than
when no tension stiffening is used.

5.2.6 Conclusions

The conclusions drawn from this part are as follows:

(1) The developed finite element model provided fairly
satisfactory agreement with experimental results for the
deep beam chosen.

(2) The shear retention parameters affect the behaviour of
the deep beam studied particularly after about 50% of the
failure load. however, this is very much interrelated with
the convergence tolerance. The results indicated that care
must be exercised when dealing with these parameters. The
same results could be obtained using different combinations
of shear retention parameters and convergence tolerance. The
most sensitive aspect of behaviour to these parameters is
the ultimate load.

(3) The theoretical strain and stress distributions obtained
showed satisfactory behaviour as did the predictions of the
post-cracking stiffness. This might seem to illustrate the
adequacy of the orthogonal smeared cracking model employed
in this study for this type of behaviour.

(4) Use of tension stiffening seems to enhance the early
portion of the theoretical curve without significantly
increasing the predicted ultimate load. Its use is generally
not desirable for this type of structure. If it is used,
however, low values of tension stiffening parameters (

$\alpha_1 = 5.0$ and $\alpha_2 = 0.5$) are recommended, coupled with low values of convergence tolerance, say Toler = 1%.

(5) Proper modelling of boundary conditions and load application was found important in this type of analysis. However, although this aspect was studied for linear elastic conditions, it showed considerable effect. This is basically because the bearing plates used at the supports and under the applied load are usually long in comparison to the beam dimensions. This greatly affect the stress distributions near the support and at load application.

5.3 Application to Shallow Beams Simulating Beam-Column Connection

5.3.1 Introduction

Beam-column connections are a common feature of reinforced concrete structures. Although the individual behaviours of the beam and column are relatively simple, the local behaviour of the junction makes the whole system much more complicated. A study was conducted by Burns and Siess (ref. 16) to investigate the load-deformation behaviour of beam-column connections of reinforced concrete frames. Tests were made on beams simply supported and loaded through a column stub at midspan.

5.3.2 Beam Chosen for the Study

Beam J4 of the test series was chosen for the purpose of this study. The beam has also been analysed by various authors (refs. 15, 17, 18) and so gives additional comparisons. Details of the beam are shown in Figure (5.11)

and the material properties are shown in Table (5.4). Two load-deflection curves were reported by the authors for this beam. The first one is a curve cut-down just beyond the yield point and up to a 2 in. (50 mm) central deflection. The second curve is one which gives the complete behaviour up to the ultimate load and in which the first part of the curve up to the yield point is approximated by a straight line. This is because the authors were concerned with the four main points of change in the behaviour of the structure namely cracking, yielding, first crushing and ultimate stage. Therefore the theoretical results of this study will be compared with both those curves for better judgement and understanding.

Because of symmetry, only half of the beam will be analysed. The finite element mesh used is shown in Figure (5.12). All steel reinforcement was placed at the exact locations and a 3x3x3 Gauss integration rule was used. The load was applied in equal increments of 16 KN until failure occured. Enough load increments were provided to ensure failure will occur.

5.3.3 Discussion of Results

In the analysis of this beam the values of the shear retention parameters were first set at $\beta_1 = 0.5$, $\beta_2 = 0.1$ and $\beta_3 \varepsilon_t' = 0.004$, and tension stiffening was set inactive to start with, following the observations of the previous section. The maximum number of iterations was taken as 15 and the stiffness was recomputed at the beginning of each load increment.

Figures (5.13) and (5.14) show load-deflection curves for different yield strengths of steel, f_y. This was reduced by 9% and 15% because it was noticed that it had the major effect on the behaviour at the yielding stage, following the reasonable prediction of both the cracking load and the post-cracking stiffness for the chosen values of shear retention parameters as can be seen in the above figures. In the experimental curves the yield point is the most definite of all four points along the load-deflection curve. It marks a complete change in behaviour.

The ultimate load predictions were higher than the experimental value by 12.2% and 4.2%, for the two reductions in the yield value of steel, respectively. The reduction of f_y can be arguably justified on the basis that a major part of bond between steel and concrete is usually lost near ultimate conditions, a behaviour not accurately handled in the present finite element model as full bond is assumed leading to overestimation of the ultimate load. This can be compared with the reasonable predictions of both the cracking load and the post-cracking stiffness as the first one is independent of bond-slip characteristics and the second one is mildly affected by bond deterioration especially in the early stages.

Because of the dominance of flexural stresses and the belief that tension-stiffening is more associated with flexural behaviour, an attempt to study the effect the tension stiffening parameters was also made to clarify this point for the present finite element model. Several values of

tension stiffening parameters, α_1 and α_2, were examined using two values of convergence tolerance (Toler), namely 10% and 1%. The coarse value of 10% is considered enough for a reasonably accurate equilibrium whereas 1% is tight enough for equilibrium for all practical purposes.

Figures (5.15) and (5.16) show the results of this study. On the whole, all values of tension stiffening parameters regardless of the value of the convergence tolerance produced a very clearly stiff post-cracking response and a gross overestimation of the ultimate load. However, the effect of the smaller value of the convergence tolerance is evident near ultimate conditions but it was not enough to give appreciable reduction on the ultimate load. Reduced values of α_1 and α_2 resulted in less stiffer post-cracking response but still with overestimation of both the post-cracking stiffness and the ultimate load. Both parameters seem to affect the behaviour markedly particularly after the yield point.

A load-deflection curve from the previous set, i.e. with no tension stiffening, is also included in Figures (5.15) and (5.16). It is clearly evident that the no-tension stiffening curve is better in predicting both the post-cracking stiffness and the ultimate load. More importantly, the main points along the load-deflection curve, in particular cracking and yielding points are more clearly defined in this case than when tension stiffening is at all used. It is not apparent, however, which combination of these parameters best suit this particular problem apart from the conclusion

that tension stiffening might not give accurate results. Clearly further study on this problem is needed but that falls beyond the scope of this study.

The following paragraphs describe the results with tension stiffening inactive and compares them with the experimental behaviour. It was observed during the experiment that the cracking started at a load level of about 40.0 KN while the reinforcing steel yielded at a load of 156.0 KN. In this analysis, cracking started at a load of 48.0 KN while yielding of reinforcement started at a load level of 144.0 KN. when f_y was reduced by 15%.

Analytical crack patterns and propagation are shown in Figure (5.17). The beam cracked first at the region of the maximum bending moment near midspan. Cracks then propagated upwards and outwards, those near the centre line remaining vertical while the ones nearer to the support inclined towards the centre of the beam. The experimental crack propagation was only described as no figure was provided in reference (16). The theoretical crack propagation agrees reasonably well with that description. The marked changes of stiffness at cracking and in particular at steel yielding are well predicted. Crushing was observed at elements 3 and 4 indicating the local behaviour, due to stress concentrations at the junction near the ultimate load, which agrees well with experiment.

Theoretical steel response is shown in Figure (5.18) at different points along the main reinforcement. Although

there were no experimental results to compare with, the general behaviour follows that of the load-deflection curve indicating an expected response. After the yield point very high steel strains were carried by the bottom bars, which lead to the redistribution of considerable amount of stresses onto the structure leading to concrete crushing and the final failure soon afterwards. Very small stresses were carried by the main bars near the supports as might be expected.

5.3.4 Conclusions

From the results discussed above the following points were concluded:

(1) Although the pre-cracking stiffness, post-cracking stiffness and crack propagation were reasonably predicted, the ultimate load was overestimated by the chosen values of shear retention parameters when no tension stiffening is used.

(2) A basic material property, namely the yield strength of steel proved to be far more important than the use or otherwise of tension stiffening. Tension stiffening resulted in gross overestimation of both the post-cracking stiffness and the ultimate load when used with either a coarse (10%) or a tight (1%) convergence tolerance.

(2) Analysis with no-tension stiffening and a reduced yield value of steel (15% reduction) was closer to the experimental results than those with tension stiffening included. The reasons were not apparent and further

investigation of this point is suggested.

5.4 Application on Rectangular Beams Subjected to Pure Torsion

5.4.1 Introduction

As a major part of this study is devoted to torsion of L-beams an investigation on the reliability of the developed computer program for torsional analysis was undertaken. The aim of this section is to set guidelines for the analysis of the complicated flanged solid sections (T, I and L) using the relatively simple case of pure torsional behaviour of rectangular sections as a starting point. Reported experimental results were used to assess the capabilities of the theoretical model. Later on the case of combined torsion and bending is dealt with using the information and experience obtained from the pure torsion study.

5.4.2 Beams Chosen for the Study

A series of tests on plain and reinforced concrete rectangular sections subjected to pure torsion were conducted by Hsu (refs. 19, 20). The tests were used to calibrate, among other tests, the first ACI torsion design criterion (ref. 21). 10 plain and 53 reinforced concrete beams were tested in all, covering a range of parameters including the effects of the following variables: concrete strength, beam size and scale effect, amount of reinforcement, solid beams versus hollow beams, ratio of volume of longitudinal bars to volume of stirrups, depth-to-width ratio of cross-sections, arrangement of longitudinal bars and spacing of stirrups.

Beams were selected from this series because: (1) a wide range of variables were investigated and (2) detailed information of all aspects of the behaviour were readily available. Thus a good range of beams could be analysed which illustrate different aspects of behaviour. Four beams were selected for the analysis, designated B2, B4, G4 and N2 by Hsu. Dimensions and material properties are given in Figure (5.19) and Table (5.5). Beams B2 and B4 are of the same size with D/B=1.5. Beam G4 is larger with D/B=2.0 and beam N2 is smaller, also with D/B=2.0. The reinforcement ratios were different in each beam.

Different finite element meshes were used for the analysis. Very little previous work on torsion of reinforced concrete using finite elements has been reported to assist in this study, reference (22), which does not contain detailed information, being the only one known to the author. Because of this lack of information linear elastic studies of the following aspects were undertaken : mesh convergence, boundary conditions and load application.

5.4.3 Mesh Convergence Study

Figure (5.20) shows different finite element meshes used for an elastic analysis of beam B4 for a mesh convergence study. The boundary conditions selected for this study were those termed B/Cs 3 as will be shown later in section (5.4.6). The angle of twist per unit length was evaluated using the procedure described in section (5.4.5). The loading was applied as four nodal point loads to produce the

desired pure torque following the conclusions of section (5.4.4). Figure (5.21) shows the average angle of twist plotted against the total number of degrees of freedom for 8, 12, 16, 20 and 27 elements. It is clear from the plot that the angle of twist for 20 elements increases by only 2.25% over that for 8 elements; the difference between the two meshes being the number of elements along the beam span. Upon further subdivison of the mesh across the section, the angle of twist for 27 elements is higher by only 1.02% over that for 12 elements; the difference being the number of elements along the sides of the cross-section. This clearly indicates that if adequate number of elements is used along the three directions, the variation of the angle of twist with the total number of elements used is very small.

Following the above observations the 12-element mesh was chosen for the nonlinear analysis as it contains sufficient number of elements along all three axes of the beam. A 3x3x3 Gauss rule was used for this study resulting in a total of 27 sampling points per element. This is considered adequate for proper monitoring of concrete and steel nonlinearities, especially cracking.

5.4.4 Load Application
To properly simulate the experimentally applied torque a set of different nodal loads, shown in Figure (5.22), was studied for elastic analysis. Boundary conditions B/Cs 3 were used, (see section 5.4.6). Table (5.6) shows the resulting angles of twist for all different cases. Clearly the best results, in terms of the minimum difference between

the angles as evaluated from both sides of the cross-section, are those when the torque is applied as a set of two equal couples (case 1 in the figure).

Another important observation concerns the effect of the concentrated loads on the calculated angles of twist per unit length. The results indicate clearly that it is more accurate to evaluate the angles of twist from the lateral displacements of the nodes that are unaffected by the concentration of the applied loading, i.e. when St. Venant's principle is satisfied.

5.4.5 Evaluation of the Angle of Twist and Effect of Depth-to-

Width (D/B) Ratio

The theoretical angle of twist is calculated from the lateral displacements of the cross-section. In Figure (5.23) a typical cross-section is shown. The section is assumed to undergo rigid rotation and the warping of the sides of the cross section was neglected to simplify calculation. Thus, angles θ_1, θ_2, θ_3 and θ_4 are calculated from D_1, D_2, D_3 and D_4, associated with nodes A, B, C and D, as follows:

$$\theta_1 = \frac{1}{L} \tan^{-1} \left(\frac{x_A}{b} \right)$$

$$\theta_2 = \frac{1}{L} \tan^{-1} \left(\frac{y_B}{d} \right)$$

$$(5.1)$$

$$\theta_3 = \frac{1}{L} \tan^{-1} \left(\frac{x_C}{b} \right)$$

$$\theta_4 = \frac{1}{L} \tan^{-1} \left(\frac{y_D}{d} \right)$$

where L is the length over which the angles are evaluated.

To compare the angles θ_1, θ_2, θ_3 and θ_4, as evaluated from the two sides of the cross-section, and to check the effect of the ratio D/B on their calculation, a theoretical study was performed using an elastic analysis for different D/B ratios. Boundary conditions B/Cs 3 were used and the torque was applied as two equal couples as discussed earlier. All cross-sections have the same area and were subjected to the same torque. Figure (5.24) shows the results of the study expressed in terms of the %DIF versus D/B ratio; %DIF being the percentage difference between the angles θ_1 and θ_2 (or θ_3 and θ_4). The same results are listed in Table (5.7).

It is evident from Figure (5.24) that it is important to evaluate the angles away from the load application. If this is done it is clear, from the same figure, that if the torque is applied as two equal couples then reasonably accepted %DIF results for all practical values of D/B (say <5.0). It must be mentioned that these conclusions were applicable to elastic analysis (i.e. before cracking of concrete). In the post-cracking region the %DIF may slightly increase due to differential cracking between the two sides of the beam. This point will be further elaborated when discussing the results of the full nonlinear analysis in the following sections.

5.4.6 Effect of Boundary Conditions

Members under torsion usually provide two types of internal

torsional resistance to withstand the externally applied torques, namely circulatory torsion and warping torsion. Circulatory torsion (also known as St. Venant's torsion) provides resistance by generating shear stresses flowing in a circulatory manner on the cross section of a member. The warping torsion, on the other hand, establishes its resistance from the differential in-plane bending and shear in the component walls of the member. Warping basically means that the sections become distorted after twisting, a phenomenon which happens in all sections subjected to torsion except circular.

Generally, both types of torsion resistance occur side by side in a member subjected to torsion. Circulatory torsion predominates in solid or hollow bulky sections, although warping torsion also exists. In open thin-walled sections warping torsion predominates and circulatory torsion is very insignificant. Reinforced concrete members generally belong to the first group, hence some warping torsional resistance is expected, the amount of which depends mostly on the type of cross section and its dimensions.

Accurate modelling of warping behaviour of a cross section is coupled directly with the boundary conditions as the stress distribution at the section is affected by its distance from the supports according to St. Venant's principle. A study of this aspect of behaviour is undertaken using the developed finite element program in order to determine the most suitable boundary conditions for the problem in hand, using elastic analysis, before applying the

full nonlinear solution.

Hsu's beam B4 was chosen for the study of the effect of boundary conditions. Half the beam was considered with the 12-element mesh (Figure 5.20). A set of five different boundary conditions were examined. These are shown in Figure (5.25): (1) all nodes at one end were completely fixed to prevent any warping of the cross-section, (2) the four corner nodes were completely fixed to allow symmetrical warping to occur, (3) was similar to (2) but instead the four middle nodes were fixed, (4) two nodes only were completely fixed, this being the minimum to prevent unconstrained movement, and finally (5) all nodes at the end fixed in the x- and z-directions with only three nodes fixed in the y-direction, this being an attempt to simulate the skew-symmetry nature of the problem. The five sets of boundary conditions were designated B/Cs (1) through B/Cs (5) respectively. A torque of 4.6 KN.m was applied in each case. The elastic solutions produced the twists per unit length shown in Table (5.8).

Figure (5.26) shows the nonlinear torque/twist curves for all boundary conditions except B/Cs (4) which produced erratic results in terms of twist angles and crack patterns. Boundary condition B/Cs (1) gives a too stiff post-cracking response and a large overestimate of the ultimate torque. Furthermore, the crack pattern was not satisfactory, being initiated at the load application propagating towards the end support. B/Cs (5) produced slightly less stiff response but erratic results were observed when considering the

distortion of the cross-section at the support as shown in Figure (5.27). Moreover, the axis of the beam was continuously shifting its position with loading resulting in a considerable difficulty in computation of the twist angle. B/Cs (2) and B/Cs (3) are fairly similar, both producing acceptable crack propagation and patterns, with B/Cs (2) slightly stiffer in the post-cracking region. Because of these reasons in addition to the fact that B/Cs (3) produced the closest fit to the experiment it was therefore used for all subsequent analyses. Clearly the selection of the appropriate boundary conditions is important and the use of the minimum constraint, B/Cs (4) for example, would not seem to be sufficient. The problem of correct simulation of boundary conditions for this type of problem is not straightforward and proved to be a difficult task.

5.4.7 Effect of Shear Retention Parameters

The shear retention factor can strongly influence a nonlinear solution, especially if shear is prominent. The torsion problem is primarily a shear dominant problem and because of this dominance, and in order to isolate the effects of shear retention from those of tension stiffening, tension stiffening was assumed inactive for the study reported in this section. Its effect will be studied in the following section.

For ease of discussion of results, the shear retention parameters (β_1, β_2 and $\beta_3 \varepsilon_t'$) are recalled here. The parameter β_1 was set at 0.5, implying an assumption that 50% of the shear stiffness is lost immediately upon cracking

following the results of the deep beam previously presented. This figure has often been used before (sometimes even as a constant shear retention factor). The parameters β_2 and $\beta_3\varepsilon_t'$ were then systematically varied to study the effect of shear retention. Figure (5.28) shows torque/twist curves for beams (B4) and (G4). Results for beam (G4) show the marked effect of varying $\beta_3\varepsilon_t'$ from 0.003 to 0.0035. This confirms the importance of the rate of decay of β with increasing crack width, and of the point at which dowel action effects are assumed to act alone, after cracks widen enough for aggregate interlocking to cease, as given by β_2. The effect of β_2 can be seen from the results of beam (B4). This seems to have most influence closer to ultimate conditions, as can be seen from comparing β_2 =0.1 and β_2=0.08 for $\beta_3\varepsilon_t'$=0.003.

Optimum values for these parameters are difficult to discern because not enough experimental data is available, and so many other unknown factors are at play. Moreover, the effects of all numerical and material parameters are interrelated and it is always extremely difficult to completely isolate them from each other in any study. From this study, however, β_1 =0.5, β_2 =0.1 and $\beta_3\varepsilon_t'$=0.003 gave satisfactory comparisons with the experimental results for both beams and so were used in all subsequent analyses. The convergence tolerance was set at 10% which reasonably maintains equilibrium. The maximum number of iterations was set at 15 for all load increments in this study, following the suggestions of Al-Manaseer (ref. 15), which proved reasonable as convergence was generally obtained within the specified number of iterations.

Crack propagation with increasing torque and final crack pattern is shown in Figure (5.29) for beam (B4). In reference (5) a general description of the crack propagation is given with the final crack pattern for one beam only. The final crack pattern for this particular beam is not provided. By comparison to the given description the theoretical propagation and final pattern are both considered satisfactory and compare reasonably well with experiment.

Figure (5.30) illustrates steel stresses in all four beams. Experimental results have been predicted reasonably well. Neither longitudinal steel nor stirrups carry any significant stresses prior to cracking, confirming that the steel percentage has negligible effect on the torsional rigidity of the beam at the pre-cracking stage. The sudden jump in the steel stresses immediately after cracking is well predicted. Note also the irregular stresses in the short legs of the stirrups, a phenomenon also observed experimentally. Hsu (ref. 20) emphasised this phenomenon giving no reasons as his theory could not explain this peculiarity. In some way it could be attributed to the redistribution of excess stresses on the structure in the progressive cracking stage; being released more on the longer faces of the cross-section. This keeps the longer legs of the stirrups under increasing stresses while relieving the shorter legs.

Lengthening of the beam with increasing torque is another

experimental observation. Figure (5.31) shows this for all four beams. Again comparison between analysis and experiment is very satisfactory. The theoretical lengthening of beam was evaluated along the beam axis as was measured experimentally. The close resemblance of the unit lengthening curves and the average strain in the longitudinal steel indicates that the lengthening of the beam is due to stretching of the longitudinal bars.

The stress distribution along a typical longitudinal bar is shown in Figure (5.32) for different load levels. It can be seen that before cracking no significant stresses are carried by the bar. After cracking, stresses increase considerably. The distribution is generally uniform along the bar, as expected from a uniform torque throughout the beam. The slight increase at the ends can be attributed to the concentration of nodal forces due to the applied loads and resulting reactions. The distribution is considered quite satisfactory and consistent with the expected behaviour.

The stress distribution around a typical stirrup, after cracking, is shown in Figure (5.33). The distribution resembles the shear stress distribution for a rectangular section under pure torsion, with maximum values occuring at the middle of the longer side. St. Venant's distribution is not applicable after cracking as tests have shown that the stress is roughly uniform along the longer legs of the stirrups (ref. 20). However, the complete picture may be more complicated. Probably the continuity requirement

imposed by the finite element model and the number of elements used across the section have caused the nonuniform prediction.

Figure (5.34) compares torque/twist curves and Table (5.9) gives ultimate torques for all beams. The agreement is acceptable. Comparing beams (B2) and (B4) it can be seen that the ultimate torque and post-cracking rigidity are strong functions of steel percentage. A comparison of beams (G2) and (N2) indicates the influence of the beam size. The D/B ratio for these beams is the same and the reinforcement ratios are nearly the same, but (G4) has a cross-sectional area 2.8 times that of (N2) producing an ultimate torque about 4.5 times higher. Hsu (ref. 20) pointed out that the law of similitude does not hold in the case of torsion of rectangular reinforced concrete sections and suggested further research in this phenomenon. Its study is of importance because in model testing the ultimate torque of a model is usually assumed to be linearly related to that of the prototype.

5.4.8 Effect of Tension Stiffening Parameters

To discuss the effect of tension stiffening on this type of analysis, the tension stiffening model described in Chapter Four is recalled. With shear retention parameters adopted from the previous section as $\beta_1 = 0.5$, $\beta_2 = 0.1$ and $\beta_3 \varepsilon'_t = 0.0035$, several values for the tension stiffening parameters (α_1 and α_2) were examined. The maximum number of iterations was specified as 15 and two values for the convergence tolerance were considered, namely 10% and 1%.

The value of 1% was used because it was noticed that using any values of tension stiffening parameters a stiff response was obtained as reflected in the torque/twist curves.

Figure (5.35) shows torque/twist curves for Hsu's beam (B4) using different values for the tension stiffening parameters and two values for the convergence tolerance. It is evidently clear from the figure that all values of tension stiffening parameters produced unacceptably stiff initial post-cracking response. However, at a later stage the curves seem to compare reasonably well with the experiment and the no-tension stiffening curves. Furthermore, the ultimate torques predicted with the inclusion of tension stiffening were only slightly higher than those predicted with no-tension stiffening. This can probably be attributed to the nature of the torsional cracking as distinctly different from flexural cracking.

Consider a simple beam subjected to an increasing central load. The flexural cracks starts at the bottom surface in the region of maximum moment, spreading out-wards. If the same beam was subjected to an increasing pure torque, "spiral" cracks are expected which can spread all over the span much quicker than flexural cracks. So, in flexural cracking the top part of the beam acts a compression zone until, possibly, very late stage of loading. This compression zone is capable of taking a great amount of stresses as a result of redistribution of tensile stresses from the cracked tensile zone during the loading process until yielding and/or crushing takes place. In torsional

cracking, on the other hand, no definite compression zone exists and cracks occur in all faces almost simultaneously. Therefore the compression zone is only represented by the planes parallel to the crack directions, where concrete is already weakened by the cracks.

Hsu and Mo (refs. 23, 24) refer to this phenomenon as softening of concrete. Hence, this explains the importance of the shear transfer model rather than the tension stiffening model in torsion analysis. Indeed the results of using a convergence tolerance of 1% (considered enough for tight equilibrium) shows clearly that tension stiffening would still result in overestimation of the torsional response anyway.

The stiff response of tension stiffening can be further demonstrated by studying the steel response. Figure (5.36) shows the steel response for beam (B4) with different tension stiffening parameters. The underestimation of the steel stresses is very clear when using tension stiffening at all.

5.4.9 Effect of Solution Algorithm

As mentioned earlier in Chapter Four, several algorithms can be chosen at will as to when to recalculate the stiffness during each load increment. This has its effect on the final results, depending on the type of the structure, type of loading, increment size etc. In all results discussed so far the stiffness is calculated at the beginning of each load increment where it remains unchanged during that increment

(Nalgo = 3). It was noticed that this procedure needed many iterations (sometimes the maximum specified number) at crack initiation despite the good behaviour following that up until failure. This is due to the severe nonlinearity that results from the quick spread of torsional cracking as already described in the previous sections. Indeed this has been reported by Hsu (ref. 20) where a horizontal plateau was noticed upon cracking.

It can be argued, however, that the clarity and existence of this horizontal plateau, depends largely on the beam size, D/B ratio and the reinforcement ratio. It is clearer in beams with lesser amount of reinforcement and/or with smaller cross-section. This trend is markedly reflected in the predicted curves and so on these basis the difficulty of solution convergence, as reflected in large number of iterations performed at crack initiation, is considered satisfactory and far from worrying. It is also well known that the steel, in the torsion problem, does not contribute to the stiffness and does not carry any significant stresses until after concrete cracks. As this was well, as shown earlier, the performance of the model was considered satisfactory.

But in order to improve the convergence process at crack initiation and further study the effect of the solution algorithm on the overall response, another solution algorithm was applied (Nalgo = 5). Here the stiffness is updated at iterations 1 and 8 of each load increment. Figure (5.37) shows the results of using this algorithm against the

previous one. Although the convergence process at cracking totally improved, it is evidently clear that there is no much improvement on the overall response despite the fact that better ultimate torque is now predicted. As recalculation of the stiffness costs much more than the resolution of the resulting simultaneous equations, and after comparing the cost of both analyses (Nalgo = 3 and Nalgo = 5) it was clear that the first is advantageous to use.

5.4.10 Conclusions

From the results presented in the previous sections the following points are concluded:

(1) The developed three dimensional nonlinear finite element model simulates the pure torsional behaviour of reinforced concrete rectangular beams within acceptable accuracy. In particular, torque/twist curves, ultimate strenghts, beam lengthening and steel behaviour were all predicted well.

(2) This indicates that the smeared fixed orthotropic crack model, used in this work, is an adequate approximation as long as proper attention is paid to selecting appropriate shear transfer properties through the shear retention factor.

(3) The results demonstrate the importance of proper modelling of shear transfer and illustrate the overestimation of the structural response that may result if tension stiffening is used where torsional shear is dominant.

(4) It is very important that the correct boundary conditions are chosen to allow appropriate warping behaviour to occur. This might seem a basic and straightforward task. However, it proved to be crucial for accurate predictions of torsional behaviour especially after concrete cracking. Improper modelling of boundary conditions results in unexpected basic responses, such as the crack propagation, because of its effect on the stress distribution near the support.

(5) The results of this section, combined with the previous two sections, indicate clearly that although the nonlinear finite element model reasonably predicts the behaviour of a variety of reinforced concrete problems, care and proper judgement must be used to identify what parameters affect the particular situation in question. Generally, when shear dominates the shear retention factor is more important and tension stiffening may be neglected alltogether or used with very small values of its parameters. On the other hand, when flexure dominates the tension stiffening may be more important and hence could be used. However, the tension stiffening parameters proved to be very difficult to assess as demonstrated by the results of the shallow beam simulating beam-column behaviour.

5.5 Application on Rectangular Beams Subjected to Combined Loading

5.5.1 Introduction

Combined loading is the reality of most reinforced concrete

structures. Many experimental studies have been conducted to investigate the behaviour of reinforced concrete beams sustaining combined bending, torsion and shear. However, this combined behaviour has apparently not been investigated by finite element models. This is mainly because of the presence of torsion which ideally needs full three dimensional modelling for complete treatment compared to flexure and shear which can be satisfactorily dealt with using two dimensional models. Therefore, the capability of the finite element model developed in this work has also been checked for such type of loading.

5.5.2 Beams Chosen for the Study

Collins et. al. (ref. 25) tested two series of rectangular reinforced concrete beams under combined bending and torsion. All beams contained both longitudinal and transverse reinforcement. Beams of one series (series RE) had equal top and bottom longitudinal reinforcement while those of the other series (series R) had unequal top and bottom reinforcement. Of the first series . the beams designated (RE4) and (RE2) were chosen for this study, because they had the same cross section and amount of reinforcement but differ only in the torque/moment ratio. There was also reasonable amount of information on their behaviour.

5.5.3 Beams Description and Finite Element Mesh

The beams have a 10x6.5 in. (254x165 mm) cross-section. They had been tested over an 8-ft (2438 mm) span, one end being clamped against torsion and the other end being free to

twist. The bending load was applied at the one-third points and the torsion was applied at the free end by means of hydraulic jacks. The jacks were hydraulically interconnected so that during the test the ratio of torsion to bending remained constant. The load was experimentally applied in about 10 increments up to failure. The only difference between the two beams was the torque to moment ratio, being 0.88 for (RE4) and 2.61 for (RE2).

Figure (5.38) and Table (5.10) show the beams details and material properties. The figure also shows different finite element meshes used in the analysis. All bars were placed at their exact positions. For Beam (RE4) the load was applied in equal increments of T=0.666 KN.m and M=0.757 KN.m (to give about 15 load increments up to the experimental failure load), the ratio T/M being automatically maintained the same during the analysis at 0.88. For beam (RE2) the load was applied in equal increments of T=0.744 KN.m and M=0.285 KN.m (for the same reason as RE4) maintaining the T/M ratio at 2.61.

5.5.4 Results and Discussions
Beam (RE4) was analysed first using 12 elements, a mesh found suitable for Hsu's beams (previously discussed). The shear retention parameters were set at β_1 =0.5, β_2 = 0.1 and $\beta_3 \epsilon'_t$ =0.0035 for all analyses, the values found suitable for pure torsion problems. Tension stiffening parameters could have actual influence in this situation because of the presence of the flexural loading, therefore a study of its effect was undertaken, following the conclusions of the previous

section. Figure (5.39) shows a comparison between the reported experimental curve and the predicted curves,for beam RE4, using different values for the tension.stiffening parameters. The no-tenstion stiffening curve shows very flexible behaviour after cracking. It is also clear that different tension stiffening parameters (α_1 and α_2) produced different post-cracking response. α_1 =0.25 and α_2 =5.0 seemed to have given the best fit to the experimental curve. However, it can be clearly seen that the ultimate load prediction was not much affected. Even the no-tension stiffening model predicted almost the same ultimate load.

In order to study the mesh size effect the 24-element mesh shown in Figure (5.38) was used. Figure (5.40) shows torque/twist curves for different tension stiffening parameters. The effect of increasing the number of elements is insignificant in the early part of the curves. However, near ultimate conditions the mesh with higher number of elements produced a more flexible response. This may well be expected. But the difference was not considered significant. It can also be seen that α_1 =0.25 and α_2 =5.0, for the 24-element mesh, predicted a failure load close to that predicted by the 12-element mesh.

The longitudinal steel response is shown in Figure (5.41) for all four corner bars at a cross-section within the constant moment region. It can be seen that initially the top bars carried compressive stresses while the bottom ones carried tensile stresses. The magnitudes of these stresses were practically equal. This agrees well with the fact that

torsion does not produce any steel stresses before cracking and hence the steel stresses were only due to flexure. So before cracking top and bottom bar stresses are expected to be the same in magnitude but of different signs (compressive top and tensile bottom). After cracking and upon further loading the torsion induces tensile stresses in all four bars. These stresses increase the bottom bar stresses (tension + tension) and decrease the top bar stresses (tension + compression). At a certain load level, very close to failure, the stresses in the top bars become tensile, though of small magnitudes. The experimental steel response was not provided in reference (25) and hence detailed comparison was not possible.

Theoretical crack pattern for the 12-element mesh is shown in Figure (5.42). When compared to the predicted crack pattern for Hsu's beam (Figure 5.29), the difference is markedly clear. The pure torsion cracking tend to spread fairly quickly all over the beam soon after crack initiation. In the case of combined loading, the top surface of the beam within the constant moment region remains intact, serving as a compression zone, until very close to failure. These distinct behaviours seemed to have been well predicted. No experimental crack pattern was given for either of the two beams to compare with.

The beams were reported to have failed by yielding of the bottom steel and formation of compression hinge at the top surface (termed mode 1 failure by the authors). The theoretical analysis showed yielding of both bottom bars and

crushing of concrete at the top Gauss points in concrete within the constant moment zone, a clear indication of good prediction of the failure mode.

Figure (5.43) shows the torque/twist curves for beam (RE2). Again the behaviour was predicted with reasonable accuracy. Only the 24-element mesh was used for this beam. Figure (5.44) shows the predicted steel response. No experimental curves were provided, however, but the predicted response was considered satisfactory. Similar to the response of beam (RE4), the bottom longitudinal bars carried tensile stresses for the whole loading stages, while the top bars carried compressive stresses first which changed sign at the ultimate conditions.

5.5.5 Conclusions

The following conclusions are drawn from the results discussed in the previous section:

(1) The finite element model predicts the behaviour of reinforced concrete rectangular beams under combined loading reasonably well. Proper attention must be paid to selecting the adequate material parameters. The choice of the shear retention parameters follows that for the case of pure torsion whereas tension stiffening parameters have been studied.

(2) The overall behaviour (torque/twist curves) is predicted within a reasonable accuracy. The distinct difference between the pure and combined loading cracking behaviour is

demonstrated.

(3) Although no experimental steel response was provided, the theoretically predicted response is reasonable. No ill-behaviour is noticed.

(4) The tension stiffening parameters can influence the post-cracking stiffness markedly with no great effect on the predicted ultimate load. Use of tension stiffening may be important in the case of combined loading because of the presence of flexure. However, low values of tension stiffening parameters are recommended (typically $\alpha_1 = 0.25$ and $\alpha_2 = 5.0$).

5.6 General Conclusions and Overall Assessment

From the results presented and discussed in this chapter, the following main conclusions are re-stated:

(1) The three dimensional nonlinear finite element model offered has the capability of being used for different applications. But, as well expected with nonlinear models, care must be taken when applying it to a particular type of analysis. Each type of application is sensitive to, and more affected by, different solution and material parameters. These have been investigated and discussed for each of the applications considered.

(2) Partially intended for the analysis of torsion of reinforced concrete, the model was found quite capable to handle both cases of pure and combined torsion.

(3) The three dimensional smeared fixed orthotropic crack model, employed throughout this work, is an adequate approximation when proper modelling for shear retention and tension stiffening is incorporated.

(4) The proper choice of boundary conditions for torsion is also important and must be taken care of to allow for proper warping effects to take place.

(5) In Chapter Three the analysis termination criterion was mentioned. For all analyses presented in this chapter, the maximum number of iterations of 15 was found adeqaute with a global search through the diagonal of the stiffness matrix for detection of zero or negative pivots. A zero or negative pivot was always detected beyond the ultimate load and was always associated with very large displacements, severe cracking, yielding and/or crushing. The criterion is, therefore, considered satisfactory.

(6) In all applications considered, cracking of concrete is found to be the major source of nonlinearity in the structural response which significantly modifies the behaviour, in particular greatly reduces the post-cracking stiffness.

(7) The force convergence criterion employed is adequate to monitor equilibrium and the nonlinear solution proved to be very stable. Different convergence tolerances were studied including the coarse 10% and the practically tight 1% values, and a value of 10% can be suitable for most applications.
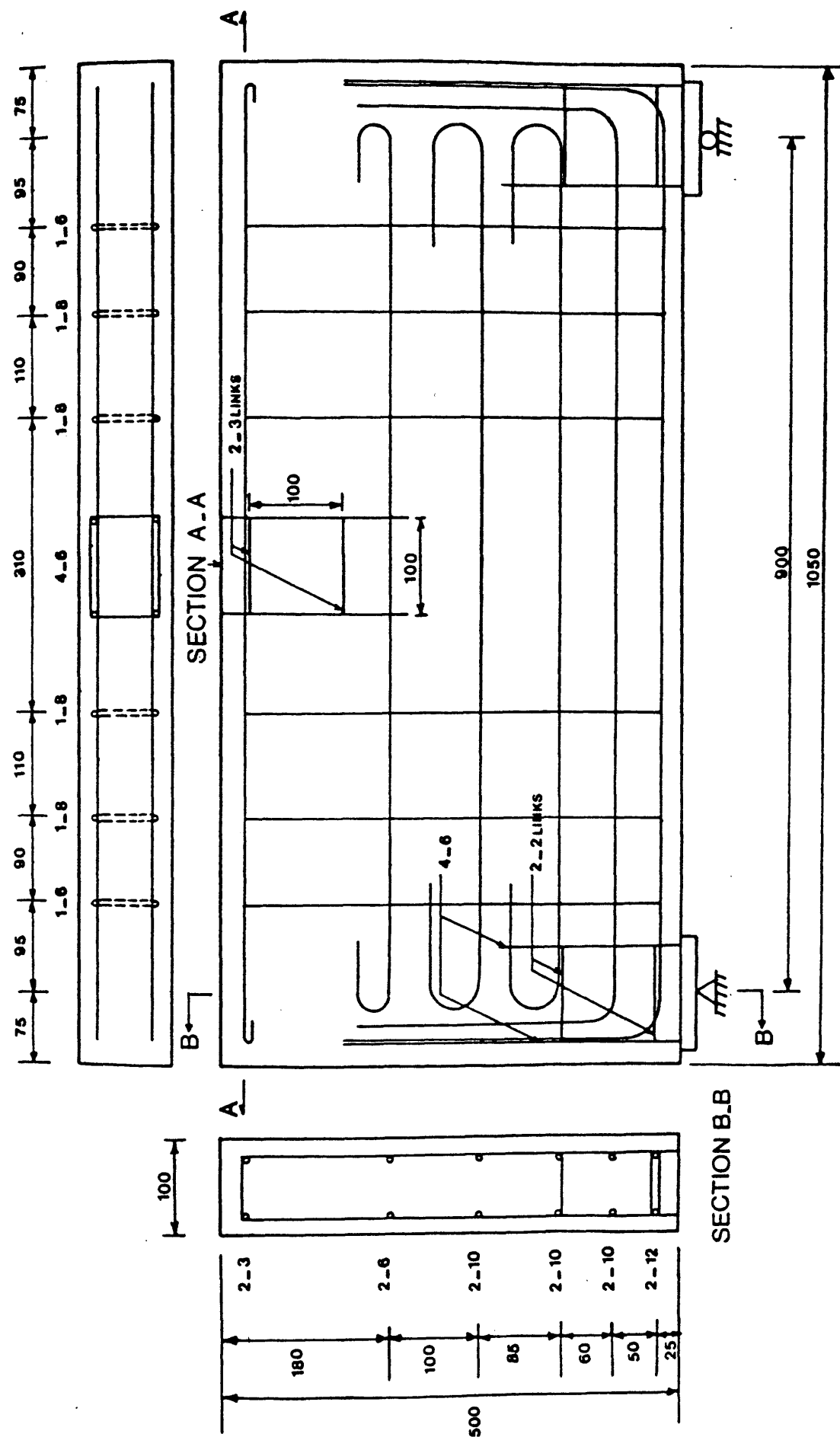
Figure (5.1) Details of Lin's deep beam 101 (ref. 13)
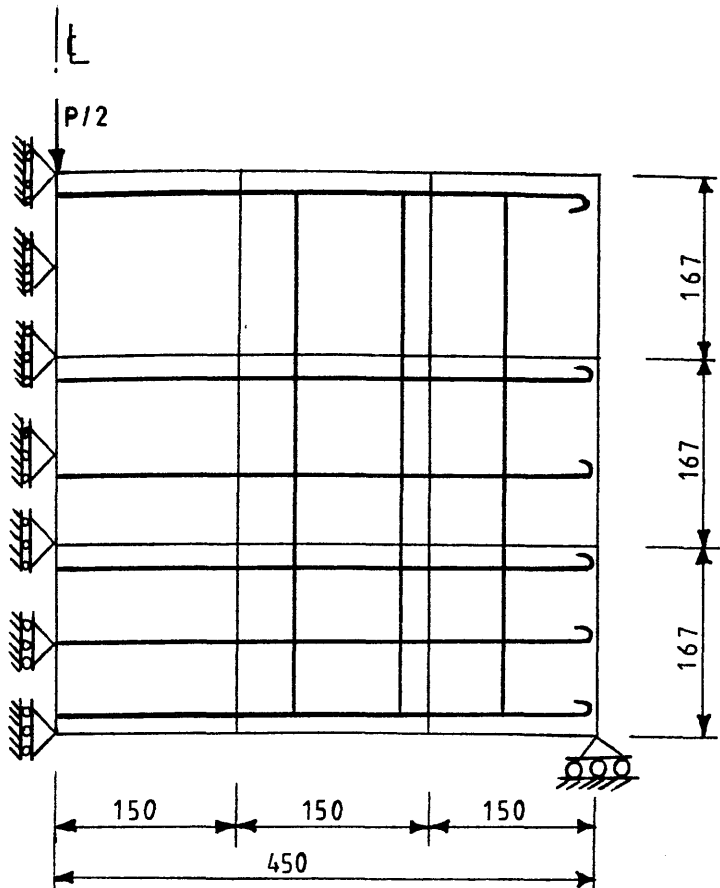
Figure (5.2) Finite element mesh for Lin's deep beam 101,
9-elements, one element across the width
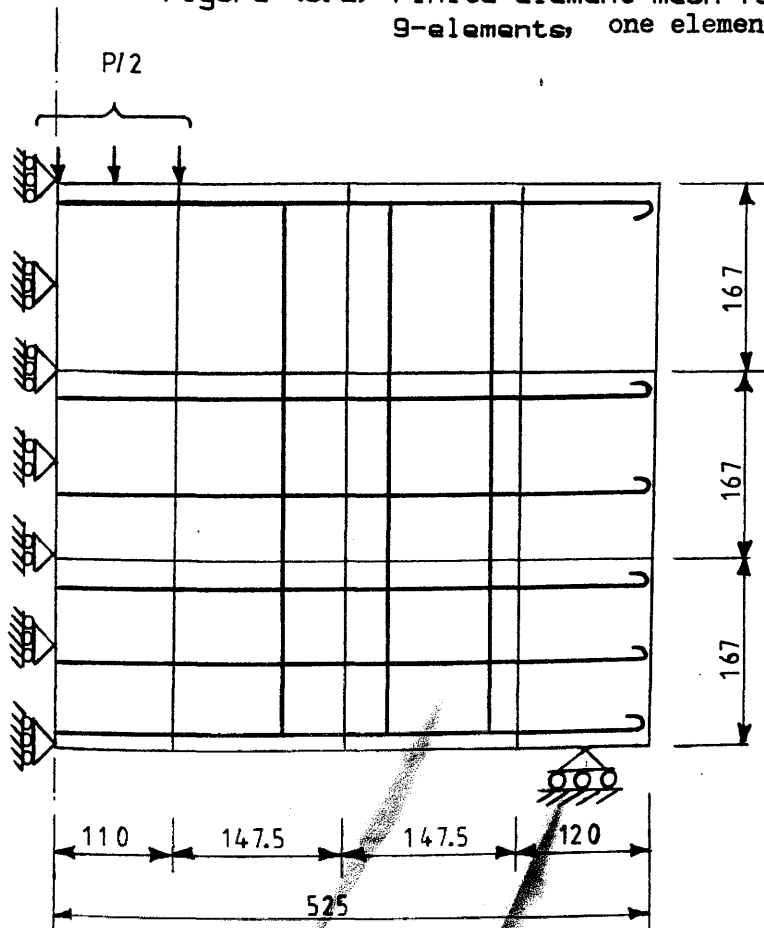
Figure (5.3) Finite element mesh for Lin's deep beam 101,
12-element mesh, one element across the width

Table (5.1) Properties of concrete for Lin's deep beam (101)

L/D	Width (b) (mm)	Depth (D) (mm)	f_{cu} (N/mm2)	f'_c (N/mm2)	f'_t (N/mm2)	E_c (KN/mm2)	ν_c
1.8	100.0	500.0	47.0	36.0	3.07	19.0	0.20

Table (5.2) Properties of steel for Lin's deep beam (101)

Bar diameter (mm)	E_s (KN/mm^2)	f_y (N/mm^2)	E_w% (N/mm^2)
6	217.3	245.8	10.0
8	188.7	225.9	10.0
10	293.6	229.7	10.0
12	263.5	323.0	10.0
16	276.7	322.5	10.0

Table (5.3) Results of the effect of boundary conditions and load application on Lin's deep beam (101). Values of the central displacement for an elastic load of 40.3 KN

	Case 1	Case 2	Case 3	Case 4	Case 5
δ	0.0809	0.0421	0.0582	0.0572	0.0430
Ratio $\dfrac{\delta}{\delta_{exp}}$	1.046	0.760	1.051	1.032	0.7760
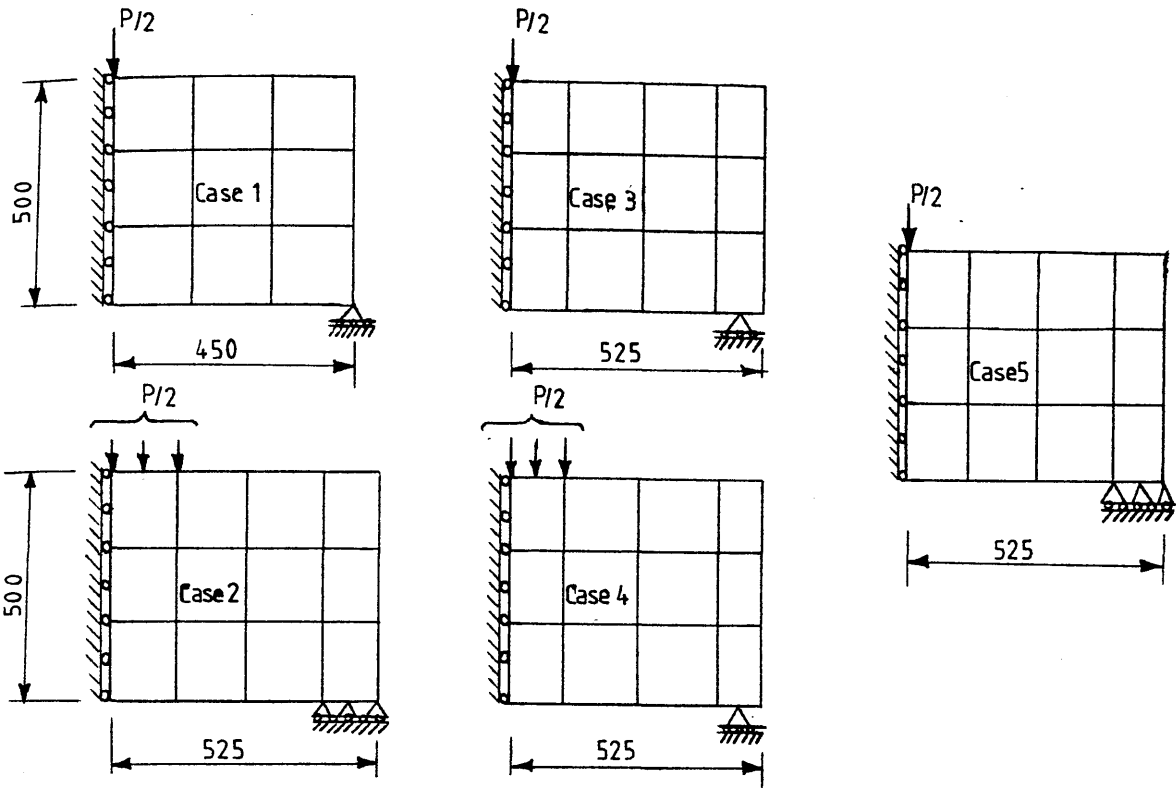
Figure (5.4) Study of boundary conditions and load application for Lin's deep beam 101
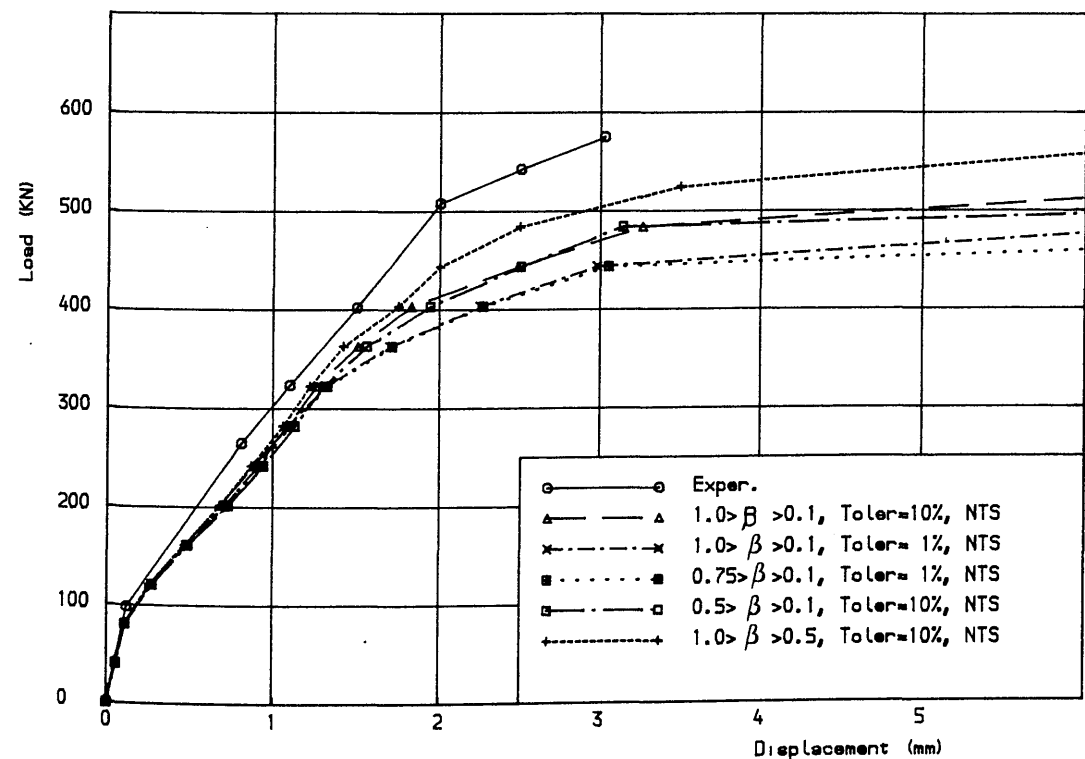
Figure (5.5) Effect of shear retention parameters on the load-deflection behaviour of Lin's deep beam (101), $\beta_3 \varepsilon'_t = 0.004$.
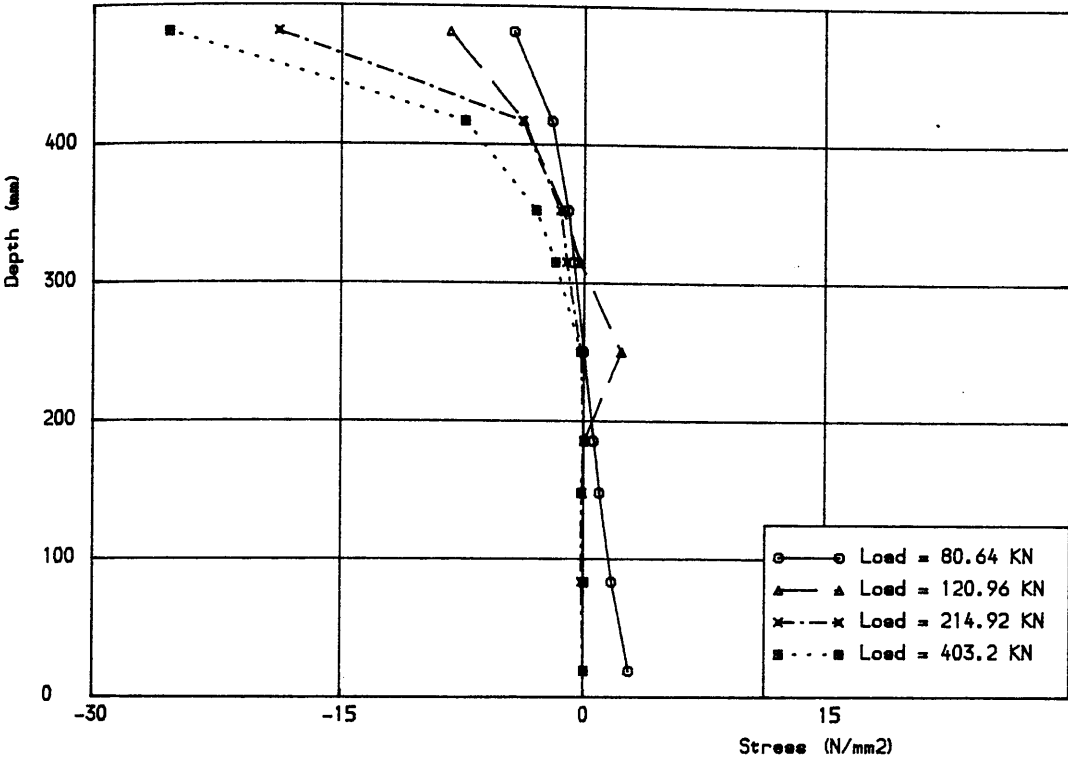
Figure (5.6 a) Stress distribution across the section at 55 mm from centre line for Lin's deep beam (101).
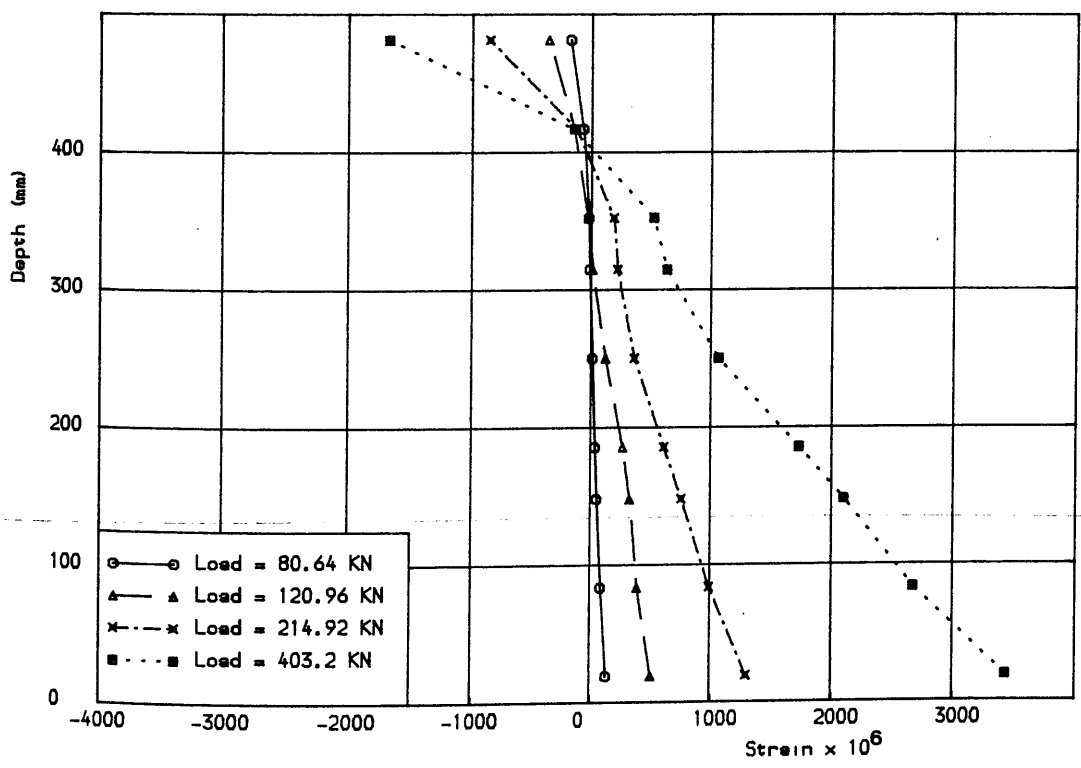
Figure (5.6 b) Strain distribution across the section at 55 mm from centre line for Lin's deep beam (101).
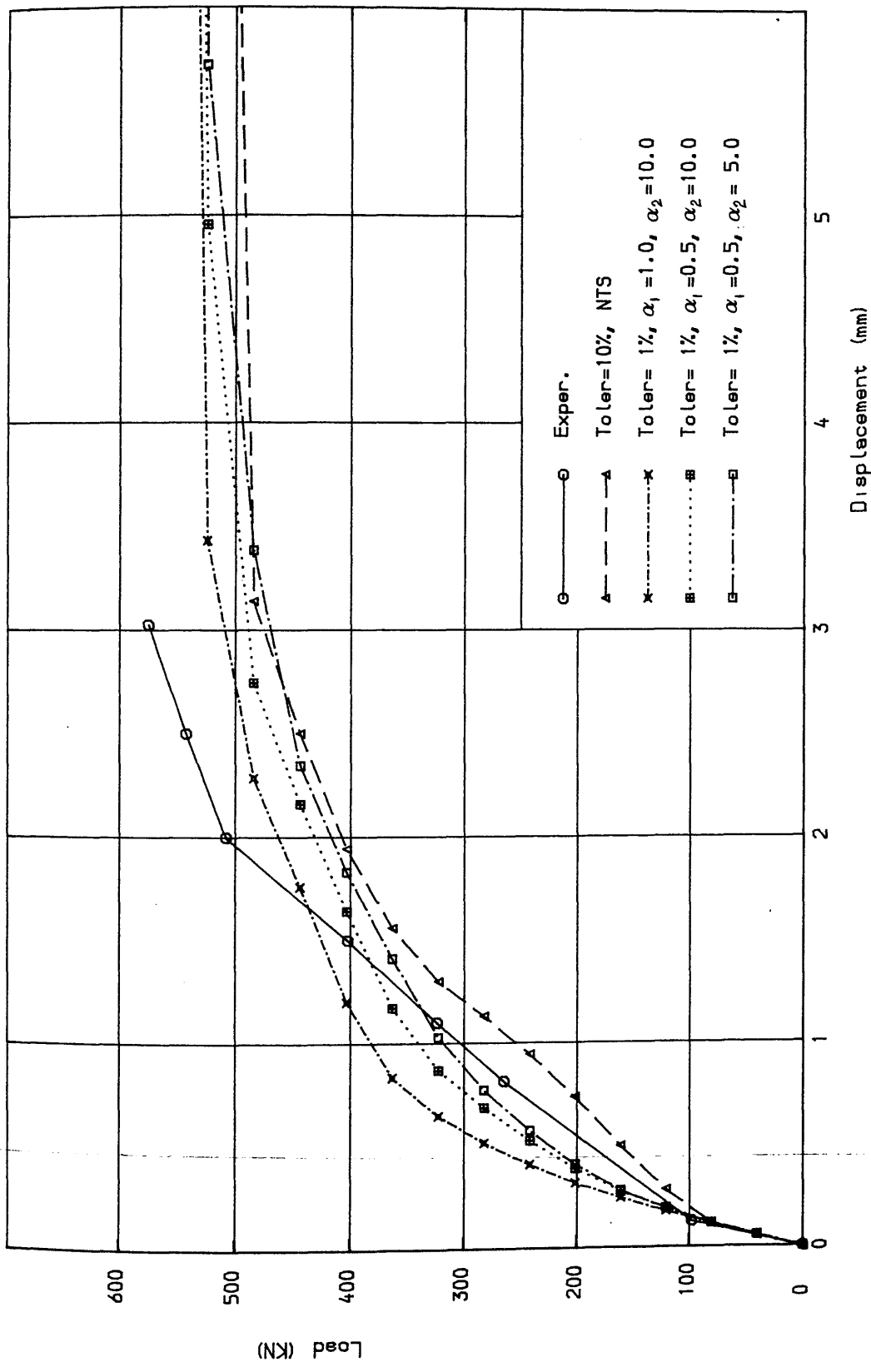
Figure (5.7) Effect of tension stiffening parameters on the load-deflection behaviour of Lin's deep beam (101), $0.5 > \beta > 0.1$, $\beta_3 \varepsilon_t' = 0.004$.

Legend:

Exper.

Toler=10%, NTS

Toler= 1%, $\alpha_1 = 1.0$, $\alpha_2 = 10.0$

Toler= 1%, $\alpha_1 = 0.5$, $\alpha_2 = 10.0$

Toler= 1%, $\alpha_1 = 0.5$, $\alpha_2 = 5.0$

Displacement (mm)

Load (KN)
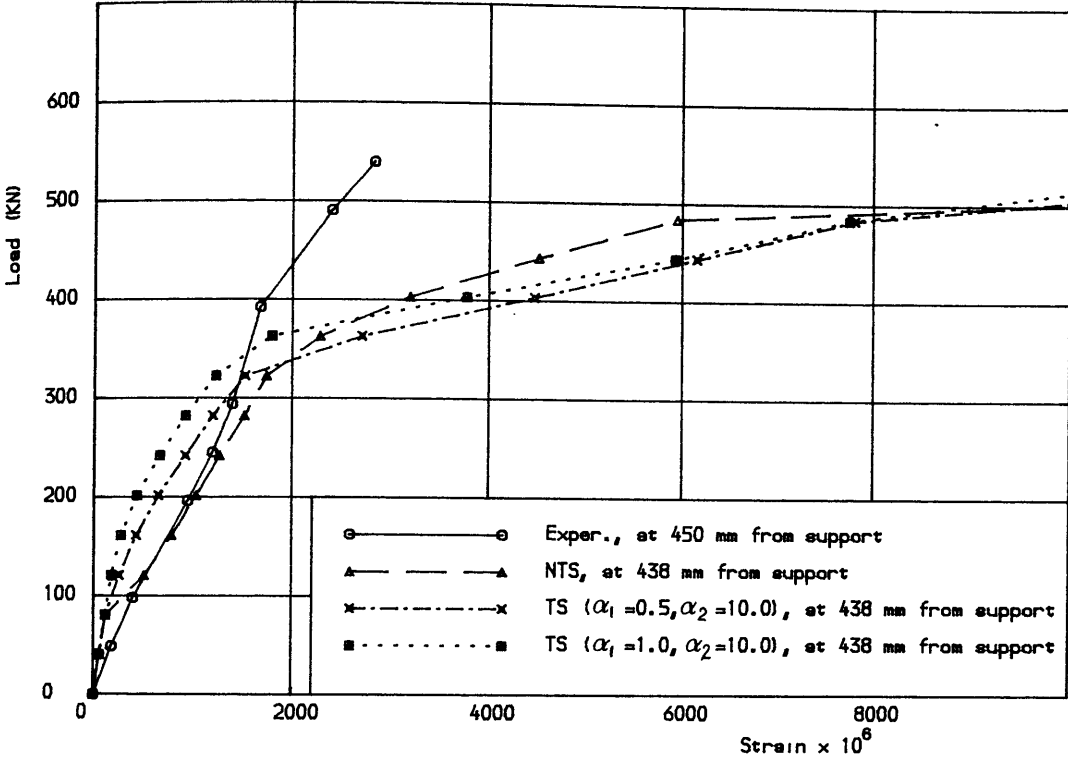
Figure (5.8 a) Effect of tension stiffening parameters on the longitudinal
bottom steel strain for Lin's deep beam (101)
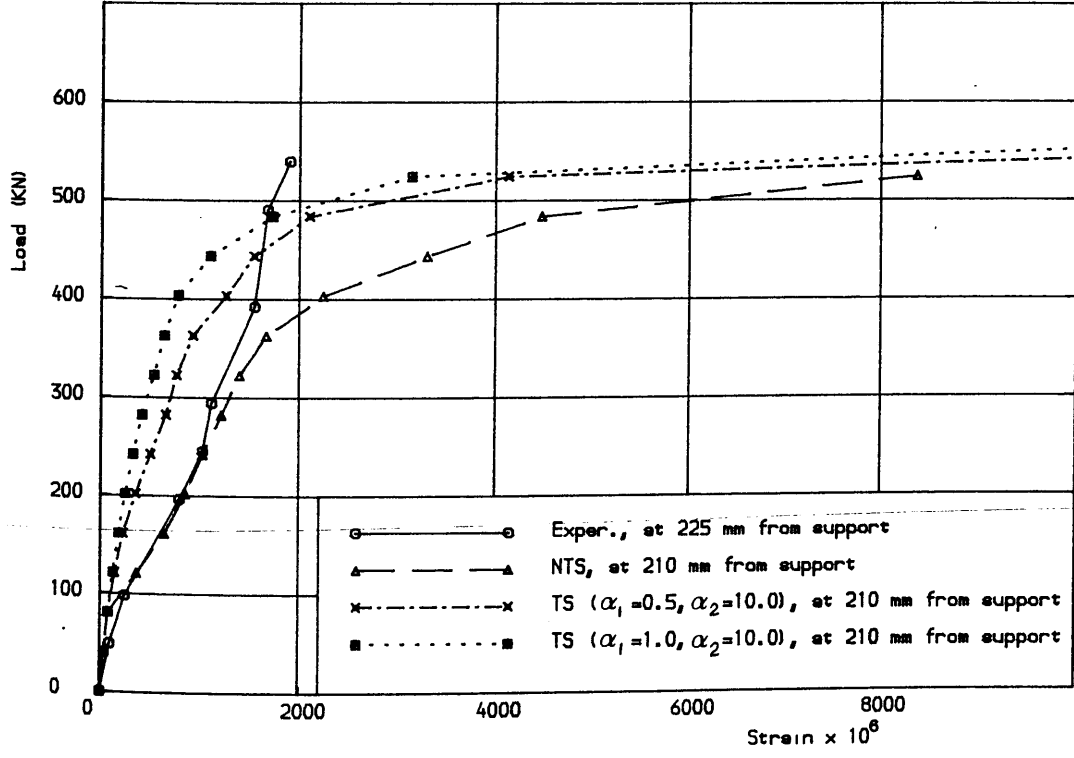
Figure (5.8 b) Effect of tension stiffening parameters on the longitudinal
bottom steel strain for Lin's deep beam (101)
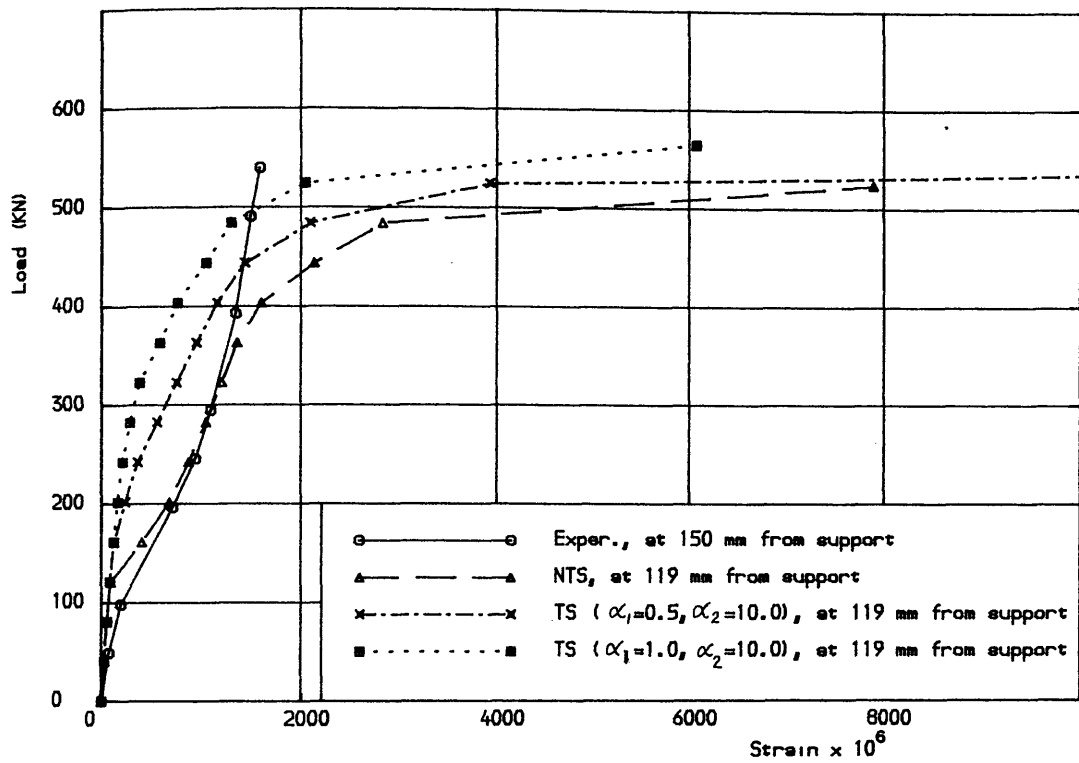
Figure (5.8 c) Effect of tension stiffening parameters on the longitudinal bottom steel strain for Lin's deep beam (101)

P=564 KN

(c)

P=161.3 KN

(a)

P=201.6 KN

(b)
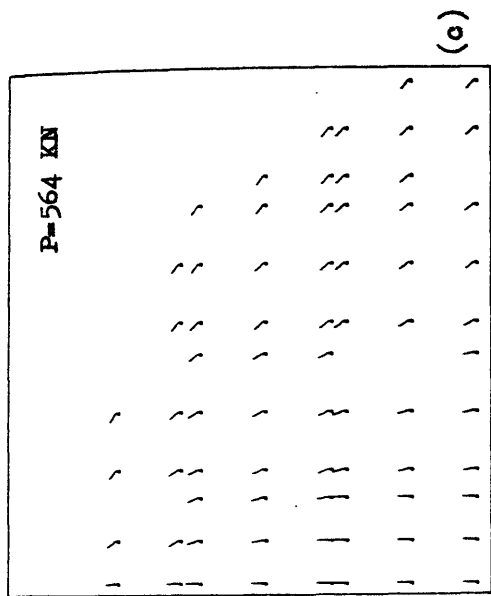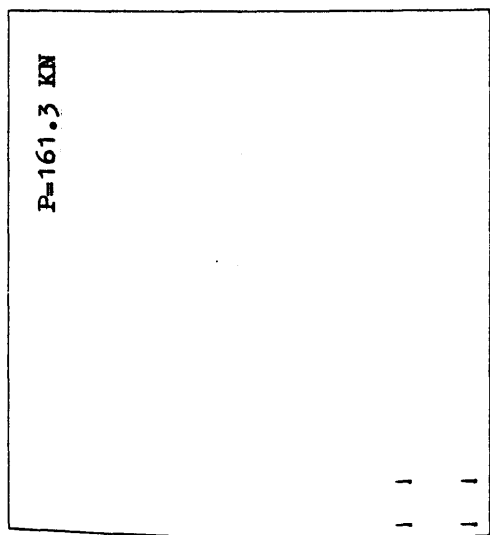
Figure (5.9) Predicted crack pattern for Lin's deep beam (101)

Lin 101

crushing
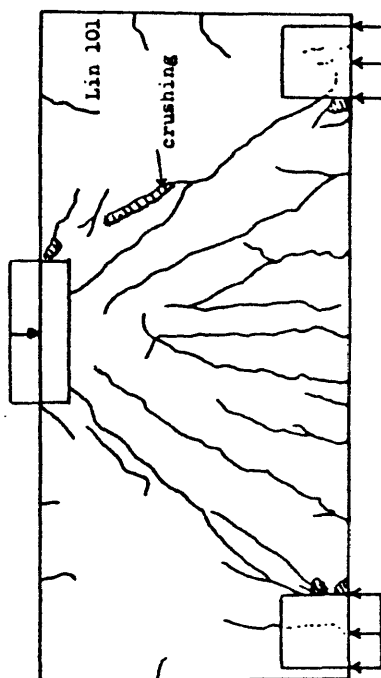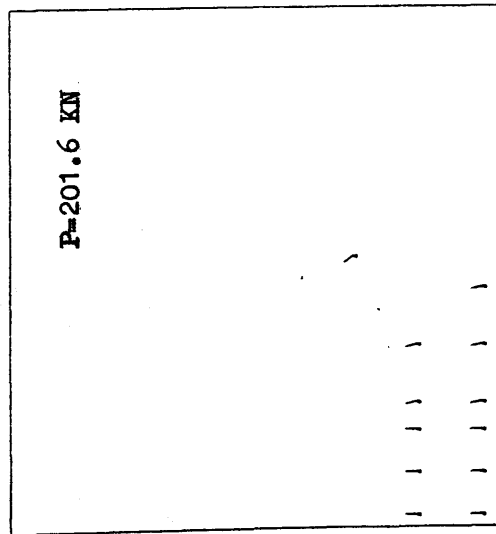
Figure (5.9 d) Experimental crack pattern at load = 575.0 KN
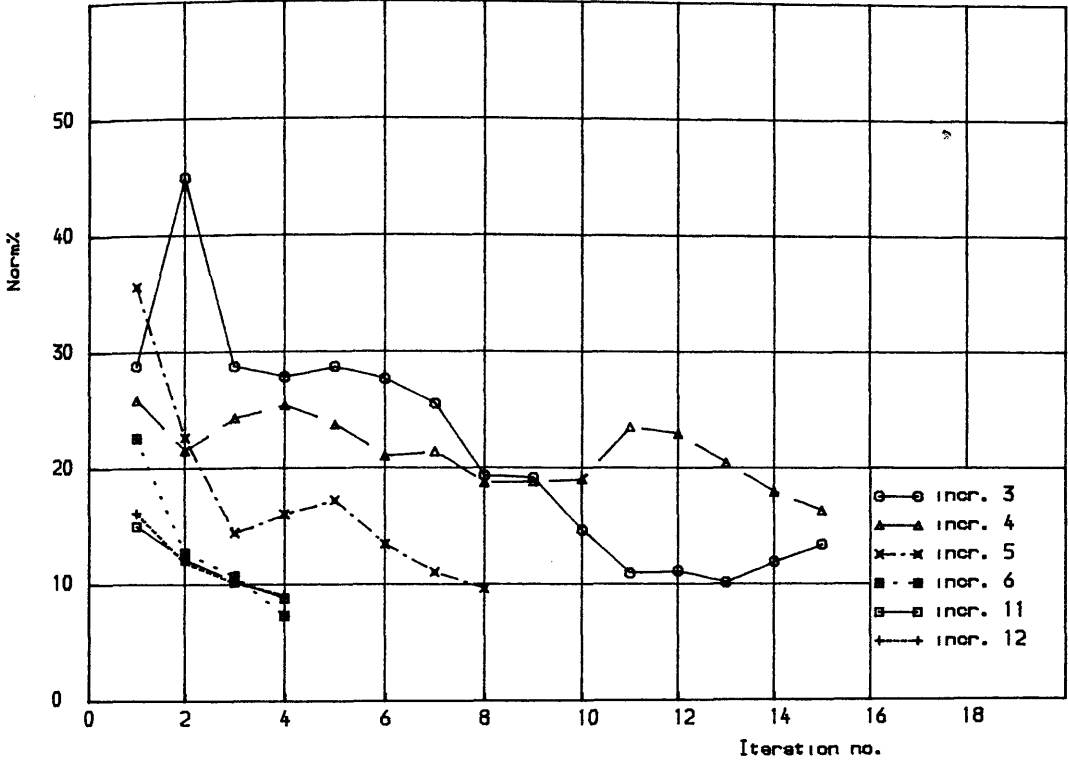
Figure (5.10 a) Study of rate of decay of residual forces for Lin's
deep beam (101). NTS (Toler=10%)
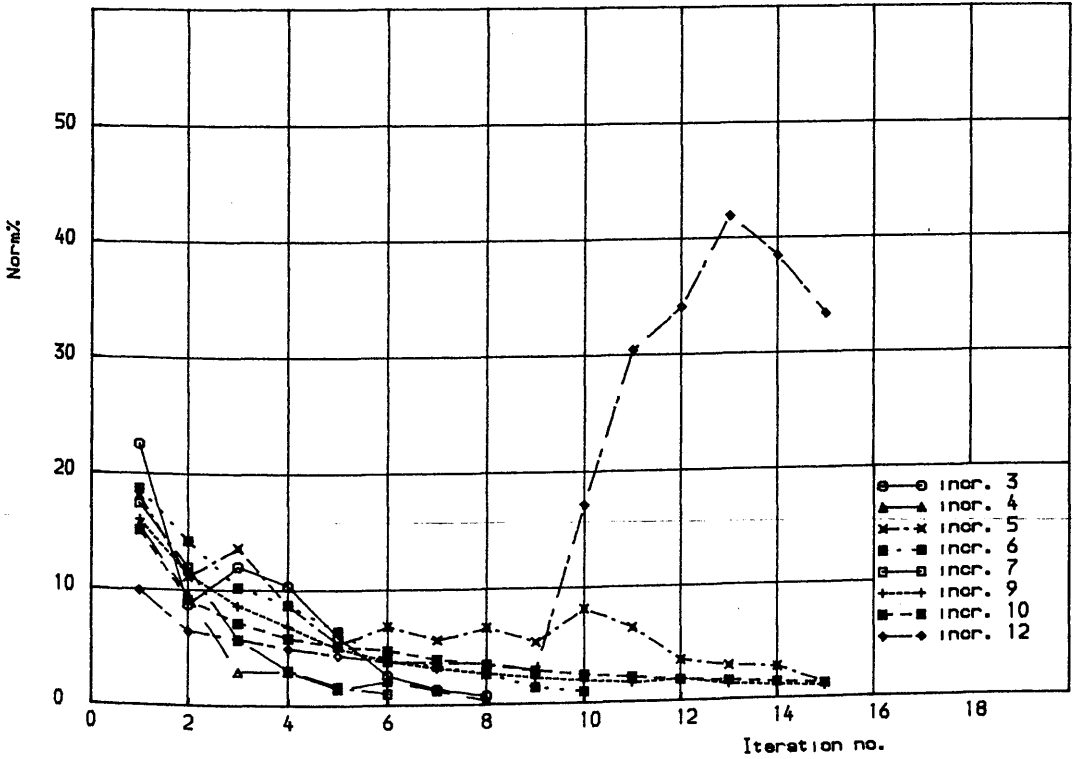
Figure (5.10 b) Study of rate of decay of residual forces for Lin's
deep beam (101), TS (α1=0.5, α2=5.0, Toler= 1%)
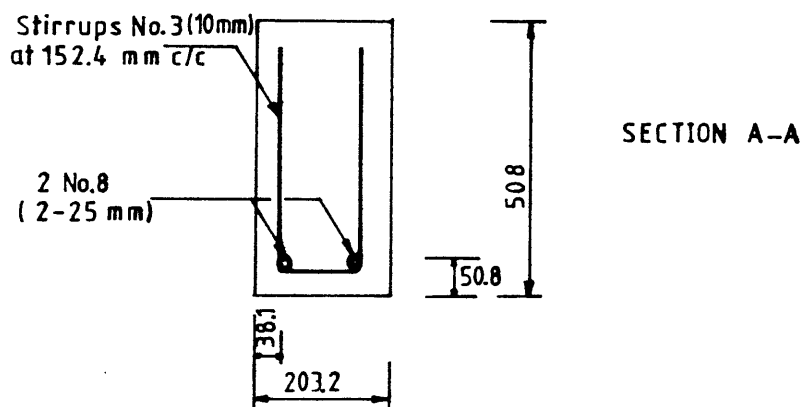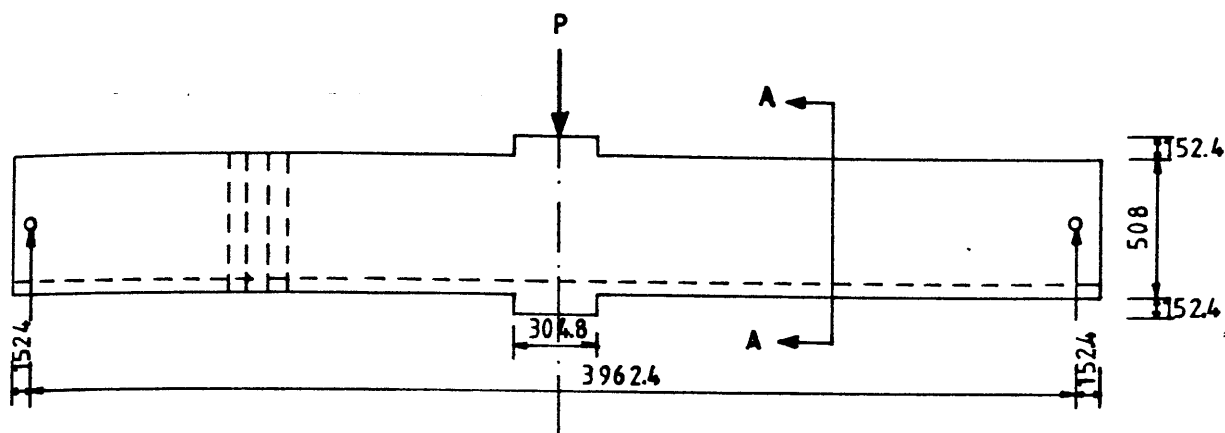
Figure (5.11) Details of Burns and Siess beam J4 (ref. 16)
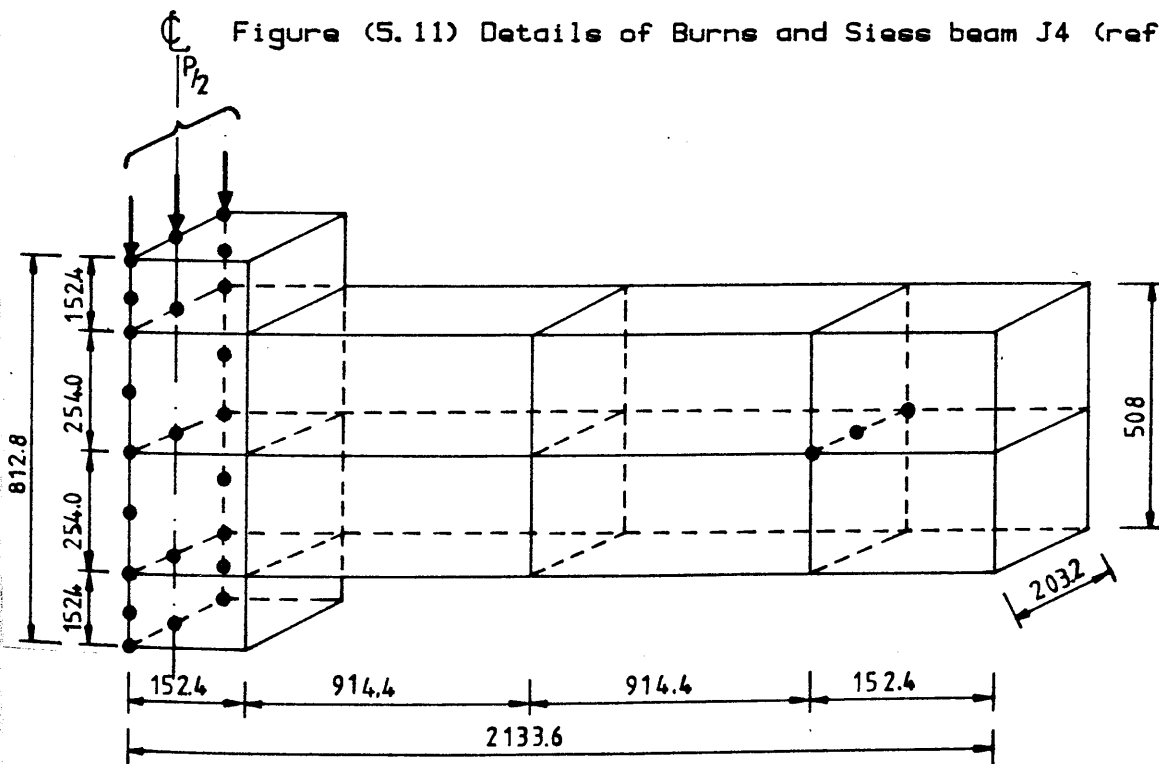
- Supported node

Figure (5.12) Finite element mesh for Burns and Siess beam J4

Table (5.4) Details of material properties for Burns and Siess
        beam (J4)

f'_c N/mm^2	f'_t N/mm^2	E_c* KN/mm^2	ν_c*	A_s mm^2	f_y N/mm^2	E_s KN/mm^2	E_w* KN/mm^2
53.0	3.77	28.4	0.20	1012.9	309.7	210.0	0.0

* assumed values
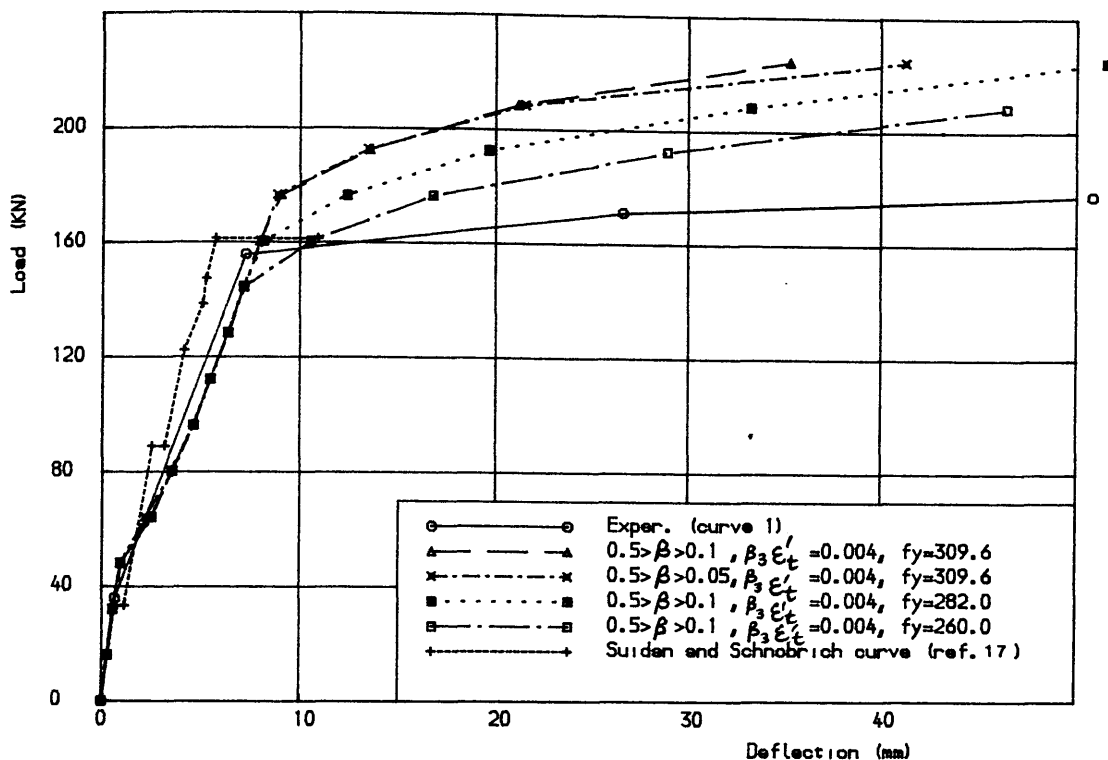
Figure (5.13) Effect of shear retention parameters and steel yield values on the load-deflection behaviour of Burns and Seiss beam (J4)
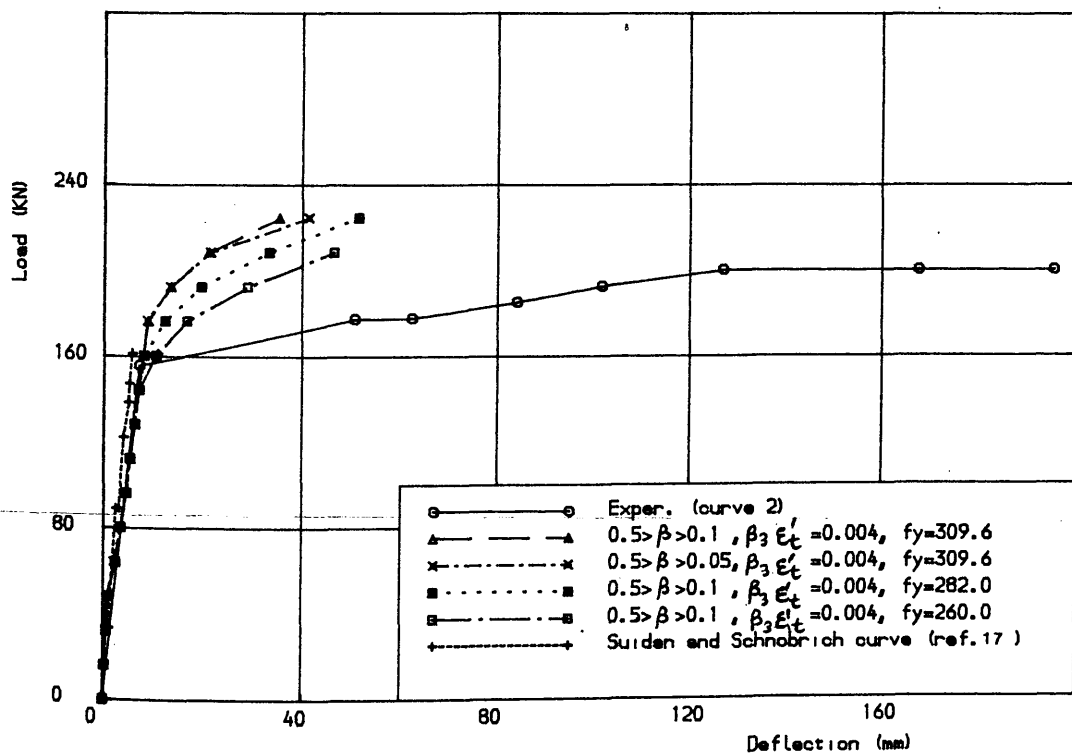
Figure (5.14) Effect of shear retention parameters and steel yield values on the load-deflection behaviour of Burns and Seiss beam (J4)
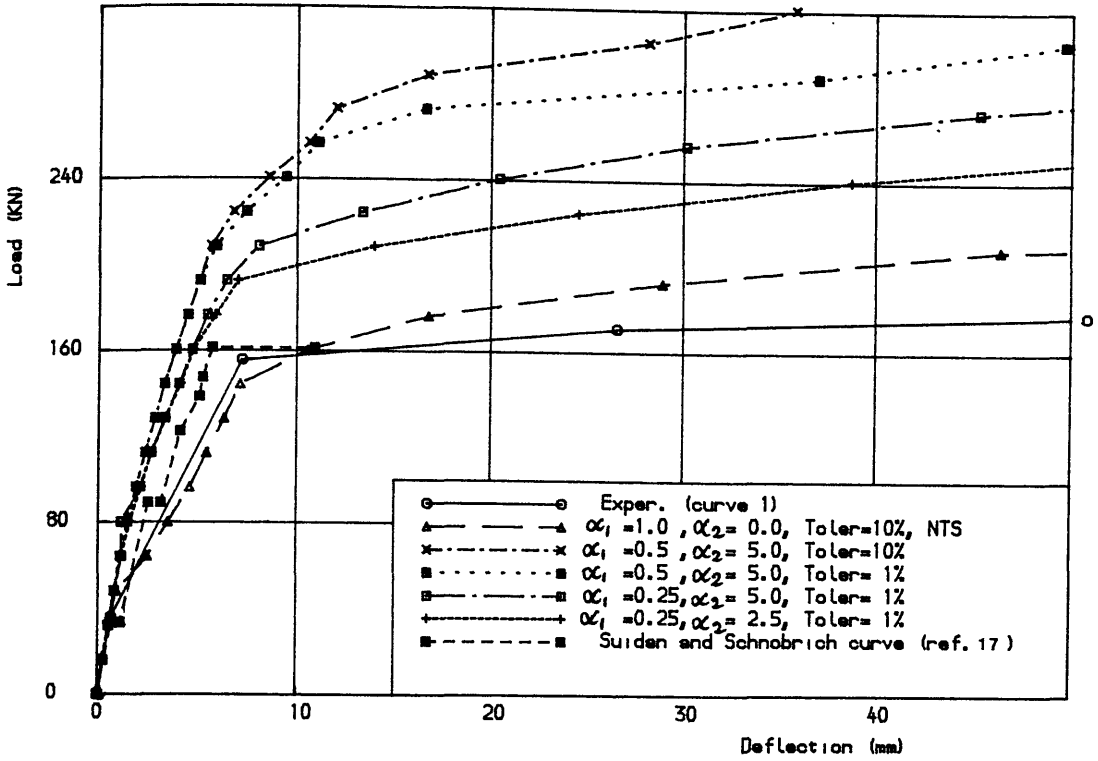
Figure (5.15) Effect of tension stiffening parameters on the load-deflection
behaviour of Burns and Seiss beam (J4)
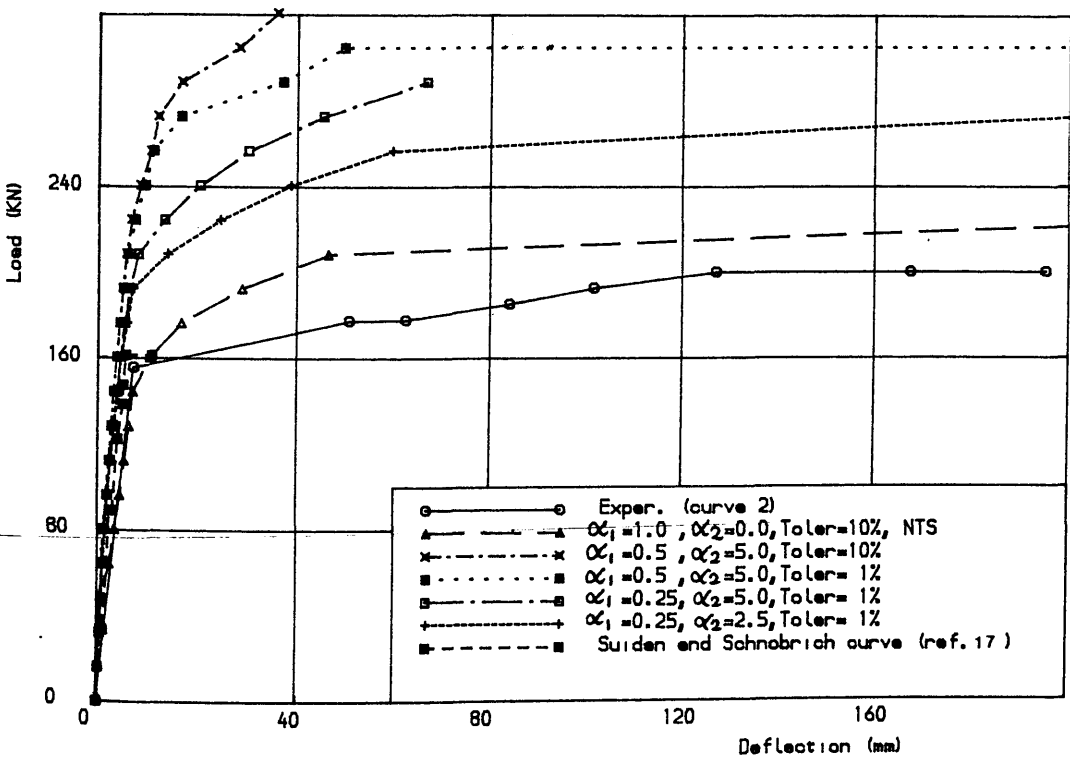
Figure (5.16) Effect of tension stiffening parameters on the load-deflection
behaviour of Burns and Seiss beam (J4)
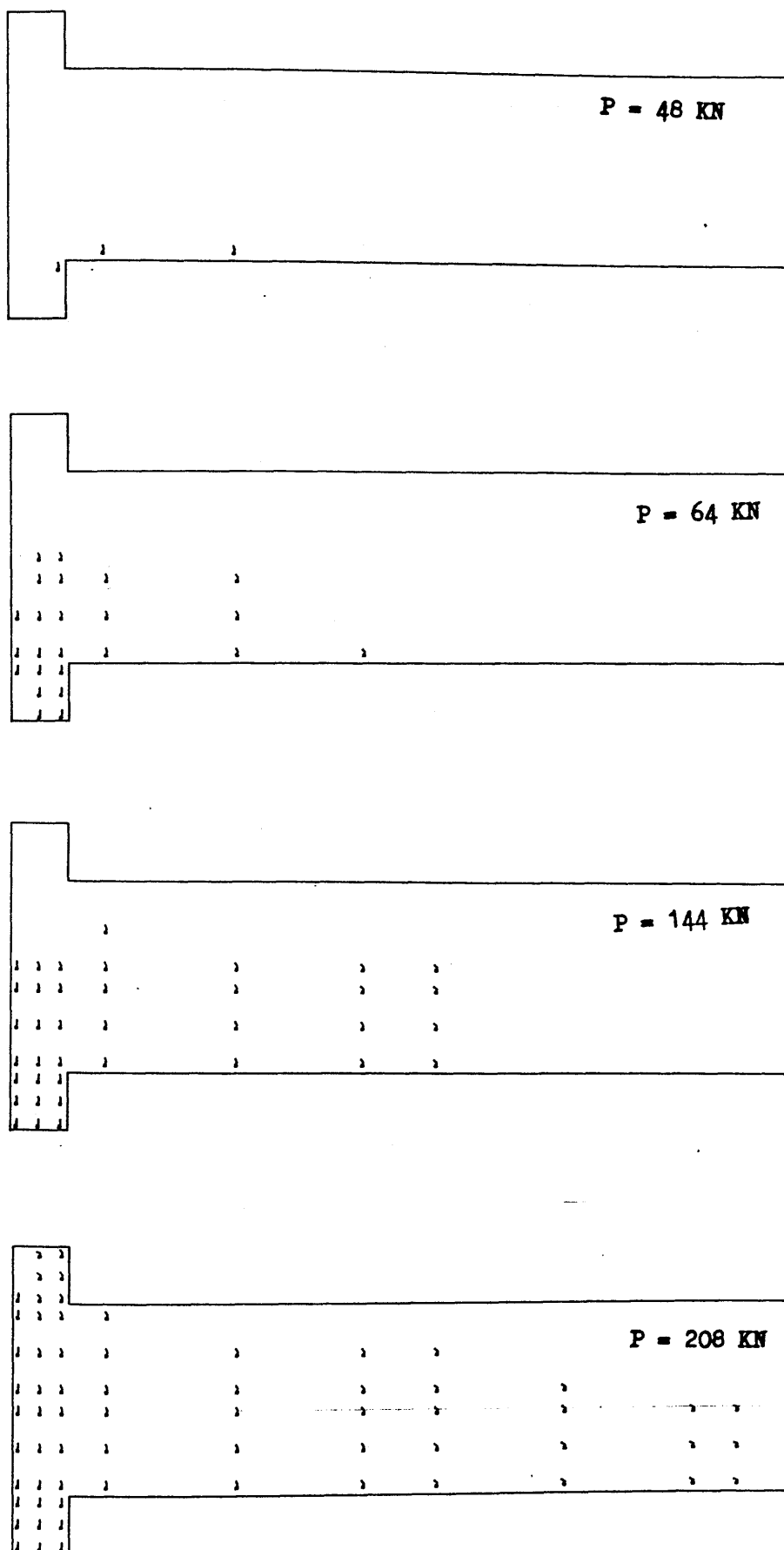
Figure (5.17) Predicted crack pattern for Burns and Siess
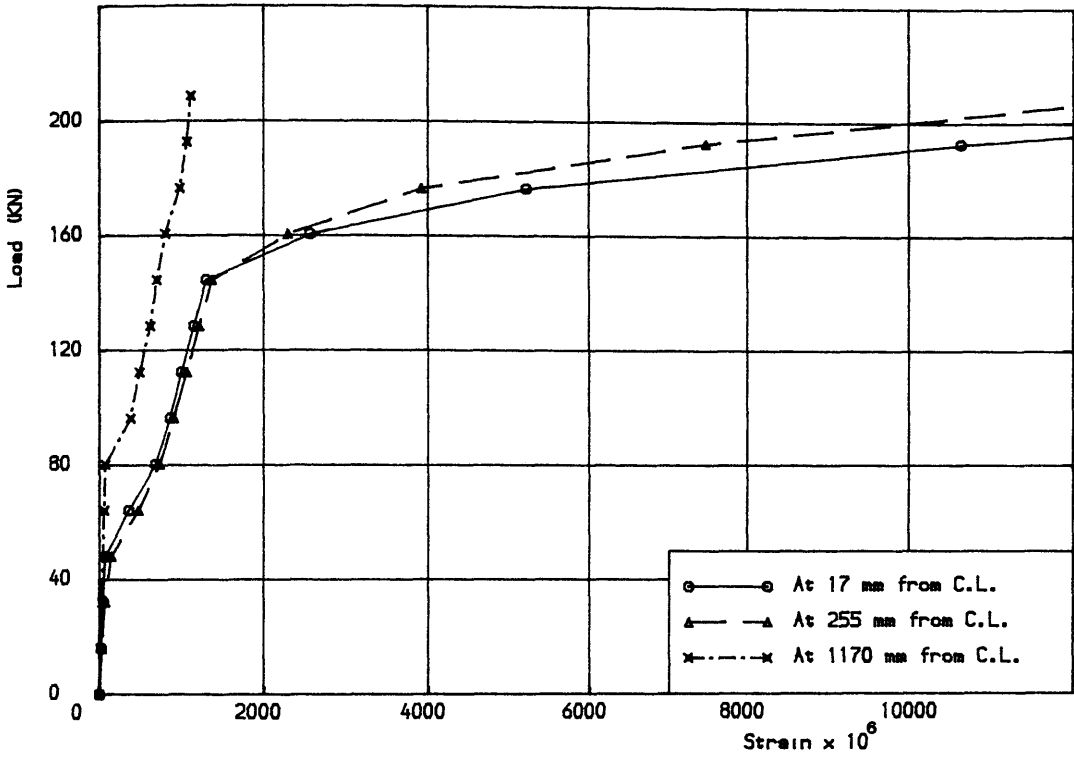
beam (J4)

*Figure (5.18) Load vs theoretical bottom longitudinal steel strain for
Burns and Seiss beam (J4)*

(b) cross section

30% additional reinforcement

Clamped in loading head
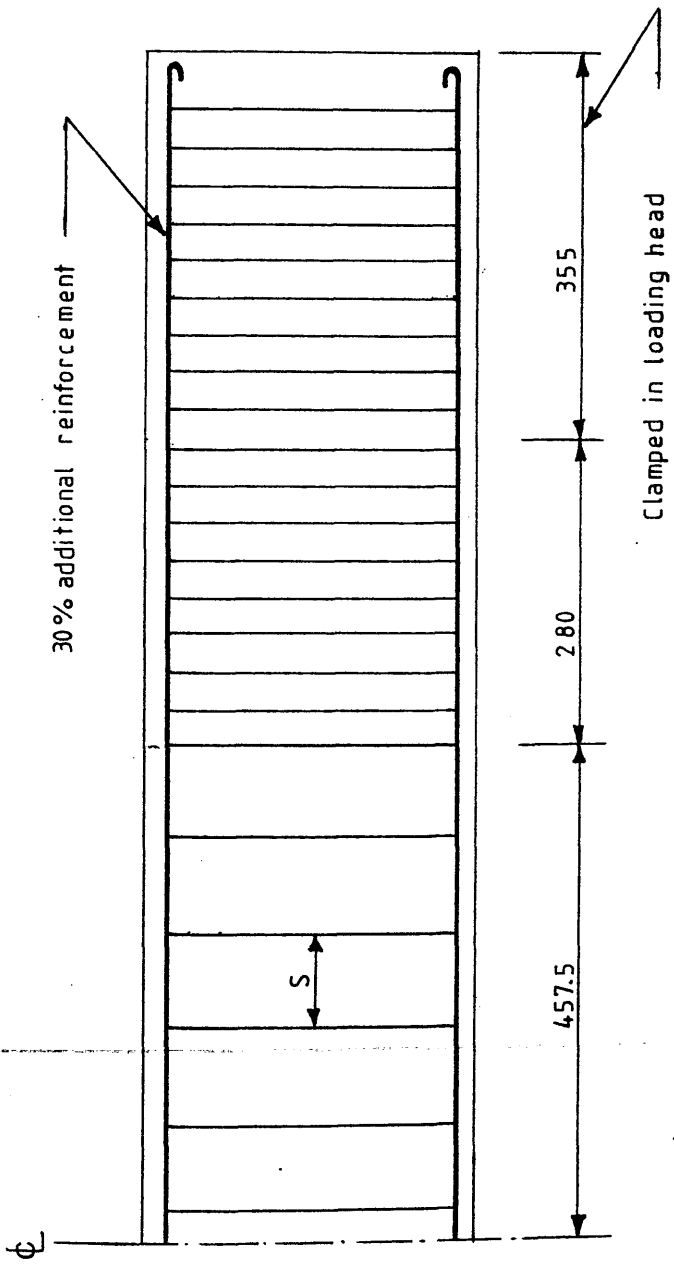
(a) dimensions and reinforcement
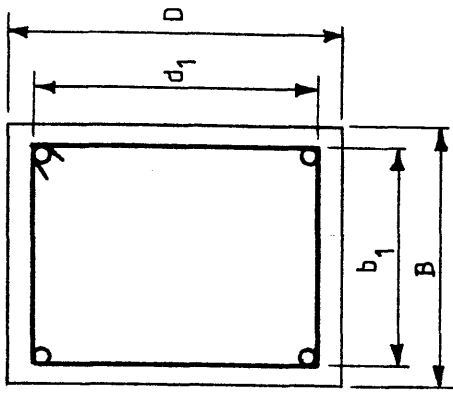
Figure (5.19) Details of Hsu's beams

Table (5.5) Details of Hsu's Beams

Beam	B (mm)	D (mm)	b_l (mm)	d_l (mm)	D/B	s (mm)	Φ_v* (mm)	Φ_l* (mm)	ρ_v %	f_{yv} (N/mm^2)	A_l %	f_{yl} (N/mm^2)	ρ_l %	E_s (KN/mm^2)	f_c' (N/mm^2)	f_t' (N/mm^2)
B2	254	381	216	343	1.5	181	12.7	15.88	0.823	320	0.827	316	1.65	196.5	28.6	3.13
B4	254	381	216	343	1.5	92	12.7	22.22	1.61	323	1.60	320	3.21	196.5	30.5	3.14
G4	254	508	216	470	2.0	114	12.7	22.22	1.20	321	1.20	325	2.40	196.5	28.3	3.08
N2	152	305	130	283	2.0	51	6.35	22.22	1.13	338	1.11	331	2.24	196.5	30.4	3.36

*Converted from psi units

Subscripts: v denotes stirrups, l denotes longitudinal steel
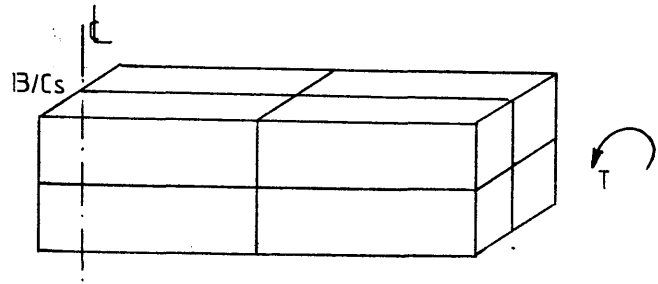
8-elements 81 nodes
243 D.O.F.
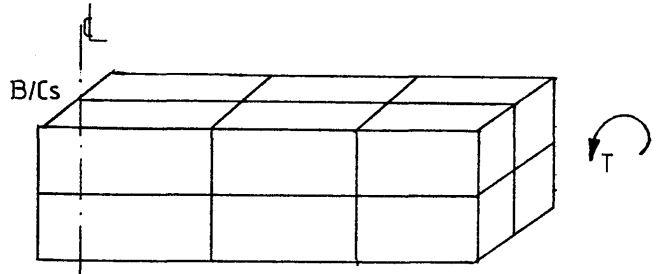
12-elements 111 nodes
333 D.O.F.
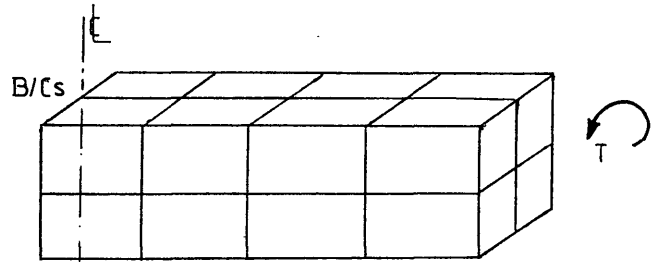
16-elements 141 nodes
423 D.O.F.
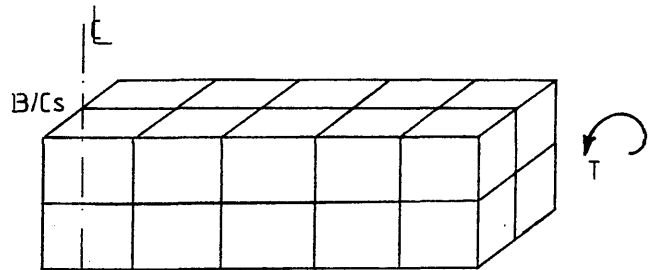
20-elements 171 nodes
513 D.O.F.
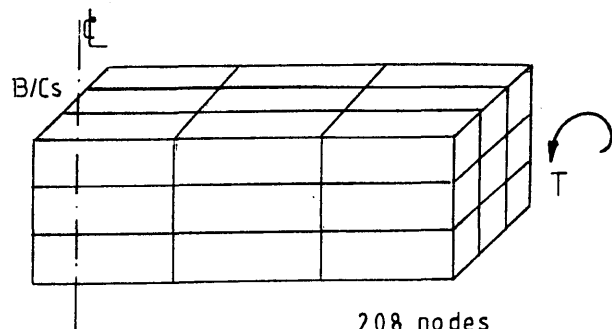
27-elements 208 nodes
624 D.O.F.

Figure (5.20) Different finite element meshes examined
for Hsu's beams
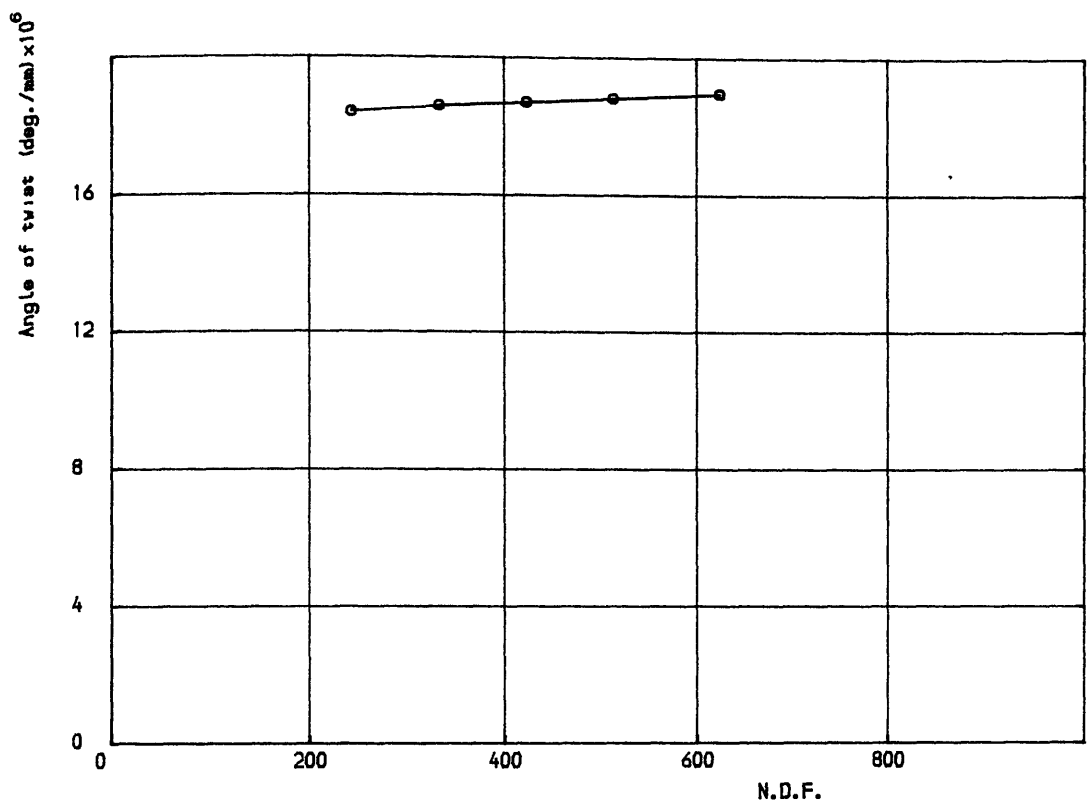
Figure (5.21) Mesh convergence study for Hus's beam (B4). Average angle of twist per unit length vs total number of degrees of freedom
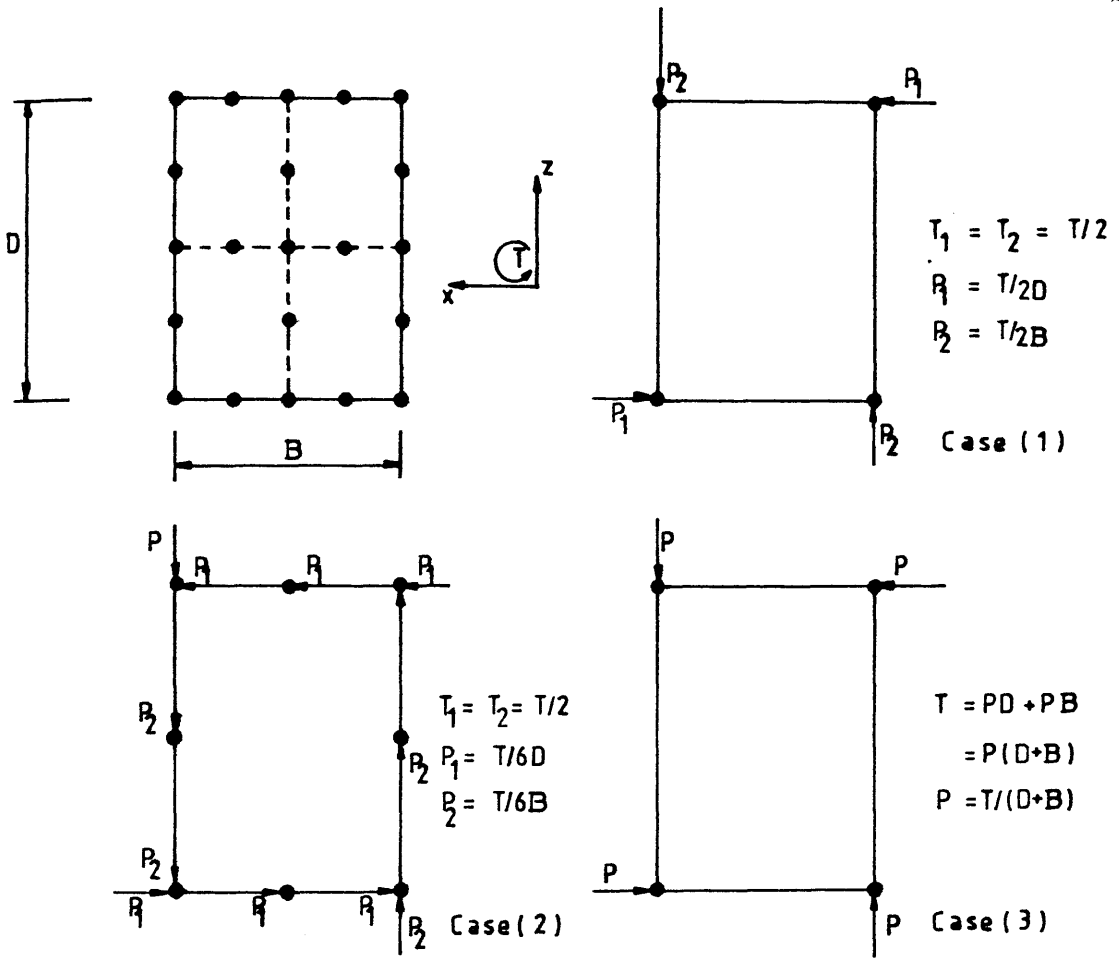
Figure (5.22) Different load applications for Hue's beams

$T_1 = T_2 = T/2$

$P_1 = T/2D$

$P_2 = T/2B$

Case (1)

$T_1 = T_2 = T/2$

$P_1 = T/6D$

$P_2 = T/6B$

Case (2)

$T = PD + PB$

$\quad = P(D+B)$

$P = T/(D+B)$

Case (3)
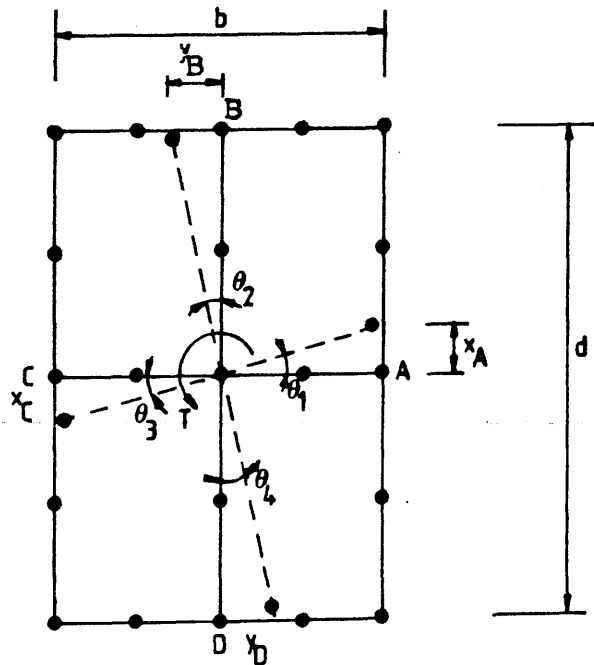
Figure (5.23) Evaluation of the theoretical angle of twist
for rectangular sections

Table (5.6) Results of the effect of load application on

Hsu's beam (B4)

	Load Case	1	2	3
Angles from displacements at free end	θ_1	17.19	17.31	16.73
	θ_2	18.94	19.33	18.88
	%DIF	10.18	11.67	12.85
Angles from displacements at 305 mm from free end	θ_1	19.44	19.56	18.53
	θ_2	19.53	20.13	19.37
	%DIF	0.46	2.91	4.53

Table (5.7) Effect of ratio D/B on evaluation of the angles of twist of rectangular sections subjected to pure torsion. Applied elastic torque = 4.6 KN.m

D/B	Angles from displacements 305 mm from free end		Angles from displacements at free end			
	θ_1	θ_2	θ_1	θ_2	%DIF(1)	%DIF(2)
1.0	18.36	18.36	16.99	16.99	0.0	0.0
1.5	19.44	19.53	17.19	18.94	0.46	9.24
2.42	23.90	24.32	20.37	24.33	1.73	16.28
4.3	34.82	36.47	29.45	36.71	4.52	19.78
6.72	48.70	53.01	41.76	53.28	8.13	21.62
10.0	***** Beam cracked *****					

%DIF(1) = % difference between the angles of twist evaluated from the longer and shorter sides 305 mm from the free end (where the load is applied)

%DIF(2) = % difference between the angles of twist evaluated from the longer and shorter sides at the free end
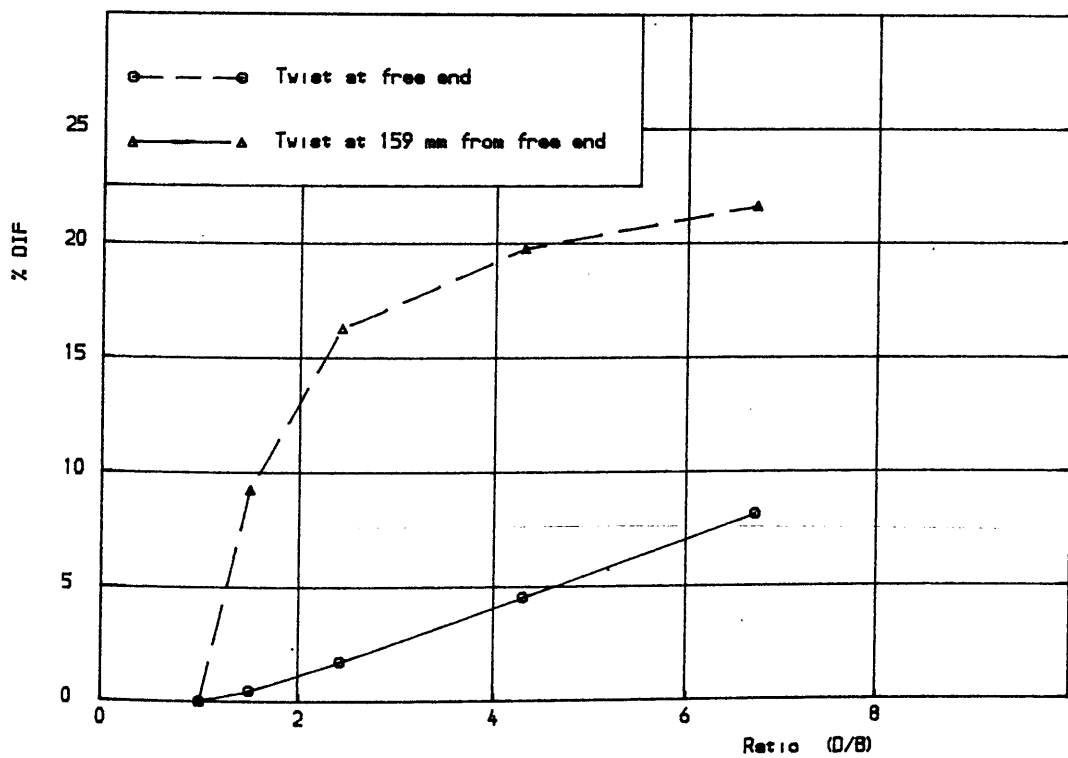
Figure (5.24) Effect of the ratio D/B on the eveluetion of angles of twist for rectangular sections
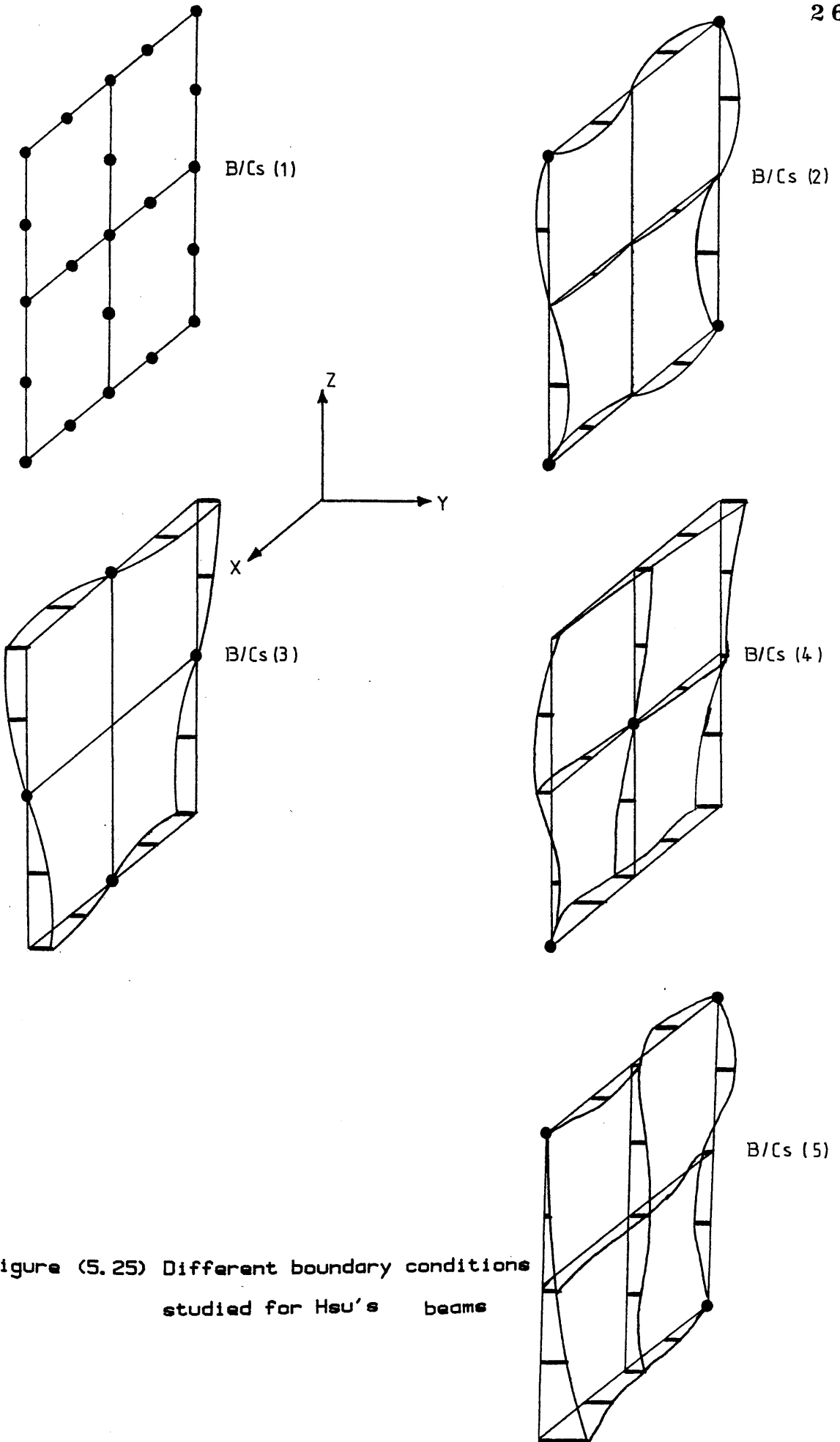
Figure (5.25) Different boundary conditions studied for Hsu's beams
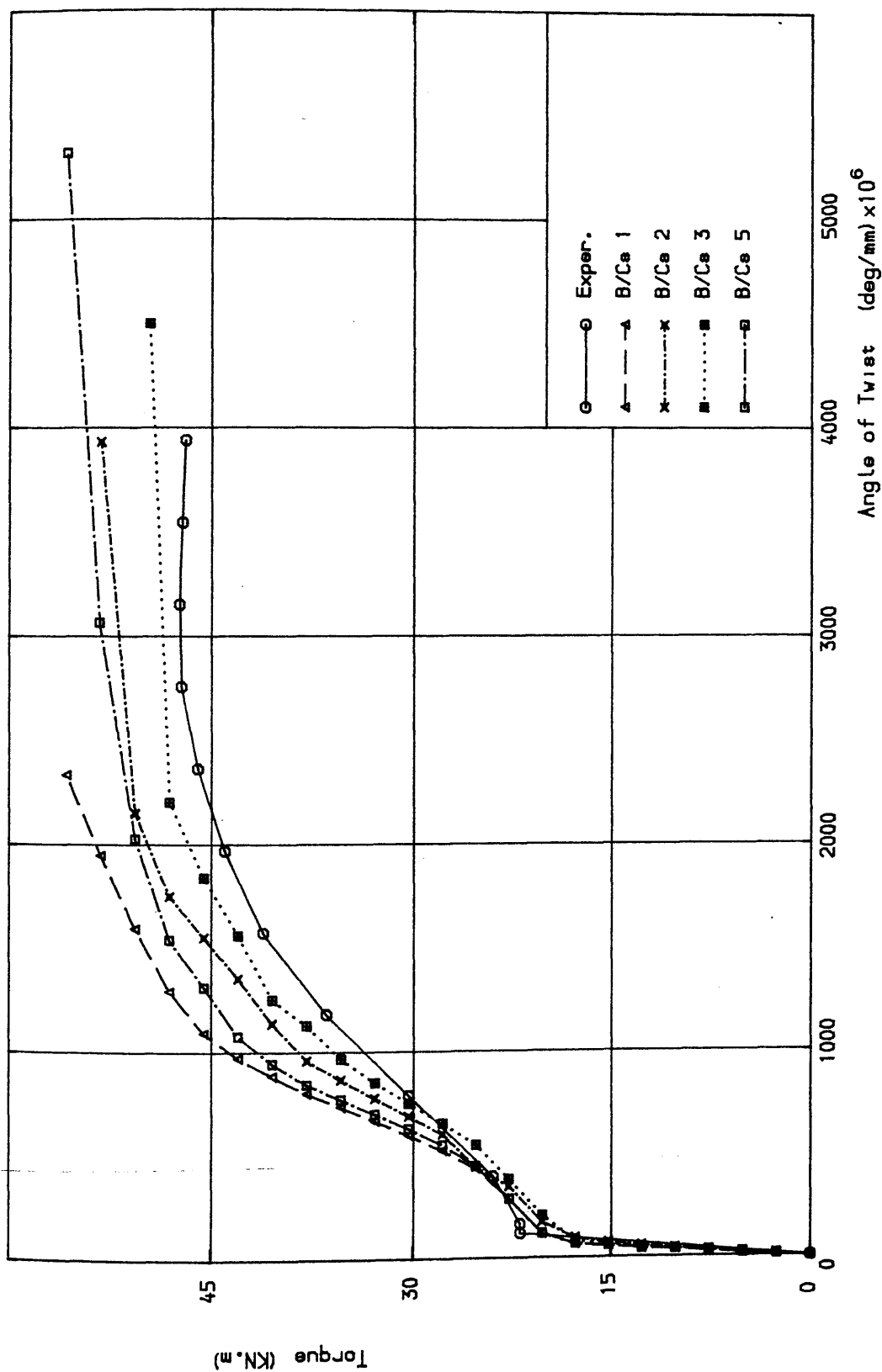
'Figure (5.26) Effect of boundary conditions on full nonlinear behaviour of Hsu's beam (B4), NTS, $0.5 > \beta > 0.1$, $\beta_3 \, \xi'_t = 0.004$
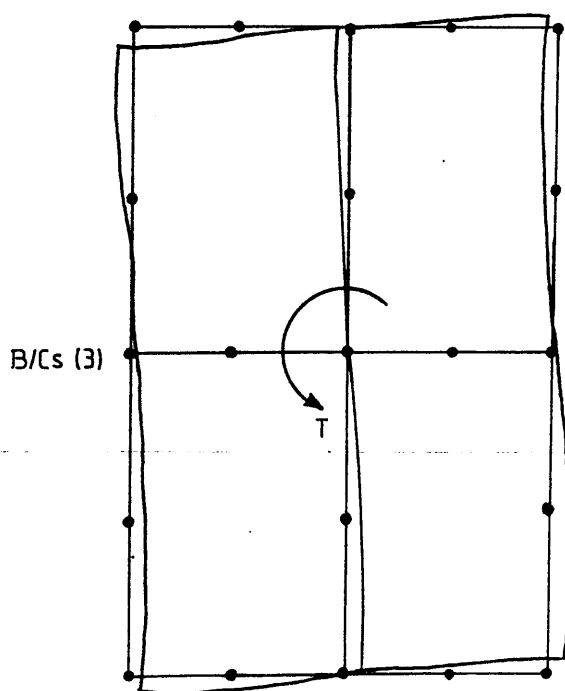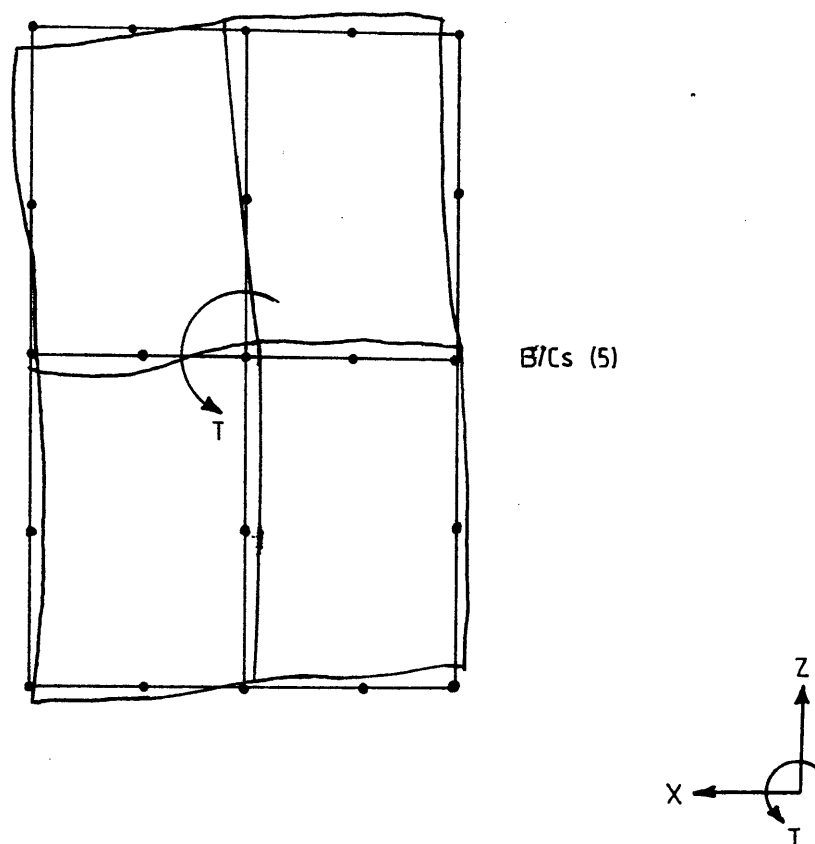
Figure (5.27) Distortion of cross section at the free ! end
for different boundary conditions. Hsu's beam B4

Table (5.8) Values of twist per unit length for an elastic torque of 4.6 KN.m for different boundary conditions, Hsu's beam (B4)

B/Cs	1	2	3	4	5
θ_1	15.73	19.51	19.44	-	-
θ_2	15.82	19.61	19.53	-	-
%DIF	0.48	0.51	0.46	-	-

Table (5.9) Comparison of ultimate torques for Hsu's beams

Beam	T_u(Exper.) KN.m	T_u(Theor.) KN.m	$\dfrac{T_u(\text{Theor.})}{T_u(\text{Exper.})}$
B2	29.26	30.13	1.030
B4	47.33	48.64	1.028
G4	64.85	61.88	0.954
N2	14.39	13.82	0.960
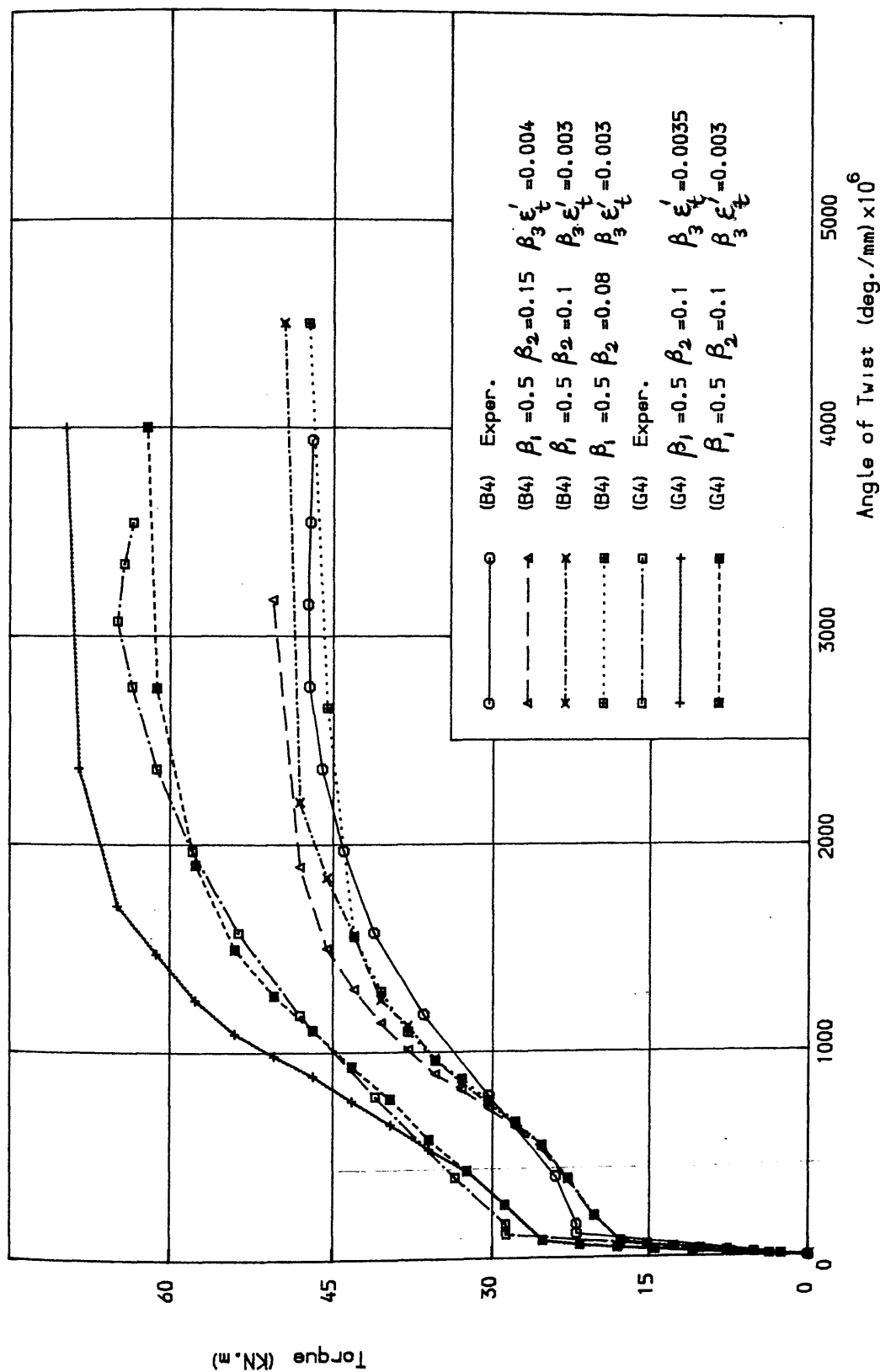
Figure (5.28) Effect of shear retention parameters on the behaviour of Hsu's beams (B4) and (G4), NTS
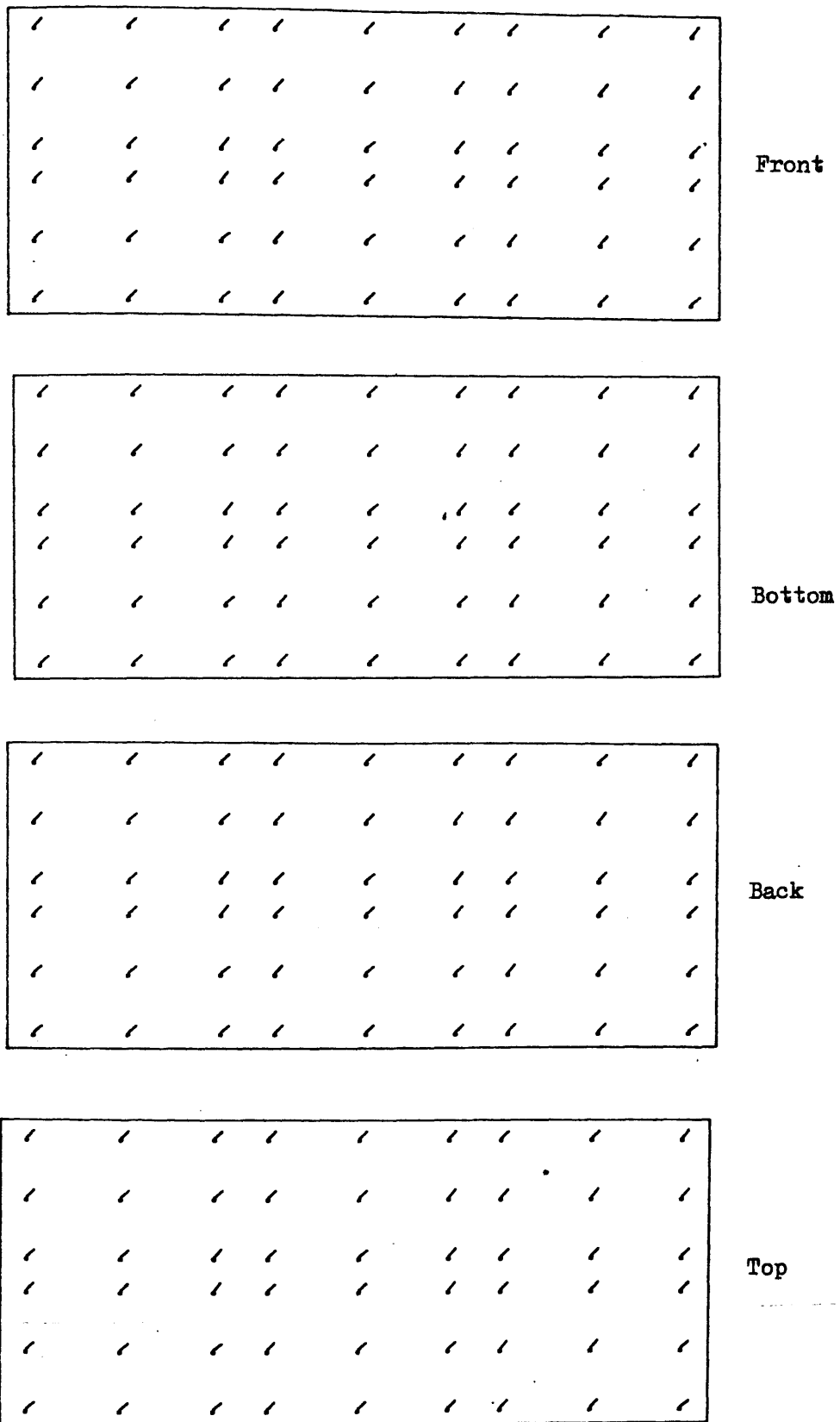
Figure (5.29) Predicted crack pattern for Hsu's beam (B4) at 0.75

failure torque
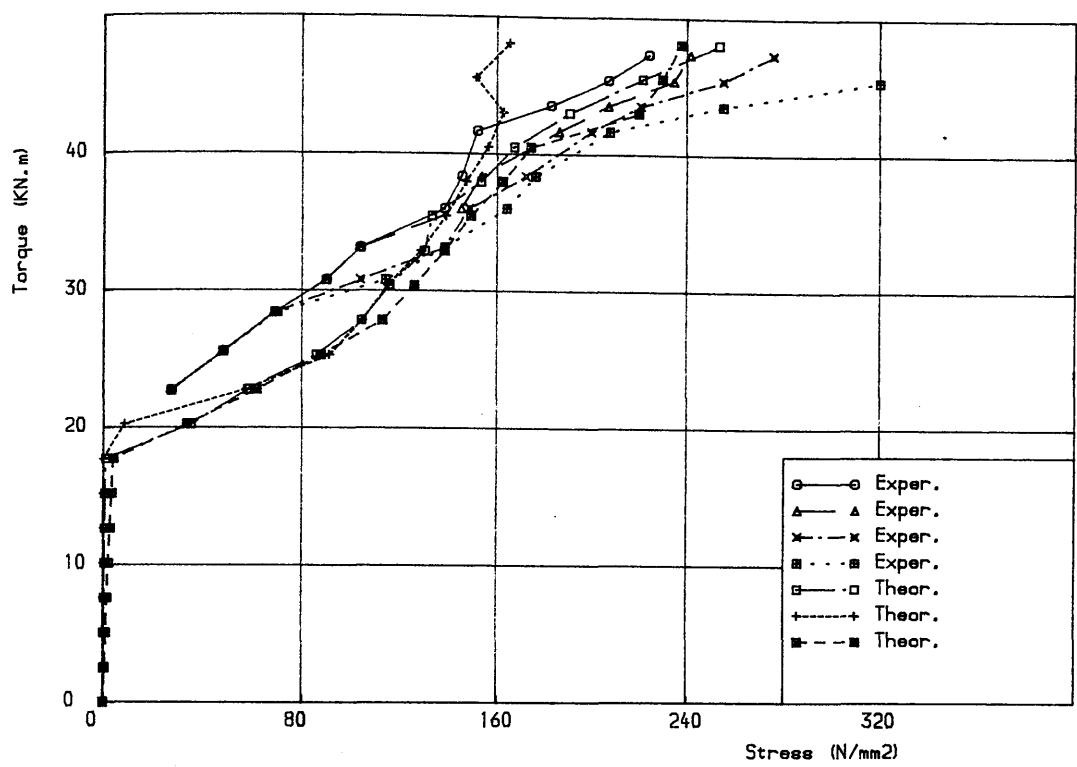
Figure (5.30 a) Torgue vs longitudinal steel stress for Hsu's beam (B4)
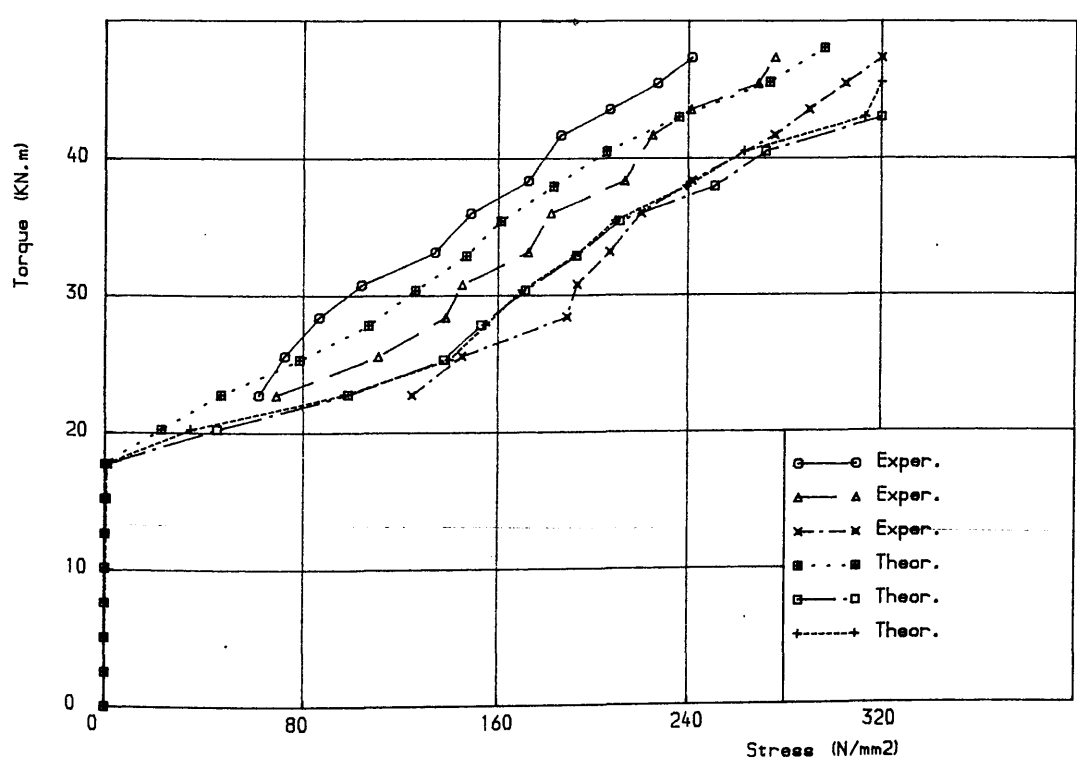
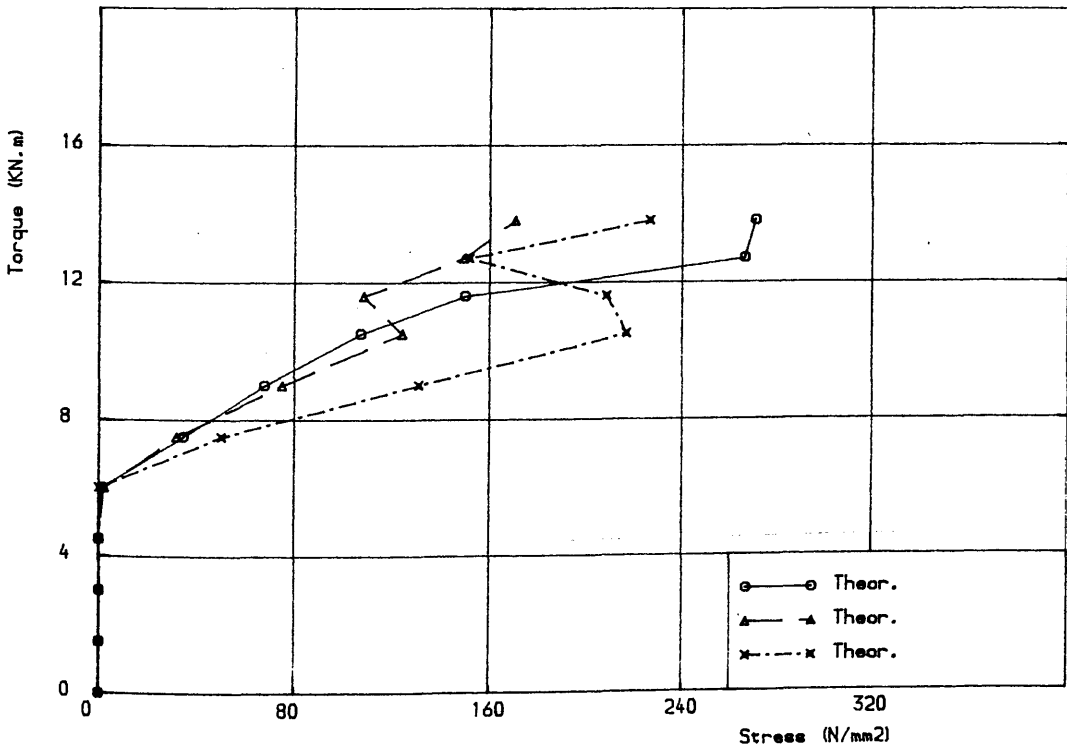Figure (5.30 b) Torgue vs stress on longer legs of stirrups for Hsu's beam (B4)
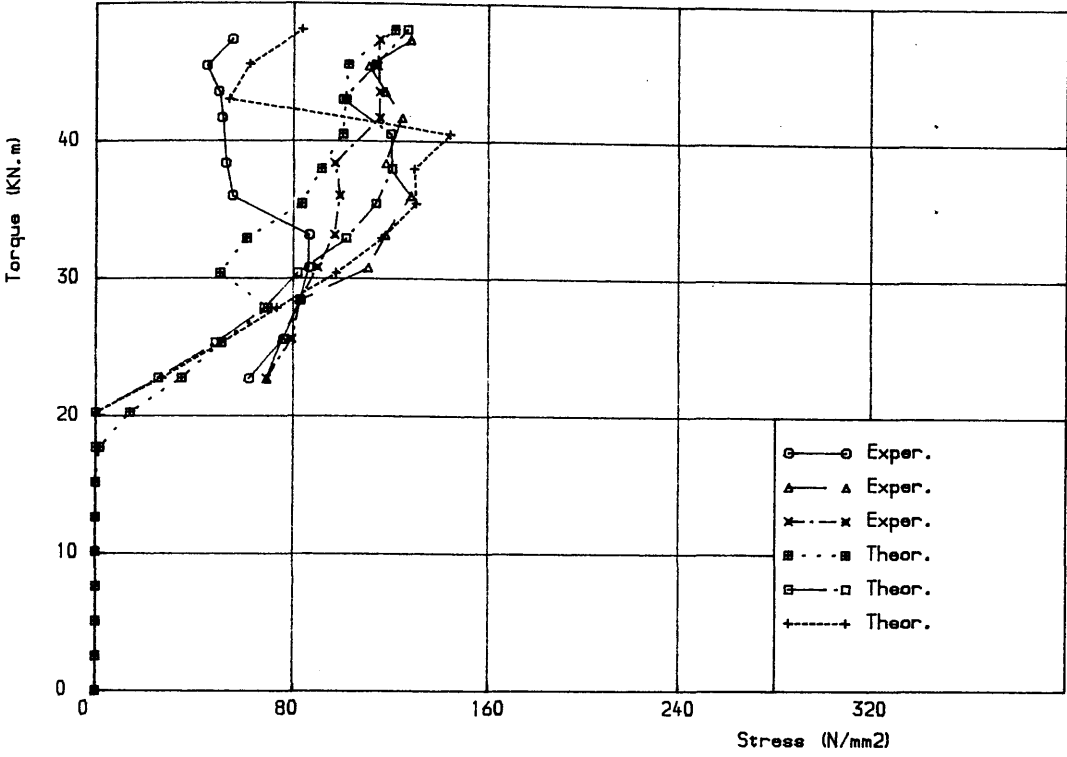
Figure (5.30 c) Torque vs stress on shorter legs of stirrups for Hsu's beam (B4)
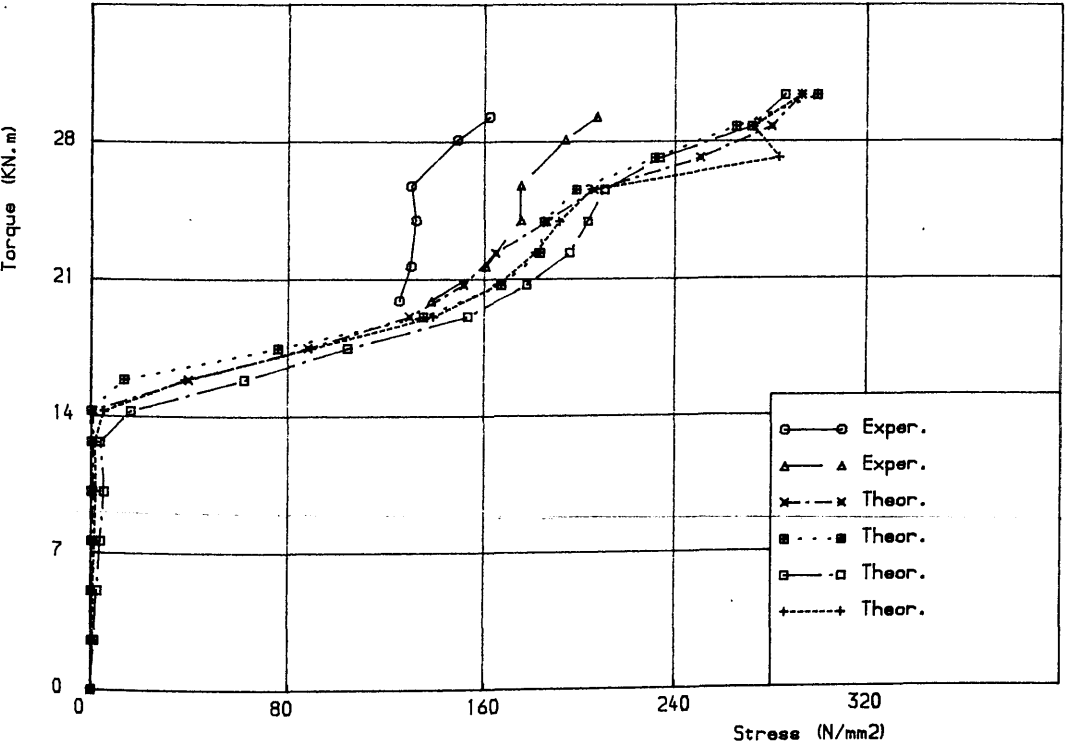
Figure (5.30 d) Torque vs longitudinal steel stress for Hsu's beam (B2)
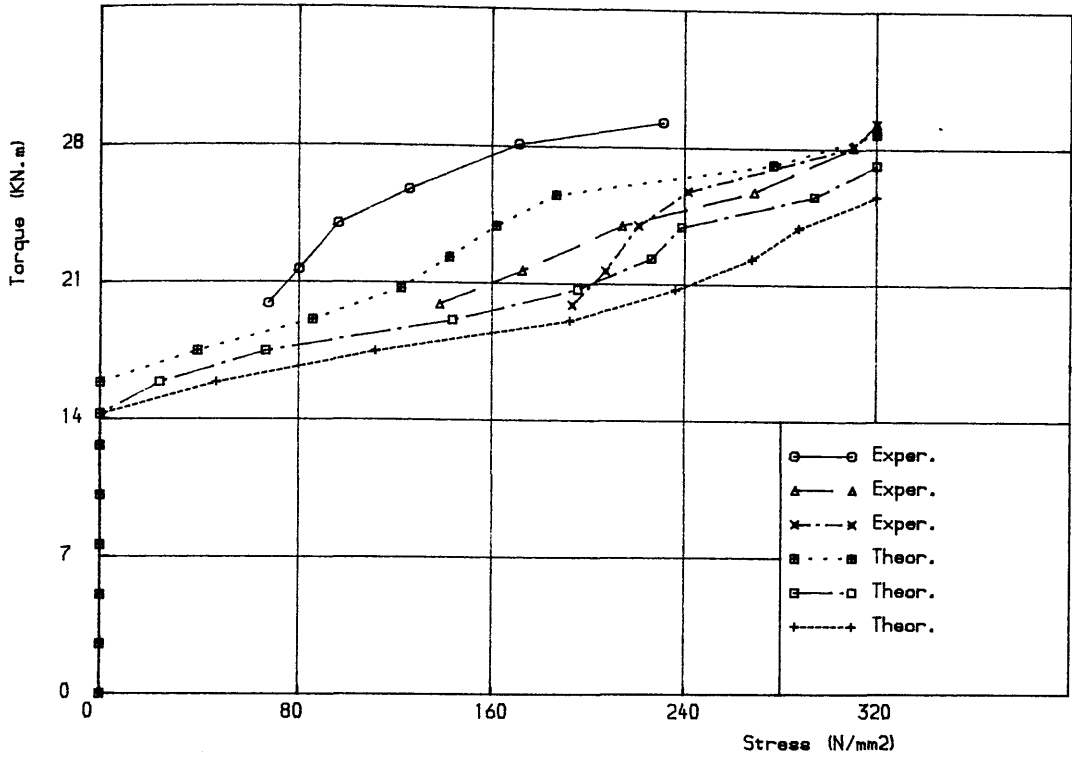
Figure (5.30 e) Torque vs stress on longer legs of stirrups for Hsu's beam (B2)
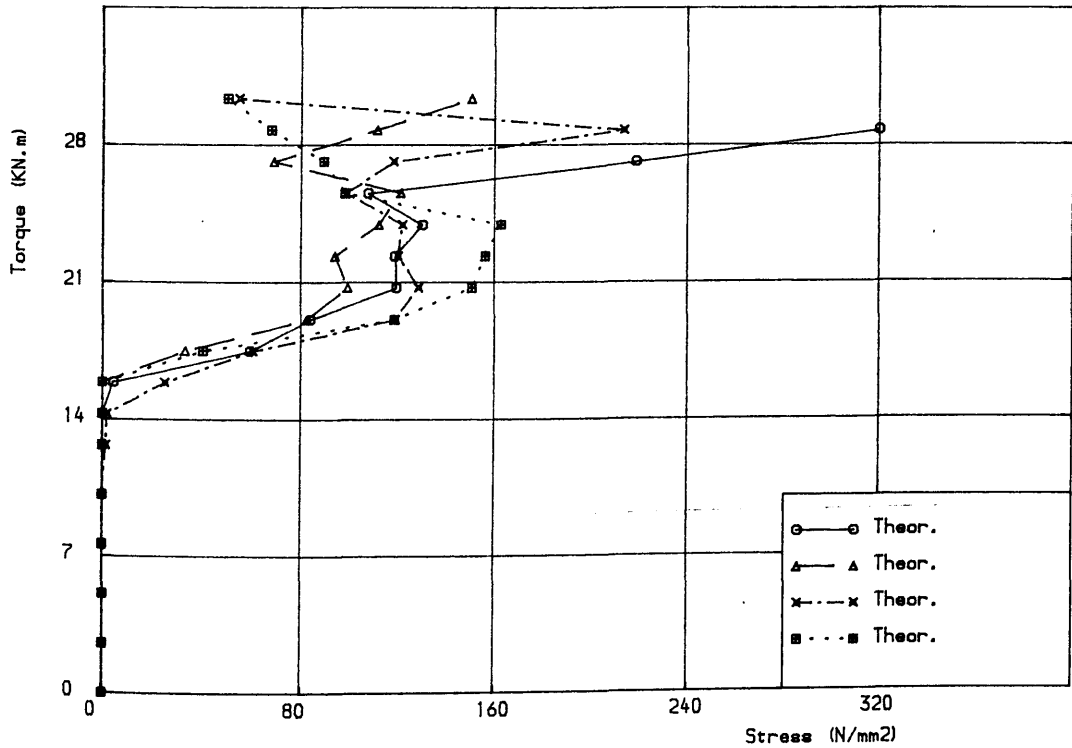
Figure (5.30 f) Torque vs stress on shorter legs of stirrups for Hsu's beam (B2)
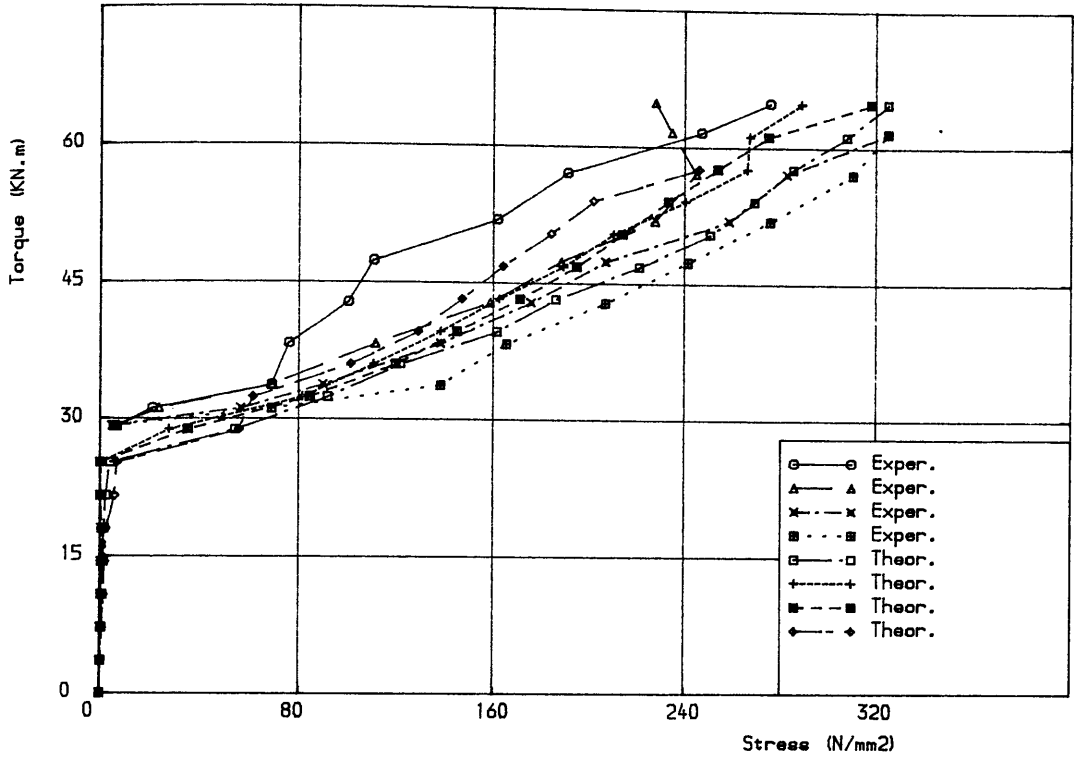
Figure (5.30 g) Torque vs longitudinal steel stress for Hsu's beam (G4)
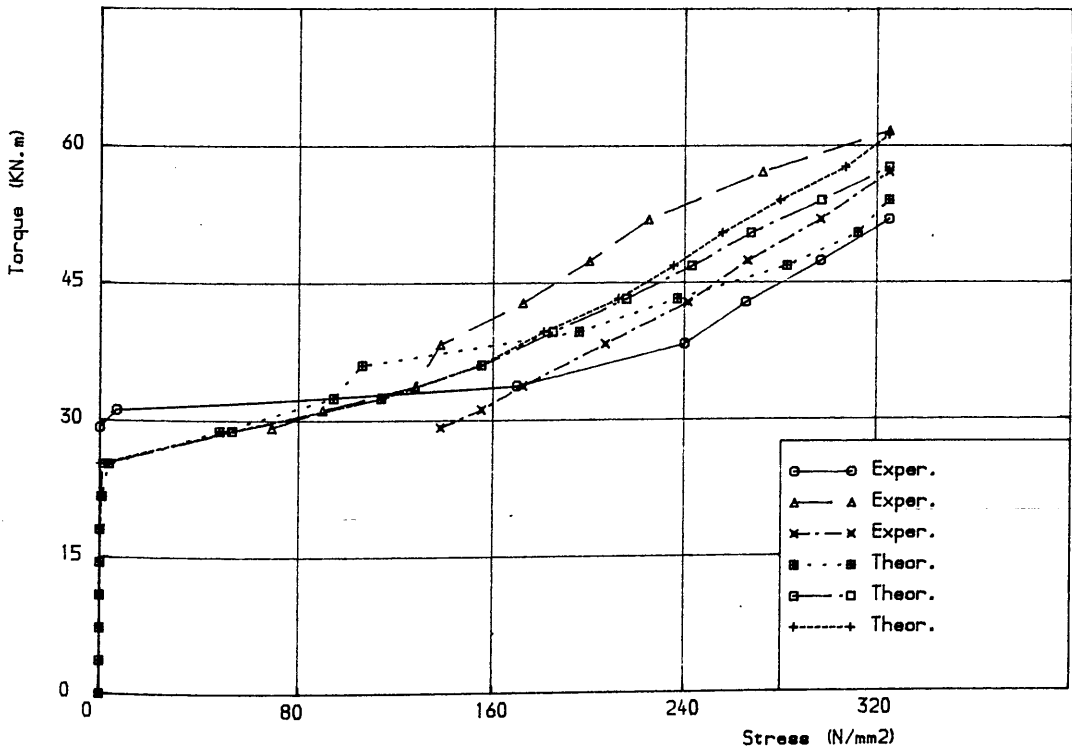
Figure (5.30 h) Torque vs stress on longer legs of stirrups for Hsu's beam (G4)
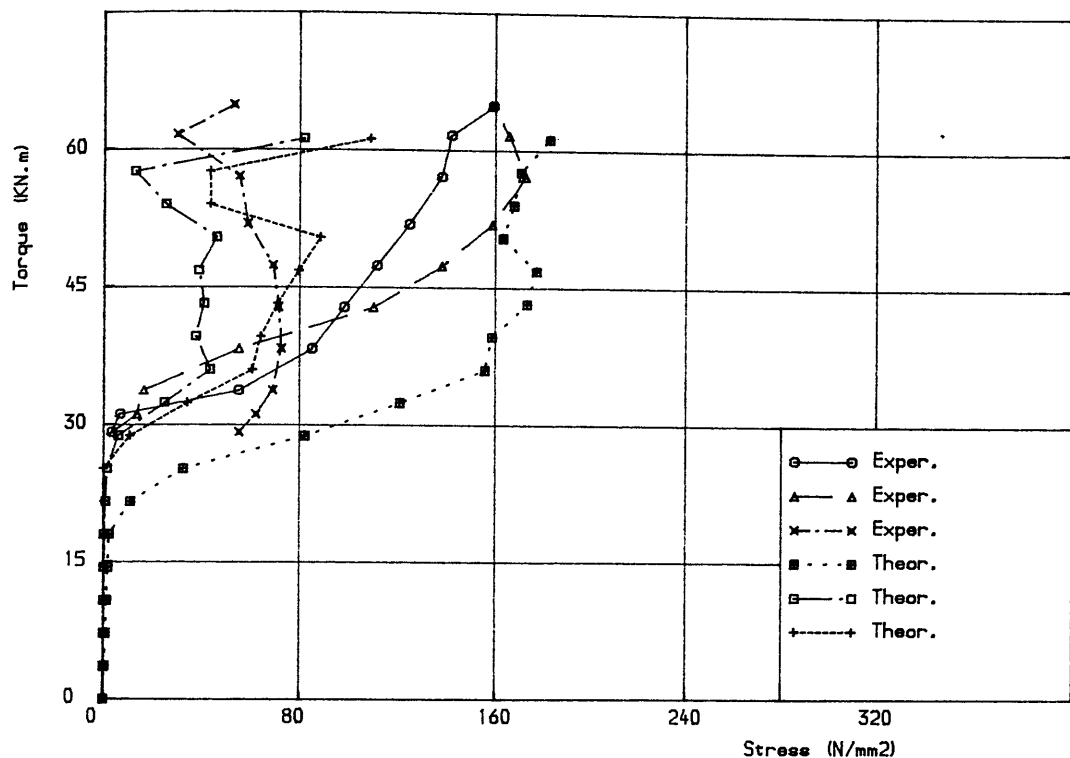
Figure (5.30 i) Torque vs stress on shorter legs of stirrups for Hsu's beam (G4)
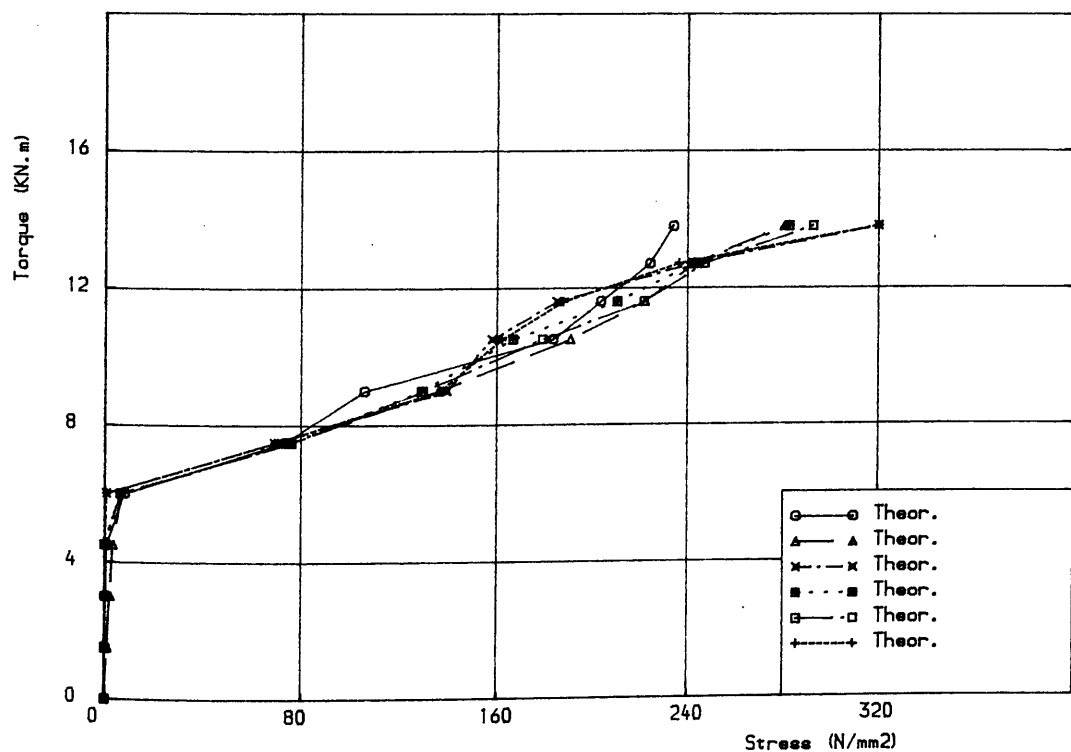
Figure (5.30 j) Torque vs longitudinal steel stress for Hsu's beam (N2)
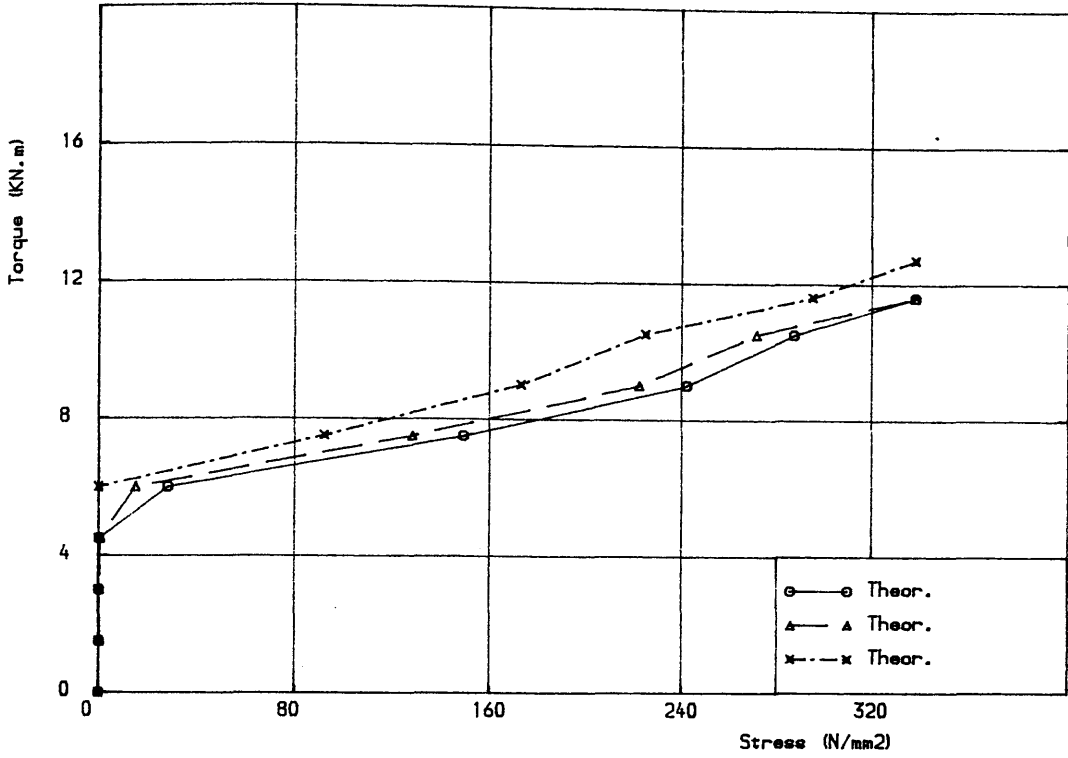
Figure (5.30 k) Torque vs stress on longer legs of stirrups for Hsu's
beam (N2)

Figure (5.30 l) Torque vs stress on shorter legs of stirrups for Hsu's
beam (N2)
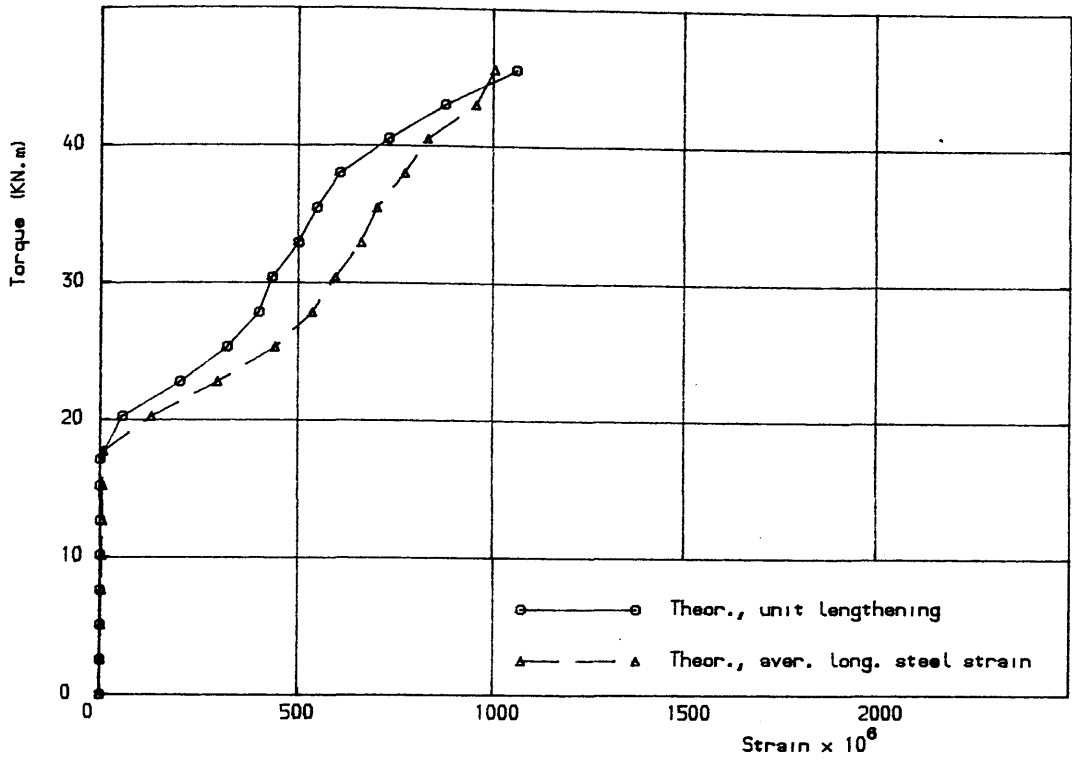
Figure (5.31 a) Torque vs unit lengthening and average longitudinal steel strain for Hsu's beam (B4)
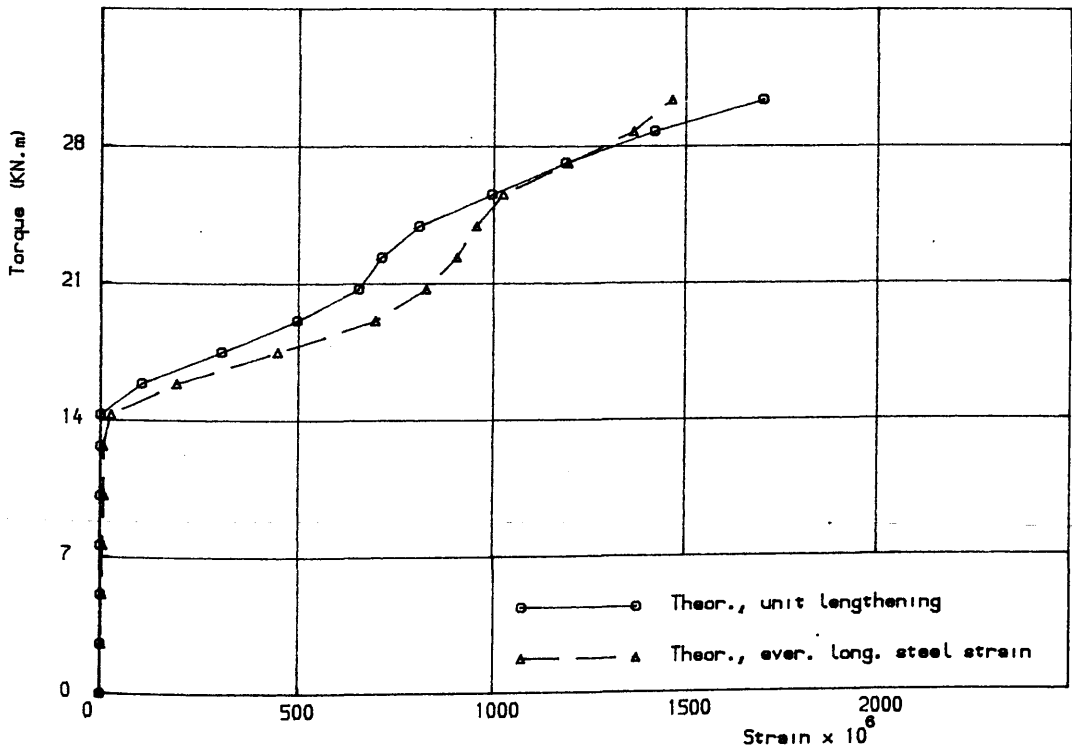
Figure (5.31 b) Torque vs unit lengthening and average longitudinal steel strain for Hsu's beam (B2)
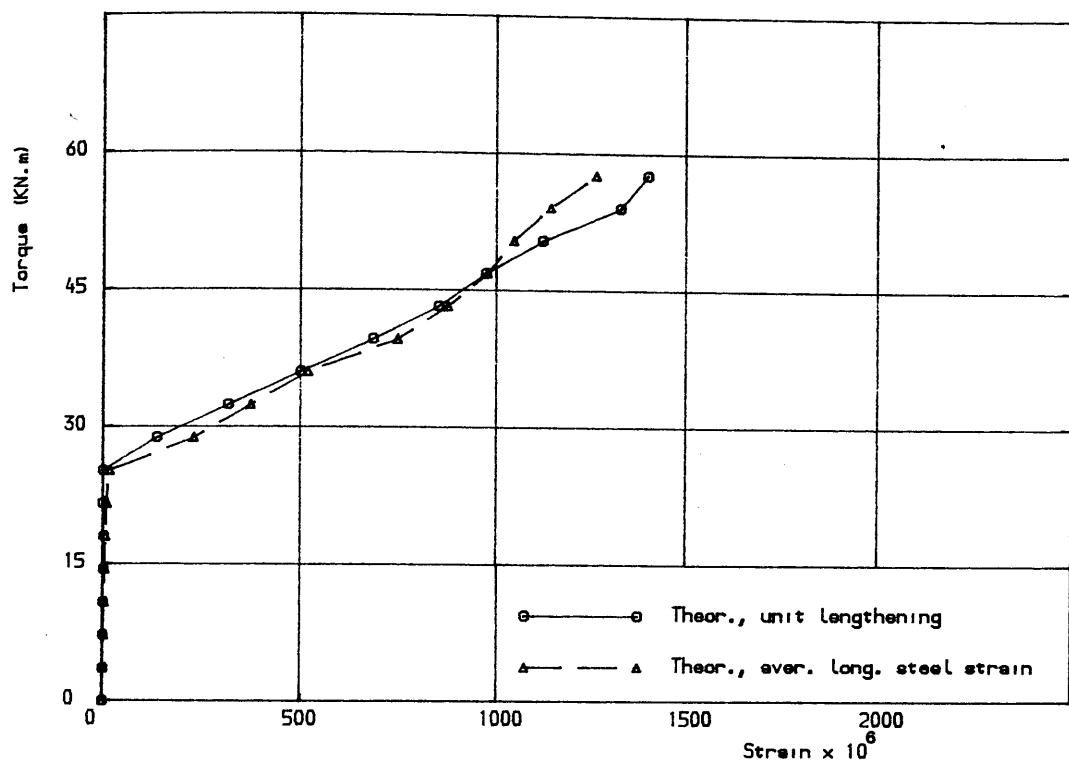
Figure (5.31 c) Torque vs unit lengthening and average longitudinal steel strain for Hsu's beam (G4)
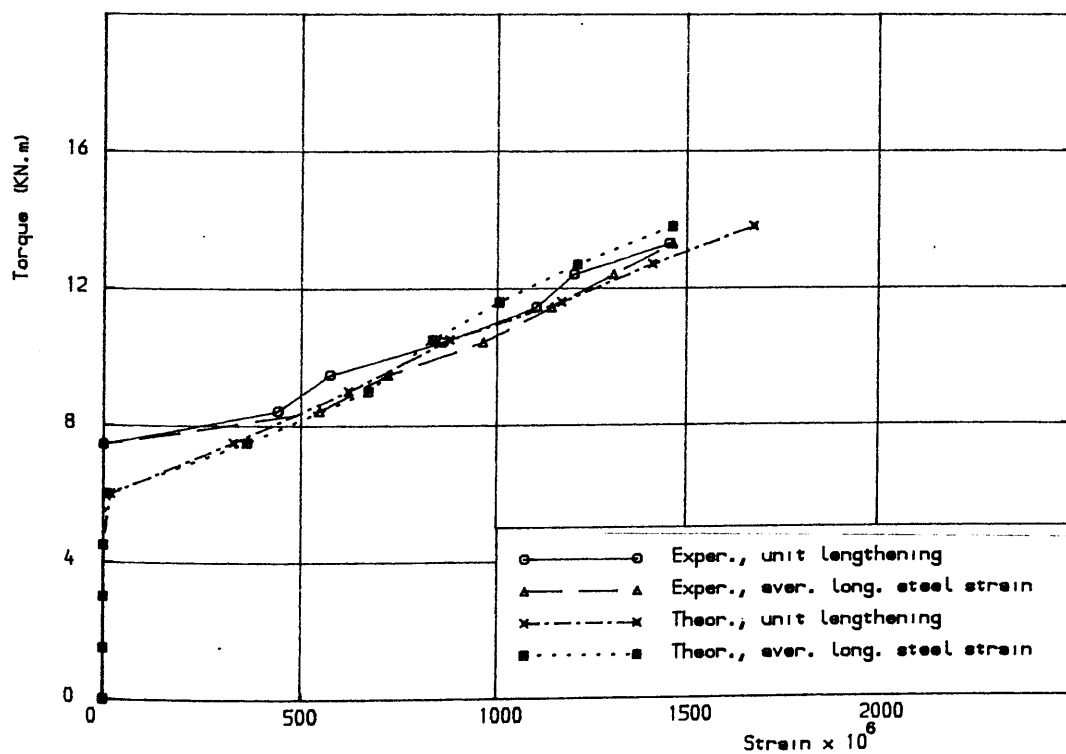
Figure (5.31 d) Torque vs unit lengthening and average longitudinal steel strain for Hsu's beam (N2)
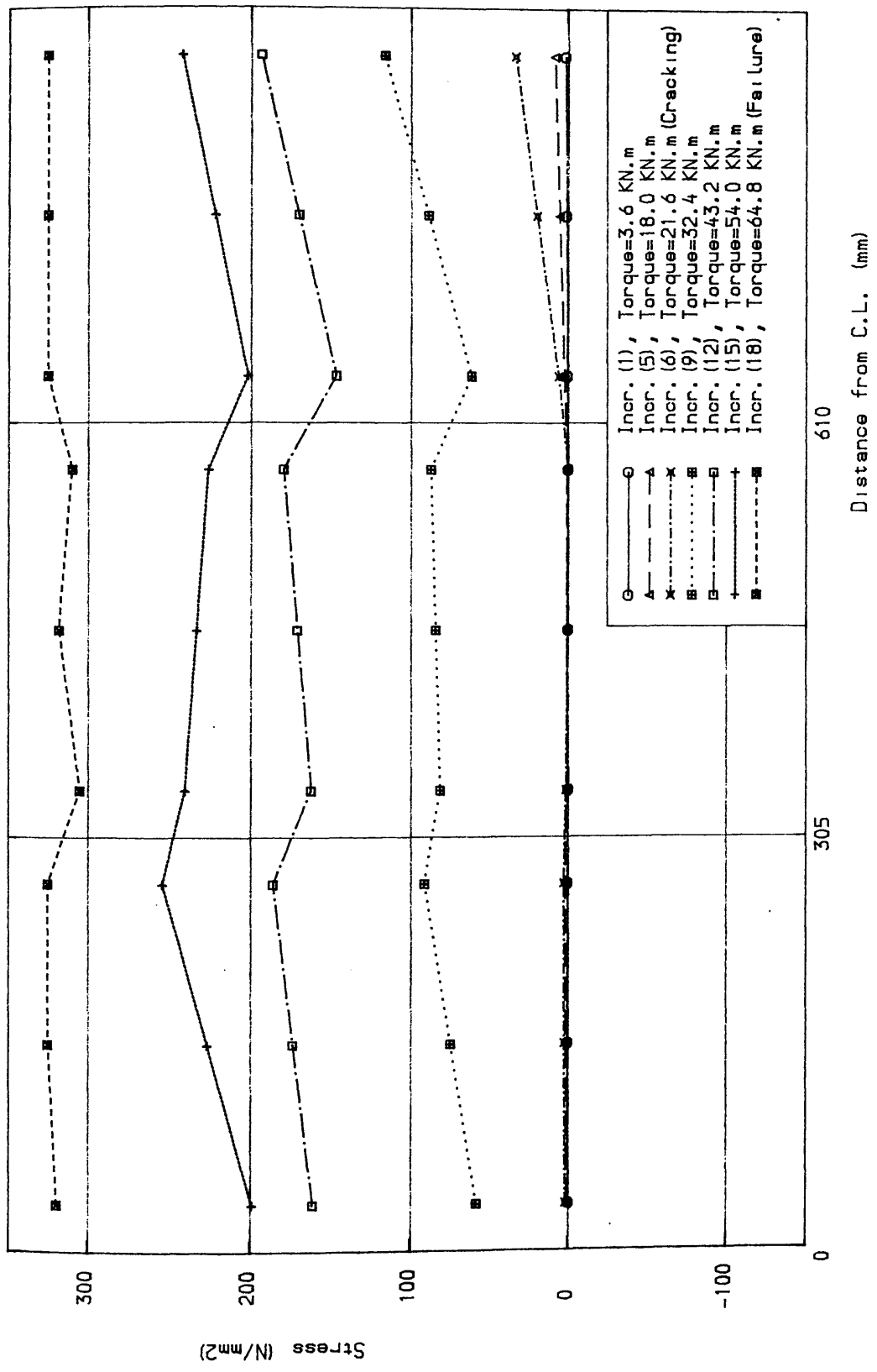
Figure (5.32) Stress distribution along a typical longitudinal bar for Hsu's beam (G4)
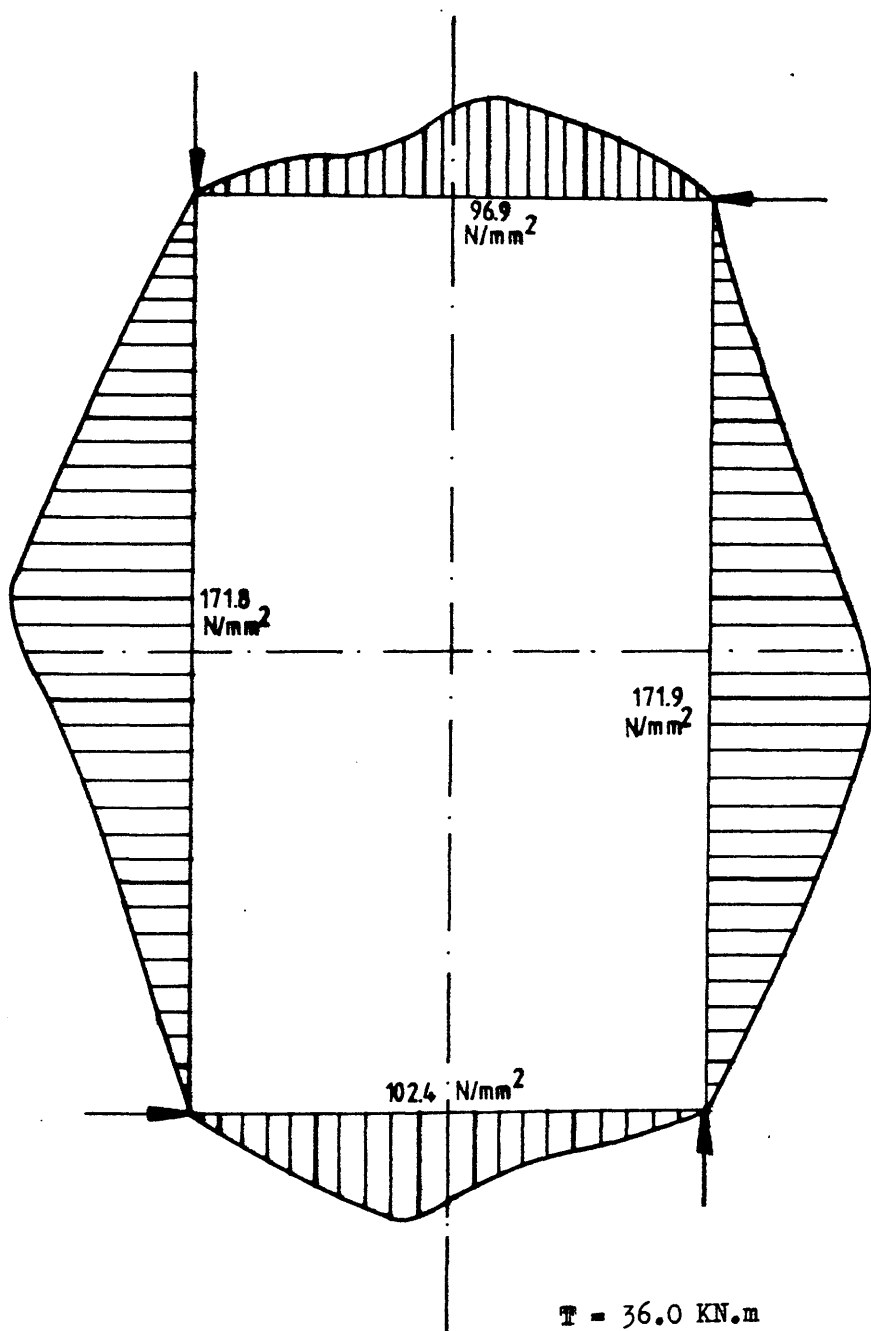
Figure (5. 33) Stress distribution along the legs of a
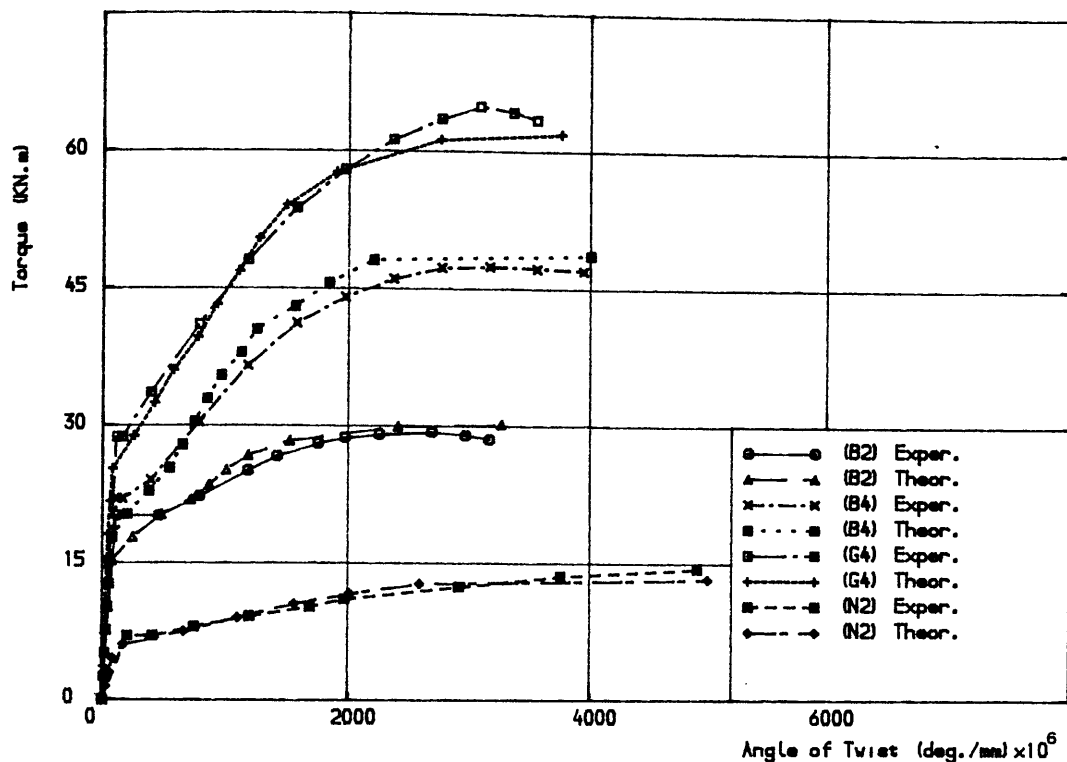typical closed stirrup for Hsu's beam G4

Figure (5.34) Torque-twist curves for Hsu's beams B2, B4, G4 and N2.
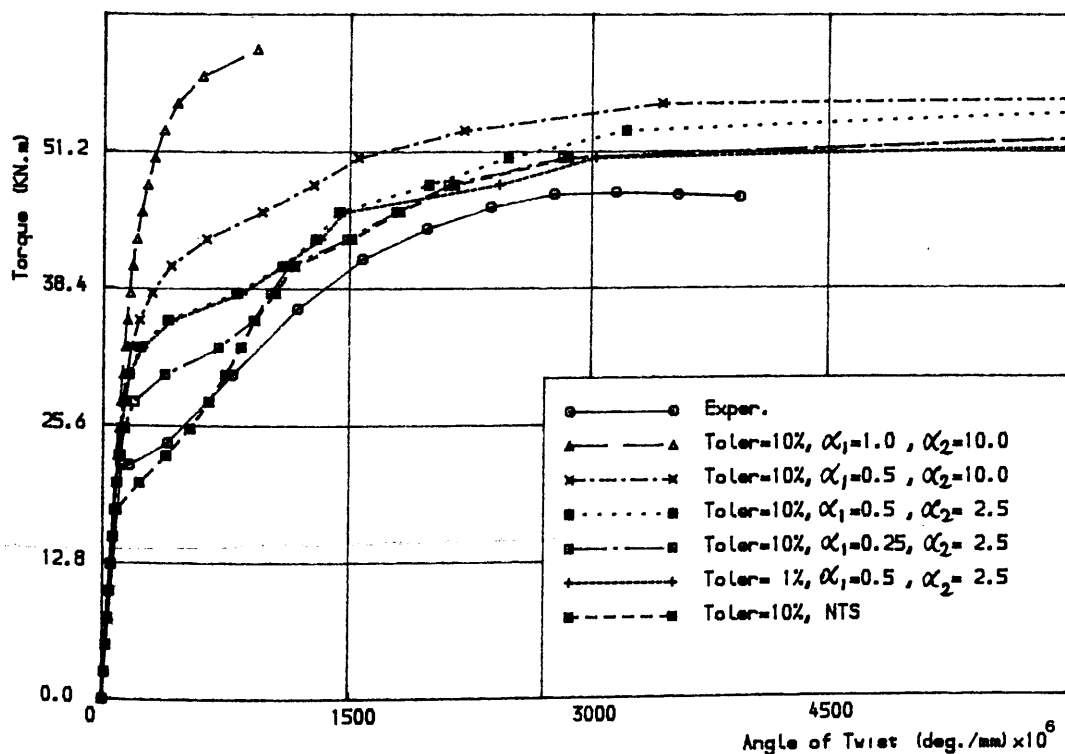NTS, $0.5 > \beta > 0.1$, $\beta_3 \mathcal{E}'_t = 0.003$

Figure (5.35) Torque-twist curves for Hsu's beams B2, B4, G4 and N2.
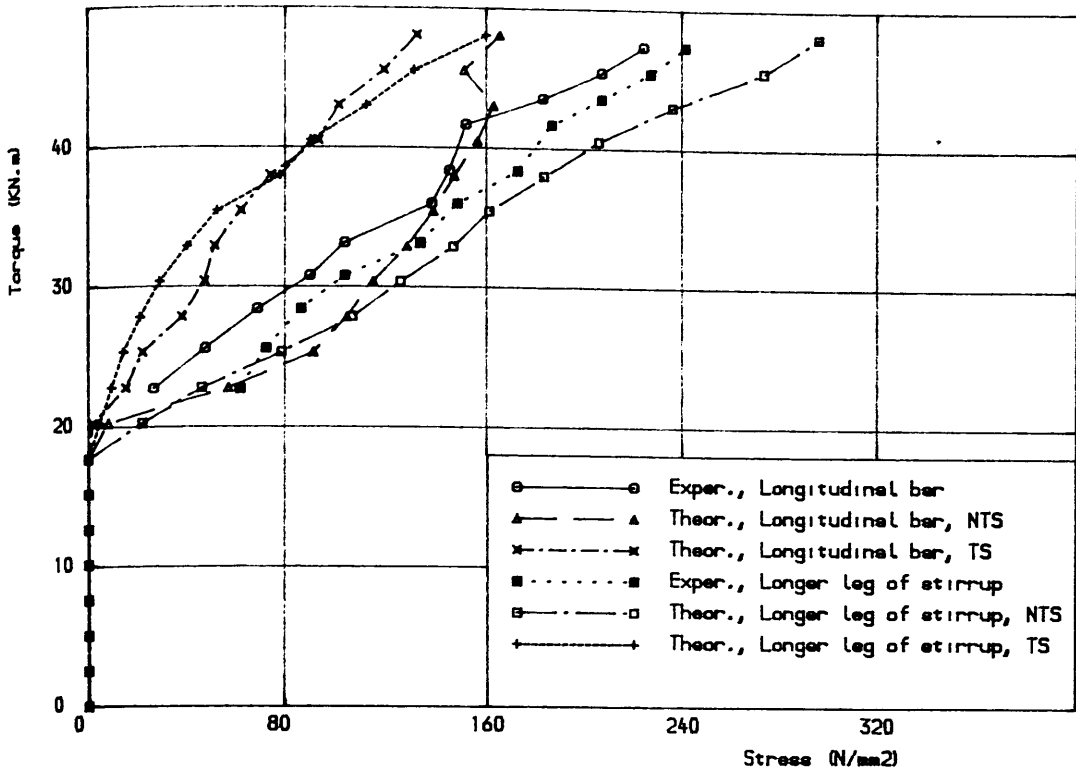TS, $0.5 > \beta > 0.1$, $\beta_3 \mathcal{E}'_t = 0.003$, Nalgo= 3

Figure (5.36) Effect of tension stiffening on steel response for
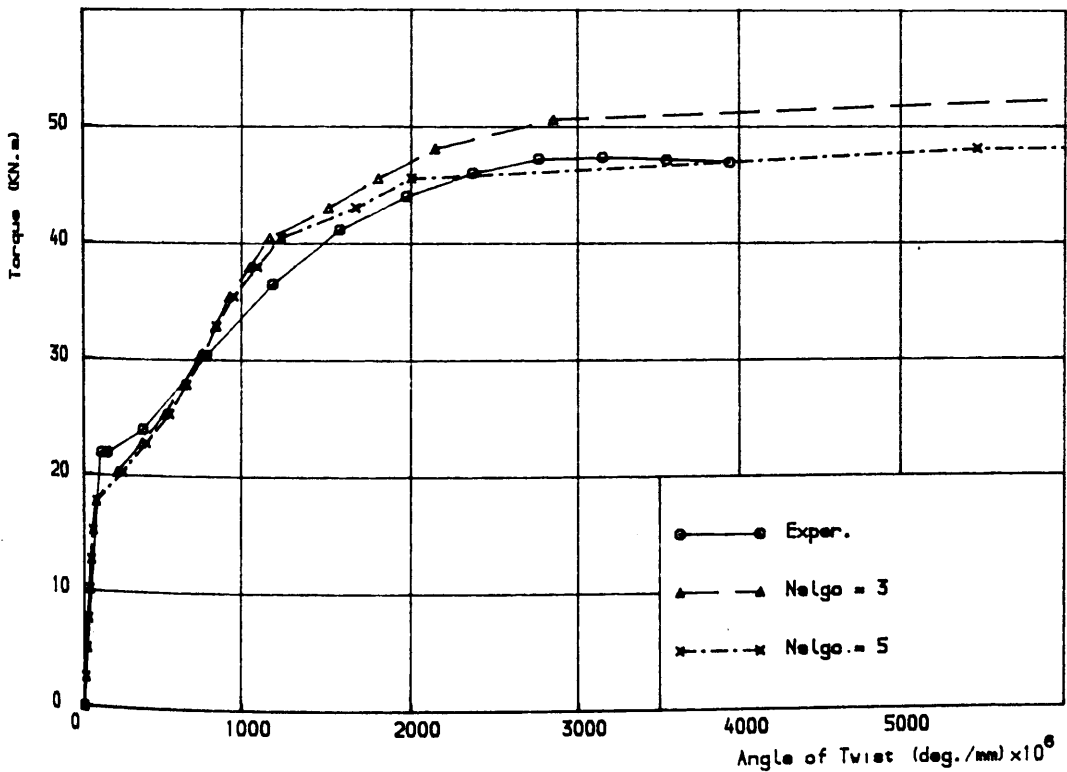Hsu's beam (B4), α_1=0.5, α_2=10.0, Toler=10%

Figure (5.37) Effect of solution algorithm on torque-twist behaviour of
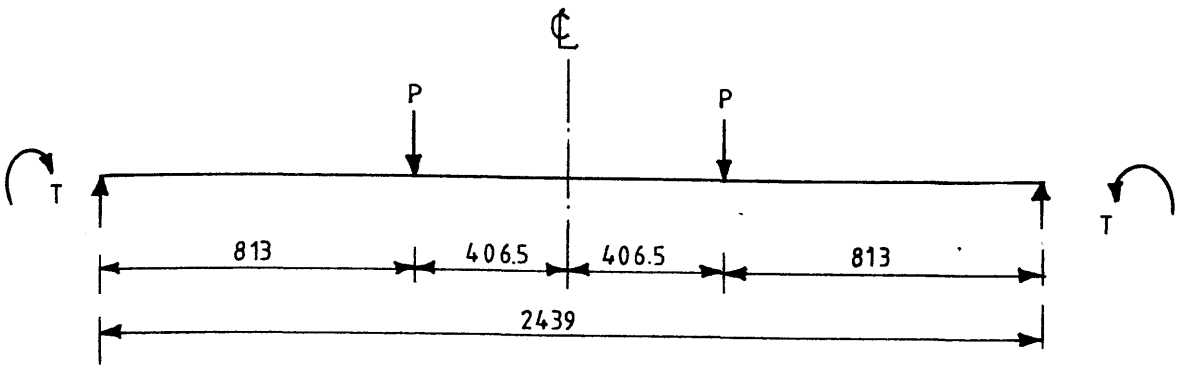Hsu's beam (4), NTS, 0.5 > β > 0.1, $\beta_3 \epsilon_t'$ =0.003, Toler=10%

Table (5.10) Details of Collins et al beams

| Beam	B (mm)	D (mm)	b_l (mm)	d_l (mm)	E_s^{*} (KN/mm²)	s (mm)	Φ_v (mm)	Φ_l (mm)	f_{yv} (N/mm²)	f_{yl} (N/mm²)	E_c^{*} (KN/mm²)	$f_c^{'}$ * (N/mm²)	$f_t^{'}$ * (N/mm²)	T/M
RE2	165	254	125	174	200	76	9.5	12.7	338	307	24	31.7	3.5	2.61
RE4	165	254	125	174	200	76	9.5	12.7	338	307	24	31.7	3.5	0.88

* Assumed values

Bar diameters converted from psi units
Subscripts: v denotes stirrups, l denotes longitudinal steel

(a) Loading

(b) Cross section

9.5 at 76 mm c/c

Φ12.7

Φ12.7

254

30

40

20

165
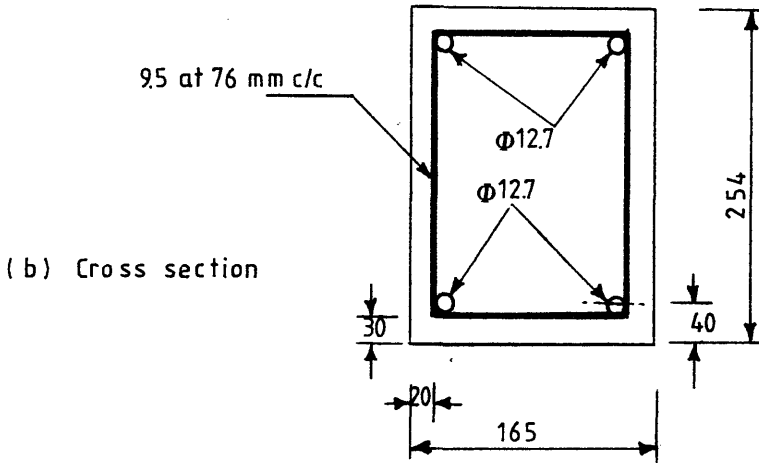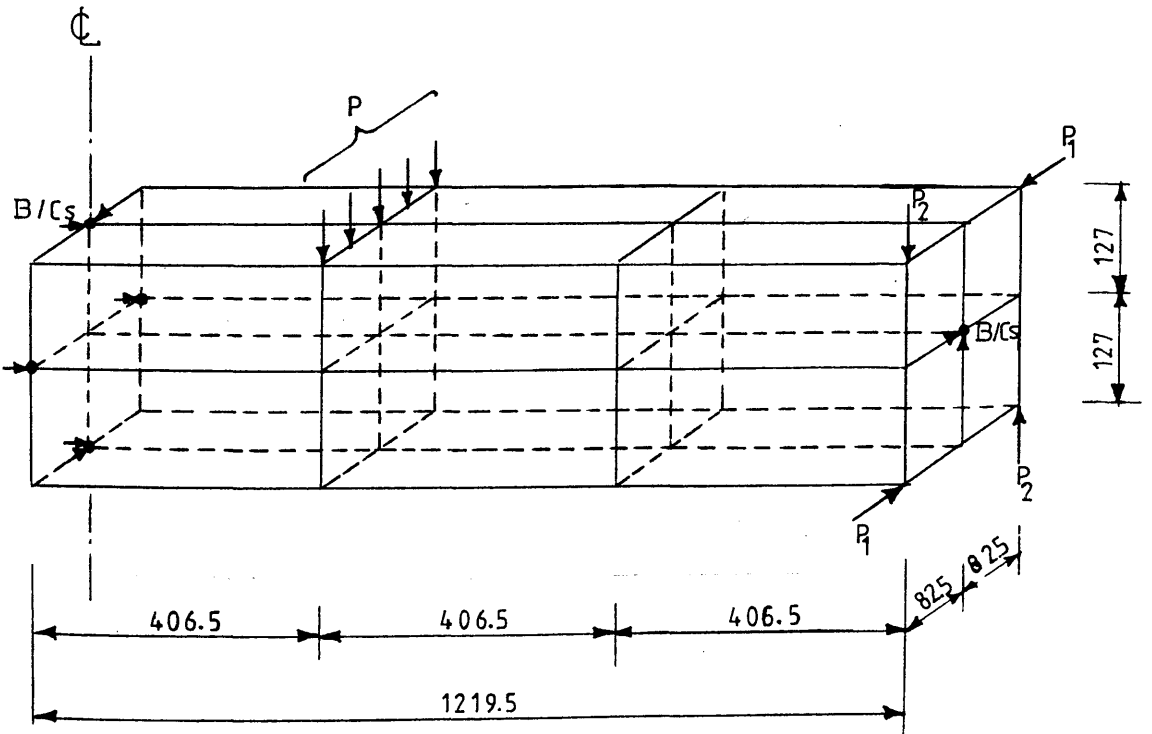
(c) 12-element mesh

● Supported node

406.5   406.5   406.5

1219.5

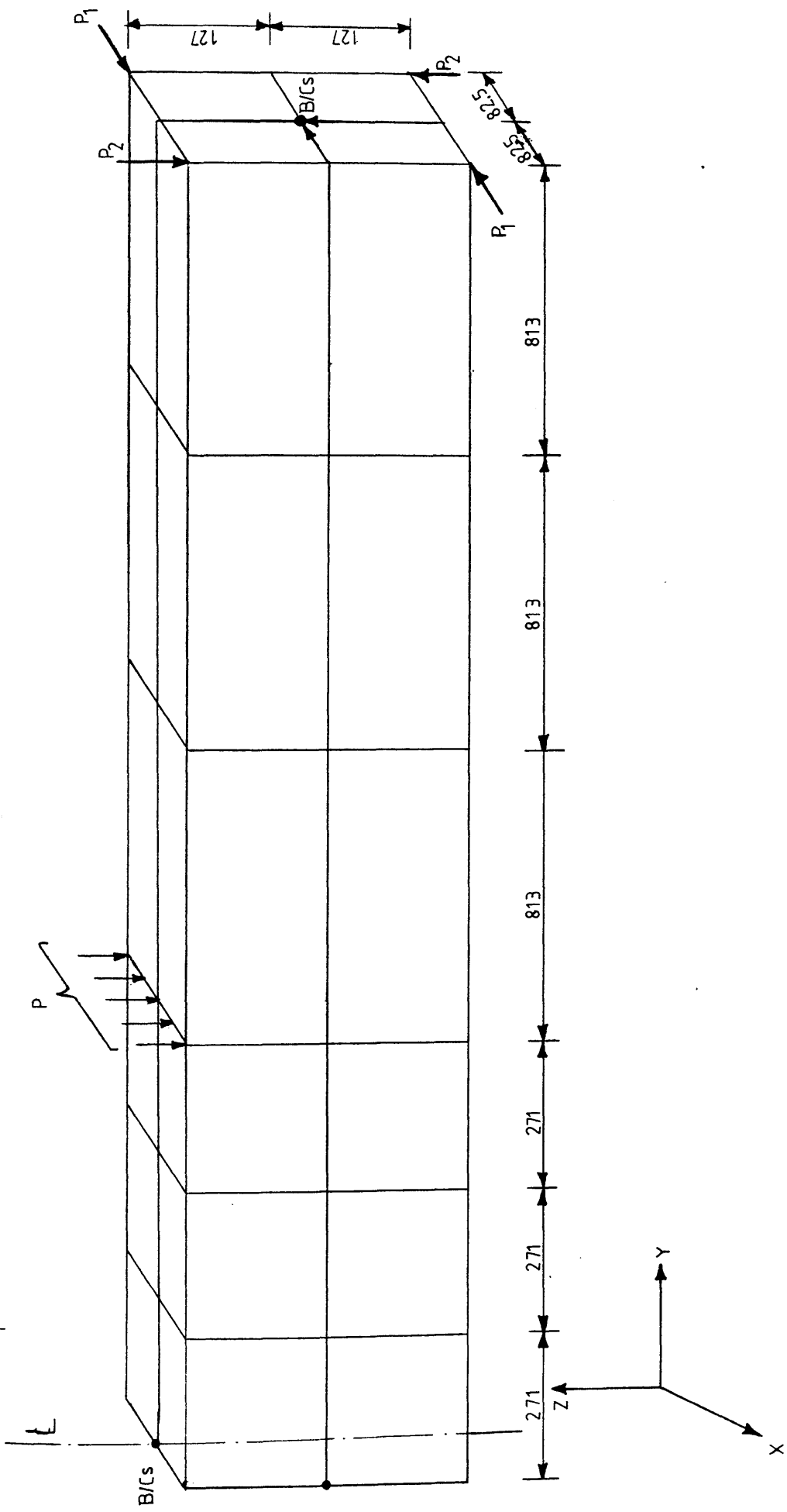Figure (5.38) Details of Collins et al Beams RE2 and RE4
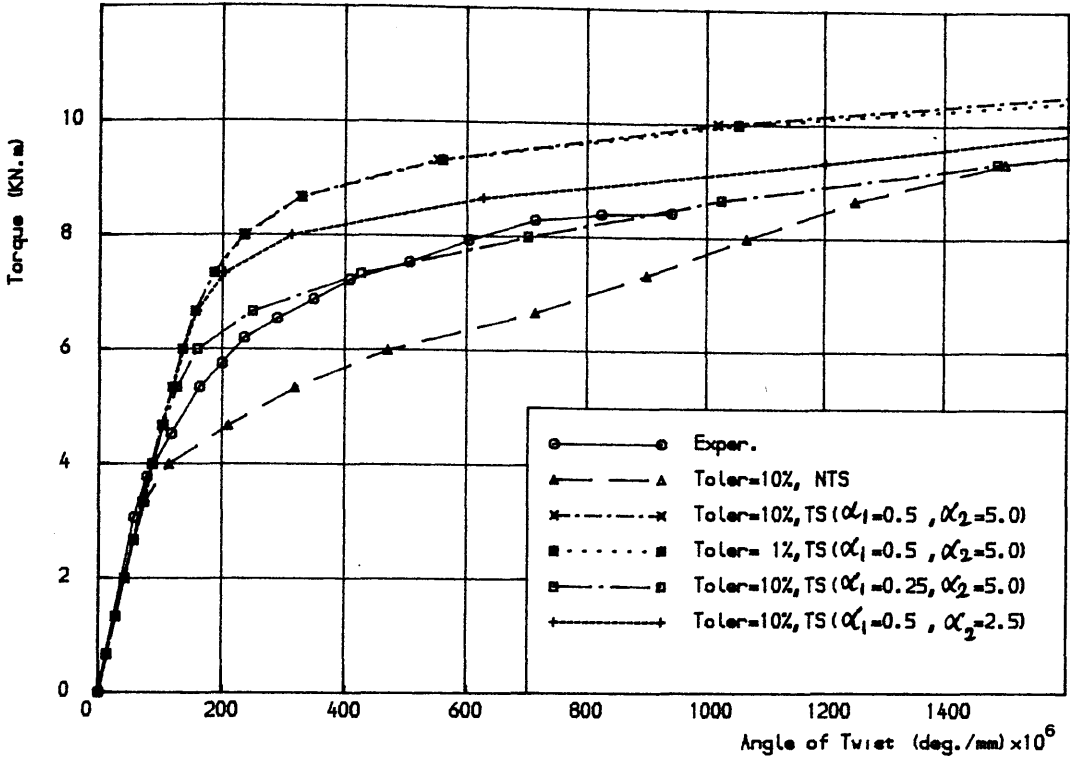
Figure (5.38 d) 24-element mesh for Collins et al beams

Figure (5.39) Torque-twist curves for different values of tension stiffening parameters for Collins et al beam (RE4), $0.5 > \beta > 0.1$, $\beta_3 \mathcal{E}_t' = 0.003$
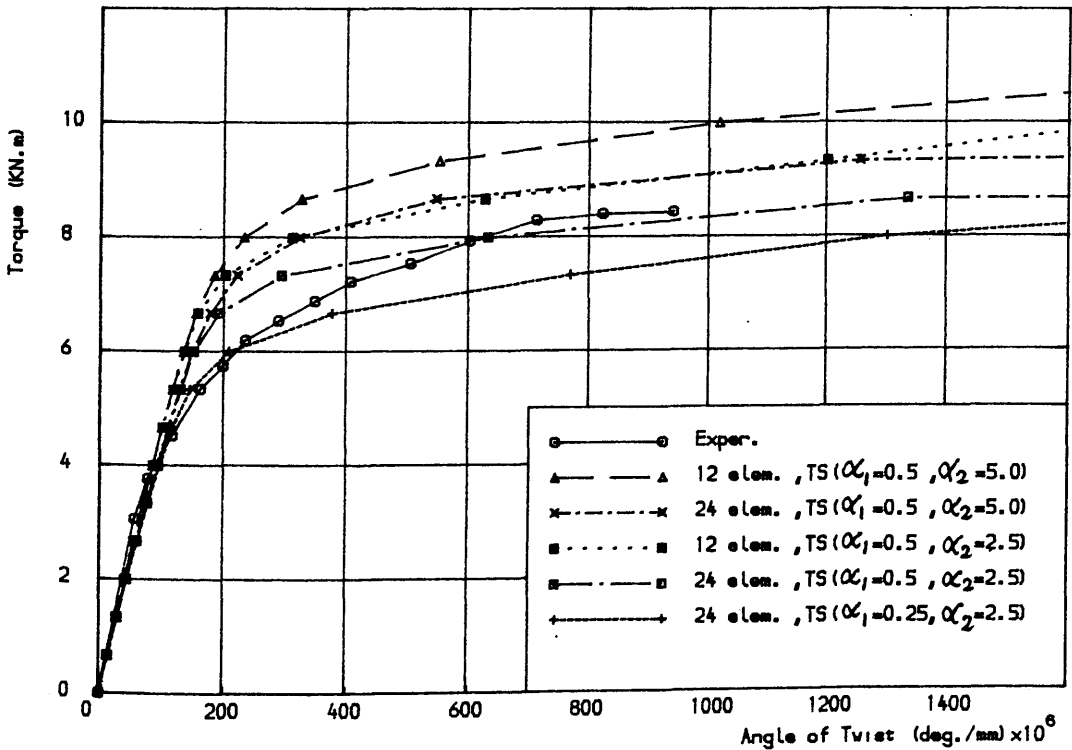

Figure (5.40) Effect of mesh size on Collins et al beam (RE4), Toler=10%, $0.5 > \beta > 0.1$, TS

Front

Bottom

Back

Top

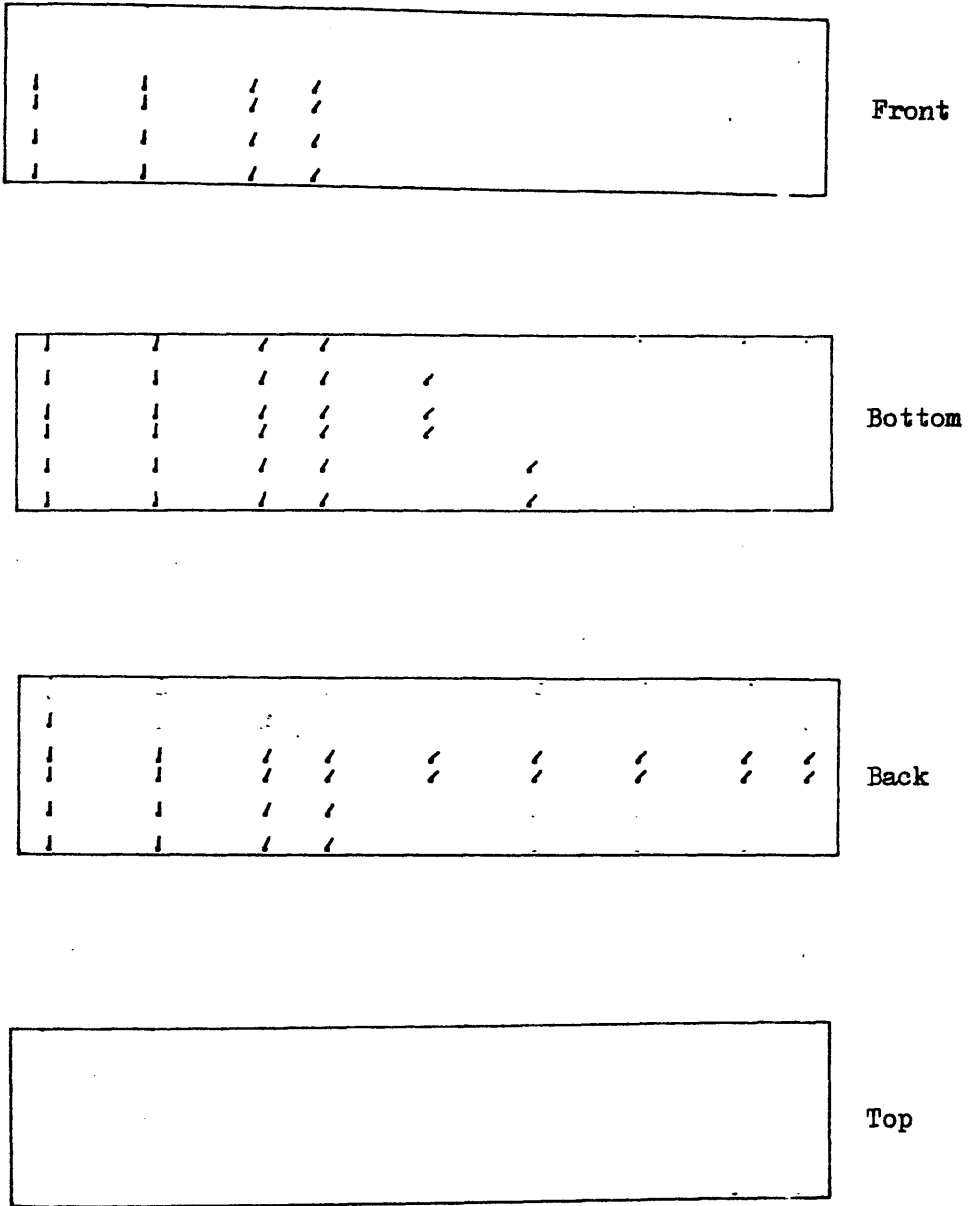Figure (5.42) Predicted crack pattern for Collins et al beam
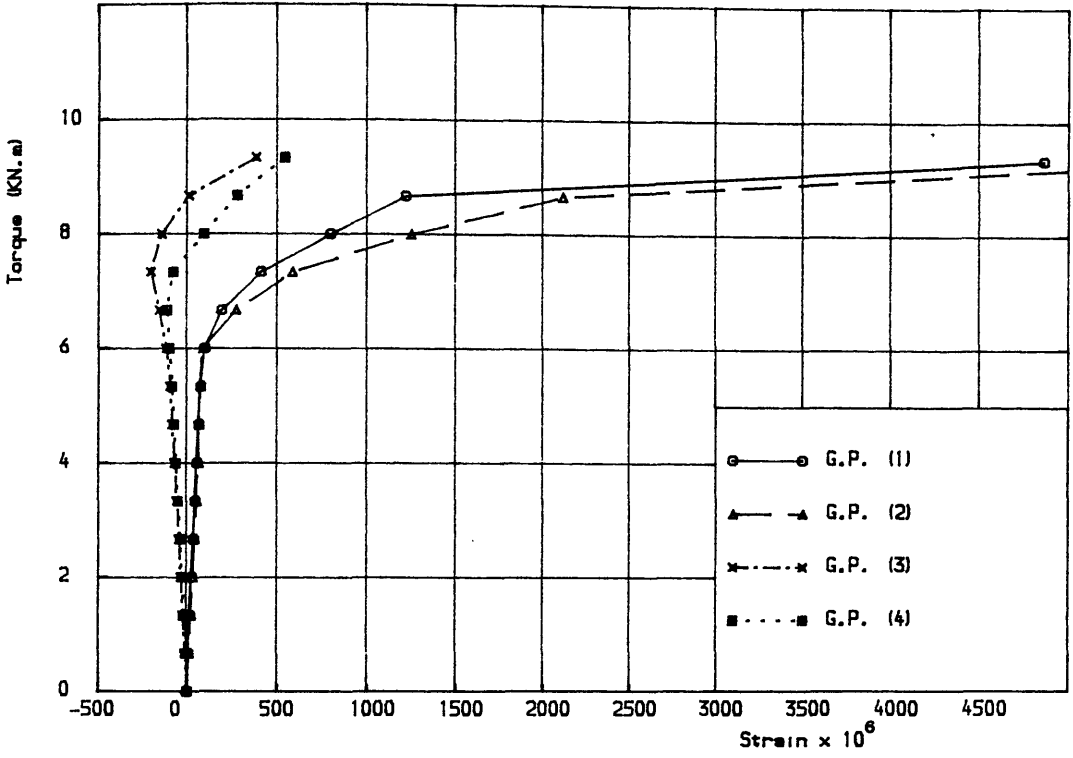
(RE4) at 0.71 failure load

Figure (5.41) Torque vs theoretical longitudinal steel strain for Collins
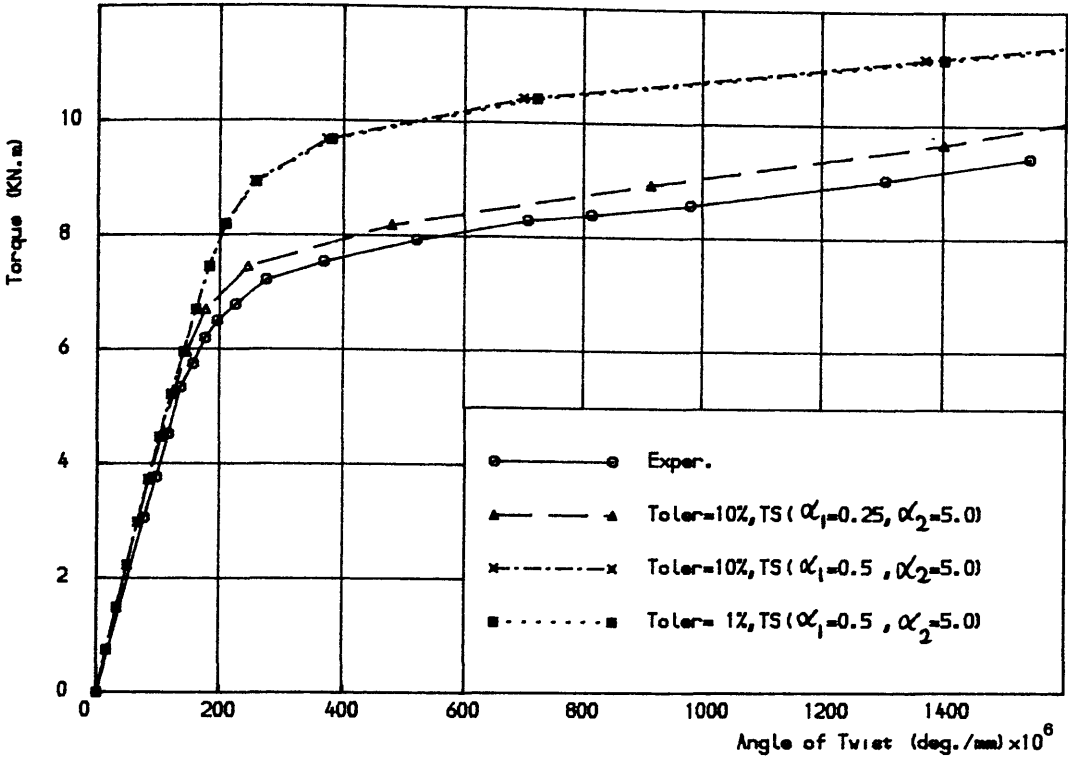et al beam (RE4)

Figure (5.43) Torque-twist curves for Collins et al beam (RE2).

$0.5 > \beta > 0.1$, $\beta_3 \mathcal{E}'_t = 0.003$, 24-element mesh
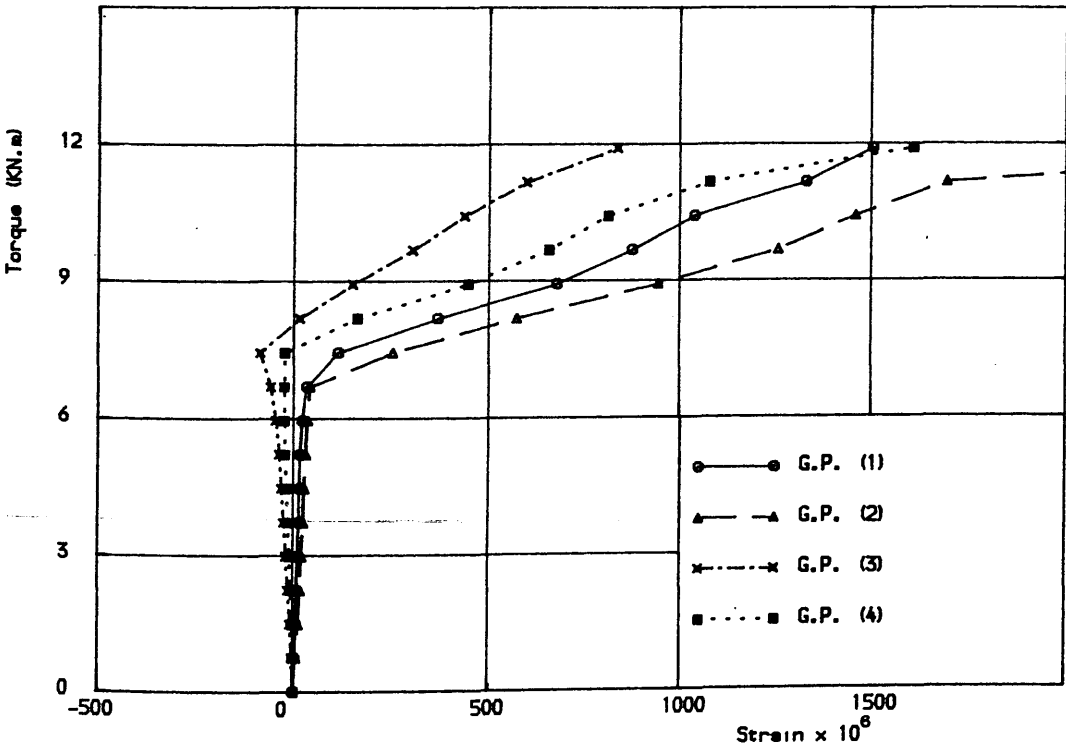

Figure (5.44) Torque vs theoretical longitudinal steel strain for Collins et al beam (RE2)

References

(1)   Gerstle,K.H.,   "Material   Modelling   of Reinforced
Concrete",   IABSE Colloquium on the Advanced Mechanics   of
Reinforced concrete, Introductory paper, Delft, 1981, pp.
41-61

(2)   Phillips,D.V.,   "Nonlinear   Analysis   of   Structural
Concrete by Finite Element Methods, Ph.D. Thesis, University
of Wales, Swansea, 1972.

(3) Cope,R.J.   and   Rao,P.V.,   "Nonlinear   Finite   Element
Strategies   for   Bridge   Slabs,   IABSE   Colloquium   on   the
Advanced Mechanics   of   Reinforced   Concrete,   Final Report,
Delft, 1981, pp. 273-288.

(4)   Crisfield,M.A.,   "Local   instabilities in the Nonlinear
Analysis   of   Reinforced   Concrete   Beams   and   Slabs",
Proceedings   Inst.   Civ.   Eng.,   Part   2, Vol. 73, 1982, pp.
135-145.

(5) Al-Manaseer,A.A.,   "A   Nonlinear Finite Element Study of
Reinforced   Concrete   Beams", Ph.D.   Thesis,   University   of
Glasgow, 1983.

(6) Park,R. and Paulay,T., "Reinforced·Concrete Structures",
Wiley, 1975.

(7) Ferguson,P.M., "Reinforced   Concrete   Fundamentals", 4th
Edition, Wiley, 1981.

(8) Crevenka,V., "Inelastic Finite Element Analysis of Reinforced Concrete Panels Under Inplane Loads", Ph.D. Thesis, University of Colorado, 1970.

(9) Ramakrishnan,V. and Ananthanaryan,Y., "Ultimate Strength of Deep Beams in Shear", ACI Journal, Vol. 65, Feb., 1968, pp. 87-98.

(10) Kong,F.K. and Robins,P.J., "Shear Strength of Reinforced Concrete Deep Beams", Concrete, Vol. 6, March, 1972, pp. 34-36.

(11) Buyukozturk,O., "Nonlinear Analysis of Reinforced Concrete Structure", Computers and Structures, Vol. 7, 1977, pp. 149-156.

(12) Phillips,D.V. and Zienkiewicz, O.C, "Finite Element Nonlinear Analysis of Concrete Structures", Proc. Inst. Civ. Engnrs., Vol. 61, Part2, 1976, pp.59-88.

(13) Lin,C.K., "Ultimate Strength Design of Deep Beams", M.Sc Thesis, University of Glasgow, 1977.

(14) Memon,G.H., "Ultimate Strength Design of Perforated Deep Beams", M.Sc. Thesis, University of Glasgow, 1980.

(15) Al-Manaseer,A.A. and Phillips, D.V., "Numerical Study of Parameters Affecting Nonlinear Solutions in Reinforced Concrete Beams", Proc. Annual Conf. Canadian Soc. Civ.

Engng, Saskatoon, Canada, 1985, pp. 163-183.

(16)   Burns,N.H.   and   Siess,C.P.,   "Load-Deformation
Characteristics of Beam-Column Connections in Reinforced
Concrete", Structural Research Series No. 234, Civil
Engineering   Studies,   University   of   Illinois,
Urbana-Champain, Illinois, Jan., 1962.

(17) Suidan,M. and Schnobrich,W.C., "Finite Element Analysis
of Reinforced Concrete", Jour. Struct. Div., ASCE, Vol. 99,
Oct., 1973, pp. 2109-2122.

(18)   Hand,F.R.,   Pecknold,D.A.   and   Schnobrich,W.C.,   "A
Layered Finite Element Nonlinear Analysis of Reinforced
Concrete   Plates   and   Shells",   Technical   Report
UILU-ENG-72-2011, University of Illinois, Aug., 1972.

(19) Hsu,T.T.C., "Torsion of Structural Concrete - Plain
Concrete Rectangular Sections", ACI Special Publication,
Torsion of Structural Concrete, SP18, 1968, pp. 203-238.

(20) Hsu,T.T.C., "Torsion of Structural Concrete - Behaviour
of Reinforced Concrete Rectangular Sections", ACI Special
Publication, Torsion of Structural Concrete, SP18, 1968, PP.
261-306.

(21) ACI Committee 318, "Building Code Requirements for
Reinforced   Concrete   (ACI   318-71)",   American   Concrete
Institute, Detroit, 1971.

(22) Melhorn,G. and Schmidt-Gonner,G., "A Calculation for Reinforced Concrete Beams Under Bending and Torsion Using Three-Dimensional Finite Elements", IABSE Colliqiuum on Advanced Mechanics of Reinforced Concrete, Delft, 1981, pp. 591-601.

(23) Hsu,T.T.C. and Mo,Y.L., "Softening of Concrete in Torsional Members", Research Report ST-TH-001-83, Dept. Civil Eng., University of Houston, Texas, 1983.

(24) Hsu,T.T.C. and Mo,Y.L., "Softening of Concrete in Torsional Members - Theory and Tests", ACI Journal, Proceedings, Vol. 82, No. 3, May-June, 1985, pp. 290-303.

(25) Collins,M.P., Walsh,P.F., Archer,F.E. and Hall,A.S., "Ultimate Strength of Reinforced Concrete Beams Subjected to Combined Torsion and Bending", ACI Special Publication, Torsion of Reinforced Concrete, SP18, 1968, pp. 379-402.

(26) Clark, L.A. and Thorogood, P., "Shear Strength of Concrete Beams in Hoging Regions", Proc. Instit. Civil Engs., Part 2, Vol. 79, June, 1985, pp. 315-326.

CHAPTER SIX

EXPERIMENTAL INVESTIGATION

6.1 Introduction

This chapter describes in detail the experimental set-up which was designed and constructed to study the strength and behaviour of the series of reinforced concrete L-sections under pure torsion. The instruments employed for measurements of the various quantities during the tests, as well as the test procedure, are also explained.

The aim of the experiments was to study the short-term torsional behaviour of reinforced concrete L-sections, containing longitudinal steel and closed stirrups, throughout all loading stages until failure. Information on the following aspects was sought:

(a) torque-twist behaviour

(b) crack initiation, propagation, and pattern

(c) strain distributions

(d) steel response

(e) failure characteristics

6.2 Test Programme

6.2.1 General

As already mentioned, part of the scope of this set of experiments was to directly assess current British Code procedure for torsion design of solid L-sections. It was considered that the direct approach of designing the specimens according to the code (BS:CP110 - 1972, now BS:8110 - 1985) requirements would give a full and more satisfactory assessment.

6.5.2 Description of Test Specimens and Parameters for Investigation

The test specimens form two groups as follows:

Group (B1): consists of five specimens. One specimen, designated B11 and termed the reference specimen, was designed strictly according to the British Code requirements (refs. 1, 2). Two specimens, B12 and B13, were provided with reduced amount of stirrups. The reduction was made by reducing the number of stirrups, and hence increasing the spacing, keeping the diameter the same as the reference specimen at 6 mm. The fourth specimen, B14 , was reinforced with a higher amount of stirrups. The increase was achieved through using 8 mm diameter stirrups keeping the spacing the same as B11. In all four specimens the amount of longitudinal reinforcement was kept the same so as to limit the number of parameters to one, namely the amount of transverse reinforcement.

The fifth specimen, designated B21, had the same amount of longitudinal and transverse reinforcement as the reference specimen B11. The difference between them was that B21 had 8 mm diameter stirrups instead of 6 mm for B11. This was meant to check the effect of stirrup spacing on the post-creaking behaviour and on the ultimate load.

Therefore the above covers a range of torsional reinforcement including that recommended by the current British Code of practice, for the chosen cross sectional dimensions.

Group (B3): consists of four specimens with smaller cross section. The steel variations of group (B1) were typically repeated in this group with specimen B31, designed to the code requirements, being the reference specimen for this group. The purpose of this group was to assess the code's design procedure for smaller cross section and study the effect of varying the amount of transverse reinforcement for the same amount and distribution of longitudinal steel.

Figure (6.1) and Table (6.1) give full details of the test specimens. Design of the reference specimens is presented in Appendix (A).

6.3 Torsion Test Set-up
6.3.1 General Description

A three dimensional steel test-rig, shown in Figures (6.2) and (6.3), was designed in which the reinforced concrete specimen is placed vertically. The total length of a specimen is fixed at 1550 mm as dictated by the height of the reaction frame. The rig can accommodate specimens of any cross section as long as their top and bottom ends are rectangular in shape. This imposes no practical difficulty whatsoever since the cross section of the test-zone can be made to any shape whilst making the ends rectangular. The specimen is fixed at the bottom and receives the applied torque at the top. A portal frame takes the resulting reaction at the top end. The rig was designed and constructed for a maximum torque of about 60 KN.m. Attention was paid to its overall stiffness, in particular the bottom

fixity and the top unit through which the torque is applied. The torque is applied independently through an arm of T-shape. All these parts will be separately described in the following sections.

Placing the beam vertically has practically no effect on the stress distribution or indeed the torsional behaviour, as very little stresses are induced, and can be directly compared with the effect of the self-weight in horizontal set-ups.

6.3.2 Bottom Fixity

The bottom supporting system (Figure 6.4) consists of a 900x500x50 mm steel plate firmly fixed to the laboratory floor. No displacement or rotation of this plate is allowed. On top of this plate two adjustable clamps (parts A in Figure 6.4) are provided. They are made of steel plates welded together to give this shape. They can easily be moved towards each other on the fixed plate until the beam is fully clamped in between. They can then be firmly bolted to the fixed plate and to each other as shown in the figure. In order to make sure that no movement takes place in this part, steel channels are placed to fully fill the gap between these clamps and the portal frame vertical supports.

Although this bottom support system can accommodate up to 500x500 rectangular sections, because of the freedom allowed through moving the clamps, the actual cross sectional size of the test specimen is normally dictated by the top unit as this is welded and has three sides fixed as will be shown

afterwards. Because all specimens tested had 300x400 rectangular ends with the 400 mm sides in the direction of the 500 mm dimension of the clamps, the remaining 100 mm gap was filled by two steel plates on the two sides of the specimen each being 50 mm thick. This ensures that the specimen under test is properly fixed on all four sides.

6.3.3 Top Unit and Load Application

The top unit consists of a 850x460x50 mm steel plate (Figure 6.5). On the bottom face three steel plates were welded to form three sides of a box into which the top of the specimen fits. The fourth side was an adjustable plate supported on another plate through two screwed steel bars as shown in the figure. The box was made such that it can accomodate a 300x400 mm rectangular section with the centre of the box coinciding with the centre of the rectangular section. Two steel cubes were welded on the top face of the steel plate to transfer the reactions received from the loading arm. This assembly is termed the "loading cap".

The loading arm is a T-shape steel plate (Figure 6.5). This rests horizontally on the horizontal beam of the loading frame and on the top of the loading cap. A groove was made so that a spindle goes through to transfer the reaction to the portal frame over the specimen being tested. Another role of the groove was to allow the lateral displacements of the specimen's axis of rotation during twist. A typical arrangement of the loading cap and the loading arm when ready for testing is shown in Figure (6.6). The figure also shows the arrangement of the two 100 KN load cells for

measurement of the two reactions that result when the load is applied. Two horizontally placed hydraulic jacks (each 200 KN capacity) placed one behind the other were used to apply the load (Figure 6.6 shows one of them). The reason of using two hydraulic jacks was to achieve a longer travel of 210 mm total. This ensures a maximum angle of rotation of about 13° . The arrangement around the load cell allows rotations to occur and ensures protection of the load cells from non-uniform pressure being applied.

Clearly the set-up as described is usable for pure torsion tests only . Further modifications could be made to allow application of combined loading if necessary. The size of the cross section to be tested could also be changed, if so desired, with only slight modifications to the loading cap.

6.3.4 Installation of Specimen

This involves the following steps:

(a) removal of the portal frame passing over the specimen,

(b) placing the specimen vertically in position,

(c) tightening the bottom fixity,

(d) placing the loading cap on top of and gripping of the specimen.

(e) placing the T-arm in position,

(f) placing the portal frame over the specimen making sure that the spindle is in position,

(g) placing the two hydraulic jacks,

(h) further checking of bolting all around, and finally

(i) connecting the load cells, transducers, and strain gauges to the datalogger for continuous measurements of the

various quantities.

6.4 Instrumentation

All specimens were instrumented to measure the applied loads, lateral and longitudinal displacements, concrete and steel strains and crack widths.

6.4.1 Measurement of the Applied Torque

As described earlier the loads were applied using two 200 KN hydraulic jacks in series and the reactions on the specimen were measured by two load cells of 100 KN capacity each placed at approximately equal distances from the spindle to give equal reactions R. The applied torque is then equal to the reaction (R) times the distance between the centres of the load cells (= 615 mm) as shown in Figures (6.6) and (6.7). In practice, however, it was difficult to get absolutely equal reactions but the difference rarely reached 2%. The average of the two load cell readings was taken to calculate the applied torque.

6.4.2 Measurement of the Lateral Displacements and
Evaluation of Angles of Rotation

One advantage of testing the specimens vertically is the ease of measurements and observation of behaviour on all four faces. In order to obtain the angles of rotation the lateral displacements over a fixed length of the "test zone" were measured. Two "levels" of linear voltage displacement transducers (LVDT) were used, each comprising of six transducers as shown in Figure (6.7). The transducers (measuring to 0.0001 mm) were mounted on an independent

frame which surrounded the specimen as shown in the figure. The frame was made of handy angles and sufficiently stiffened to prevent any movement.

Each pair of transducers was placed "over" each other so that the relative displacement is equal to the difference in their readings. Hence six relative displacements were obtained for each specimen as shown in Figure (6.8). In calculating the angles of twist it is assumed that the two sides of the cross section remain undistorted as shown in the figure. This allows the following relationships to be derived using similarity of triangles:

$$d_1 = \frac{\delta_1 x_1}{(\delta_1 + \delta_3)} \tag{6.1}$$

$$d_2 = \frac{\delta_2 d_1}{\delta_1} \tag{6.2}$$

$$\theta_1 = \tan^{-1} \frac{\delta_1}{d_1} = \tan^{-1} \frac{\delta_2}{d_2} = \tan^{-1} \frac{\delta_3}{x_1 - d_1} \tag{6.3}$$

$$d_4 = \frac{\delta_4 x_2}{(\delta_6 + \delta_4)} \tag{6.4}$$

$$d_5 = \frac{\delta_5\, d_4}{\delta_4} \qquad\qquad (6.5)$$

$$\theta_2 = \tan^{-1}\frac{\delta_4}{d_4} = \tan^{-1}\frac{\delta_5}{d_5} = \frac{\delta_6}{(x_2 - d_4)} \qquad (6.6)$$

The angles of twist, θ_1 and θ_2 were found to differ slightly before cracking and in a more noticeable way after cracking. However, for practical purposes and also in comparing experimental with finite element results the average angle is considered as the differences did not suggest otherwise.

6.4.3 Measurement of Unit Lengthening

It was reported in Chapter Two that an important phenomenon associated with torsional behaviour of reinforced concrete members is unit elongation after cracking. To enable measurement of this quantity a vertical transducer was placed on top of the loading cap and fixed on the portal frame passing over the specimen such that it measured vertical displacement at the centre of the rectangular part.

Because of the stiff end rectangular parts of the test specimens, the elongation is assumed to have been due to the elongation of the L-section part of the specimens. In support of this assumption no cracking of the specimen ends was observed as will be shown in Chapter Seven. This is because these ends were heavily reinforced and clamped along 2/3 of their lengths in either the loading cap or the bottom fixity.

6.4.4 Measurements of Steel Strains

strains in longitudinal and transverse steel were measured by means of 6 mm long electrical resistance strain gauges connected to a linear voltage processing data logger (Type Orion A). because two types of steel strains gauges were used during the course of the experimental programme, namely (Student EA.06.2401Z-120 and Jurvis Cu45Ni), due to availability, comparisons were made between these two types and the extensometer used for the standard tensile test of steel. Results of this comparison are presented in section (6.5.3).

6.4.5 Measurements of Concrete Surface Strains

Demec gauges were used for measuring concrete surface strain. The average concrete strains were measured over a gauge length of 100 mm. Because the torsional cracking was expected to form at an angle of about 45 degrees with the longitudinal axis, two pairs of demec gauges were mounted at 7 locations around the specimen as shown in Figure (6.16). The pair parallel to the crack direction would measure the compressive strain while the pair normal to the crack measures the tensile strain.

6.4.6 Crack Widths, Spacings and Inclinations

Crack widths were measured by means of a hand crack width measuring microscope (measuring to 0.02 mm). Two cracks were selected on each face of the specimen, after crack initiation, and their widths were measured at each load increment. The selection of the cracks, however, was based on the most dominant cracks at the early stages of crack

development.

Crack spacings were measured on all faces of each specimen. The spacing is taken as the normal distance between each two major cracks. It is often difficult to define the most major crack at failure of a specimen but as a general rule adopted here every well and distinctly defined crack is taken as a major crack. Five crack spacings were measured on each side of the specimen covering the whole test zone.

Angles of cracks on the faces of the specimens were recorded and the crack patterns were followed from the first stages up to failure and clearly marked. Every effort was made to record the failure characteristics of each specimen in order to identify the effects of the test parameters.

6.5 Materials

6.5.1 Concrete

The concrete mix consisted of rapid hardening portland cement (RHPC) for all specimens except B14 where ordinary portland cement (OPC) was used because of availability. However, B14 was tested at an older age to compensate for the strength. 10 mm Hynford gravels and zone 2 Hynford sand, obtained from Lanarkshire, were the coarse and fine aggregates used. A mix proportion of 1:1.5:3 was designed for an average cube strength of 40 N/mm^2 at 7 days. A minimum slump of 100 mm was specified. Six cubes and at least four cylinders were cast with each specimen. The cubes were used to determine the cube strength, two cylinders for the splitting strength, and two cylinders for the concrete

Young's modulus (and the stress-strain curve) and the cylinder strength. Figure (6.9) shows a typical concrete stress-strain curve obtained for specimen (B31).

6.5.2 Reinforcing Steel

High yield deformed bars of diameter 6, 8, 10, 12, and 16 mm were used for longitudinal and transverse reinforcement. Random samples were cut off from the batches of steel bars for all different sizes and were tested in Tinus Olsen Universal Class A testing machine, fitted with an S-type electronic extensometer. The testing procedure followed the manufacturer's instruction manual. Stress-strain curves for all bar sizes used are shown in Figure (6.10). It can be seen from the curves that not all bars followed the behavioural characteristics expected from high yield steel. For 6, 12 and 16 mm bars well defined yield points were observed. For 8 and 10 mm bars, because the yield point was not well defined as shown in the figure, the yield stress was taken as the stress corresponding to 0.2% proof strain. Table (6.2) shows the steel properties for all the bar sizes used.

6.5.3 Comparison of Extensometer with the Two Types of
      Strain Gauges

It was mentioned earlier that two types of strain gauges were used to record the steel strains due to availability at the time. Because of this and also because an extensometer was used for the steel tensile tests a comparison was carried out. This was done in the Olsen machine with an 8 mm diameter bar. Six strain gauges (three of each type) were

mounted on the bar as shown in Figure (6.11) together with the extensometer. The test followed the same procedure as for the standard tensile test of steel.

Figure (6.12) shows the results of the comparison which indicates clearly that the three instruments measured the same strain up to a value of about 3500 microstrain. Between 3500 and about 6000 microstrain there are deviations, although of little practical significance. Beyond this value the extensometer curve is above the rest indicating smaller values of strain than that measured by the strain gauges for the same load. The value of 6000 microstrain is well beyond the yield value of steel and all specimens failed while the steel strains were well below this value. Therefore it was not thought necessary to make any correction to strain values obtained from the experiments.

6.6 Preparation of Specimens and Test Procedure
6.6.1 Strain Gauging

Figure (6.13) shows the various levels of the measurement devices on a typical specimen. The first step towards specimen preparation was mounting of the steel strain gauges on the selected positions. Figure (6.14) shows the positions chosen on longitudinal bars and stirrups for all specimens, which give a total of 20 strain gauges per specimen. Of interest is the positions on the closed stirrups in an attempt to record the steel response on most legs of the stirrup. Two stirrups and six of the main bars were strain gauged as shown in the figure.

The preparation of the strain gauge installation area required the surface to be filed and smoothened with sand paper. Care was taken not to remove considerable area of steel during the operation. The surface was thereafter treated with M-prep conditioner and M-prep neutralizer (ref. 3). To cement the strain gauge and terminal strip to the bar, M-bond 200 adhesive was employed. For gauge protection against moisture and mechanical damage during casting, air drying protective coating type M-coat D and epoxy resin were applied on the gauge and terminal. A final voltmeter check was carried out for each strain gauge.

6.6.2 Reinforcing Cages and Formwork

Figure (6.15) shows a typical reinforcing cage placed inside the formwork ready for casting. The net cover was normally 20 mm. The formwork was made from 20 mm thick plywood strengthend by external 50x50 mm timber battens at the corners. The internal dimensions were 1550x400x300 mm. To achieve flexibility and reuse of one mould for more than one specimen, polystyrene blocks were used to give the desired L-shape at the test-zone and the rectangular ends. After removal of the specimen from the shuttering the polystyrene block could easily be removed. Hence the change in the cross-sectional dimensions was achieved through changing the polystyrene block dimensions.

6.6.3 Casting and Curing

Casting was normally done in two concrete batches because of the amount of concrete required. Care was taken to ensure distribution of the two mixes and collection of the control

specimens (cubes and cylinders) from both batches. The specimens were placed horizontally for casting because of practicality. Internal 12 mm poker vibrator was used during casting of all specimens for about 30 minutes until all the concrete was placed.

After casting, the specimens, cubes and cylinders were cured under damp hessian for the first three days before removing the formwork for final curing under laboratory conditions until the time of testing.

6.6.4 Demec Gauges on Concrete Surface

When cured the specimen was white painted in order to enable clear tracing of cracks and demec gauge were glued to the concrete surface using Araldite. Figure (6.16) shows the location of demec gauges on the cross section of a typical specimen. The specimen was then installed in position ready for testing (section 6.3.4).

6.6.5 Loading and Recording of Readings

About 15-20 load increments were applied on a typical specimen. Two readings were taken for each load increment, one before the demec gauge readings were manually recorded and one afterwards. The process of reading all demec gauges took about 5 minutes, on average, before cracking. After cracking, however, this time increased to an average 10 minutes. It was noticed that a slight drop in all readings took place between the two sets of readings for each load increment. However, the first (higher values) were considered for all analysis and comparison purposes because

that loading was considered to have been carried by the
section anyway. Loading was continued until failure was
noted by either a continuous drop of applied load value or a
sudden fall of that value combined by a physically
noticeable failure.

During loading, crack propagation was closely followed and
marked as the corresponding load increment was recorded on
the concrete surface at the tip of each crack. The total
duration of a test averaged between 2 to 3 hours depending
on the total number of load increments applied. It was
noticed that the maximum travel provided by using the two
hydraulic jacks was sufficiently enough for all specimens to
reach their ultimate loads. A few more readings were taken,
whenever possible, in an attempt to trace the falling branch
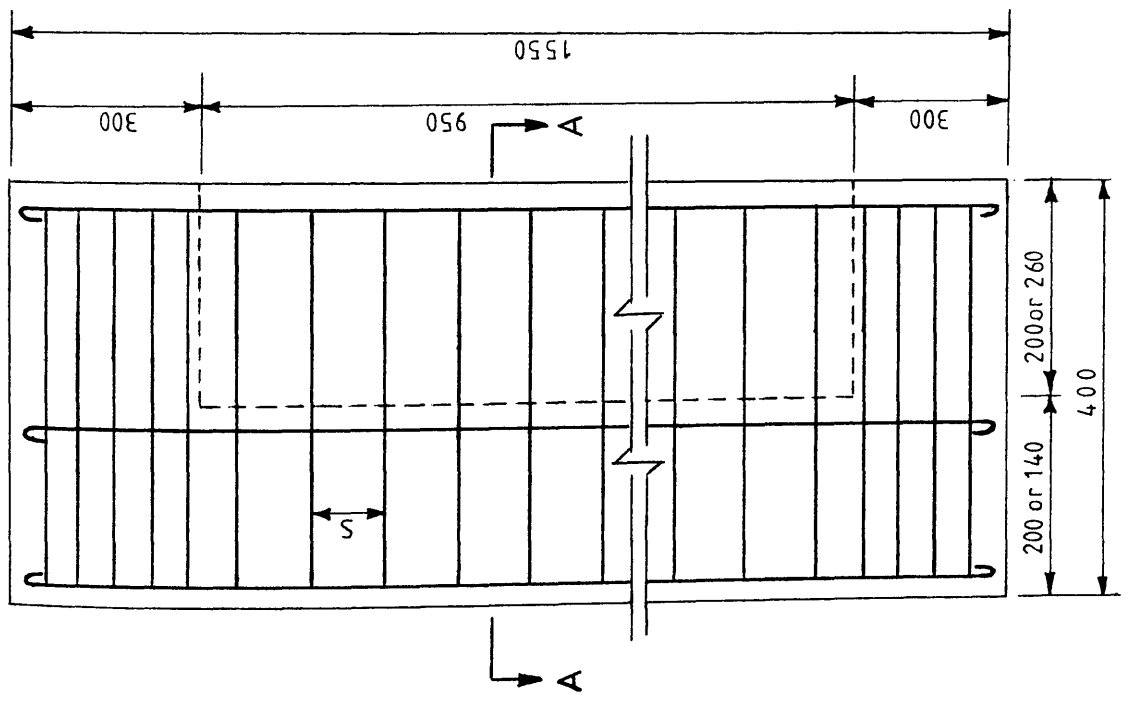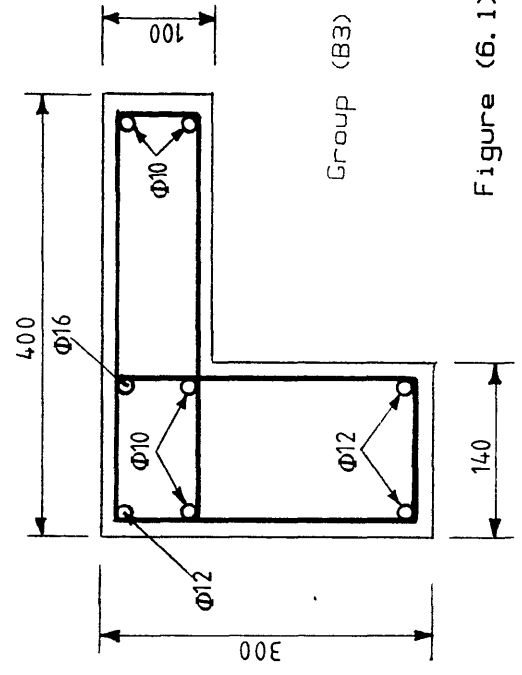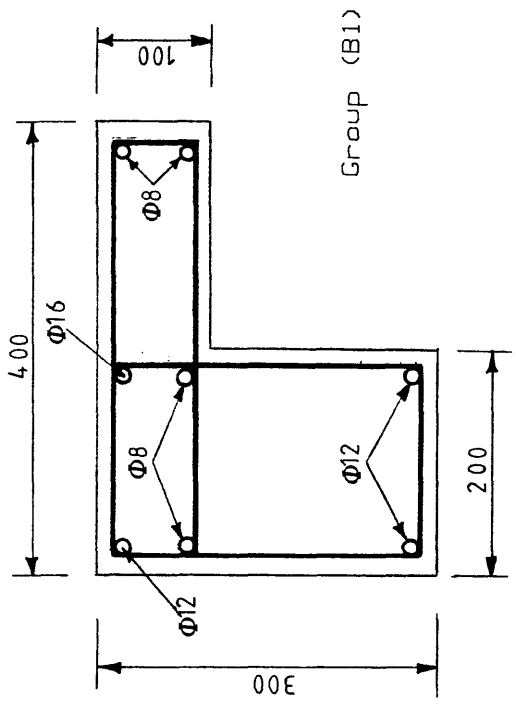of the torque-twist curve.

(a) Isometric view

Cross section
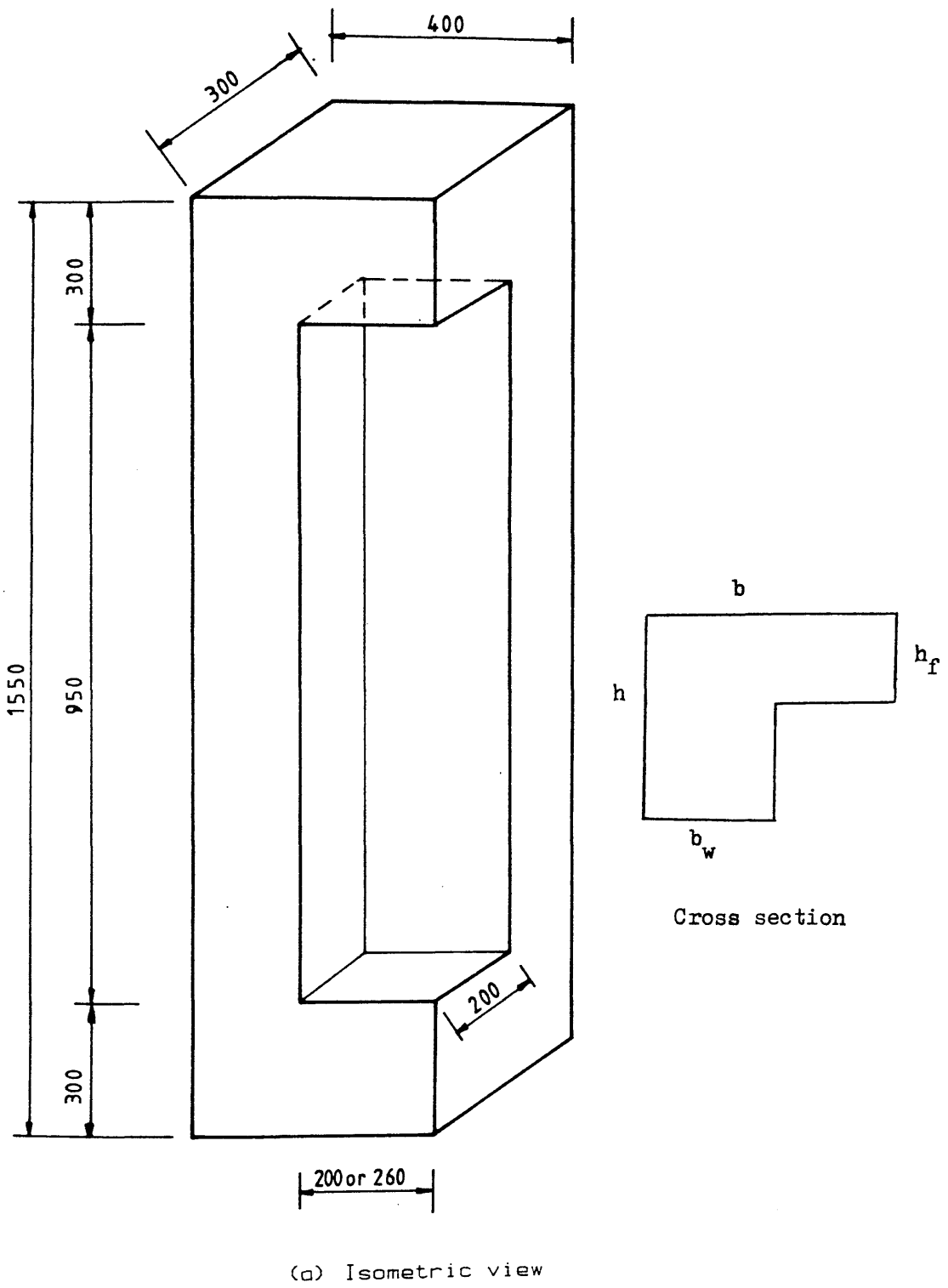
Figure (6.1) Details of test specimens

Group (B1)

Group (B3)

Figure (6.1) Continued

(b) Dimensions and reinforcement

Table (6.1) Details of specimens for the present test series

Model	b (mm)	b_w (mm)	h (mm)	h_f (mm)	h/b_w	ℓ_l %	ρ_v %	ρ_t %	ϕ_v (mm)	s* (mm)	f_{cu} (N/mm²)	f'_c (N/mm²)	f_{sp} (N/mm²)	E_c (KN/mm²)	Age (days)
B11	400	200	300	100	1.5		1.073	2.0	6	50	42.8	33.4	2.9	23.0	28
B12							0.790	1.717	6	70	50.3	39.6	2.9	21.5	14
B13						0.927	0.565	1.492	6	100	40.7	35.2	2.8	20.7	14
B14							1.906	2.833	8	50	52.3	39.4	3.2	23.0	39
B21							1.073	2.0	8	90	41.0	33.2	3.0	22.8	25
B31	400	140	300	100	2.143		1.156	2.355	6	50	44.7	35.0	2.8	23.0	14
B32						1.199	0.852	2.051	6	70	50.2	33.4	2.9	21.0	10
B33							0.609	1.808	6	100	42.3	33.1	2.7	21.1	14
B34							2.243	3.5	8	50	38.4	35.7	2.9	22.9	9

* See Figure (6.10) and Table (6.2) for full reinforcement properties
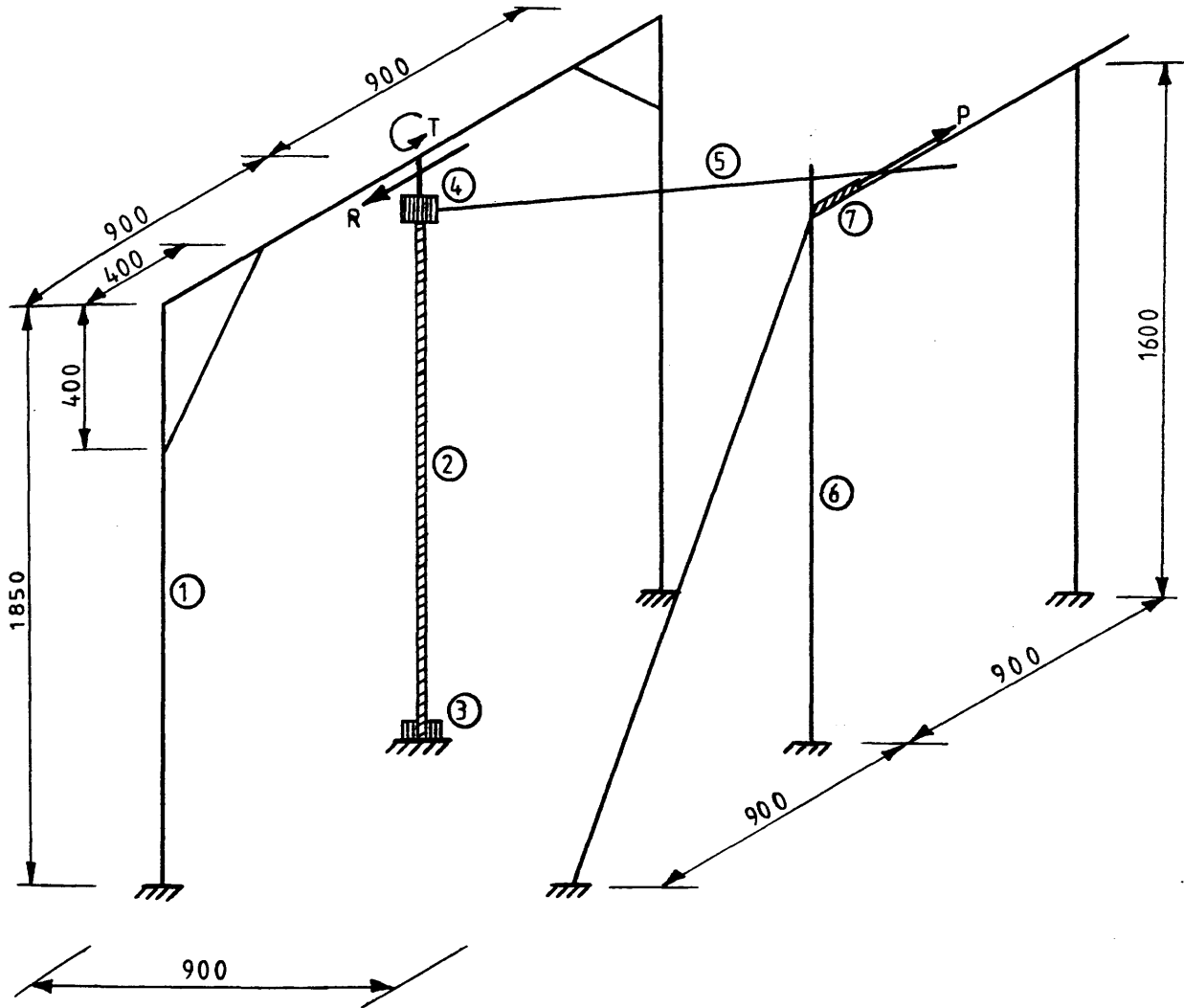
Figure (6.2) Isometric view of test-rig

(1) portal frame   (2) RC test specimen
(3) bottom fixity   (4) top unit (loading cap)
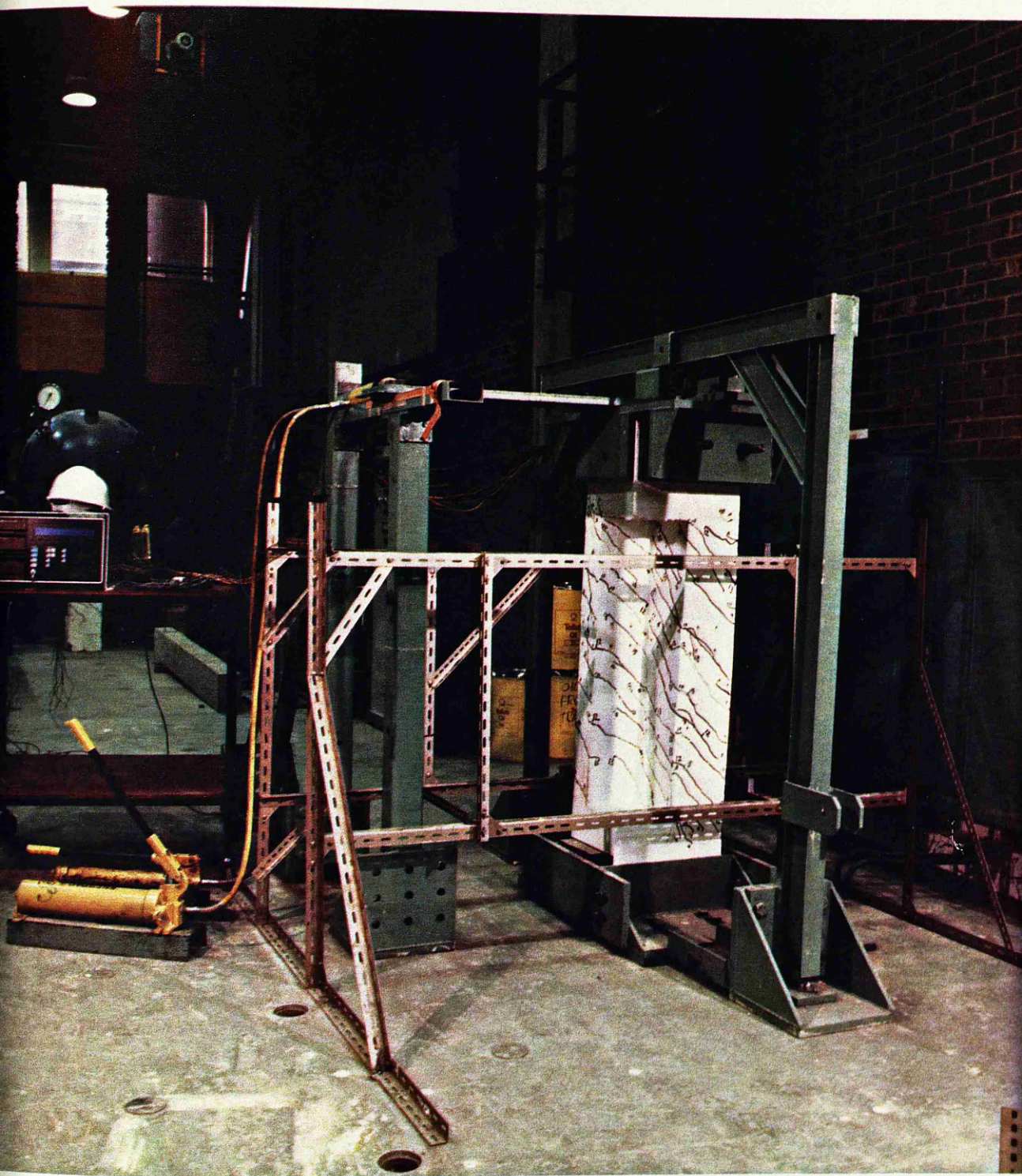(5) loading T-arm   (6) support system for hydraulic jacks
(7) 2 hydraulic jacks

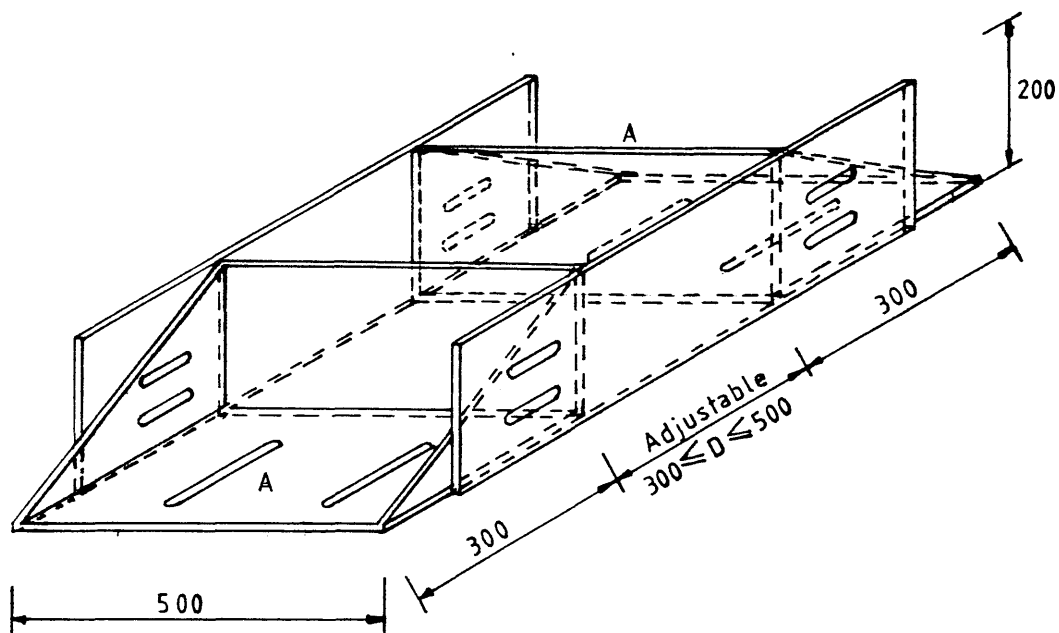Figure (6.3) Photograph of test-rig with specimen (B14) after test
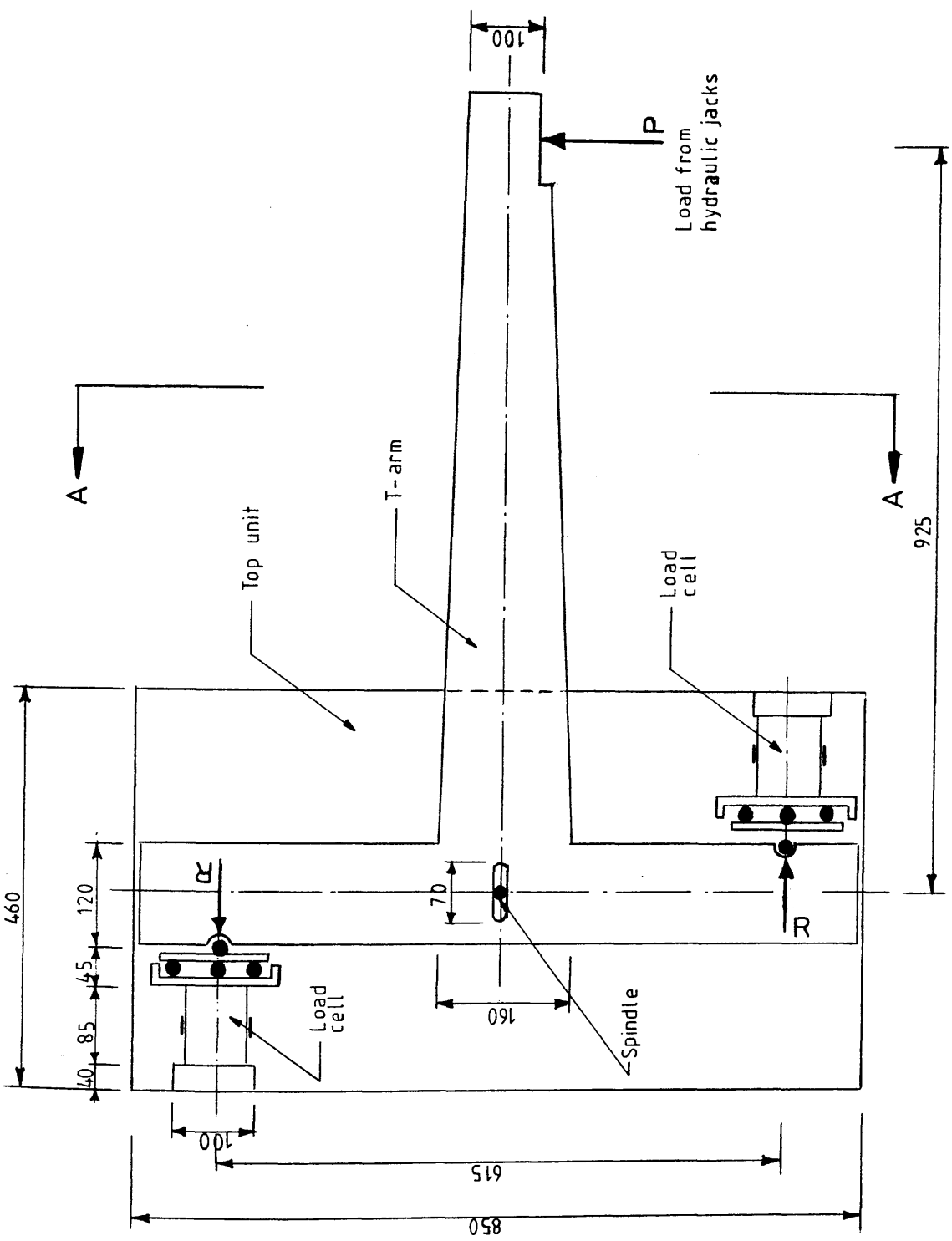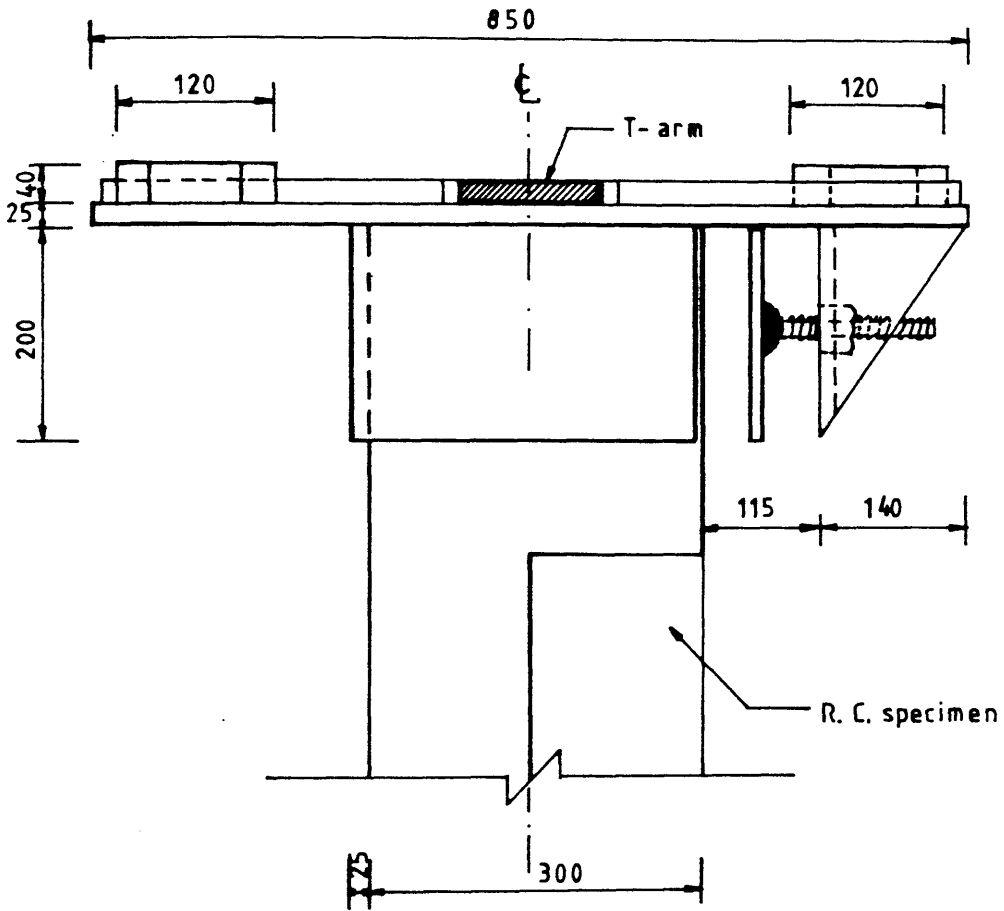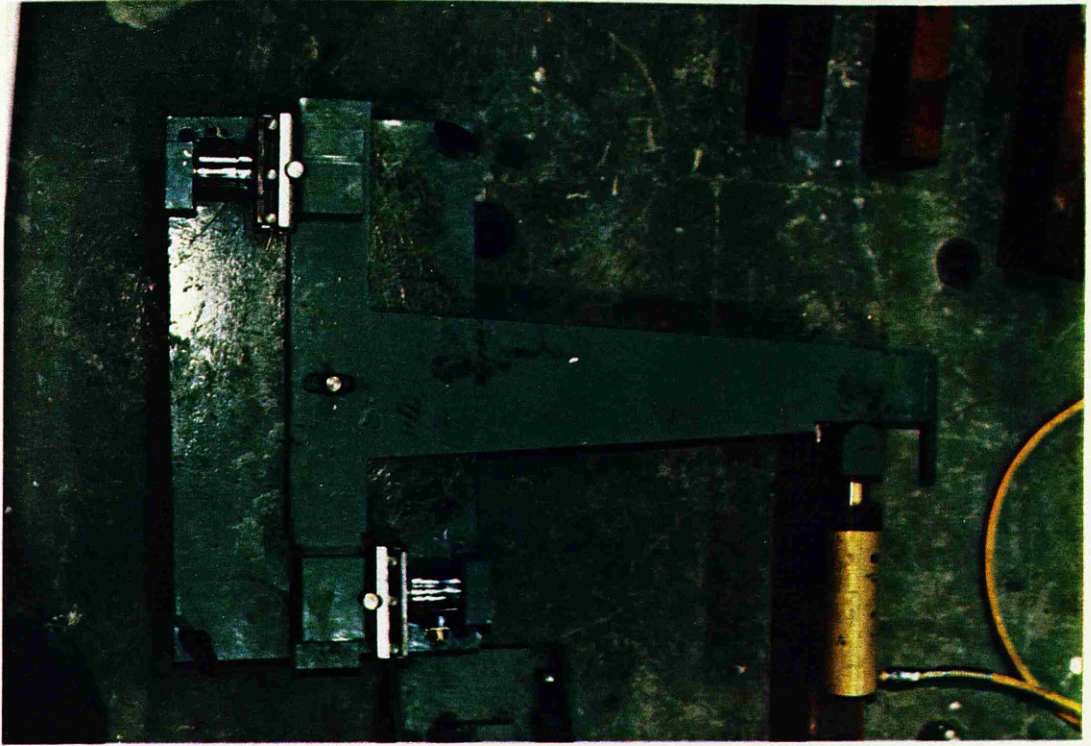
Figure (6.4) Details of bottom fixity

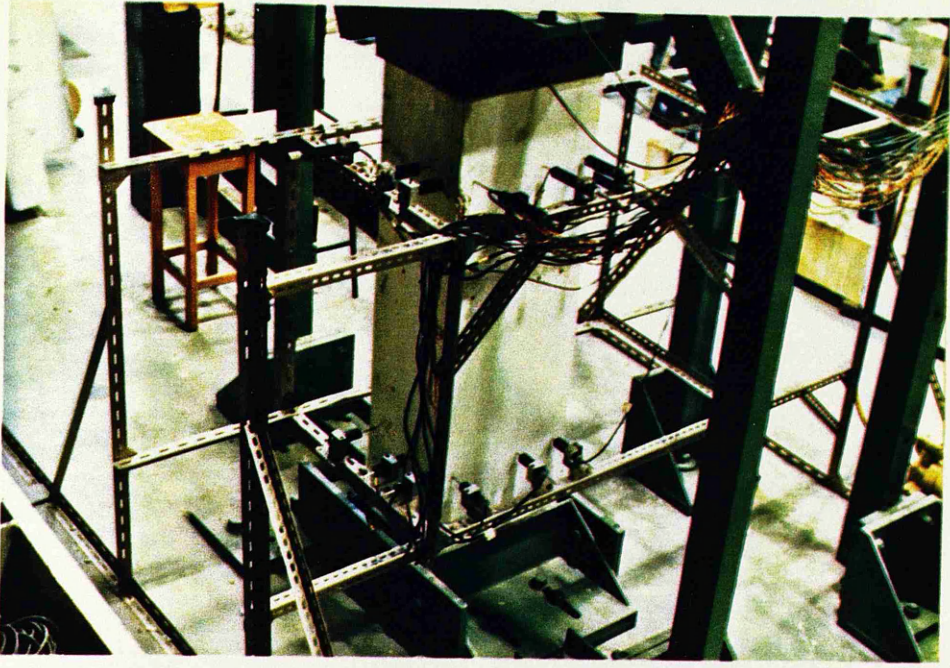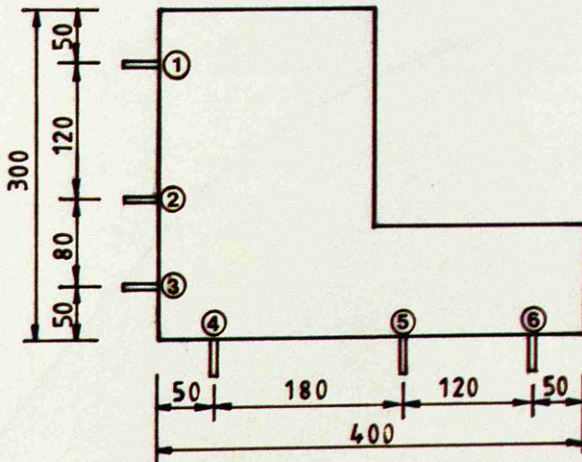Figure (6.5) Top view of loading cap and T-arm

Section AA

Figure (6.5) Continued

Top view

Figure (6.6) A typical arrangement of loading cap, T-arm, load
cells and hydraulic jack(s)

(a) Isometric view

(b) Top view

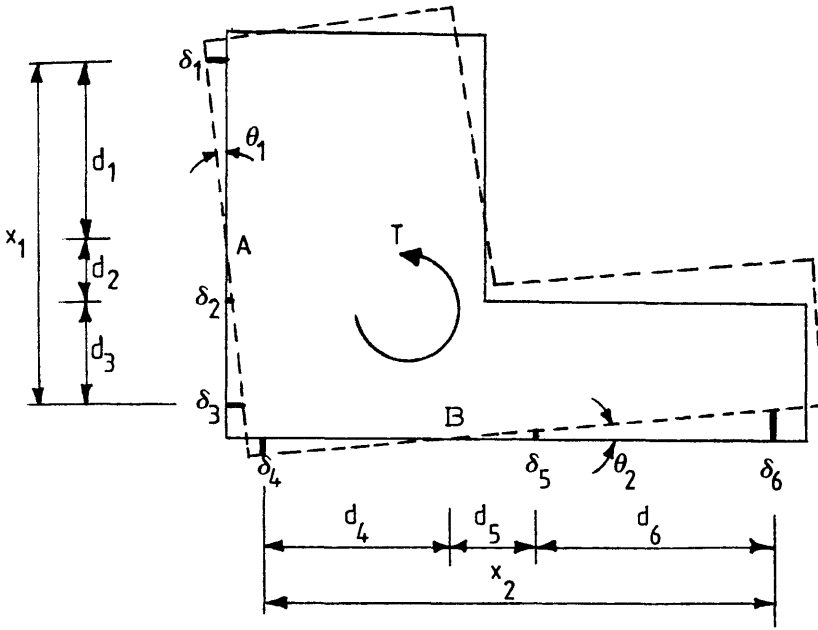Figure (6.7) Arrangement of transducers

Figure (6.8) Assumed rotation of cross section for evaluation of angles of rotation
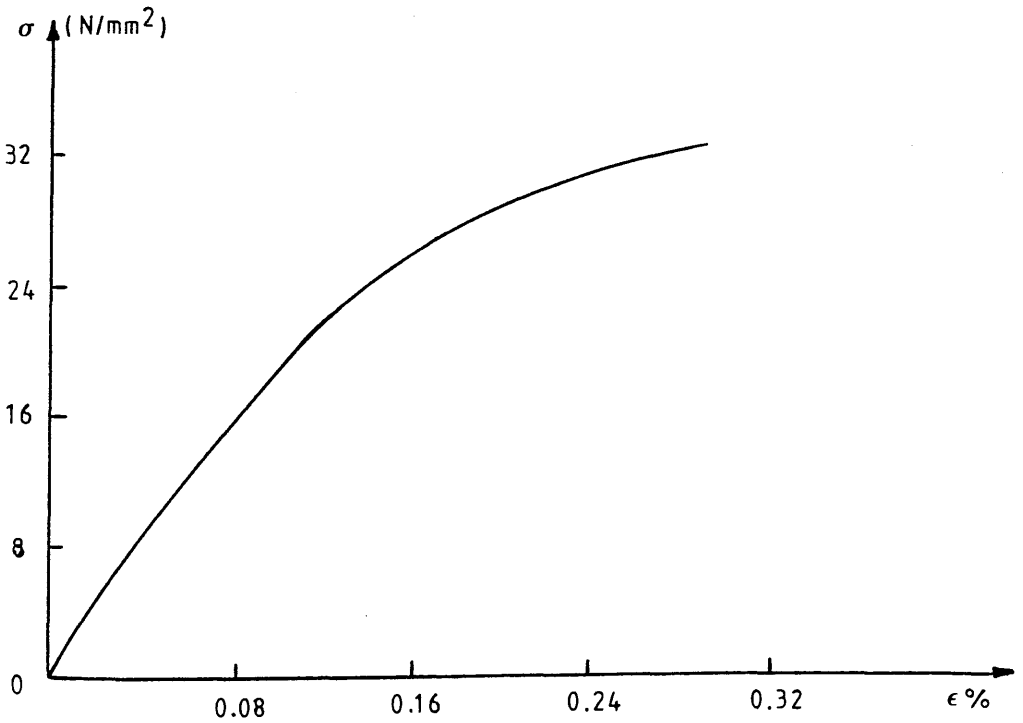
Figure (6.9) Typical concrete stress-strain curve (for specimen B13)

Table (6.2) Steel properties of the present series

Bar size mm	Area mm^2	E_s KN/mm^2	f_y N/mm^2	ϵ_y mm/mm	0.2% proof stress N/mm^2	E_w KN/mm^2
6	28.0	180.0	465.0	0.0026	-	-
8	50.0	214.0	-	-	536.0	10.0
10	79.0	206.6	-	-	500.0	7.0
12	113.0	199.2	518.0	0.0026	-	-
16	201.0	181.0	542.0	0.0030	-	-
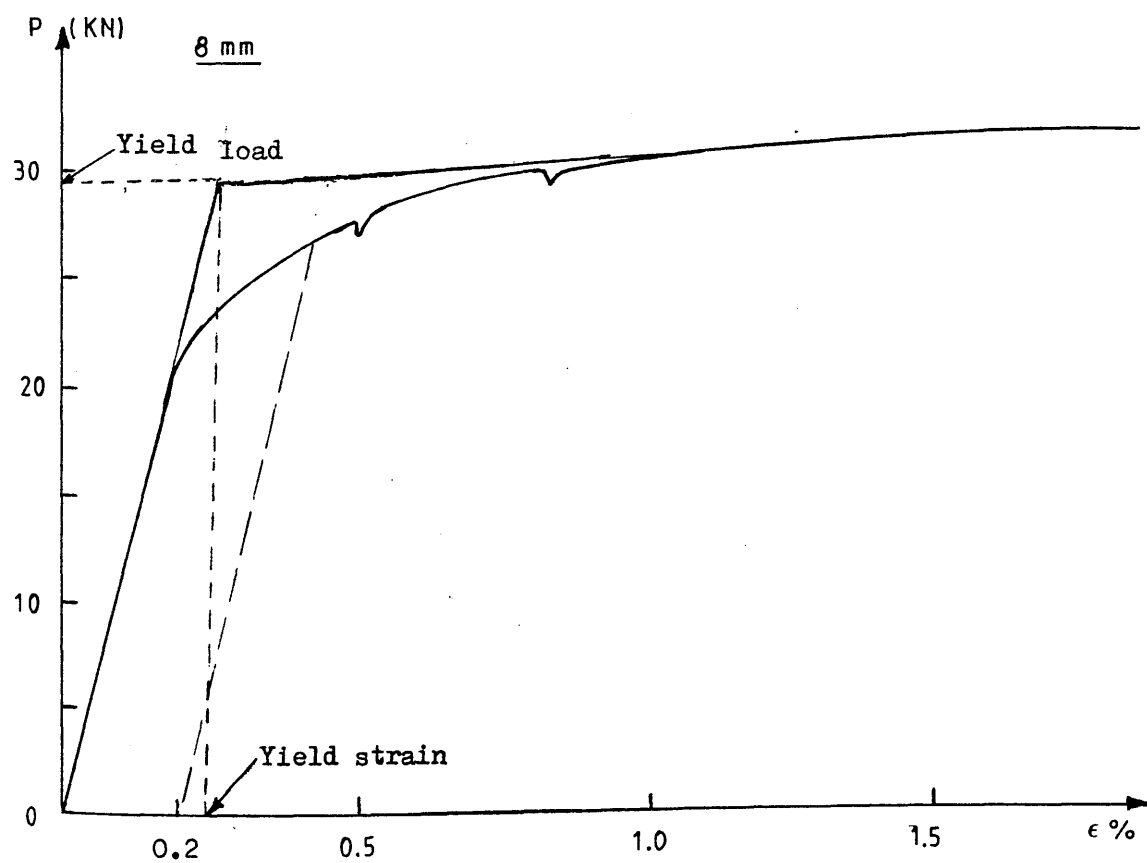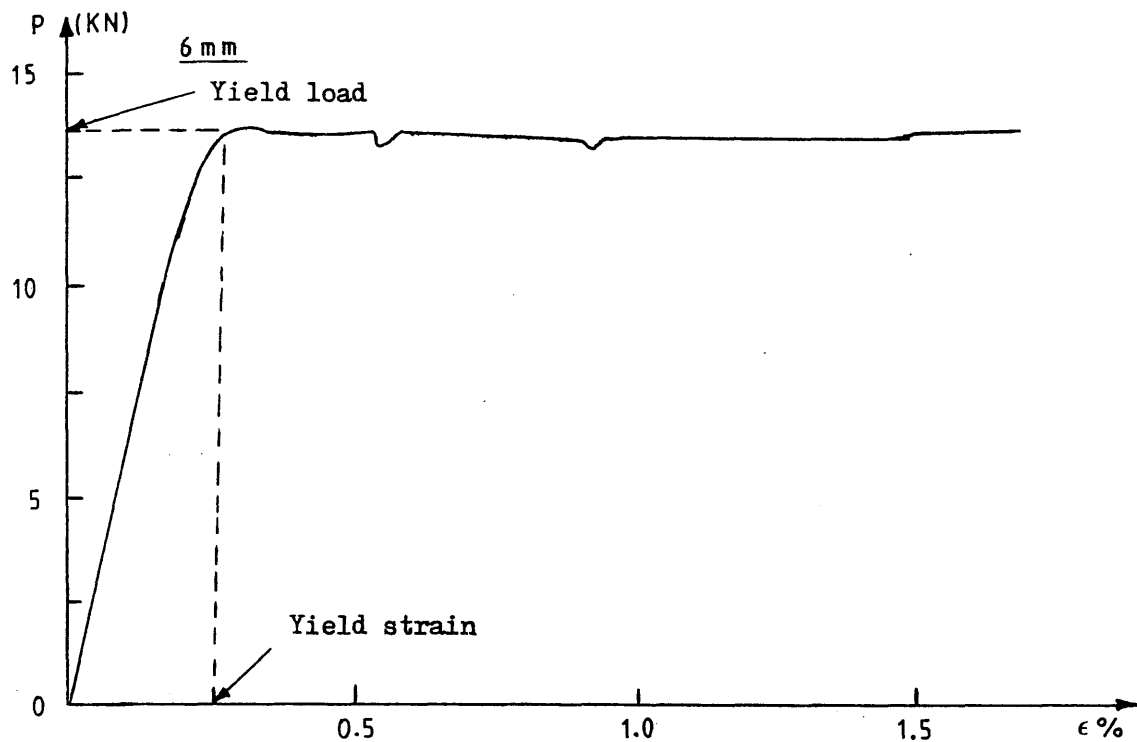
Figure (6.10) Steel stress-strain curves
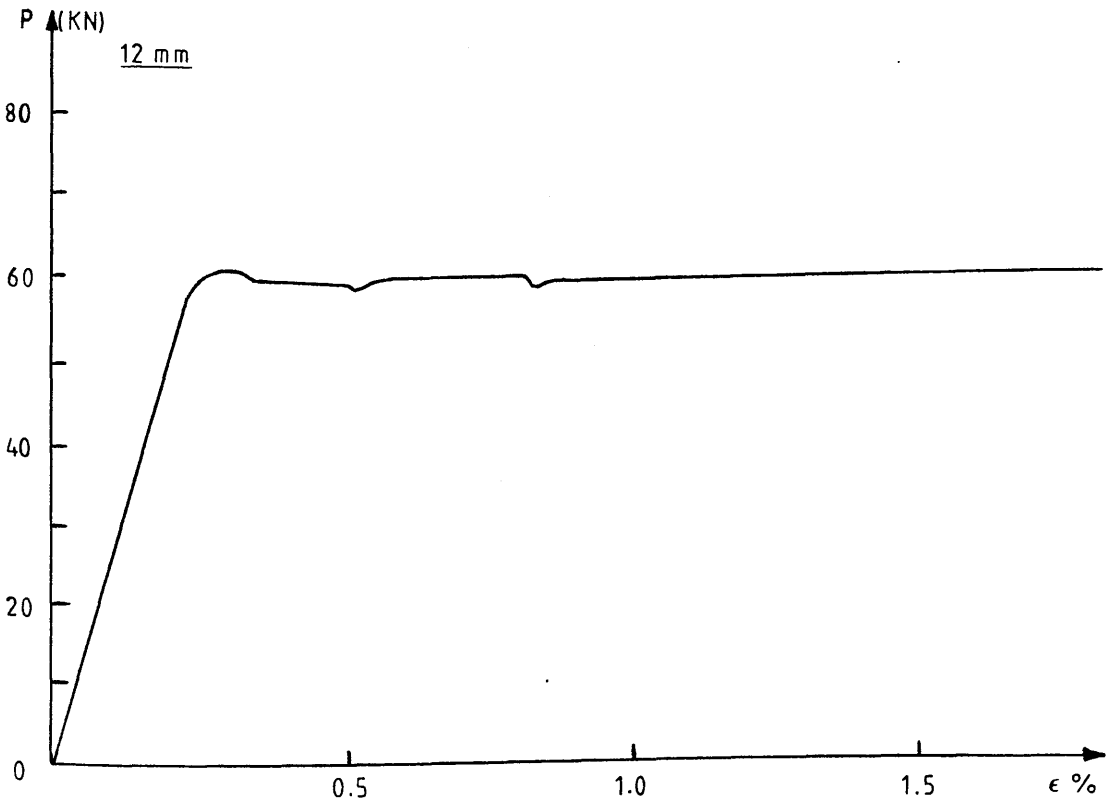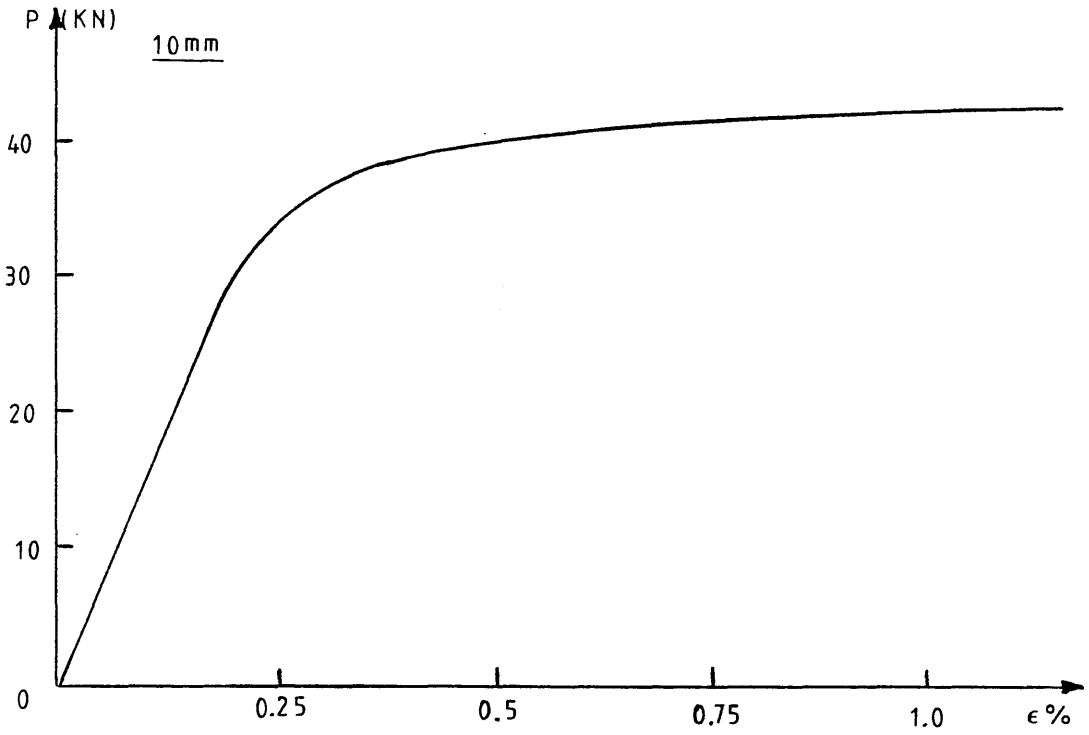
Figure (6.10) Continued
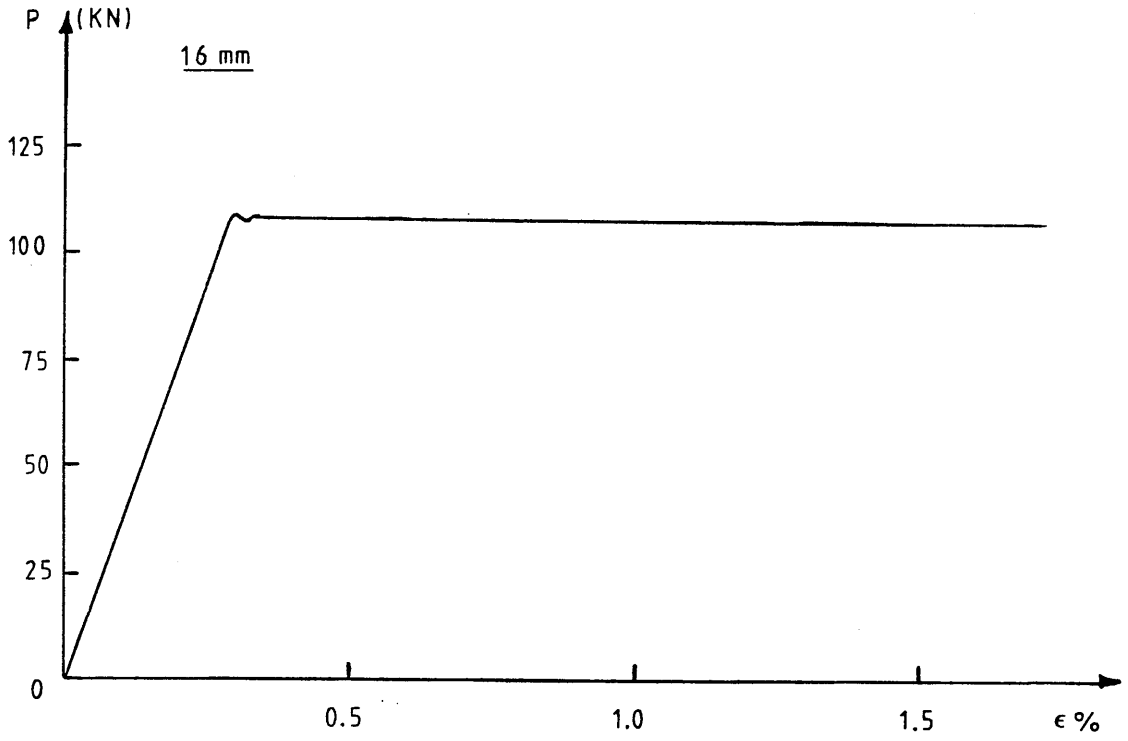
Figure (6.10) Continued
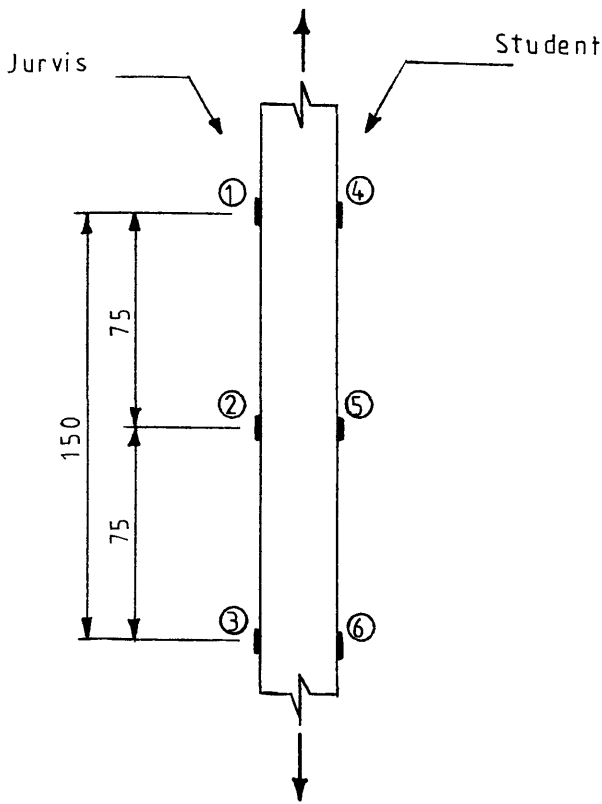
Figure (6.11) Arrangement of extensometer and strain gauges for comparison
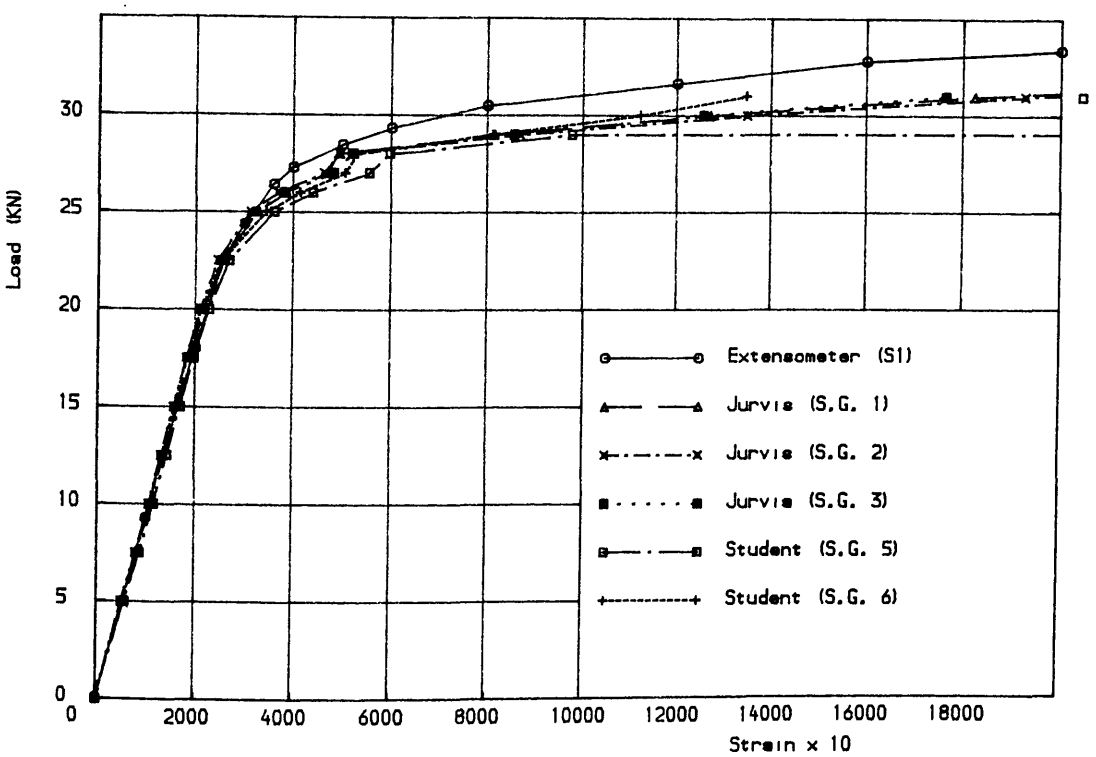
Figure (6.12) Comparison of extensometer with the two types of strain gauges
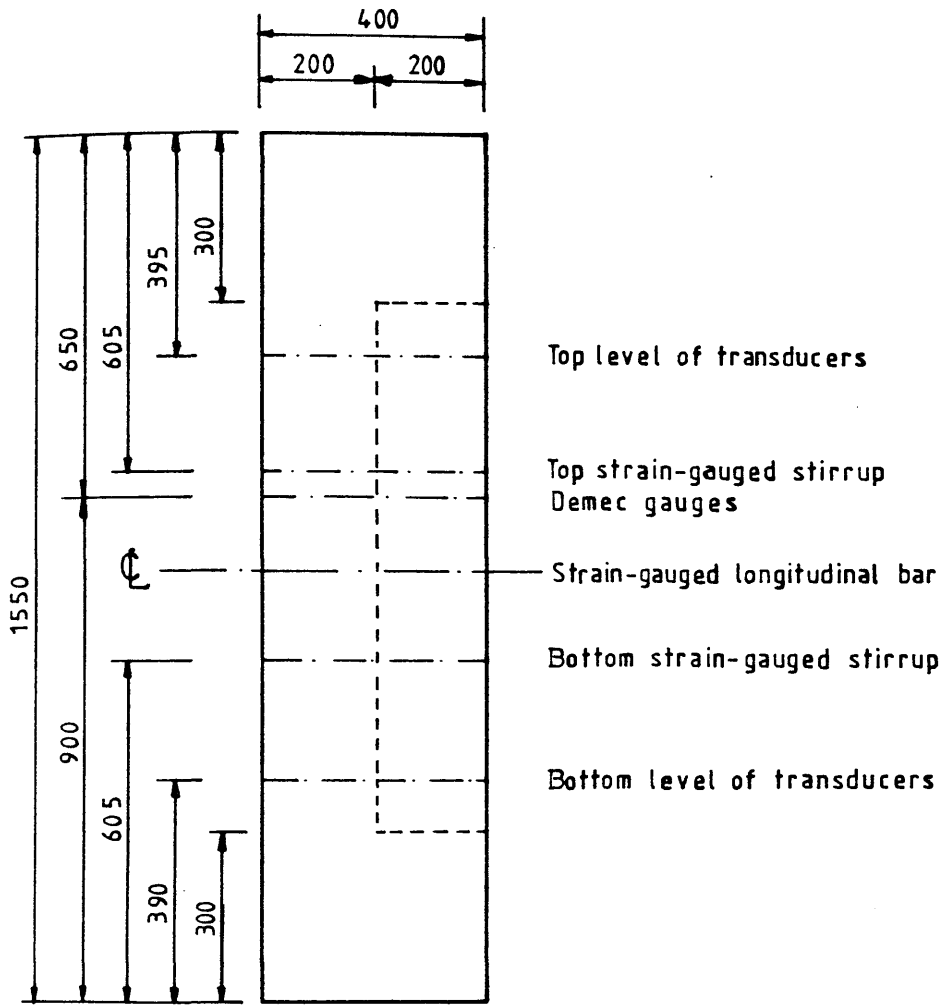
Figure (6.13) Elevation of a typical specimen showing various levels of measurement devices

(a) Stirrups

(b) Longitudinal bars
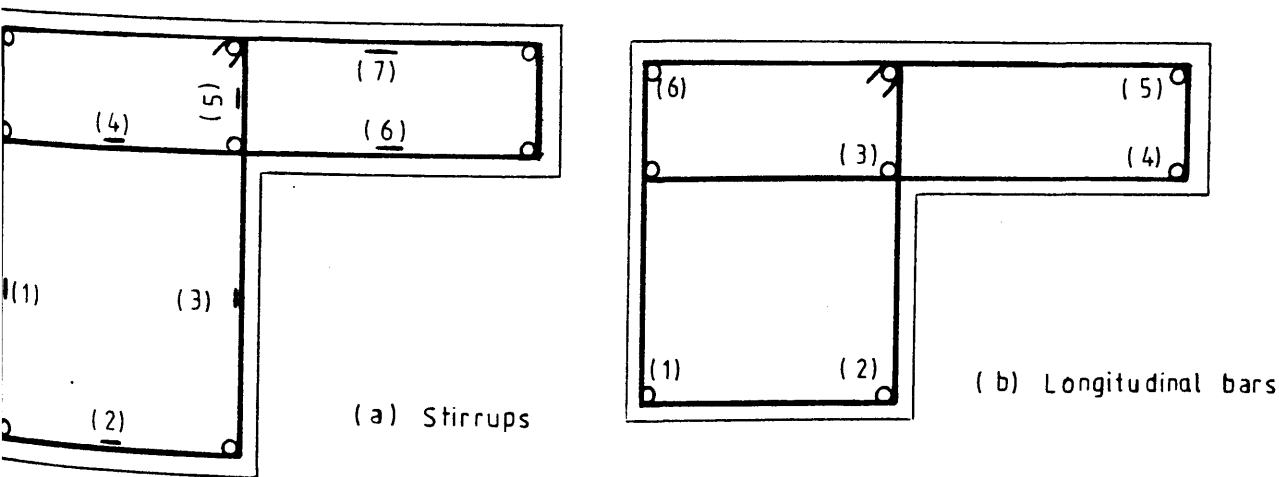
Figure (6.14) Location of steel strain gauges

Figure (6.15) Reinforcing cage for a typical model ready for casting
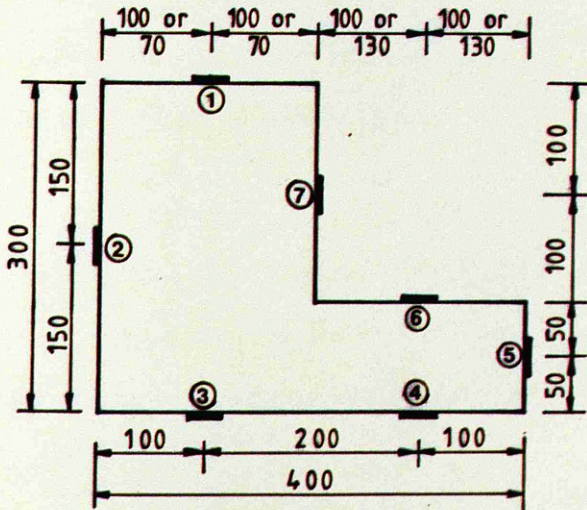
Figure (6.16) Location of demec gauges on the concrete surface

References

(1) a. CP110-1972, "Code of Practice of the Structural Use of Concrete ", Part 1, Design, Material and Workmanship, Brit. Stand. Instit., London, 1972.

(1) b. BS:8110-1985, "British Standard Structural Use of Concrete", Part 2, Code of Practice for Special Circumstances, Brit. Stand. Instit, London, 1985.

(3) Khul Harald, "Strain Gauges; theory and handling", Philips Elektronik Industrie GmbH-Hamburg.

CHAPTER SEVEN

EXPERIMENTAL RESULTS AND DISCUSSIONS

7.1 Introduction

In this chapter the experimental results are presented and discussed. For completeness, the objectives of the tests are restated as follows:

(1) To assess the validity of some aspects of the current British Code (BS8110) design procedure for torsion with special reference to solid L-sections. The reference specimen of each group was designed and detailed strictly according to the code's recommendations as explained in Chapter Six.

(2) To obtain a better insight into the torsional behaviour of properly reinforced concrete L-sections (i.e. having closed stirrups for both web and flange). The main variables for investigation were: (a) cross sectional size, (b) amount of transverse reinforcement and (c) stirrup spacing.

(3) To use these results to check the reliability of the nonlinear three dimensional finite element model for the analysis of these types of cross sections under torsion.

(4) To complement these results with the results of a parametric study, to be presented in Chapter Nine, in order to make some recommendations for the torsion design of L-sections.

7.2 Results and Discussions

The principal test results are summarised in Table (7.1). Experimental curves will be presented while they are discussed.

As described earlier the specimens B11 and B31 were designed and detailed according to the British Code procedure and were designated the reference specimens of their respective groups. The design torque for each of the two specimens was 8 KN.m, assuming f_y = 410 N/mm^2 and concrete grade 40. At the time of experiment, however, the steel yield values were higher at f_{yv} = 465 N/mm^2 and f_{yl} = 525 N/mm^2 (average). The concrete characteristics were slightly higher at f_{cu} = 42.8 N/mm^2 (f'_c = 33.4) for B11 and f_{cu} = 44.7 N/mm^2 (f'_c = 35.0) for B31. The amount of stirrups provided was governed by the limitation on the maximum stirrup spacing and was therefore much higher than the values obtained from the code's design equation. To account for these variations and to adequately assess the code's provisions, the ultimate torques for the two sections were recalculated for the actual material properties and the amount of steel provided, with three different combinations of the safety factors used in the Code's design equation. These are shown in Table (7.2) and are given by the following equations:

$$T_{R1} = \sum \left(\frac{A_{sv}}{s}\right) 0.8 x_1 y_1 (0.87 f_{yv}) \qquad (7.1)$$

$$T_{R2} = \sum \left(\frac{A_{sv}}{s}\right) x_1 y_1 (0.87 f_{yv}) \qquad (7.2)$$

$$T_{R3} = \sum \left(\frac{A_{sv}}{s}\right) x_1 y_1 f_{yv} \qquad (7.3)$$

where:

A_{sv} = area of tow legs of a stirrup

s = stirrup spacing

x_1, y_1 = shorter and longer dimensions of the stirrup

f_{yv} = yield strength of the stirrups

7.2.1 Group B1

This group consisted of five specimens B11, B12, B13, B14 and B21 and had the same cross section. Specimen B12 and B13 were reinforced with less stirrups than B11 while B14 had more stirrups. B21 was reinforced with the same volume ratio of transverse steel as B11 but 8 mm bars were used for the stirrups instead of the 6 mm bars used for B11, resulting in a larger stirrup spacing. The amount and locations of longitudinal reinforcement were kept the same as B11 throughout.

7.2.1.1 Reference Specimen B11

The load was applied in small increments of about 1.3 KN.m on average resulting in a total of 19 increments up to the failure torque. For clarity of presentation, the sides of the section are designated "face" 1, 2, 3 and 4 as shown in Figure (7.1) with the interior as "inside".

The first visible crack was observed at a load of 12.4 KN.m. Cracking started on face 2 (the longer side) at approximately 45° to the longitudinal axis and soon propagated towards the junction where faces 1 and 2 meet at about the middle of the test zone. Upon further loading the crack spreaded almost simultaneously on the outer sides (face 1 and 2) maintaining the same angle of inclination while new cracks appeared within the test zone also on the outer faces. It was noticed that the steel strains started to increase after cracking and the displacements were considerably higher than their pre-cracking values. This occured one increment after cracks were seen by the naked

eye, probably indicating that the transfer of forces from concrete to steel is not a very sudden event as cracks start to appear and propagate.

As loading increased, the "spiral" nature of torsional cracking became apparent as the cracks circulated on all faces; the last side to have suffered cracking was the interior side of the web . At a load of 23.95 KN.m the specimen failed as the load indicator began to drop with further loading. All the test zone had suffered severe cracking by this stage. Readings were also taken after the ultimate torque in an attempt to obtain the falling branch of the torque-twist curve.

Figure (7.2) shows the process of crack propagation on the four faces of a typical specimen, folded as indicated in the previous figure. The quick propagation of torsional cracking is clearly seen as loading progresses.

Figure (7.3) shows the final crack pattern on all faces of specimen B11. The inclination of the cracks to the longitudinal axis varied between 40° to 50° as can be seen from the figure. It can also be seen that cracking did not spread outside the test zone. This observation was important because it indicated that the rectangular ends had been sufficeintly reinforced.

At failure the cracks widths were large and some small cracks appeared on all faces connecting the major well defined inclined cracks, presumably as a result of bending of the sides of the cross section, in particular the flange. It also appeared that face 4 had apparently suffered

crushing as can be seen in Figure (7.3).

Crack widths are plotted in Figure (7.6) for specimen B11. Four cracks were selected on face 1 and face 2 for the crack width measurements. It is clear from the figure that 0.3 mm crack width (for serviceability limit state according to BS8110) corresponds to an average applied torque of about 16.2 KN.m.

Figure (7.4) shows the torque-twist curve for specimen B11. It is clear from the figure that the behaviour is essentially linear up to the cracking torque. This confirms the well known observation that a reinforced concrete beam under pure torque behaves like a plain concrete beam up to initial concrete cracking. This is also reflected in the steel strains, both in the longitudinal bars and stirrups, as shown in Figure (7.5). All bars carried insignificant strains before cracking, indicating the negligible contribution of steel towards the overall stiffness in the pre-cracking stage. Similar behaviour is also noted for the concrete surface strains which unfortunately were not properly recorded for this specimen but will be shown later for all remaining specimens.

Figure (7.4) also indicates that the angles of twist as measured from the lateral displacements on the shorter and longer sides (faces 1 and 2 respectively), are not quite the same. The angle of twist from the shorter face is slightly smaller than that from the longer face for the same applied torque. This indicates a stiffer response from the web compared to the flange and can be attributed to local

It was also observed during the experiment that a wide discrete crack appeared on specimen B13, the one with the least total torsional reinforcement of all specimens of this group. The actual failure of this particular specimen was sudden, accompanied by a loud bang, and was caused primarily because of this crack opening very wide resulting in a sudden large rotation of the part above it relative to the lower part. These are characteristics of a brittle failure which have undesirable practical consequences as it occurs without enough warning signs. Figure (7.8) shows torque-twist curves of the first four specimens of group B1, where generally similar behaviour as B11 can be seen.

The dowel effect of the longitudinal reinforcement was clear as the failure load was approached. At the last stages of loading, roughly at about 85% - 90% of the failure torques, cracks were significantly wide. Also, the surfaces at both sides of major crack were no longer in the same plane, showing that the steel bars were subjected to dowel action. This can be clearly seen for specimen B33, the results of which will be shown later on.

The steel response for specimens B12, B13 and B14 is given in Figure (7.9). Again, in general terms, similar behaviour as for B11 can be clearly seen.

Figure (7.10) shows torque vs crack width for remaining four specimens of this group. The crack width was larger for the specimens with small percentages of reinforcement. It decreased with increasing reinforcement.

The demec gauges, for concrete surface strain measurements,

were oriented at 45° to the longitudinal axis as shown earlier in Chapter Six. The angles of cracks with longitudinal axis were measured for all specimens and found between 40° and 50° , averaging 45° . Therefore demec gauges parallel to the cracks recorded compressive strains while those perpendicular to the cracks recorded tensile strains. These values will be close to the principal stresses but because of the irregularity and variation in the angle of inclination of the cracks they will be dealt with only as the compressive strains parallel to the cracks and the tensile strains normal to the cracks and not as the true principal stresses.

Figure (7.11) shows the measured concrete surface compressive strains plotted against the applied torque for specimens B12, B13 and B14. The figure indicates clearly that their values were small before the cracking torques and increased suddenly upon cracking as was the case with steel stresses/strains. They also generally follow the overall behaviour of the torque-twist curves, in that there is an initial straight part followed by a sudden change in slope after cracking and a continuous increase with loading up until failure. There are, however, noticeable irregularities, i.e. increase followed by a sudden temporary decrease and so on. This is due to crack propagation effect when a pair of demec gauges was affected, say, by a new crack/s forming nearby. It also reflects the instantaneous local instabilities that occur at a position where cracks either propagate to or passes by during loading.

The concrete surface tensile strains, however, were measured

but not plotted. They could be a reasonable measure for crack widths. But because the cracks chosen for the crack width measurements were different from those propagated between the demec gauges, no direct comparison could be made. The reasons are that selection of the cracks, for measurements of crack widths, was always made at the early stages of crack initiation. Furthermore, the passing of a single crack between the two terminals of a particular pair of demec gauges was never a controlled event and could never be guaranteed.

For specimen B21 cracking started and propagated in a similar fashion as specimen B11 but it was clear that they were at a larger spacing. Figure (7.12) shows the final crack patterns for specimen B21 where this is clearly evident by comparison with Figure (7.3).

The failure torque for specimen B21 was 24.95 KN.m (about 3.9% higher than B11). Several factors might have played a part in bringing this about e.g. rate of loading especially at the final stages, variation in steel yield values (6mm bars had 465 N/mm^2 definite yield value, 8mm showed strain hardening behaviour and had 536 N/mm^2 0.2% proof stress). Also, there might be more contribution of dowel action near failure due to the larger 8mm stirrup diameter. The amount of this contribution is difficult to quantify from this limited observation.

Figure (7.13) shows the torque-twist curves for specimens B11 and B12. It can be seen that before cracking the stiffness of both specimens   is the same as might be expected. In the post-cracking region, however, the curve

for B21 is slightly stiffer than that for B11. The reasons stated above with regard to the variation of ultimate torque are also valid here. Furthermore, and more importantly, the Young's modulus of elasticity of the 8mm stirrups is 214 KN/mm^2 while that for the 6mm stirrups is 180 KN/mm^2, a difference of about 16%. This is a major factor because the post-cracking torsional stiffness is known to be a strong function of the steel properties (Chapter Two). The nature of cracking (spacing and width) might have also contributed. The main conclusion from this comparison is that use of larger spacing caused wider spaced cracks but did not significantly affect the ultimate torque for the same amounts of longitudinal and transverse reinforcements.

Figure (7.14) shows the steel response for specimen B21 where again similar behaviour, as for all previous specimens, is evident. The concrete surface principal compressive strains are shown in Figure (7.15) for the same specimen. These behaved linearly, and were small in value up to the cracking torque. A sudden increase is noticed after cracking. The general trend follows that of the torque-twist behaviour.

7.2.3 Group B3

This group consisted of four specimens designated B31, B32, B33 and B34. The specimens had the same cross sectional area, which was smaller than the first group. B31 was the reference specimen for this group. The amount of transverse reinforcement was varied in a similar way as for group B1 for the same amount and distribution of longitudinal steel.

For all specimens small load increments were applied until failure. The average increment size was 1.3, 1.1, 1.2 and 2.6 K.m for B31, B32, B33 and B34, respectively. These resulted in a total number of increments of 16, 16, 16 and 11 up to the failure torque.

The observations during the experiments were fairly similar to group B1. The crack inclinations with the longitudinal axes were between 39° and 49°, in general. The same crack did not necessarily continue round the corner as a continuous crack during its propagation to form a helix; concrete is not an ideal material after all.

Figure (7.16) shows the torque-twist curves for all four specimens of this group. The ultimate torque increased with increase in reinforcement. The reference specimen, B31, failed at 20.88 KN.m.

A comparison of the final crack patterns for specimens B31, B32 and B33 is shown in Figure (7.17). The effect of the larger spacing of stirrups is clearly reflected in specimens B32 and B33 where an increased crack spacing can be observed.

The dowel effect can be seen in Figure (7.18) for specimen B33. The bending of the longitudinal steel bars, where they meet the stirrup, indicate this effect. Also the crushing of concrete is clearer for this specimen, being reinforced with the least amount of steel. Crushing occurred at the centre of the test zone in the flange as can be seen in the same figure.

The reinforcement response for all four specimens of this

group is shown in Figure (7.19) where again similar response, as for the first two groups, can be observed. Insignificant strains were recorded before cracking, followed by a large increase after cracking and a continuous increase thereafter until failure.

Figure (7.20) shows the concrete surface compressive strains plotted against the applied torque for this group. Torque vs crack width is presented in Figure (2.21). The applied torque corresponding to 0.3mm crack width is about 15.0 KN.m, 12.64 KN.m and 9.64 KN.m for specimen B31, B32 and B33 respectively.

7.3 Summary

This section aims to summarise the results under the following headings:

(1) Pre-cracking stiffness

(2) Cracking torque

(3) Post-cracking torsional stiffness

(4) Angles of twist at cracking and failure

(5) Crack propagation, spacing and width

(6) Steel response and unit lengthening

(7) Concrete surface strains

(8) Failure torques and failure modes

(9) Assessment of Some Aspects of BS8110 Torsion Design Procedure.

Following the observed behaviour described above the torque-twist curve for a typical specimen is idealised as shown in Figure (7.22), with various important quantities defined. The slope of the initial linear part of the torque-twist

curve is the pre-cracking torsional stiffness (K_o) and the angle of twist at the end of this part is termed "angle of twist at craking θ_{cr}". After cracking of concrete the first part of the nonlinear curve is approximated by a straight line and the slope of this part is taken as the "post-cracking torsional stiffness K_{cr}". The curve bends afterwards up to the ultimate torque T_u (peak point) before descending again. The angle of twist at the peak point is termed "angle of twist at failure θ_u".

7.3.1 Pre-cracking Stiffness

As can be seen in all experimental torque-twist curves the behaviour is essentially linear before cracking. The reinforced concrete members of L-shaped cross section behave like plain concrete members before cracking, regardless of the amount of torsional reinforcement. Indeed, the pre-cracking torsional stiffness was almost the same for all specimens with different reinforcement contents when the cross section was the same as shown in Table (7.3).

The effect of concrete strength might have resulted in slight variations. The variation obtained in this study does not suggest corrections, for comparison purposes, as the elastic modulus of concrete varied within a limited range (20.0 KN/mm^2 - 23.0 KN/mm^2).

7.3.2 Cracking Torques

As the reinforcement has insignificant contribution to the behaviour before cracking, the cracking torque is mainly a function of concrete strength for the same size. However, it is found that the cracking torque does increase slightly

with the increase in the amount of transverse reinforcement. Table (7.1) lists cracking torques for all specimens of this series. These values are plotted against the percentage volume of transverse reinforcement in Figure (7.23). Examination of the figure reveals a mildly increasing trend. The effect of the size of the cross section is very clear as the cracking torques of the specimens of group B1 are higher than the corresponding specimens of B3.

7.3.3 Post-cracking Torsional Stiffness

Torsional stiffness is greatly reduced after cracking occurs (Figures 7.4, 7.8, 7.13 and 7.16). Table (7.3) compares the post-cracking torsional stiffness expressed as a percentage of the pre-cracking value for all specimens. The post-cracking portion of the torque-twist curve is never a full straight line, because of the continuous process of crack propagation followed later by yielding of steel and/or crushing of concrete. However, for the above comparison the post-cracking torsional stiffness is obtained from the early part of the post-cracking portion of the curve (as shown in the idealized torque-twist curve of Figure 7.22) approximated to a straight line so as to give a comparative measure of the sharp reductions that take place after concrete cracking.

The table reveals that the ratio of the post- to pre-cracking torsional stiffness ranges between 7% to 13%, a very small proportion. This is because of the nature of torsional cracking which spread all round the section fairly soon after crack initiation. It also reflects the role of reinforcement in taking over the major role, at this stage,

of resisting the applied torque. The values of these stiffnesses, however, are approximate because of the nature of idealization but generally fall within reasonable accuracy for this type of comparison.

Figure (7.24) shows the ratio of post- to pre-cracking torsional stiffness plotted against the volume ratio of transverse reinforcement for all specimens. The behaviour is fairly linear indicating a general trend which needs further experimental evidence to allow establishment of a more widely applicable relationship between these two quantities.

7.3.4 Angles of Twist at Cracking and Failure Torques

In Table (7.3) the angles of twist at two significant stages during the loading process, namely the cracking and failure stages, are listed for all specimens. The ratios of the value at failure (peak of the torque-twist curve) to that at cracking give a clear indication of the very large rotations that are required for the section to develop its ultimate capacity. This ratio could be as high as 20 in some cases as can be seen in the table. For the specimens tested in this study the ratio varied between 12 - 21%. Figure (7.25) shows this ratio plotted against the volume ratio of transverse reinforcement for the two groups of specimens, where an approximately linear relationship can be seen.

The high value of the ratio of twist at failure to that at cracking is likely to play a major role in determining the service load. The code does not specify a value for the service load (torque) based on rotation, as analogous to deflection in case of flexure. Therefore a code provision dealing with a limiting maximum rotation may be necessary.

7.3.5 Crack Propagation, Spacing and Width

Torsional cracks are distinguished by their "helical" nature and also by their rapid propagation compared to flexural cracking. An inclination of 40° - 50° to the longitudinal axis was observed for all specimens tested in this series. The spacings of the cracks were found to be directly influenced by the stirrups spacing. Closely spaced stirrups resulted in closer, but finer cracks whereas widely spaced stirrups produced widely spaced cracks but with larger width. For specimens B13 and B33, the least reinforced in each group, the failure has actually resulted from a distinct "helical" crack causing sudden collapse; a brittle type of failure.

As crack width plays an important role in determining the service load according to the code, the applied torques corresponding to 0.3 mm crack width were determined from the torque vs crack width curves (Figures 7.6 and 7.21) and are listed in Table (7.5). Comparison of these values with the design and experimental failure torques will be made in section (7.3.9) for assessment of some of the Code's provisions.

7.3.6 Steel Response and Unit Lengthening

Both longitudinal bars and closed stirrups did not carry any measureable strains before cracking. After cracking, large increases in steel strains were observed as shown in Figures (7.5, 7.9, 7.14 and 7.19). This confirms the well established fact that reinforced concrete members behave like identical plain concrete members before cracking. The increase in steel strains indicates that the equilibrium

condition that existed in the uncracked reinforced member was upset by cracking so that the member sought a new equilibrium condition by transfering load to the reinforcement.

The steel strains, after cracking, were found to continuously increase with loading on all legs of a closed stirrup. Although in most curves the behaviour can be approximated to a straight line there are a lot of nonlinearities. The torque vs steel strain curves show that at failure of all specimens yielding had occured in at least one of the longitudinal or transverse reinforcement as also shown in Table (7.1). Better utilization of reinforcement was achieved when lesser amount of stirrups was used. This is clear when comparing the steel response of specimens B11, B12 and B13 (Figures 7.5, and 7.9).

Hsu (ref. 2) tested rectangular reinforced concrete beams under pure torsion and reported that after cracking the stirrup stresses at the centre of the wider face increased approximately linearly with loading up to failure. The steel stresses in the shorter legs of the stirrup increased at first and then acted irregularly, often decreasing when ultimate conditions were approached. In general no such peculiar behaviour was observed for the L-sections tested in the present series.

Comparison of steel response for specimens B11 and B21 (Figures 7.5 and 7.14) shows that, although the failure torque is practically the same for both specimens the longitudinal steel strains at failure are much higher for

B21. This may be attributed to the increased stirrup spacing or increased stirrup diameter, being the only differences between the two specimens. However, this point needs further investigation as it is directly linked with the maximum limitation on stirrup spacing. The comparison seems to indicate that this limitation can be made less stringent as it only affected the crack spacing and width, but not to the extent that prevents slight relaxations in these limitations.

Because of the type of cross section and the fact that the longitudinal bars are of different diameter, as dictated by the design procedure, warping of the cross section is not expected to be the same in flange and web. Also differential cracking is expected, because of the different stiffnesses of web and flange, resulting in unequal strains in the longitudinal bars and also unequal lengthening along the cross section. Therefore, the unit lengthening of each specimen is plotted with the longitudinal steel strains without averaging these strains. These are shown in Figures (7.5, 7.9, 7.14, and 7.19). The similarity is evident as no measurable lengthening can be seen before cracking. A large increase follows after cracking of concrete and continues thereafter up to failure.

7.3.7 Concrete Surface Strains

As the demec gauges were oriented at 45° to the longitudinal axis, it was possible to record roughly both the compressive strains parallel to the cracks and the tensile strains normal to the cracks on the concrete surface. The compressive strains are shown in Figures (7.11, 7.15 and

7.20) where, similar to steel strains, a large increase upon cracking is clear, resulting in two distinct regions, before and after cracking. The tensile strains could be quite useful to measure. They give an indication of the crack width. But it is extremely difficult to estimate crack width from these values because of the following reasons:

(1) The positions of the demec gauges were pre-selected to cover all sides of the cross section. As cracks propagated, either more than one crack passed between the terminals of the demec gauges or the terminal itself was affected by the process of crack propagation.

(2) Not all the deformation recorded by the demec gauge is due to the crack width alone, part of it must be due to the concrete strains in between the terminals being 100 mm apart. Detailed study of this aspect of behaviour is important but may require small size specimen where such local behavior can be closely monitored.

7.3.8 Failure Torques and Failure Modes

The failure (or ultimate) torque is defined as the maximum torque which can be resisted by the member, in other words the peak of the torque-twist curve. Table (7.1) shows the measured ultimate torques for all specimens. These are also plotted in Figure (7.26) against the volume ratio of transverse reinforcement, where it is clear that the failure torque increased with the increase in transverse reinforcement.

Comparison of failure torques of specimens B11, B12 and B13 reveals that a reduction of 26.4% and 47.3% of transverse reinforcement resulted in a reduction of only 5.0% and 18.0%

in the failure torque, taking B11 as a reference. Similar comparison of B31, B32 and B33 shows that a reduction of 26.3% and 47.3% produced a reduction of only 13.1% and 17.4%. This must be directly combined with the steel response where better utilization of longitudinal steel was achieved when largely reduced amounts of stirrups were used, as reflected in the longitudinal steel strains previously discussed. This tend to indicate that the principle of equal volume through which the longitudinal steel is determined (which is also employed by the ACI code) could be slightly relaxed.

Hsu (ref. 2) investigated this particular point and reported that when the total reinforcement is less than about 2.3%, the volume ratio of longitudinal steel to stirrups, m, can vary between 1.0 and 1.5 and both reinforcements will nevertheless yield. Two of his beams (B2 and B9), for example, had roughly the same total amount of reinforcement (= 1.65% and 1.71%) but different values of m (=2.18 and 1.0). Yet they failed practically at the same torque (=259 and 264 in-kips). This is interpreted as reasonable because both beams were underreinforced so that all reinforcement was utilized. He also found that although the fully effective value of m can vary widely for beams with small percentage of reinforcement, it becomes very sensitive for beams with high percentage of reinforcement. As no variation of the longitudinal reinforcement was made in this study an attempt has been made to look into it using the developed finite element model as will be reported in Chapter Nine

The failure modes of the test specimens can best be studied through the crack propagation and patterns together with the steel response. The skew-bending type of torsional failure has been widely accepted as a theoretical model to facilitate calculation of a section torsional capacities. The space truss model, on the other hand, serves the same purpose by clearly defining the functions of both longitudinal and transverse steel and concrete in resisting the applied torque.

As already described the present experiments clearly showed the spiral 45° nature of torsional cracking. Crushing of concrete was clearly observed at the flange in two of the specimens, namely B13 and B33. This is an indication of a skew-bending failure. However, there is no clear cut signs in all specimens as to the occurrence of crushing at that particular location. It occured and was seen clearly for specimens with reduced amonut of steel.

7.3.9 Assessment of Some Aspects of the Code's Design Procedure in the Light of the Present Test Results

Table (7.5) and Figure (7.27) shows comparison of the following torques:

(1) BS8110 design torque (T_d) of the reference specimens

(2) Recalculated values of the torque (T_{R1}, T_{R2} and T_{R3}) using the actual material properties and the steel amount, for the three different combinations of the factors employed in the Code's design equation, previously defined .

(3) Cracking torques

(4) Experimental failure torques and

(5) Applied torque corresponding to 0.3 mm crack width

Examination of the above table and figure reveals the following points:

(1) The recalculated torques of the reference specimens immediately indicate that the code's provisons are far too conservative. The root cause of this is the restriction on the maximum stirrup spacing as this was governed by the smallest dimension of the flange. This led to a substantially increased stirrups in the web as can be seen in Appendix (A). Column 15 of the table reveals that this is of lesser magnitude in the smaller cross section B13 as the smallest dimension of web and flange are closer. Appreciation of this point can lead to a less stringent stirrup spacing and hence much more economical design. Currently the stirrup spacing is based on the least of x_1, $y_1/2$ or 200 mm, whichever the lesser. It is suggested that this limit could be $(x_1+y_1)/2$, $y_1/2$ or 200 mm. This suggestion is put forward among some "tentative design recommendations" later in Chapter Nine.

(2) The experimental failure torque of the reference specimen B11 is practically equal to T_{R2} whilst that of B31 is closer to T_{R3}. This suggests that in principle the equation is reasonably applicable.

(3) The applied torques corresponding to 0.3 mm crack width for the two groups of specimens shows that these torques are all higher than the design torque (T_d) even for the specimens with much reduced transverse reinforcement. This observation substantiates point (1) above.

(4) On the whole, the results indicate that the code's

torsion design provisions can be improved to reduce its current conservative nature. Suggestions for improvements will follow after further variables are investigated through a parametric study reported in Chapter Nine.

7.4 Conclusions

The following conclusions are drawn from the present results on reinforced concrete sections subjected to pure torsion:

(1) The code procedure is found conservative as it grossly underestimates the section torsional capacity. An immediate reason for this is the limit on stirrup spacing as this is based on the smallest dimension of the component rectangles. Relaxation of this limit would result in a more economical use of reinforcement.

(2) The design equation is, in principle, quite applicable but an increase in the permissible shear stresses and a modification of the factor 0.8 appears to be necessary to reduce its present conservative nature especially if the present procedure of calculating the amount of reinforcement from the total design torque is to be used.

(3) The applied torques at 0.3 mm crack width were found higher than the design torque of the reference specimen of each group even for the reduced volume ratios of stirrups, an observation that supports the above two points.

(4) The behaviour was found to be essentially linear until cracking of concrete. For all practical purposes the slope of this linear part of torque-twist curve is independent of the amount of torsional reinforcement. After cracking the steel strains/stresses and the concrete surface strains

increased largely and continued to increase thereafter until failure.

(5) Reduction of transverse reinforcement, for the same amount of longitudinal steel, was found to reduce both the post-cracking torsional stiffness and the ultimate torque. However, a particular percentage reduction resulted in a lesser percentage reduction of ultimate torque, allowing more utilization of longitudinal steel. This is another demonstration of the uneconomical amount of steel according to the code, where even sections with the reduced amount of reinforcement developed ultimate torques well above the design torque of their corresponding reference specimens (designed and detailed according to the Code's provisions).

(6) The stirrup spacing was found to effect both the crack width and spacing. Closely spaced stirrups resulted in closely spaced fine cracks. Larger stirrup spacing resulted in widely spaced cracks but with larger crack widths.

(7) Use of larger stirrup diameter with larger spacing instead of smaller stirrup diameter, giving the same amount of transverse reinforcement, with the same amount and distribution of longitudinal steel, was found to produce practically the same ultimate torque (specimens B11 and B21). Only the crack width and spacing were affected as described above.

(8) The cracking torque was found to increase slightly with the increase in the volume ratio of transverse reinforcement.

(9) Large reduction of torsional stiffness occured after cracking of concrete. The ratio of post- to pre-cracking stiffness ranged between 7% - 13%.

(10) Very large rotations were necessary for the torsional members to develop their ultimate torques. The ratio of twist at failure to that at cracking was found to vary between 12 - 20.

(11) Finally, the experimental tests yielded sufficiently consistent data for assessing the developed finite element model in the analysis of reinforced concrete solid flanged sections subject to torsion.

References

(1 a) BS CP110 - 1972, "Code of Practice for the Structural Use of Concrete", Part 1, Design, Material and Workmanship, British Standard Institution, London, 1972.

(1 b) BS8110 - 1985, "British Standard Structural Use of Concrete", Part 2, Code of Practice for Special Circumstances, British Standard Instiution, 1985.

(2) Hsu, T.T.C., "Torsion of Structural Concrete - Behaviour of Reinforced Concrete Rectangular Members", ACI Special Publication, Torsion of Structural Concrete, SP18, 1968, pp. 261-306.

Table (7.1) Summary of principal test results

Model	Cracking		Ultimate		Stiffness		Yielding of Reinforcement	
	T_{cr} (KN.m)	θ_{cr} (Deg./mm)x10^{-6}	T_u (KN.m)	θ_u (Deg./mm)x10^{-6}	K_o (KN.mm^2/deg)x10^6	K_{cr} (KN.mm^2/deg)x10^6	Longit.	Stirrups
B11	12.43	245.2	23.95	3825	69.5	7.1	Y	N
B12	13.18	249.6	22.75	3650	72.6	6.2	N	Y
B13	11.31	230.0	19.66	3350	67.4	4.8	N	Y
B14	14.57	275.0	34.54	4335	72.6	7.4	N	Y
B21	12.33	250.0	24.89	3500	67.6	8.9	Y	Y
B31	9.21	296.7	20.88	4500	32.1	4.0	Y	Y
B32	10.11	290.0	18.14	4100	35.9	2.7	Y	Y
B33	8.04	265.0	17.25	5300	31.3	2.5	Y	Y
B34	9.43	241.0	28.43	5075	40.1	5.0	Y	N

K_o = pre-cracking torsional stiffness

K_{cr} = post-cracking torsional stiffness

N = steel did not yield Y = steel yielded

Table (7.2) Recalculation of reference specimens using actual material
properties and amounts of steel provided

Specimen	BS8110 Design Torque T_d (KN.m)	Values (KN.m)		
		T_{R1}	T_{R2}	T_{R3}
B11	8.0	18.49	23.1	26.56
B31	8.0	13.48	16.85	19.37

Table (7.3) Pre- and Post-cracking torsional stiffness for all
specimens

Specimen	K_ex10^6 KN.mm^2/deg.	K_ox10^6 KN.mm^2/deg.	K_{cr}x10^6 KN.mm^2/deg.	K_{cr}/K_o%
B11	87.8	69.5	7.1	10.2
B12		72.6	6.2	8.5
B13		67.4	4.8	7.1
B14		72.6	7.4	10.2
B21		67.6	8.9	13.2
B31	38.9	32.1	4.0	12.5
B32		35.9	2.7	7.5
B33		31.3	2.5	8.0
B34		40.1	5.0	12.5

K_e = St. Venant's elastic torsional stiffness assuming ν_c = 0.2

K_o = Experimental pre-cracking torsional stiffness

K_{cr} = Experimental post-cracking torsional stiffness

Table (7.4) Comparison of angles of twist at cracking and failure
for all specimens

Specimen	$\theta_{cr} \times 10^6$ deg./mm	$\theta_u \times 10^6$ deg./mm	θ_u / θ_{cr}
B11	245.2	3825	15.6
B12	249.6	3650	17.41
B13	230.0	3350	11.55
B14	275.0	4335	15.76
B21	250.0	3500	14.0
B31	296.7	4500	15.17
B32	290.0	4100	14.14
B33	265.0	5300	20.0
B34	241.0	5075	21.58

θ_{cr} = angle of twist at cracking torque

θ_u = angle of twist at failure torque

Table (7.5) Comparison of Various Values of torques

(1)	(2)	(3)	(4)	(5)	(6)	(7)	(8)	(9)	(10)	(11)	(12)	(13)	(14)	(15)
Specimen	BS8110 Design Torque T_d (KN.m)	Redesign Torques (KN.m)			T_u (Exp) (KN.m)	$T_{0.3}$ (KN.m)	$\frac{T_u}{T_d}$	$\frac{T_u}{T_{R1}}$	$\frac{T_u}{T_{R2}}$	$\frac{T_u}{T_{R3}}$	$\frac{T_{0.3}}{T_d}$	$\frac{T_{0.3}}{T_{R1}}$	$\frac{T_{0.3}}{T_u}$	$\frac{T_{R1}}{T_d}$
		T_{R1}	T_{R2}	T_{R3}										
B11	8	18.49	23.10	26.56	23.95	16.0	3.0	1.3	1.04	0.90	2.0	0.86	0.67	2.31
B12	-				22.75	17.14	2.84	1.23	0.98	0.86	2.14	0.93	0.75	
B13	-				19.66	13.5	2.46	1.06	0.85	0.74	1.69	0.73	0.69	
B14	-				34.54	20.0	2.50	1.87	1.50	1.30	2.5	1.08	0.58	
B21	-				24.89	-	3.11	1.35	1.07	0.94	-	-	-	
B31	8	13.48	16.85	19.37	20.88	16.0	2.60	1.55	1.24	1.08	2.0	1.19	0.77	1.69
B32	-				18.14	12.0	2.27	1.35	1.08	0.94	1.5	0.89	0.66	
B33	-				17.25	9.64	2.16	1.28	1.02	0.89	1.21	0.72	0.56	
B34	-				28.43	-	3.55	2.11	1.69	1.47	-	-	-	

$T_{0.3}$ = Applied torque corresponding to o.3 mm crack width
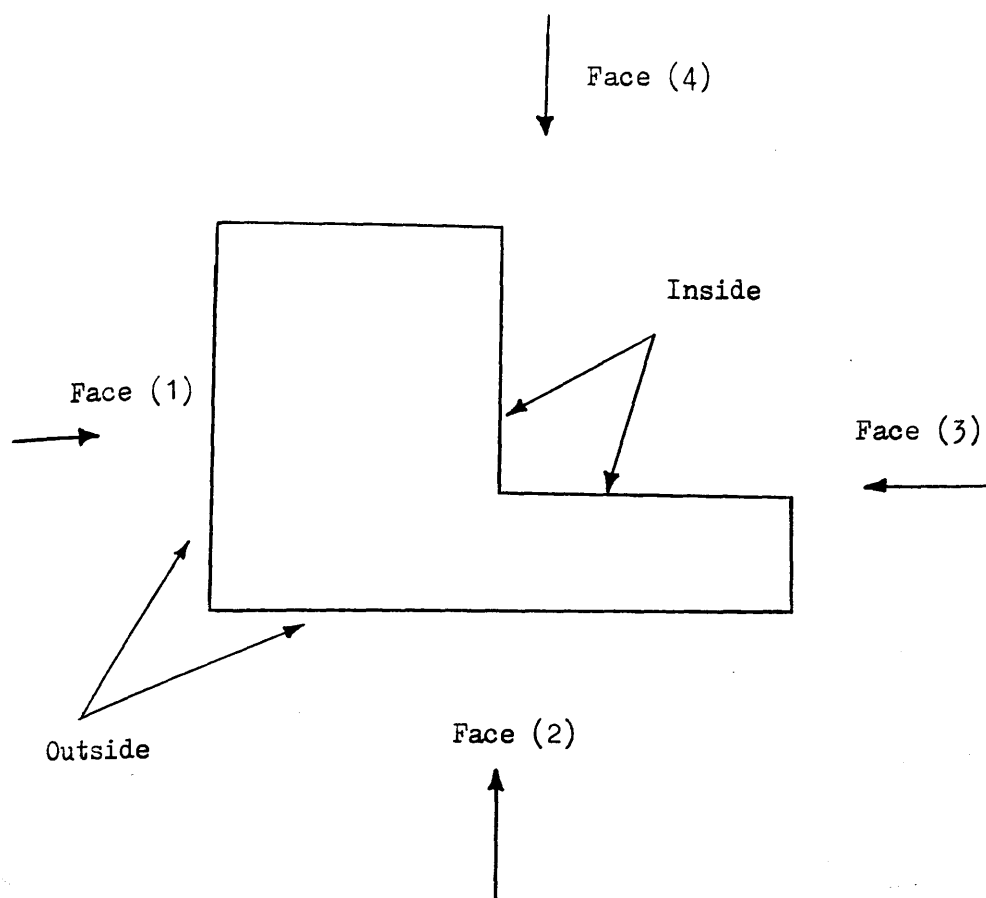
Figure (7.1) Designation of specimen sides for clarity of crack propagation and patterns
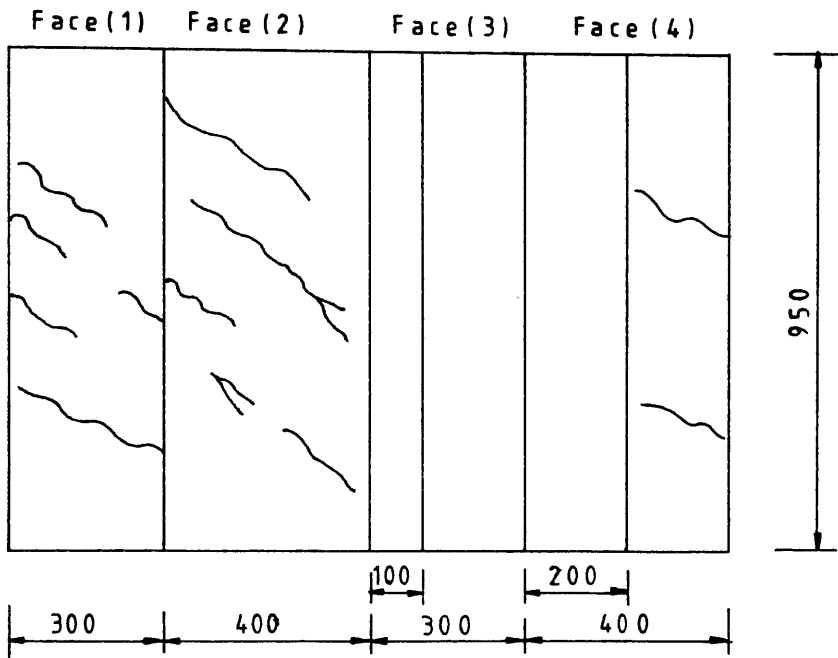
Face(1)   Face(2)   Face(3)   Face(4)

950

|100| |200|
300   400   300   400

T = 13.0 KN.m = 0.38 T$_u$

Face(1)   Face(2)   Face(3)   Face(4)

950

|100| |200|
300   400   300   400
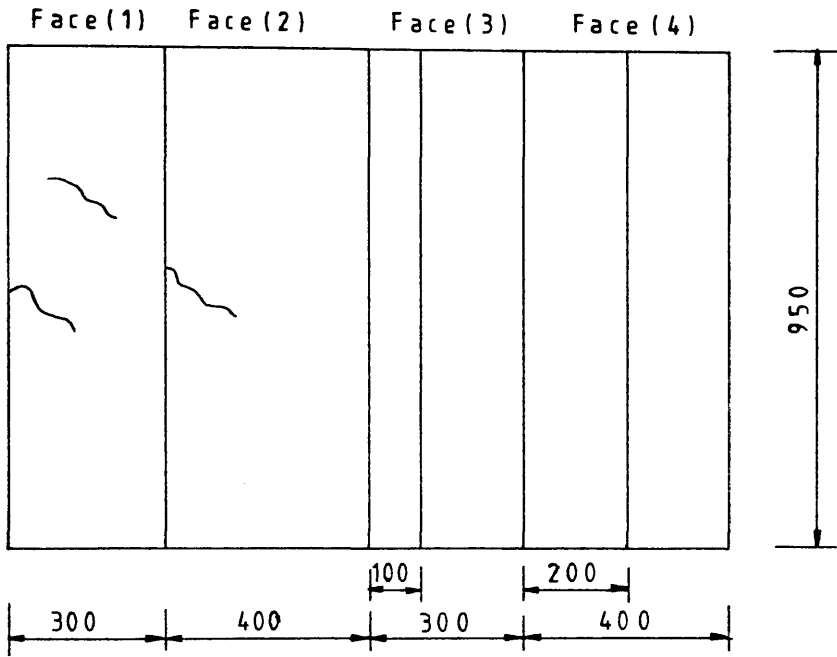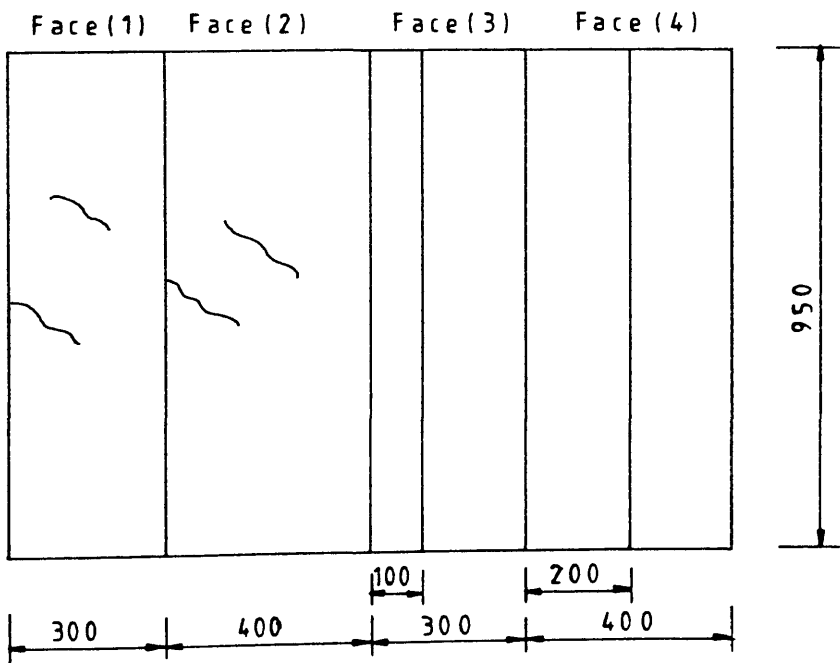
T = 14.5 KN.m = 0.42 T$_u$

Figure (7.2) Crack propagation during the loading process for specimen (B14)

Face(1)   Face(2)   Face(3)   Face(4)

950

100   200

300   400   300   400

T = 16.4 KN.m = 0.47 T$_u$

Face(1)   Face(2)   Face(3)   Face(4)

950

100   200

300   400   300   400
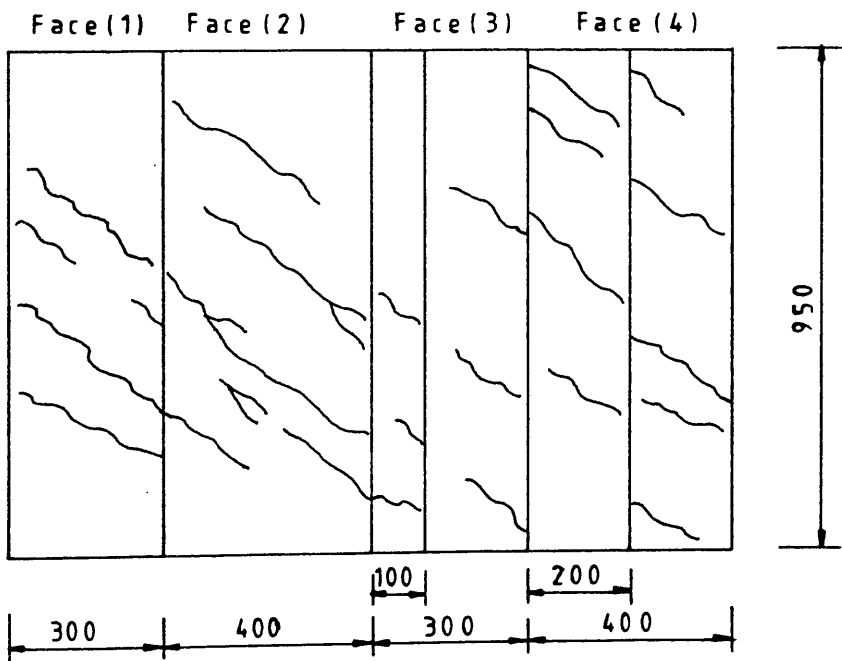
T = 18.3 KN.m = 0.53 T$_u$

Figure (7.2) Continued

Face(1) Face(2)   Face(3)   Face(4)

950

100   200

300   400   300   400

T = 19.90 KN.m = 0.58 T_u

Face(1)   Face(2)   Face(3)   Face(4)

950

100   200

300   400   300   400
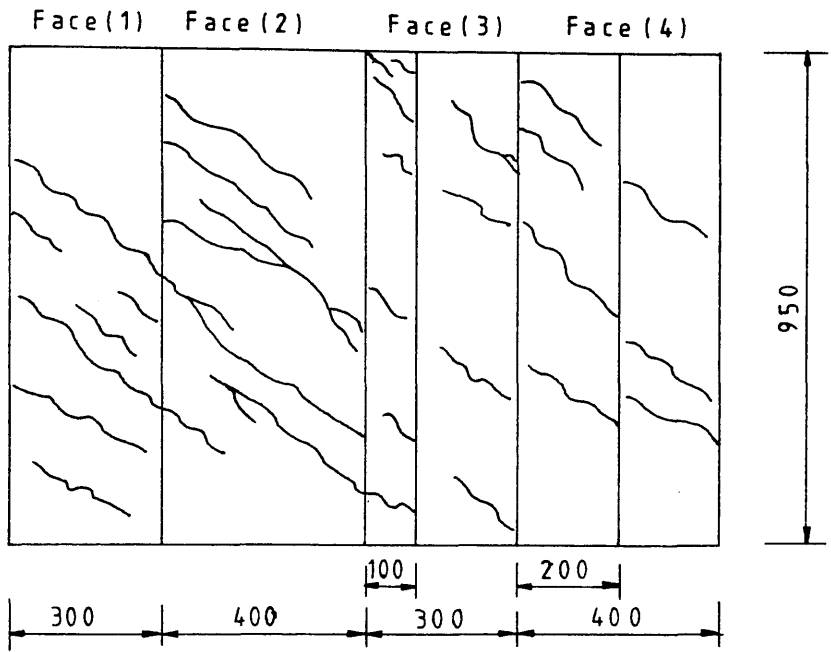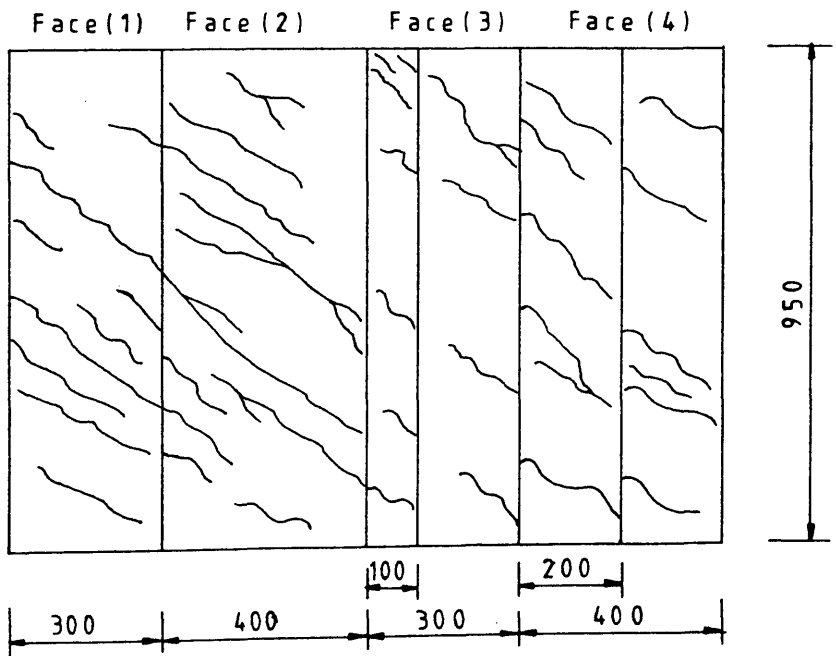
T = 21.7 KN.m = 0.63 T_u

Figure (7.2) Continued
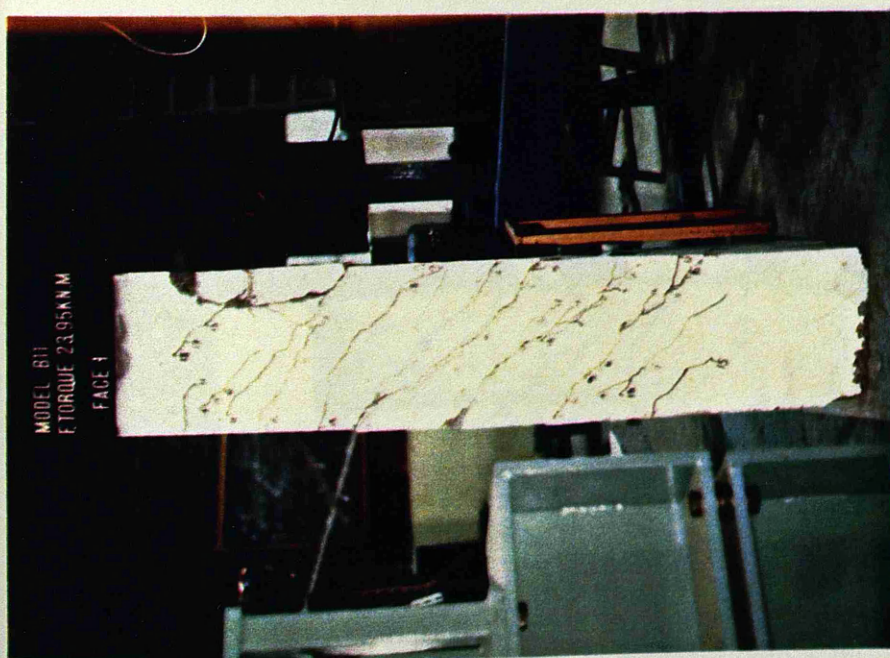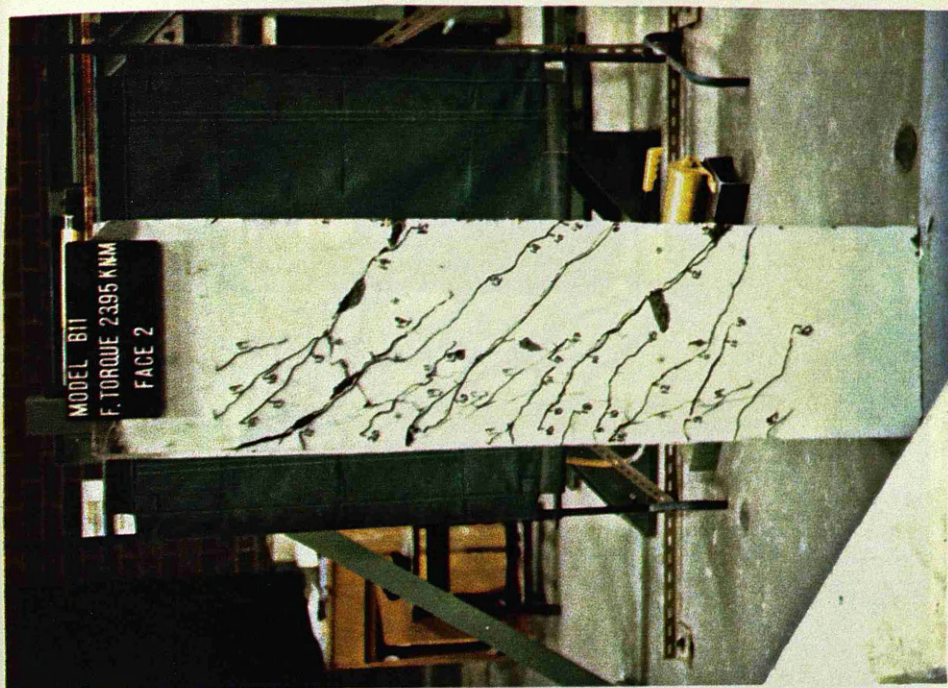
Figure (7.3) Final crack pattern for specimen (B11)
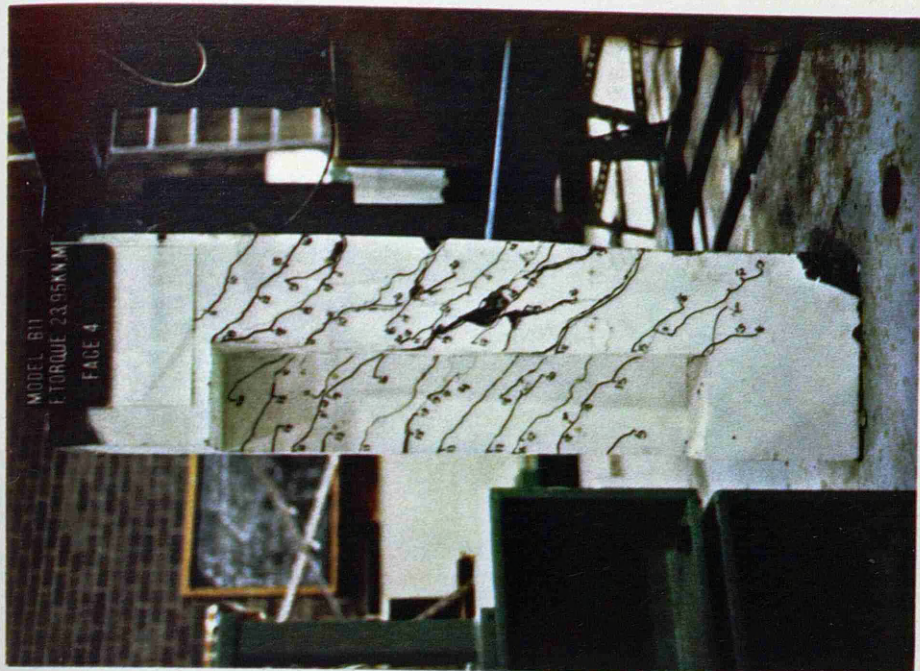
Figure (7.3) Continued

Figure (7.3) Continued
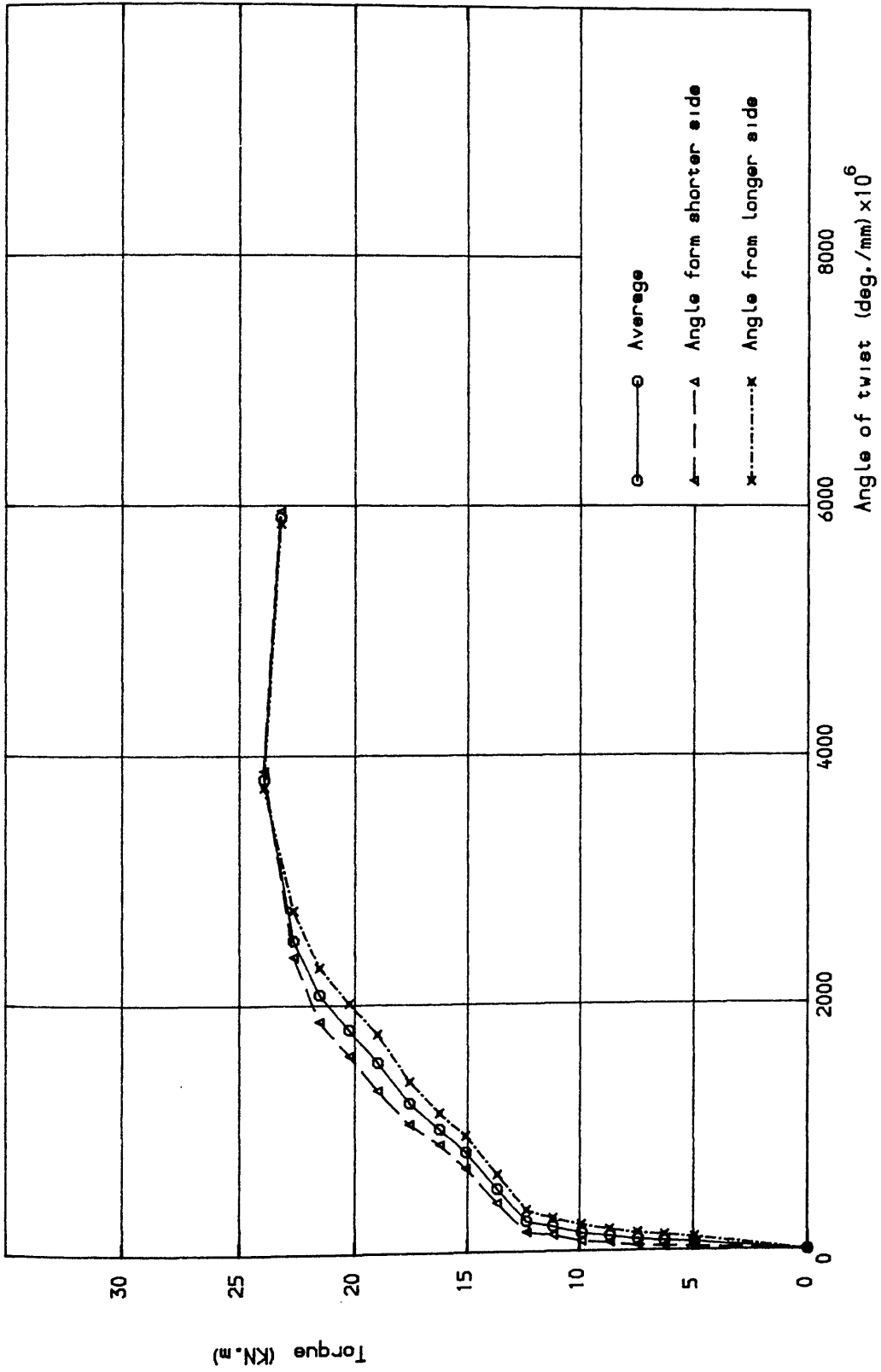
Figure (7.4) Torque-twist curves for specimen B11
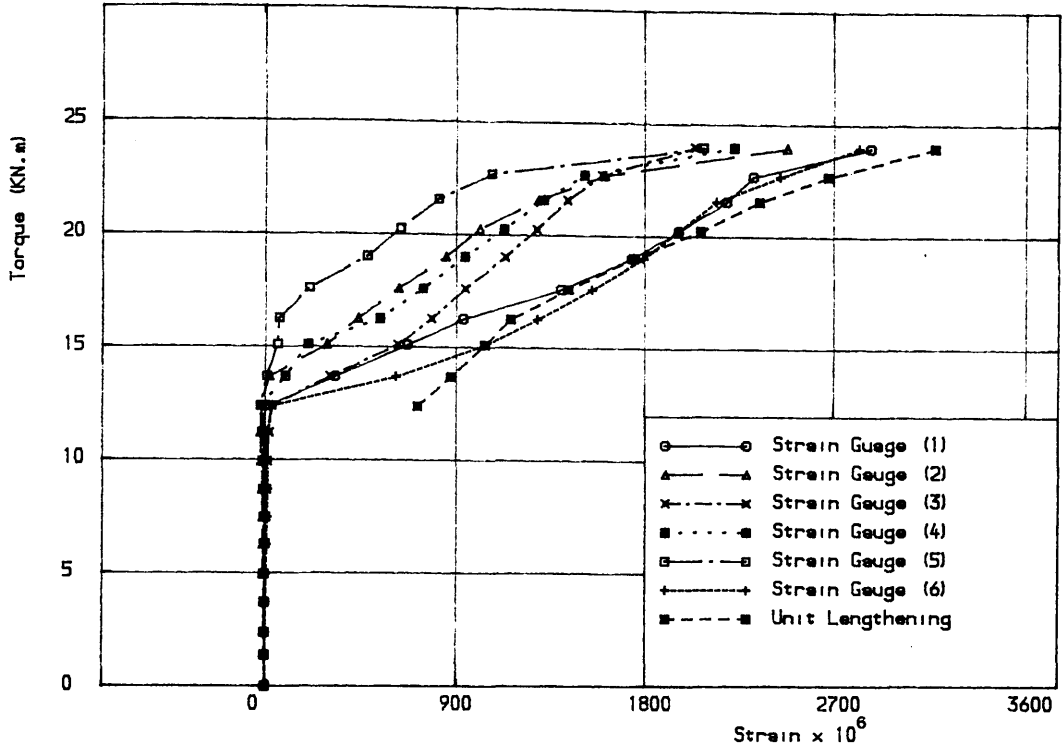
Figure (7.5 a) Torque vs longitudinal steel strains and unit
lengthening for specimen B11
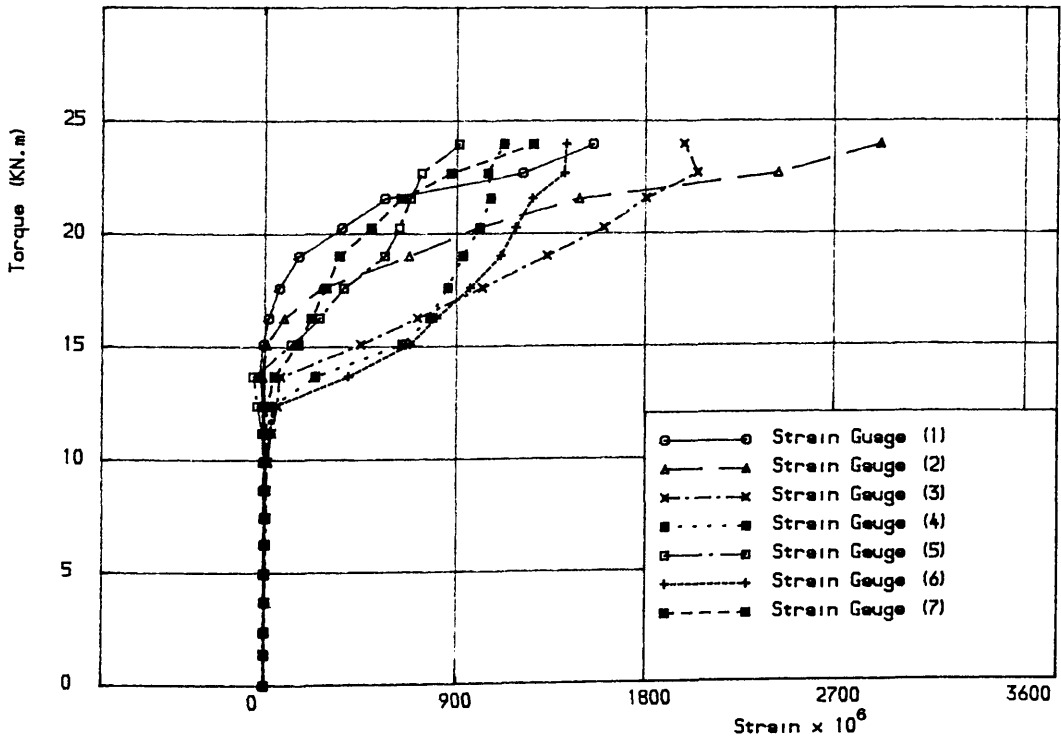
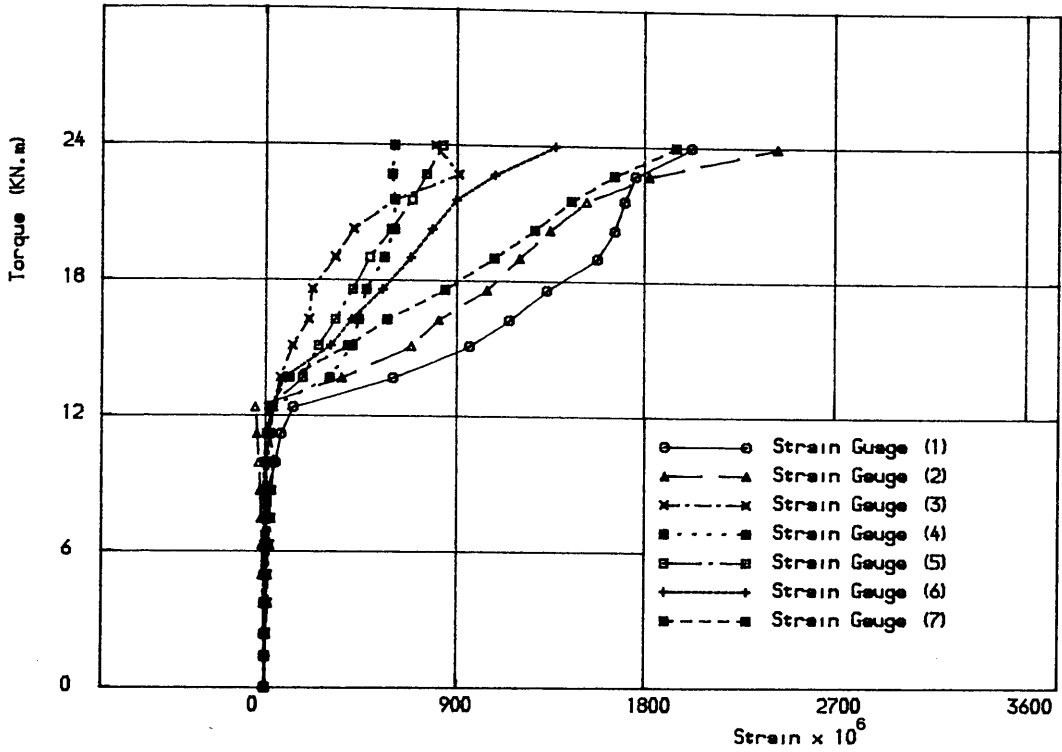Figure (7.5 b) Torque vs top stirrup strains for specimen B11

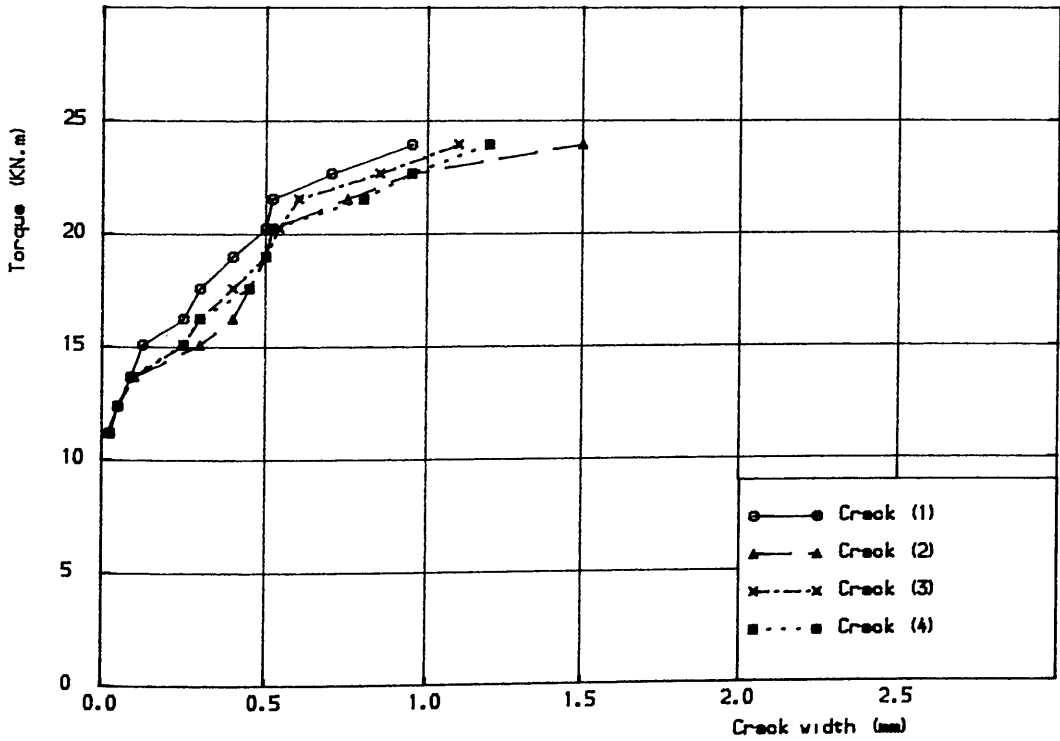Figure (7.5 c) Torque vs bottom stirrup strains for specimen B11

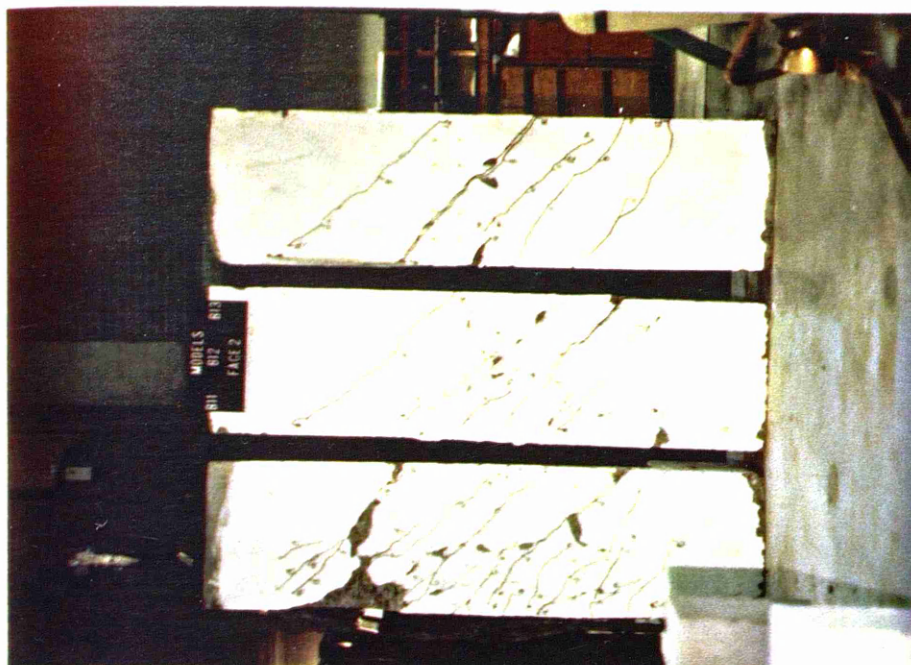Figure (7.6) Torque vs crack width for specimen B11

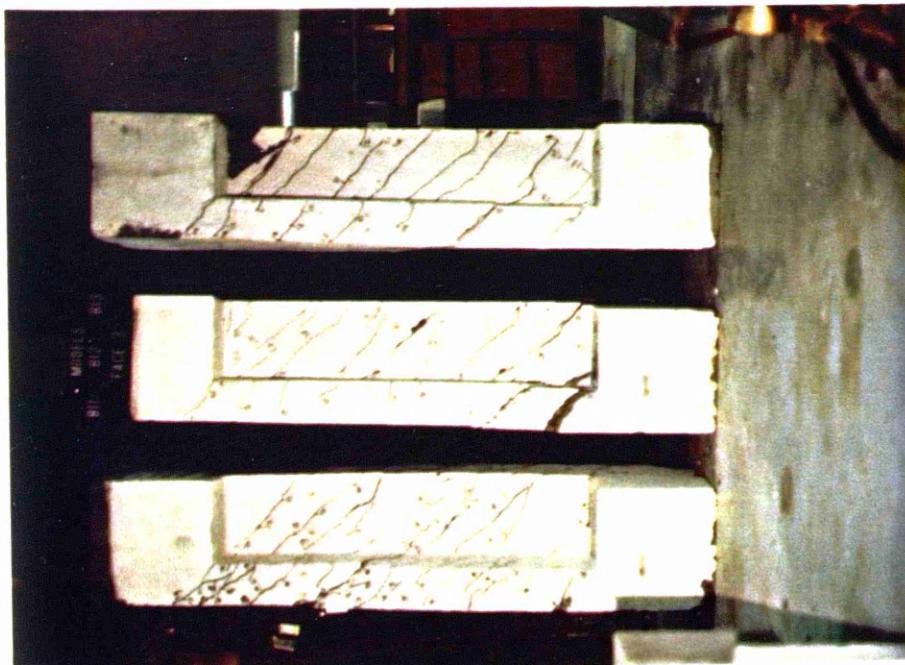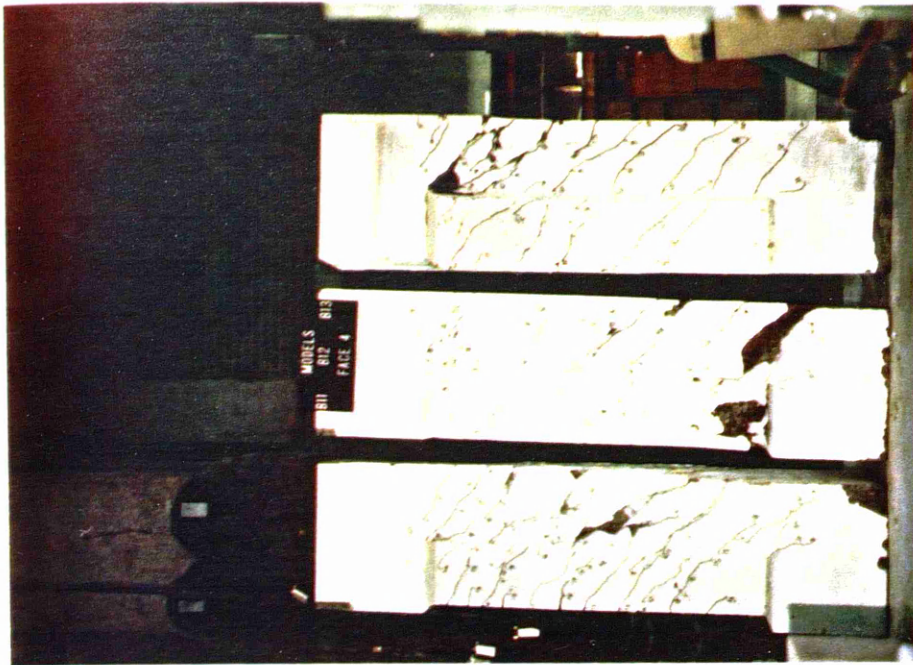Figure (7.7) Final crack patterns for specimens B11, B12 and B13
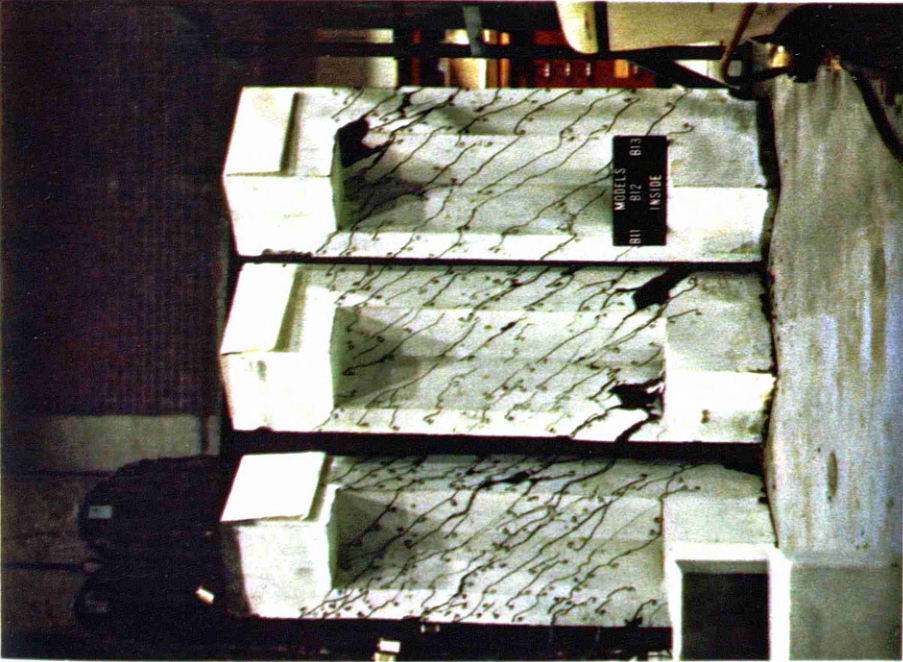
Figure (7.7) Continued

Figure (7.7) Continued
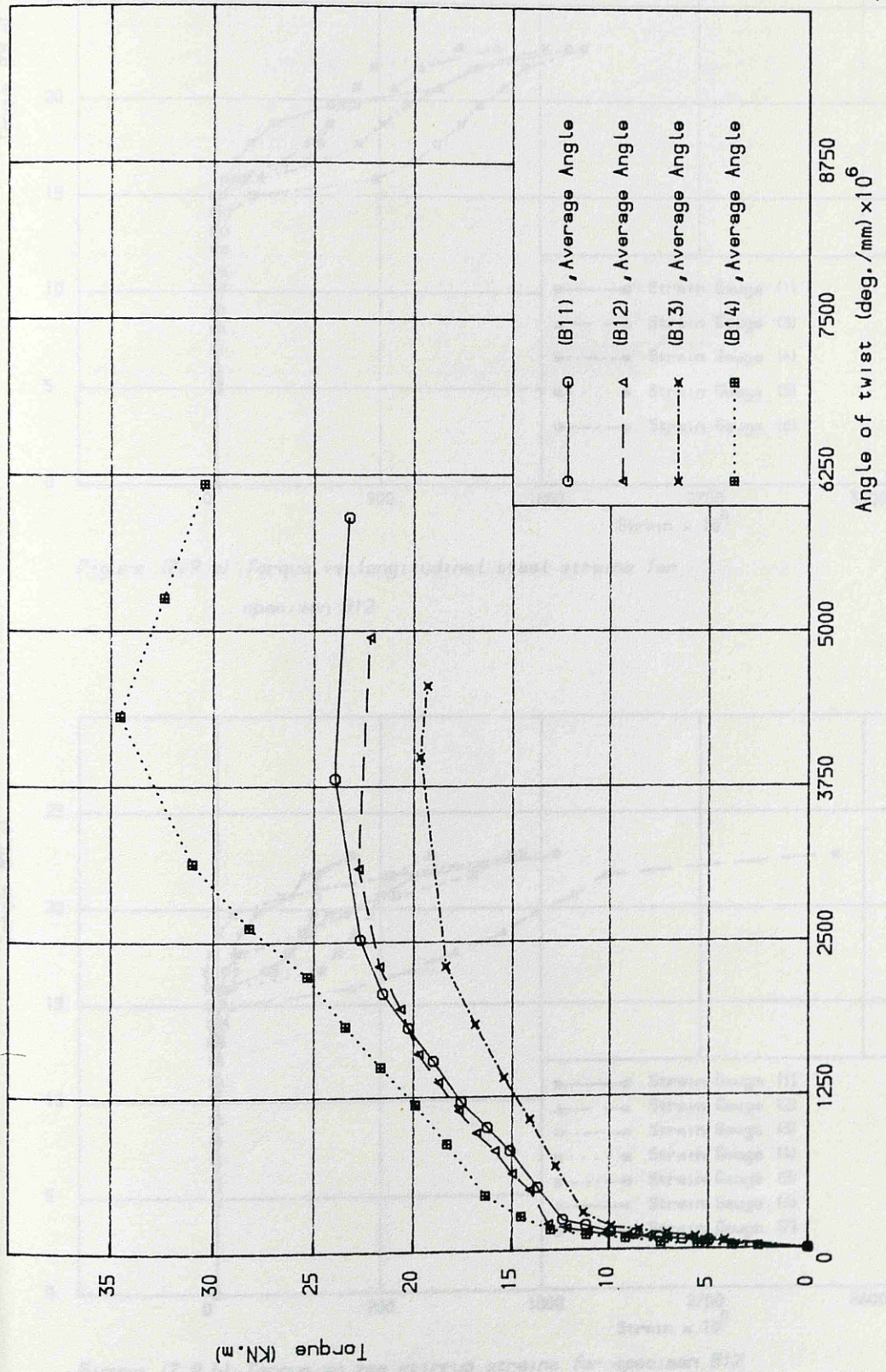
Figure (7.8) Torque-twist curves for specimens B11, B12, B13 & B14

Figure (7.9 a) Torque vs longitudinal steel strains for specimen B12

Figure (7.9 b) Torque vs top stirrup strains for specimen B12
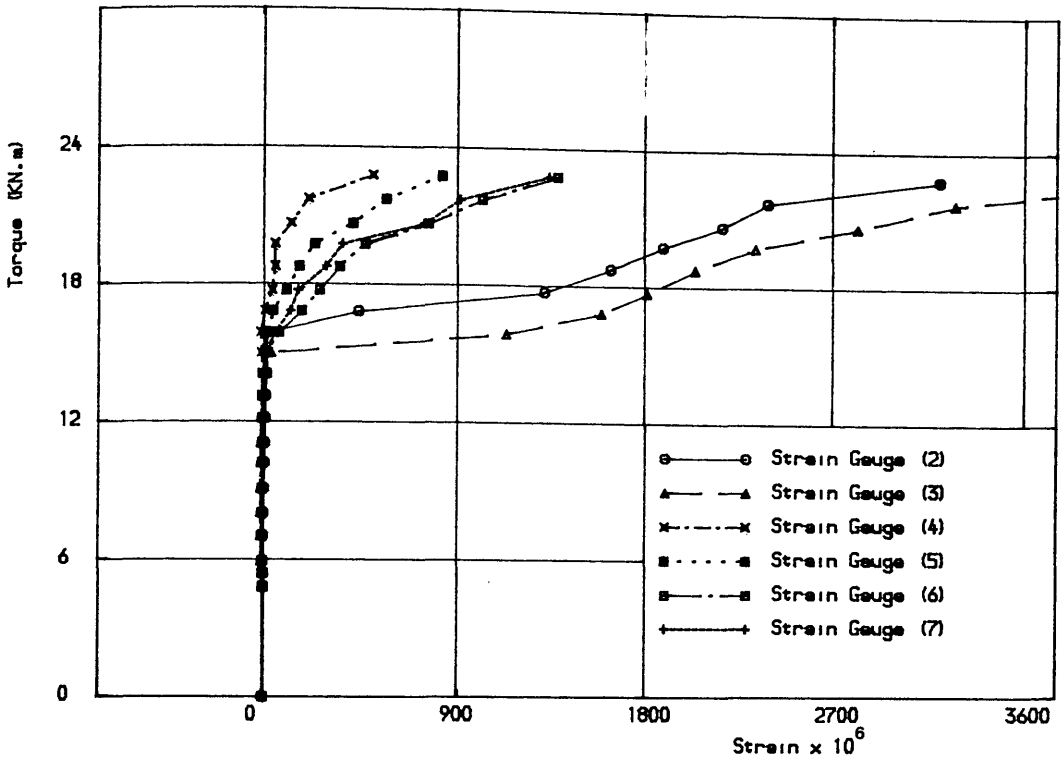
Figure (7.9 c) Torque vs bottom stirrup strains for specimen B12

Figure (7.9 d) Torque vs longitudinal steel strains for
specimen B13

Figure (7.9 e) Torque vs top stirrup strains for specimen B13

Figure (7.9 f) Torque vs bottom stirrup strains for specimen B13

Figure (7.9 g) Torque vs longitudinal steel strains and unit
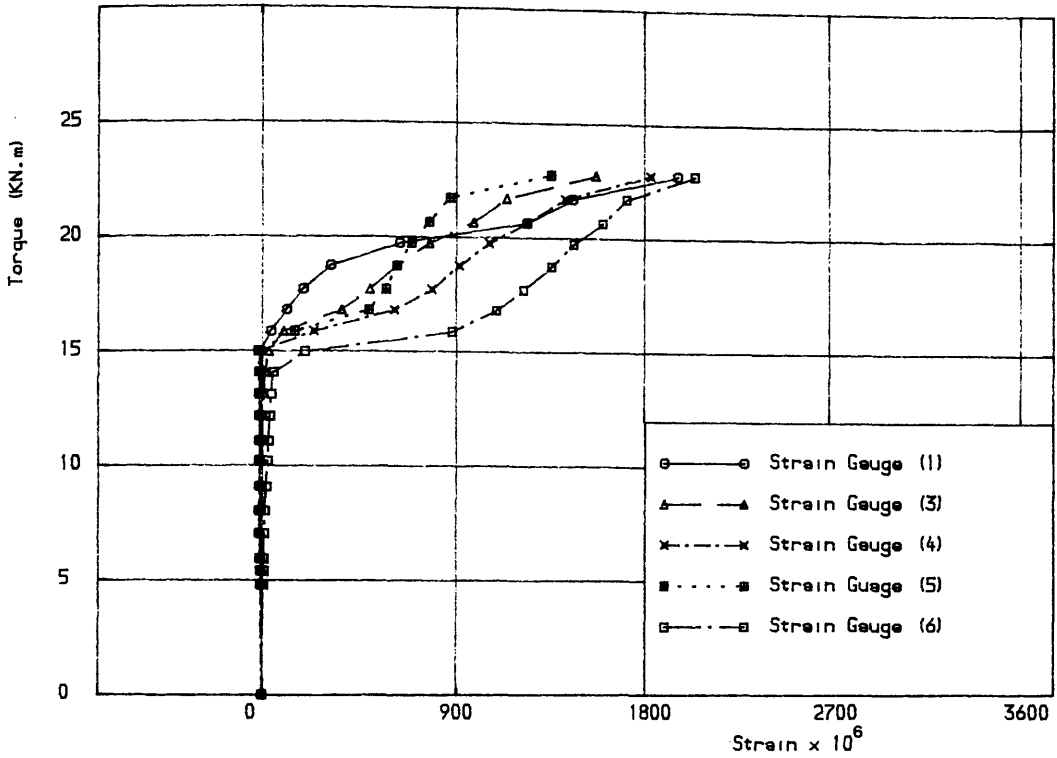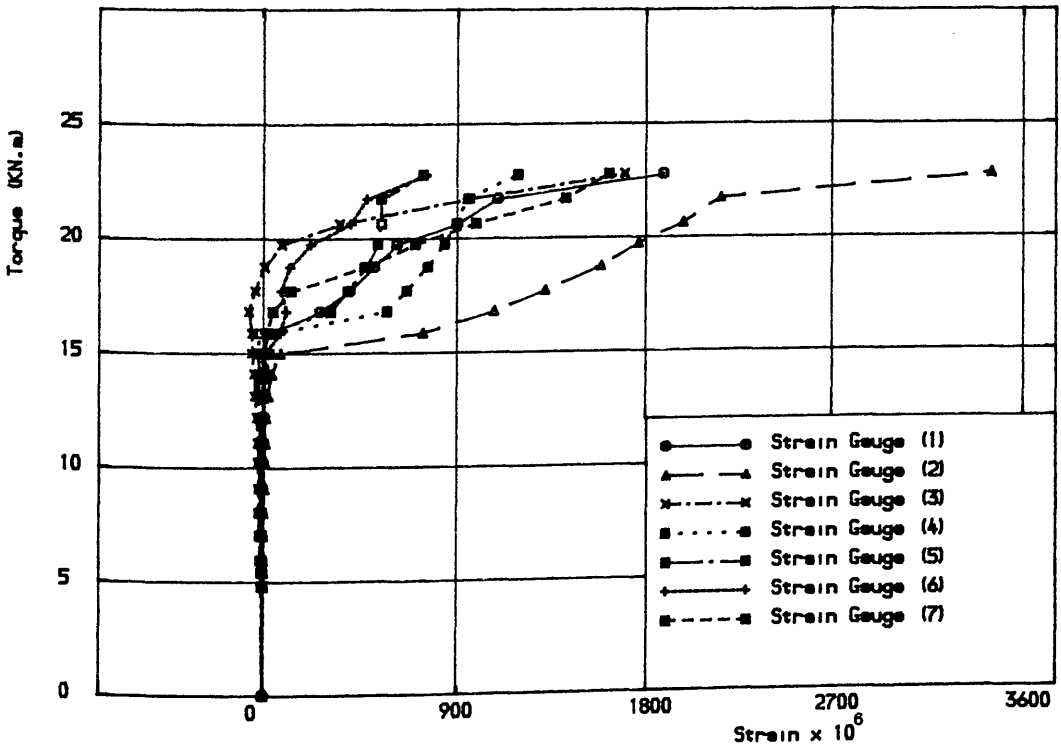lengthening for specimen B14

Figure (7.9 h) Torque vs top stirrup strains for specimen B14

Figure (7.9 i) Torque vs bottom stirrup strains for specimen B14

Figure (7.10 a) Torque vs crack width for specimen B12

Figure (7.10 b) Torque vs crack width for specimen B13

Figure (7.10 c) Torque vs crack width for specimen B14
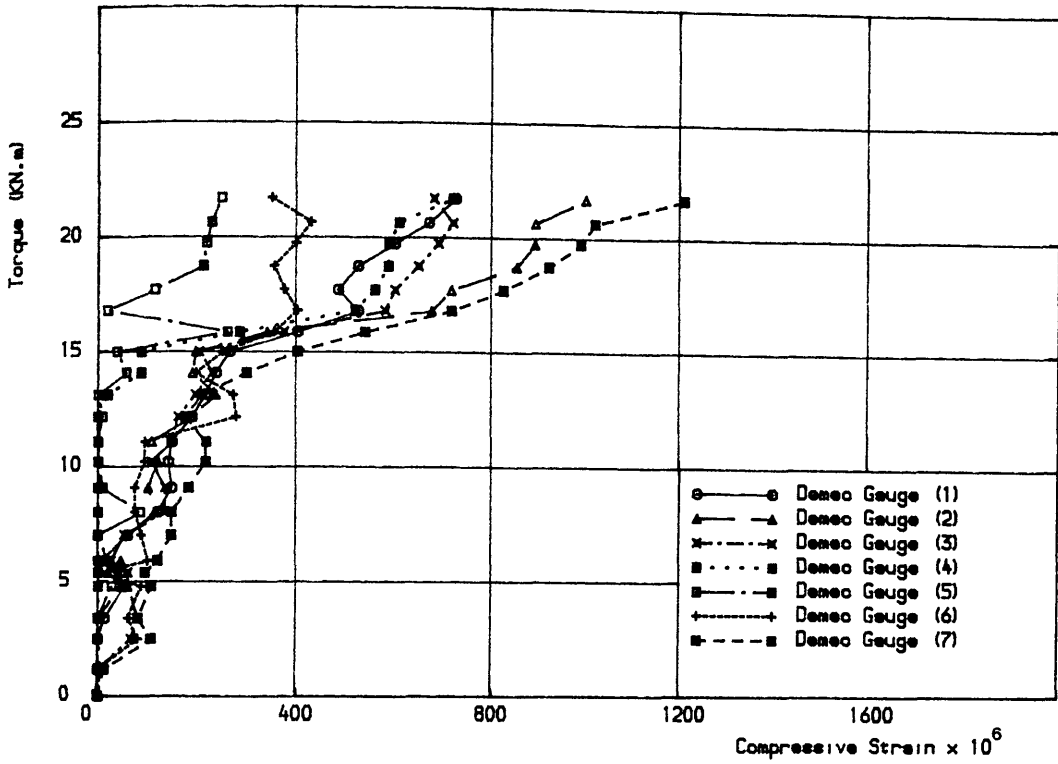
Figure (7.11 a) Torque vs concrete surface compressive strains for
specimen B12
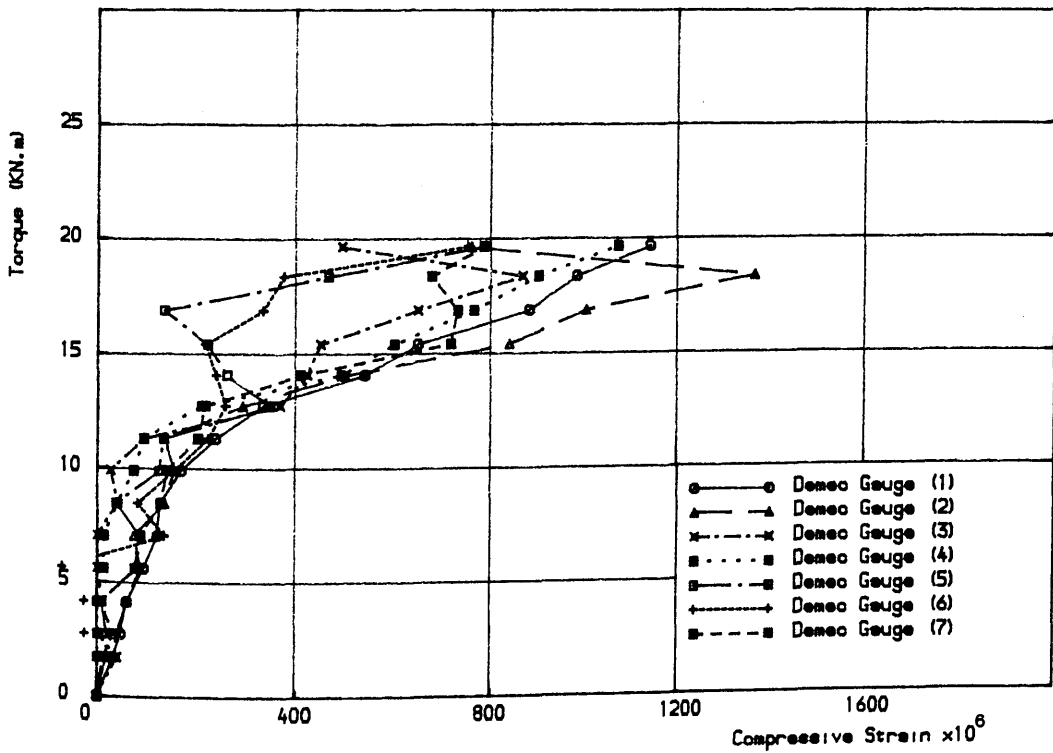
Figure (7.11 b) Torque vs concrete surface compressive strains for
specimen B13
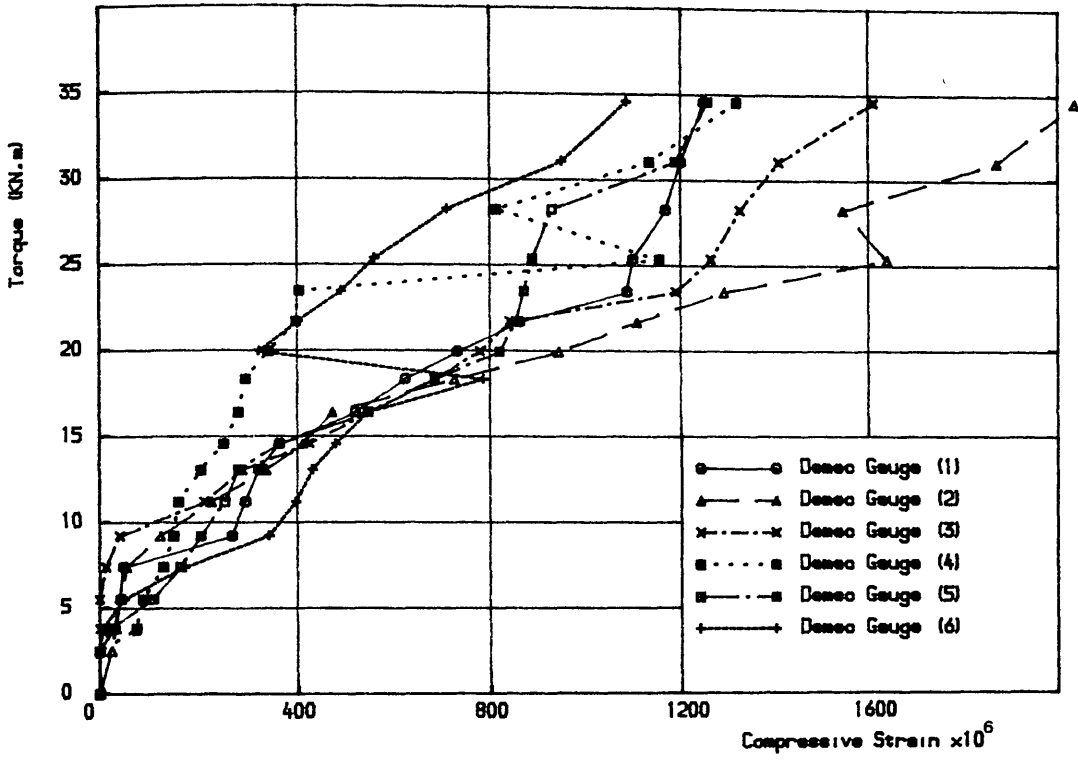
Figure (7.11 c) Torque vs concrete surface compressive strains for
specimen B14
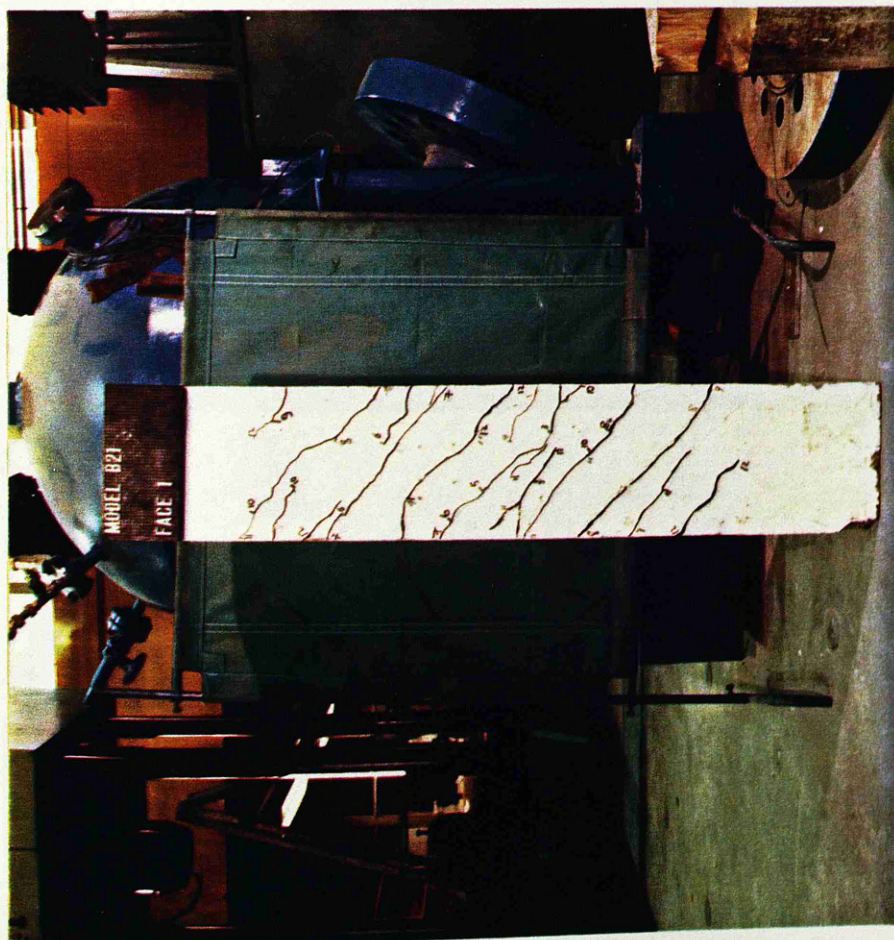
Figure (7.12) Final crack pattern for specimen B21

Figure (7.12) Continued

Figure (7.12) Continued
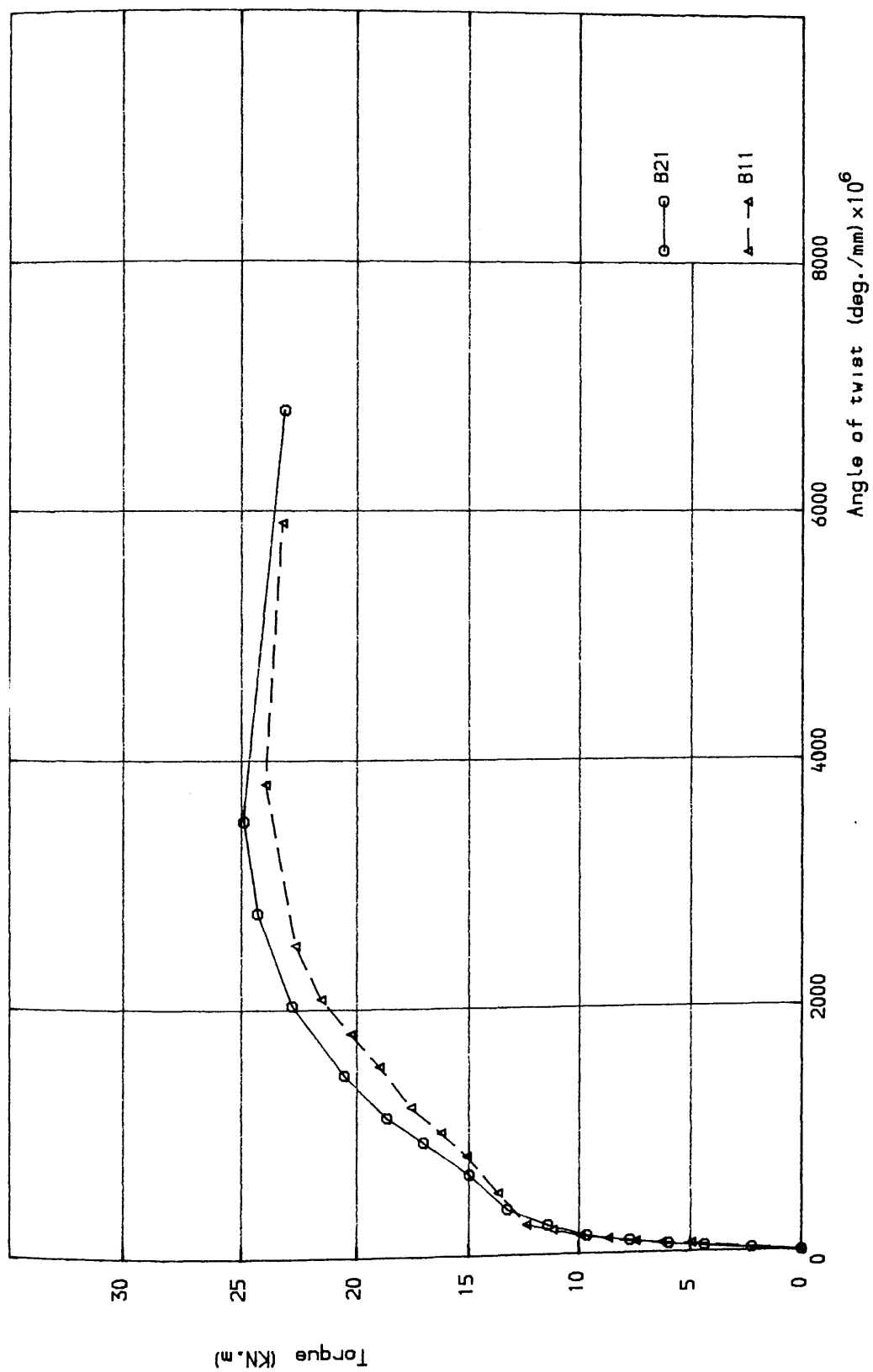
Figure (7.13) Torque-twist curves for specimens B11 and B21
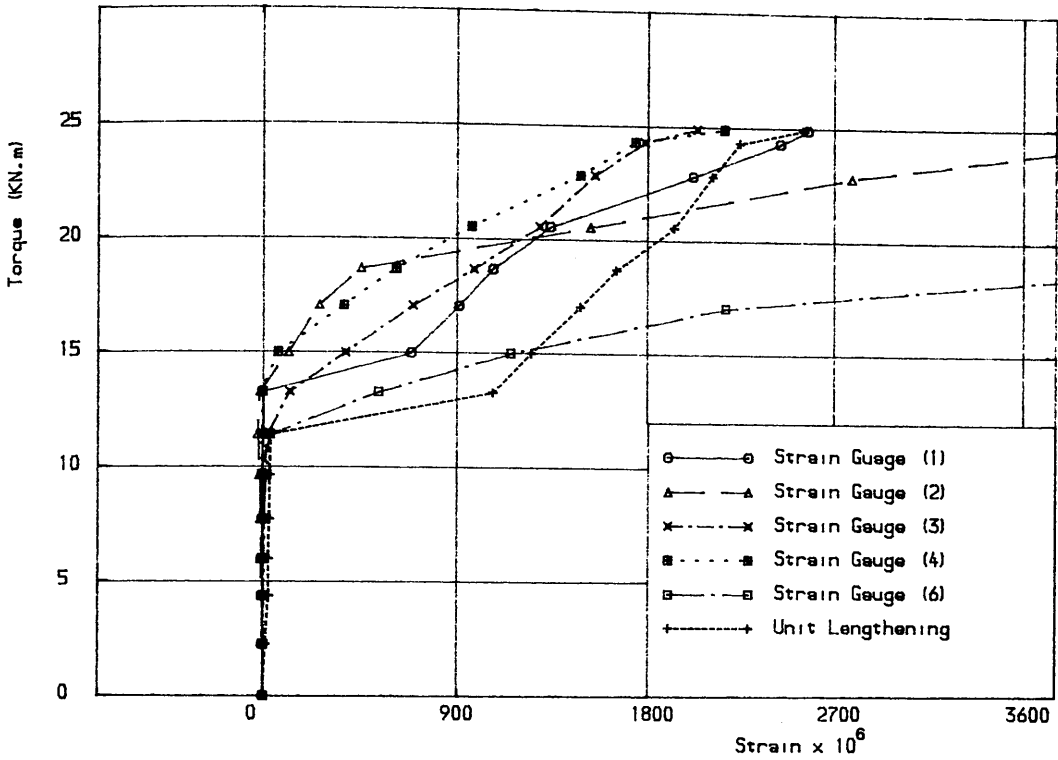
Figure (7.14 a) Torque vs longitudinal steel strains and unit
lengthening of specimen B21
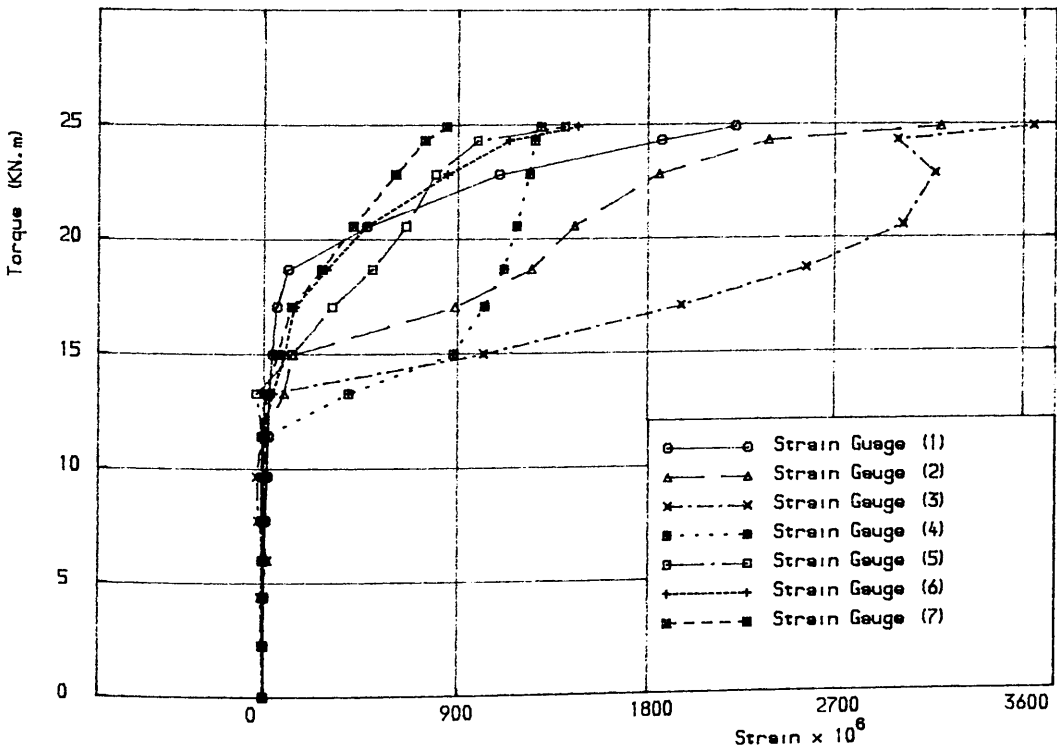
Figure (7.14 b) Torque vs top stirrup strains for specimen B21
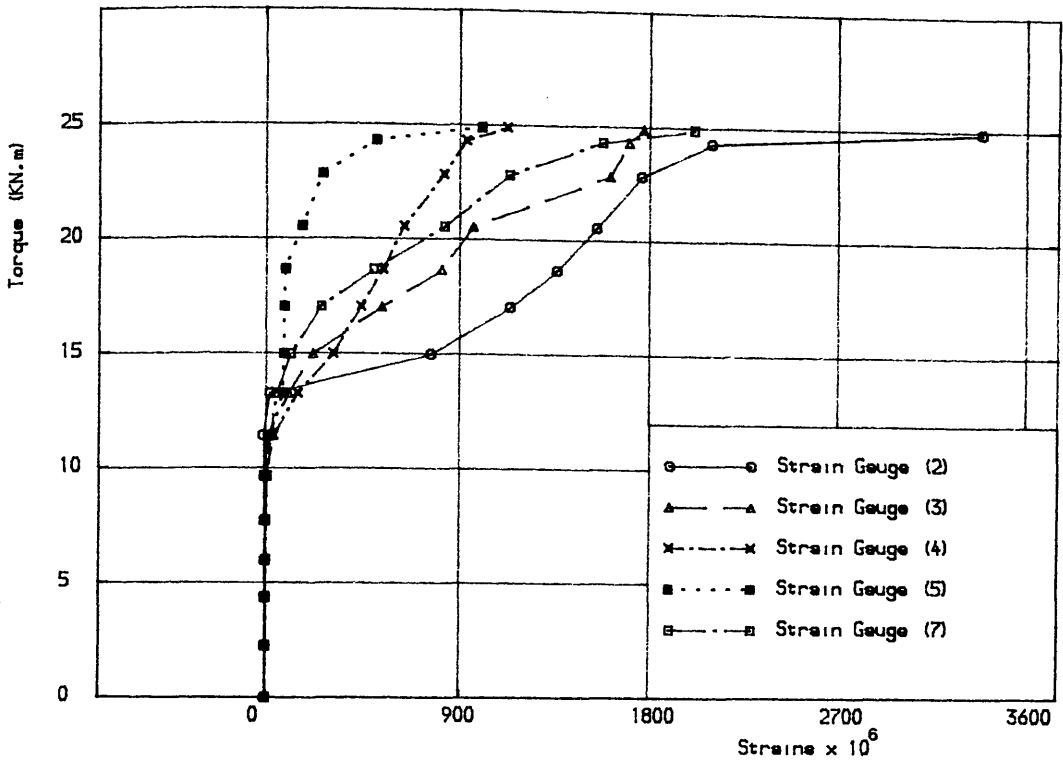
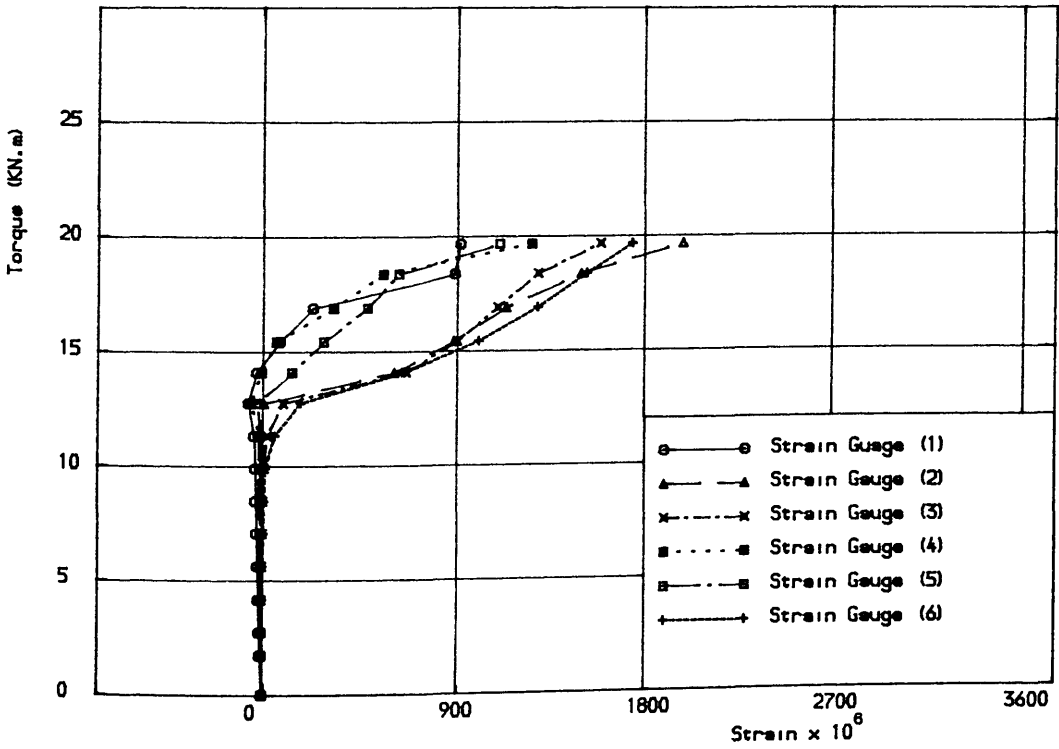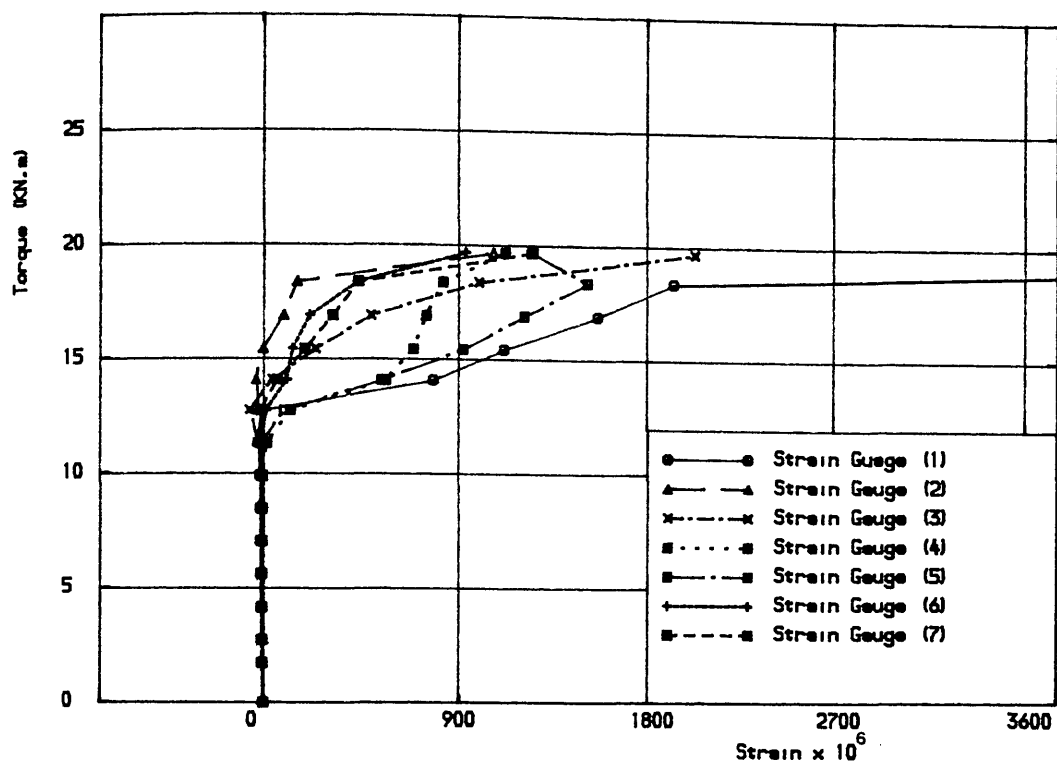Figure (7.14 c) Torque vs bottom stirrup starins for specimen B21
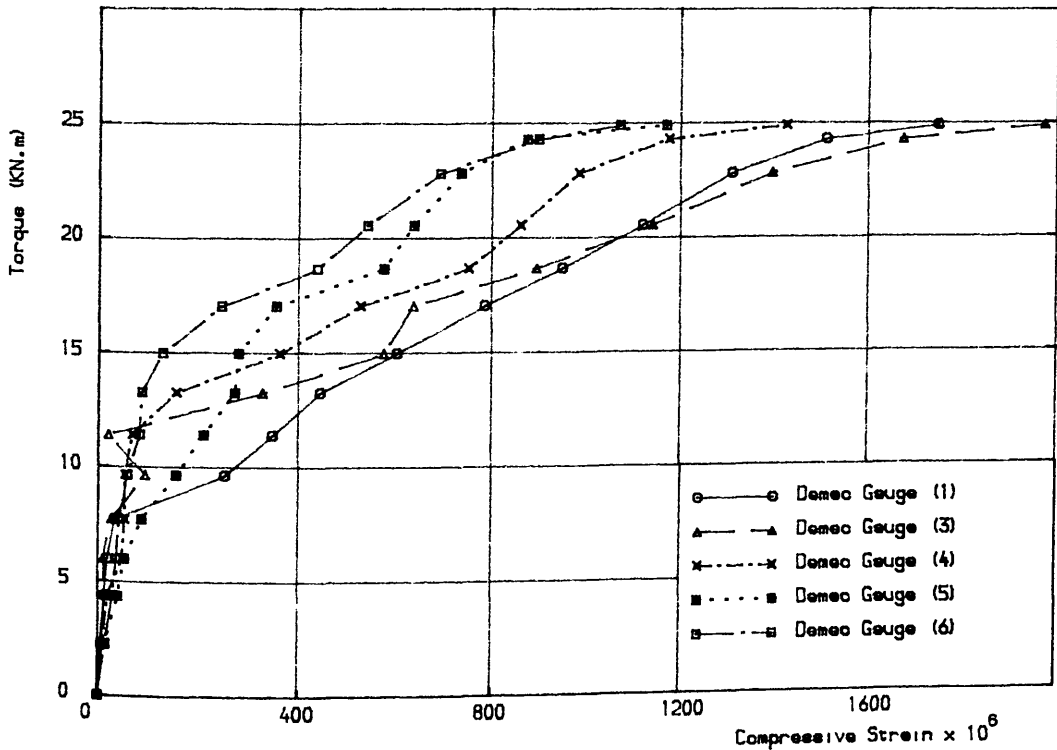
Figure (7.15) Torque vs concrete surface compressive strains for
specimen B21

Figure (7.16) Torque-twist curves for specimens B31, B32, B33 and B34
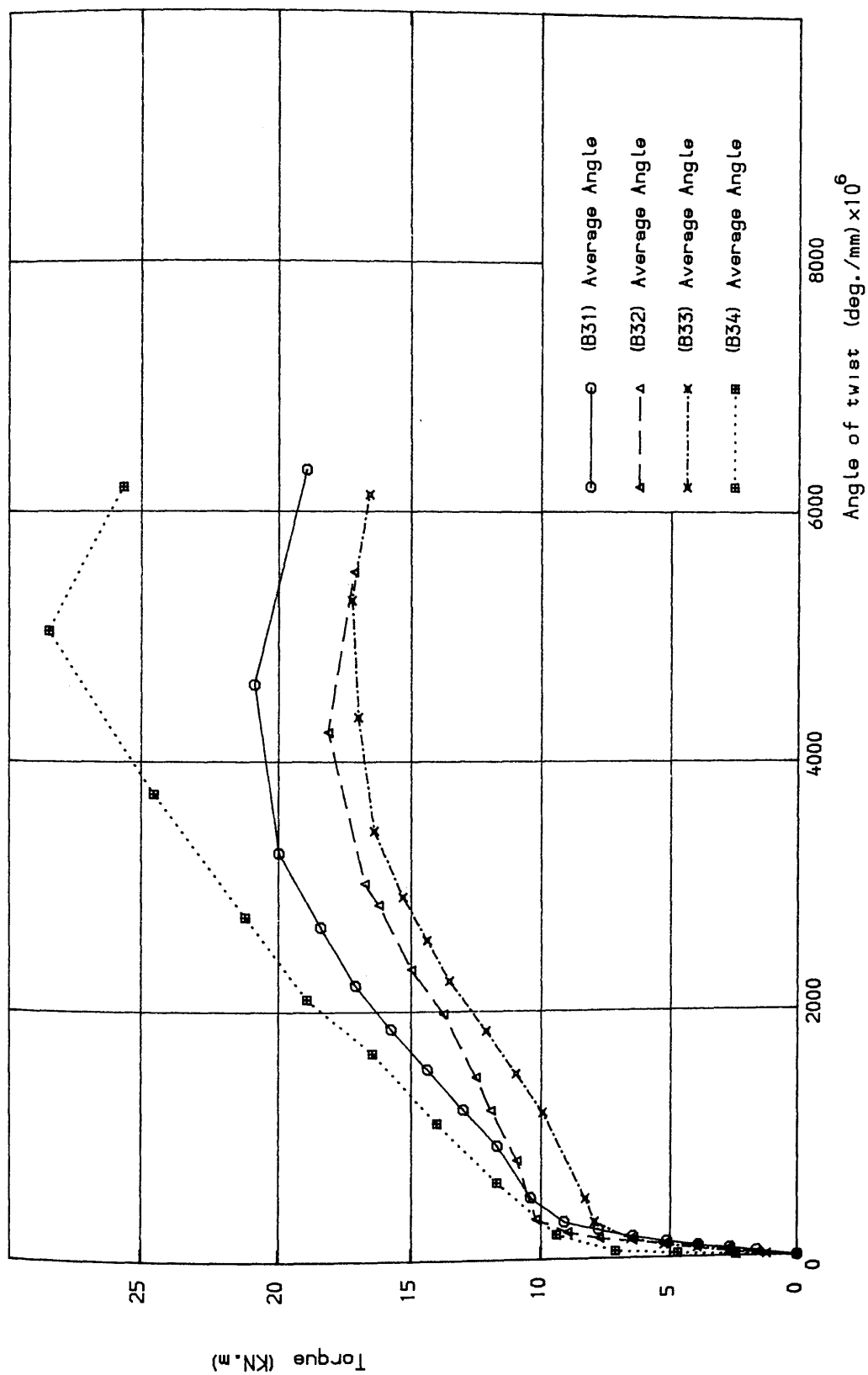
Figure (7.17) Final crack pattern for specimens B31, B32 and B33
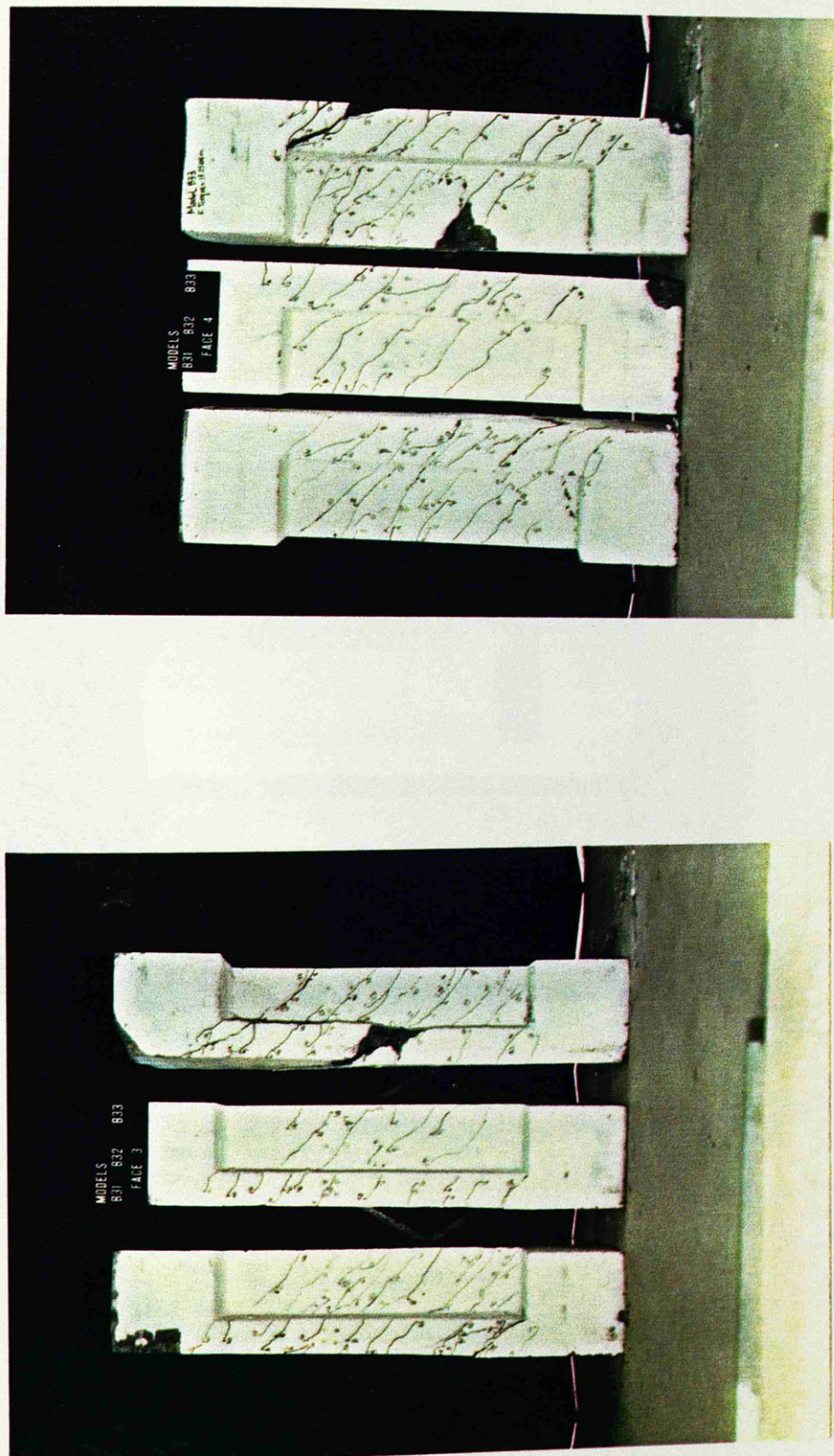
Figure (7.17) Continued
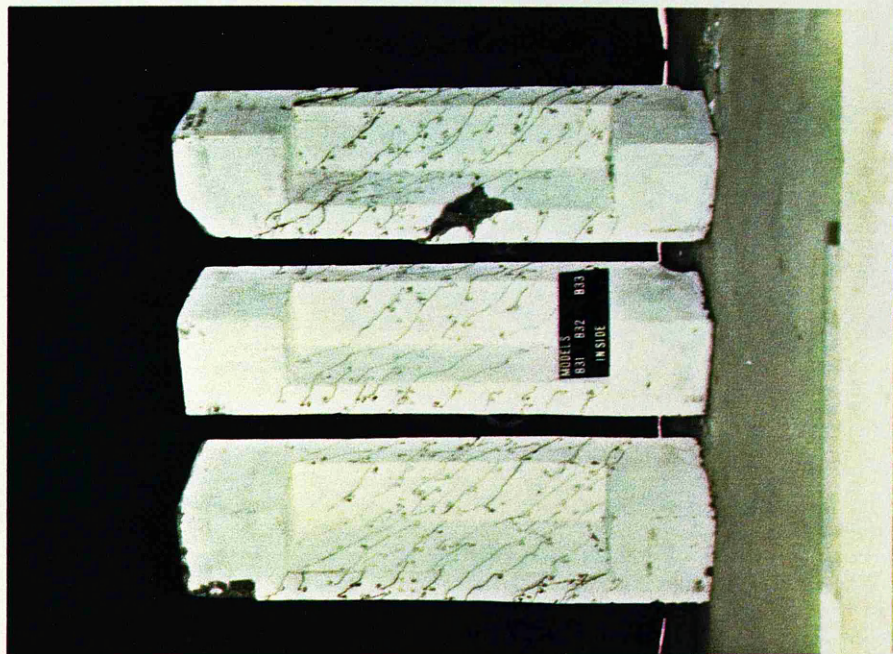
Figure (7.17) Continued
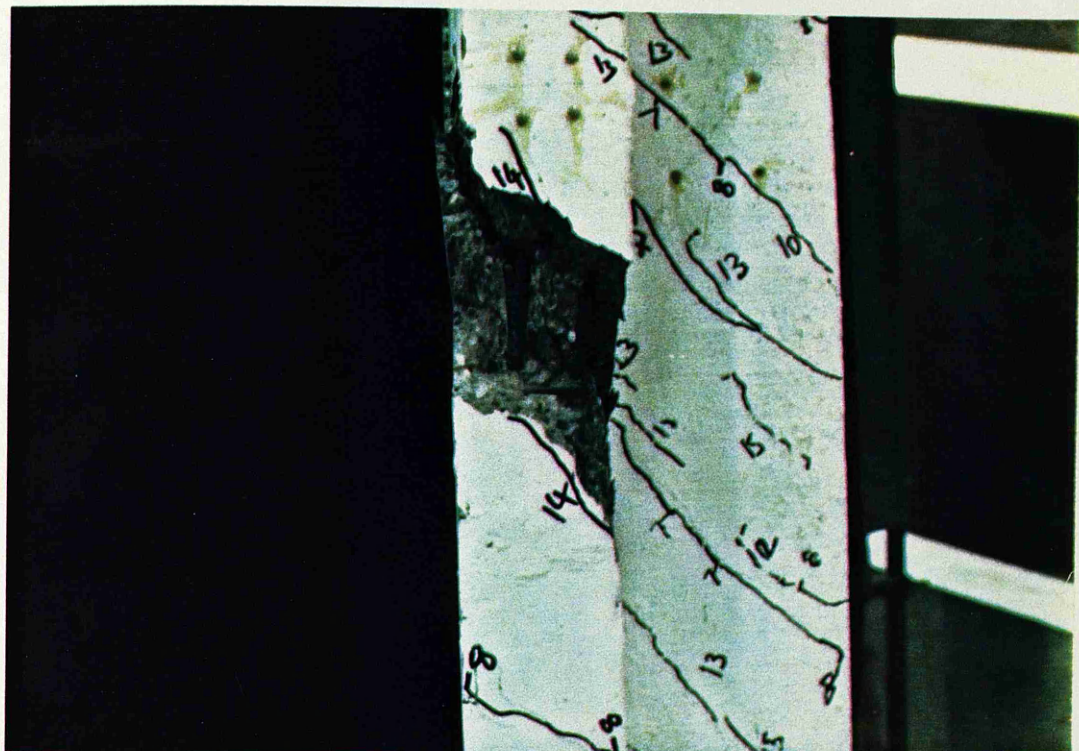
Figure (7.18) Dowel effect on the longitudinal bars
of specimen B33
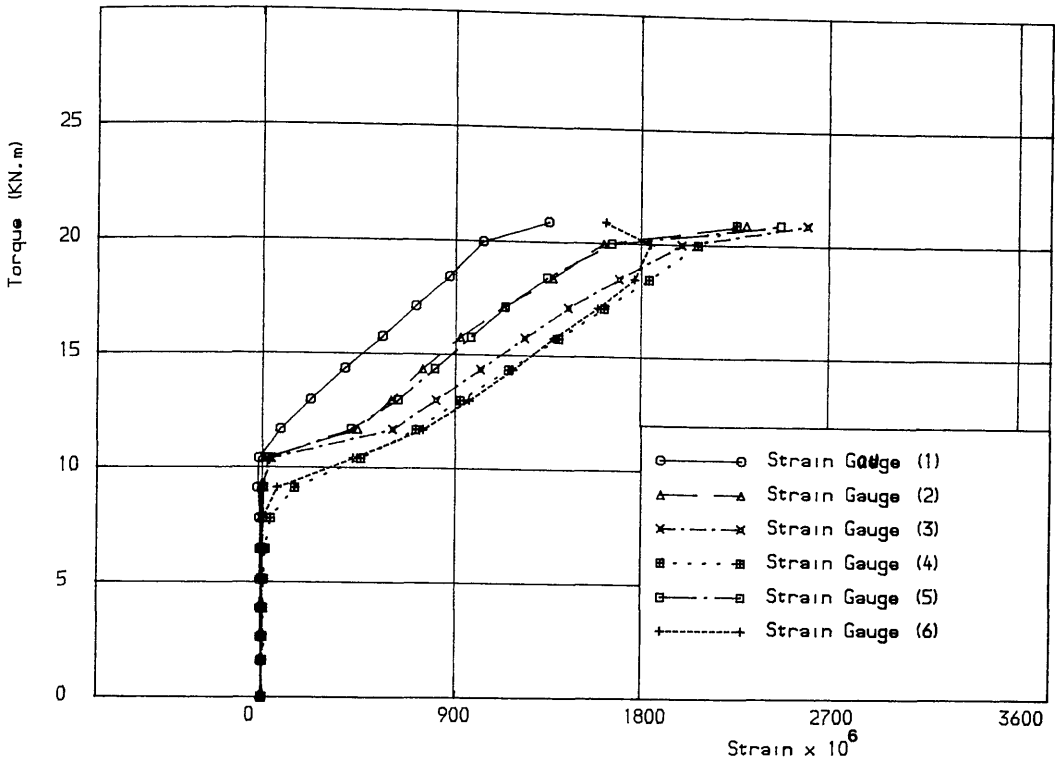
Figure (7.19 a) Torque vs longitudinal steel strains for specimen B31
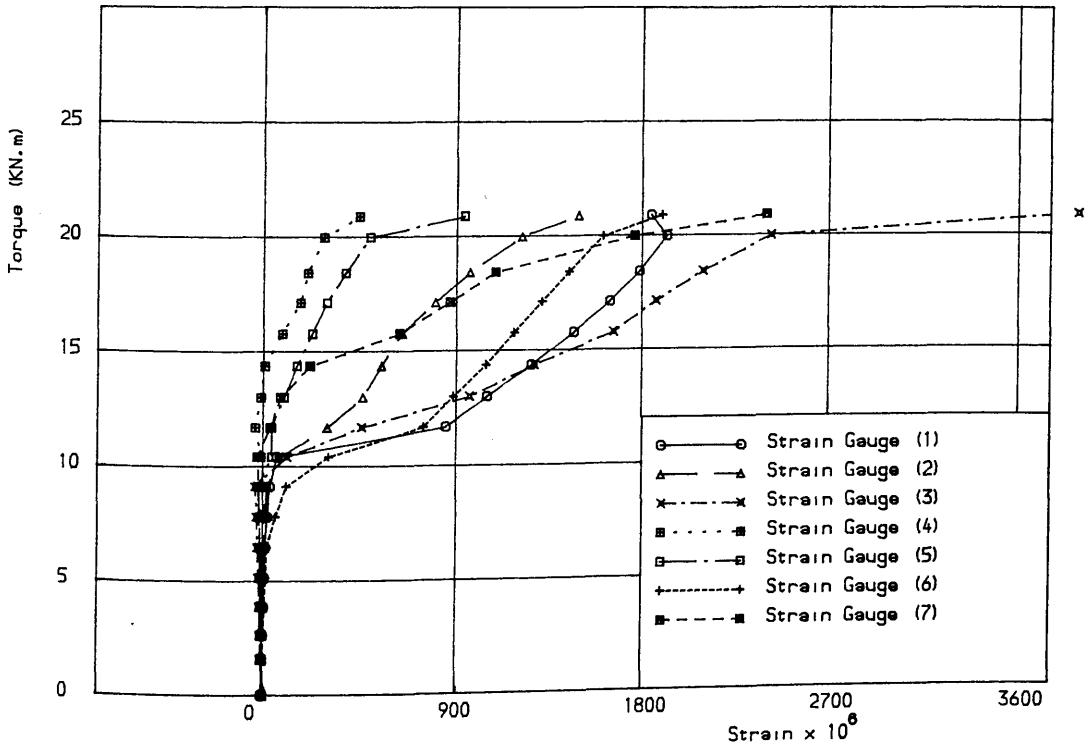
Figure (7.19 b) Torque vs top stirrup strains for specimen B31

Figure (7.19 c) Torque vs bottom stirrup strains for specimen B31

Figure (7.19 d) Torque vs longitudinal steel strains for specimen B32
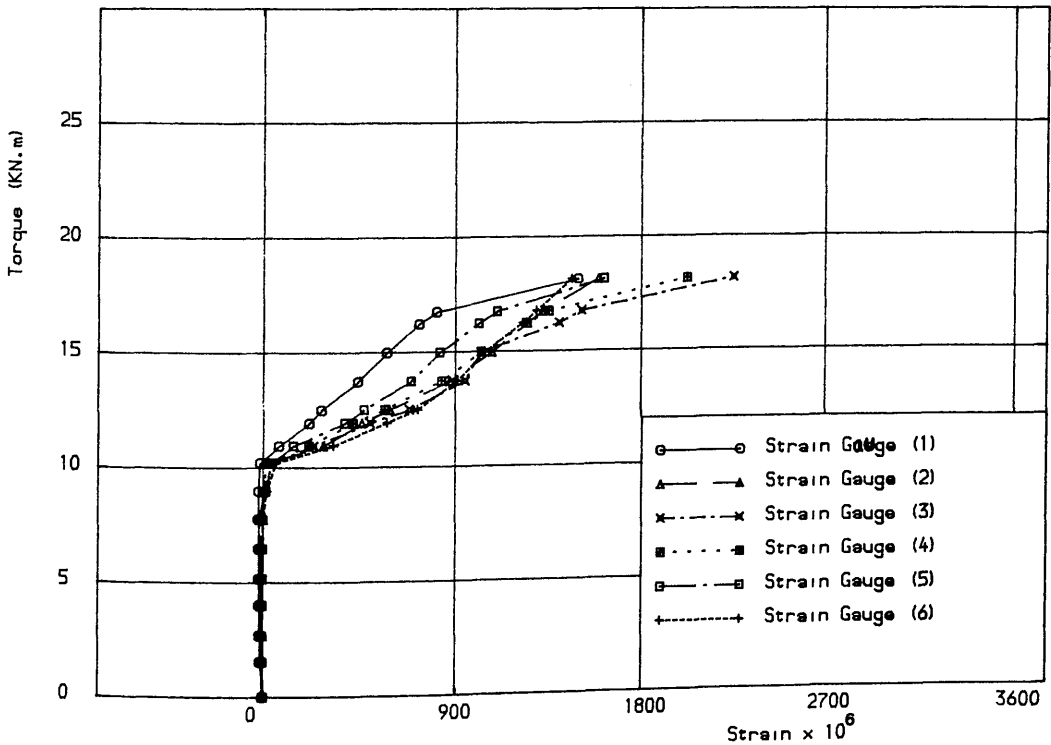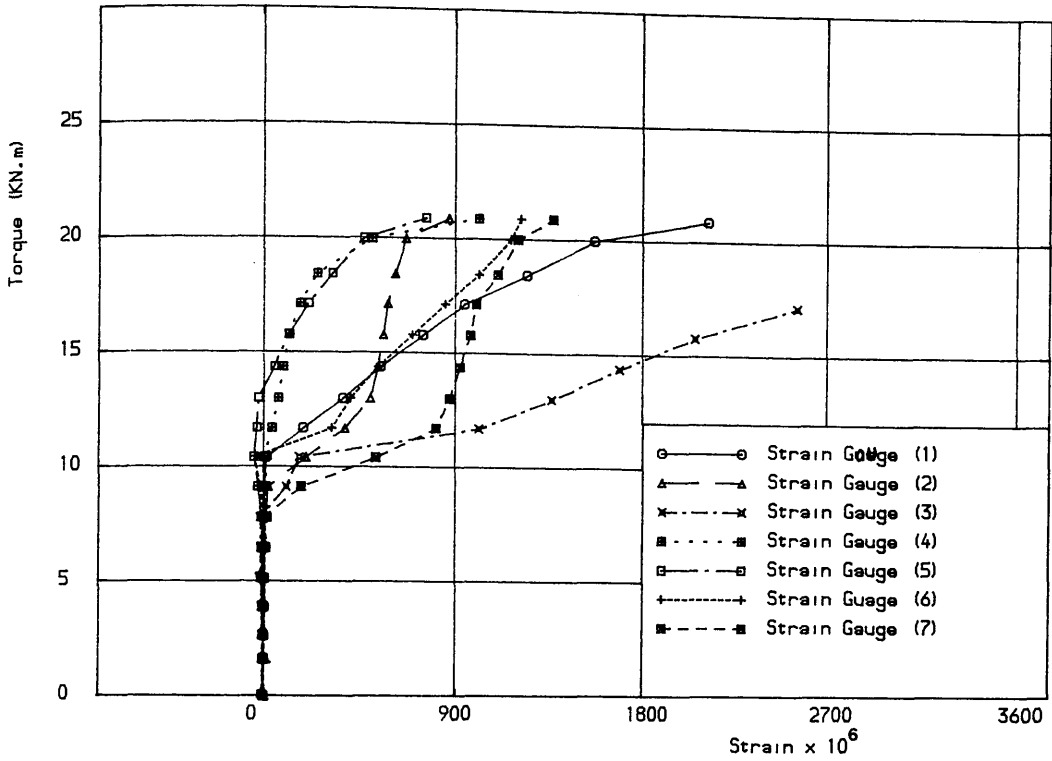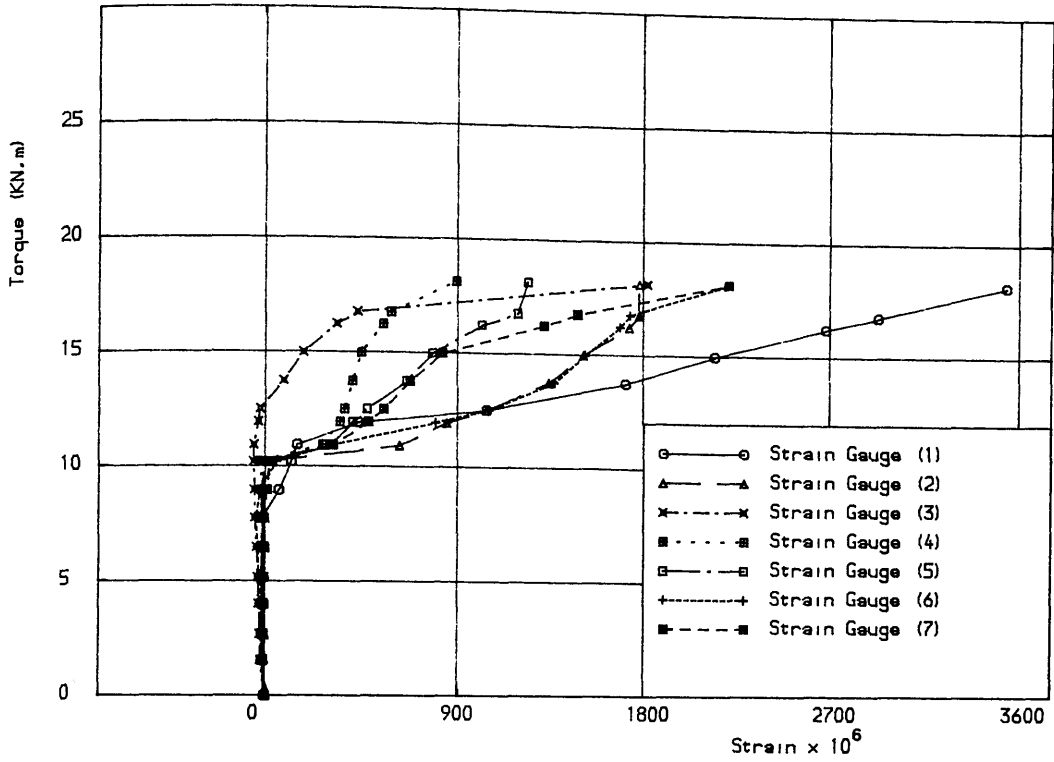
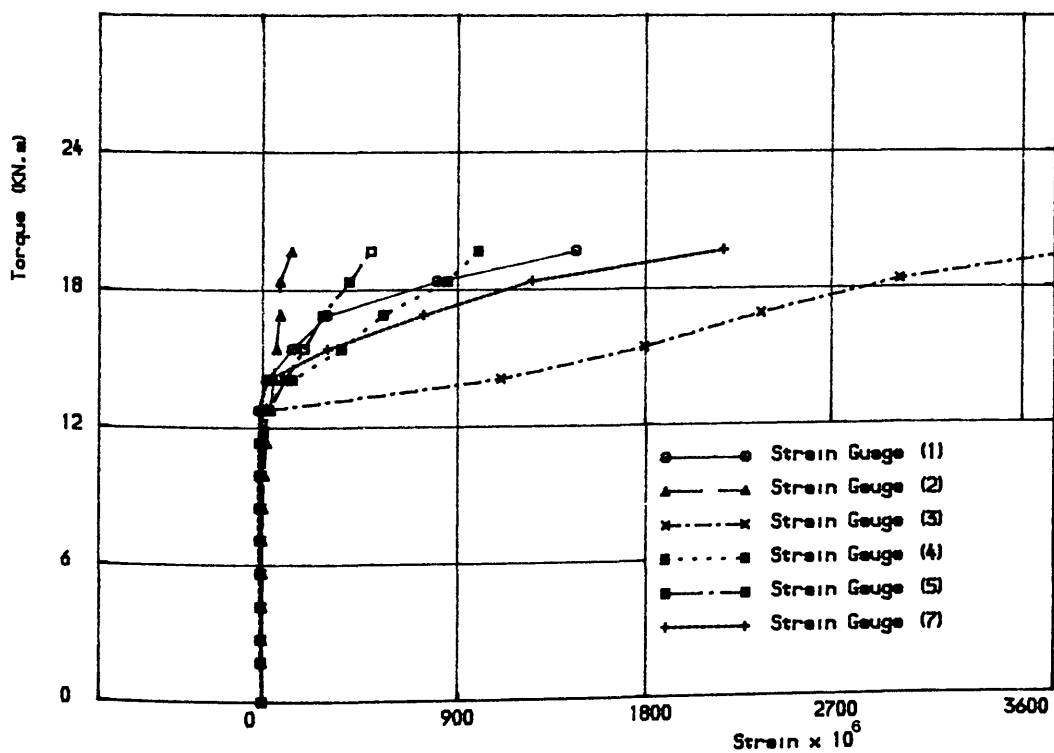Figure (7.19 e) Torque vs top stirrup strains for specimen B32
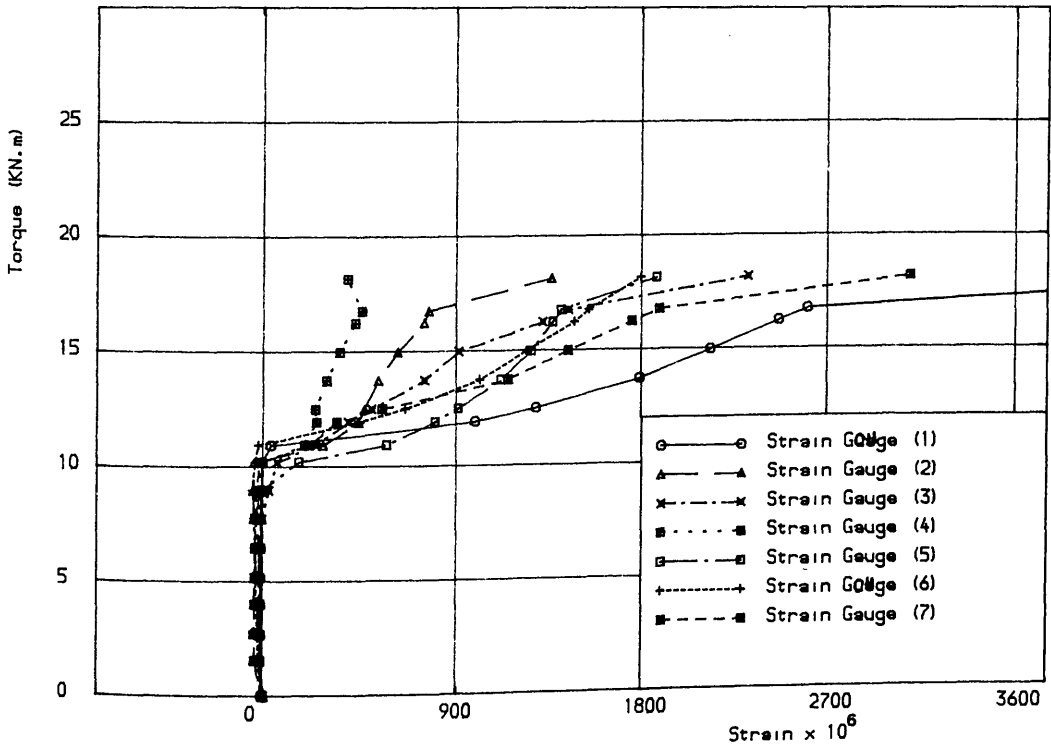
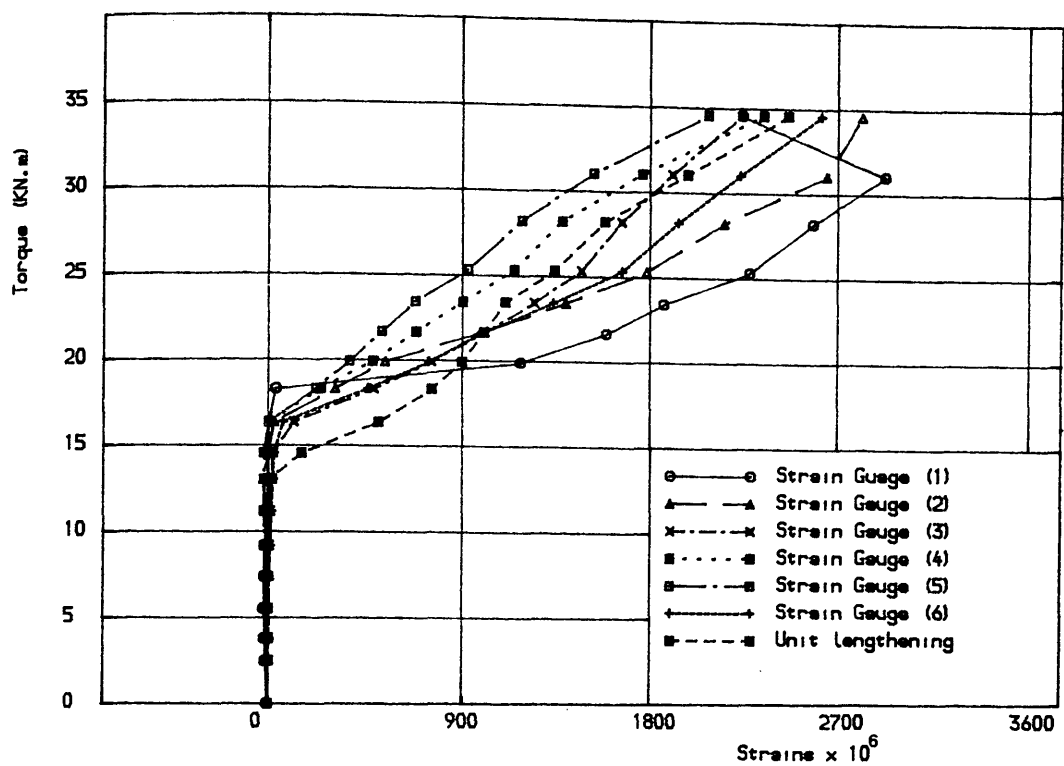Figure (7.19 f) Torque vs bottom stirrup strains for specimen B32
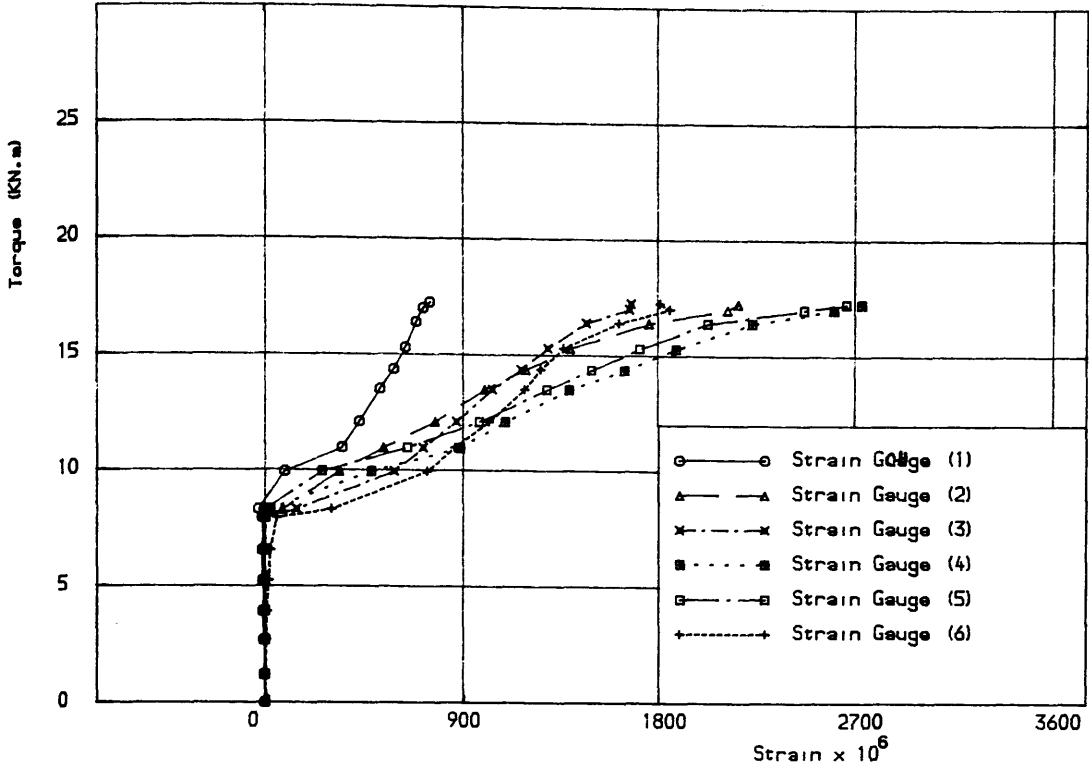
Figure (7.19 g) Torque vs longitudinal steel strains for specimen B33
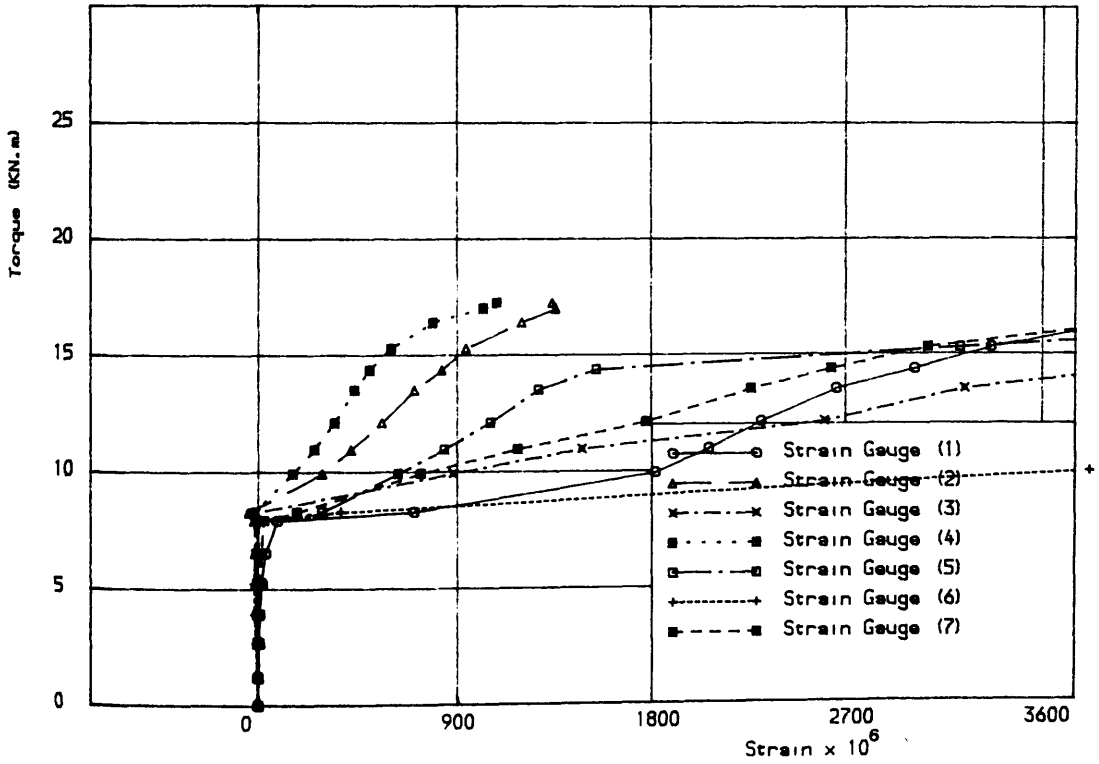
Figure (7.19 h) Torque vs top stirrup strains for specimen B33
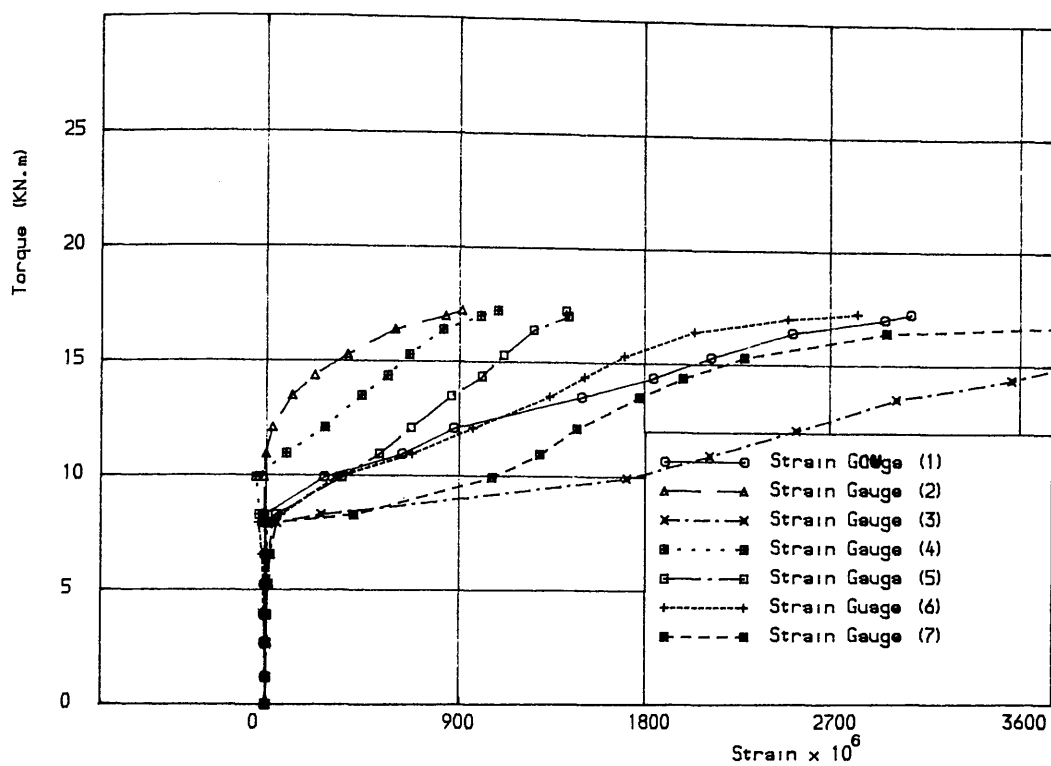
Figure (7.19 ı) Torque vs bottom stirrup strains for specimen B33
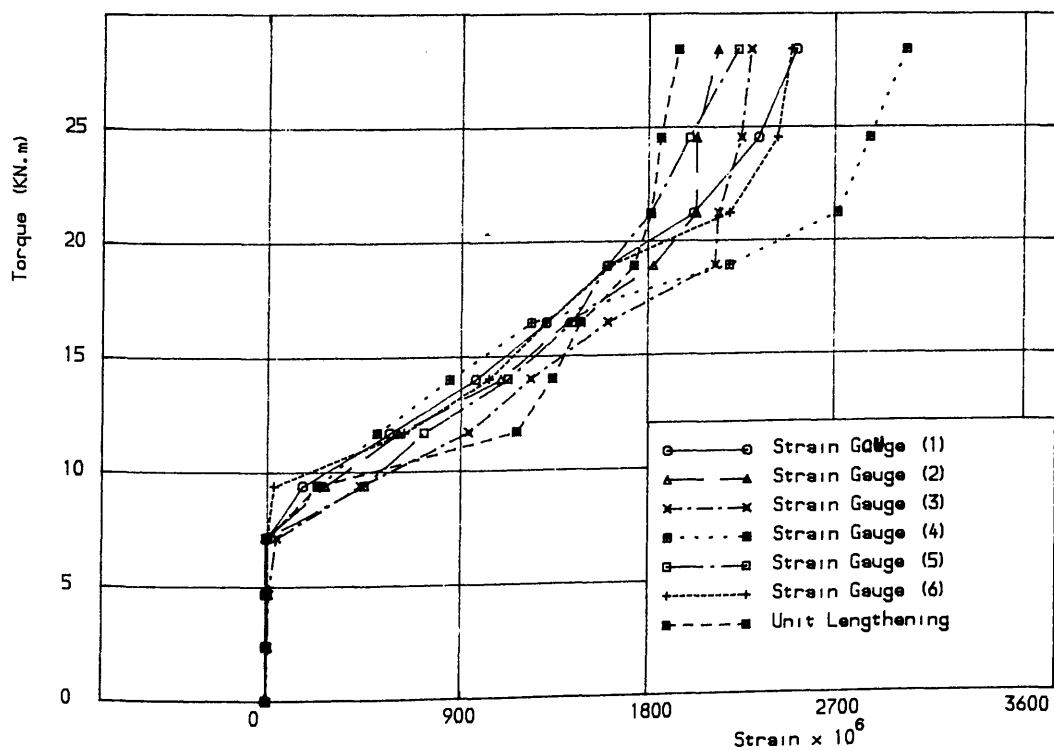
Figure (7.19 j) Torque vs longitudinal steel strains and unit
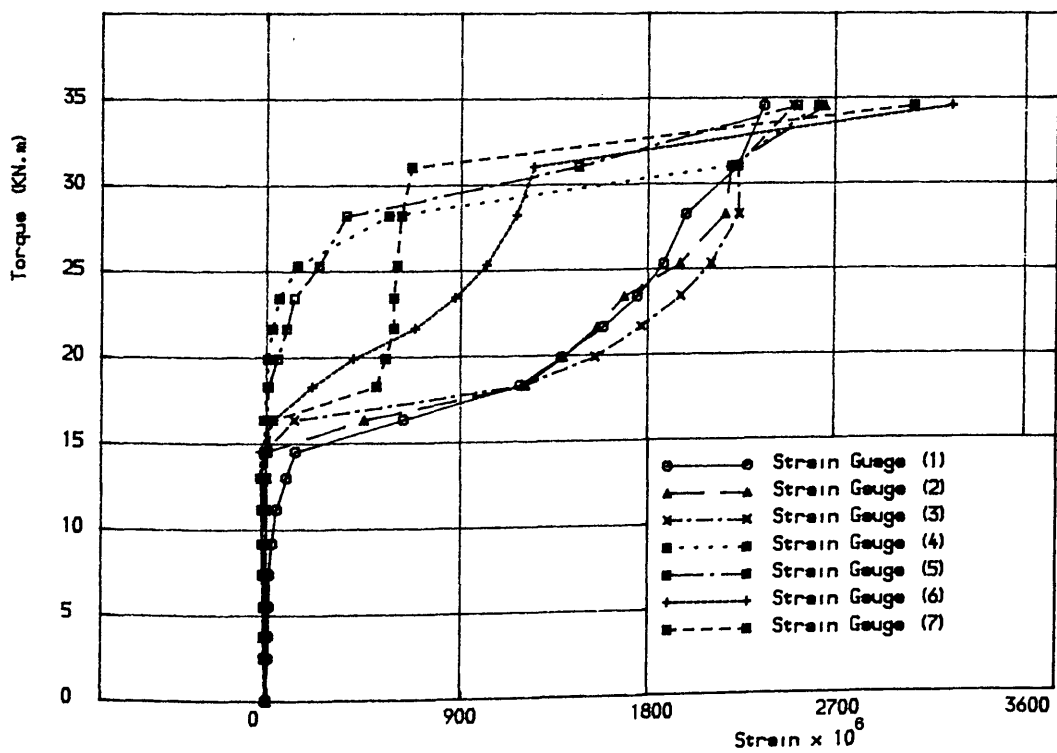lengthening for specimen B34
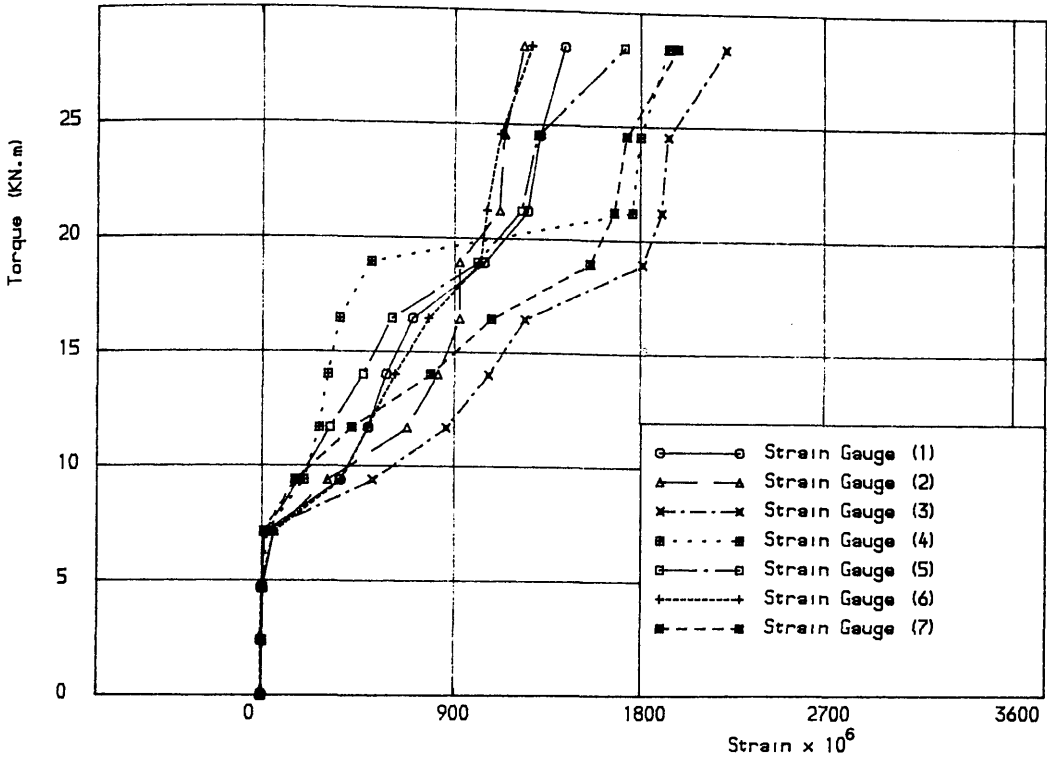
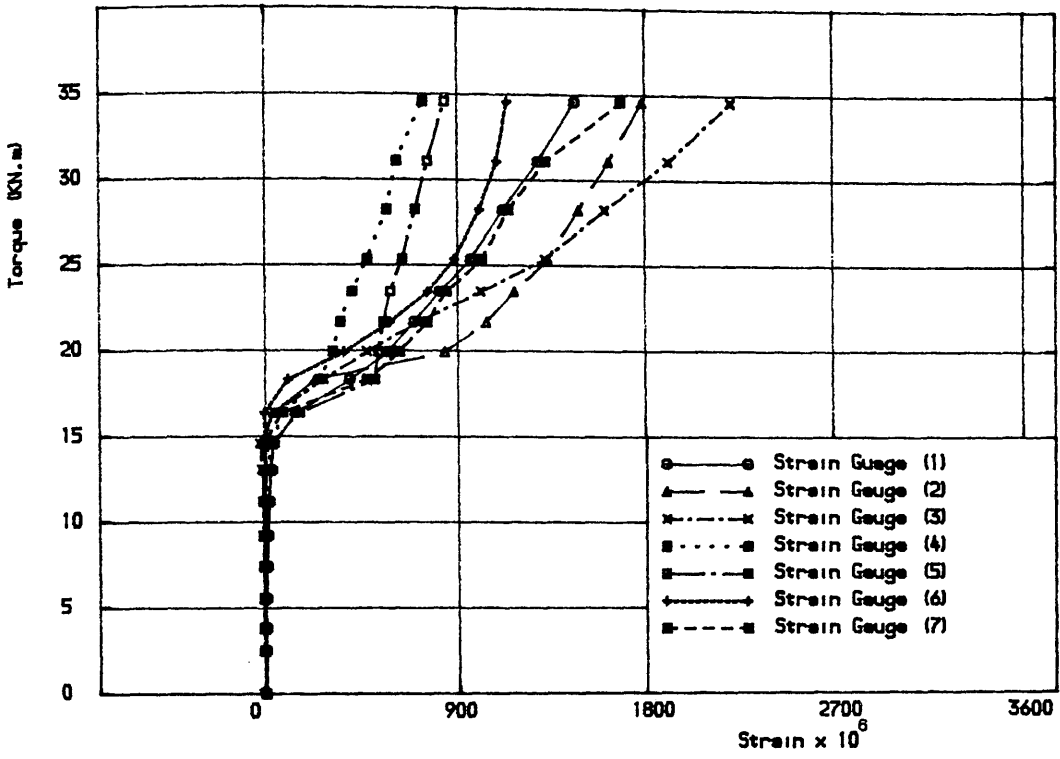Figure (7.19 k) Torque vs top stirrup strains for specimen B34
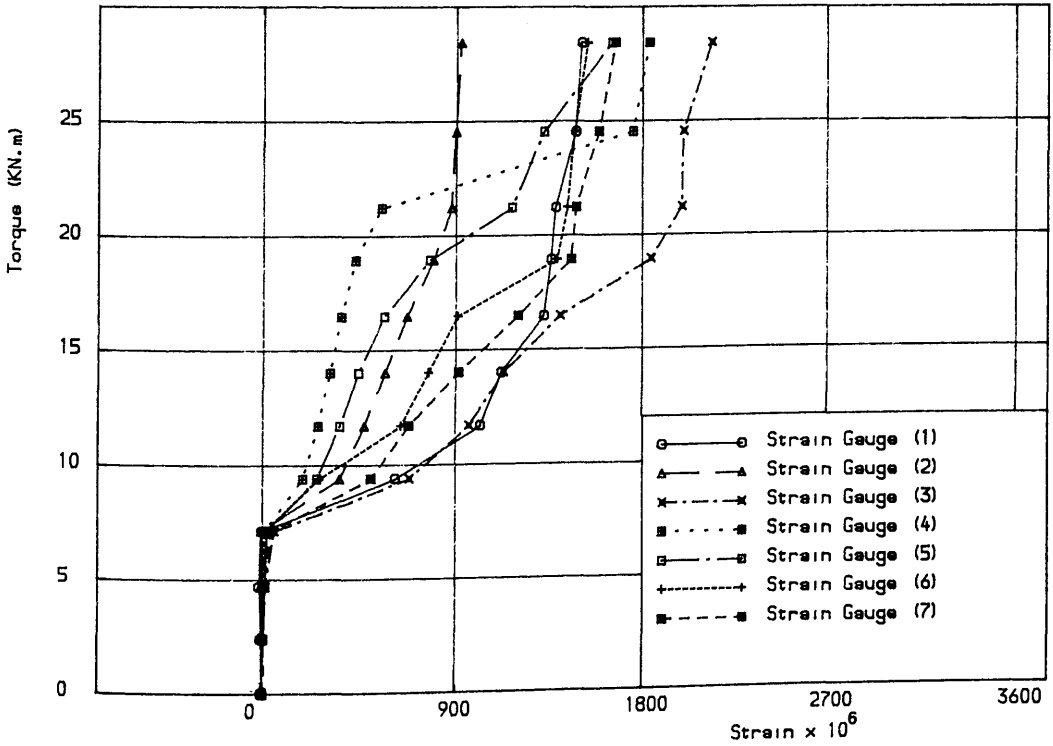
Figure (7.19 l) Torque vs bottom stirrup strains for specimen B34
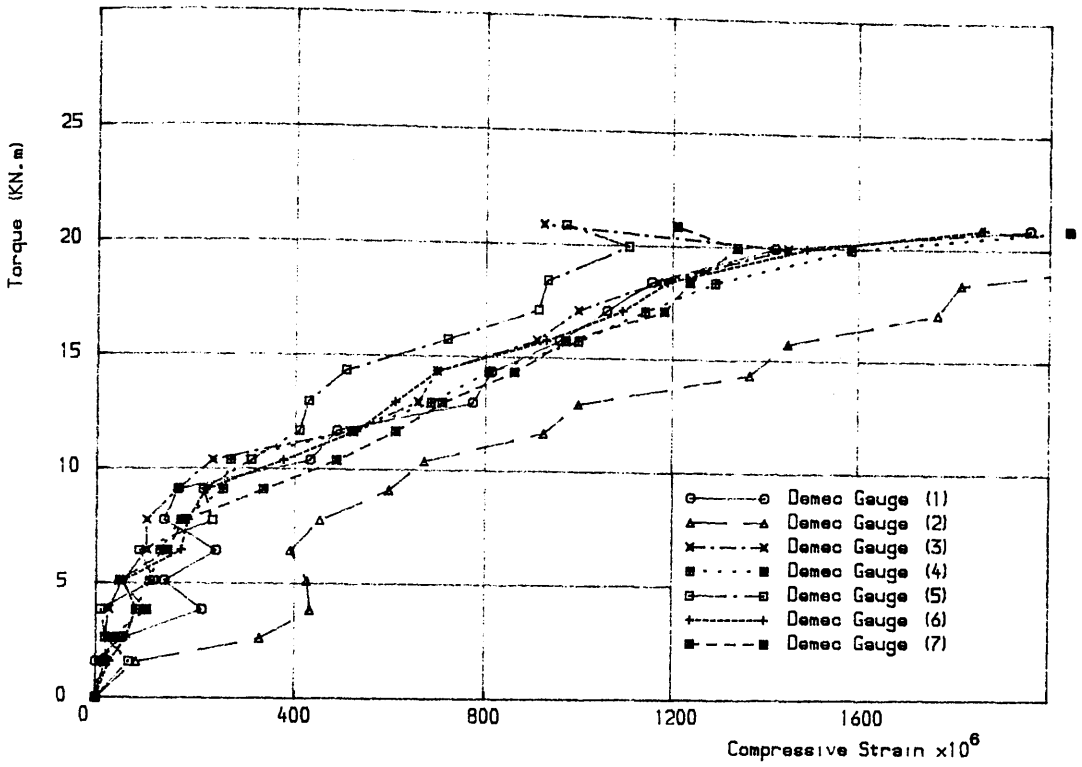
Figure (7.20 a) Torque vs concrete surface compressive strains for specimen B31
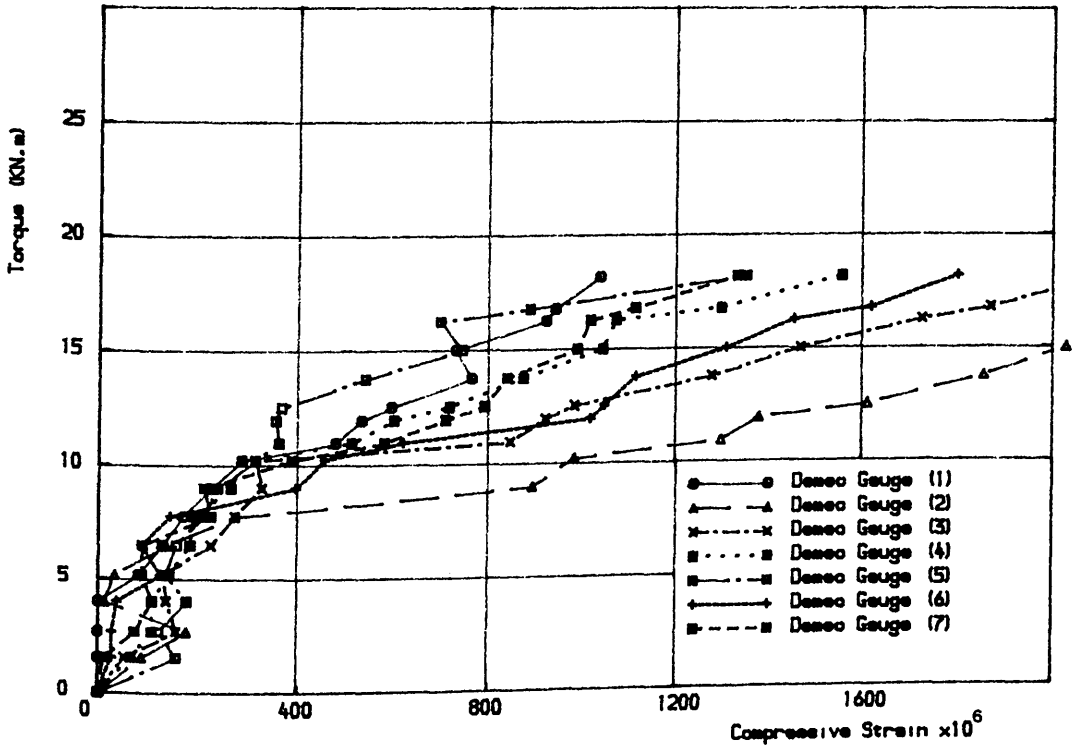
Figure (7.20 b) Torque vs concrete surface compressive strains for specimen B32
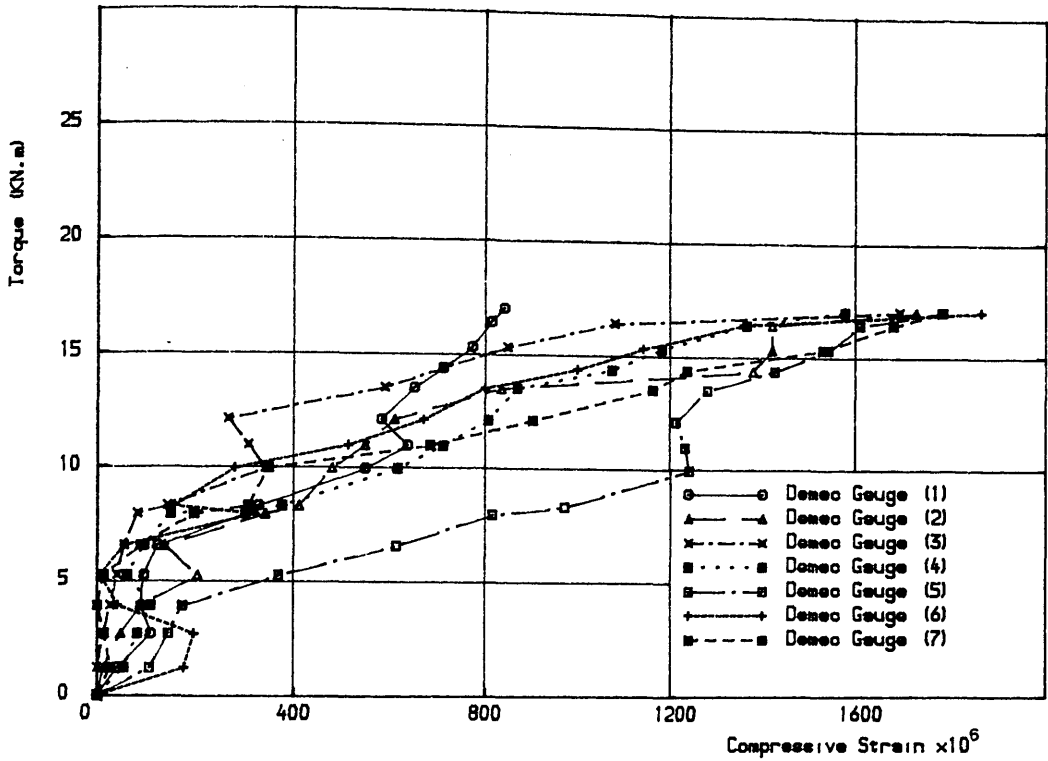
Figure (7.20 c) Torque vs concrete surface compressive strains for specimen B33
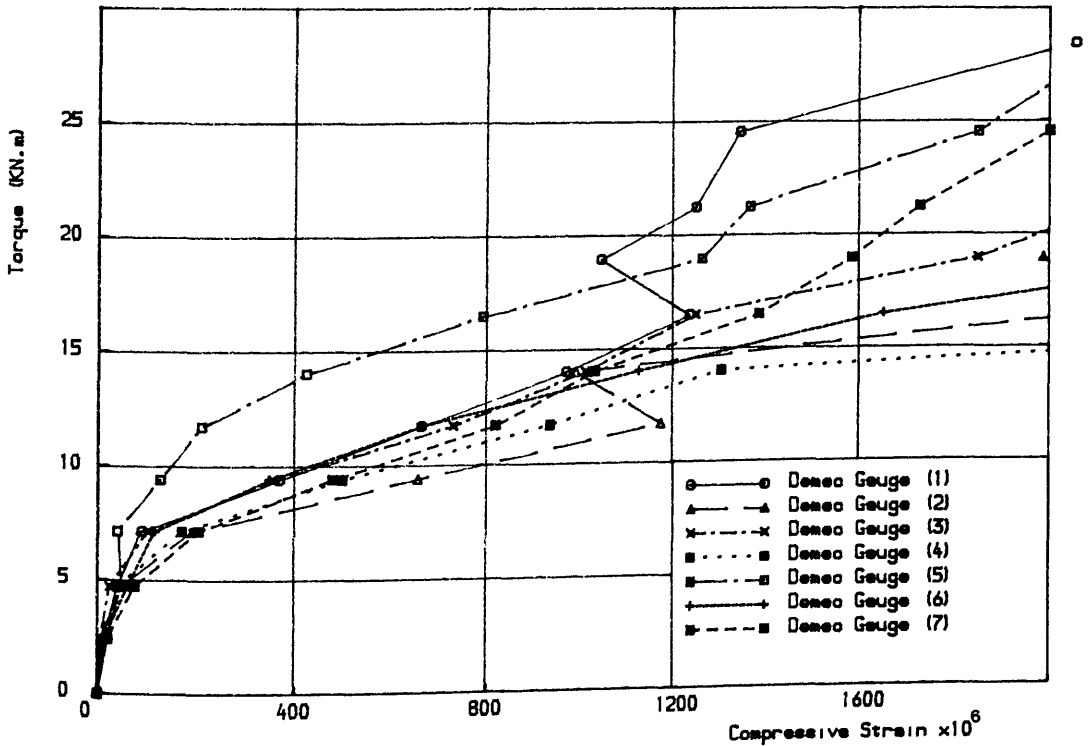
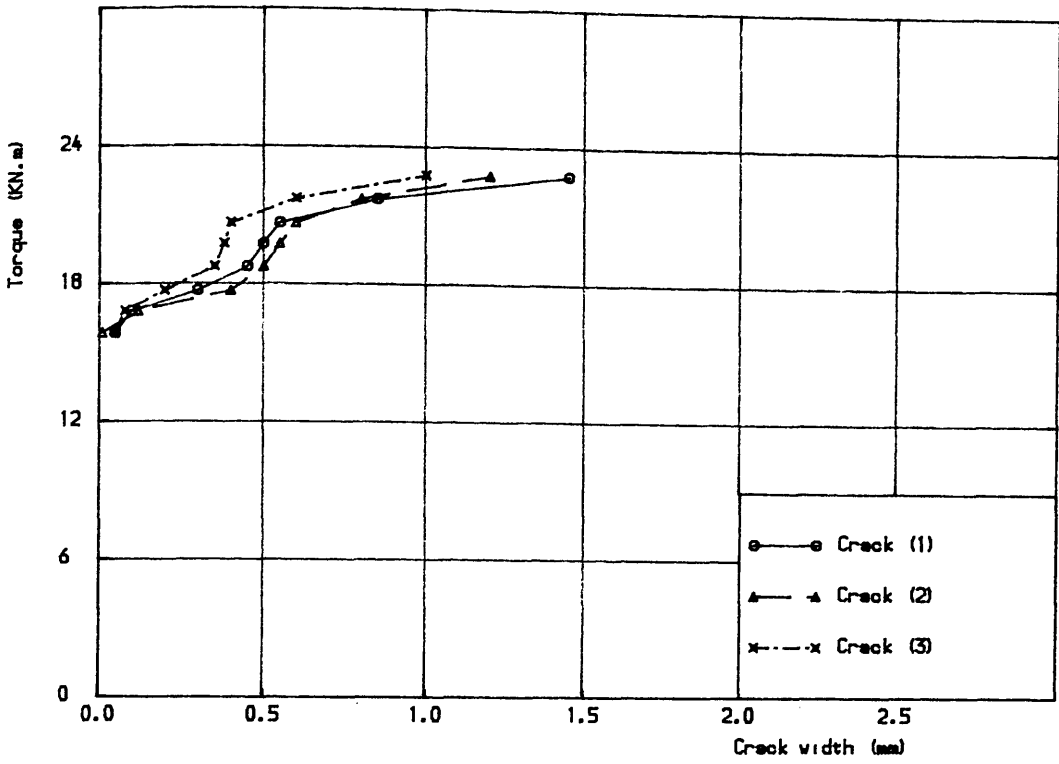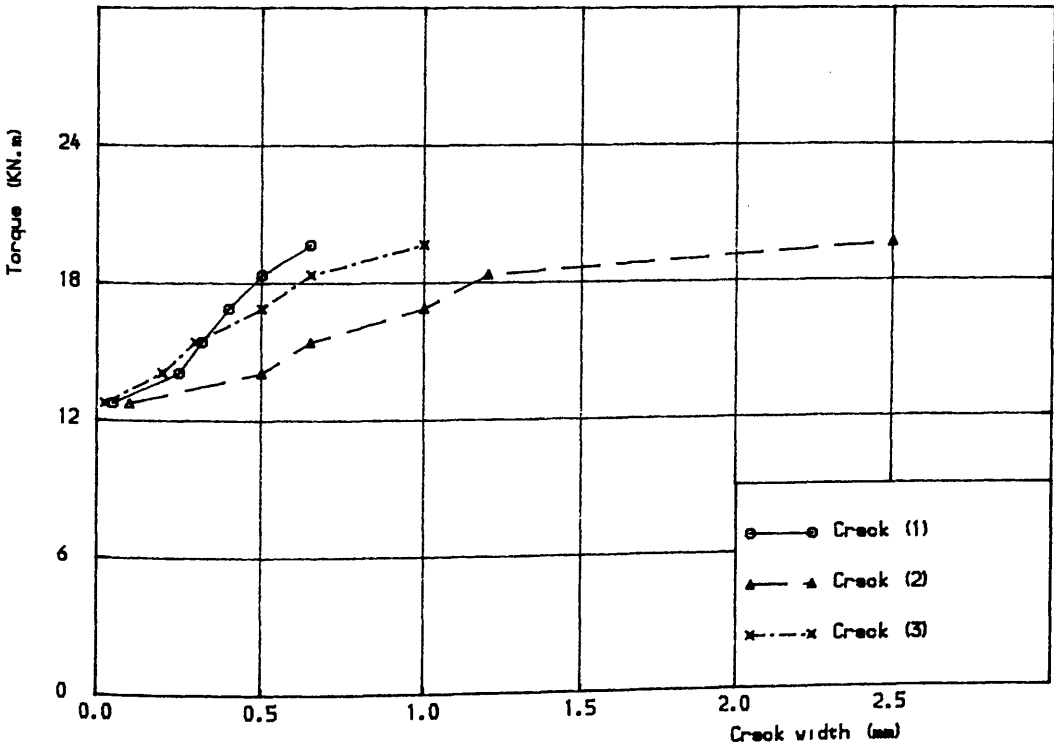Figure (7.20 d) Torque vs concrete surface compressive strains for specimen B34
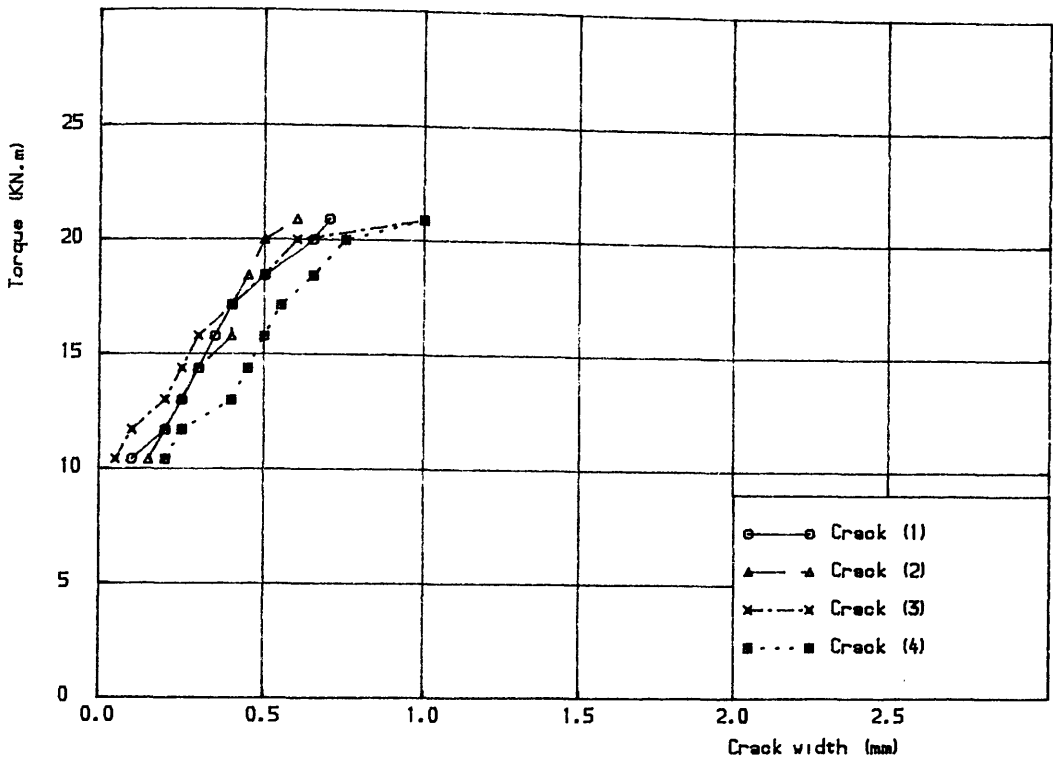
Figure (7.21 a) Torque vs crack width for specimen B31
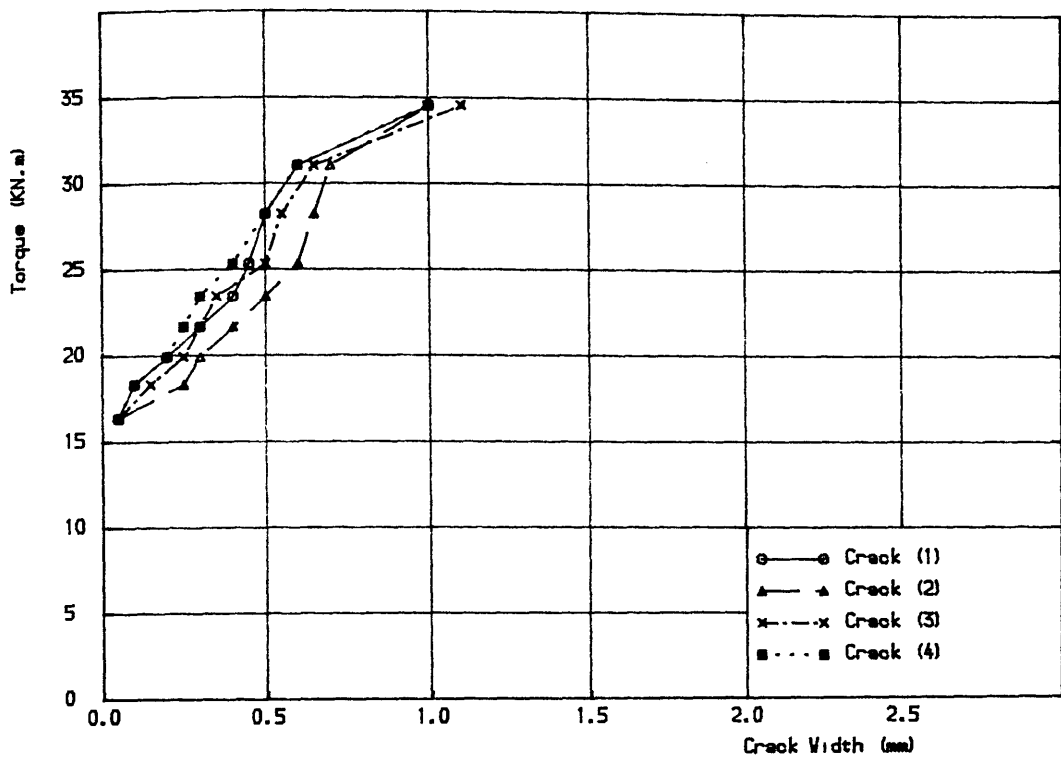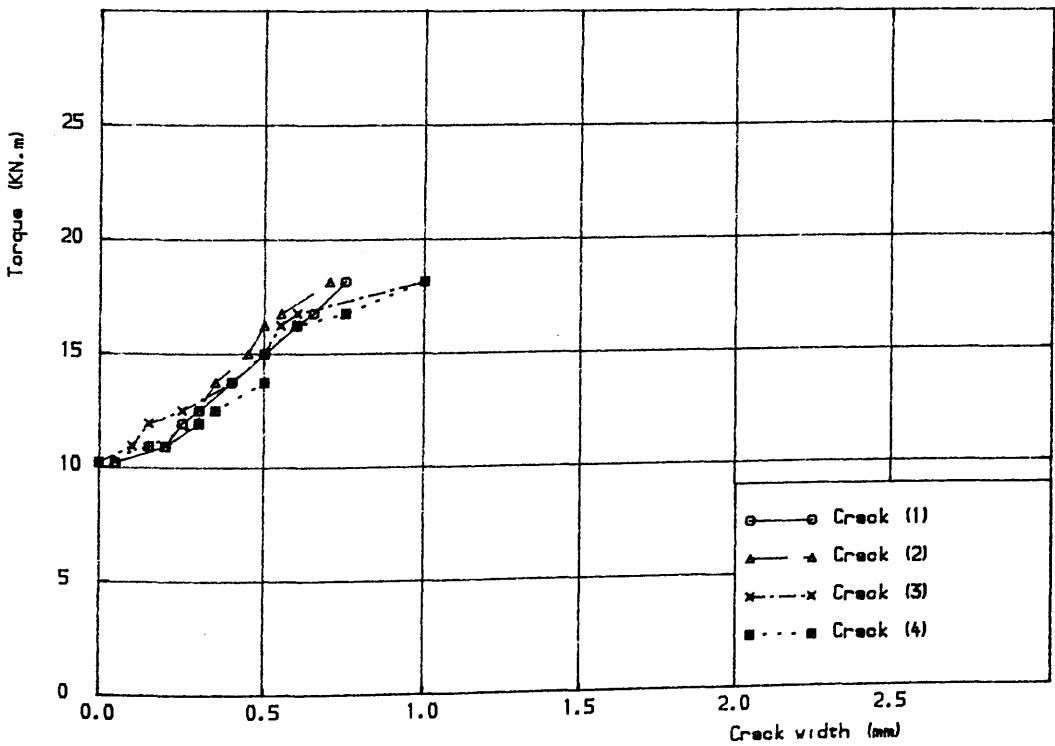

Figure (7.21 b) Torque vs crack width for specimen B32
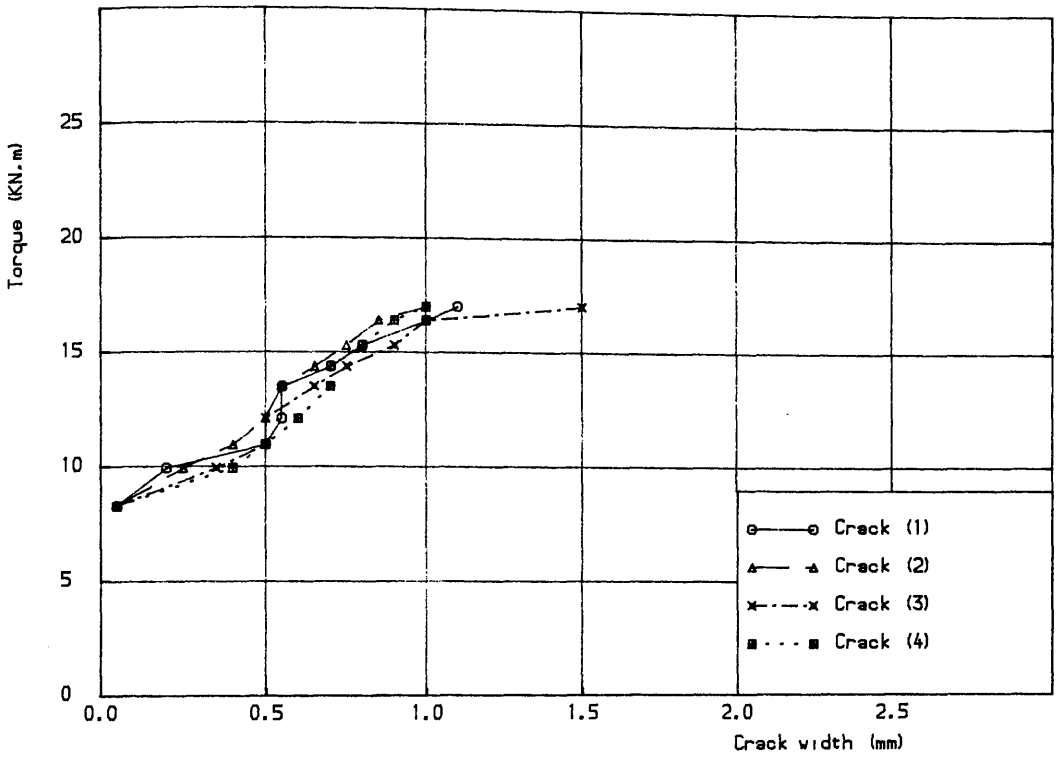
Figure (7.21 c) Torque vs crack width for specimen B33
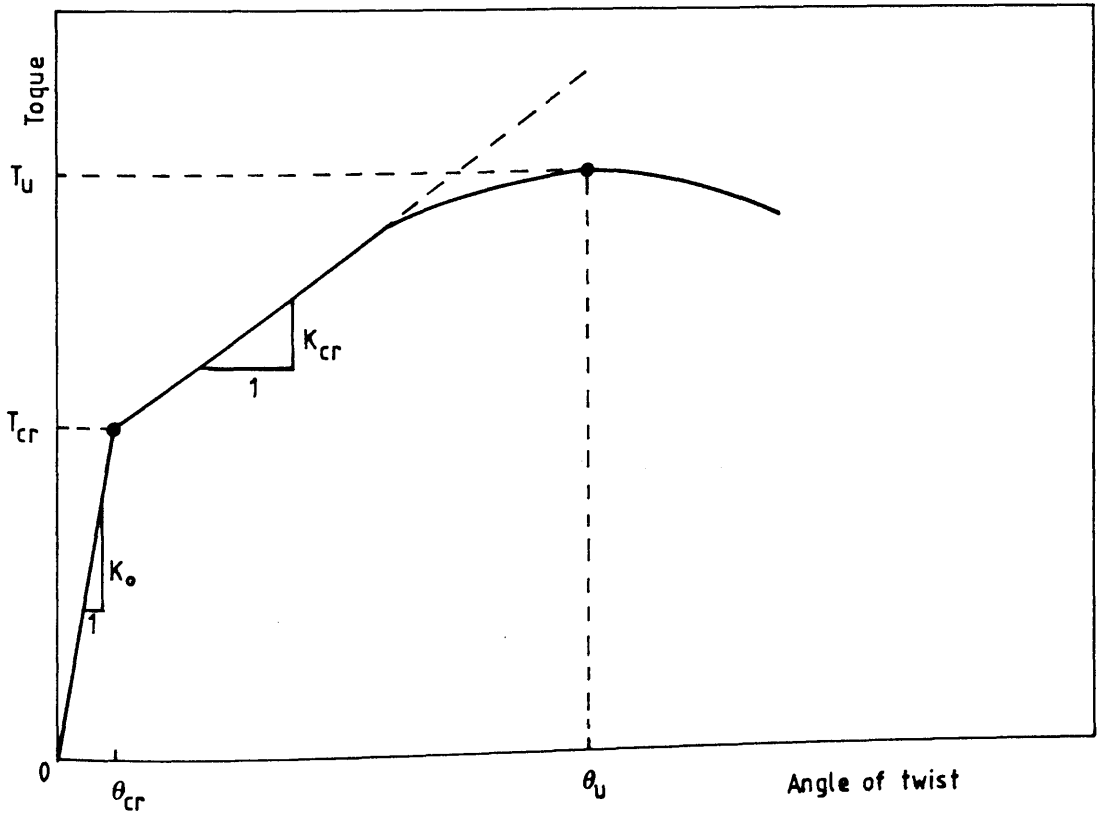
Figure (7.22) Idealised torque-twist curve for a typical
specimen
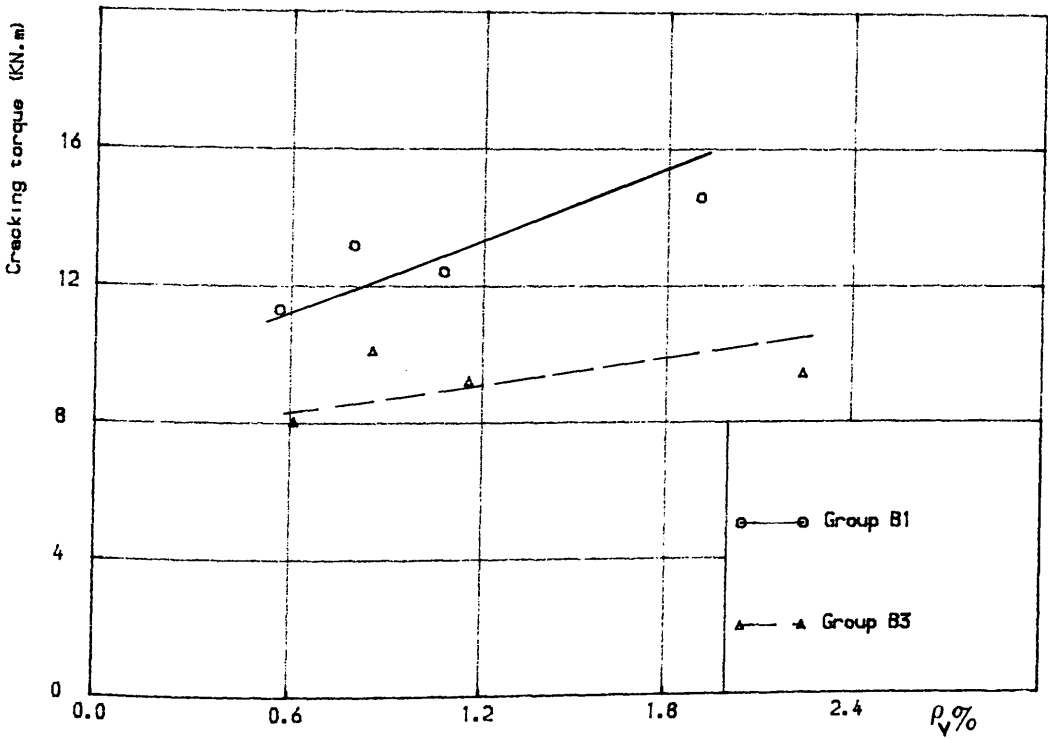
Figure (7.23) Cracking torque vs volume ratio of transverse reinforcement
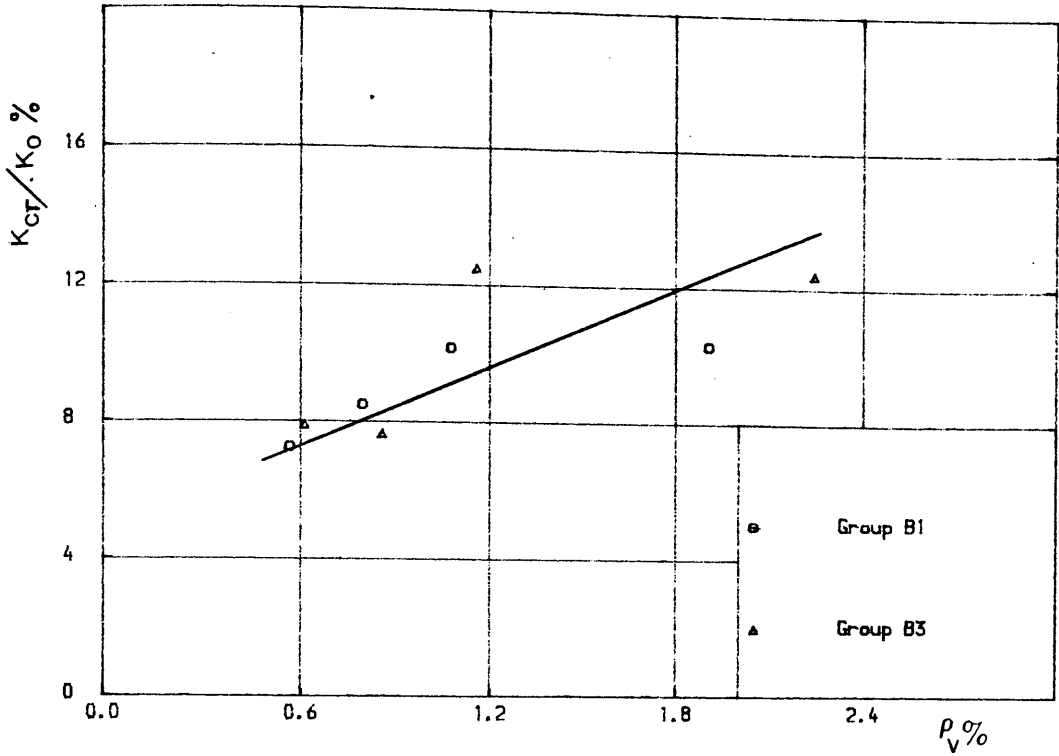
Figure (7.24) Ratio of post- to pre-cracking torsional stiffness vs
volume ratio of transverse reinforcement
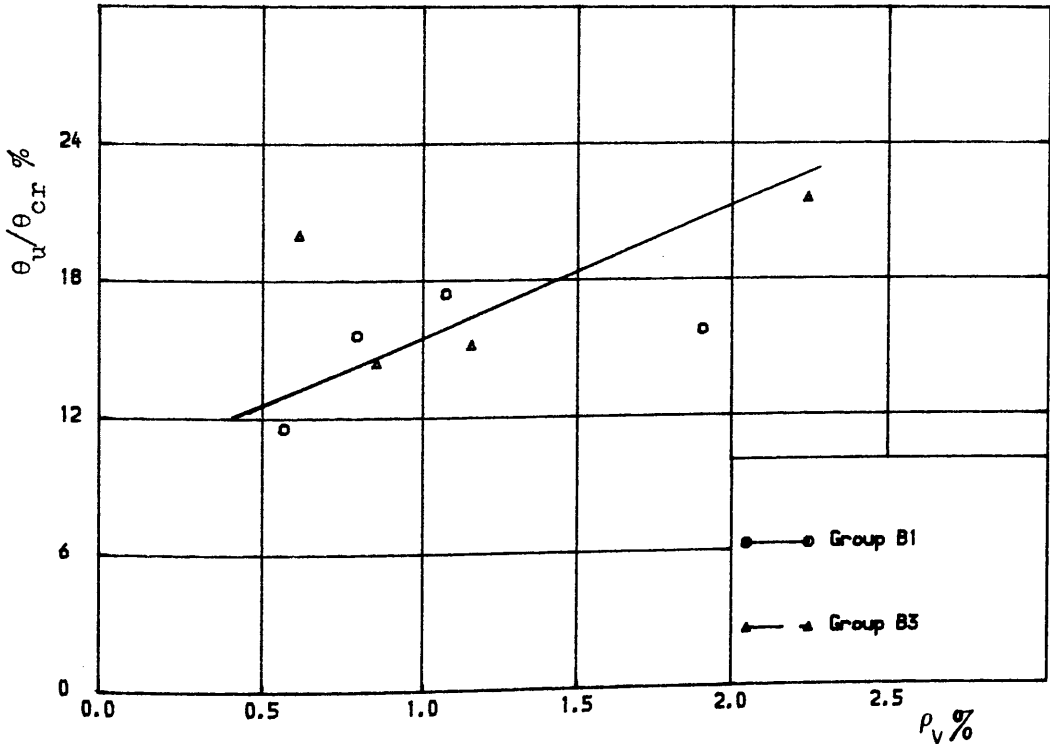
Figure (7.25) Ratio of angle of twist at failure to angle of twist at
cracking vs volume ratio of transverse reinforcement
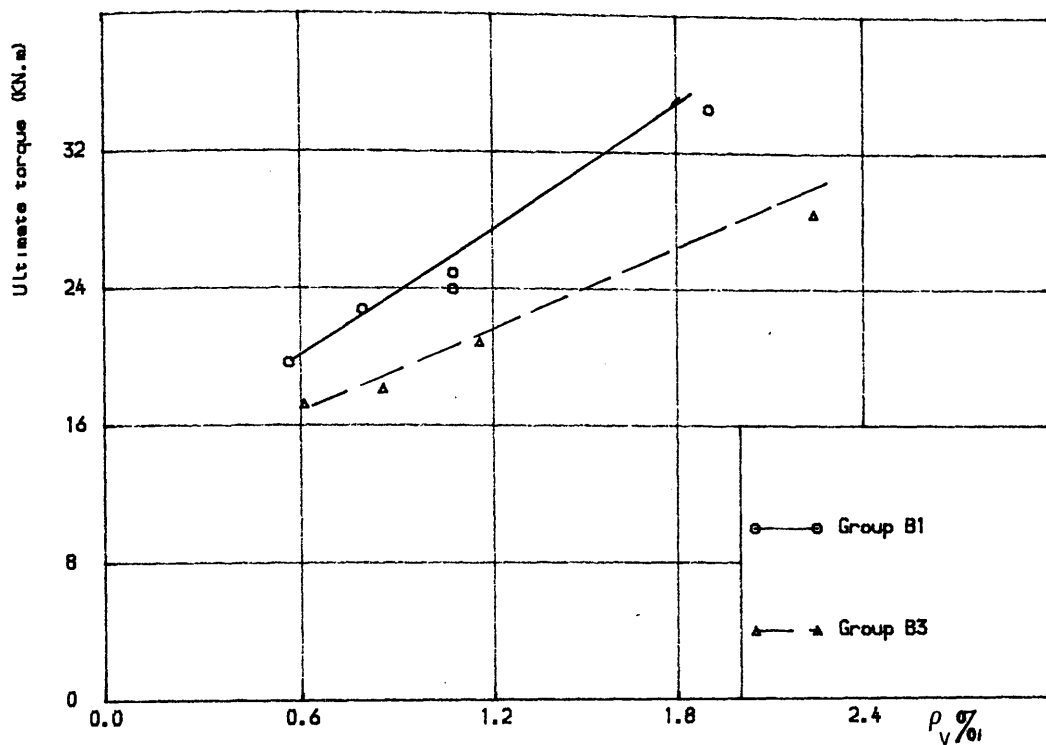
Figure (7.26) Ultimate torque vs volume ratio of transverse reinforcement
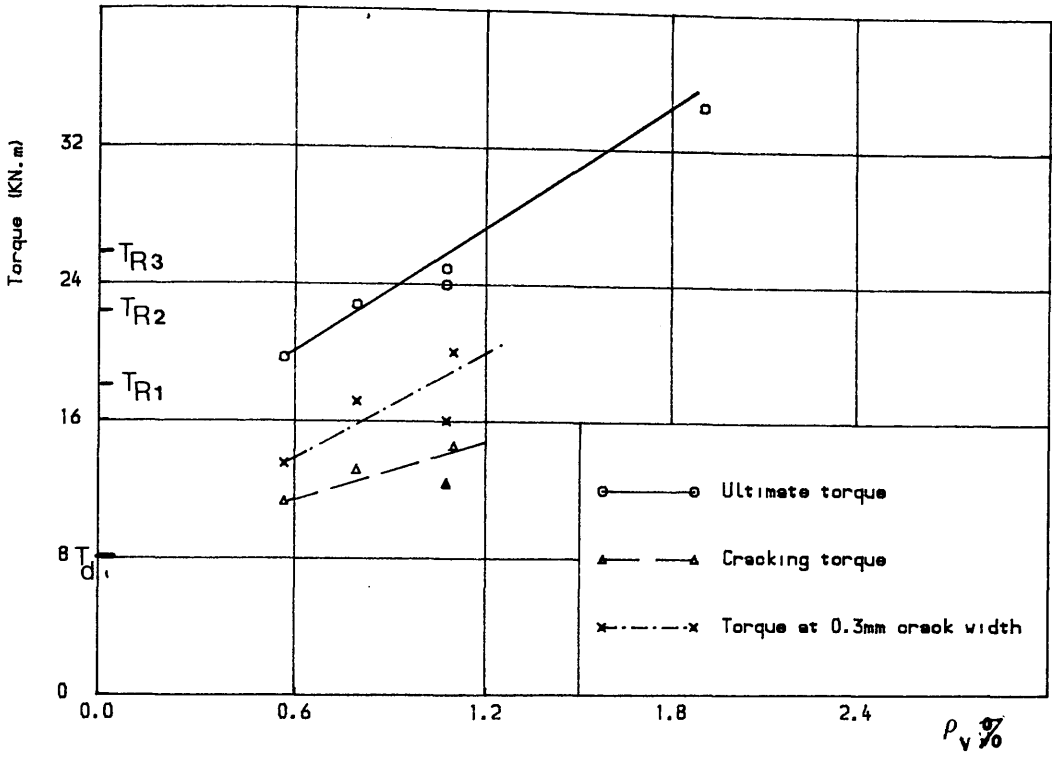
Figure (7.27 a) Comparison of various torques for group B1
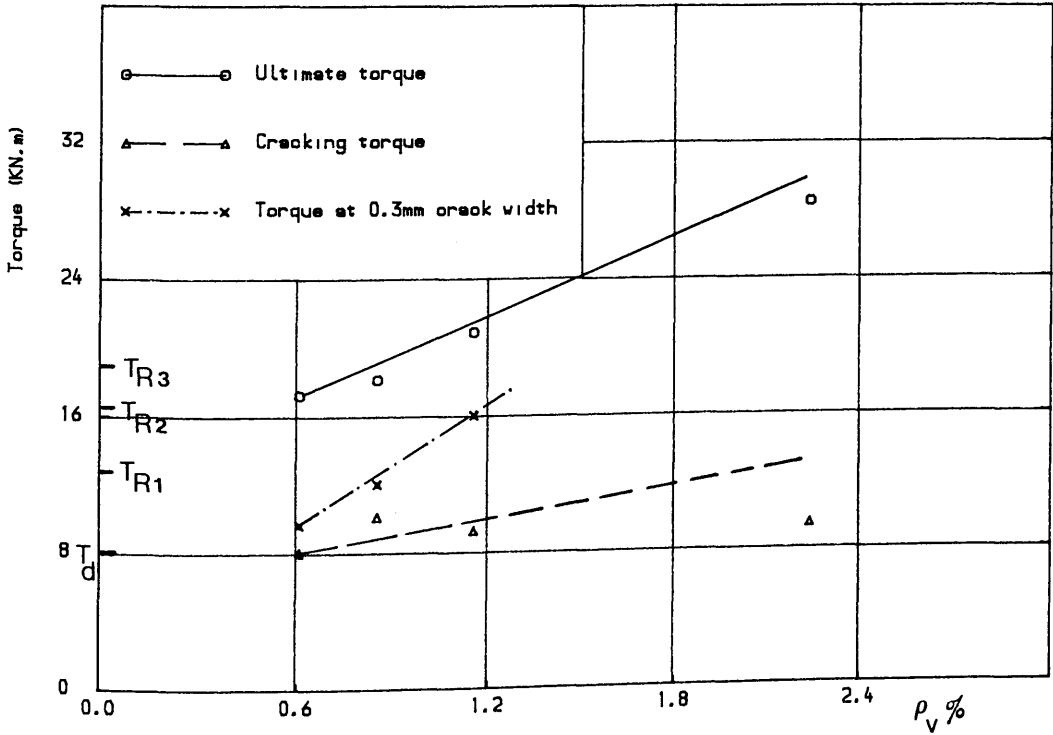
Figure (7.27 b) Comparison of various torques for group B2

References

(1 a) BS CP110 - 1972, "Code of Practice for the Structural Use of Concrete", Part 1, Design, Material and Workmanship, British Standard Institution, London, 1972.

(1 b) BS8110 - 1985, "British Standard Structural Use of Concrete", Part 2, Code of Practice for Special Circumstances, British Standard Instiution, 1985.

(2) Hsu, T.T.C., "Torsion of Structural Concrete - Behaviour of Reinforced Concrete Rectangular Members", ACI Special Publication, Torsion of Structural Concrete, SP18, 1968, pp. 261-306.

CHAPTER EIGHT

FINITE ELEMENT ANALYSIS OF THE TEST SPECIMENS

AND COMPARISON WITH EXPERIMENTAL RESULTS

8.1 Introduction

The aim of this chapter is to analyse all nine test specimens using the developed nonlinear finite element program. Comparisons of theoretical and experimental results are performed to demonstrate the applicability of the finite element model in the analysis of reinforced concrete L-sections subject to pure torsion. Use is made of the experience gained in Chapter Five for rectangular reinforced concrete beams under pure and combined torsion. Part of these results has already been reported (ref. 1), where good agreement between experimental and predicted results was shown for the cases studied. Table (8.3) lists all predicted ultimate torques and the values obtained experimentally. As already mentioned above, the predictions are quite satisfactory for all specimens except B14 and B34, for which the total volume reinforcement ratio (longitudinal steel ÷ stirrups) is highest in each respective group.

In Chapter Five it was shown that the shear retention parameters affect the torsional response of reinforced concrete. The values of $\beta_1 = 0.5$, $\beta_2 = 0.1$ and $\beta_3 \epsilon_t' = 0.003$ were found to suit the case of pure torsion and were therefore adopted in this case. It was also concluded in that chapter that tension stiffening results in stiff initial post-cracking response in the case of pure torsion and was recommended to be set inactive. The case here is again pure torsion and so the tension stiffening model was set inactive

for all analyses (i.e $\alpha_2 = 0.0$).

The analysis will focus on the following aspects of the torsional behaviour: (1) overall behaviour as reflected in the torque-twist curves, (2) steel response for both longitudinal bars and stirrups, (3) crack patterns and (4) failure modes.

Specimen B11 is analysed in detail, others will follow as they are similar. The following aspects of finite element analysis were studied using B11 before applying them to the rest of the specimens:

(1) Mesh study

(2) Effect of boundary conditions and load application

In all analyses a 3x3x3 Gauss integration rule is used. The element stiffnesses are recomputed at the beginning of each load increment. A maximum number of iterations of 15 was specified and the convergence tolerance was set at 10%. All reinforcing bars were embedded at their exact positions within the 20-noded isoparametric brick element used for concrete representation.

8.2 Finite Element Mesh Study

In Chapter Five it was shown that a 12-element mesh was adequate for the analysis of Hsu's rectangular beams under pure torsion and Collins et al. rectangular beams subjected to combined torsion and bending. The conclusion there was that it is essential to isolate a group of elements along the span to free them from the effects of both the load application and boundary conditions. While this conclusion is immediately employed here, further investigation on the

mesh size effect is undertaken because of the flanged nature of the sections.

Because of the skew-symmetry, one half of the specimen was considered for analysis. Three different meshes of 9, 12 and 32- elements, shown in Figure (8.1), were examined. They all had a group of isolated free elements between the boundary conditions at the centre line and the loaded nodes at the free end. The 9- and 12-element meshes are basically the same in the number of elements along the sides of the cross section but the number of isolated elements along the axis is different, being 3 and 6 for the two meshes respectively. The 32-element mesh differs from the other two in the further subdivision across the section. This was to allow more sampling points across the section to assess whether it is important to provide for this.

The total pure torque was applied as two equal couples (Figure 8.2), similar to the case of rectangular sections. Table (8.1) and Figure (8.3) shows the resulting angles of twist for the three meshes for an elastic torque of 2.7 KN.m. The results show slight increase of the angle of twist with the increase in the mesh size, as expected. The 32-element mesh produced 8.7% higher angle than the 12-element mesh and 11.4% higher angle than the 9-element mesh. The difference between the 12-element and 9-element meshes is only 2.5% increase. It was thus considered satisfactory to use the 12-element mesh for the full nonlinear analysis as this will produce analyses considerably cheaper than the 32-element mesh whilst still giving reasonable predictions. The reduced boundary conditions, discussed in the following

section, were employed in this investigation. The angles of twist were evaluated using the procedure of section (8.4)

8.3 Study of Boundary Conditions

The importance of proper modelling of boundary conditions, for torsion analysis with finite elements, has been discussed in Chapter Five. It was shown that a set of reduced boundary conditions, where 4-centre nodes are restrained to allow for proper warping behaviour to take place, is the most suitable. To check this point further for L-sections, two sets of boundary conditions, designated case 1 and case 2 as shown in Figure (8.4), were examined. The same elastic torque of 2.7 KN.m was applied to both cases using the 12-element mesh. The torque is applied as two equal couples.

Table (8.2) and Figure (8.5) shows the results of this part. The full fixity produced a 9.7% lesser angle of twist than the reduced fixity. This indicates the stiffer response when full fixity at the centre line is used and confirms the earlier finding on rectangular sections. Therefore, and similar to the case of rectangular sections, the reduced set of boundary conditions is chosen as it allows proper warping of the cross section to take place.

8.4 Evaluation of Angles of Twist from Lateral Displacements

The approach followed here is similar to that adopted for the evaluation of the angles of twist from the experimental lateral displacements as reported in Chapter Six. The lateral nodal displacements were used for this purpose as shown in Figure (8.6). For simplicity of mathematical

handling it was assumed that the edges of the cross section remain straight after twisting. This allows the following set of equations to be derived (refer to Figure 8.6) using similarity of triangles:

$$x_1 = \frac{D_1 S_1}{(D_1 + D_2)} \tag{8.1}$$

$$\theta_1 = \frac{1}{S_3} \tan^{-1} \left(\frac{D_1}{x_1} \right) \tag{8.2}$$

$$x_2 = \frac{D_3 S_2}{(D_3 + D_4)} \tag{8.3}$$

$$\theta_2 = \frac{1}{S_3} \tan^{-1} \left(\frac{D_3}{x_2} \right) \tag{8.4}$$

$$\theta_A = \frac{(\theta_1 + \theta_2)}{2} \tag{8.5}$$

where θ_1 = angle of twist per unit length obtained from the shorter side of the cross section

θ_2 = angle of twist per unit length obtained from the longer side of the cross section

θ_A = average angle of twist

S_1, S_2 = dimensions of shorter and longer sides of the cross section

S_3 = length over which the twist angle is to be computed

x_1, x_2 = dimensions along the shorter and longer sides shown in Figure (8.6)

D_1, D_2, D_3, D_4 = the relevant nodal displacements obtained from the finite element analysis

This procedure is considered adequate for the following two reasons: (1) it is fairly similar to that used for the evaluation of the experimental twist, therefore the comparsions are straightforward and (2) with the adopted load application it produced acceptably close twist as obtained from shorter and longer sides, the difference being about 11% maximum for elastic analysis as shown in Table (8.1).

8.5 Comparison of Theoretical and Experimental Results

In the following analyses the prediction of the overall behaviour, i.e. torque-twist curves, cracking and ultimate torques, pre- and post-cracking torsional stiffnesses will be assessed first. Local behaviour, such as steel strains at the sampling points, will be considered second to that as it proved difficult to obtain good predictions for all aspects of the behaviour using the same set of material/solution parameters.

Figure (8.7) shows torque-twist curves for specimen B11. Examination of the figure reveals that the torque-twist behaviour is well predicted. Indeed the early linear parts of the experimental and the predicted curves are practically identical. This confirms the earlier findings regarding the boundary conditions. It also provides satisfaction over the material modelling (i.e. the concrete stress-strain laws in particular) as the material properties experimentally obtained were all used for the finite element analysis. After cracking, the post-cracking torsional stiffness is predicted with reasonable accuracy, despite the fact that the predicted curves give slightly higher values of twist

than the experimental curve for the same applied torque. This difference is considered insignificant because of the difficulties and scatter associated with reinforced concrete behaviour. This deviation is mainly because of the earlier cracking in the theoretical curve. The ultimate torque is well predicted, the ratio of predicted to experimental torque being 1.035. Therefore, the overall assessment of the finite element model seems reasonable.

Steel strain predictions are examined for both longitudinal and transverse reinforcement, both of which were placed exactly at their locations as in the experiments. Figure (8.8) shows comparison of steel strains for longitudinal steel while Figure (8.9) shows that for a closed stirrup for specimen B11. Again overall reasonable agreement can be seen, as neither the longitudinal steel nor the stirrups recorded any significant strains prior to concrete cracking. After cracking, there is a considerable increase in the recorded experimental strains and this is well predicted. However, the two figures indicate that the predictions vary between remarkable to fairly acceptable.

The simulation of steel reinforcement by single embedded bars has shown its importance very evidently in torsional applications. This is because in torsion of reinforced concrete both the longitudinal bars and stirrups have a major role after concrete cracking and indeed they act as individual bars in a sort of framework, therefore their position within the concrete is of particular importance.

Crack propagation and final crack pattern is shown in Figure (8.10) for specimen B11. The quick propagation of torsional

crcaking is clear and the predictions are in reasonable agreement with the experimental behaviour described in Chapter Seven.

The process of steel yielding of a typical stirrup and concrete crushing for specimen B11 is shown in Figure (8.11). Yielding started at the top of the flange near the junction and propagated first towards the free end and later inwards, indicating the greater bending of the flange. At ultimate conditions further yielding occured within the web and both flange and web crushed. This tend to indicate that although crushing was the eventual cause of fialure, it has been essentailly initiated by yielding of the stirrups for this particular specimen. However, this may not be the case for all specimens.

The above results show the adequacy of the boundary conditions, load application and the material parameters, namely the shear retention and tension stiffening parameters, for the case in consideration. Hence these values will be used for the analysis of all subsequent specimens.

Figure (8.12) shows torque-twist curves for specimens B11, B12, B13 and B14. Fairly acceptable predictions are evident for the first three specimens. Both the post-cracking stiffnesses and the ultimate torques were reasonably predicted. However, for specimen B14, the one with the highest torsional reinforcement, the ultimate torque is overestimated by about 13.2%. The volume ratio of stirrups for this specimen is 1.96% and the total volume ratio of steel is 2.83%. It is thought that this increased amount of

stirrup reinforcement is the reason behind the model not being able to predict the behaviour well, due to bond deterioration. In the experiment, a lot of bond is lost due to progressive torsional cracking at later stages of loading and as the ultimate load is approached. In the finite element model, however, full bond is assumed between concrete and steel. This observation is important when applying the developed finite element for torsion analysis of members with high volume ratios of reinforcement.

Figures (8.13) through (8.18) show the comparisons of the predicted and experimental steel strains for specimens B12, B13 and B14. Reasonable predictions are obtained but of a lesser accuracy than the torque-twist curves. The variation of the amount of stirrups did not affect the pre-cracking behaviour of steel as no strains were recorded in any of the specimens as also occured in the experiments. This is taken as a critical assessment of the model's behaviour for torsion analysis because it is a distinguishing characteristic of torsion behaviour of reinforced concrete members. It is also taken as a good sign of the reasonable behaviour of the embedded bars for simulation of steel reinforcement developed in the finite element model.

Model B21 had the same cross section and reinforcement as B11. The only difference being that the stirrups were 6mm diameter at 50 mm spacing for B11 and 8mm diameter at 90mm spacing for B21. The experiments showed that this difference affected only the crack width and spacing but not the ultimate torque, this increased by only 3.9%.

Figure (8.19) shows comparison of torque-twist curves for

specimens B11 and B12. The finite element model seem to predict the post-cracking behaviour of B11 better than B21, although the ultimate load predictions for both specimens are good. For B21 the post-cracking part of the theoretical curve shows a larger rotation than the experimental curve for the same applied torque. It is interesting, however, to notice that the two theoretical curves are more closer to each other than the two experimental curves, a reflection perhaps of how reinforced concrete is a rather far from perfect material.

Comparisons of steel strains for specimen B21 are shown in Figures (8.20) and (8.21). Strain gauge (6) on the longitudinal steel (Figure 8.20) shows strange response as it recorded very high strains soon after cracking. It is suspected that this was because the strain gauge itself was damaged or affected by friction against another steel bar and so the results can be discarded. Otherwise the predictions fall within acceptable limits and confirm the earlier observations.

Figure (8.22) shows comparison of the torque-twist curves obtained for specimens B31, B32, B33 and B34. As can be seen, the behaviour of the first three specimens was predicted within acceptable accuracy similar to the first three specimens of the previous group. The predicted behaviour of B34, however, shows an overestimation of about 14% of the ultimate torque for the adopted material and solution parameters. Similar to specimen B14 of group B1, this is attributed to bond effects not being catered for in the finite element model as full bond is assumed between

concrete and steel. This overestimation occured despite the reasonable prediction of the post-cracking torsional stiffness which tend to support the previous reasoning regarding the bond-slip behaviour at the late stages of loading. The specimen contained an amount of reinforcement higher than B14, being 3.5% for the total steel and 2.24% for stirrups per volume. Comparisons of the predicted and experimental steel strains are shown in Figures (8.23) through (8.30) where fairly reasonable agreements can be seen.

A reasonable conclusion on the behaviour of the finite element program in the analysis of specimens B14 and B34 would be that proper modelling of bond seem to be required if the program is to be used for such high reinforcement ratio. No attempt was made to vary the shear retention parameters to get closer prediction of the ultimate torque for these two specimens in favour of offering general conclusions as to the recommended values for the shear retention parameters. However, reduced values of shear retention parameters and/or convergence tolerance would result in better predictions. This needs further analyses in which these parameters are systematically varied to establish the proper combination to suit the case of high reinforcement ratios.

8.6 Conclusions

The following conclusions can be drawn from the analytical study:

(1) The results indicate the applicability of the developed nonlinear finite element model in analysing the more

complicated case of pure torsion of solid reinforced L-sections. The basic characteristics of the behaviour, namely the pre-cracking torsional stiffness, cracking torque, post-cracking torsional stiffness, ultimate torque and steel response were all predicted with reasonable accuracy for the majority of the specimens analysed. All these results were obtained using the same material and solution parameters.

(2) The results demonstrate that all conclusions and guidelines drawn from the parts dealing with torsional behaviour of rectangular sections, in Chapter Five, are also applicable to the more complicated situation of solid L-sections. These concern the boundary conditions, material parameters in particular the shear retention and tension stiffening effects and mesh selection schemes. Reduced boundary conditions suit the case of pure torsion to allow proper warping to take place. Tension stiffening must be set inactive (α_2 = 0.0), and the following values of shear retention parameters are recommended: $\beta_1 = 0.5$, $\beta_2 = 0.1$ and $\beta_3 \epsilon'_t$ = 0.003. The finite element mesh to be used needs to have sufficient number of elements, along the span, isolated from the effects of both boundary conditions and load application.

(3) A major observation is that for high reinforcement ratios, say about 2.5% for the total amount of steel (longitudinal + transverse steel) per volume, the finite element model tend to overestimate the ultimate torque despite the reasonable predictions otherwise. This is attributed to the unsuitability of the full bond assumption used in the finite element model. With high steel ratios the

behaviour seems to be more sensitive to the bond-slip phenomenon which did not affect the analysis of all sections with steel ratios lower than 2.5%. This point needs further investigation both experimentally and with finite element analysis. With the present finite element model lower values of the shear retention parameters than those given in (3) above may be used to reduce the degree of overestimation. It may also be required to modify the program to provide better simulation of bond-slip behaviour. The modification can be achieved by incorporating a bond-slip law to substitute the assumption of full bond used to derive the governing equations for steel simulation presented in Chapter Three.

(4) The predicted steel response indicate the importance of the proper simulation of reinforcing steel, achieved here through embedded bars placed at their exact positions as they appear in the structure.

(5) Finally, it is concluded that the finite element program is adequate for use in parametric studies where actual physical testing can be substituted by numerical studies, provided clear guidelines are set and more importantly the effects of the important solution and material parameters are already established through comparisons of experimental and predicted results as has been done in this chapter.
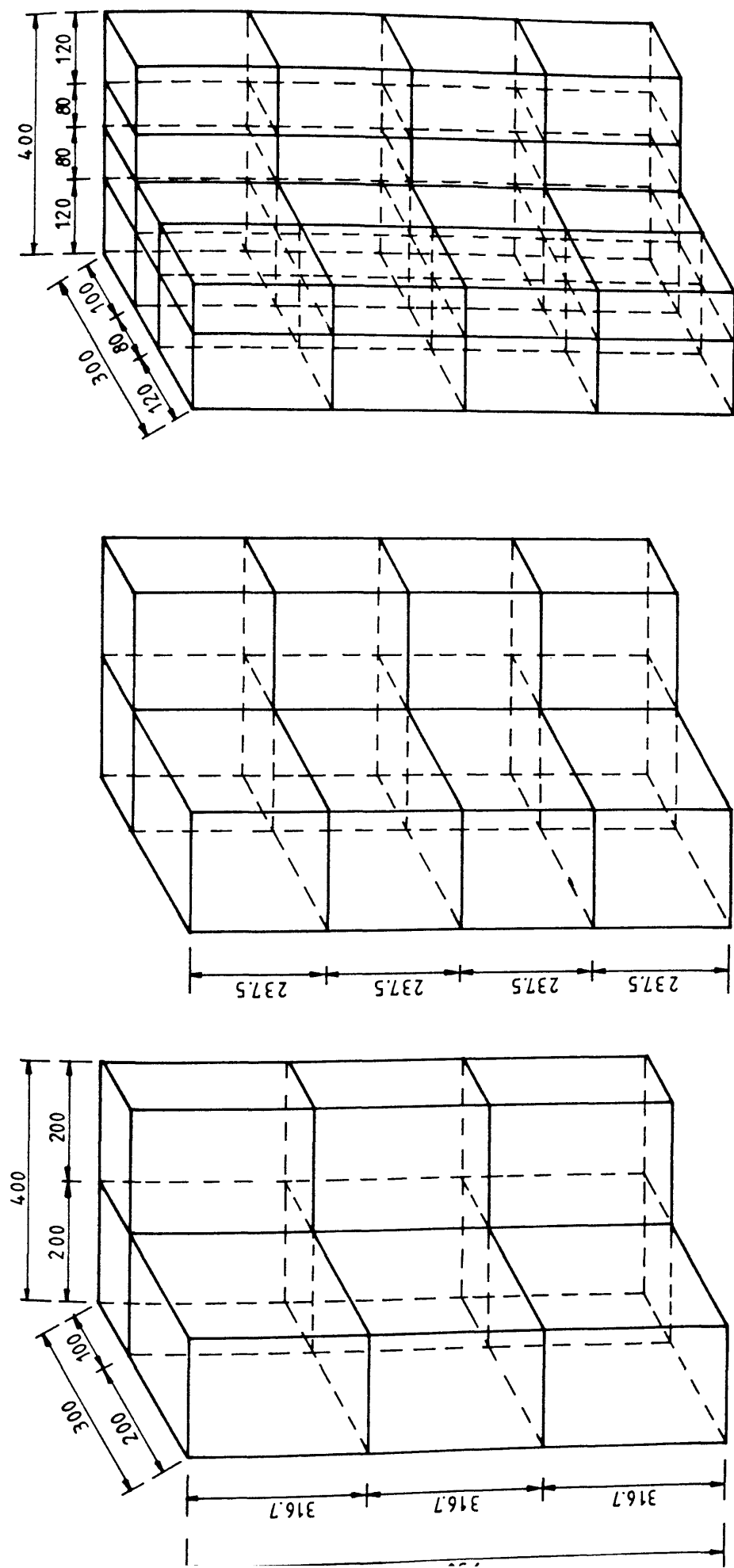
Figure (8.1) Different finite element meshes examined
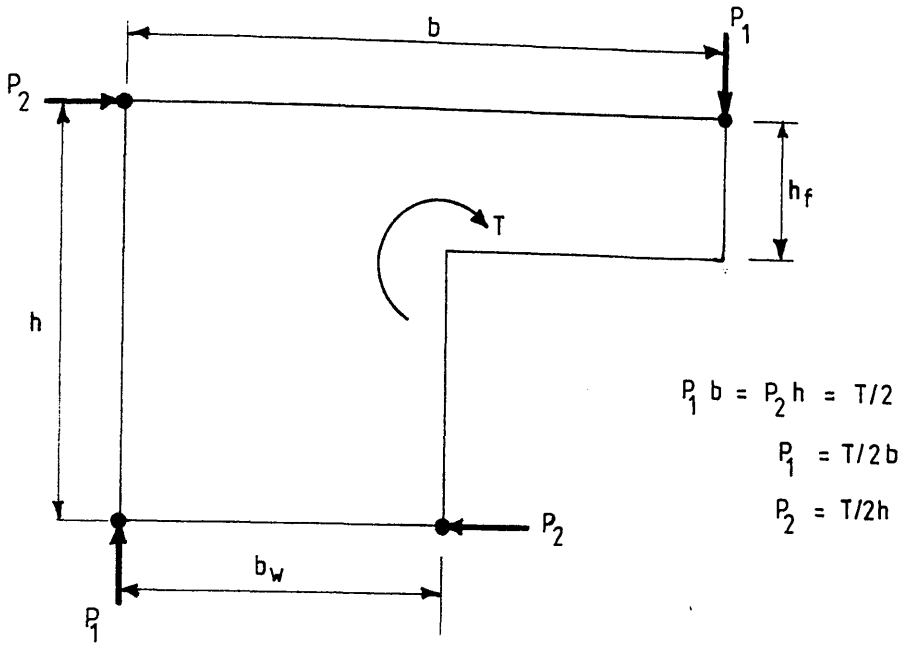
Figure (8.2) Load application to produce the required pure torque

$$P_1 b = P_2 h = T/2$$

$$P_1 = T/2b$$

$$P_2 = T/2h$$
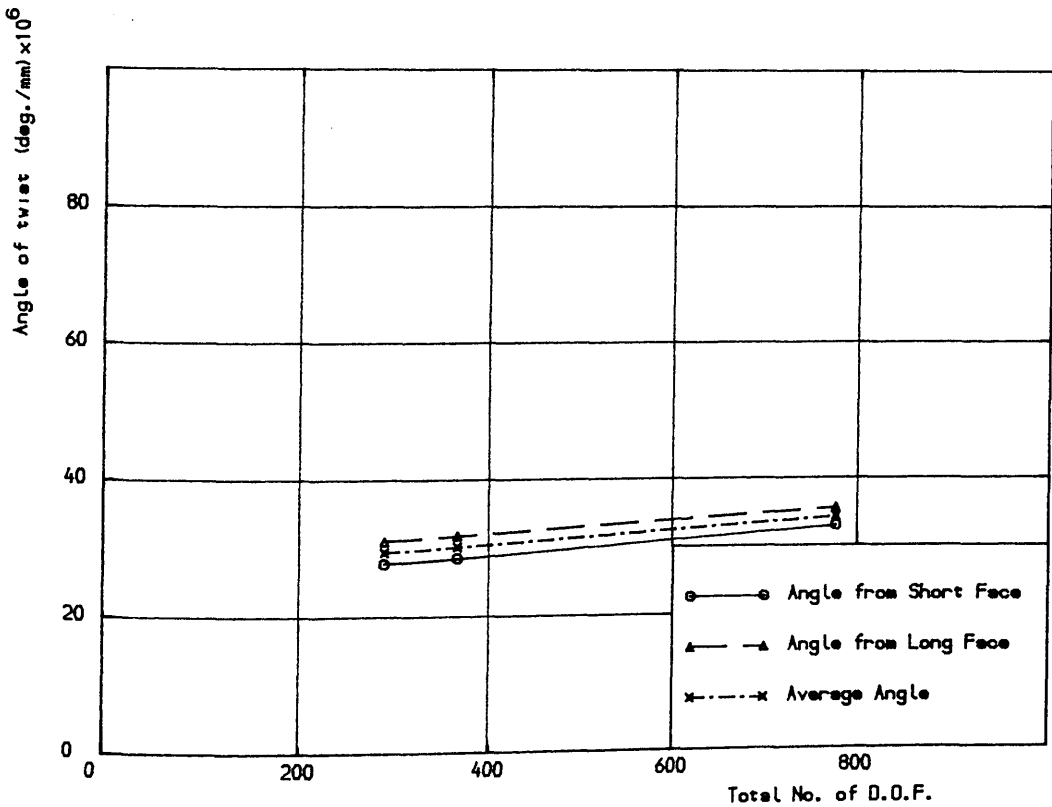
Figure (8.3) Mesh convergence study for model B11

Case (1)

Case (2)

• Fixed node
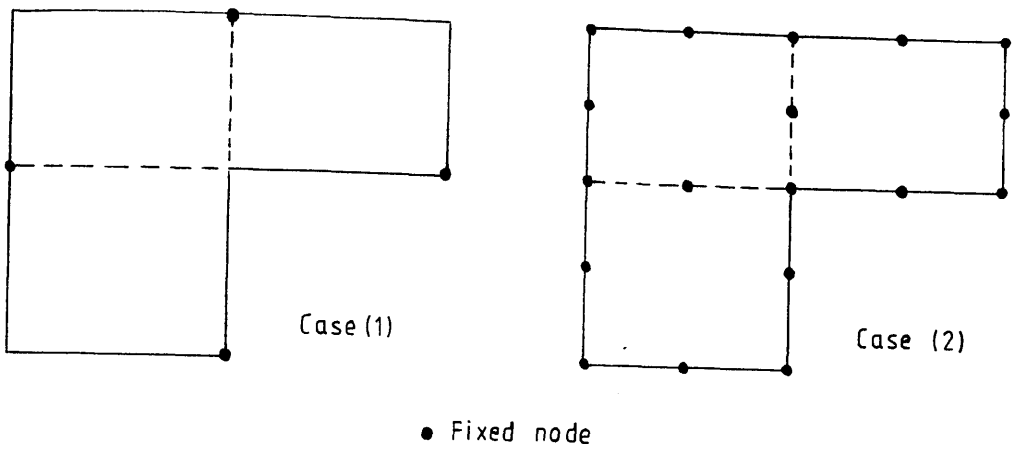
Figure (8.4) Different boundary conditions studied
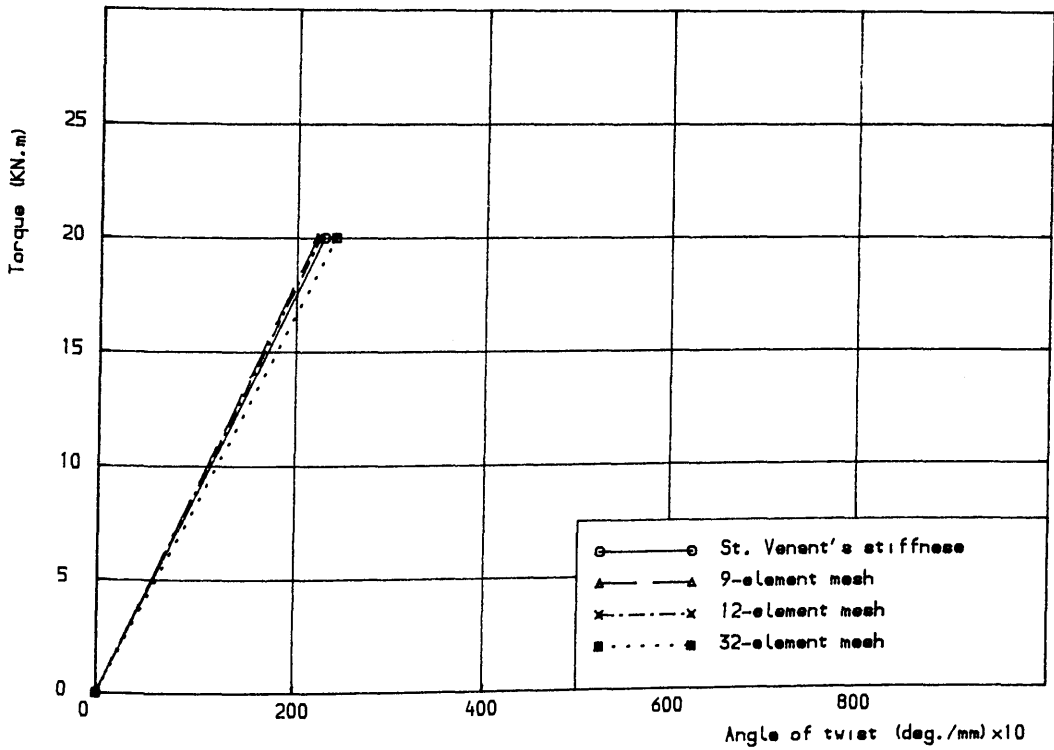
Figure (8.5) Comparison of elastic stiffnesses for specimen B11

Table (8.1) Effect of mesh size on the angles of twist

for L-sections. Applied elastic torque =

2.7 KN.m, boundary conditions case 1.

No. of elements	D_1 mm	D_2 mm	D_3 mm	D_4 mm	θ_1	θ_2	%DIF
9	0.0991	0.0390	0.0352	0.1708	27.753	31.653	10.63
12	0.1003	0.0414	0.0352	0.1758	28.479	31.819	10.50
32	0.1182	0.0458	0.0426	0.1964	31.964	33.579	7.35

θ_1 and θ_2 in deg./mm x 10^6

Table (8.2) Effect of boundary conditions on the angle of

twist for L-sections, 12-element mesh

Boundary conditions	D_1 mm	D_2 mm	D_3 mm	D_4 mm	θ_1	θ_2	%DIF
Case 1	0.1003	0.0414	0.0352	0.1758	28.479	31.819	10.50
Case 2	0.0787	0.0497	0.0425	0.1509	25.817	29.156	11.25

θ_1 and θ_2 in deg./mm x 10^6
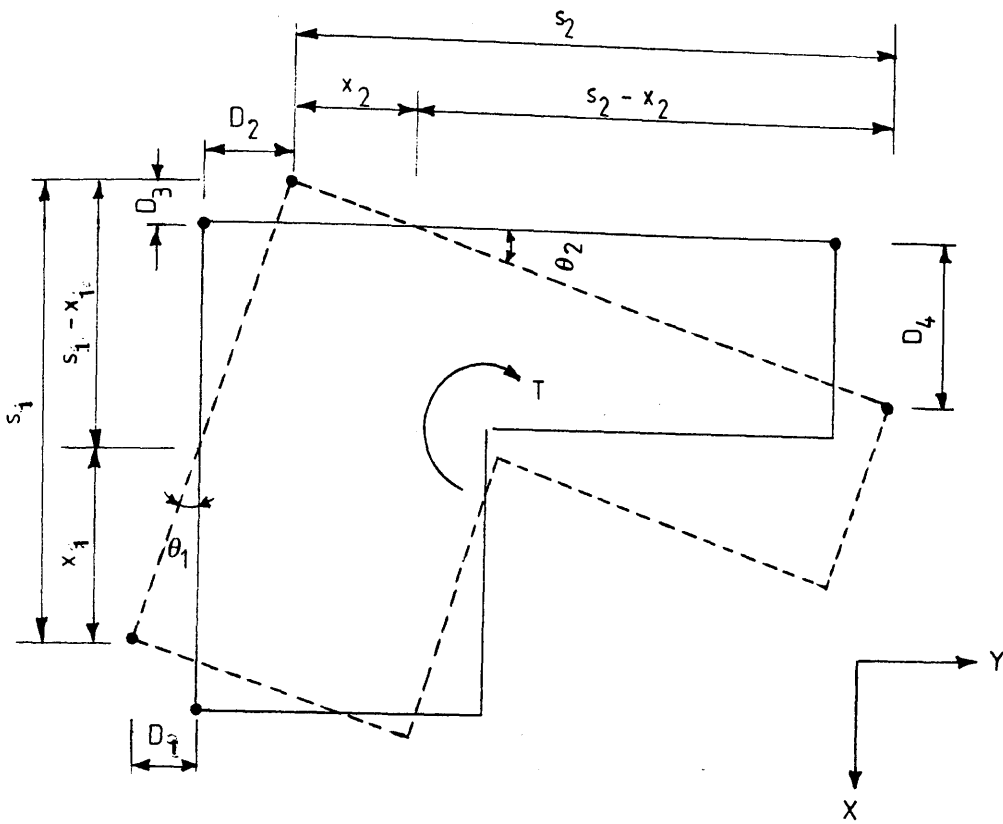
Figure (8.6) Evaluation of angles of twist from lateral nodal
displacements
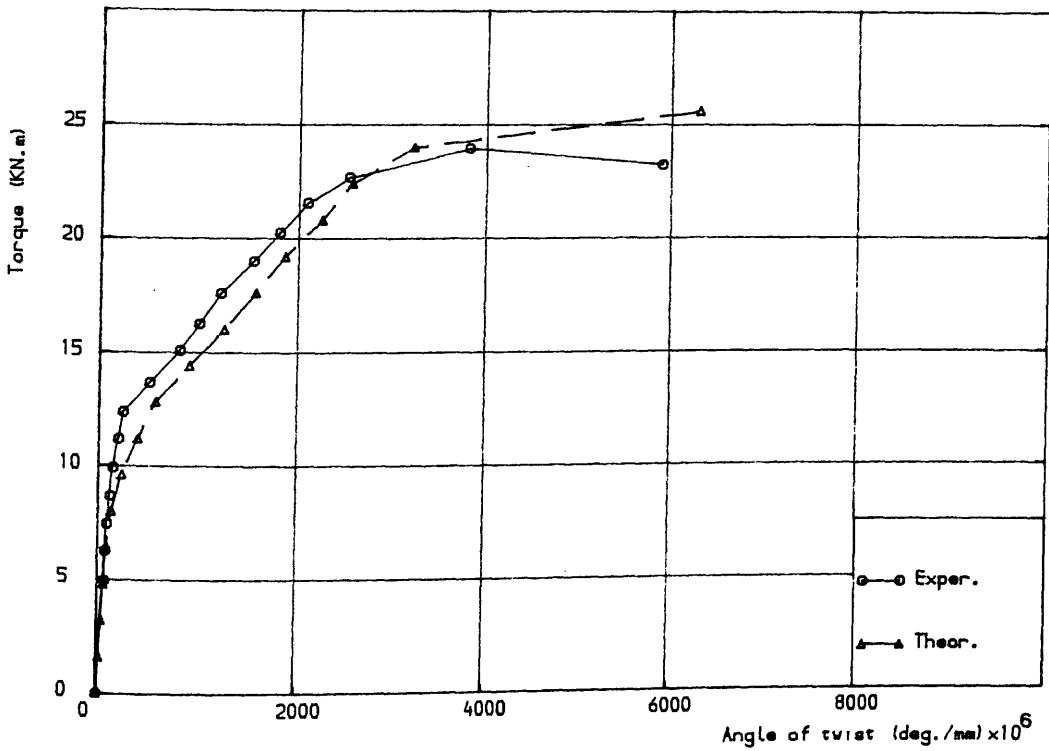
Figure (8.7) Torque-twist curves for model B11, 12-element mesh, Toler=10%
$0.5 > \beta > 0.1$, $\beta_3 \varepsilon_t' = 0.003$, NTS
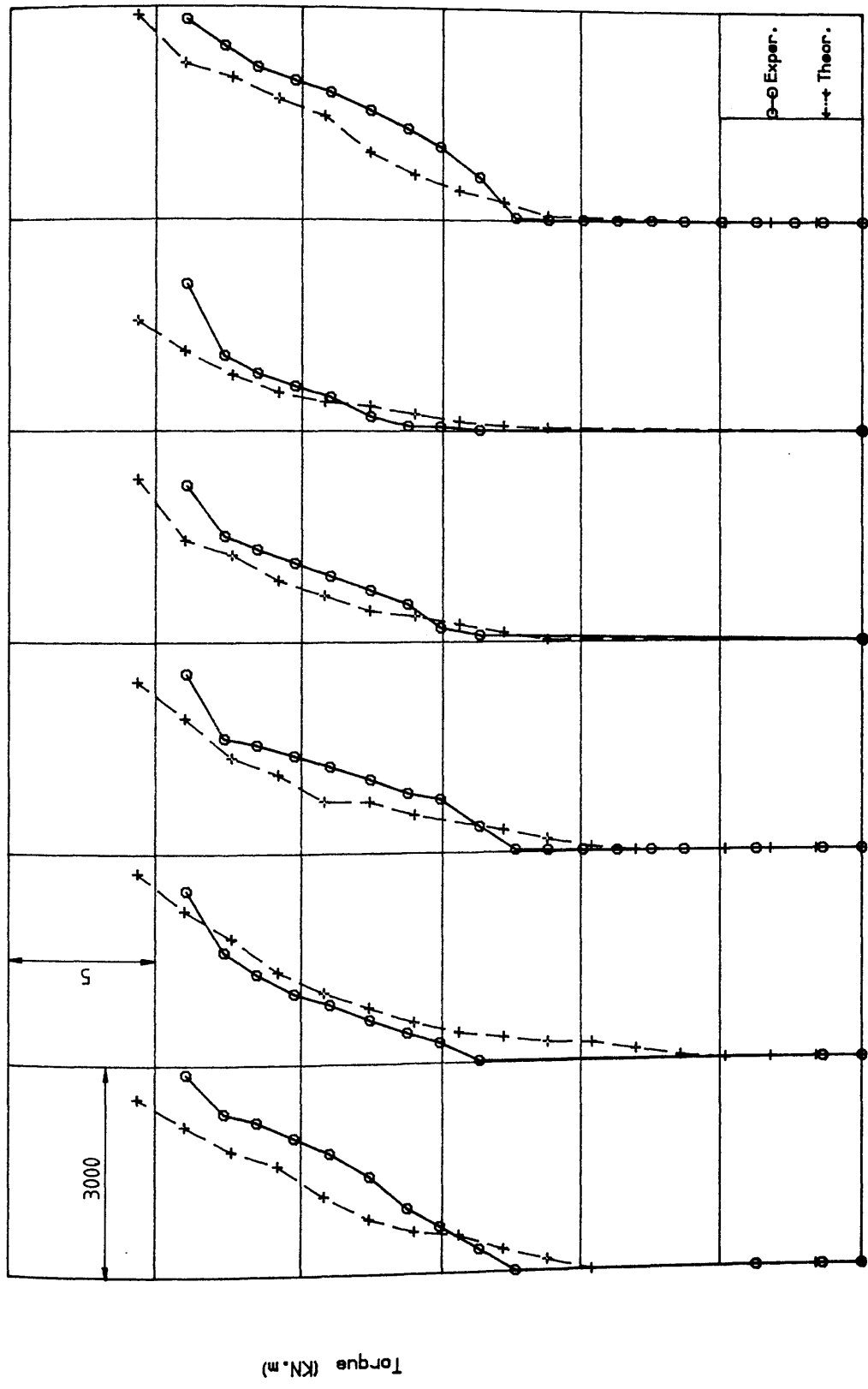
Figure (8.8) Comparison of longitudinal steel strain for model (B11)
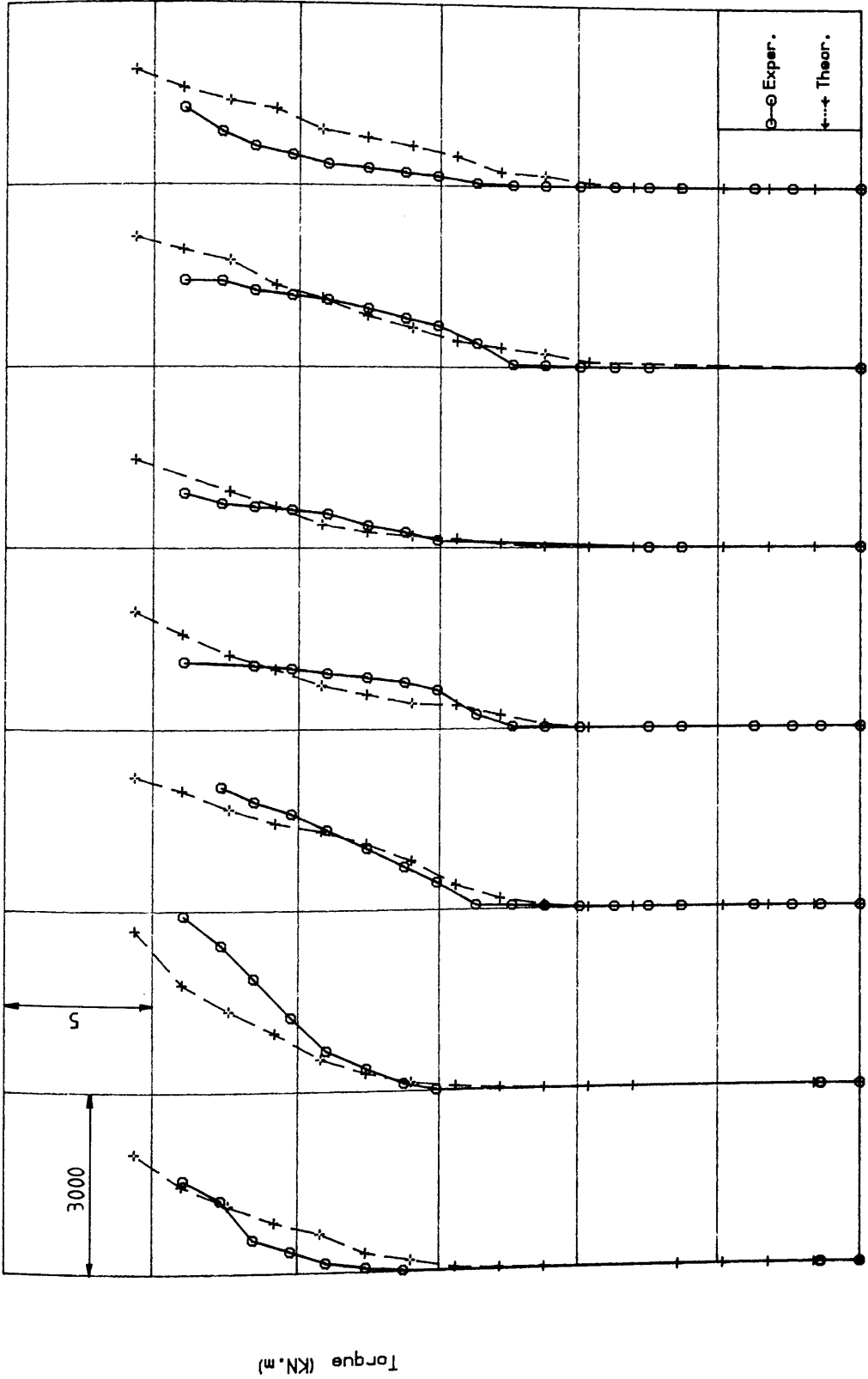
Figure (8.9) Comparison of top stirrup strain for model B11

Strain × 10^6

Torque (KN.m)

Face(1)   Face(2)   Face(3)   Face(4)

T = 5.4 KNm = 0.23 T$_u$

Face(1)   Face(2)   Face(3)   Face(4)

T = 13.5 KNm = 0.56 T$_u$
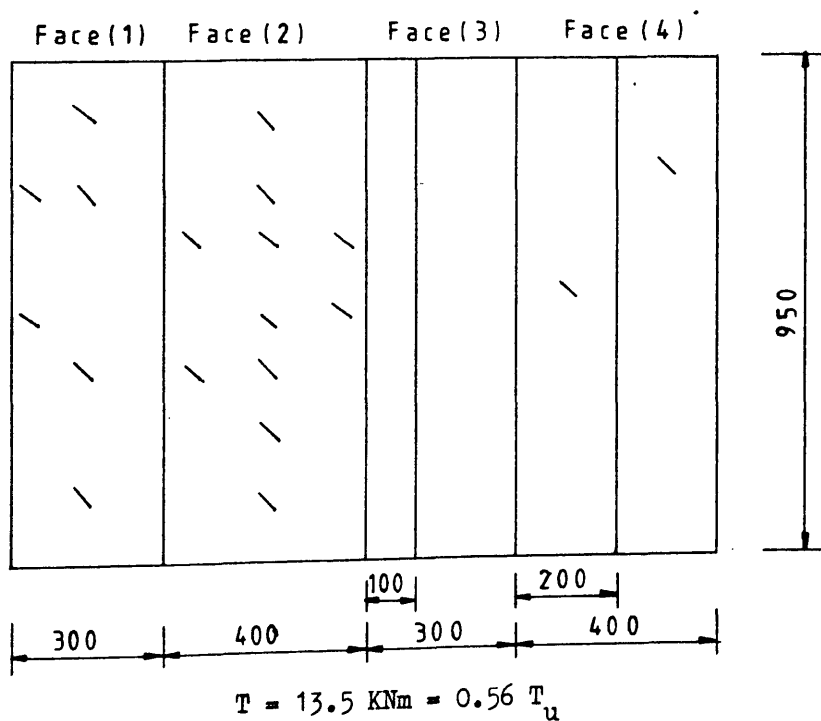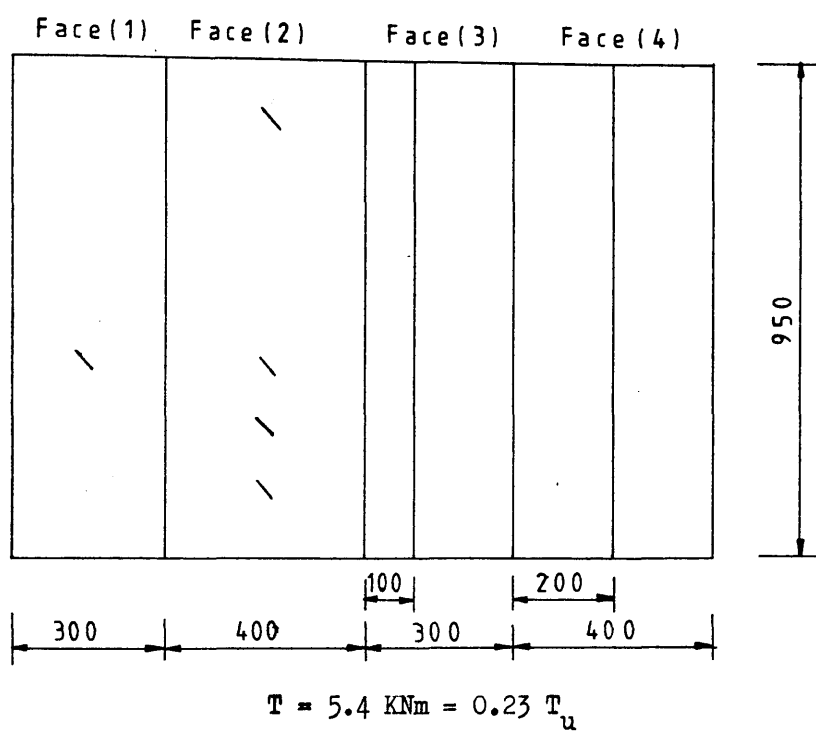
Figure (8.10) Predicted crack Propagation for specimen
(B11)

Face(1) Face(2)   Face(3)   Face(4)

950

|100| 200

300   400   300   400

T = 18.9 KNm = 0.79 T_u

Face(1) Face(2)   Face(3)   Face(4)

950

|100| 200

300   400   300   400
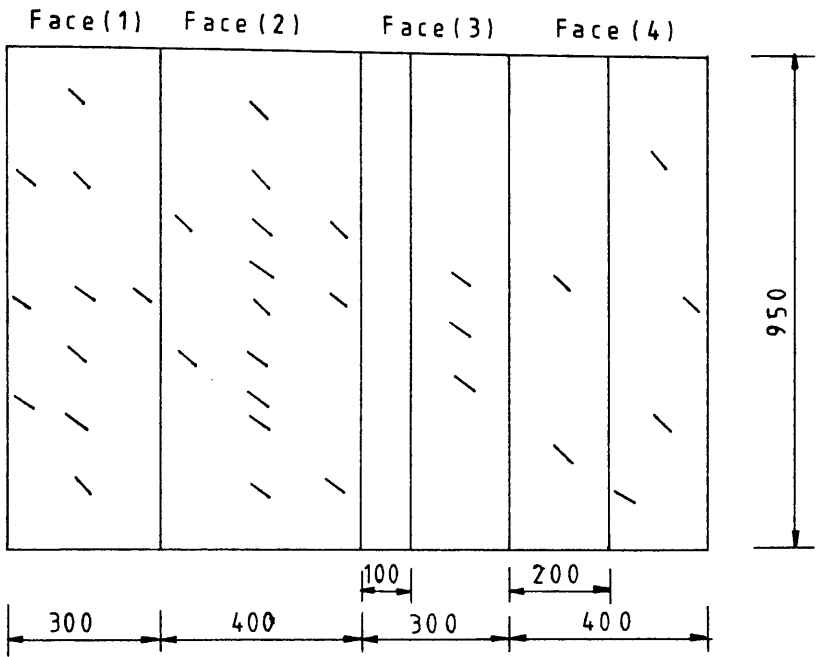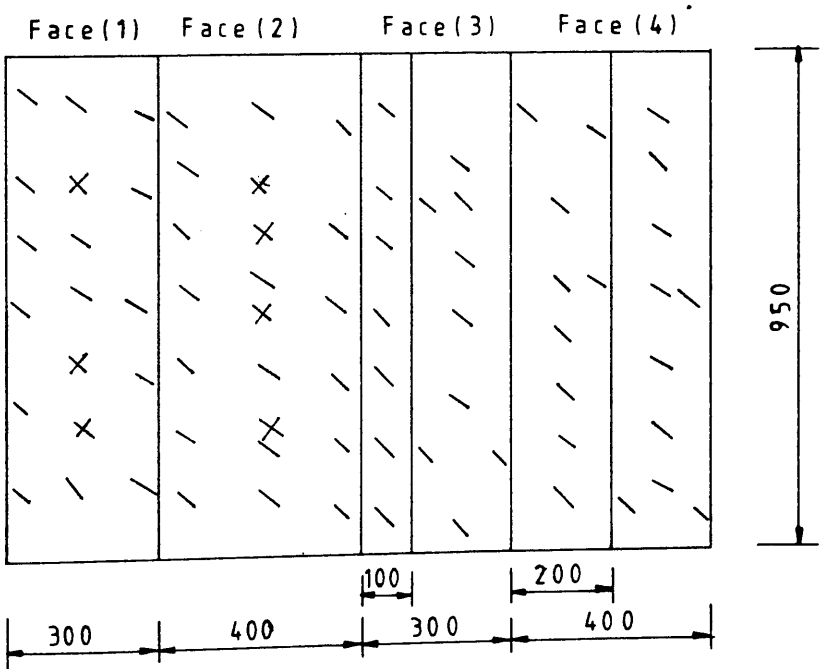
T = 22.8 KNm = 0.95 T_u

Figure (8.10) Continued

(1)

T=18.9 KN.m

(2)

T=21.6 KN.m

(3)

T=22.8 KN.m

(4)

T=24.0 KN.m

● Yielding

///// Crushing
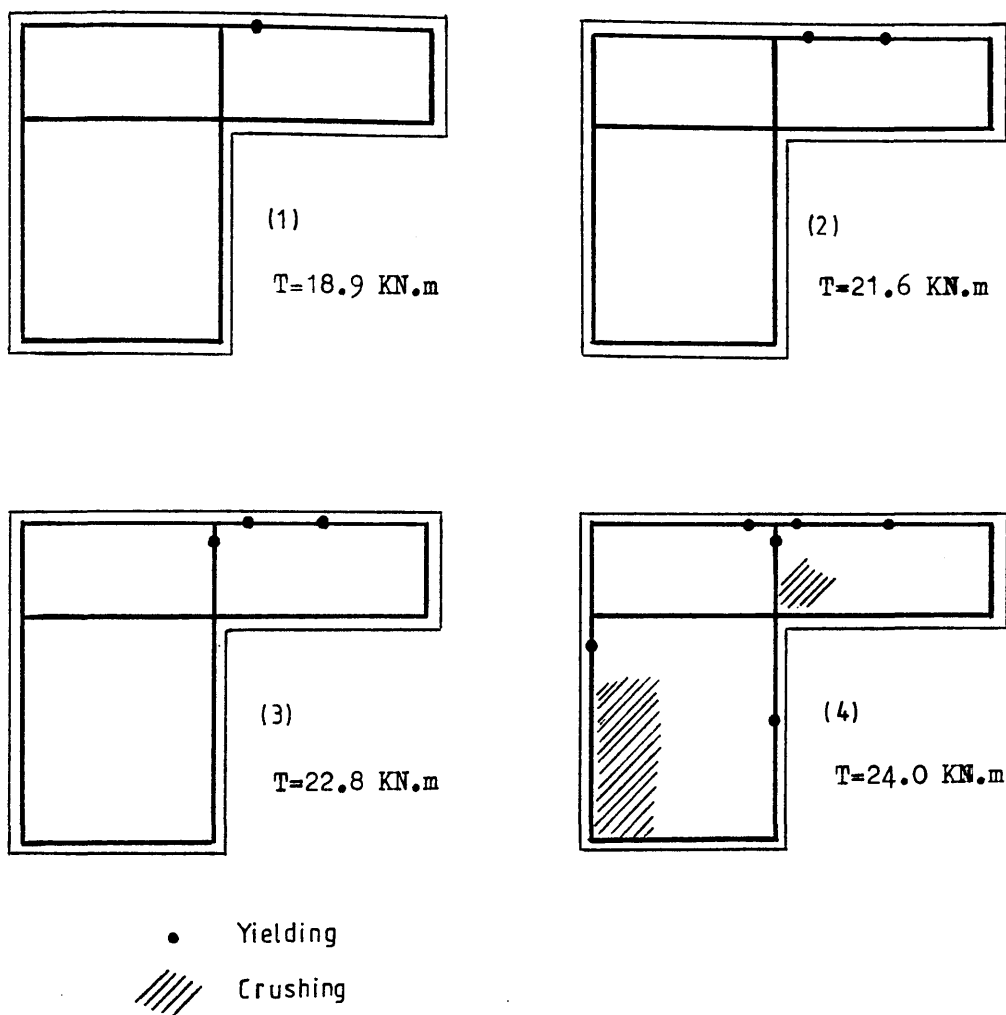
Figure (8.11) Process of yielding of reinforcement for
          specimen (B11)
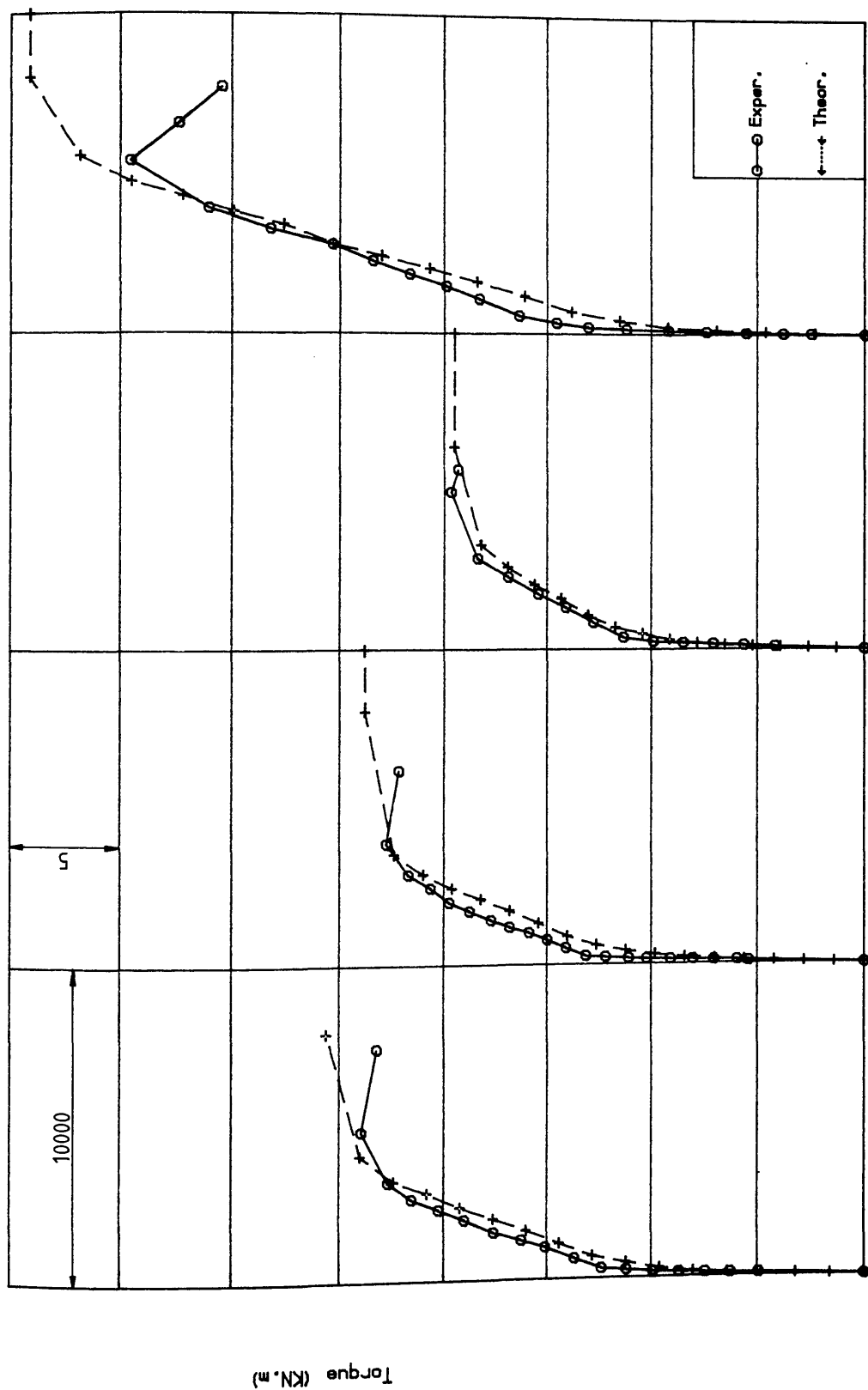
Figure (8.12) Torque-twist curves for models B11, B12, B13 and B14
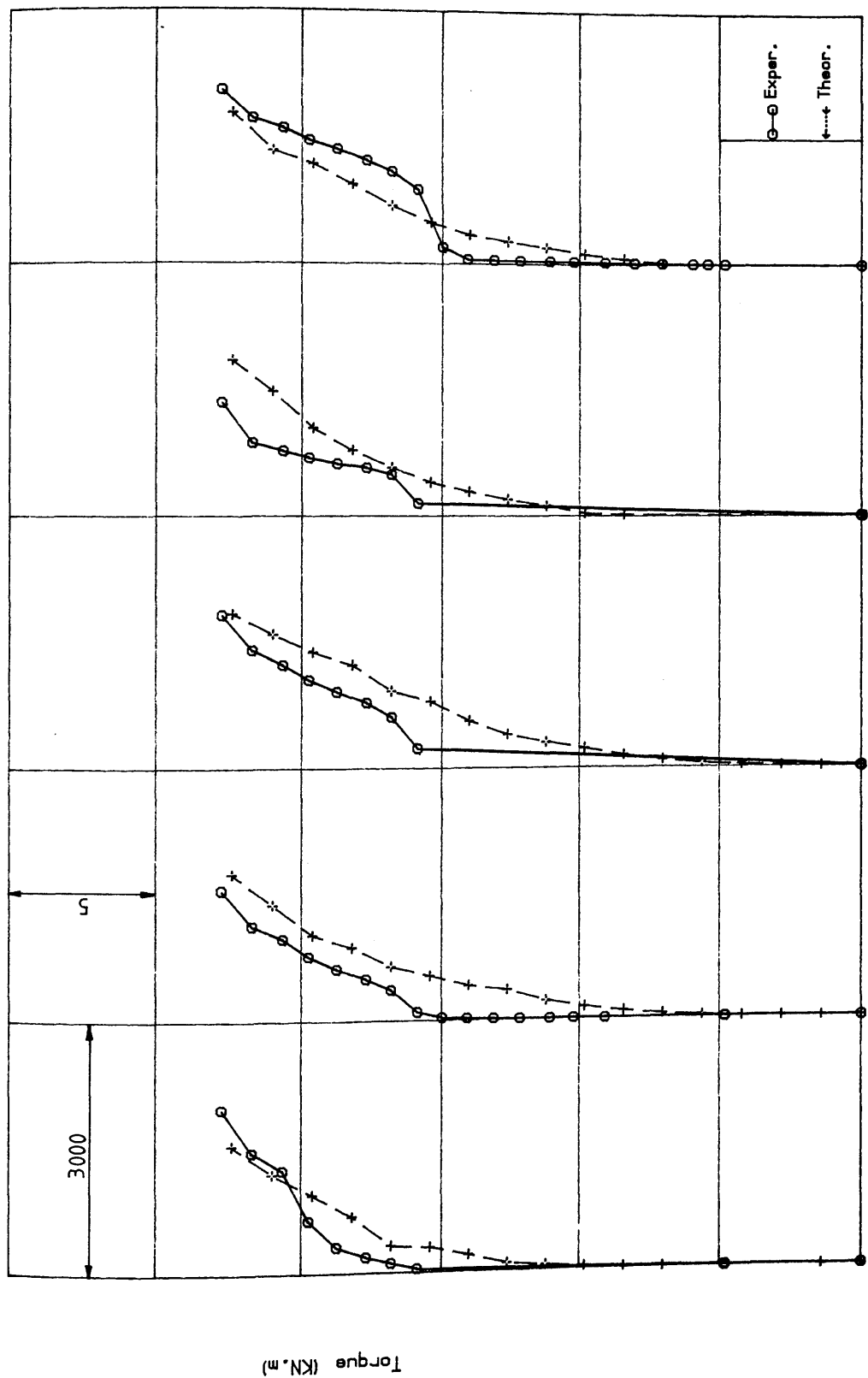
Figure (8.13) Comparison of longitudinal steel strain for model (B12) at strain gauges 1, 3, 4, 5, 6
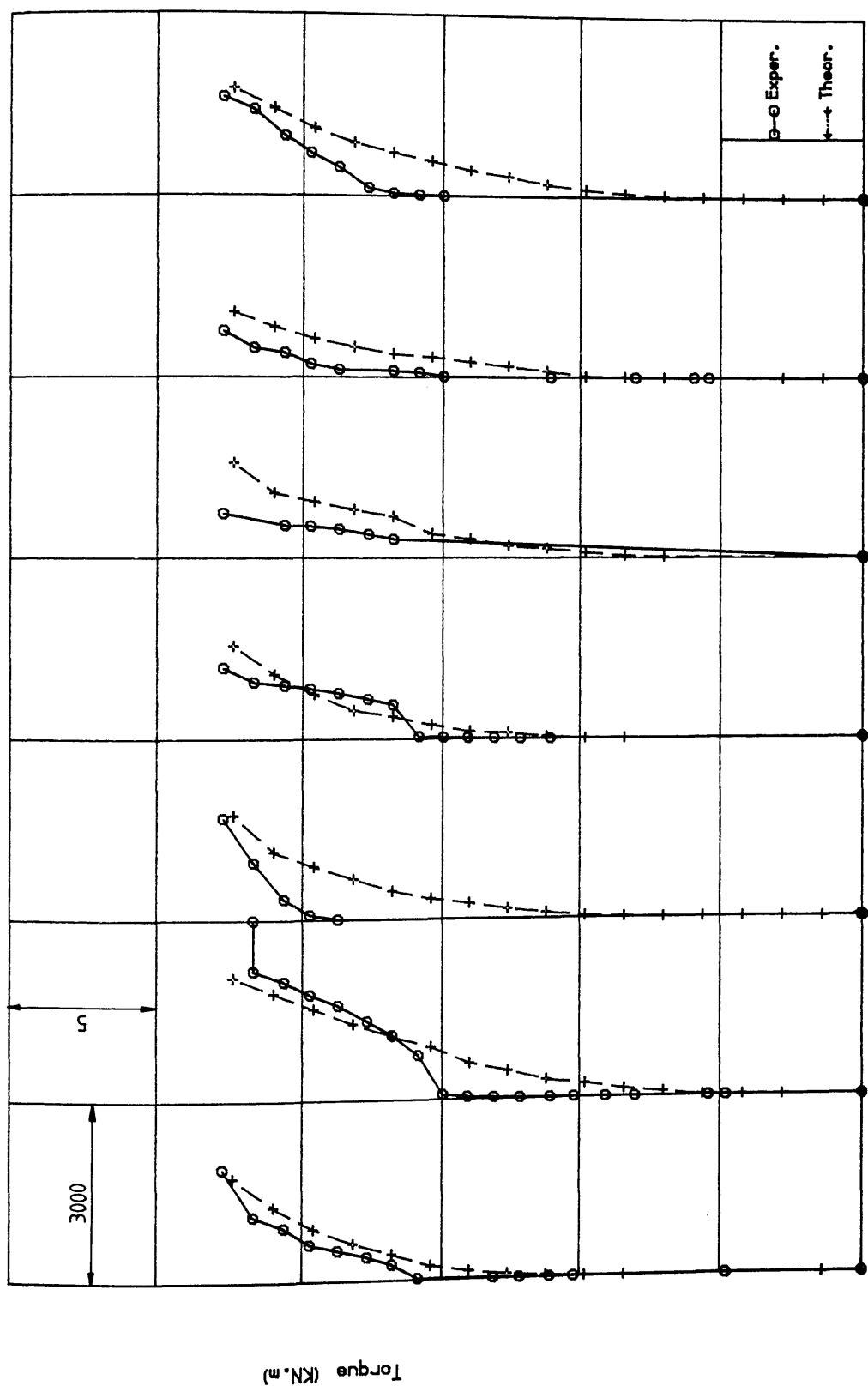
Figure (8.14)   Comparison of top stirrup strain for model B12

Strain x 10^6

Torque (KN.m)
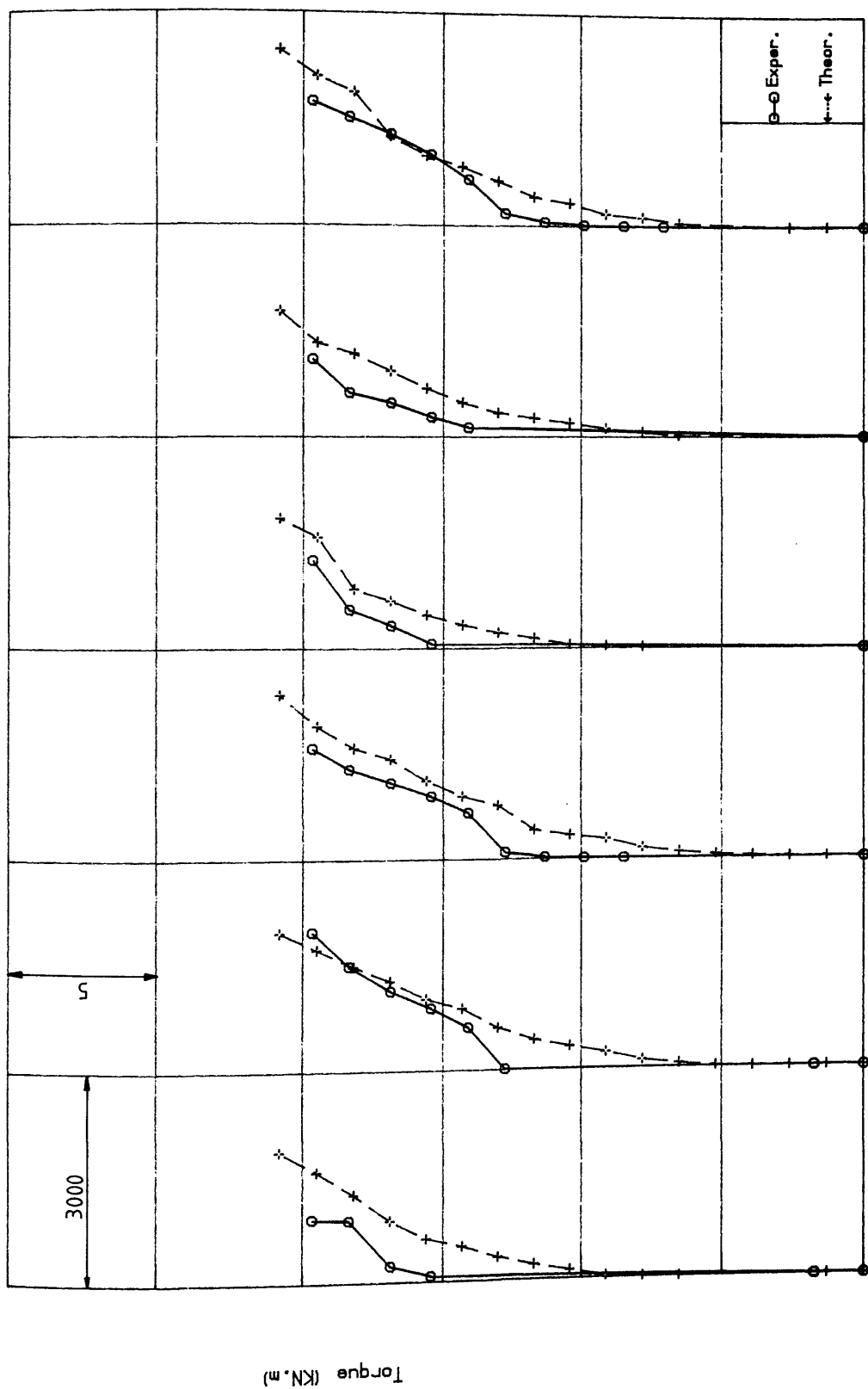
Figure (8.15) Comparison of longitudinal steel strain for model (B13)
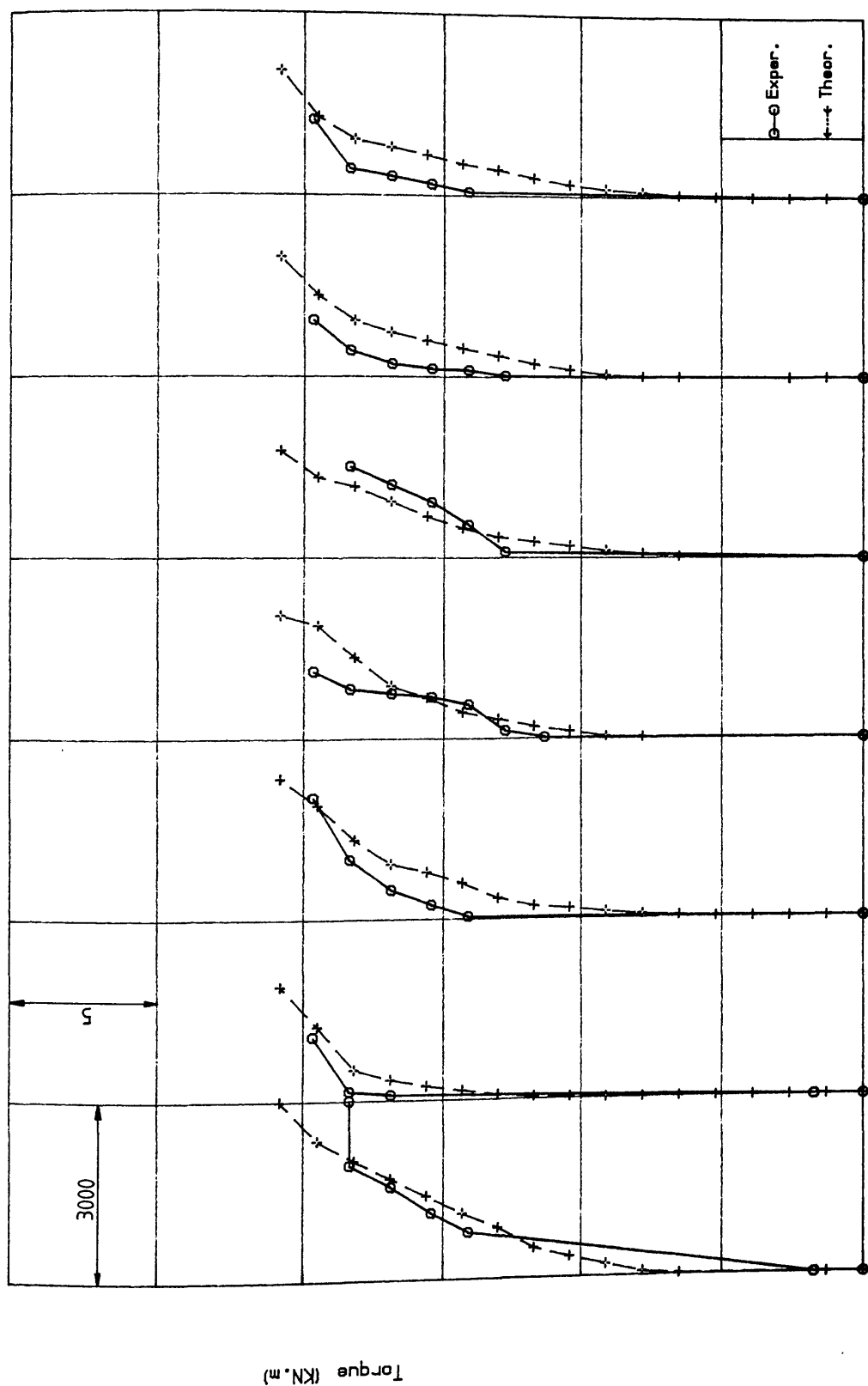
Figure (8.16) Comparison of top stirrup strain for model B13

Strain × 10^6

Torque (KN.m)
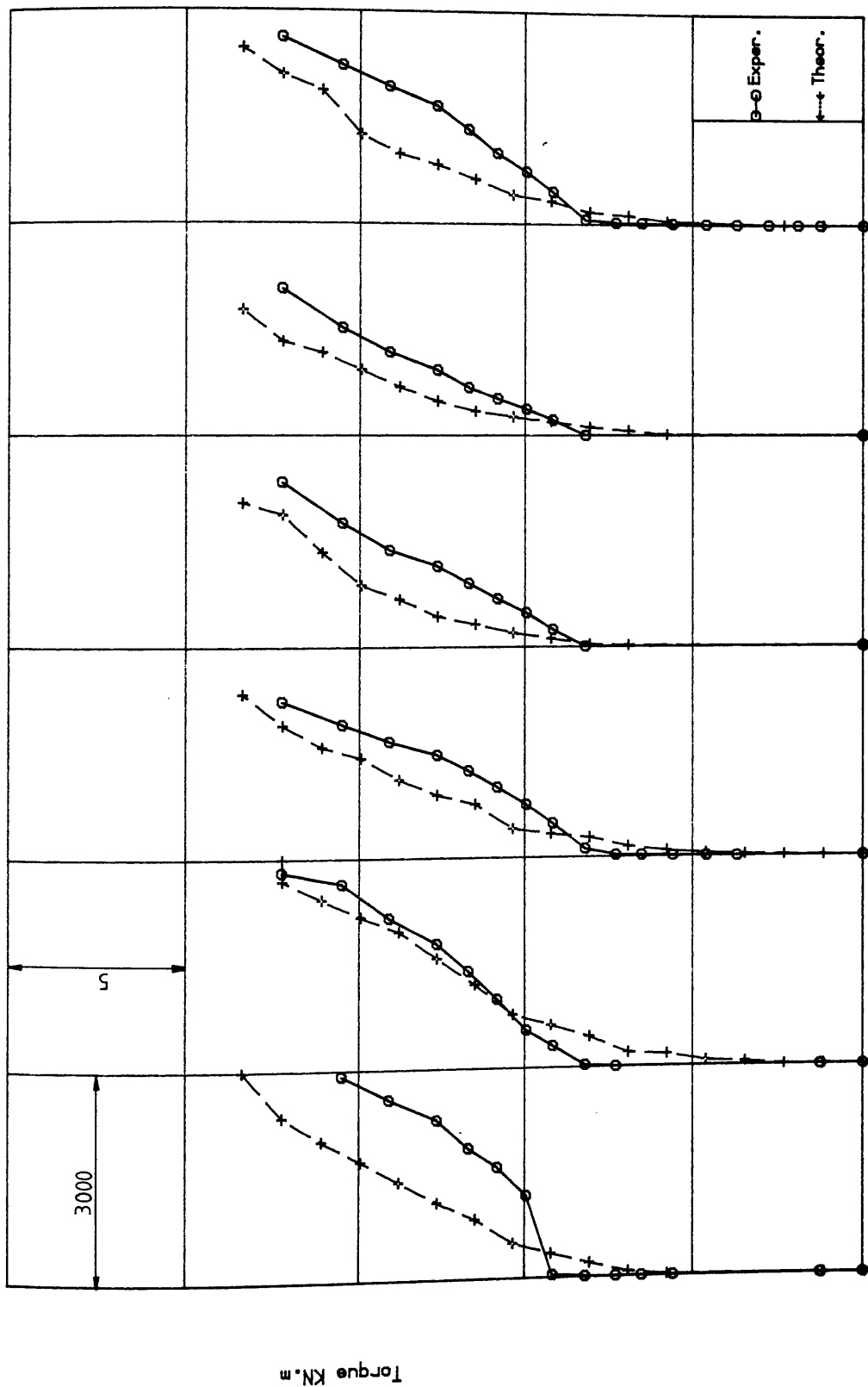
Figure (8.17) Comparison of longitudinal steel strain for model B14
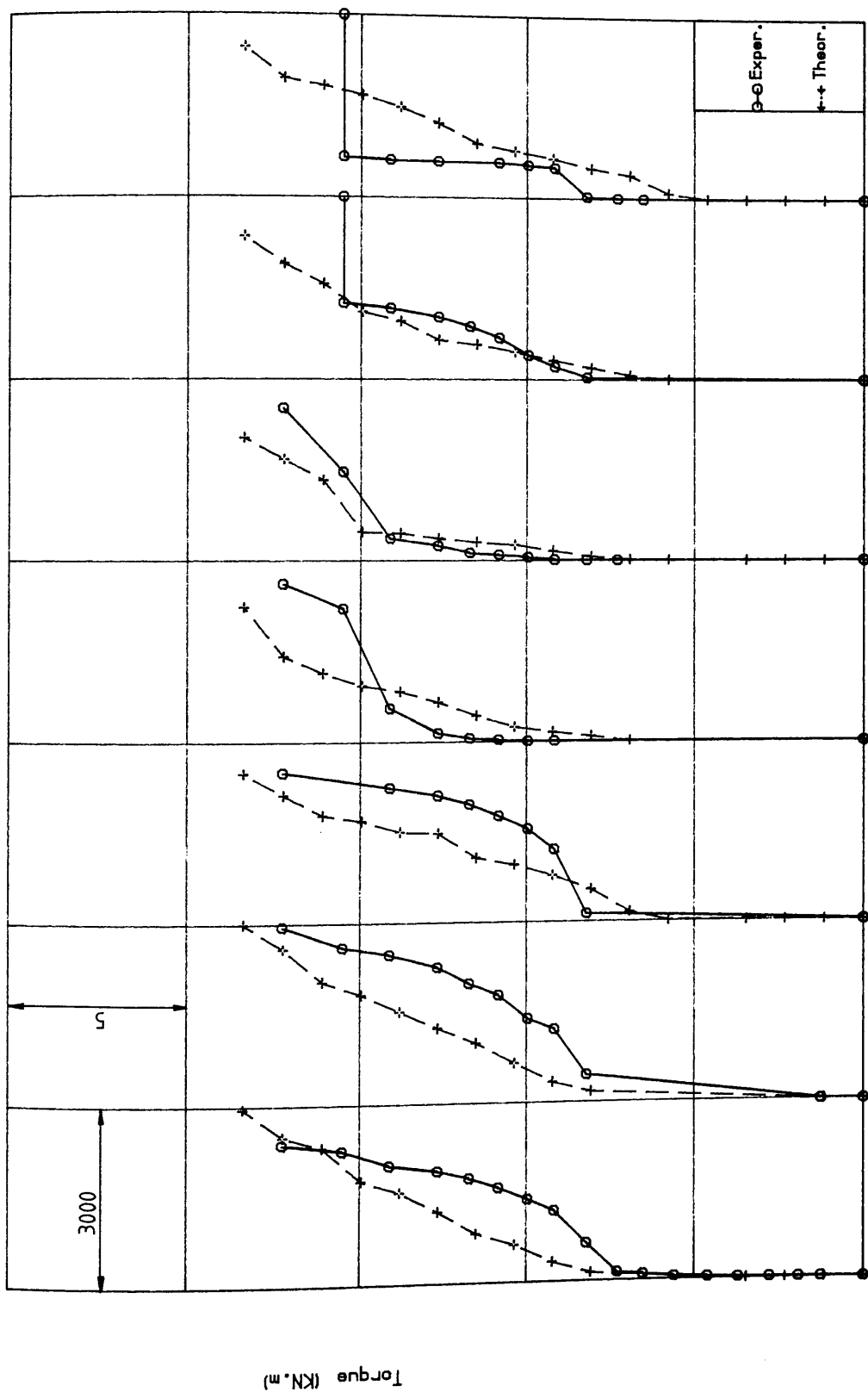
Figure (8.18) Comparison of top stirrup strain for model B14
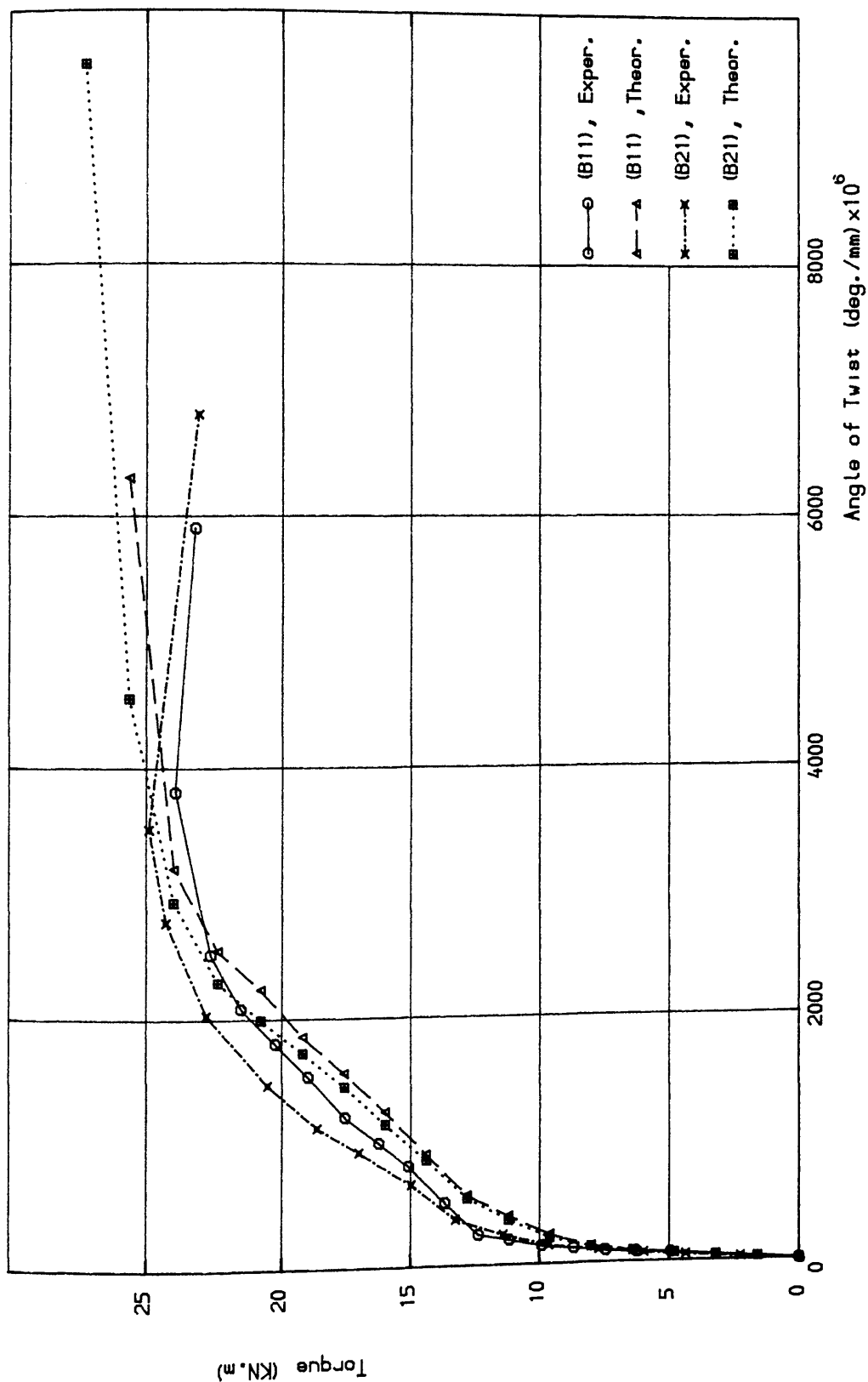
Figure (8.19) Torque-twist curves for models B11 and B12
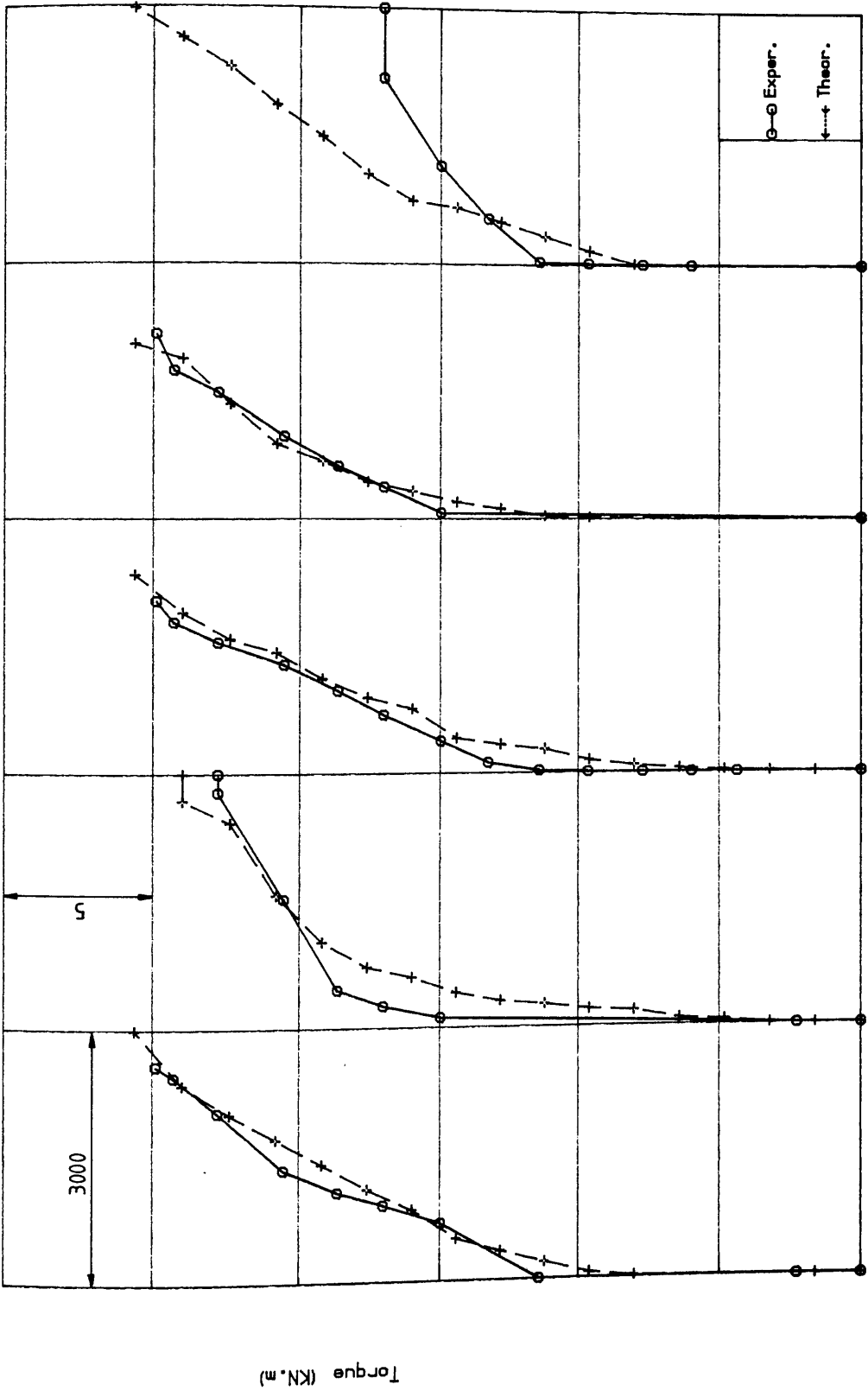
Figure (8.20) Comparison of longitudinal steel strain for model (B21)
at strain gauges 1, 2, 3, 4 and 6

Strain x10^6

Torque (KN.m)
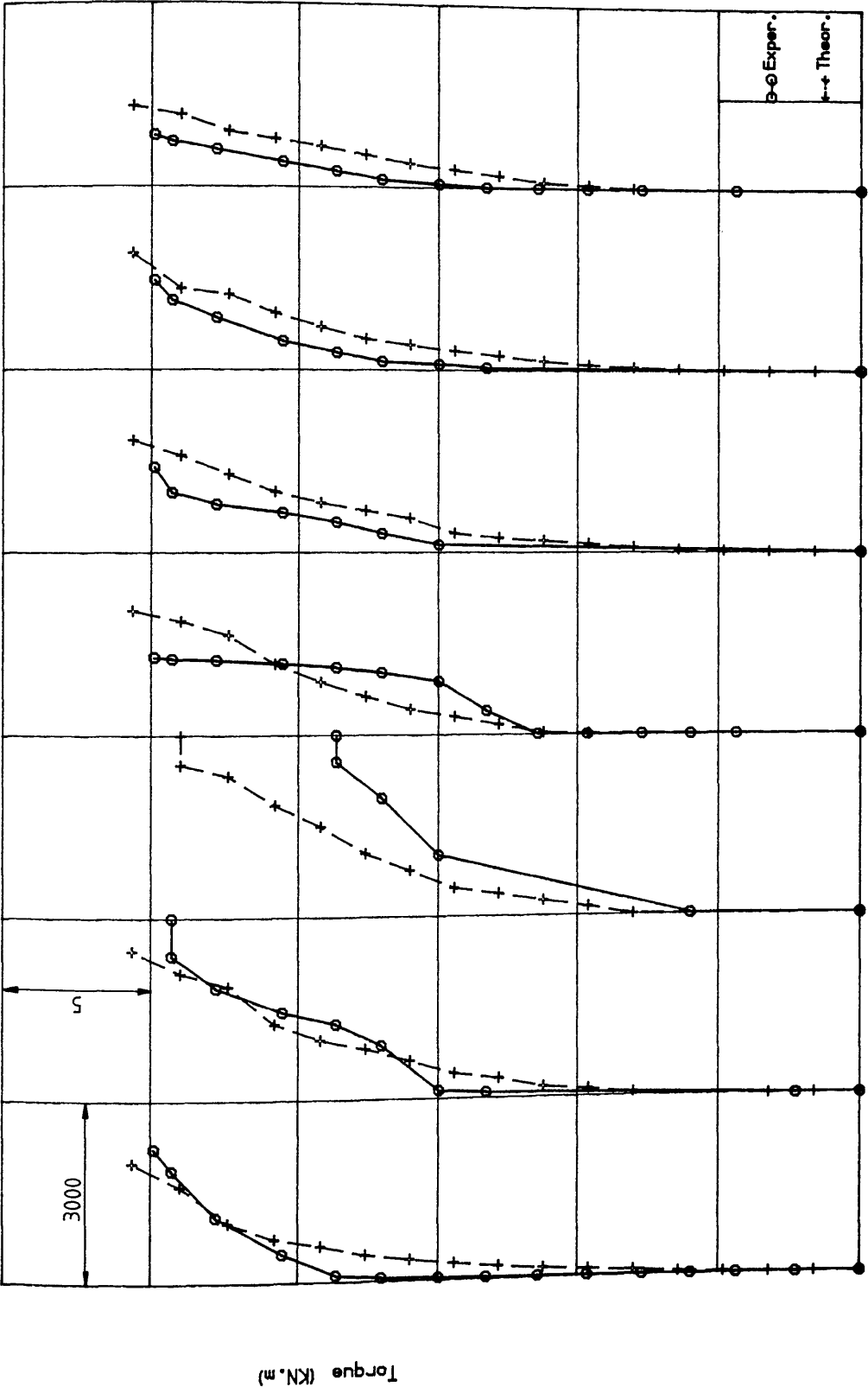
Figure (8.21) Comparison of top stirrup strain for model (B21)

Strain ×10^6

Torque (KN.m)
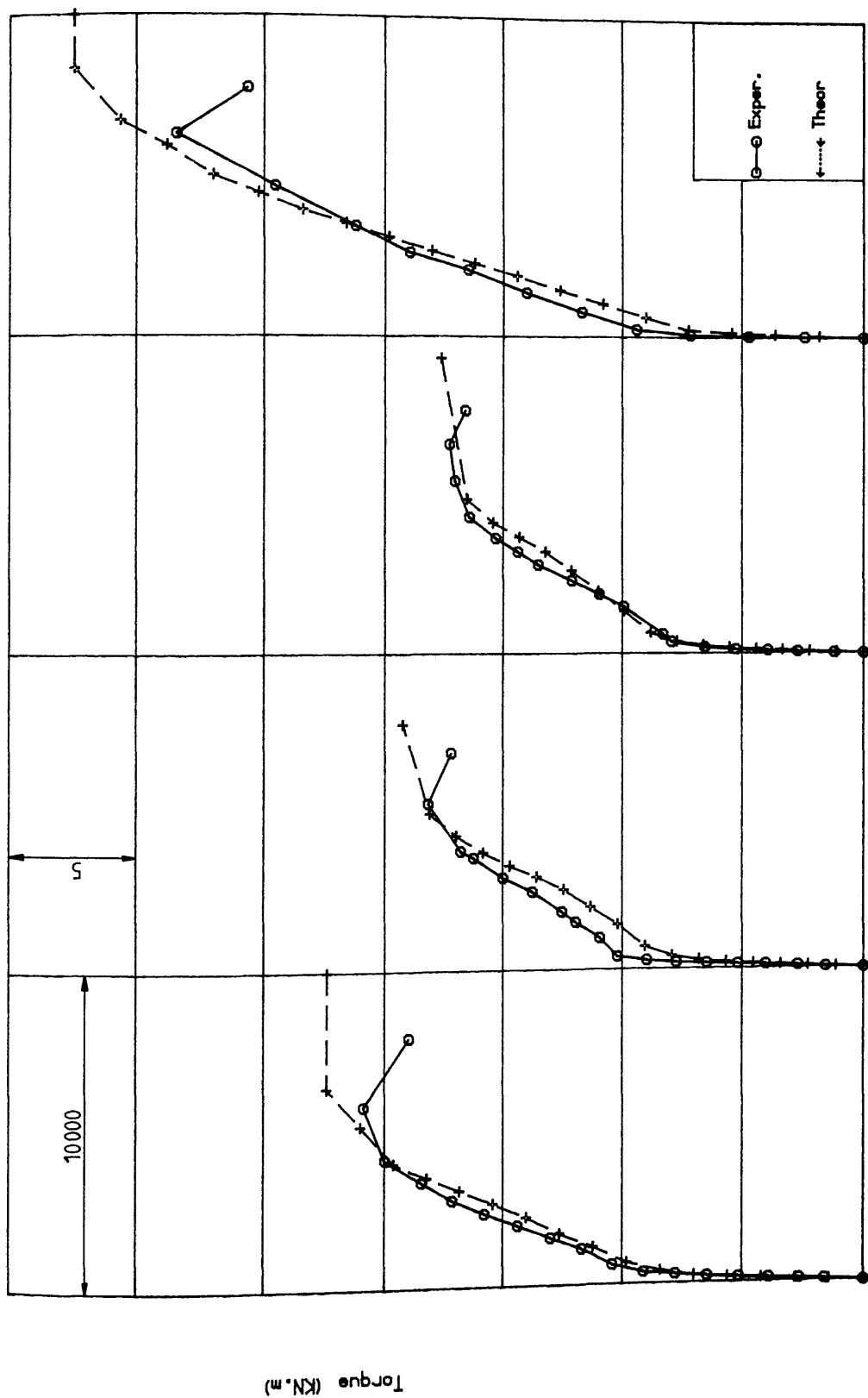
Figure (8.22) Torque-twist curves for models B31,
B32, B33 and B34
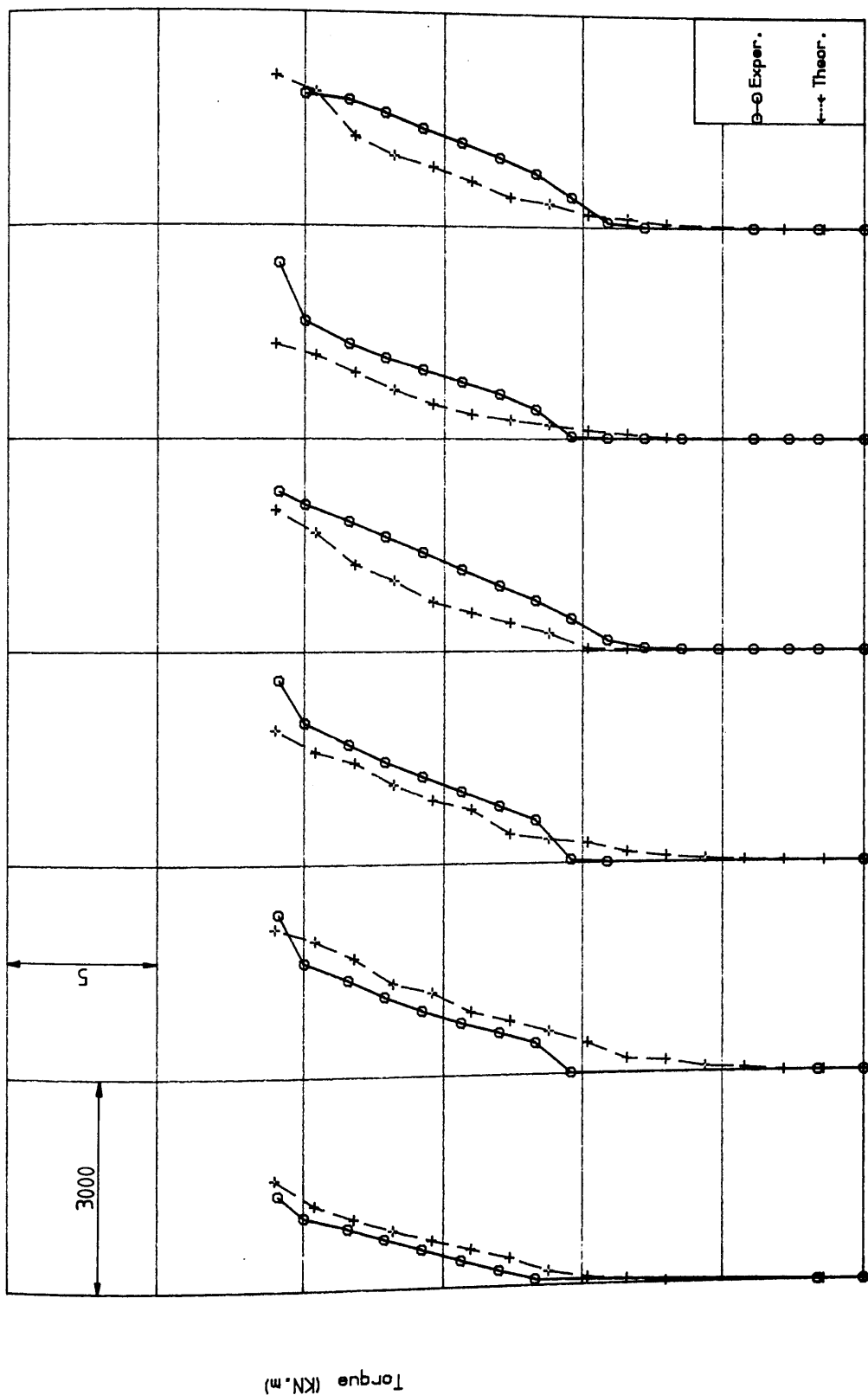
Figure (8.23) Comparison of longitudinal steel strain for model B31
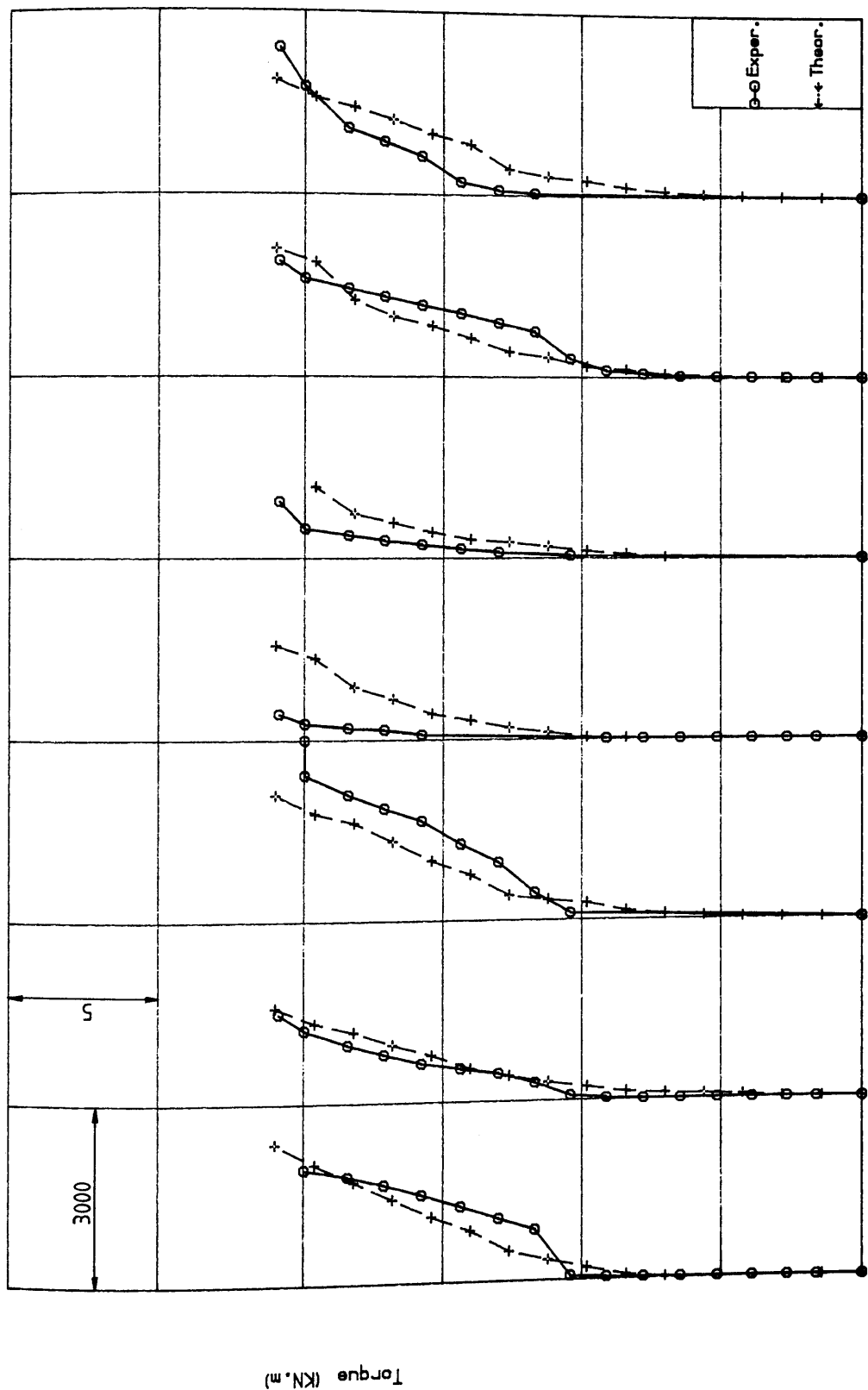
Figure (8.24) Comparison of top stirrup strain for model B31
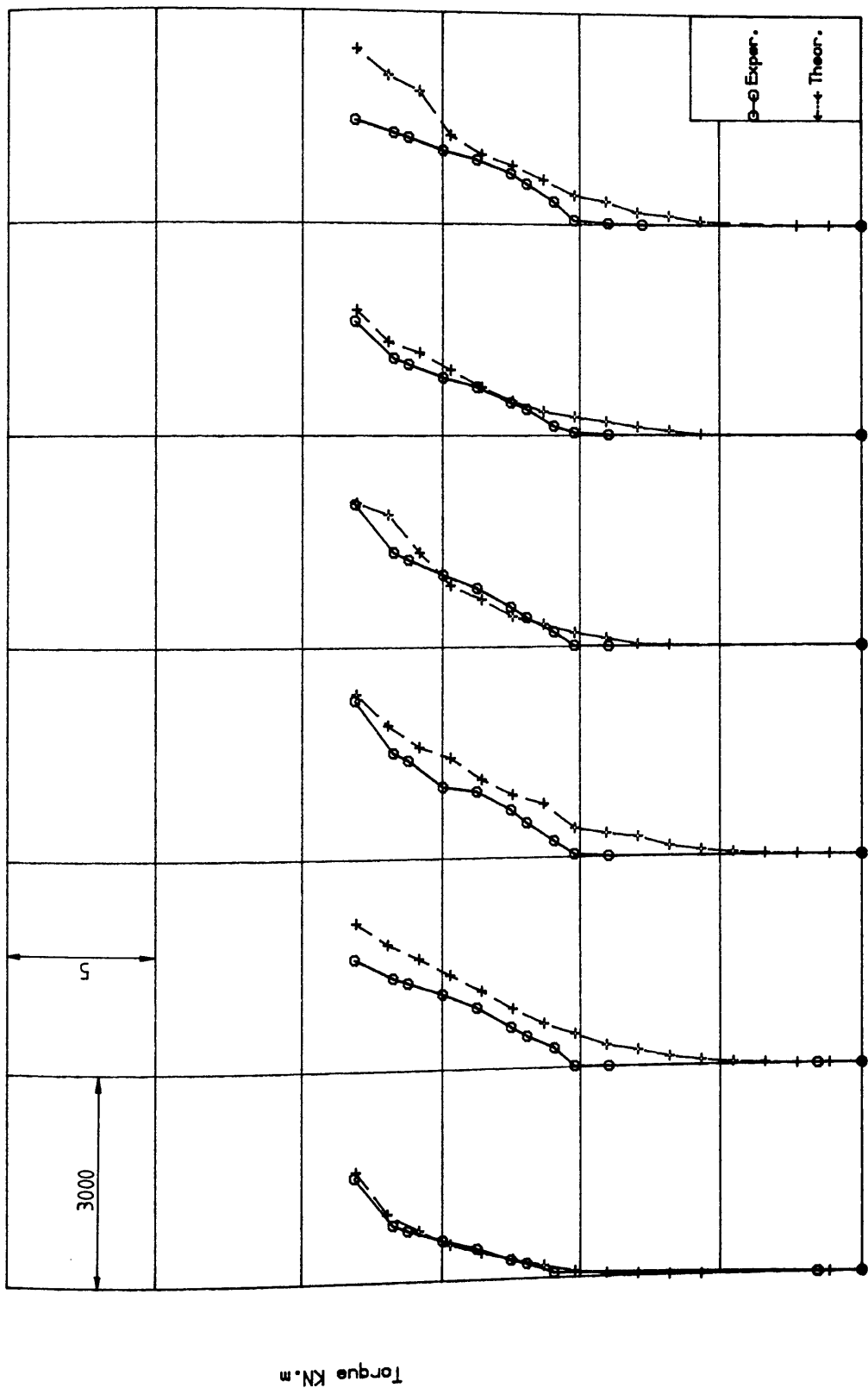
Figure (8.25) Comparison of longitudinal steel strain for model B32

Strain x10^6

Torque KN.m
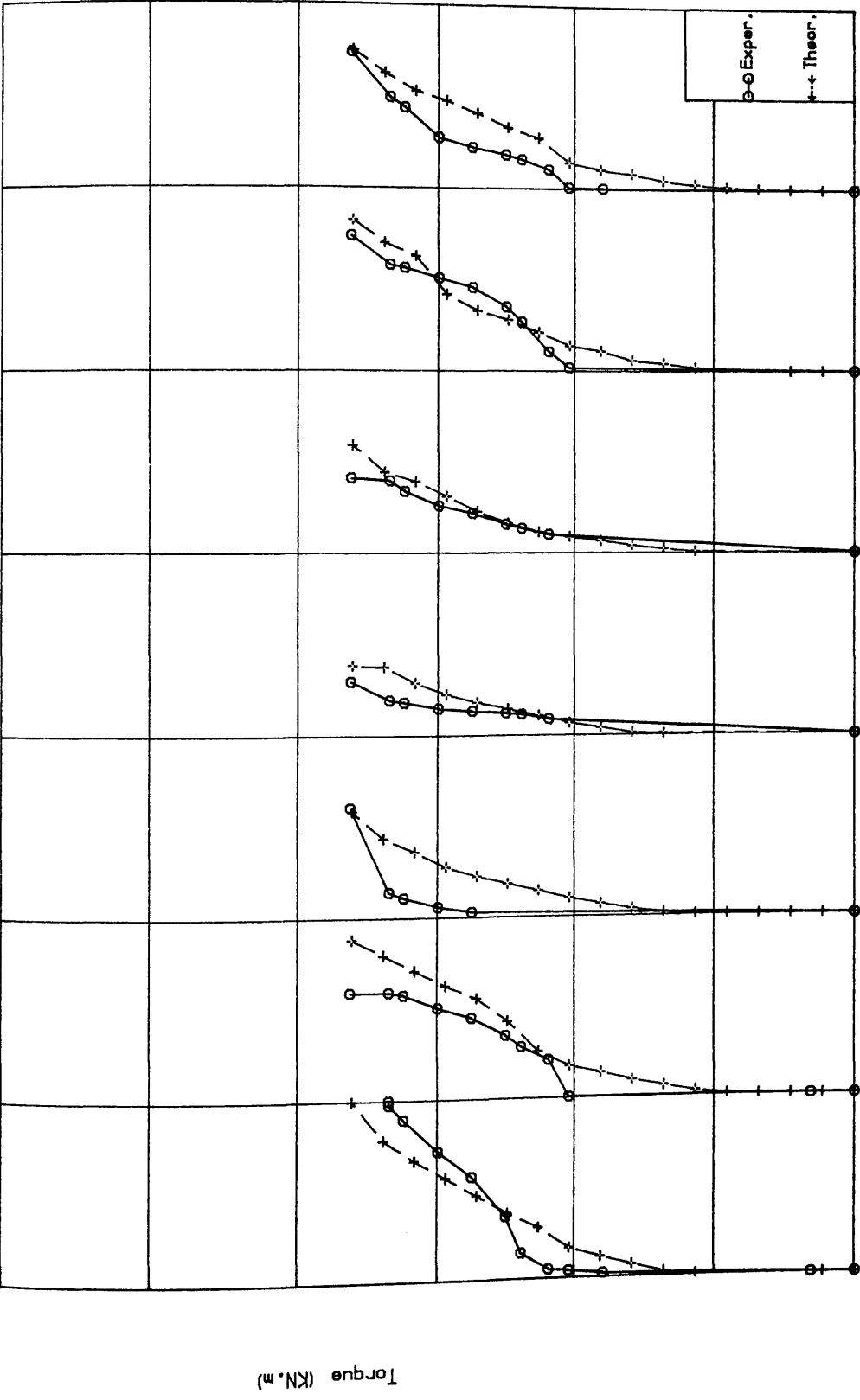
Figure (8.26) Comparison of top stirrup strain for model B32
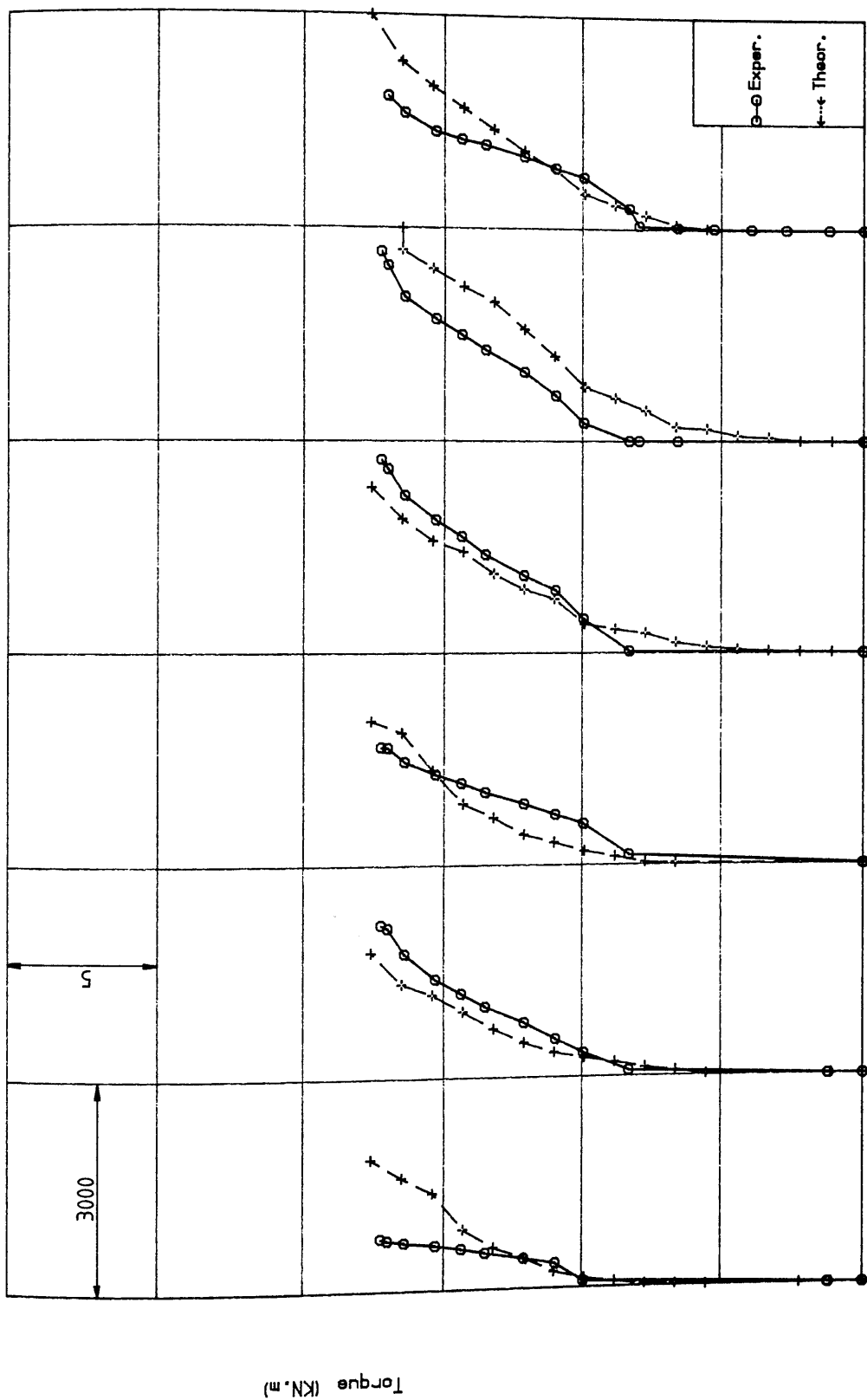
Figure (8.27) Comparison of longitudinal steel strain for model B33

Torque (KN.m)

Strain x10^6

Exper.

Theor.

5

3000
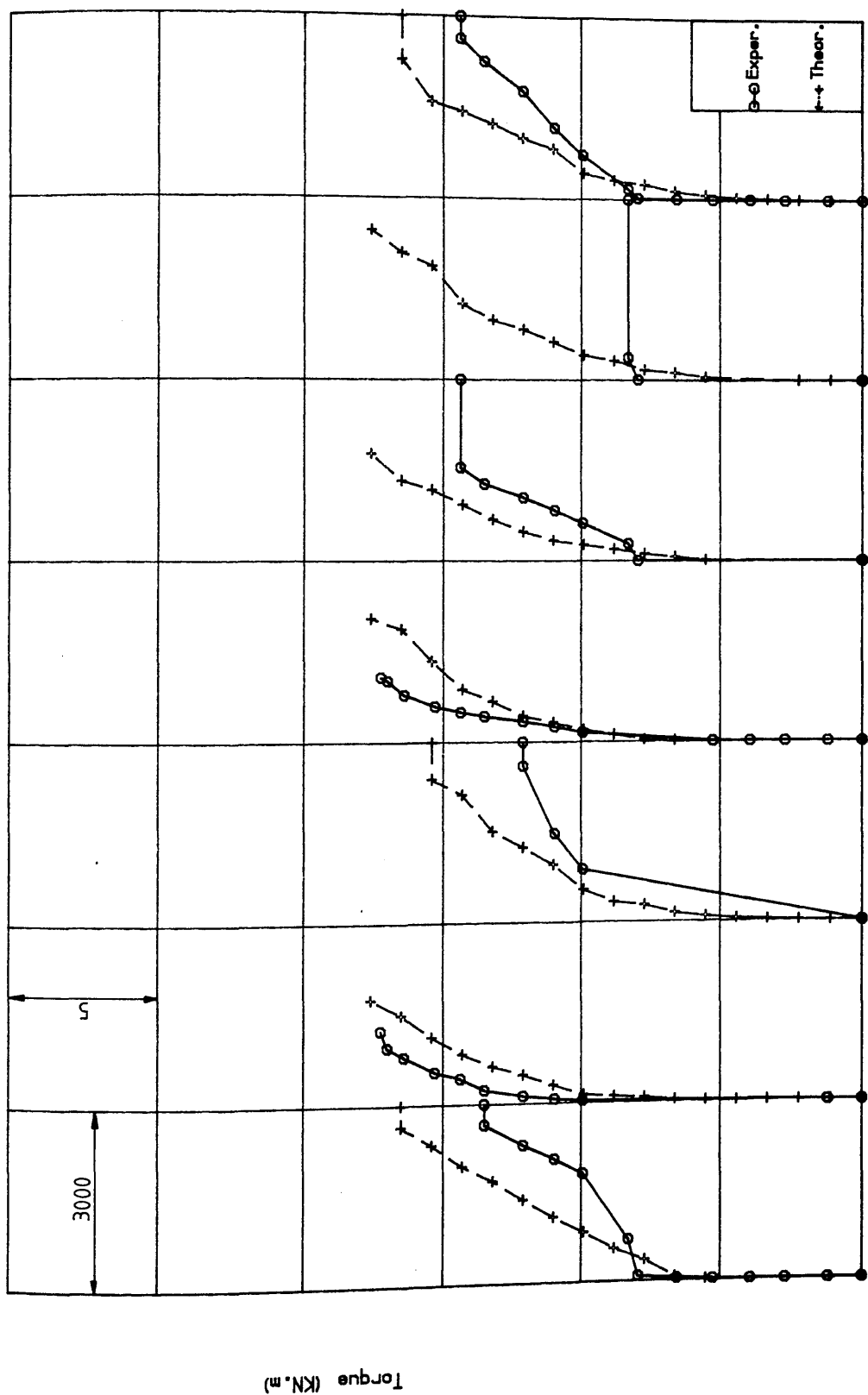
Figure (8.28) Comparison of top stirrup strain for model B33
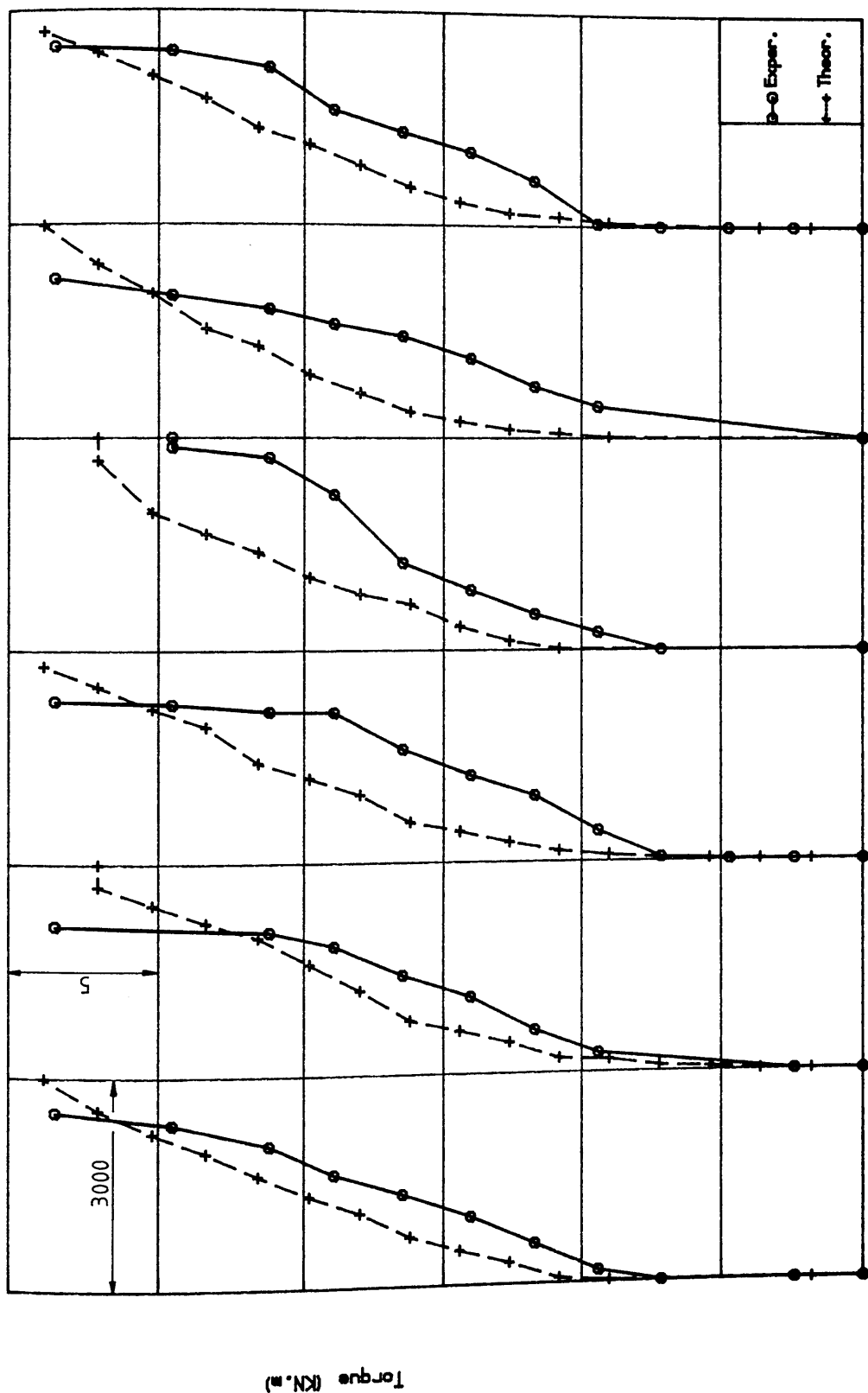
Figure (B.29) Comparison of longitudinal steel strain for model B34
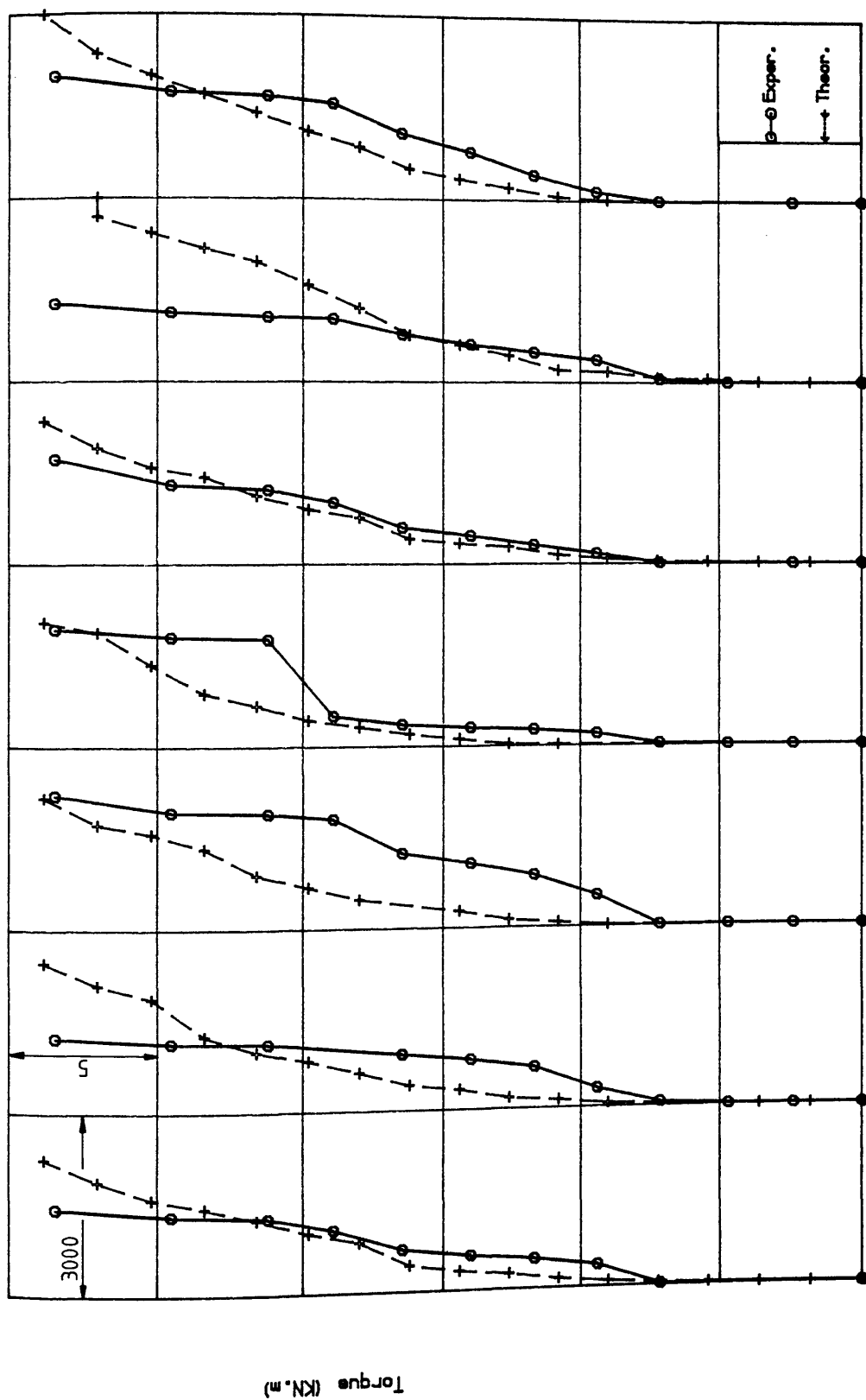
Figure (8.30) Comparison of top stirrup strain for model B34

Strain × 10^6

Torque (KN.m)

Table (8.3) Comparison of experimental and predicted ultimate torques of the test specimens

Group	Specimen	T_u(Exper.) KN.m	T_u(Theor.) KN.m	$\dfrac{T_u(\text{Theor.})}{T_u(\text{Exper.})}$
	B11	23.95	24.8	1.035
	B12	22.75	23.8	1.046
B1	B13	19.66	20.0	1.017
	B14	34.54	39.1	1.132
	B21	24.89	24.8	0.996
	B31	20.88	23.8	1.106
B3	B32	18.14	19.2	1.059
	B33	17.25	18.7	1.084
	B34	28.43	32.4	1.140

Mean = 1.068

S.D. = 0.048

References

(1) Phillips, D.V. and Mohamed, M.S., "Analysis of Reinforced Concrete Beams in Torsion", Proc. Second Inter. Conf. Civil and Struct. Engng. Computing, Civil-Comp 85, ICE, London, 3-5 Dec., 1985, pp. 305-311.

CHAPTER NINE

PARAMETRIC STUDY AND DESIGN RECOMMENDATIONS

9.1 Objectives and Scope

The aim of this chapter is to present and discuss results of a numerical parametric study on reinforced concrete solid L-sections subjected to pure torsion using the developed nonlinear three dimensional finite element program. These results will be combined with the experimental results of Chapter Seven in order to investigate more structural variables which where not possible to include in the experimental programme for practical reasons and to clarify and amplify the experimental study.

The material and solution parameters, found suitable for torsion analysis in Chapters Five and Eight, are again used here. The 12-element mesh, "reduced" boundary conditions and method of load application are also used with a standard length of 950 mm. The total reinforcement ratio for all numerical models is less than 2.5% to avoid the undesired overestimation of the ultimate torque observed in Chapter Eight for values of reinforcement volume ratios above this value.

9.2 Parameters Chosen for Investigation

Table (9.1) and Figure (9.1) show details of the numerical models which include two specimens of the experimental programme to aid comparison. Models denoted N relate to the numerical study; those denoted B are the ones experimentally tested. The main variables investigated are as follows:

(1)Effect of the size of cross section for the same
     ratios of longitudinal and transverse reinforcement

This was chosen to check the applicability or otherwise of the law of similitude as it is customary to test the behaviour on small scale laboratory specimens and assume afterwards that identical behaviour can be expected in real life, large scale structural elements. An example of this is the ultimate torque which is normally taken as linearly related to the cross sectional size when the reinforcement ratios are the same. This aspect has been experimentally checked for rectangular sections by Hsu (ref. 1)

Models B11, N81, N31 and N41 have increasing size of cross section with the same side ratios (i.e. h/b_w etc.). The reinforcement ratios, both longitudinal and transverse, are practically the same for all models. Models B13, and N43 study similar parameters except a smaller reinforcement ratio was used (same longitudinal reinforcement ratio as the previous group but half the ratio of transverse reinforcement). All material properties of B11 were used in the finite element analysis of N81, N31 and N41; those of B13 were used for the analysis of N43.

(2)Effect of detailing of reinforcement for the same
     cross section and amount of steel

This aspect was considered because of the importance, stressed by the codes of practice, of the use of closed stirrups to resist torsional stresses for both flange and web of a solid flanged section. It has also been pointed out in Chapter Two that the majority of experimental studies on torsional behaviour of reinforced concrete flanged sections

have been conducted on sections reinforced with only one layer of steel in the flange or even with an unreinforced flange.

Models N21 and N51 have the same cross section and volume ratios of both the longitudinal and transverse reinforcement as B11. The detailing of this reinforcement is, however, different. N21 has the web properly reinforced with longitudinal bars and closed stirrups while the flange has only one layer of steel provided at the top. N51 has all the steel lumped in the web leaving the flange unreinforced. In the analysis of N21 and N51 all material properties of B11 were used.

(3) Effect of varying the amount of longitudinal steel
      for the same amount of transverse reinforcement

This particular parameter is considered because only the variation of the transverse reinforcement was studied in the experimental part of this work. Both longitudinal and transverse steel has an important role to play, a fact which has been well established in this study as well as elsewhere.

Model N71 is of the same cross section and amount of stirrups as B11, but the amount of longitudinal steel is halved. However, the distribution of reinforcement is the same, having been provided in both web and flange. All material properties of B11 were used in the analysis of N71.

9.3 Results and Discussions

9.3.1 Introduction

The principal quantity to be considered in this parametric

study will be the ultimate torque. This will be used for each group of models in order to establish the trend caused by the particular variable being considered. The other aspect will be the general behaviour of each group (reflected in the torque-twist curve) which will be used for two purposes:

(1) to study the effect of the variable in question on the overall behaviour, and

(2) to assess the degree of acceptability of the results so that the values of the ultimate torques obtained can be safely taken as if the model has actually been experimentally tested. The predicted ultimate torque of a numerical model is accepted after its torque-twist curve shows no peculiar behaviour during the various stages, i.e. pre-cracking, post-cracking and ultimate conditions.

9.3.2 Effect of the Size of the Cross Section for the Same Ratios of Longitudinal and Transverse Reinforcement

Table (9.2) shows comparison of the ultimate torques obtained for group 1 (models B11, N81, N31 and N41) and group 2 (models B13 and N43). Each of the models B11 and B13 is considered as a reference for its group to which the parameter $\Sigma x^2 y$ and ultimate torque, T_u, of the other models are referred. The parameter $\Sigma x^2 y$ (where x and y are the shorter and longer dimensions of the component rectangles) is chosen because it reflects the concrete contribution towards the ultimate torque of the reinforced concrete section as it appears in the elastic, plastic and the skew-bending theories to predict the ultimate torque of a plain concrete section (Chapter Two). The table indicates clearly that for the same ratios of longitudinal and transverse

reinforcement, a certain increase in the size of the section does not produce the same increase in the ultimate torque. This indicates that the law of similitude does not hold for reinforced concrete L-sections subjected to pure torsion. Hsu (ref. 1) found similar behaviour for reinforced concrete rectangular sections under pure torsion.

Figure (9.2) shows the results plotted against the line which indicates the applicability of the law of similitude. The upper- and lower-limit of the numerical ultimate torque denote, respectively, the numerical torque one load increment above and one increment below that predicted by the finite element model. This is because of the uncertainty associated with the finite element prediction of the failure torque. However, because small load increments are normally aplied, the values taken are reasonably acceptable. The parameter $\sum(x^2y)^*$ and the ultimate torque T_u^* are those of the reference models B11 and B13. It can be seen from the figure that a certain increase in the size of the cross section produces a larger increase in the ultimate torque. This can be attributed to greater contribution of concrete to the ultimate torque of the reinforced concrete section. The results of group 2, despite being plotted with only two points, confirm this finding which is very clear from the results of group 1.

This observation can have important implications on the current British Code torsion design procedure. At present no concrete contribution is considered in the code's design equation as already mentioned in Chapter Two. This is one of the reasons behind the procedure being far too conservative

and appreciation of this point will lead to less uneconomical designs.

Figure (9.3) shows the torque-twist curves obtained for group 1. The size increase is evident in other aspects of the behaviour, namely: the pre- and post-cracking torsional stiffness and the cracking torque, all of which increased, as expected. The post-cracking stiffnesses, defined in Chapter Seven (Figure 7.22), are listed in Table (9.3) where it this clear that the post-cracking stiffness increases with the increase in the size of the cross section.

9.3.3 Effect of Detailing of Reinforcement for the Same Cross Section and Steel Amount

Table (9.4) lists the ultimate torques and the post-cracking torsional stiffnesses obtained for models B11, N21 and N51. Figure (9.4) shows the torque-twist curves for the same models. Examination of these results reveals the following:

(1) Provision of one layer of reinforcement in the flange resulted in a reduction of about 25% of the ultimate torque (model N21) accompanied by a reduced post-cracking torsional stiffness and a reduced ductility. The post-crcaking stiffness is reduced to about 50%. The final failure of this model was caused by yielding of the flange reinforcement followed by crushing at the junction of web and flange.

(2) Completely unreinforced flange (model N51) reduced the post-cracking stiffness to only about 18% and further reduced the ultimate torque. The reduction in the ultimate torque is about 33% resulting from a large rotation of the

flange about the web causing crushing of concrete at the junction. This crushing can be expected but it emphasizes the need for closed stirrups in the flange. Acting as a short cantilever supported by the web, the flange will have compression at the bottom and tension at the top, thus the crushing that resulted.

(3) The above gives clear evidence of the effect of improper detailing of torsional reinforcement for the same amount of steel in solid flanged sections. The lack of proper detailing means uneconomical use of the torsional reinforcement. Use of closed stirrups in all component rectangles is an important factor to ensure better performance of a flanged section after cracking of concrete and at ultimate conditions. The same amount of stirrups can be better utilized if it is well distributed.

Figure (9.5) shows strain distribution along all sides of a closed stirrup well after cracking of concrete for model B11 obtained from the finite element analysis. Plotting of this distribution involves the strain values at 30 Gauss points, a number practically impossible to mount as strain gauges on the closed stirrup because of the small dimensions of some of the sides of the stirrup (being about 50mm long), leaving aside economy considerations. The distribution resembles to a large extent the shear stress distribution on the sides of each rectangle. The most important observation, however, is that the junction provides a continuity of strain over the rectangle common to both web and flange. This may support the view expressed earlier in Chapter Seven concerning the "junction effect"

for flange sections, as codes of practice generally consider that the torsional capacity of a solid flanged section is the sum of the torsional capacities of its rectangular components.

The strain continuity indicates that a flanged section actually acts to a large extent as one unit and not as separate rectangles as implied by the codes. This is believed to increase the torsional capacity of a flanged section. However, it may be extremely difficult to quantify the contribution of this "junction effect".

9.3.4 Effect of Varying the Amount of Longitudinal Reinforcement

Figure (9.6) shows torque-twist curves for models B11, B13 and N71. B13 is similar to B11 except that the transverse reinforcement is 52.7% of that for B11. It is clear from the figure that the curves for all three models are practically identical before cracking. This is expected as the steel does not contribute to the torsional stiffness at this stage. After cracking, however, B13 and N71 show practically identical behaviour until just before the ultimate conditions where N71 produced a slightly higher ultimate torque (only about 3.7% higher than B13).

These results are also shown in Table (9.5) where it can be seen that a 47.3% reduction in the stirrup amount (model B13) resulted in 17.9% reduction of the ultimate torque, for the same cross section and longitudinal steel, B11 being the reference. A 49.9% reduction in the longitudinal reinforcement (model N71) produced a 14.8% reduction of the ultimate torque, for the same cross section and transverse

steel, B11 again being the reference.

Table (9.6) and Figure (9.7) show similar results for models N41 and N43, which have the same cross section (the largest of the cross sections) and the same longitudinal reinforcement. N43 has a reduced amount of transverse reinforcement. It can be seen from the table that a reduction of 47.3% in transverse reinforcement (model N43) resulted in a 37.5% decrease in the ultimate torque, N41 taken as the reference.

The above results indicate the following points:

(1) Reduction of either of the longitudinal or transverse reinforcement results in a reduction of the ultimate torque for the same cross section and material properties. The amount of the reduction is hard to determine as it depends on many factors, in particular the size of the cross section, reinforcement ratios and material properties.

(2) The reduction in reinforcement also produces a reduced post-cracking torsional stiffness, a quantity much dependent on the amount of torsional reinforcement. The pre-cracking stiffness, however, remains the same as steel plays insignificant role before concrete cracking in torsion of reinforced concrete.

(3) Equal percentage reductions of longitudinal and transverse steel seem to result in practically the same post-cracking behaviour for the same cross section and material properties. This tends to emphasize the importance of both longitudinal and transverse reinforcement in

resisting the applied torque on a reinforced concrete section. It is difficult to determine the precise ratio of longitudinal steel to stirrups for both of them to yield simultaneously for better utilization of reinforcement. This ratio, normally termed the balanced volume ratio, m_b, has been investigated on reinforced rectangular beams under pure torsion by Hsu (refs. 1, 3) who found that m_b may vary within a range depending on the total percentage of steel. He suggested the following approximate range:

$$0.7 < m_b \, f_{yl}/f_{ys} < 1.5 \qquad\qquad (9.1)$$

where f_{yl}, f_{ys} = yield values of longitudinal and transverse reinforcement respectively

The ACI and British codes determine the required area of longitudinal steel by employing the principle of equal volume whereby the longitudinal reinforcement is taken as equal in volume to that of the stirrups, suitably adjusted for any differences in yield strengths. Although this is simple and hence attractive for design purposes it may not result in the most effective utilization of the reinforcement. However, this point needs more investigation, in particular using physical experiments.

9.4 Conclusions and Design Recommendations
9.4.1 Conclusions
From the main points discussed at the end of each of the previous sections, the following conclusions are drawn:
(1) Numerical parametric studies are some of the most useful applications of properly tried and tested nonlinear finite element models. In a time of continuously decreasing

computing cost the finite element method can provide a powerful and relatively economical means of investigating the behaviour of reinforced concrete elements and structural systems subject to various stress resultants. Structural variables can be studied to complement experimental results to broaden the scope of the investigation before arriving at additional conclusions.

(2) Size effect is important in pure torsion of reinforced concrete solid L-sections. The law of similitude is not applicable in this case. For the same reinforcement ratio, same material properties and same ratios of cross sectional dimensions (i.e. flange width-to-depth etc.), a particular percentage increase in the cross sectional area results in a higher percentage increase in the ultimate torque.

(3) Proper detailing of torsional reinforcement is vital for solid flanged sections in order to ensure the desired ductility and the ultimate torques. For the same quantity of longitudinal and transverse steel, one layer of steel in the flange results in a substantially reduced ductility and a considerably less ultimate torque than if the same amount of stirrups were provided as closed stirrups in both web and flange. Completely unreinforced flange results in a brittle failure caused by crushing of the flange at the junction of web and flange.

(4) The variation of the longitudinal reinforcement indicated the importance of both longitudinal bars and stirrups in resisting the applied torque. For the same total volume ratio of reinforcement, the ultimate torque for two

similar models was practically the same despite them having
different allocations of longitudinal and transverse steel.
This point, however, needs further investigation which must
involve physical experiments, because the codes of practice
generally use the principle of equal volumes to determine
the amount of longitudinal reinforcement from that of the
stirrups. This may not necessarily result in the best
utilization of reinforcement.

9.4.2 Design Recommendations

The following suggestions arise from both the experimental
results and the results of the parametric study. Because of
the limitted number of the experiments they are only
"Tentative Design Recommendations" associated directly with
the current British Code (BS8110-1985) torsion design
procedure and will certainly require additional supportive
results.

(1) The permissible torsional shear stress v_{tmin} can be
increased to become the splitting strength of concrete
divided by a factor of safety of say 2.0.

(2) The minimum stirrup spacing might be increased to become
$(x_1+y_1)/2$, $y_1/2$ or 200 mm whichever the less, instead of the
present limit of x_1, $y_1/2$ or 200 mm for small sections.

(3) A separate term accounting for concrete contribution is
necessary similar to the ACI Code and the CEB-FIP Model
Code. This term could be based on the elastic ultimate
torque of plain concrete. It is suggested that half the
elastic ultimate torque is to be considered (implying a

factor of safety of 2). Therefore:

$$T_e = \alpha(x^2 y f'_t)/2 \qquad (9.2)$$

It follows that the code's design equation becomes:

$$T_s = \sum \left(\frac{A_{sv}}{s_v}\right) 0.8 x_1 y_1 (0.87 f_y) \qquad (9.3)$$

where T_s is the steel contribution, i.e. the ultimate torque
for the reinforced concrete L-section is given by:

$$T = \sum T_s + \sum T_e \qquad (9.4)$$

(4) For large sections, more concrete contribution is
expected as indicated by the results of the parametric
study. Therefore suggestion (3) becomes more necessary in
this case otherwise uneconomical use of steel will result.

(5) Use of closed stirups in all rectangular components is
vital and hence it is important to follow the code's
recommendation of this type of stirrups.

* Reference specimen B11 is redesigned following these
suggestions and this is given in Appendix D.

Table (9.1) Details of the parametric study

Model	h (mm)	b_w (mm)	b (mm)	h_f (mm)	$\frac{h}{b_w}$	$\frac{b}{b_w}$	$\frac{h_f}{b_w}$	$\frac{b}{h_f}$	ρ_l	ρ_v	ρ_t	Φ (mm)	s (mm)	A_c (mm²)	Longitudinal Bar Diameters		
															1	2	3
B11	300	200	400	100	1.5	2.0	0.5	4.0	0.927	1.073	2.0	6	50	80	16	12	8
B13										0.565	1.492	6	100		16	12	10
N21	300	200	400	100	1.5	2.0	0.5	4.0	0.927	1.073	2.0	6	42	80	15.4	-	15.4
N31	400	250	500	130	1.6	2.0	0.52	3.85	0.929	1.073	2.002	8	54	132.5	20	16	10
N41	450	300	600	150	1.5	2.0	0.5	4.0	0.950	1.073	2.02	8	40	180	20	20	12
N43										0.565	1.515	6	42				
N51	300	200	400	100	1.5	2.0	0.5	4.0	0.927	1.073	2.0	6	35	80	15.4	-	15.4
N71	300	200	400	100	1.5	2.0	0.5	4.0	0.464	1.073	1.537	6	50	80	11.3	8.5	5.7
N81	350	230	460	115	1.5	2.0	0.5	4.0	0.940	1.073	2.013	8	67	106.95	16	16	8
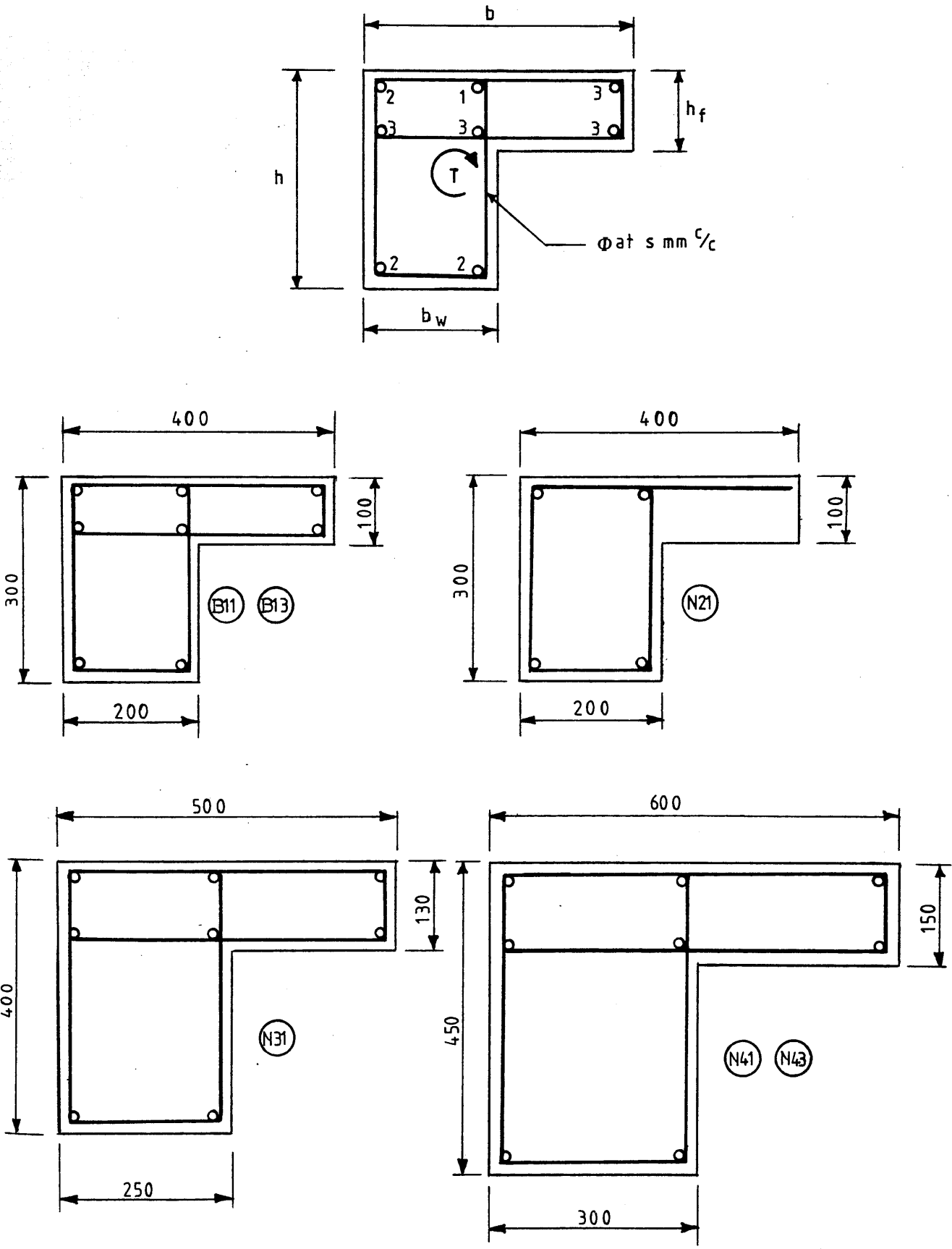
Figure (9.1) Details of cross sections used for the parametric study
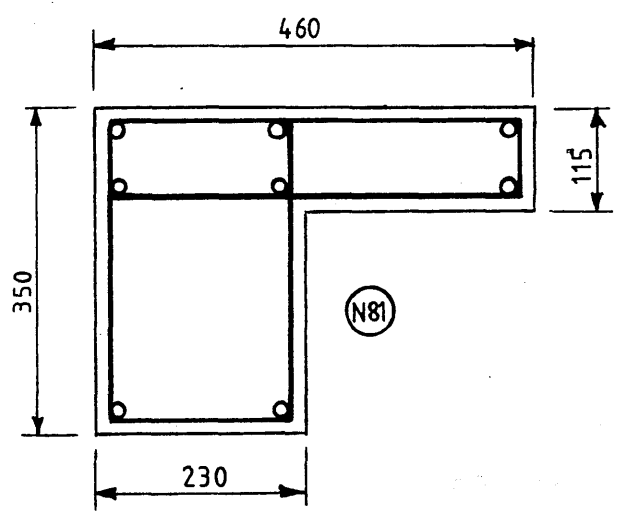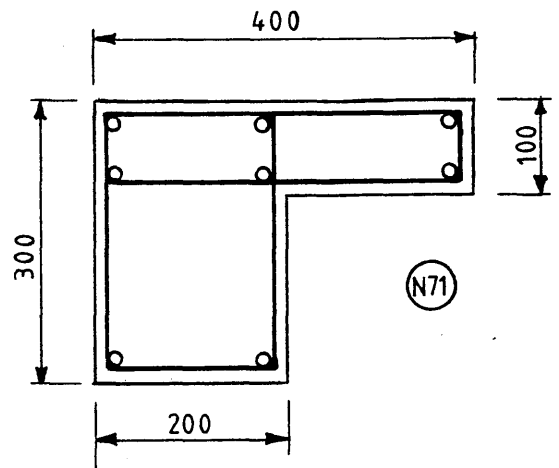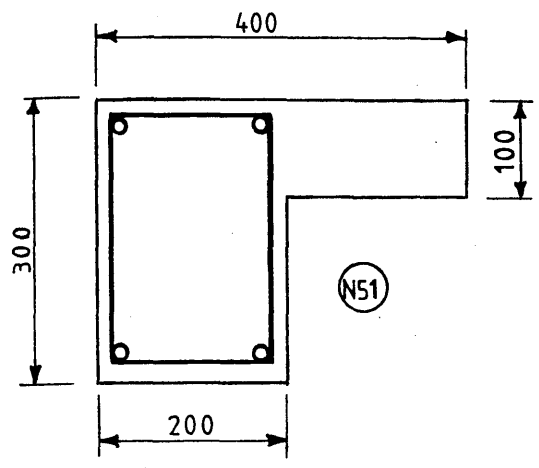
Figure (9.1) Continued

Table (9.2) Effect of the size of cross section, for the same volume ratios of longitudinal and transverse reinforcement, on the ultimate torque

Model	$\sum x^2 y \times 10^6$ mm^3	$\dfrac{\sum x^2 y}{\sum (x^2 y)}*$	T_u KN.m	$\dfrac{T_u}{T_u}$	ρ_v	ρ_l	ρ_t
B11	14.00	1.00	23.95	1.000	1.073	0.927	2.000
N81	21.56	1.54	49.0	2.046	1.073	0.940	2.013
N31	29.23	2.09	80.0	3.340	1.073	0.929	2.002
N41	47.25	3.38	96.0	4.008	1.073	0.950	2.023
B13	14.00	1.00	19.66	1.000	1.073	0.565	1.492
N43	47.25	3.38	76.0	3.866	0.950	0.565	1.515

Table (9.3) Pre- and post-cracking torsional stiffnesses of specimens B11, N81, N31 and N41

Specimen	B11	N81	N31	N41
$K_{cr} \times 10^6$ KN.mm^2/deg.	6.12	8.93	15.14	36.91
$K_\theta \times 10^6$ (St. Venant's)	87.80	152.64	225.40	436.06
$K_o \times 10^6$ (Predicted)	73.92	142.67	213.78	401.33

Table (9.4) Effect of detailing the same amount of reinforcement
on the ultimate torque and the post-cracking
torsional stiffness for the same cross section

Specimen	T_u KN.m	$\dfrac{T_u}{T_u(B11)}$	K_{cr} x10^6 KN.mm^2/deg.
B11	23.95	1.000	7.100
N21	18.0	0.752	3.563
N51	16.0	0.668	1.281

Table (9.5) Effect of varying the longitudinal and transverse
reinforcement by the same amount on the ultimate
torque and the post-crcaking torsional stiffness

Specimen	T_u KN.m	$\dfrac{T_u}{T_u(B11)}$	K_{cr} x 10^6 KN.mm^2/deg.	ρ_l	ρ_v	ρ_t
B11	23.95	1.000	7.100	1.073	0.927	2.000
B13	19.66	0.821	4.800	0.565	0.927	1.492
B71	20.4	0.852	4.438	1.073	0.464	1.537

Table (9.6) Ultimate torque for specimens N41 and N43

Specimen	T_u KN.m	$\dfrac{T_u}{T_u(N41)}$	ρ_l	ρ_v	ρ_t
N41	96.0	1.0	1.073	0.950	2.023
N43	76.0	0.625	0.565	0.950	1.515
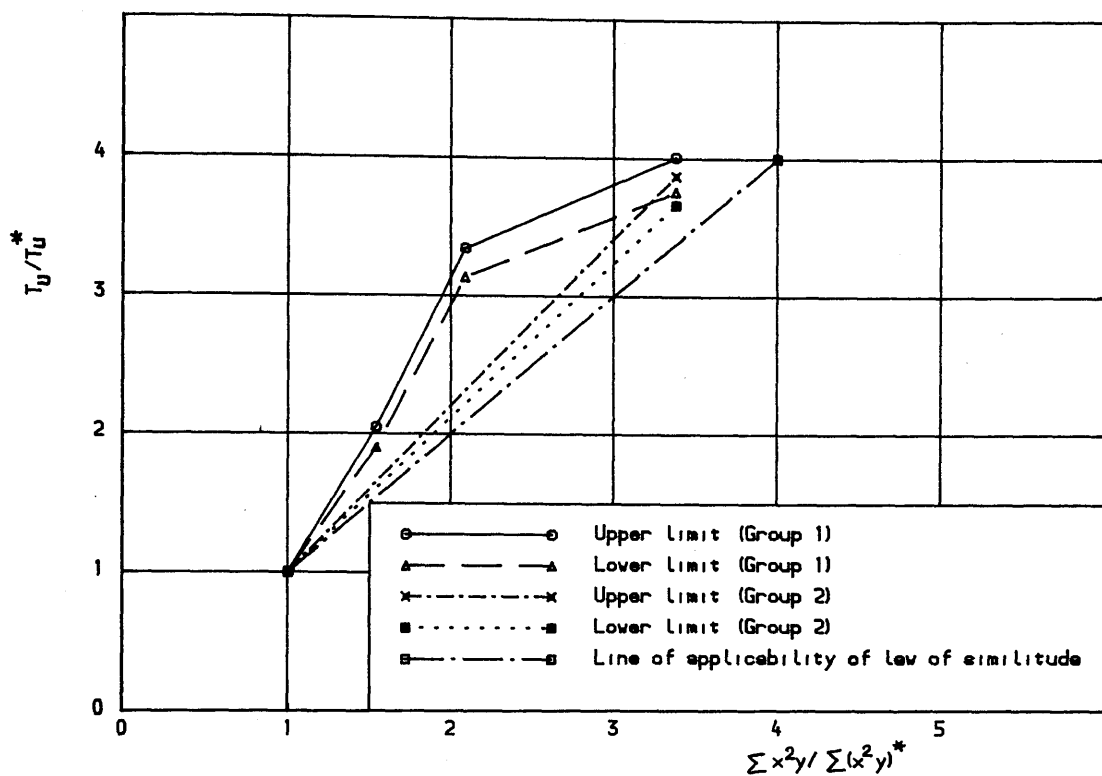
Figure (9.2) Size effect for the same ratios of longitudinal and
transverse reinforcement
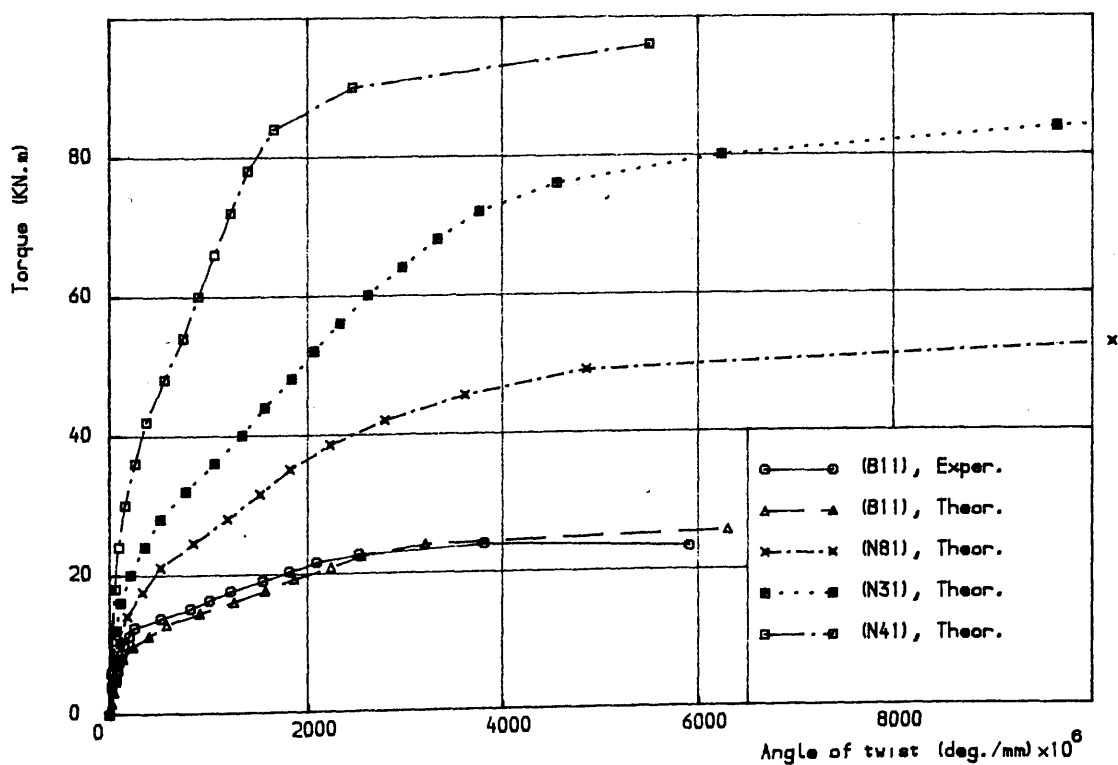
Figure (9.3) Torque-twist curves for models B11, N81, N31 and N41
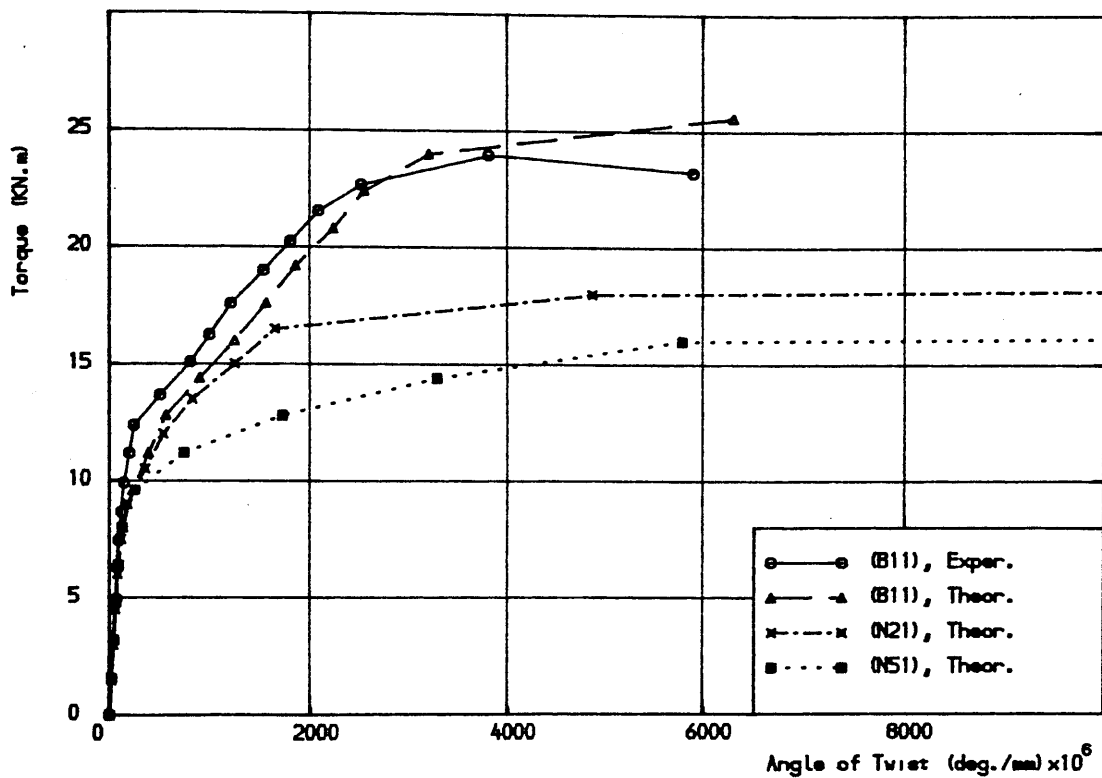
Figure (9.4) Torque-twist curves for models B11, N21 and N51

Max.= 337.0 N/mm^2

T = 18.9 KN.m

● Experimental values
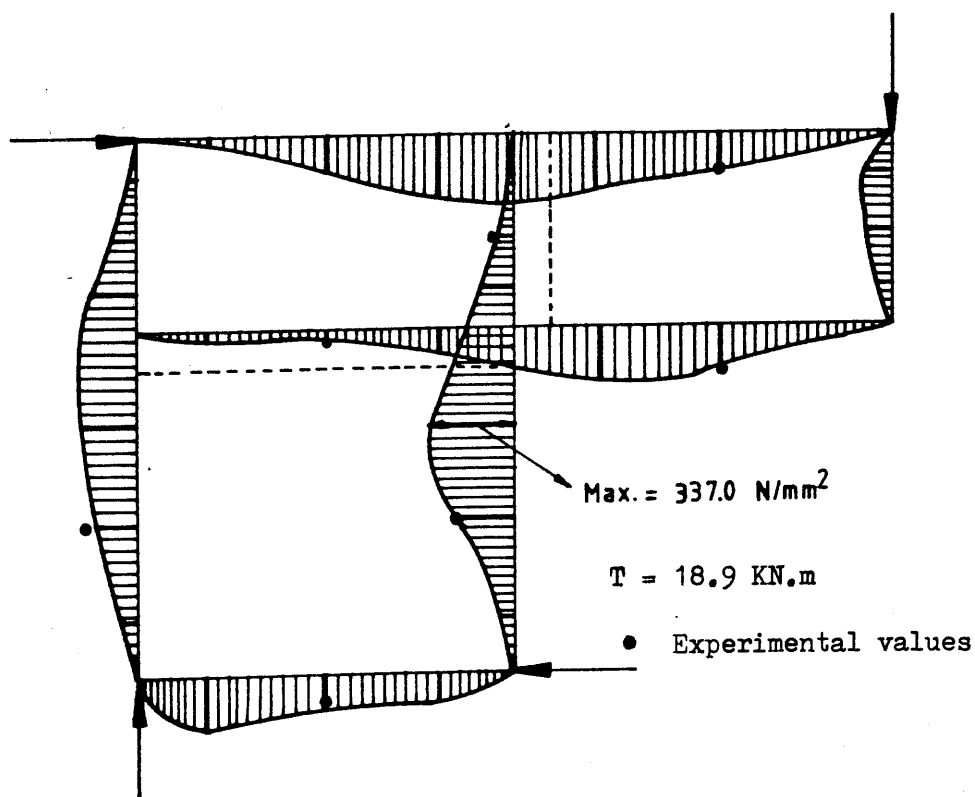
Figure (9.5) Strain distribution along all legs of a closed
stirrup for specimen (B11)
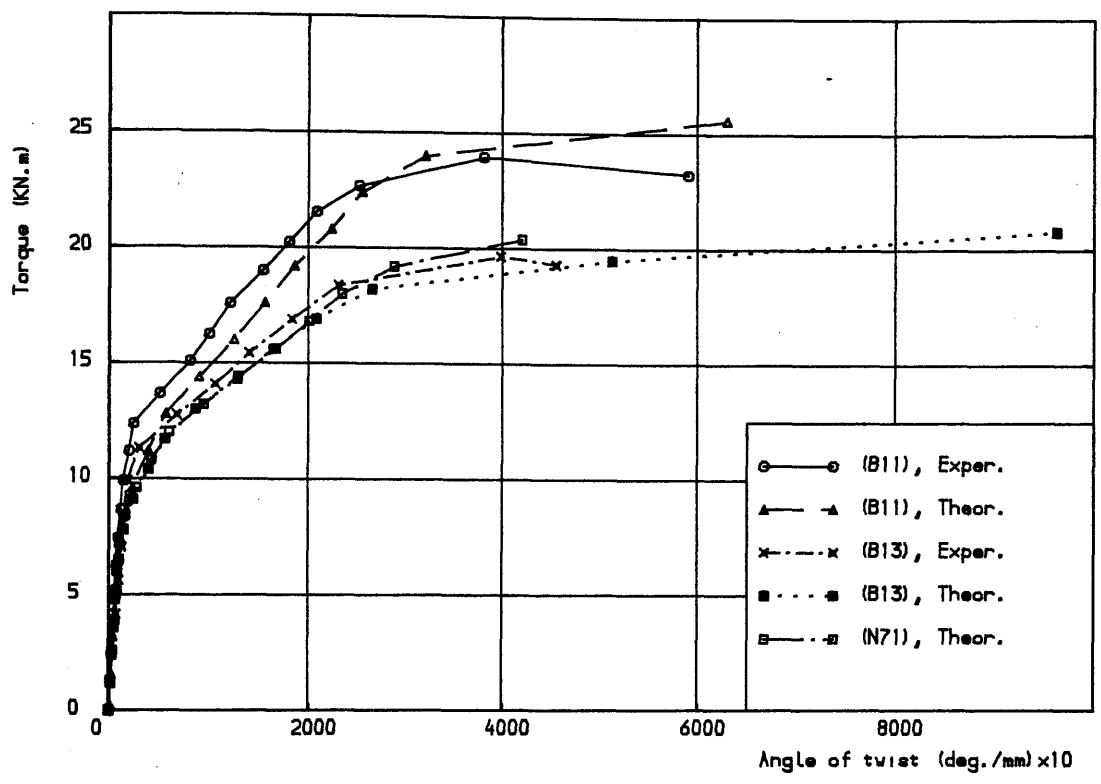
Figure (9.6) Torque-twist curves for models B11, B13 and N71
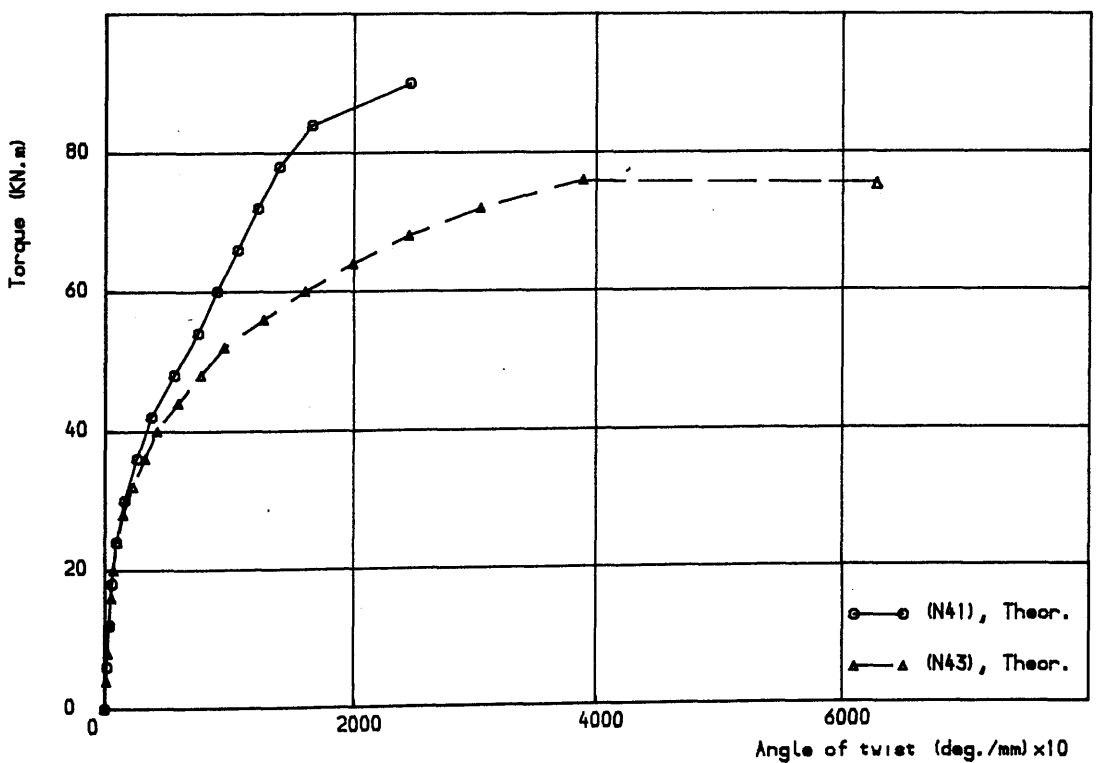
Figure (9.7) Torque-twsit curves for models N41 and N43

References

(1) Hsu, T.T.C., "Torsion of Structural Concrete - Behaviour of Reinforced Concrete Rectangular Members", ACI Special Publication, SP18, Torsion of Reinforced Concrete, Detroit, 1968, pp. 261-306.

(2) BS8110-1985, "British Standard Structural Use of Concrete", part 2, Code of Practice for Special Circumstances, London, 1985.

(3) Hsu, T.T.C., "Torsion of Reinforced Concrete", Van Nostrand Reinhold Co., 1984.

(4) Hsu, T.T.C., "Ultimate Torque of Reinforced Rectangular Beams", Jour. Struct. Div., ASCE, Vol. 94, No. ST2, Feb., 1968, pp. 485-510.

(5) Park, R. and Paulay, T., "Reinforced Concrete Structures", Wiley, 1975.

CHAPTER TEN

CONCLUSIONS, COMMENTS AND SUGGESTIONS FOR FURTHER WORK

10.1 General Conclusions

On the basis of the different analyses carried out it is concluded that the nonlinear three dimensional finite element model developed in this work predicts within acceptable accuracy the short-term behaviour of a variety of reinforced concrete structures as long as certain conditions are observed. In particular the pure and combined torsional behaviour of rectangular beams and the pure torsional behaviour of L-sections were all predicted well.

From the experimental investigation it is concluded that the current British Code torsion design provisions are too far on the conservative side. It results in underestimation of the torsional capacity of properly reinforced concrete L-sections and therefore an uneconomical use of reinforcement.

Numerical parametric studies are some of the most useful applications of properly tried and tested nonlinear finite element models, where structural variables can be studied to complement experimental results to broaden the scope of the investigation before arriving at additional conclusions.

10.2 Detailed Conclusions

The main detailed conclusions from the various aspects of this study are summarised as follows:

(A) Applications of the Finite Element Model

(1) Satisfactory predictions can be obtained by the finite element model provided that attention is paid to the guidelines set regarding tension stiffening, shear retention

parameters and other numerical parameters e.g. increment size, convergence tolerance, mesh size and boundary conditions.

(2) For torsional applications the boundary conditions must be carefully chosen to allow for proper warping behaviour to take place. "Reduced" boundary conditions at the supported end of a beam allow such behaviour to occur and are therefore recommended. For example, four nodes one at the centre of each side of a rectangular section are adequate.

(3) The shear retention factor plays a major role in the analysis of structures subjected to torsional stresses, and for the shear retention model used the following values are recommended: $\beta_1 = 0.5$, $\beta_2 = 0.1$ and $\beta_3 \epsilon_t' = 0.003$.

(4) Care must be exercised when applying the model in a particular situation. In general, when shear dominates the shear retention factor is more important and the tension stiffening model can be made inactive or used with very small values of its parameters ($\alpha_1 < 0.5$ and $\alpha_2 < 5.0$). When flexure dominates the tension stiffening parameters may be important and hence could be used but again with small values of α_1 and α_2. Tension stiffening overestimates the stiffness in the early part of the load-deflection curves (or torque-twist curves) and underestimates steel strains without significantly affecting the ultimate load predictions

(5) The smeared fixed orthotropic crack model is an adequate approximation as long as the above points regarding the tension stiffening and shear retention models are observed.

(6) All conclusions and guidelines for torsion analysis of rectangular sections are also applicable to the more complicated situation of solid L-sections. These concern the boundary conditions, material parameters in particular the shear retention and tension stiffening effects and mesh selection schemes.

(7) A major observation is that for high volume reinforcement ratios, above about 2.5% for the total amount of steel, the finite element model tend to overestimate the ultimate torque despite the reasonable predictions otherwise. This is attributed to the unsuitability of the full bond assumption used in the finite element model. With high steel ratios the behaviour seems to be more sensitive to the bond-slip phenomenon which did not affect the analysis of all sections with steel ratios lower than 2.5%. With the present finite element model lower values of the shear retention parameters than those recommended above may be used to reduce the degree of overestimation. It may also be required to modify the program to provide better simulation of bond-slip behaviour. This needs reformulation of the embedded bars.

(8) The predicted steel response indicate the importance of the proper simulation of reinforcing steel, achieved here through embedded bars placed at their exact positions as they appear in the structure.

(B) Experimental Study

(1) The code torsion design procedure is found too conservative as it grossly underestimates the section torsional capacity. An instant reason is the limit on

stirrup spacing as this is based on the smallest dimension of the component rectangles. Relaxation of this limit would result in a more economical use of reinforcement.

(2) The design equation:

$$T = \left(\frac{A_{sv}}{s_v}\right) 0.8 x_1 y_1 (0.87 f_{yv})$$

is, in principle, quite applicable but modification of the factor 0.8 appears to be necessary to reduce its present conservative nature. The results indicate that the factor 0.8 may be eliminated.

(3) The applied torques at 0.3 mm crack width were higher than the design torque of the reference specimen of each group even for the reduced volume ratios of stirrups, an observation that supports the above two points.

(4) Behaviour was essentially linear until cracking of concrete. The slope of this linear part of torque-twist curve is independent of the amount of torsional reinforcement. After cracking the steel strains/stresses and the concrete surface strains increase rapidly and continue to increase thereafter until failure.

(5) Reduction of transverse reinforcement, for the same amount of longitudinal steel, reduces both the post-cracking torsional stiffness and the ultimate torque. However, a particular percentage reduction results in a lesser percentage reduction of ultimate torque, allowing more utilization of longitudinal steel.

(6) Stirrup spacing effects both the crack width and

spacing. Closely spaced stirrups results in closely spaced fine cracks. Larger stirrup spacing results in widely spaced cracks but with larger crack widths. Sudden failures and crushing of concrete may occur in torsional specimens with large stirrup spacing (larger than about 100 mm for small sections).

(7) Use of larger stirrup diameter with larger spacing instead of smaller stirrup diameter, giving the same amount of transverse reinforcement, with the same amount and distribution of longitudinal steel, produces practically the same ultimate torque.

(8) The cracking torque increases slightly with the increase in the volume ratio of transverse reinforcement, for the same cross section and longitudinal steel. A 1% increase in the volume ratio of transverse reinforcement results in about 15%-25% increase in the crcaking torque.

(9) Large reductions of torsional stiffness occur after cracking of concrete. The percentage ratio of post- to pre-cracking stiffness may fall within the range 7% - 13%.

(10) Very-large rotations are necessary for the torsional members to develop their ultimate torques. The ratio of twist at failure to that at cracking was found to vary between 12 and 20.

(C) Parametric Study

(1) The size effect is important in pure torsion of reinforced concrete solid L-sections. The law of similitude is not applicable. For the same reinforcement ratio, same material properties and same ratios of cross sectional

dimensions (i.e. flange width-to-depth etc.), a particular percentage increase in the cross sectional area results in a higher percentage increase in the ultimate torque.

(2) Proper detailing of torsional reinforcement is vital for solid flanged sections in order to ensure the desired ductility and the ultimate torques. For the same quantity of longitudinal and transverse steel, one layer of steel in the flange results in a substantially reduced ductility and a considerably less ultimate torque than if the same amount of stirrups were provided as closed stirrups in both web and flange. Completely unreinforced flange results in a brittle failure caused by crushing of the flange at the junction of web and flange.

(3) The variation of the longitudinal reinforcement indicates the importance of both longitudinal bars and stirrups in resisting the applied torque. For the same total volume ratio of reinforcement, the ultimate torque for two similar models was practically the same despite them having different allocations of longitudinal and transverse steel. This point, however, needs further investigation which must involve physical experiments, because the codes of practice generally use the principle of equal volumes to determine the amount of longitudinal reinforcement from that of the stirrups. This may not necessarily result in the best utilization of reinforcement.

10.3 Suggestions for Further Work

Extensions of this study can be conveniently grouped as follows:

(1) Further Applications of the Finite Element Program:

(a) The program in its present state is readily available for detailed study of various reinforced concrete structures. In particular, the influence of many parameters can be isolated and studied.

(b) Detailed parametric studies can also be performed to investigate other parameters not covered in Chapter Nine. One immediate suggestion is the case of combined torsion and bending where the ratio of moment to torque is varied.

(c) Applications to other cases of pure and combined torsion include T- and I-sections. The guidelines regarding boundary conditions, load application, shear retention and tension stiffening parameters will be very useful in these cases.

(2) Developments of the Finite Element Program:

(a) The program requires a fully automatic mesh generator to be incorporated. This will considerably reduce time spent in data preparation and serve as a first step for automatic plotting of crack patterns and distorted shapes of the structure during the various loading stages.

(b) The various plotting routines, which are now separate programs, can also be incorporated in the analysis program.

(c) Some of the recent numerical techniques can be used in conjunction with the material models instead of the Newton-Raphson method. Eexamples of such techniques are the so-called BFGS method and the arc-length method.

(d) A re-start facility would also be of good benefit as it allows intermediate checkpoints during the analysis process.

(e) Proper modelling of bond-slip behaviour can be tried. This might be done by either modifying the set of matrices derived in Chapter Three for simulation of steel reinforcement or incorporating a suitable bond-slip law.

(f) The reinforcement is at present restricted to run parallel to the local coordinates of the embedded concrete element. Although this did not affect any of the applications undertaken, it may be necessary to include for the likely case of inclined bars or when the mesh subdivision requires some element boundaries to make angles with the embedded bars. Such a development requires a new derivation of the governing equations of Chapter Three assuming the general case of inclined embedded bars.

(g) Automatic load incrementation scheme might be a useful inclusion for monitoring behaviour near ultimate conditions.

(3) Experimental Studies

(a) More variables to expand the present set of experiments include variation of longitudinal reinforcement, size effect for the same volume ratio and distribution of longitudinal and transverse steel, concrete strength and detailing of the same amount of reinforcement.

(b) Combined torsion and bending is undoubtedly the first obvious expansion after (a) above.

(c) Other properly reinforced flanged sections (I and T) need detailed experimental studies under both pure and combined torsion.

APPENDIX A

DESIGN OF REFERENCE SPECIMENS

Specimen B11

Design ultimate torque = 8.0 KN.m

Assume:

high yield steel f_y = 410 N/mm^2,

6 mm stirrups (area of two legs = 56 mm^2)

concrete grade 40 - v_{tmin}=0.42 N/mm^2 and v_{tu}=4.75 N/mm^2

Flange

x_1 = 100-2x20-6 = 54 mm, y_1 = 200-2x20-6 = 154 mm

$h^3_{min} h_{max}$ = 100^{3}x200 = 2.0 x 10^8

T_1 = (2/25.2) x T = 0.635 KN.m

$$v_t = \frac{2T}{h^2_{min}(h_{max}-h_{min}/3)} = \frac{2 \times 0.635 \times 10^6}{100^2[200 - 100/3]} = 0.762 > v_{tmin}$$

.. torsion reinforcement required

y_1 = 154 < 550 i.e. section is small

v_{tu} x y_1/550 = 4.75 x (154/550) = 1.33 N/mm^2

.. v_t < 1.33   .. section is feasible

$$\text{Links:} \quad \frac{A_{sv}}{s_v} > \frac{T_1}{0.8x_1y_1(0.87f_y)} = \frac{0.635 \times 10^6}{0.8 \times 54 \times 154(0.87 \times 410)} = 0.268$$

.. s_v < 56/0.268 = 209 mm

but s_v should be least of x_1, y_1/2 or 200 mm

.. **Provide 6 mm links @ 50 mm c/c**

Longitudinal Steel: A_{sl} > $(A_{sv}/s_v)(f_{yv}/f_{yl})(x_1+y_1)$

> (56/50)x 1x(54+154) = 233 mm^2

.. **Provide 4 bars 8 mm dia. (A = 200 mm^2)**

<u>W e b</u>

$x_1 = 200 - 2 \times 20 - 6 = 154$ mm, $y_1 = 300 - 2 \times 20 - 6 = 254$ mm

$h^3{}_{min}h_{max} = 200^3 \times 300 = 23.2 \times 10^8$

$T_2 = (23.2/25.2) \times T = 7.365$ KN.m

$$v_t = \frac{2T}{h^2{}_{min}(h_{max} - h_{min}/3)} = \frac{2 \times 7.365 \times 10^6}{200^2[300 - 200/3]} = 1.578 > v_{tmin}$$

.. torsion reinforcement required

$y_1 = 254 < 550$ i.e. section is small

$v_{tu} \times y_1/550 = 4.75 \times (254/550) = 2.194$ N/mm^2

.. $v_t < 2.194$ .. section is feasible

Links: $\dfrac{A_{sv}}{s_v} > \dfrac{T_1}{0.8 x_1 y_1 (0.87fy)} = \dfrac{7.365 \times 10^6}{0.8 \times 154 \times 254 (0.87 \times 410)} = 0.660$

.. $s_v < 56/0.687 = 84$ mm

but sv should be least of x1, y1/2 or 200 mm

.. <u>Provide 6 mm links @ 50 mm c/c</u>

Longitudinal Steel: $A_{sl} > (A_{sv}/s_v)(f_{yv}/f_{yl})(x_1 + y_1)$

$> (56/50) \times 1 \times (154 + 254) = 457$ mm^2

.. <u>Provide 4 bars 12 mm dia. ($A = 452$ mm^2)</u>

Arrangement of longitudinal steel reinforcement involved provision of a 16 mm bar instead of (8mm + 12mm) bars at the junction of web and flange.

<u>Specimen B31</u>

Design ultimate torque = 8.0 KN.m

Assume:

high yield steel fy = 410 N/mm^2,

6 mm stirrups (area of two legs = 56 mm^2)

concrete grade 40 - $v_{tmin} = 0.42$ N/mm^2 and $v_{tu} = 4.75$ N/mm^2

<u>Flange</u>

$x_1 = 100-2 \times 20-6 = 54$ mm, $y_1 = 260-2 \times 20-6 = 214$ mm

$h^3_{min} h_{max} = 100^3 \times 260 = 2.6 \times 10^8$

$T_1 = (2.6/10.65) \times T = 1.953$ KN.m

$$v_t = \frac{2T}{h^2_{min}(h_{max}-h_{min}/3)} = \frac{2 \times 1.953 \times 10^6}{100^2[260 - 100/3]} = 1.723 > v_{tmin}$$

.. torsion reinforcement required

$y_1 = 214 < 550$ i.e. section is small

$v_{tu} \times y_1/550 = 4.75 \times (214/550) = 1.848$ N/mm^2

.. $v_t < 1.848$ .. section is feasible

Links: $\dfrac{A_{sv}}{s_v} > \dfrac{T_1}{0.8 x_1 y_1 (0.87 f_y)} = \dfrac{1.953 \times 10^6}{0.8 \times 54 \times 214 \times 0.87 \times 410)} = 0.592$

.. $s_v < 56/0.592 = 95$ mm

but s_v should be least of x_1, $y_1/2$ or 200 mm

.. <u>Provide 6 mm links @ 50 mm c/c</u>

Longitudinal Steel: $A_{sl} > (A_{sv}/s_v)(f_{yv}/f_{y1})(x_1+y_1)$

$> (56/50) \times 1 \times (54+214) = 300$ mm^2

.. <u>Provide 4 bars 10 mm dia. (A = 314 mm^2)</u>

<u>Web</u>

$x_1 = 140-2 \times 20-6 = 94$ mm, $y_1 = 300-2 \times 20-6 = 254$ mm

$h^3_{min} h_{max} = 140^3 \times 300 = 7.96 \times 10^8$

$T_2 = (7.96/10.56) \times T = 6.030$ KN.m

$$v_t = \frac{2T}{h^2_{min}(h_{max}-h_{min}/3)} = \frac{2 \times 6.030 \times 10^6}{140^2[300 - 140/3]} = 2.429 > v_{tmin}$$

.. torsion reinforcement required

$y_1 = 254 < 550$ i.e. section is small

$v_{tu} \times y_1/550 = 4.75 \times (254/550) = 2.107$ N/mm^2

.. $v_t > 2.107$ but only slightly

Links: $\dfrac{A_{sv}}{s_v} > \dfrac{T_1}{0.8x_1y_1(0.87f_y)} = \dfrac{6.030 \times 10^6}{0.8 \times 94 \times 254 \times (0.87 \times 410)} = 0.885$

$\therefore s_v < 56/0.885 = 63$ mm

but s_v should be least of x_1, $y_1/2$ or 200 mm

$\therefore$ Provide 6 mm links @ 50 mm c/c

Longitudinal Steel: $A_{sl} > (A_{sv}/S_v)(f_{yv}/f_{yl})(x_1 + y_1)$

$> (56/50) \times 1 \times (94 + 254) = 390$ mm^2

$\therefore$ Provide 4 bars 12 mm dia. (A = 452 mm^2)

Arrangement of longitudinal steel involved the provision of a 16 mm bar instead of (10mm ÷ 12mm) bars at the junction of web and flange.

APPENDIX (B)

BRIEF DESCRIPTION OF THE DEVELOPED FINITE ELEMENT PROGRAM

The program analyses nonlinear three dimensional stress problems using 20-noded isoparametric elements for concrete and embedded bars for reinforcing steel. The bars can be of any number and can be embedded anywhere within the concrete elements, the only restriction being that they must be parallel to the local coordinates (ξ, η, ζ) of the basic concrete element.

The incremental-iterative method is used to solve the nonlinear equations. The resulting linear equations are solved by a Frontal technique, earlier described[1] and later modified[2] by Hinton and Owen to include buffer storage area in order to reduce the cost of the analysis. The program includes a triaxial short-term constitutive equations for concrete, due to Ottosen, a three dimensional cracking model, and a bilinear stress-strain law for steel which accounts for strain-hardening effects. Post-cracking behaviour of concrete is treated through shear retention and tension stiffening models.

Fully automatic mesh generation is not included. Instead a semi-automatic generator is included for regular solid meshes only. Coordinates of midside nodes are always automatically generated. Because of the enormous amount of output that can result, the output required is generally left to be chosen at will. The displacements of all nodal points are always printed. The cracking situation, crushing

situation and steel strains and stresses are printed for all elements. Output of normal, shear and principal stresses and strains in concrete can be chosen for each element at will within a very flexible scheme, this being the major source of the lengthy output.

A list of all subroutines is shown next, followed by a brief description of their role. A chart illustrating the relationship between each subroutine is provided at the end of this section followed by a data preparation user manual. The program is full of comment statements to ensure easy follow-up of all operations for any future developments.

(1) Hinton, E. and Owen, D.R.J, "Finite Element Programming", Academic Press, 1977.

(2) Owen, D.R.J. and Hinton, E., "Finite Elements in Plasticity - Theory and Practice", Pineridge Press, Swansea, 1980.

List of Subroutines

1.	NONL3D	18.	RESIDU
2.	INPUT	19.	LINEAR
3.	ZERO	20.	SECYP
4.	CORNER	21.	BASTSS
5.	MIDSID	22.	SURF1
6.	ALGOR	23.	SURF2
7.	GAUSSQ	24.	PRINCI
8.	STIF3D	25.	PSARR
9.	BASTIF	26.	DIRECT
10.	LOAD3D	27.	CRACRU
11.	INCREM	28.	CONVER
12.	SFR3	29.	TRANSF
13.	JACOB3	30.	OUTPUT
14.	BMAT3D	31.	CHECK1
15.	MOD3D	32.	ECHO
16.	DBE	33.	CHECK2
17.	FRONT		

(1) Program NONL3D

This is the master subroutine from which all other subroutines are called.

(2) Subroutine INPUT

This reads the required information for geometry, boundary conditions, material properties for concrete and steel, and calls the required subroutines for data checking. The initial values for all material property constants are also set up and stored for later use.

(3) Subroutine ZERO

This initializes various arrays to zero for accumulation of loads, reactions, displacements, stresses etc.

(4) Subroutine CORNER

This generates coordinates of corner nodes for a solid regular mesh in a semi-automatic fashion.

(5) Subroutine MIDSID

This computes the coordinates of the midside nodes for the 20-noded isoparametric brick elements.

(6) Subroutine ALGOR

This sets the equation resolution index. The index indicates whether or not the system of equations is to be accompanied by a full reformulation of the element stiffnesses depending on the algorithm chosen, the current load increment and the current iteration.

(7)_Subroutine_GAUSSQ

This sets up the sampling (Gauss) point positions and weighting factors for numerical integration. The order of Gauss rule is restricted to either 2x2x2, 3x3x3 or 4x4x4.

(8)_Subroutine_STIF3D

This computes the stiffness matrix for the 20-noded isoparametric brick element accounting for the cracking, crushing and the material laws of concrete, as dictated by the components of the D-matrix passed on by subroutine MOD3D, and yielding of reinforcement treated in subroutine BASTIF.

(9)_Subroutine_BASTIF

This computes the stiffness of all the bars embedded within the basic concrete element and adds them into the appropriate places in the stiffness matrix before returning control back to subroutine STIF3D for storage.

(10)_Subroutine_LOAD3D

This computes the consistent nodal forces after reading the relevant data for any combination of five load types, namely: (1) nodal point loads, (2) gravity loading, (3) distributed loads on element edge, (4) thermal loading and (5) distributed loads on element face.

(11)_Subroutine_INCREM

This increments the load applied in subroutine LOAD3D. The total load applied during a typical load increment is the accumulative load of all the previous increments including

the current one.

(12)_Subroutine_SFR3

This calculates the shape functions and their derivatives for the 20-noded element.

(13)_Subroutine_JACOB3

This calculates the coordinates of all Gauss points, and the Jacobian matrix, its determinant and inverse for the the 20-noded element.

(14)_Subroutine_BMAT3D

This subroutine calculates the strain matrix [B] for the 20-noded element. It is also used for the bar elements as a special case of the main element.

(15)_Subroutine_MOD3D

This subroutine evaluates the material property matrix, [D], accounting for the stress state prevailing at the Gauss point in question ready for stiffness calculations.

(16)_Subroutine_DBE

This calculates the stress matrix [DB] for the 20-noded element.

(17)_Subroutine_FRONT

This solves the simultaneous equations by means of Gauss elimination and back substitution. The Frontal technique is used with a buffer storage facility to reduce the cost.

(18) Subroutine RESIDU

This subroutine reduces the stresses to the failure surface and evaluates the equivalent nodal forces.

(19) Subroutine LINEAR

This evaluates incremental stresses and strains assuming linear elastic behaviour.

(20) Subroutine SECYP

This reads in the current state of stress then computes and store secant values of Young's modulus and Poisson's ratio of concrete using Ottosen's constitutive equations.

(21) Subroutine BASTSS

This evaluates reinforcing bar stresses and brings down the stresses to the yield value or along the strain-hardening part in case yielding of steel occured.

(22) Subroutine SURF1

This evaluates, by direct internal iteration, the value of the third principal stress, σ_{3f}, and the second invariant of the deviatoric stress tensor at failure for the current state of stress using Ottosen's failure criterion.

(23) Subroutine SURF2

This evaluates the value of the third principal stress, σ_{3f}, and the second invariant of the deviatoric stress tensor at failure for the current state of stress using the Modified Coulomb failure criterion. This is an economically cheaper alternative to Ottosen's failure criterion (subroutine

SURF1), as no iteration is needed, though with lesser accuracy.

(24) Subroutine PRINCI

This calculates the principal stresses and strains and their directions at all Gauss points of the element.

(25) Subroutine PSARR

This simply arranges the principal stresses so that $\sigma_1 > \sigma_2 > \sigma_3$, required for Ottosen's constitutive equations.

(26) Subroutine DIRECT

This solves the three simultaneous equations needed for the evaluation of the direction cosines of the second and third principal stresses (σ_2 and σ_3) had the material cracked in one direction due to the first principal stress σ_1.

(27) Subroutine CRACRU

This deals with cracking and crushing of concrete using the appropriate criteria. For cracking, the offending principal stress is set to zero and the appropriate crack directions are fixed. For crushing, all stresses are set to zero.

(28) Subroutine CONVER

This checks the convergence of the iteration process using the residual forces method.

(29) Subroutine TRANSF

This subroutine sets up the transformation matrices used to transform the stresses and strains to the required

directions.

(30) Subroutine OUTPUT

This outputs displacements, reactions, stresses in concrete and steel, Gauss point coordinates, concrete cracking and crushing situations, and yielding situation of reinforcement. To avoid excessive amount of output selective items can be chosen at will.

(31) Subroutine CHECK1

This checks the control parameters read in subroutine INPUT to ensure that they all have values ranging within the specified description in the manual. Any error detected is given an appropriate number which can be checked to indicate the source.

(32) Subroutine ECHO

This is called if any error is detected in CHECK1 or CHECK2. The main purpose is to stop the program execution and to print any remaining unread data cards.

(33) Subroutine CHECK2

This checks any identical information given with regard to coordinates and nodal connections. The most useful check in this subroutine is the one which ensures that the maximum frontwidth does not exceed the value specified in subroutine FRONT.

Chart showing the relationship between the subroutines of the developed
nonlinear three dimensional finite element program

DATA PREPARATION MANUAL FOR PROGRAM NONL3D
FOR THREE DIMENSIONAL NONLINEAR ANALYSIS
OF REINFORCED CONCRETE STRUCTURES

CARD SET 1 TITLE CARD(12A6)-One Card

| Cols. 1-72 TITLE | Title of the problem - limited to 72 alphanumeric characters |

CARD SET 2 CONTROL CARD(13I5)-One Card

Cols. 1-5 NPOIN	Total number of nodal points
6-10 NELEM	Total number of elements
11-15 NVFIX	Total number of restrained boundary points - where one or more degrees of freedom are restrained
16-20 NMATS	Total number of different materials
21-25 NGAUS	Order of integration formula for numerical integration (2, 3 or 4 Gauss Rules can be used but 3 is recommended for monitoring nonlinear behaviour especially cracking)
26-30 NALGO	Parameter controlling nonlinear solution algorithm: 1-Initial stiffness method. The element stiffnesses are computed at the beginning of the analysis and remain unchanged thereafter 2-Secantial stiffness method. The element stiffnesses are recomputed during each iteration of each load increment 3-Combined algorithm. The element stiffnesses are recomputed for the first iteration of each load increment only 4-Combined algorithm. The element stiffnesses are recomputed for the second iteration of each load increment only (of course for the first load increment, the element stiffnesses must be calculated for the first iteration also) 5-Combined algorithm. The element stiffnesses are recomputed for the first and eighth iteration of each load increment. For the purpose of this work a maximum number of iteration of 15 was adopted 6-Combined algorithm. The element stiffnesses are recomputed at the first, sixth, eleventh and fifteenth iteration of each load increment.
31-35 NCRIT	The failure criterion to be employed in conjunction with Ottosen Constitutive Equations for concrete: 1-Ottosen four-parameter failure criterion 2-Modified Coulumb criterion
36-40 NINCS	The total number of load increments to be applied
41-45 NCORN	Parameter for semi-automatic mesh

generation:

0-When the mesh is for irregular solid structure (I,L,T beams, or rectangular beams and slabs when irregular mesh is to be used). In this case the coordinates of all corner nodes must be input and Card Sets 5 and 6 must be omitted

1-When the mesh is for regular solid structure (rectangular beams and slabs). In this case no nodal coordinates of any point are to be input, instead Card Sets 5 and 6 must be used

46-50 NSTYP   Number of steel types used (different bar diameters or different material properties)

51-55 NREPL   Parameter controlling the use of the whole program for plain or reinforced concrete:

0-For plain concrete. In this case Card Sets 8 and 11 must be omitted

1-For reinforced concrete. In this case Card Sets 8 and 11 must be used

56-60 NTSTI   Parameter controlling the use or otherwise of the tension stiffening model:

0-Tension stiffening model not to be used

1-Tension stiffening model to be used

61-65 NCMOD   Parameter controlling the crushing model to be used:

1-The first model where crushing is assumed when the minimum principal compressive stress exceeds the uniaxial value for concrete regardless of whether the Gauss point has already cracked or not

2-The second model where crushing is checked by using Von Mises failure envelope in strain space for any Gauss point with at most one crack present, otherwise the uniaxial value is used as in the first model

<u>CARD SET 3 ELEMENT CONNECTION, REINFORCEMENT, AND OUTPUT</u>
<u>CARDS(16I5)</u>-Two cards for each element, from column 1 to 80 in the first card and from column 1 to 55 in the second card. Total = 2*NELEM cards.

<u>First card:</u>

Cols. 1-5   NUMEL   Element number

      6-10   MATNO(NUMEL)   Material property number

      11-15   LNODS(NUMEL,1)   1st Nodal connection number

      16-20   LNODS(NUMEL,2)   2nd Nodal connection number

      21-25   LNODS(NUMEL,3)   3rd Nodal connection number

              .   .

              .   .

              .   .

      76-80   LNODS(NUMEL,14) 14th Nodal connection number

<u>Second card:</u>

```
Cols.  1-5   LNODS(NUMEL,15)15th Nodal connection number
       6-10  LNODS(NUMEL,16)16th Nodal connection number
              .                      .
              .                      .
              .                      .
      26-30  LNODS(NUMEL,20)20th Nodal connection number
      31-35  MATNO1(NUMEL)   Element reinforcement identifier:
                             0-The element contains no bars passing
                             through
                             1-The element contains bar(s) passing
                             through
      36-40  MATNO2(NUMEL)   Number of reinforcing bars parallel
                             to the x-direction
      41-45  MATNO3(NUMEL)   Number of reinforcing bars parallel
                             to the y-direction
      46-50  MATNO4(NUMEL)   Number of reinforcing bars parallel
                             to the z-direction
      51-55  NRESU(NUMEL)    Element output control parameter:
                             (This is because the amount of output
                             from a full nonlinear run is
                             enormous and usually the output of
                             certain elements is of more interest
                             than others)
                             0-Output element cracking and crushing
                             situation, reinforcement stresses and
                             strains and yielding situation
                             1-Output element Gauss point
                             coordinates, normal and shear stresses
                             and strains, cracking and crushing
                             situation, reinforcement stresses and
                             strains and yielding situation
                             2-Output element Gauss point
                             coordinates, principal stresses and
                             strains and their directions,
                             reinforcement stresses and strains
                             and yielding situation
                             3-Output element Gauss point
                             coordinates, normal and shear stresses
                             and strains, principal stresses and
                             strains and their directions,
                             cracking and crushing situations,
                             reinforcement stresses and strains
                             and yielding situation
```

Note: The nodal connection numbers for each element must be
      listed in the anticlockwise sequence shown in Figure (1)
      starting from any corner node.

CARD SET 4 NODAL COORDINATES CARDS(I5,3F10.3)-One card for
            each node whose coordinates are to be input. If
            NCORN=1 in Card Sets 2, omit this set and instead
            Card Sets 5 and 6 must be used to generate the mesh.
```
Cols.  1-5   IPOIN          Nodal point number
       6-15  COORD(IPOIN,1) X-coordinate of the node
      16-25  COORD(IPOIN,2) Y-coordinate of the node
      26-35  COORD(IPOIN,3) Z-coordinate of the node
```

Notes: 1) The coordinates of the highest numbered node must be
          input, regardless of whether it is a midside node or
          not.

2) The total number of cards in this set will generally
   differ from NPOIN in card set 2 since for element
   sides which are linear it is only necessary to specify
   data for corner nodes; intermediate nodal coordinates
   being automatically interpolated if on a straight
   line.

CARD SET 5 REGULAR SOLID MESH GENERATION CONTROL
CARD(3F10.3,3I5)-One card (used for regular solid mesh only). if
                 NCORN=0 in Card Set 2, omit this set.
Cols. 1-10 XINCR   Increment of length in x-direction
      11-20 YINCR   Increment of length in y-direction
      21-30 ZINCR   Increment of length in z-direction
      31-35 NDIVX   Number of equal divisions in
                           x-direction
      36-40 NDIVY   Number of equal divisions in
                           y-direction
      41-45 NDIVZ   Number of equal divisions in
                           z-direction

CARD SET 6 REGULAR SOLID MESH GENERATION NODE CARDS(I5)-One
           card for each corner node. If NCORN=0 in Card Set 2,
           omit this set. Total = number of corner nodes.
Cols. 1-5 IPOIN   Nodal point number

CARD SET 7 RESTRAINED NODE CARDS(I5,2X,3I1,3F10.3)-One card for
           each restrained node. Total of NVFIX cards specified
           in Cars Set 2.
Cols. 1-5 NOFIX   Restrained node number
      8   IFPRE(IVFIX,1) Condition of restraint on
                           x-displacement
                           0-No displacement restraint
                           1-Nodal displacement restraint
      9   IFPRE(IVFIX,2) Condition of restraint on
                           y-displacement
                           0-No displacement restraint
                           1-Nodal displacement restraint
      10   IFPRE(IVFIX,3) Condition of restraint on
                           z-displacement
                           0-No displacement restraint
                           1-Nodal displacement restraint
      11-20 PRESC(IVFIX,1) The prescribed value of the x
                           component of the nodal displacement
      21-30 PRESC(IVFIX,2) The prescribed value of the y
                           component of the nodal displacement
      31-40 PRESC(IVFIX,3) The prescribed value of the z
                           component of the nodal displacement

CARD SET 8 ELEMENT REINFORCEMENT CARDS(2I5,3F10.3,2I5)-One card
           for each bar passing through the element. Total in
           each element = NBARE = MATNO2(IELEM)+MATNO3(IELEM)+
           MATNO4(IELEM) as specified in Card Set 3. If NREPL=0
           in Cars Set 2 (i.e. when the whole structure is plain
           concrete), omit this set. If NBARE = 0 for a certain
           element then omit the cards corresponding to that
           element in this set.
Cols. 1-5 IELMR   Reinforced element number
      6-10 NBARN(IELMR,IBARE) Bar number
      11-20 BARXP(IELMR,IBARE) X-local coordinate of the bar
                               (=0.0 if the bar is parallel to

```
                                    the x-direction)
    21-30  BARYP(IELMR,IBARE)  Y-loacl coordinate of the bar
                               (=0.0 if the bar is parallel to
                               the y-direction)
    31-40  BARZP(IELMR,IBARE)  Z-local coordinate of the bar
                               (=0.0 if the bar is parallel to
                               the z-direction)
    41-45  NBMAT(IELMR,IBARE)  Bar material number
    46-50  NBDIR(IELMR,IBARE)  Bar direction:
                               1-If the bar is parallel to the
                               local x-axis
                               2-If the bar is parallel to the
                               local y-axis
                               3-If the bar is parallel to the
                               local z-axis
```

CARD SET 9 CONCRETE MATERIAL PROPERTY CARDS(I5,2F10.3,2F5.3, 2F7.3,2F12.8,F5.3)-One card for each different type of concrete. Total of NMATS cards specified in Card Set 2.

```
Cols.  1-5   NUMAT               Material property number
       6-15  PROPS(NUMAT,1)      Initial modulus of elasticity,Ei,
                                 from uniaxial stress-strain curve
      16-25  PROPS(NUMAT,2)      Secant value of Young's modulus
                                 at uniaxial compressive failure
      26-30  PROPS(NUMAT,3)      Initial value of Poisson's ratio
      31-35  PROPS(NUMAT,4)      Secant failure value of Poisson's
                                 ratio
      36-42  PROPS(NUMAT,5)      Cylinder crushing strength of
                                 concrete
      43-49  PROPS(NUMAT,6)      Tensile Strength of concrete
      50-61  PROPS(NUMAT,7)      Mass density of concrete
      62-73  PROPS(NUMAT,8)      Coefficient of thermal expansion
      74-78  PROPS(NUMAT,9)      Ratio of uniaxial tensile to
                                 compressive strength of concrete
                                 (this must be 0.08, 0.1 or 0.12
                                 as Ottosen constants are tabulated
                                 for these three values only)
```

Note: 1) The initial Young's modulus is about (2.0-2.5) x secant failure value.

CARD SET 10 FIRST ADDITIONAL CONCRETE PROPERTIES CARD(4F8.5) One card. Data for Ottosen model, modified Coulumb criterion and uniaxial crushing strain of concrete.

```
Cols.  1-8   OTTOD               Ottosen parameter,D, for concrete
                                 constitutive equation (0.0 to 1.0)
       9-16  OTTBA               Ottosen Parameter,Ba, for concrete
                                 constitutive equation (=0.8)
      17-24  PHIMC               Angle of internal friction for
                                 the modified Coulumb criterion
                                 for concrete (=37.0 degrees)
      25-32  UCRSN               The value of the uniaxial crushing
                                 strain of concrete
```

CARD SET 11 SECOND ADDITIONAL CONCRETE PROPERTIES CARD(6F8.5) One card. Data for shear retention factor, tension stiffening and the ratio of allowable cracking strength of concrete to its tensile strength.

```
Cols.  1-8   BETA1               The value to which the shear
```

		retention factor drops immediately upon cracking (0.0 - 1.0)
9-16	BETA2	The value to which the shear retention factor finally settles (0.0 - BETA1)
17-24	BETA3	The ratio of the final normal tensile strain, after which the shear retention factor remains a constant (=BETA2), to the cracking strain
25-32	ALFA1	The ratio of the value to which the normal stress across the crack drops immediately at cracking to the tensile strength of concrete for the tension stiffening model
33-40	ALFA2	The value of the final tensile strain at which the tension stiffening effect becomes zero to the cracking strain
41-48	RATFT	Ratio of the allowable (cracking) stress to the tensile strength of concrete

CARD_SET_12_REINFORCEMENT_PROPERTY_CARDS(I5,4F15.8)-One card
for each type of steel. Total of NSTYP specified
in Card Set 2. If NREPL = 0 in Card Set 2 (i.e.
when the whole structure is plain concrete), omit
this set.

Cols.	1-5	NREIN	Reinforcing steel type number
	6-20	STPRO(NREIN,1)	Young's modulus of elasticity
	21-35	STPRO(NREIN,2)	X-sectional area of the bar
	36-50	STPRO(NREIN,3)	Yielding stress
	51-65	STPRO(NREIN,4)	Work hardening factor after yielding (specified as the percentage ratio of Young's modulus after yielding to that before yielding)

Note: 1) If two steel types (i.e. mild and high tensile) having
the same diameter are used they can be input as two
different materials. In fact this is a more versatile
representation of steel behaviour, as each bar is
individually modelled and hence follows its own
stress-strain law.

CARD_SET_13_LOAD_TITLE_CARD(12A6)-One card

Cols.	1-72	TITLE	Title of the load - limited to 72 alphanumeric characters

CARD_SET_14_LOAD_TYPE_INDICATOR_CARD(5I5)-One card

Cols.	1-5	IPLOD	Applied point load control parameter: 0-No applied nodal point loads to be input 1-Applied nodal point loads to be input
	6-10	IGRAV	Gravity loading control parameter: 0-No gravity loads to be considered 1-Gravity loads to be considered
	11-15	IEDGE	Distributed edge load control parameter:

                                    0-No distributed edge loads to be
                                    input
                                    1-Distributed edge loads to be
                                    input
        16-20 ITEMP   Thermal loading control parameter:
                                    0-No thermal loading to be input
                                    1-Thermal loading to be input
        21-25 IFACE   Distributed loads on the face
                                    control parameter:
                                    0-No distributed loads on the face
                                    to be input
                                    1-Distributed loads on the face to
                                    be input

CARD_SET_15_APPLIED_POINT_LOAD_CARDS(I5,3F15.2)-One card for
              each loaded nodal point.
Cols. 1-5   LODPT   Node number
      6-20 POINT(1)   Load component in x-direction
      21-35 POINT(2)   Load component in y-direction
      36-50 POINT(3)   Load component in z-direction

Notes: 1) The last card should be that for the highest numbered
          node whether it is loaded or not.
       2) If IPLOD = 0 in Card Set 14, omit this set.

CARD_SET_16_GRAVITY_LOADING_CARD(3F10.3)-One card
Cols. 1-10 GRAVX   Component of gravity in
                                    x-direction
      11-20 GRAVY   Component of gravity in
                                    y-direction
      21-30 GRAVZ   Component of gravity in
                                    z-direction

Notes: 1) The component of the gravity loading must be specified
          as multiple of the gravitational acceleration g.
       2) If IGRAV = 0 in Card Set 14, omit this set.

CARD_SET_17_DISTRIBUTED_EDGE_LOAD_CARDS
16(a)_CONTROL_CARD(I5)-One card
Cols. 1-5   NEDGE   Number of element edges on which
                                    distributed loads are to be
                                    applied
16(b)_ELEMENT_EDGE_TOPOLOGY_CARDS(4I5)
Cols. 1-5   NEASS   The element number with which the
                                    element edge is associated
      6-10 NOPRS(1)   List of nodal points, in an
                                    anticlockwise sequence, of the
                                    nodes forming the element edge on
                                    which the distributed load acts
16(c)_DISTRIBUTED_LOAD_CARDS(9F8.4)
Cols. 1-8   PRESS(1,1)   Value of x-component of the
                                    distributed load at node NOPRS(1)
      9-16 PRESS(2,1)   Value of x-component of the
                                    distributed load at node NOPRS(2)
      17-24 PRESS(3,1)   value of x-component of the
                                    distributed load at node NOPRS(3)
      25-32 PRESS(1,2)   Value of y-component of the
                                    distributed load on node NOPRS(1)
      33-40 PRESS(2,2)   Value of y-component of the
                                    distributed load on node NOPRS(2)

```
41-48 PRESS(3,2)          Value of y-component of the
                          distributed load on node NOPRS(3)
49-56 PRESS(1,3)          Value of z-component of the
                          distributed load on node NOPRS(1)
57-64 PRESS(2,3)          Value of z-component of the
                          distributed load on node NOPRS(2)
65-72 PRESS(3,3)          Value of z-component of the
                          distributed load on node NOPRS(3)
```

Notes: 1) Subsets 17(b) and 17(c) must be repeated in turn for
           every element edge on which a distributed load acts.
           The element edges can be considered in any order.
       2) If IEDGE = 0 in Card Set 14, omit this set.

CARD_SET_18_TEMPERATURE_CARDS(I5,F10.3)
Cols. 1-5 NODPT   Node number
       6-15 TEMPE(NODPT)   Temperature at node

Notes: 1) Datum temperature is taken to be zero.
       2) Only nodal temperature which are non-zero need be
          input. The card set must terminate with the highest
          numbered node regardless of the temperature value at
          this node.
       3) If ITEMP = 0 in Card Set 14, omit this set.

CARD_SET_19_DISTRIBUTED_LOAD_ON_ELEMENT_FACE_CARDS
19(a)_CONTROL_CARD(I5)-One card
Cols. 1-5 NFACE   Number of element faces on which
                                distributed loads are to be input
19(b)_ELEMENT_FACE_TOPOLOGY_CARDS(9I5)
Cols. 1-5 NEASS   The element number with which the
                                element face is associated

       6-10 NOPRS(1)
      11-15 NOPRS(2)
      16-20 NOPRS(3)   List of nodal points, in an
      21-25 NOPRS(4)   anticlockwise sequence, of the
      26-30 NOPRS(5)   nodes forming the face on which
      31-35 NOPRS(6)   the distributed load acts
      36-40 NOPRS(7)
      41-45 NOPRS(8)
19(c)_DISTRIBUTED_LOAD_CARDS(8F10.4/8F10.4/8F10.4)-Three cards
       for each loaded face as clear in the format.
First_Card:
Cols. 1-10 PRESS(1,1)
      11-20 PRESS(2,1)
      21-30 PRESS(3,1)   Values of x-component of the
      31-40 PRESS(4,1)   distributed load at nodes NOPRS(1),
      41-50 PRESS(5,1)   NOPRS(2),NOPRS(3),......,NOPRS(8)
      51-60 PRESS(6,1)
      61-70 PRESS(7,1)
      71-80 PRESS(8,1)
Second_Card:
Cols. 1-10 PRESS(1,2)
      11-20 PRESS(2,2)
      21-30 PRESS(3,2)   Values of y-component of the
      31-40 PRESS(4,2)   distributed load at nodes NOPRS(1),
      41-50 PRESS(5,2)   NOPRS(2),NOPRS(3),......,NOPRS(8)
      51-60 PRESS(6,2)
      61-70 PRESS(7,2)
      71-80 PRESS(8,2)
```

Third Card:
Cols. 1-10 PRESS(1,3)
     11-20 PRESS(2,3)
     21-30 PRESS(3,3)          Values of z-component of the
     31-40 PRESS(4,3)          distributed load at nodes NOPRS(1),
     41-50 PRESS(5,3)          NOPRS(2),NOPRS(3),......,NOPRS(8)
     51-60 PRESS(6,3)
     61-70 PRESS(7,3)
     71-80 PRESS(8.3)

Notes: 1) Subsets 19(b) and 19(c) must be repeated in turn for
          every element face on which a distributed load acts.
          The element faces can only be on the x-y plane.
       2) If NFACE = 0 in Card Set 14, omit this set.

CARD SET 20 LOAD INCREMENT CONTROL CARDS(2F10.5,3I5)-One card
          for each load increment. Total of NINCS cards as
          specified in Card Set 3.
Cols. 1-10 FACTO              Applied load factor for this
                              increment specified as a factor
                              of the loading input in Card Sets
                              14 to 19
     11-20 TOLER              Convergence tolerance factor as
                              a percentage
     21-25 MITER              Maximum number of iterations
                              allowed for this load increment
     26-30 NOUTP(1)           Parameter controlling output of
                              results after the first iteration
                              (may be needed for investigation):
                              0-No output needed
                              1-Output displacements
                              2-Output displacements and
                              reactions
                              3-Output displacements, reactions
                              and stresses
     31-35 NOUTP(2)           Parameter controlling output of
                              the converged results (and the
                              results after the last iteration
                              had the solution not converged at
                              maximum number of iterations):
                              0-No output needed
                              1-Output displacements
                              2-Output displacements and
                              reactions
                              3-Output displacements, reactions
                              and stresses
Notes: 1) The applied loading factors are accumulative. If FACTO
          is specified as 0.6, 0.3, 0.2 for the first three load
          increments, then the total load acting during the
          third increment is 1.1 times that specified in Card
          Sets 14 to 19.
       2) The output control parameters NOUTP(1) and NOUTP(2)
          must not be mixed up with the element output control
          parameter NRESU specified in Card Set 3. NRESU is only
          relevant when NOUTP(1) or NOUTP(2) is equal to 3.

## APPENDIX C

The following set of equations is used to obtain the value of $\sigma_{3f}$ (the minimum compressive stress at failure) for a particular stress state ($\sigma_1$, $\sigma_2$, $\sigma_3$) using Ottosen's failure criterion described in Chapter Four.

$$I_1 = \sigma_1 + \sigma_2 + \sigma_3 \tag{1}$$

$$J_2 = \frac{1}{6}[(\sigma_1 - \sigma_2)^2 + (\sigma_2 - \sigma_3)^2 + (\sigma_1 - \sigma_3)^2] \tag{2}$$

$$\cos\theta = \frac{2\sigma_1 - \sigma_2 - \sigma_3}{2\sqrt{3}\sqrt{J_2}} \tag{3}$$

$$\cos3\theta = 4\cos^3\theta - 3\cos\theta \tag{4}$$

$$f(I'_1, J'_2, \cos3\theta) = a\frac{J_2}{\sigma_c^2} + \frac{J_2}{\sigma_c} + b\frac{I_1}{\sigma_c} - 1 \tag{5}$$

The computation procedure involves internal iteration and this is performed as follows:

(1) Start with a value DELIN = ($\sigma'_2 - 10$)/2

(2) Assume an arbitrary value for $\sigma'_{3f} = \sigma'_2 + $ DELIN

(3) Calculate $I_1$ using Equation (1)

(4) Calculate $J'_2$ using Equation (2)

(5) Calculate $\cos\theta$ from Equation (3)

(6) Calculate $\cos3\theta$ using Equation (4)

(7) Check if $\cos3\theta > 0$ then $= K_1\cos(\arccos(K_2\cos3\theta)/3)$

(8) Check if $\cos3\theta < 0$ then $= K_1\cos(\pi/3 - \arccos(-K_2\cos3\theta)/3)$

(9) Obtain $f(I'_1, J'_2, \cos3\theta)$ from Equation (5)

(10) Check if $f(I'_1, J'_2, \cos3\theta) < 10^{-6}$ then execute step (15)

(11) Make DELIN = DELIN/2

(12) Check if $f(I'_1, J'_2, \cos 3\theta) > 0$ then $\sigma'_{3f} = \sigma'_{3f}$ - DELIN

(13) Check if $f(I'_1, J'_2, \cos 3\theta) < 0$ then $\sigma'_{3f} = \sigma'_{3f}$ + DELIN

(14) Back to step (3) for a new value of $\sigma'_{3f}$

(15) terminate the process and accept last value of $\sigma'_{3f}$

## APPENDIX D

## DESIGN OF REFERENCE SPECIMEN B11 ACCORDING TO THE

## "TENTATIVE DESIGN RECOMMENDATIONS" - Chapter Nine

Two examples will be given here; the first example is a redesign of reference specimen B11 for the design torque of 8.0 KN.m. used in the experimental programme, whilst the second example is a calculation of the ultimate torque for the same specimen following the "Tentative Design Recommendations" using the actual amount of steel provided.

Steel and concrete characteristics:

high yield steel of $f_y$ = 410 N/mm$^2$

6 mm stirrups (area of two legs = 56 mm$^2$)

concrete grade 40 -

$v_{tmin}$ = $f_{sp}$/3.0 = 3.0/2 = 1.5 N/mm$^2$

($f_{sp}$ is the experimentally obtained value). This value is also used as the tensile strength of concrete $f'_t$.

Example (1)

Flange:

$x_1$ = 100-2x20-6= 54 mm,    $y_1$ = 200-2x20-6 = 154 mm

$h^3_{min}$ $h_{max}$ = $100^3$x200 = 2.0 x $10^8$ mm$^4$

$T_1$ = (2/25.2)xT = 0.635 KN.m

$$v_t = \frac{2T}{h^2_{min}(h_{max}-h_{min}/3)} = \frac{2x0.635x\,10^6}{100^2(200-100/3)} = 0.762 < v_{tmin}$$

∴ torsion reinforcement not required

St. Venant's coefficient* $\alpha$= $\alpha$(y/x) = $\alpha$(1.5) = 0.246

∴   $T_e$ = 0.5 (0.246x$100^2$x200x3.0x$10^{-6}$) = 0.738 KN.m

Web:

$x_1$ = 200-2x20-6 = 154 mm,    $y_1$ = 300-2x20-6 = 254 mm

* see Chapter 2, ref. 10 for example

$$h^3_{min} h_{max} = 200^3 \times 300 = 23.2 \times 10^8 \ mm^4$$

$$T_2 = (23.2/25.2) \times T = 7.365 \ KN.m$$

$$v_t = \frac{2T}{h^2_{min}(h_{max}-h_{min}/3)} = \frac{2 \times 7.365 \times 10^6}{200^2(300-200/3)} = 1.578 > v_{tmin}$$

$$\therefore \ \text{torsion reinforcement required}$$

$$y_1 = 254 < 550 \ \therefore \ \text{section is small}$$

$$v_{tu} \times y_1/550 = 4.75 \times (254/550) = 2.194 \ N/mm^2$$

$$\therefore \ v_t < 2.194 \quad \therefore \ \text{section is feasible}$$

St. Venant's coefficient $\alpha = \alpha(y/x) = \alpha(2.0) = 0.2305$

$$\therefore \ T_e = 0.5 \ (0.2305 \times 200^2 \times 300 \times 3.0 \times 10^{-6}) = 4.149 \ KN.m$$

$$\therefore \ T_s = 8.0 - 4.149 - 0.738 = 3.113 \ KN.m$$

$$\text{Links:} \quad \frac{A_{sv}}{s_v} > \frac{T_2}{0.8 x_1 y_1 (0.87 f_y)} = \frac{3.113 \times 10^6}{154 \times 254 \times 0.87 \times 410} = 0.279$$

$$\therefore \ s_v < 56/0.279 = 201 \ mm$$

but $s_v$ must be $< (x_1+y_1)/2$, $y_1/2$, 200 mm

$$< 204mm, \ 127mm, \ 200mm$$

say $s_v = 100 \ mm \quad \therefore \ \text{Provide 6mm links at 100 mm c/c}$

<u>Longitudinal steel:</u> $A_{sl} > (A_{sv}/s_v) \ (f_{yv}/f_{yl})(x_1+y_1)$

$$> (56/100) \ (1) \ (154+254)$$

$$> 229 \ mm^2$$

$$\therefore \ \text{Provide 4 bars 10 mm dia. (A 314 mm}^2)$$

## Comparison of volume ratios of reinforcement:

$\rho_v = 0.301\%$

$\rho_l = 0.393\%$

$\rho_t = 0.694\%$     This is about 35% of the total reinforcement ratio of specimen B11 which only cracked at a torque of 12.43 KN.m and failed at a torque of 23.95 KN.m.

.. saving in steel amount of specimen B11 is 65%.

## Example (2)

Calculation of the ultimate torque of specimen B11 using the actual amount of steel provided according to the suggested provisions.

$$T = \sum (T_e + T_s) = (T_e + T_s)_{web} + (T_e + T_s)_{flange}$$

$$= 0.5 \times (0.2305 \times 200^2 \times 300 \times 3.0 \times 10^{-6}) +$$

$$(56/50) \times 0.8 \times 154 \times 254 \times 0.87 \times 410 \times 10^{-6} +$$

$$0.5 \times (0.246 \times 100^2 \times 200 \times 3.0 \times 10^{-6} +$$

$$(56/50) \times 0.8 \times 54 \times 154 \times 0.87 \times 410 \times 10^{-6}$$

$$= 4.149 + 12.502 + 0.738 + 2.658 \qquad = 20.05 \ KN.m$$

Comparison of this torque and the experimental ultimate torque (23.95 KN.m) reveals that this procedure is still reasonably conservative.

The following table shows comparisons of the ultimate torques for all specimens according to the above procedure and the experimental failure torques. It can be seen that the procedure is still reasonably conservative.

## Table (D.1)

| Specimen | $T$ KN.m | T(Exper.) KN.m | $\dfrac{T(Exper.)}{T}$ |
|---|---|---|---|
| B11 | 20.05 | 23.95 | 1.19 |
| B12 | 15.72 | 22.75 | 1.45 |
| B13 | 12.47 | 19.66 | 1.58 |
| B14 | 31.96 | 34.54 | 1.08 |
| B21 | 19.93 | 24.89 | 1.25 |
| B31 | 14.38 | 20.88 | 1.45 |
| B32 | 11.14 | 18.14 | 1.63 |
| B33 | 8.72 | 17.25 | 1.98 |
| B34 | 25.40 | 28.43 | 1.12 |